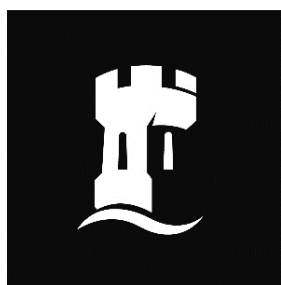


Flow Heck Reactions and Photocatalysed C-O Coupling Reactions

Toby H. Waldron Clarke

University of Nottingham and Johnson Matthey iCASE



Supervisors: Prof. Michael W. George and Prof. Sir Martyn Poliakoff
Industry Supervisor: Dr. Peter R. Ellis

*Thesis submitted to the University of Nottingham for the Degree of
Doctor of Philosophy*

September 2021

Declaration

I hereby declare that this Thesis and the work presented in it are my own, unless acknowledged otherwise.



Toby Waldron Clarke,
September 2021.

Acknowledgments

Firstly, I would like to thank my academic supervisors, Prof. Michael W. George and Prof. Sir Martyn Poliakoff, for their longstanding support both before and during my PhD, and for the continued opportunities to develop and execute research ideas, allowing me to develop as a scientist and an individual.

The work described in this Thesis was made possible by the help and support of many colleagues and collaborators. The project, as a collaboration between the University of Nottingham and JM, would also not have been possible without the support, input and assistance from collaborators. My industrial supervisor, Peter R. Ellis, has been immensely helpful in coordinating the project, communicating the interests of JM, and involving a brilliant team at JM, as well as offering numerous helpful discussions and meetings allowing for me to develop and learn whilst also gaining industrial insights. I would also like to thank Chris Zalis, Carin C. C. Johansson Seechurn and Rachel Kahan who have all had important inputs into the project, offering useful insights and allowing me hugely beneficial access to materials from JM.

Much of the work described in this Thesis could not have been completed without technical assistance and support from many members of technical staff at the University of Nottingham. Richard Wilson, Ben Clarke, Matthew McAdam and Richard Meehan for mechanical engineering inputs, mostly in fabrication of equipment used for the flow reactor used in Chapters 2, 3 and 4 without which, the work would not have been possible, and for frequently fixing/maintaining various pieces of equipment throughout this project. I also thank David Litchfield for similar assistance, useful discussions and electrical/electronic engineering inputs, allowing for equipment in both flow reactors built in this project to be used and maintained, again without which, the work in this project would not have been possible. Also, glassblowing technicians Clive Dixon and Conor Howell-Bennett have been hugely helpful throughout the project in constructing and fixing glassware used in general laboratory work and for building of the flow photochemical reactor as well as always offering helpful discussions. Mark Guylar has also been hugely helpful in ensuring efficient lab operations and always being able to offer advice and inputs on a huge variety of aspects over the course of the project. Analytical staff, particularly Shazad Aslam for NMR assistance and Ben Pointer-Gleadhill with GC-MS assistance are thanked for their help.

Huge thanks are owed to all members of the George & Poliakoff Group throughout my time there for both help and inputs into my development and research. In particular, to Bryan Tambosco, Jonathan Moore, Hamza Boufroua and Marcos Veguillas for helping me to develop as a synthetic chemist; Darren Lee, Rowena Howie and Ke Jie for helping me develop the skills needed to undertake work in flow chemistry; Rodolfo Teixeira, Xue Zhong Sun and Surajit Kayal for assisting and participating in time-resolved spectroscopic investigations who the work would not have been possible without; as well as Ashley Love, Katherine Reynolds and Genevieve Garwood who have all had valuable inputs. Importantly, I have had the privilege to guide and work alongside a number of project students, Adam Lee, Georgia Briscoe and Benjamin Lugg as well as collaborating with and mentoring Wagma Ayub in continuous flow PGM catalysed synthesis and I hope that they were able to learn as much from me as I was from them.

I would lastly like to thank any organisations/individuals who I have received useful support from, such as the Royal Society of Chemistry for the award of a Researcher Development Grant, the Nature Communications Chemistry journal for the award of an Early Career Researcher Training Grant Award, Scientific Update for the recognition of a Young Chemist Award for work in continuous flow Pd-catalysis and the EPSRC for funding this iCASE studentship as well as for a Doctoral Prize to continue pursuing my passion following the work described in this Thesis.

Abbreviations

Commonly used abbreviations used in this Thesis are as follows:

BPR	Backpressure Regulator
Butac	<i>n</i> -butyl acrylate
ButCin	<i>n</i> -butyl cinnamate
CGE	1-(cyclohexyloxy)-2-methoxybenzene
dF(CF ₃)ppy	2-(2,4-Difluorophenyl)-5-(trifluoromethyl)pyridine
DHB	1,2-dihydroxy but-3-ene
DIPEA	Diisopropyl ethylamine
dtbbpy	4,4'-Di- <i>tert</i> -butyl-2,2'-dipyridyl
FEP	Fluorinated ethylene propylene
FID	Flame ionisation detector
GC	Gas chromatography
Gcl	Guaiacol
GVL	γ -valero lactone
HPBO	1-hydroxy-4-(3-pyridyl)butan-2-one
HPLC	High pressure liquid chromatography
IB	Iodobenzene
ID	Inner diameter
Ir-125	[Ir(ppy) ₂ (dtbbpy)]PF ₆
Ir-126	[Ir{dF(CF ₃)ppy} ₂ (dtbbpy)]PF ₆
JM	Johnson Matthey
LED	Light emitting diode
MeButCin	butyl (E)-3-(<i>p</i> -tolyl)acrylate
MLCT	Metal-to-ligand charge transfer
NHPI	1,3-dioxoisindolin-2-yl cyclohexanecarboxylate
OD	Outer diameter
PGM	Platinum group metal
ppm	Parts per million
ppy	2-phenyl pyridine
PTFE	Polytetrafluoroethylene
RHR	Reductive Heck Reaction
RHP	Reductive Heck Product
RRHR	Redox Relay Heck Reaction
SCE	Saturated calomel electrode
SS	Stainless steel (316)
TMG	<i>N,N,N',N'</i> -tetramethyl guanidine
TRIR	Time-resolved infrared
TWV	Three-way valve
<i>w.r.t.</i>	With respect to
WT	Wall thickness
1-Hex	1-hexanol
3IP	3-iodo pyridine
4BrAP	4-bromo acetophenone
4HOAP	4-hexyloxy acetophenone
4IA	4-iodo anisole
4PBO	<i>trans</i> -4-Phenyl-3-buten-2-one

Thesis Summary

The work described in this Thesis involves a collaborative project between the University of Nottingham and Johnson Matthey (JM). JM operate in many aspects related to platinum group metals (PGMs, Pt, Pd, Ir, Rh, Os and Ru),¹ an important application of which is in catalysis,^{2,3} particularly for chemical manufacturing. The remit for this project involves the application of flow synthesis and PGM catalysis, for developing thermal Pd-catalysed C-C coupling reactions and photochemical Ir-catalysed C-O coupling reactions, in flow.

Chapter 1

This Chapter introduces the background concepts to the work conducted, namely, synthetic process chemistry, flow chemistry and platinum group metal catalysis and how these are combined for developing more efficient processes.

Thermal Continuous Flow Pd-Catalysed C-C Coupling Reactions

A thermal flow reactor was built and used to investigate Heck-type Reactions. Low loadings of simple Pd salts (with no added ligands) were employed in short residence times, at >200 °C, for Heck Reactions, Redox Relay Heck Reactions and Reductive Heck Reactions, described in Chapters 2-4.

Chapter 2 – Heck Reaction

The Heck Reaction between iodobenzene and *n*-butyl acrylate was used to benchmark the reactor. Following optimisation, good yields at 250-270 °C (in MeCN), were observed using Pd(OAc)₂ (no added ligand) at 0.0005 mol% (5 ppm), in short timescales (5-10 min).

Chapter 3 – Redox Relay Heck Reaction Towards a Pharmaceutical Intermediate

The reactor was then applied to a Redox Relay Heck Reaction (coupling of an aryl halide and alkenyl alcohol, furnishing an aryl-alkyl ketone), towards a pharmaceutical intermediate, prepared from a heterocyclic substrate and allylic alcohol coupling partner. Following optimisation in flow, in only 15 min residence time using low 0.05 mol% PdCl₂ (no added ligand), a yield of 73% (>95% conv.) was observed, at 225 °C.

Chapter 4 – Reductive Heck Reaction

The reactor was used for the development of the first (to our knowledge) flow Reductive Heck Reaction, adapting a batch method between aryl halides and enones, using excess diisopropylethylamine as a hydride source. Using 0.05 mol% loading of Pd(OAc)₂ (no added ligand), 70-75% yield was observed at 200 °C, in 10 min residence time. In this, an unexpected side-product was observed representing the first (to our knowledge) enone C=C reduction, using Pd(OAc)₂ and a tertiary amine, a potential avenue for further investigation of homogeneous “hydrogenations”, without using flammable H₂.

Photochemical Continuous Flow Ir-Catalysed C-O Coupling Reactions

A photochemical flow reactor was built and used to investigate metallaphotoredox C-O coupling reactions. Two processes for alkyl-aryl ether synthesis were developed, allowing either disconnection of the Ar-O-R motif to be performed synthetically, in flow, adapting previously described procedures. The mechanism of one was investigated using time-resolved infra-red spectroscopy, described in Chapters 5-7.

Chapter 5 – Ir/Ni C-O Coupling of Aryl Bromides and Alcohols

A previously reported Ir/Ni dual catalytic C-O formation was translated into flow following screening in batch to determine suitable conditions for flow processing. *N,N,N',N'*-tetramethylguanidine (TMG) was found to replace quinuclidine *and* K_2CO_3 , whilst maintaining homogeneity. In the flow photoreactor, it was observed that Ir-photocatalyst loading, Ni-catalyst loading and solvent demand could be reduced (relative to batch reactions). Productivities approaching 200 g day^{-1} , with yields around 90%, in short residence times following optimisation were observed.

Chapter 6 – Ir/Cu C-O Coupling of Phenols and NHPI-Esters

A second metallaphotoredox alkyl-aryl etherification reaction, involving Ir/Cu decarboxylative coupling was translated into flow. This involved the opposite retrosynthetic disconnection to the Ir/Ni approach, with redox-active esters and phenols as coupling partners. Already homogeneous, this was straightforwardly translated into flow where optimisation of Ir/Cu loadings, reaction time/temperature, added amine equivalents and concentration resulted in yields of ~90% being observed, again in short timescales and allowing for reduced Ir loadings (1 mol% to 0.1-0.5 mol%) and reduced Cu loadings (20 mol% to 10 mol%) to be applied. Productivities of $\sim 80 \text{ g day}^{-1}$ were observed.

Chapter 7 – TRIR Mechanistic Investigations of Ir/Ni C-O Coupling

The Ir/Ni C-O coupling mechanism was also investigated using time-resolved infrared spectroscopy, involving acquiring transient IR spectra on the ns- μ s timescale following photoexcitation. Evidence supporting a reductive quenching pathway by quinuclidine or TMG, and subsequent reduction (presumably by the reduced photocatalyst) of the Ni co-catalyst was observed. This forms a better mechanistic picture, assisting in reaction optimisation, or developing new reactions.

Table of Contents

Chapter 1 Background and Introduction	10
1.1 Introduction	11
1.2 Synthetic Organic Process Chemistry	11
1.3 Green Chemistry and Engineering in Synthetic Processes	13
1.4 Catalysis in Synthetic Processes	15
1.5 Continuous Flow Chemistry	19
1.6 Project Aims & Strategy	25
Thermal C-C Coupling Reactions <i>Flow Heck-Type Reaction Processes</i>	26
Chapter 2 Heck Reactions in Flow with Novel Processing Conditions	27
2.1 Abstract	28
2.2 Strategy & General Aims	28
2.3 Introduction	29
2.3.1 Palladium-Catalysed Cross-Coupling Reactions	29
2.3.2 Continuous Flow Palladium-Catalysed Cross-Coupling Reactions in Process Chemistry	32
2.3.3 Further Examples of Continuous Flow Heck Reactions	35
2.4 Results & Discussion	39
2.4.1 Initial Investigations Using a Vapourtec Reactor	39
2.4.2 Building a New Reactor to Enable Access to Novel Process Windows	45
2.4.3 Applying the Custom-Built Reactor to Model Heck Reactions	48
2.4.4 Catalyst Screen Involving Pre-Formed Pd Catalysts	53
2.4.5 Investigating >300 °C Reaction Conditions	56
2.4.6 Screening High Boiling Solvents as Potentially Greener Alternatives	58
2.4.7 Investigating GVL as a Green Reaction Solvent Enabling Access to Temperatures >300 °C	59
2.5 Conclusions & Further Work	60
Chapter 3 Flow Redox Relay Heck Reaction Towards a Pharmaceutical Intermediate	62
3.1 Abstract	63
3.2 Strategy & General Aims	63
3.3 Introduction	64
3.3.1 Redox Relay Heck Reaction Basic Principles	64
3.3.2 Developments and Applications of Redox Relay Heck Reactions	69
3.3.3 Summary	73
3.4 Results & Discussion	73
3.4.1 Redox Relay Heck Reaction in the Synthesis of a Pharmaceutical Intermediate	73
3.4.2 Continuous Flow Optimisation of a Redox Relay Heck Reaction	74
3.5 Conclusions & Further Work	81
Chapter 4 Reductive Heck Reactions in Continuous Flow	83
4.1 Abstract	84
4.2 Strategy & General Aims	84
4.3 Introduction	84
4.3.1 Traditional and Reductive Heck Reactions	84
4.3.2 Applications of Reductive Heck Reactions	86
4.3.3 Conditions for Reductive Heck Reactions	87
4.4 Results & Discussion	90
4.4.1 Selection of an Appropriate Reductive Heck Reaction for Developing a Flow Process	90
4.4.2 Initial Batch Reactions	91
4.4.3 Initial Flow Temperature Dependence Investigation	96
4.4.4 Determining the Identity of an Unexpected Side-Product	98
4.4.5 Attempts to Increase Reaction Selectivity	98
4.5 Conclusions & Further Work	105
Photocatalysed C-O Coupling Reactions <i>Flow Ir/Ni and Ir/Cu Reaction Processes</i>	107
Chapter 5 Photocatalysed C-O Bond Synthesis in Continuous Flow: Ir/Ni-Catalysed C-O Coupling	108
5.1 Abstract	109
5.2 Strategy & General Aims	109
5.3 Introduction	110
5.3.1 Photochemistry and Photoredox Catalysis	110
5.3.2 Photoredox Catalysis	111
5.3.3 Dual Metallaphotoredox Catalysis	117
5.3.4 C-O Bond Forming Reactions in Organic Synthesis	120
5.3.5 Photocatalytic Developments in C-O Bond Forming Alky-Aryl Etherification Reactions	123
5.4 Results & Discussion	128
5.4.1 Determination of a Suitable Reaction to Investigate in Flow	128

5.4.2 Initial Investigations in Batch to Determine Conditions Suited to Flow Processing	129
5.4.3 Construction of a Flow Reactor for Investigating Continuous MacMillan C-O Coupling.....	140
5.4.4 Initial MacMillan C-O Bond Formations in Flow	141
5.4.5 Considerations for Optimisation of MacMillan Coupling Conditions in Flow	142
5.4.6 Investigating Temperature Dependence of MacMillan C-O Coupling in Flow.....	143
5.4.7 An Assessment of Reactor Fouling and Control Experiments.....	145
5.4.8 Investigations into Reduced Ir and Ni Catalyst Loadings in Continuous Flow	148
5.4.9 Concentration Dependence Investigations.....	151
5.4.10 Investigation of the Process Productivity and Scalability.....	152
5.5 Conclusions & Further Work.....	155
Chapter 6 Photocatalysed C-O Bond Formation in Continuous Flow: Ir/Cu-Catalysed C-O Coupling.....	156
6.1 Abstract	157
6.2 Strategy & General Aims	157
6.3 Introduction	158
6.3.1 Decarboxylative Metallaphotoredox C-O Coupling Reaction	158
6.3.2 Redox-Active NHPI-Esters	159
6.3.3 Issues with Cu-Catalysis in Synthesis.....	160
6.3.4 Works Exploiting Redox-Active NHPI-Esters	161
6.3.5 Other Works Circumventing Cu-Catalysis Issues	163
6.3.6 Other Works Circumventing Cu-Catalysis Issues with Redox-Active NHPI-Esters	164
6.4 Results & Discussion.....	166
6.4.1 Initial Reactions in Batch.....	166
6.4.2 Initial Development of Flow Processing Conditions – Residence Time and Temperature.....	169
6.4.3 Catalyst Loading Screen	170
6.4.4 Optimising Amine Additive Equivalents	171
6.4.5 Optimising Concentration.....	172
6.4.6 Catalyst Screen	173
6.4.7 Assessment of the Reaction Scalability and Productivity.....	173
6.5 Conclusions & Further Work.....	175
Chapter 7 Investigating the Dual Ir/Ni Etherification Mechanism with Time-Resolved Infrared Spectroscopy.....	176
7.1 Abstract	177
7.2 Strategy & General Aims	177
7.3 Introduction	178
7.3.1 Time-Resolved Spectroscopy for Mechanistic Investigation	178
7.3.2 Time-Resolved Infrared Investigations Related to Photoredox Catalysis	180
7.3.3 Mechanistic Proposals for the MacMillan C-O Coupling Reaction	185
7.3.4 Previous Investigations of Mechanisms for the MacMillan C-O Coupling Reaction.....	187
7.3.5 Summary.....	192
7.4 Results & Discussion.....	192
7.4.1 Assigning the Excited State Photocatalyst	192
7.4.2 Investigations with Quinuclidine as a Reaction Additive	195
7.4.3 Investigations with TMG as a Reaction Additive	200
7.4.4 TMG and Quinuclidine Comparison	207
7.4.5 Mechanistic Proposal	208
7.5 Conclusions & Further Work.....	209
Chapter 8 Summary	210
References.....	213
Experimental	221
Exp.1 General Experimental Detail	221
Exp.2 Flow Reactors.....	222
Exp.2.1 Thermal Tubular Flow Reactor	222
Exp.2.2 Photochemical FEP Coil Flow Reactor	224
Exp.3 Light Sources.....	228
Exp.3.1 Variable Colour LED Block.....	228
Exp.3.2 White LED Block.....	229
Exp.3.3 Lightsabre LEDs.....	230
Exp.4 TRIR Experimental Detail.....	231
Exp.4.1 General Detail	231
Exp.4.2 Detail of the Time-Resolved Infrared Spectroscopy Equipment.....	231
Exp.4.3 Data Processing, Analysis and Fitting	233
Exp.5 Characterisation/Isolation Data for Compounds Synthesised	233
Exp.5.1 Chapter 2	233
Exp.5.2 Chapter 3	234

Exp.5.3 Chapter 4	234
Exp.5.4 Chapter 5	235
Exp.5.5 Chapter 6	236
Exp.6 Experimental Synthesis Procedures	236
Exp.6.1 Chapter 2	236
Exp.6.2 Chapter 3	251
Exp.6.3 Chapter 4	256
Exp.6.4 Chapter 5	265
Exp.6.5 Chapter 6	279
Appendix	289
Ap.1 Spectral Data	289
Ap.1.1 Chapter 2	289
Ap.1.2 Chapter 3	291
Ap.1.3 Chapter 4	294
Ap.1.4 Chapter 5	296
Ap.1.5 Chapter 6	297
Ap.2 Analytical Yield Quantification (GC or ¹ H NMR)	299
Ap.2.1 Chapter 2	299
Ap.2.2 Chapter 3	301
Ap.2.3 Chapter 4	302
Ap.2.4 Chapter 5	304
Ap.2.5 Chapter 6	308
Ap.3 Spectroelectrochemistry Data	309
Ap.3.1 Ir-126 Spectroelectrochemistry Data	310
Ap.3.2 TMG Spectroelectrochemistry Data	311
Ap.3.3 Quinuclidine Spectroelectrochemistry Data	311
Ap.3.4 NiCl ₂ .glyme/dtbbpy Spectroelectrochemistry Data	312
Ap.4 Reactor Standard Operating Procedures	313
Ap.4.1 Thermal Flow Reactor Standard Operating Procedure	313
Ap.4.2 Photochemical FEP Flow Reactor Standard Operating Procedure	315
Ap.5 GC Chromatograms	317
Ap.5.1 Chapter 2	317
Ap.5.2 Chapter 3	318
Ap.5.3 Chapter 4	319
Ap.5.4 Chapter 5	321
Ap.5.5 Chapter 6	322

Chapter 1

Background and Introduction

1.1 Introduction

This project involves the development of synthetic processes in flow, involving PGM catalysis, with the principles of Green Chemistry and Green Engineering in mind. The overarching aims of the project involve the development of flow processes for thermal Pd-catalysed C-C coupling reactions, and photochemical Ir-catalysed C-O coupling reactions, as a collaboration between the University of Nottingham and JM.

Applying flow reactors for thermal, catalytic reactions can offer significant benefits.⁴⁻⁷ Due to continuously replenishing the mixture inside a flow reactor, small reactor volumes can be used whilst still achieving good throughput, leading to efficient heat transfer across narrow channels in flow reactors.⁴ Furthermore, small volumes can be efficiently heated without excessive energy requirements. Heating a large-volume batch reactor requires significant energy-input and often results in non-uniform heating.^{4,8} Furthermore, again due to the small volumes of flow reactors, superheated (above boiling point) conditions can be achieved efficiently and safely.⁵ This is because in flow and with a small volume, pressurised conditions can be achieved and, even in the event of *e.g.*, over-pressure, rupture *etc.*, small volumes minimise the associated safety hazard.⁴ Therefore, efficiently and safely accessing such novel processing windows in flow reactors can lead to processing benefits for synthetic chemistry.⁵ The work in Chapters 2, 3 and 4 looks towards applying the benefits of thermal flow reactors towards Heck-type processes.

Flow reactors also act as an enabling tool for photochemical reactions.^{4,9-11} Photochemistry offers a synthetic route towards products that can be difficult to prepare thermally.¹² In batch, however, photochemical reactions are difficult to scale-up due to issues with non-uniform irradiation. Using flow reactors, narrow channel transparent tubing can lead to efficient irradiation of mixtures containing chromophores.^{10,11} Photocatalysis has emerged as a field where mild conditions can be applied and powerful synthetic transformations performed.¹³ Being able to scale-up photochemical processes, enabled by efficient irradiation and simplified scalability using flow reactors, can realise the advantages of photochemistry.^{10,11} The work in Chapters 5 and 6 looks to develop continuous flow processes for Ir-photocatalysed C-O coupling reactions. The work in Chapter 7 looks towards a mechanistic investigation of one of these reactions, using time-resolved spectroscopy as a novel approach.

1.2 Synthetic Organic Process Chemistry

Synthetic chemistry has been described by K. C. Nicolaou as “*the art and science of constructing substances, natural or designed, whose primary element is carbon*”.¹⁴ This involves not only academic interest, but also has industrial applications *e.g.* in the synthesis/production of pharmaceuticals, agrochemicals, materials, fragrances/flavourings, amongst others. The development of efficient processes for the large-scale synthesis of such chemicals is therefore important.

The chemical synthesis/process industry can be traced back to the initiation of the synthetic dye industry, with the accidental synthesis of the artificial purple dye mauveine (by Perkin in 1865, while attempting to prepare the anti-malarial natural product quinine).¹⁴ This was followed by the syntheses of the naturally occurring dyes alizarin (Perkin, 1869, amongst others) and indigo (Baeyer, 1870), which were products already used, but until then had been extracted from plants, rather than prepared *via* synthetic processes (**Fig 1.1**).¹⁴ Typically, the extraction of chemical products (with a known useful

application) from nature is inefficient for meeting demand and/or would require the destruction/interference with natural eco-systems or habitats. Therefore, synthetic processes are important for obtaining such products, or for the development and production of non-natural chemical products with a required application.¹⁵

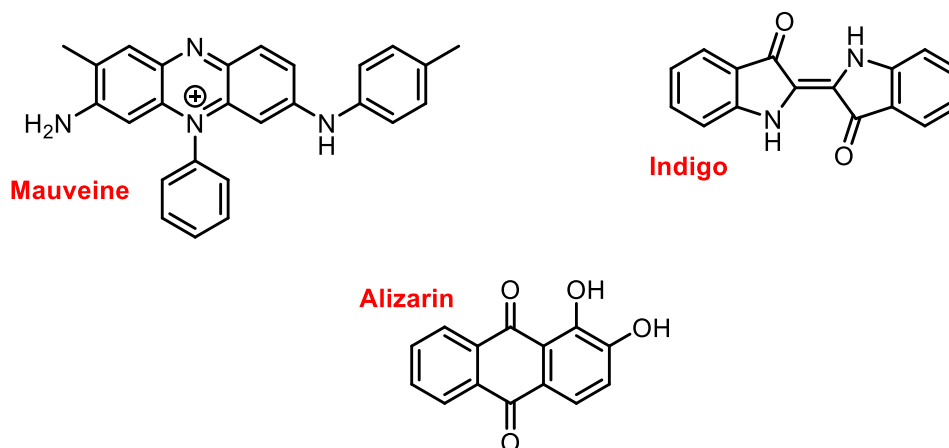
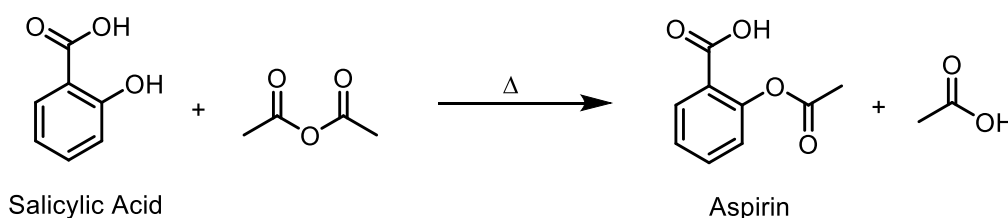


Fig 1.1 examples of dye chemicals that began the synthetic chemical industry.¹⁴

The beginning of the pharmaceutical industry followed the synthetic dye industry. Again, this was somewhat accidental, with Hoffmann synthesising Aspirin (acetylsalicylic acid) whilst working on the structural determination of the anti-inflammatory natural product, salicin.¹⁴ Hoffmann's synthesis involved heating salicylic acid, with acetic anhydride (**Scheme 1.1**).¹⁶



Scheme 1.1 Hoffmann's Aspirin synthesis from which, the pharmaceutical industry began.^{14,16}

Such examples represent perhaps the most obvious reason for performing synthesis and developing processes - that the target molecule is *needed*.¹⁵ Synthetic chemistry has been hugely important in developing society and changing the world.¹⁷ For example, pharmaceuticals vital for healthcare, agrochemicals needed to ensure adequate food supply, as well as sanitation chemicals, cosmetics, fragrances, flavourings, dyes and materials (present in applications such as clothes, plastics, electronics, amongst many others) are all produced *via* synthetic chemistry processes.^{14,15,17,18}

Traditionally, organic syntheses have been performed using conventional batch methodologies, in both the lab and the manufacturing plant.^{7,8} This involves the addition of reagents required to bring about a desired reaction into a single vessel, where they are then mixed and subjected to the necessary conditions to bring about the reaction.^{8,19} Typically, in a research lab, reactions are performed on small scales (<1 mL to around 10 L).⁷ On a manufacturing scale, however, processes may require being carried out on a much larger scale (up to 1000's of L).⁸ Despite the difference in scale, the approaches traditionally used to perform reactions on a manufacturing scale are not wholly unrecognisable from

the approaches traditionally used for much smaller lab scale reactions.⁸ In the research lab, reactions are typically performed using glass reaction vessels. However, in the chemical manufacturing industry, glassware does not offer the physical strength required to perform reactions on the required scales.⁸ Reaction vessels used for larger scale chemical manufacturing traditionally involve steel-jacketed, glass-lined vessels (to infer the same properties as methods used in the research lab). Typically, the vessel will be fitted with relevant apparatus for heating/cooling, addition of chemicals and control and monitoring of conditions.⁸

However, batch approaches suffer limitations⁷. Flow processing has emerged as a possibly more efficient route for the synthesis of *e.g.*, pharmaceuticals. This is a key concept of the work here, described later in this Chapter. Moreover, also key here is the field of catalysis, particularly using PGMs. Catalysis, also described in more detail later, can offer a more efficient approach for the synthesis and production of target chemicals. Both continuous flow processing and catalysis are key aspects of Green Chemistry which, as described in the next Section, outlines aspects important in the development of sustainable and efficient chemical processes.

1.3 Green Chemistry and Engineering in Synthetic Processes

Production of chemicals such as medicines and agrochemicals responsible for treating illnesses and ensuring adequate food supply, respectively, must be able to meet the required demand.^{20,21} Unfortunately, the synthetic processing industry can historically be considered inefficient in terms of energy and resource requirements, as well as, in some instances, polluting and occasionally even dangerous.²¹ The required demand for important synthetic chemicals should be met without detriment to the population or environment in terms of safety, energy demand and resource usage. That is, the production of crucial chemical products should be satisfied in a safe, clean and resource efficient manner.²¹ Therefore, chemical production should be undertaken with a holistic, cyclical approach where key concepts (such as waste generation, energy/resource usage, *etc.*) are considered. Green Chemistry has been developed with such considerations in mind.

The term Green Chemistry was coined in the early 1990's and is a philosophical approach towards developing a chemical-involving process.²⁰ Central to the concept of Green Chemistry is that by making a process greener, it should follow that the process is made cheaper *i.e.* it becomes environmentally *and* economically more attractive.^{20,21} To illustrate, a green process should, for example, minimise the resources required to generate a desired amount of product. By minimising the resources required, not only does the process become less resource intensive and hence can be considered "greener", but the cost of the process should be reduced, as, effectively, more product is made from less raw material, maximising the process economics. Green Chemistry is defined by the US Environmental Protection Agency as "*the design of chemical products and processes that reduce or eliminate the use or generation of hazardous substances*" and that it must apply across the entire life-cycle of a chemical product (*i.e.* in design, manufacture, use and disposal).²² Green Chemistry, however, may more suitably be defined by the Twelve Principles, which have come to represent it.²⁰ These were developed by Anastas and Warner and later summarised by the mnemonic **PRODUCTIVELY (Fig 1.2)**.²³

P – Prevent waste,
R – Renewable materials,
O – Omit derivatisation steps,
D – Degradable chemical products,
U – Use safe synthetic methods,
C – Catalytic reagents,
T – Temperature, pressure ambient,
I – In-process monitoring,
V – Very few auxiliary substances,
E – E-Factor, maximise feed in product,
L – Low toxicity of chemical products,
Y – Yes, it is safe!

Fig 1.2 *PRODUCTIVELY* mnemonic for the 12 principles of Green Chemistry.²³

The principles cover a variety of aspects important to a chemical process, including safety, resource/energy demand and aspects of chemical reactivity.^{20,21,23} Numerous metrics exist to attempt to quantify how green a process is. The simplest of these are the yield and selectivity of a reaction, which have been traditionally used metrics in quantifying the outcome of a chemical reaction.²¹ Other important metrics to consider include those related to the efficiency/economy of the synthetic reactions and conditions themselves. Baran analysed the concepts of atom-economy, step-economy and redox-economy of a synthesis, describing them as guidelines for the execution of an efficient synthesis.²⁴ Atom-economy was developed by Trost and is essentially a measure of the weight of atoms in the reactants which end up as atoms in the product.^{21,24,25} The concept of step-economy is that a multi-step synthetic process should be made more efficient by minimising the number of steps required to obtain a desired target, particularly from a cost and time perspective. This metric can simply be evaluated in the number of steps used to achieve a given target.^{24,26} The redox-economy is linked to this and is the principle that eliminating/reducing the number of reduction/oxidation steps by a judicious choice of reactions in a process should lead to an efficient process, unless, those redox reactions used are important for constructing the skeleton or correct stereochemistry of the target. Minimising this, like step-economy, should lead to a shorter, more efficient synthesis.^{24,27} Another metric used for attempting to quantify how green a process is the E-Factor. This was developed by Sheldon and, similarly to atom-economy, considers how wasteful a process is, and is defined as the mass ratio of waste to desired product, where waste is everything but the desired product (including waste solvent, spent catalysts *etc.*).^{21,28} Many of these metrics contribute towards an “*ideal synthesis*”, originally considered by Hendrickson, and analysed by Baran.^{29,30}

Such metrics mainly focus upon the efficiency of the chemical transformations in a synthesis. They do not account, for example, for the nature of the waste (*i.e.* whether it is hazardous or not), other hazards involved for a process user/operator or end consumer, or what the ultimate fate of the product is.²⁸ It is not always straightforward, therefore, to quantify some features which contribute towards how green the process is.^{20,21} The consideration of whether a process is green involves all these aspects, amongst others, across the entire life-cycle. As such, a life-cycle analysis is important,²¹ in which, some of the previously mentioned metrics can be used for comparison of different processes. After attempting to quantify the greenness of alternative processes, the “greenest” route should be adopted

by a manufacturer. This route *should* have the least overall impact on the environment and human health. In principle, this *should* also make the “greenest” route the most economically attractive – particularly where reduced environmental demand on energy and resources is considered.^{20,21} Adopting the “greenest” route, however, may not always be straightforward and compromises could be necessary.²¹ For example, a choice between a route which minimises waste, or which minimises generation of hazardous materials, might be required. Furthermore, attention should be paid to the quantity of chemical required for meeting a certain need, *i.e.* can another chemical achieve the need, with less quantity?^{31,32} As well as this, the facilities, infrastructure and instrumentation used should all be considered.³¹

An important factor related to Green Chemistry and the involvement of hazardous substances in a process, is what the *risk* involved is. The risk can be defined as a function of the hazard of the substance and the likelihood of exposure to the substance – this therefore depends on much more than just the nature of hazard of the substance. Here, hazard is considered as a situation that could lead to harm, and the risk is the probability that harm will occur.^{20,21}

$$\text{Risk} = f(\text{Hazard} \times \text{Exposure})$$

Eqn 1.1 *risk of a process - probability that harm will arise from a process that has potential to do harm.*

For example, a particularly hazardous substance might be generated and consumed during a reaction in a synthetic process. If this is the case, it is unlikely that the operating chemist would encounter/handle the hazardous substance. The likelihood of exposure, and hence risk, could be low. Alternatively, if the hazardous substance is produced in one step, then requires isolation for use in a subsequent step, such that the operator would be exposed to it, the risk might be high.

Green Engineering is also important for managing the risk of a process. This is defined to be “*the design, commercialisation and use of processes and products, which are feasible and economical while minimising generation of pollution at the source and risk to human health and the environment*”.²¹ This is important as, in the design of an efficient synthetic process, which is also safe and environmentally benign, not only are aspects related to the inherent chemistry of the reactions chosen important, but also the design and selection of equipment used to perform the processes in. For some hazardous chemicals (*e.g.*, explosive) employing logical and well-thought-out reactor engineering processes might allow for the presence of hazardous substances, whilst still operating with a low risk.

Overall, Green Chemistry and Engineering represents how improvements to synthetic processes might be made and implemented. This involves considerations of the chemistry associated with the process of interest, the nature of the chemical compounds involved in the transformations, as well as with the apparatus and demands required to perform the process.

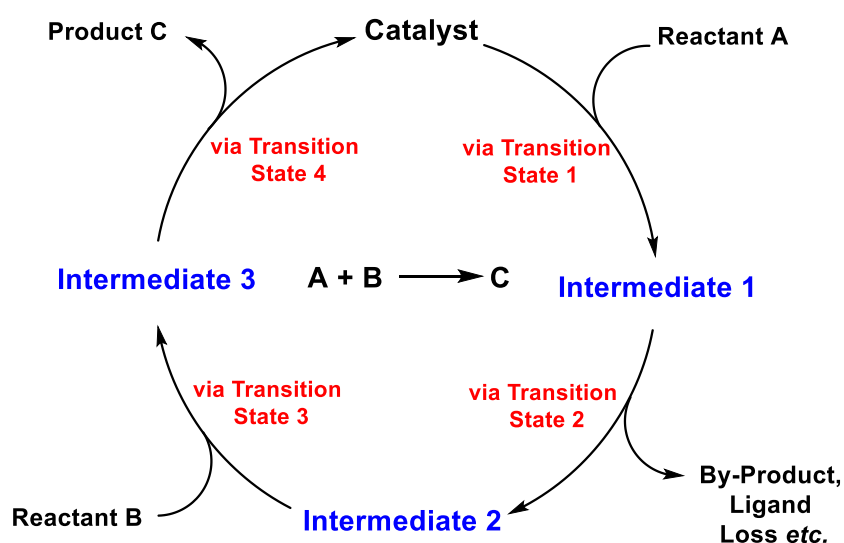
1.4 Catalysis in Synthetic Processes

The term catalysis was first coined by Berzelius and a catalyst was later defined by Ostwald as “*a substance that changes the rate of a chemical reaction, without itself appearing in the products*”.³³ This definition allows for a catalyst to be described as a substance that can speed up, or slow down a reaction. A subtly different definition is that a catalyst is “*a substance that increases the rate of*

approach to equilibrium of a chemical reaction without being substantially consumed in the reaction".³³ This definition invokes some important features of catalysis. Firstly, it focuses on the reaction *rate*, so is inherently related to kinetics, without altering significantly the position of equilibrium for the reaction.³³ Also, that the catalyst should not be substantially consumed implies the involvement of a catalytic cycle where the catalyst should mostly be regenerated when ending the cycle (hence able to undergo multiple cycles).³³ Therefore, the amount of a catalyst required for a catalytic reaction should be sub-stoichiometric, if the catalyst is efficient.

Catalysis is important in synthetic processes – particularly for industrial scale manufacturing.³³ By incorporating (often) only small quantities of a catalyst in a reaction, rates can be significantly increased, allowing for the production greater amounts of desired chemical products in shorter time-scales.³³ Catalysis is a broad field, and encompasses a variety of sub-categories, perhaps the two widest sub-categories of catalysis would be homogeneous and heterogeneous catalysis. This is where the catalyst is in the same phase as the reacting material, or in a different phase to the reacting material, respectively.³⁴ There can be further separations, for example whether the catalyst is a metallic catalyst, an enzyme catalyst, an organometallic catalyst, amongst others, and many of these can overlap. The application of metal-based catalysts in production of many manufactured chemicals has historically been exceptionally important.³⁵

A catalyst can achieve increased reaction rates in a number of ways, for example, by providing alternative reaction pathways with a lower energy route to the product than would be possible in the absence of the catalyst.³³ Such a route would typically proceed *via* a catalytic cycle. A typical catalytic cycle (**Scheme 1.2**) often consists of a number of intermediate species, leading to the final product(s) with regeneration of the active catalyst to complete the cycle (which then repeats).³⁴ In the cycle, the starting materials, intermediates and final product(s) are connected by transition states. Therefore, the nature of the transition state, particularly in the rate-limiting step of the catalytic cycle, is important for catalytic mechanisms.^{33,34,36}



Scheme 1.2 general cycle for a catalytic reaction of $A + B \rightarrow C$, showing various intermediates before forming the products with regeneration of the active catalyst.³⁷

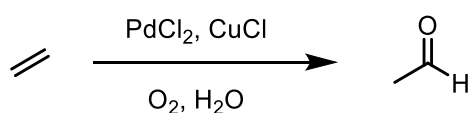
For catalyst efficacy, important aspects include the reaction yield, the time taken to achieve that yield and the amount of catalyst required to give that yield (loading) and product selectivity (particularly when side-products form *via* competing reactions).^{21,35} Turnover Frequency (TOF), **Eqn 1.2**, can also be used to quantify catalyst performance, developed originally from a statement from Boudart.³⁸ One of the broadest definitions applying to TOF arising from this statement is that TOF is the “*amount of product formed in a catalytic reaction, divided by the amount of catalyst and reaction time*”.^{35,39}

$$TOF = \frac{\text{Number of Moles of Desired Product Formed (mol)}}{\text{Number of Moles of Catalyst Added (mol)} \times \text{Reaction Time (s)}}$$

Eqn 1.2 calculation of TOF, based upon a broad definition of the term.³⁵

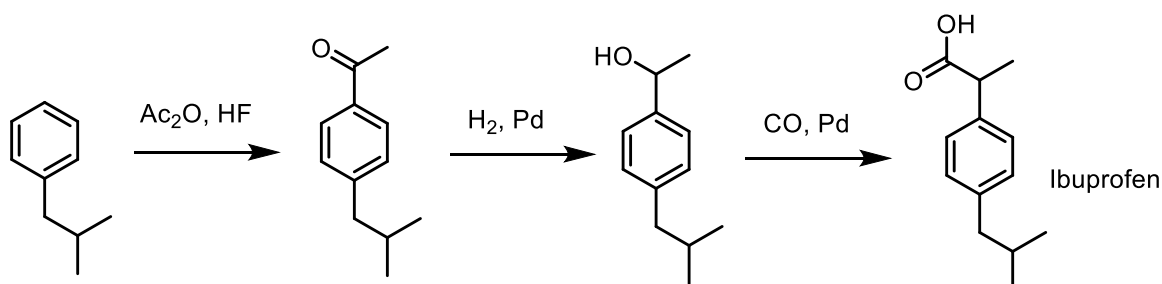
Applying catalytic reactions can allow for efficient processing of organic chemicals.^{40,41} The uses of catalysis in process chemistry include the production of bulk/commodity chemicals (typically large-scale, heterogeneous or homogeneous catalysis), as well as for production of fine/specialty chemicals *e.g.* pharmaceuticals (often using homogeneous catalysis).⁴⁰ Homogeneous catalysts *e.g.* organometallic catalysts with specifically designed ligands, are often able to impart more specific transformations in reactions, hence finding usefulness in production of finer products.⁴²

Synthetic processes involving homogeneous PGM catalysis is important to the work in this Thesis. The origins of which can be traced back to the development of the Wacker Process (**Scheme 1.3**),^{43,44} employing a Pd/Cu co-catalytic system for the oxidation of ethene to acetaldehyde (a fine chemical, used for the manufacture of specialty chemicals).



Scheme 1.3 the Wacker Process, co-catalysed by Pd and Cu salts, a crucial aspect in the history of the development of PGM catalysis in organic manufacturing.⁴⁴

An example of specialty chemical production involving metal-based catalysis is that employed in two important stages of the synthesis of Ibuprofen, developed by Hoechst Celanese, **Scheme 1.4**.⁴⁵ The first of these steps is ketone hydrogenation, catalysed by a heterogeneous Pd/C, followed by homogeneously catalysed alcohol carbonylation.⁴⁵



Scheme 1.4 the Hoechst Celanese route to Ibuprofen, involving HF-catalysed acylation (avoiding stoichiometric waste from more conventionally used AlCl_3), a heterogeneous Pd-catalysed hydrogenation of a C=O, followed by a homogeneous Pd-catalysed carbonylation.⁴⁵

Following the Wacker Process, PGMs have found use in a huge range of catalysed reactions. For example, hydrogenation, dihydroxylation, oxidation, cross-coupling, photoredox catalysis, hydroformylation, carbonylation and metathesis, amongst many others. Some of which are summarised below in **Fig 1.3**, highlighting the broad array of uses of the PGMs in synthesis and these are typically important reactions in the Synthetic Chemist's Toolkit.

Platinum Group Metals in Synthesis

Group 8	Group 9	Group 10
44 Ru 101.1 Hydrogenation (Noyori) Metathesis (Grubbs) Alcohol Oxidation Photoredox Catalysis	45 Rh 102.9 Alkene Hydrogenation Hydrosilylation Carbonylation Hydroformylation Cyclopropanation Transfer Hydrogenation	46 Pd 106.5 C-C or C-X Coupling Carbonylation Allylic Substitution Hydrogenation
76 Os 190.2 Dihydroxylation Aminohydroxylation	77 Ir 192.2 Carbonylation Hydrogenation (Crabtree) Imine Hydrogenation Photoredox Catalysis	78 Pt 195.1 Hydrosilylation Hydrogenation

Fig 1.3 broad uses of PGMs in synthesis.

Catalysis is represented as one of the Green Chemistry principles (and can contribute towards others), as it leads to increased reaction rates, meaning processes should require less processing time, and are typically used sub-stoichiometrically, generating less waste.²¹ To establish whether a catalytic route is beneficial compared to a non-catalytic route to the same target, a full life-cycle analysis of both possibilities would be required, to truly determine if the catalysis offers an improvement in the "greenness" of the process. For example, arguments can be made to the detriment of PGM catalysis as PGMs are rare and energy intensive to mine and process.^{46,47} The advantage of a catalyst is that,

typically, it is required only in a small amount, as it should be regenerated in the mechanistic cycle. Often, this makes the catalyst advantageous over a stoichiometric reagent which, typically, would generate more waste and can complicate purification processes.²¹ A further advantage is that catalysts can be designed to be highly selective for a desired transformation. The Hoechst Celanese Ibuprofen synthesis (**Scheme 1.4**) involves two PGM catalysed steps (Pd-catalysed hydrogenation and carbonylation) yet is often considered a Green Chemistry success. This is due to a high atom economy and small amount of waste generated, enabled by the Pd-catalysed steps.⁴⁵

Important developments in PGM catalysis, relevant to this Thesis, involve the widely-used cross-coupling reactions, including the Suzuki Reaction, Heck Reaction and Sonogashira Reaction.^{43,48,49} These are hugely important in synthesis and manufacturing and are described in Chapters 2, 3 and 4. Using a PGM catalyst for such reactions can often save a number of steps in a multi-step reaction sequence towards a desired target. Despite the rarity of PGMs, it can frequently be seen that the nature of such transformations carried out in a single-step using a PGM catalyst often would require multiple reactions to achieve the same target when using an alternative route which does not require a PGM catalyst. Therefore, by not using a PGM catalyst, longer processing times and generation of more waste is often an issue which, from a commercial perspective, can become more costly, with greater environmental strain. This highlights how having to choose one chemical process over another often requires compromise and full consideration to determine the “best” route.²¹

1.5 Continuous Flow Chemistry

Improving synthetic processes includes designing syntheses towards ideality,^{29,30} applying the principles of Green Chemistry,²⁰ considering the utility of the synthetic product,³² reasonable application of facilities/instrumentation³¹ and designing reactors following the principles of Green Engineering.²¹ Continuous flow reactors have emerged as an important enabling technique for improving the efficiency and scalability of laboratory and industrial-scale syntheses, offering numerous possible benefits for chemical processing.^{4,11,50,51}

Traditionally, both lab and industrial-scale syntheses of specialty chemicals (*e.g.* pharmaceuticals) is performed in batch.⁸ A batch process can be defined as one where the reactant materials are charged into the reaction system, and the product discharged all at once, sometime later.¹⁹ The reactants in the system are typically mixed and heated and, upon scaling batch processes, the conditions can change dramatically, *e.g.* going from the mg scale, to kg scale.⁸ In part, this is due to the inherent issues associated with heating a larger vessel – heat transfer can be inefficient due to smaller surface-to-volume ratios, which can lead to unwanted side-reactions occurring.⁸ Other issues include that glass, being a weak material, cannot be scaled up to the size required for manufacturing. Typically, glass-lined stainless steel vessels would be required. However, due to the opaque nature of steel, this imparts difficulty in aspects such as separations, due to not being able to directly observe the contents of the vessel (though reactor tanks often have an observation point to ease this somewhat).⁸ Moreover, due to the large volumes on the manufacturing scale, there is an inherently greater safety risk. This is because, for example, if the reaction is exothermic, much more heat is generated at scale. There are therefore associated issues with runaway reactions.⁸

A continuous process can be defined as one where the reactant material(s) and product(s) are continuously charged and discharged, respectively, from the reactor system, throughout the process duration.¹⁹ These can be performed in flow reactors (**Fig 1.4**), which offer a potential solution to the issues associated with traditional batch processing.⁴ These reactors involve pumping reagents through a series of pipework/tubing, which contains a reactor unit/manifold, where the reaction occurs (which could be thermal, photochemical, biochemical, etc.). Flow reactors can be commercially obtained, or homemade, where typically commercially available reactors are better for reproducibility between labs, whereas homemade reactors can often be designed for a specific purpose.⁵²

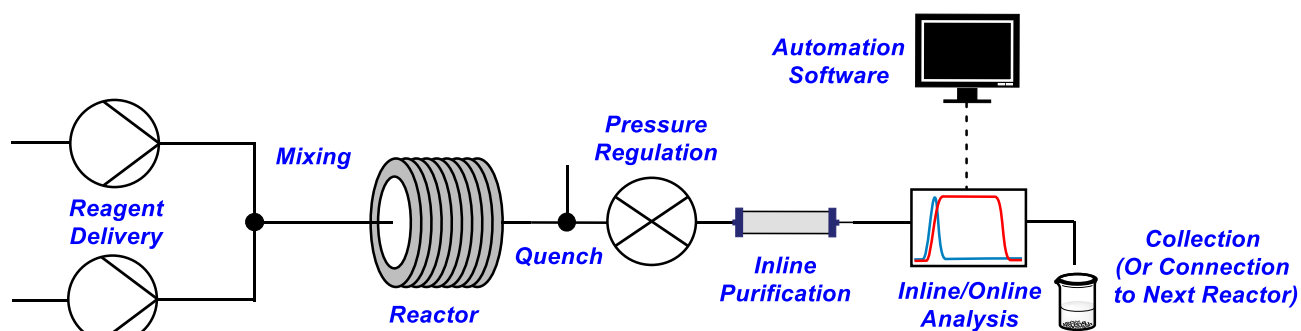


Fig 1.4 anatomy of a generic continuous flow reactor system.^{4,53}

Reagent solutions are delivered into the system by pumps. Typically, for lab-scale reactors (which can be easily scaled-up), syringe pumps,^{6,53,54} peristaltic pumps,⁵⁴ or repurposed HPLC pumps⁵²⁻⁵⁴ are used. The reagent materials can be pre-mixed or can be mixed within the system of tubing, if pumped from separate sources. A simple T-piece or Y-piece (for mixing of two fluid streams), or a cross-piece (for mixing of three fluid streams) can be used for mixing of multiple fluid streams.⁵⁴ For improved mixing, a static mixer can be used, which would be placed inline of the fluid stream and involves a specific geometrical construction placed within the hollow tubing, to influence the flow structure, enhancing heat and mass transfer.⁵⁵ The static mixer could involve *e.g.* a PTFE coil, a sand-packed bed or glass beads.⁵⁴ Alternatively, reactors such as vortex reactors⁵⁶⁻⁵⁸ and spinning disk reactors^{59,60} have been designed for efficient mixing within the reactor manifold.

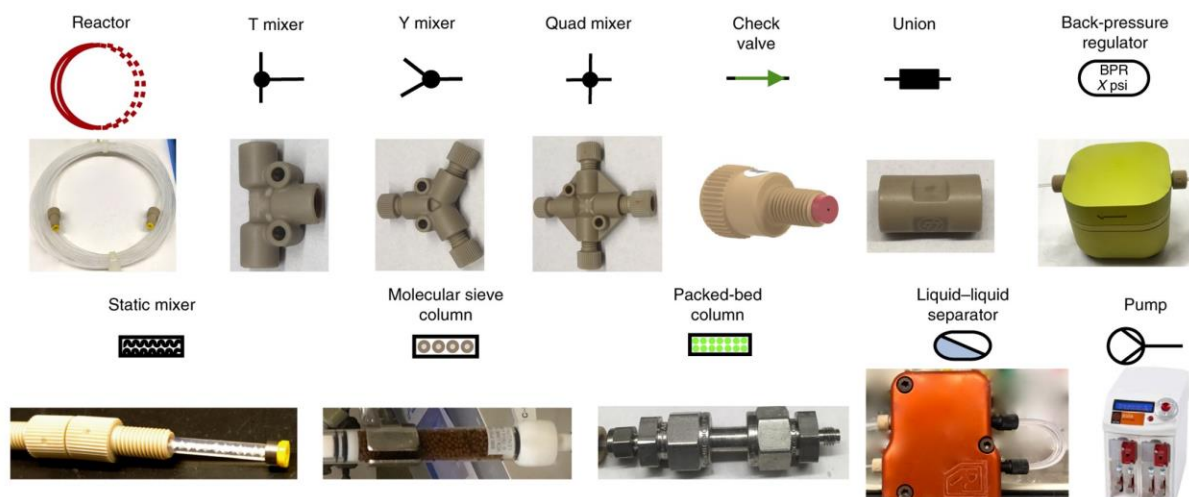


Fig 1.5 example equipment used in constructing a flow reactor, for pumping, mixing, reacting and separating fluid streams. Reproduced with permission from J. Britton and T. F. Jamison, *Nature Protocols*, 2017, **12**, 2423-2426.

When the reactant material reaches the reactor unit, the chemical reaction takes place. The rate at which the material is pumped through the reactor (the flow rate) can be chosen to give the desired range of residence times for the reactant material within the reactor section of the system.⁵⁴ That is, by dividing the volume of the reactor unit (mL) by the fluid flow rate (mL min^{-1}), the reaction residence time, *i.e.* planned time the reactants spend in the reactor manifold (min), can be calculated. This can also influence the flow regime, *i.e.* the turbulence of the flow, or whether slug/bubble-flow is observed in a biphasic mixture.⁴ Typically, reactor units can be classified as coils, chips and packed-beds,^{4,53} though other reactor manifold designs exist, such as vortex or spinning disks, mentioned previously. Generally, coils, chips and packed-beds can all be heated/cooled by conventional (or unconventional) methods, and can also be designed for allowing more unconventional activation methods, such as photochemical or electrochemical activation.⁴ The design of the reactor and material choice must be considered, for the intended application. Chip reactor units are typically on a milli/micro-scale and involve machined silicon, glass, ceramics, or stainless steel.^{4,61} Due to the small volume and very narrow channels on the machined chip, they usually have extremely high surface-to-volume ratios, making heat transfer very efficient, although, clogging can be an issue and typically they have low throughput. Therefore, these are typically well suited to process development.⁴ Coil reactor units typically involve a coiled length of tubing, with the tubing material chosen to reflect the chemical compatibility and condition requirements, typically including stainless steel, Hastelloy, PEEK or transparent fluoropolymers.⁴ These can be constructed on a milli/micro-scale, but simply scaled-up by using a larger length of tubing. These units can be heated/cooled by immersion in a heating/cooling bath, or by mounting on a heated/cooled unit, and can also be irradiated with a light source, given the right choice of tubing material.⁴ Packed-bed reactor units involve a column/cartridge, usually made from stainless steel, glass, or polymers and which is filled with a solid material embedded between filters at the inlet/outlet to the column/cartridge.⁴ The reaction solution is passed through the packed-bed to facilitate the reaction, and the solid material is well-suited to being a heterogeneous catalyst, though it could also be, *e.g.* glass beads to encourage mixing in a reactor unit.⁴ For these units, appropriate selection of, *e.g.* solid particle size is important for controlling aspects such as backpressure, and sometimes the packed-bed can give a chromatographic effect.⁴

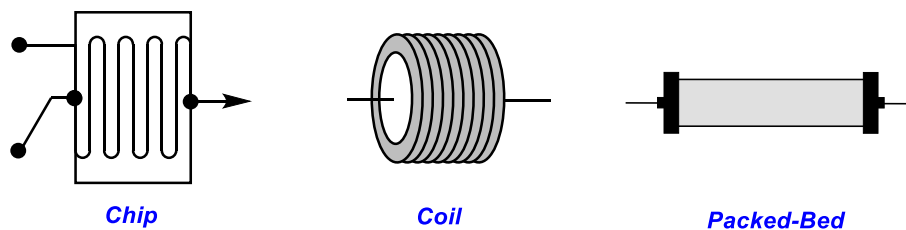


Fig 1.6 chip, coil and packed-bed flow reactor units - used commonly used in flow chemistry.^{4,53}

Due to the nature of pumping reagents through a system including a reactor, the volume of material undergoing a reaction at any time is small compared to the total volume that may need to be processed. This is because the reagents are continually being pumped in to the reactor manifold, where they undergo a reaction, and then are also continually being pumped out of the reactor section (after they have reacted to the desired conversion) and being replaced by fresh reactant material.^{4,62} Moreover, typically, a small (micro-scale or milli-scale) reactor can be employed for both research and manufacturing purposes, allowing the volumes of material being processed to be kept small even upon scale-up.⁶³

The benefits that this flow chemistry can offer are numerous.⁴ To begin, safety is a key factor. This is because batch processing involves a large volume of reactant solution being processed, whereas, in flow, a much smaller volume is being reacted at any one time. This can minimise the potential effects of *e.g.* runaway reactions.^{4,62} Moreover, being able to control where reagents mix in the fluid stream can avoid generation of any possible reactive intermediates that form upon the reagents mixing until they are desired, minimising the contact of the operator with potential hazards.⁴

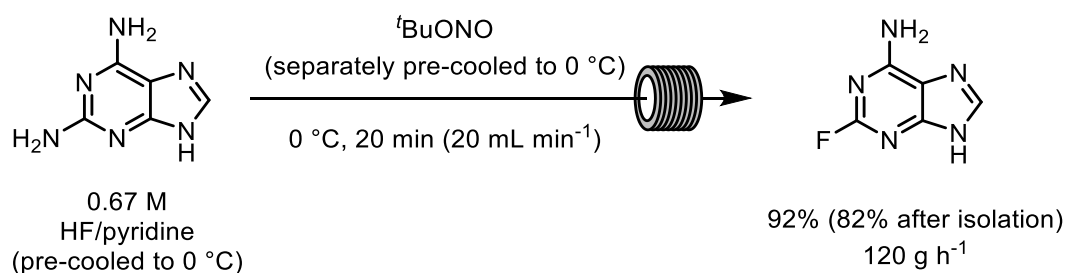
Other benefits include better control over reaction conditions. As mentioned, the flow rate of reagent solutions can be controlled to give a precise residence time of the solution in the reactor part of the system. This can negate the impact of any undesired side-reactions, reducing waste formed.^{4,64} Also, inherent to the technology due to the larger surface-to-volume ratios inside reactor tubing, transfer of heat and mass is generally efficient. That is, the heat supplied to the system is efficiently conducted, and due to the nature of flowing the reactant solution through small channels, mixing is efficient.^{4,65}

Scale-up of reactions from the laboratory to manufacturing is typically more straightforward. This is because, in principle, it is possible to scale-up a flow process simply by having more reactors performing the same process ("numbering-up"), or, the length/volume of tubing where reactions take place can simply be increased (dimensioning).^{4,63} However, the dimensioning approach in practice, is typically not as straightforward, due to considerations of effective reactor designs. Numbering-up may be more straightforward, but also involves a number of engineering choices to be made (*e.g.* parallel or series, one feedstock or many, reproducibility across each system *etc.*).⁶³ It is also possible, with extensive optimisation, to establish a process of a multi-step reaction whereby each reaction can be performed in a fully telescoped system.⁶⁶ That is, where the products of one reaction are fed in to a flow reactor where a second reaction is undertaken. This, from a scale-up and manufacturing perspective, would be highly attractive as an efficient means of chemical manufacturing.^{51,67}

The ability to monitor processes using inline/online technologies is also possible using continuous flow.⁶⁸ Inline monitoring involves a process analytical instrument in the fluid flow, at a point downstream of the reactor.^{4,68} This allows for continuous monitoring of the process, allowing to ensure the smooth running of reactions and the formation of expected products. Online monitoring involves sample removal from the flowing stream for analysis.⁶⁸ These, in turn, allow for the possibility of self-optimised flow reactors/processes. This is where the result of the monitoring process is fed back to a computer, where an algorithm can process the data and, given any changes, can automatically adjust the system conditions to maintain the maximum efficiency (which could be in terms of yield, productivity *etc.*).^{7,50,69}

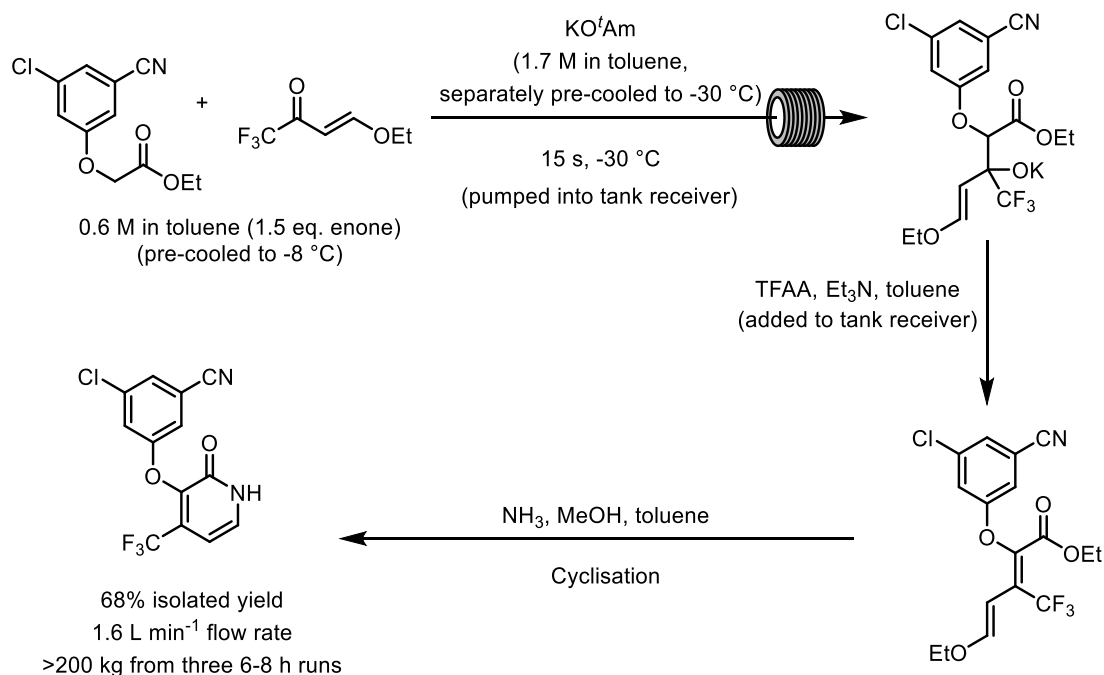
One of the key benefits of continuous flow as an enabling technology for chemical manufacturing is the access to “novel process windows”, *i.e.* extreme or novel reaction conditions, such as high temperatures.⁵ Such conditions are more difficult/unsafe to achieve in batch.^{4,5} Mostly, this is due to the volume of material being reacted at any one time in flow being relatively small.^{4,5,66} This means that there are less safety concerns associated, and less processing techniques employed, in applying conditions such as super-heated temperatures, where the mixture must also be pressurised to prevent solvent boiling.⁴ Using traditional batch methods, this would require a substantial energy input to heat and pressurise batch vessels to such elevated temperatures, and also would likely lead to detrimental observations due to poorer mixing and heat transfer when compared to flow.⁸ Moreover, in batch, applying a large amount of heat and pressure to a large volume of reactant material can be inherently dangerous in the event of a system failure, *i.e.* a lot of pressure and heat would be released at once.

Due to these benefits outlined, particularly in terms of safety, scalability, and improving process efficiency, continuous flow is attractive for manufacturing processes, fitting in with the principles of Green Chemistry.^{20,21} Moreover, it is typically an option to finetune these advantages offered using flow, by integrating process engineering and reactor design considerations in order to maximise the benefits offered by a flow system for a specific process.⁶⁶ As such, flow chemistry has attracted attention from the pharmaceutical industry.^{70,71} For example, researchers from Merck have used a flow platform for the preparation of (selectively) 2-fluoroadenine, from 2,6-diaminopurine (**Scheme 1.5**), of interest for anti-virals and cancer treatments.^{72,73} The reaction, known to be temperature sensitive and exothermic, was well-suited to flow processing, due to the ability to tightly control reaction temperatures.⁴ Also, using two pumps, it was possible to keep separate the reagents until the desired point of mixing in the flow reactor, avoiding unexpected exotherms. The flow synthesis was optimised using a small-scale flow reactor, at 0.2 mL min⁻¹, then, using larger dimension tubing, the reaction was scaled to 20 mL min⁻¹. This resulted in production of 120 g h⁻¹ synthesis of their target.⁷²



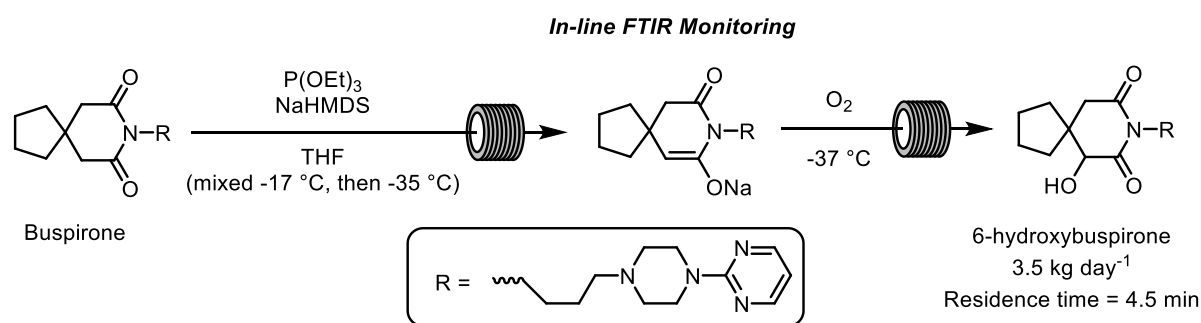
Scheme 1.5 large-scale flow synthesis of 2-fluoroadenine.⁷²

Researchers from Merck have also exploited flow chemistry in the synthesis of a key intermediate en route to Doravirine (**Scheme 1.6**), an HIV/AIDS treatment.⁷⁴ The flow synthesis involved aldol-type chemistry to form an intermediate, which was then pumped directly into a tank reactor, to which, TFAA and Et₃N were charged to for an elimination-cyclisation process (upon addition of NH₃/MeOH), in a streamlined process.⁷⁴ This was optimised to 20 mL min⁻¹ in a lab, then, was applied to scale-up at 1.6 L min⁻¹, allowing for the production of over 200 kg (68% isolated yield) of the intermediate from three 6-8 h runs.⁷⁴



Scheme 1.6 continuous flow synthesis of a pharmaceutical intermediate producing over 200 kg from three 6-8 h runs.⁷⁴

In an early example of the application of continuous flow chemistry for pharmaceutical preparation, researchers from Bristol-Myers Squibb synthesised 6-hydroxybuspirone (the active metabolite of psychotropic agent Buspirone).⁷⁵ They achieved this by performing α -hydroxylation at a C=O present in buspirone, *via* a streamlined enolization-oxidation process (**Scheme 1.7**).⁷⁵ Molecular oxygen was applied as the oxidant, representing one of the benefits of flow chemistry in that multi-phase reactions are often more efficient, due to enhanced mixing.⁴ Furthermore, inline FTIR analysis was integrated to monitor the enolization step, representing a further benefit of flow chemistry for implementing analytical techniques.⁴



Scheme 1.7 large-scale synthesis of 6-hydroxybuspirone using a multi-step flow process with integrated inline analysis.^{71,75}

1.6 Project Aims & Strategy

The work in this Thesis aims to develop flow syntheses and processes involving PGM catalysis. Two distinct classes of reaction were of interest: C-C and C-O coupling reactions. The remit for reactions involving C-C coupling were those using thermal Pd-catalysis and it was decided during this work to investigate Heck-type processes. The remit for reactions involving C-O coupling were those involving photochemistry, and it was decided to explore Ir-photocatalysis (alongside Ni and Cu co-catalysis). The reasons for choosing the reactions investigated are outlined in the relevant Chapters.

To allow these reactions to be investigated/developed in continuous flow, suitable apparatus was required. With these points, the work here followed the general strategy:

- Identification of suitable reactions, or the possibility for development of suitable reactions in the literature, following the outlined remit.
- Designing and constructing suitable flow reactor equipment for investigating/developing reaction processes.
- Optimising reaction conditions for the identified/developed reaction using the constructed flow reactor.

Alongside this, a mechanistic investigation into a photocatalysed C-O coupling reaction was performed, using time-resolved infrared spectroscopy, which also allowed for a comparison between adapted conditions for the reaction developed in this work, and existing protocols. As such, the aims were as follows:

- To build suitable equipment for performing thermal and photochemical flow reactions.
- To identify/develop conditions for the reactions of interest, suitable to flow processing.
- To determine whether flow processes for the reactions of interest could be developed and, if so, whether the unique features of flow chemistry could provide any benefits.
- To determine whether the mechanisms of photocatalysed reactions could be investigated using time-resolved infrared spectroscopy.

Thermal C-C Coupling Reactions

Flow Heck-Type Reaction Processes

Chapter 2

Heck Reactions in Flow with Novel Processing Conditions

2.1 Abstract

In this Chapter, flow Heck Reactions were investigated under novel processing conditions. Firstly, a suitable flow system was required for performing the reactions (and related reactions in Chapters 3 and 4). To begin, a commercial flow system was used, however, it was later determined that a system allowing access to higher temperatures and pressures was desired. As such, a small volume (3.0 mL) tubular coil flow reactor was designed and constructed, based on stainless steel tubing and repurposed HPLC pump/pressure regulation apparatus to allow for, in principle, temperatures up to 400 °C. Model Heck Reactions have been reported in the literature in flow with segmented-flow conditions^{76,77} and at temperatures ~200 °C, low Pd loadings of 0.05 mol% have been shown to be applied successfully under such conditions.⁷⁶ In this work, using the home-made reactor, temperatures >200 °C were studied. It was found that at 250<x<300 °C, low (5-10 ppm) loadings of Pd(OAc)₂ could be applied to model Heck Reactions of iodobenzene and butyl acrylate, affording yields of ~90% at full conversion (*c.f.* 14% under analogous conditions at 200 °C). Furthermore, it was also shown that MeCN, commonly used as a polar aprotic solvent for Heck Reactions and previously used in flow literature on the Heck Reaction, can be replaced by γ -valero lactone, a greener alternative solvent, previously used for Heck Reactions in batch.^{78,79} At 300 °C, decomposition appeared to predominate unless at extremely short ~1 min residence times, in which case, observed yields were low, at ppm loadings and would likely require higher catalyst amounts to achieve reasonable yields/conversions, so was not investigated further in this work. At temperatures >300 °C, decomposition was apparent even at short 1 min residence times.

2.2 Strategy & General Aims

The remit for Chapters 2-4 was to develop flow processes for thermally activated, Pd-catalysed C-C bond forming reactions. The preliminary aim was to investigate an established C(sp²)-C(sp²) coupling, and the Heck Reaction was chosen to investigate in this Chapter. This was used to obtain/benchmark a suitable flow reactor and to investigate the potential benefits offered by access to novel processing windows, in flow. In particular, the Heck Reaction was chosen as a C(sp²)-C(sp²) coupling reaction as other related reactions (discussed in Chapters 3 and 4) involve C(sp²)-C(sp³) bond formations, which formed the remit of work presented in later Chapters.

The general aims of the work in this Chapter were to investigate the use of high temperature conditions, enabled by using a flow reactor, for the Heck Reaction. Specifically, the aims were to investigate whether processing benefits such as reduced Pd catalyst loadings and decreased reaction times could be obtained by using such conditions, offering scalable, improved processing.

To explore these aims, the following strategy was adopted:

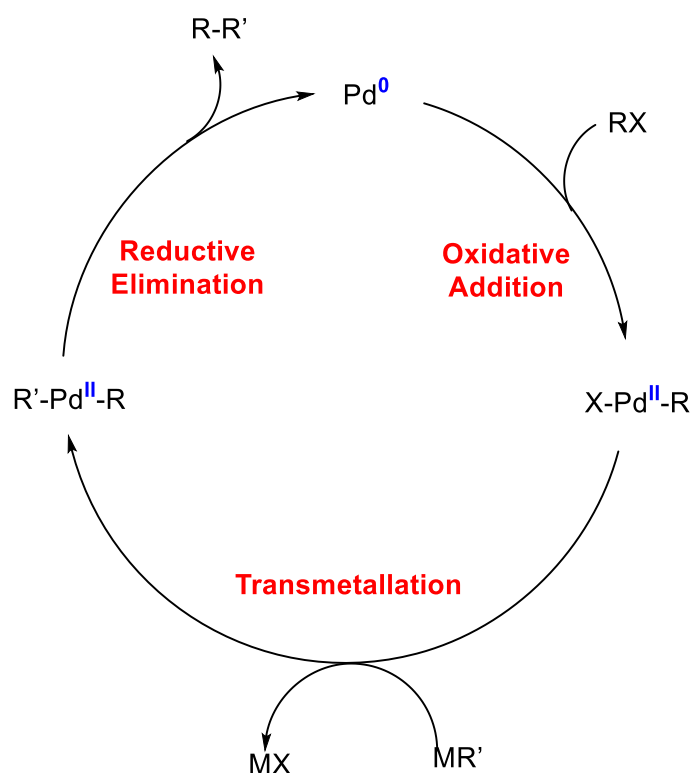
- A suitable reaction was to be identified and it was considered that a model Heck Reaction should be used to benchmark the conditions against previous literature. The reaction mixture flowing through the reactor was required to be homogeneous so considerations were made with this in mind, and a starting point where a simple Pd catalyst could be used without identifying Pd precipitation was taken as a starting point.
- A suitable piece of apparatus was required for performing such reactions in flow. A commercially available flow reactor was acquired and used for initial investigations, due to ready availability.

- Due to certain considerations for ongoing work, a reactor was built as part of the work in this Chapter to allow for exploring a wider range of processing windows.
- The custom-built reactor was used to explore high temperature/pressure conditions, studying the effect of such conditions, as well as different catalysts and solvents, on the required catalyst loading, reaction yield and processing times for the model Heck Reactions.

2.3 Introduction

2.3.1 Palladium-Catalysed Cross-Coupling Reactions

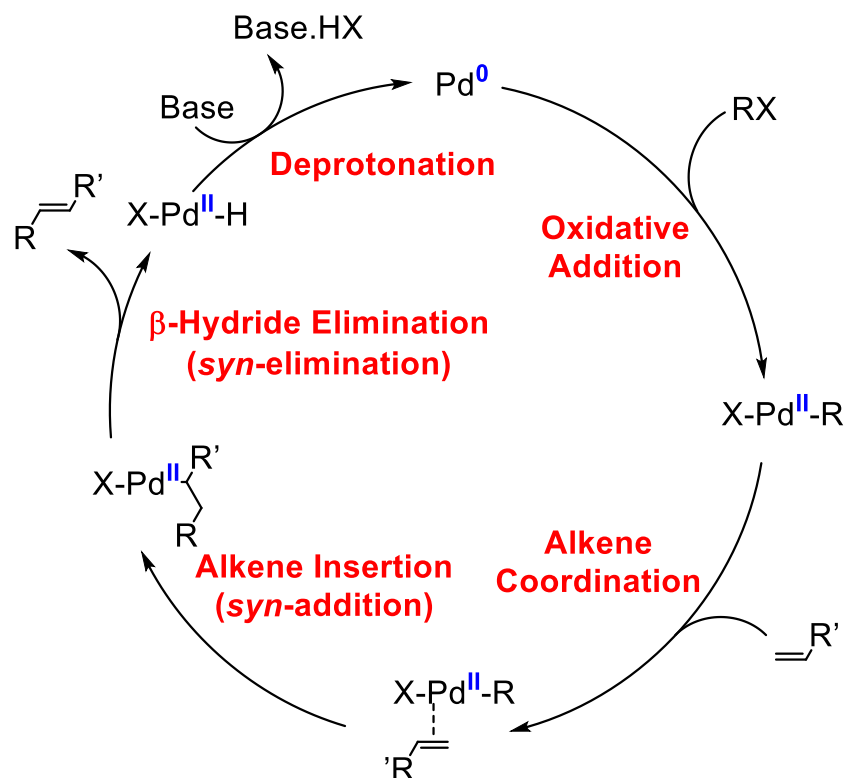
Pd-catalysed cross-coupling reactions are hugely important in the Synthetic Chemist's Toolkit, frequently applied in laboratories and in chemical manufacturing. Cross-coupling reactions typically involve the substitution of, *e.g.* aryl/vinyl/alkyl halide (or *pseudo*-halide) species with a nucleophile, in the presence of (often) a transition metal catalyst. In general, these reactions involve oxidative addition of the organohalide (or *pseudo*-halide) to the catalyst, followed by transmetalation, then reductive elimination to furnish the coupled product (**Scheme 2.3.1**).^{43,80}



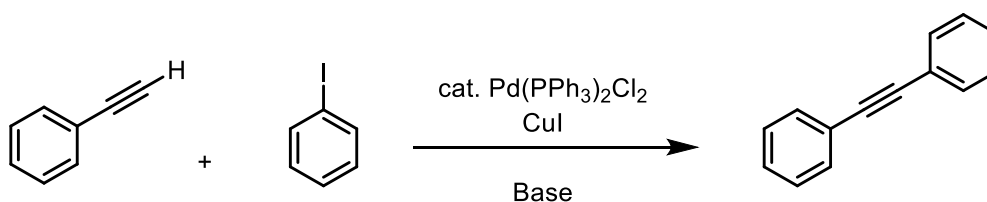
Scheme 2.3.1 generalised catalytic cycle for a Pd-catalysed cross-coupling reaction. *R* is typically an aryl group, *R'* can typically be an aryl/vinyl group, the nature of *M* depends on the coupling type employed, *e.g.* Suzuki $M = B(OR)_2$, Stille, $M = SnR_3$.⁸¹

Following the application of Pd-catalysis in the Wacker Process (mentioned in Chapter 1),⁴⁴ developments from Richard Heck began to broaden the scope of applying Pd in catalytic reactions. Heck's initial research, in the late 1960's and early 1970's, focussed on the reactions of organomercurial compounds in the presence of a Pd salt and an alkene.⁴³ However, due to the toxicity of organomercury

compounds, interest turned towards reactions of organic halides and alkenes, again in the presence of Pd salts. These developments culminated in the now well-known Heck Reaction (**Scheme 2.3.2**).⁴³

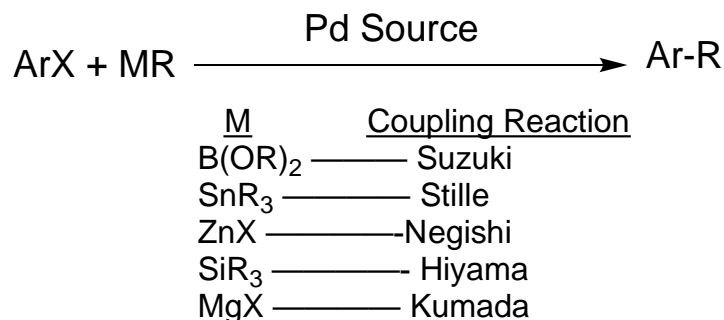


The work of Heck and others paved the way for Pd taking a crucial role in catalysis for organic synthesis and many new types of coupling reaction were discovered following this. The Sonogashira Reaction (**Scheme 2.3.3**) was demonstrated shortly following the Heck Reaction.^{43,48} This typically involves an aryl halide being coupled with an alkyne, with a copper co-catalyst allowing for more mild conditions to be employed.⁴⁸ In general, such discoveries in organo-palladium chemistry are termed the First Wave of the field and generally involve the discovery of the catalytically useful properties of Pd complexes.⁴³



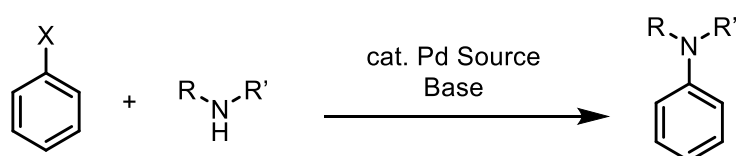
Following this, the Second Wave of organo-palladium chemistry involved expanding the scope to involve a variety of organometallic coupling partners.⁴³ In the late 1970's, Negishi reported the Pd-catalysed cross-coupling of organo-zinc and organo-aluminium partners with aryl halides.⁴⁸ Shortly afterwards, organo-tin reagents were also successfully employed (Stille Coupling).^{43,48} Despite the synthetic utility, organo-tin reagents have toxicity concerns which have limited their process chemistry application.⁸¹ Due to such concerns, the Suzuki Reaction was developed. Under mild conditions, an arylboronic acid (or ester) and an aryl or alkenyl halide undergo cross-coupling reactions, using a Pd

catalyst. Organo-boron reagents are typically stable, easy to handle, non-toxic and react under mild conditions.⁴⁸



Scheme 2.3.4 general scheme for Pd-catalysed coupling reactions.

The Second Wave of organo-palladium chemistry involved expanding the scope of coupling partners other than the organometallic species. For example, the Buchwald-Hartwig Coupling Reaction (Scheme 2.3.5), involving the formation of C-N bonds between an aryl halide and an amine, was developed. Similar reactions have also been reported for C-O, C-S and C-P bond formations.^{43,48}



Scheme 2.3.5 general scheme for a Buchwald-Hartwig Reaction.⁴⁸

The Third Wave of organo-palladium chemistry followed, involving broad efforts to improve upon the methodologies.⁴³ This includes developing new catalysts/ligands⁴³ and altering traditional reaction conditions, *e.g.* using environmentally-friendly solvents,⁸² or *pseudo*-halide coupling partners, *e.g.* phenol derivatives (Fig 2.3.1).⁸³ The Third Wave of organo-palladium chemistry also involves the industrialisation and large-scale use of cross-coupling chemistry, relevant to the application of flow reactors for Pd-catalysed cross-coupling.^{43,48}

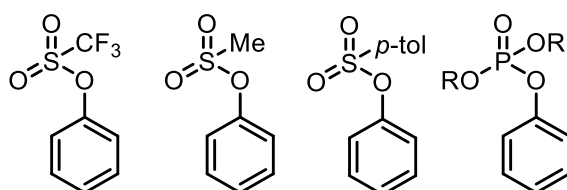


Fig 2.3.1 phenol-derived “pseudo-halide” coupling partners. From left to right, the species are aryl triflates, mesylates, tosylates and phosphates.⁸³

The widespread use of Pd-catalysed cross-coupling reactions in both industry and in academia culminated in the awarding of the 2010 Chemistry Nobel Prize to Heck, Suzuki and Negishi for their crucial roles in developing this field of chemistry. Pd-catalysed couplings have found application in the production processes of pharmaceuticals, and other commercial targets. Examples of these include Boscalid and Vemurafenib, which are a fungicide and anti-cancer agent respectively, manufactured using Suzuki Coupling Reactions in their processes.⁸⁴

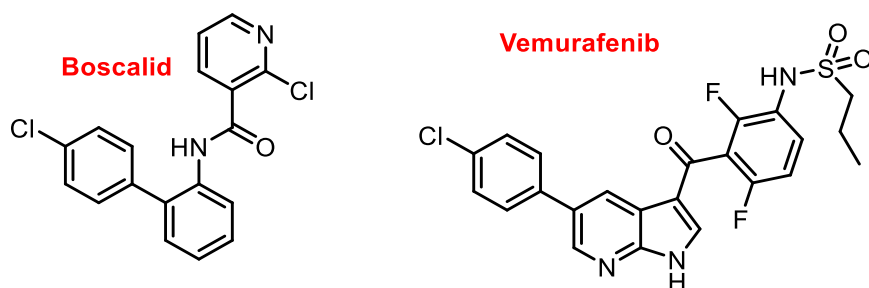


Fig 2.3.2 commercial chemicals produced using Suzuki Coupling.

Montelukast and Naproxen, both pharmaceuticals, involve Heck Reactions in their production.⁸⁴

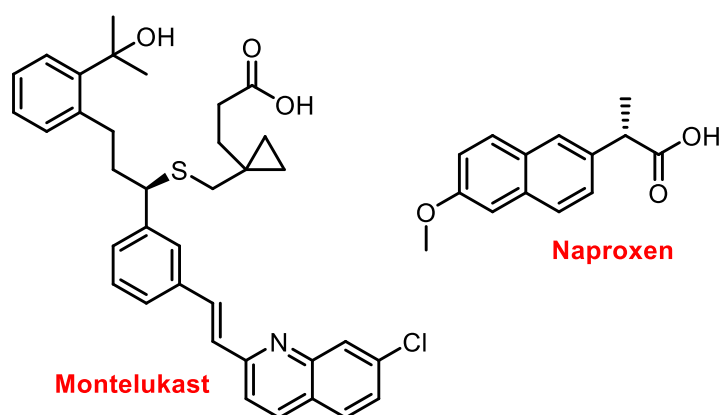


Fig 2.3.3 commercial chemicals produced using Heck Coupling.

Other commercial examples employing other Pd cross-coupling reactions include the production of Diflunisal and Terbinafine, prepared in processes involving a Kumada Coupling and Sonogashira Coupling, respectively.⁸⁴

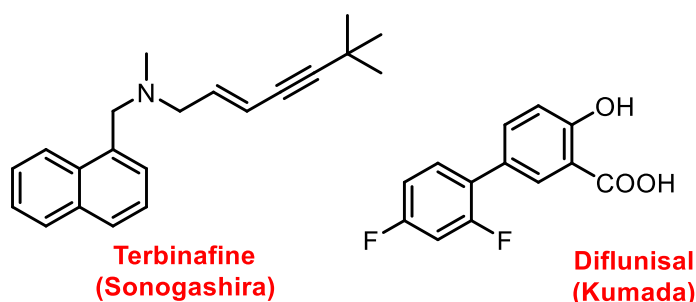


Fig 2.3.4 commercial chemicals produced using Sonogashira and Kumada Coupling Reactions.

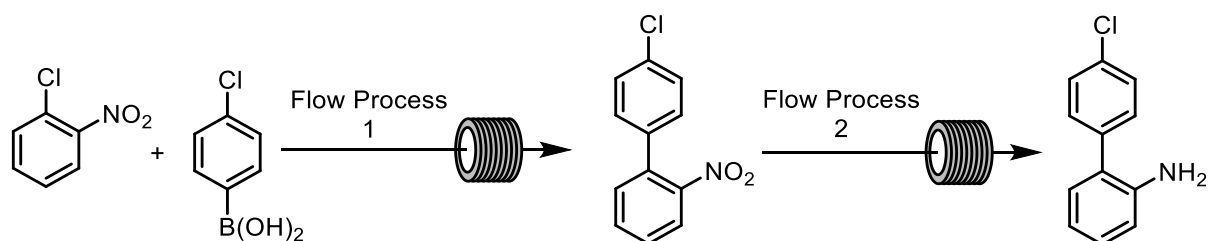
2.3.2 Continuous Flow Palladium-Catalysed Cross-Coupling Reactions in Process Chemistry

Pd-catalysed cross-couplings are therefore important in process synthesis.^{43,84} In Chapter 1, it was explained how flow reactors offer benefits for chemical manufacturing. As such, continuous flow reactors have previously been applied to Pd-catalysed coupling reactions.

Some of the advantages of flow processing particularly benefit catalytic organic reactions.^{65,85} For example, simplified access to novel processing windows, such as superheated reaction conditions, may

lead to accelerated rates,⁵ therefore allowing to reduce catalyst loadings. Other advantages include that due to scale-up being simplified, it is attractive for manufacturing processes, which catalytic reactions are highly important for.^{4,33} Moreover, implementing spectroscopic monitoring and automating processes could allow for maximising usage from the (typically expensive) catalyst.^{4,21} Other considerations include that multi-step processing, favourable in flow, lends itself well towards integrating systems whereby catalysts could be recovered and reused.⁸⁵ There are potential drawbacks of performing organometallic catalytic reactions in flow, however. For example, metal-based catalysts can have issues with solubility.^{86,87} In batch, this is typically not an issue, unless precipitation leads to catalyst deactivation and the reaction failing. However, in flow, solid formation can result in blockages, causing the process to fail.⁸⁵ The examples below highlight the application of flow processing for Pd-catalysed cross-coupling reactions, towards products of interest for process synthesis.

Kappe and co-workers have previously reported the multi-step synthesis of an intermediate in the synthesis of Boscalid, in flow.⁸⁸ Boscalid is a fungicidal agrochemical involving a Suzuki Coupling in the manufacturing process.⁸⁴ Kappe and co-workers investigated whether an integrated flow approach could be used towards a key intermediate *via* the Suzuki Reaction, followed by nitro group reduction (Scheme 2.3.6).⁸⁸



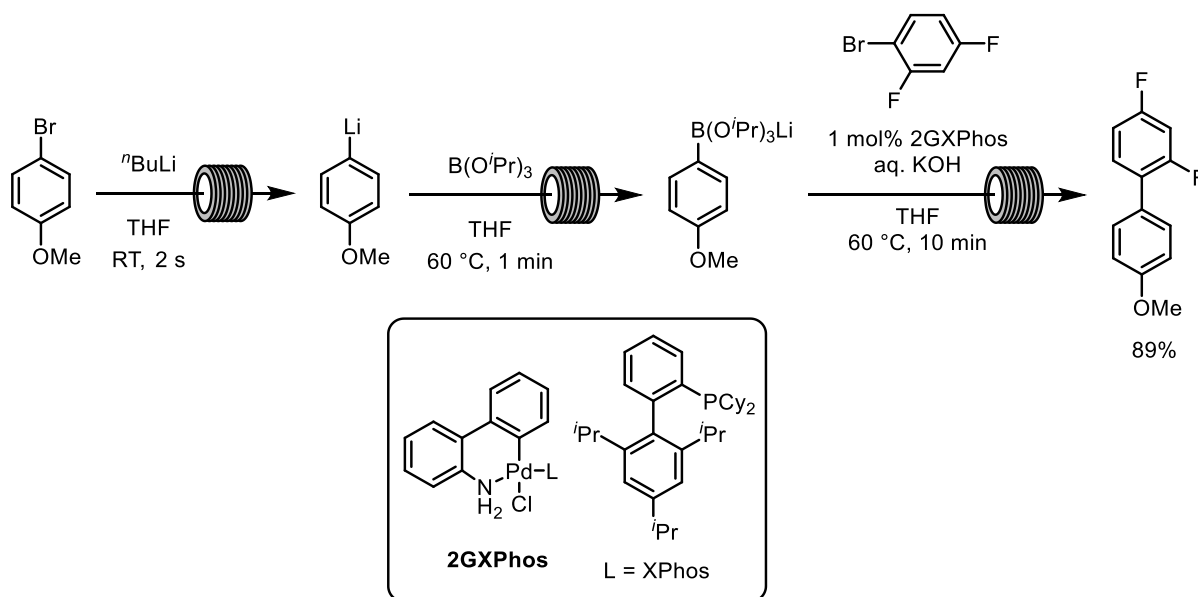
Flow Process 1: ^tBuOK, 0.25 mol% Pd(PPh₃)₄, ^tBuOH:H₂O, 160 °C, 15 min, 99%.

Flow Process 2: Pt/C, H₂, ^tBuOH/H₂O (4:1, 0.1 M), 30 °C, 1 mL min⁻¹, 99%.

Scheme 2.3.6 telescoped (multi-step, where one step feeds directly into the next) flow synthesis of an intermediate, towards the agrochemical Boscalid.⁸⁸

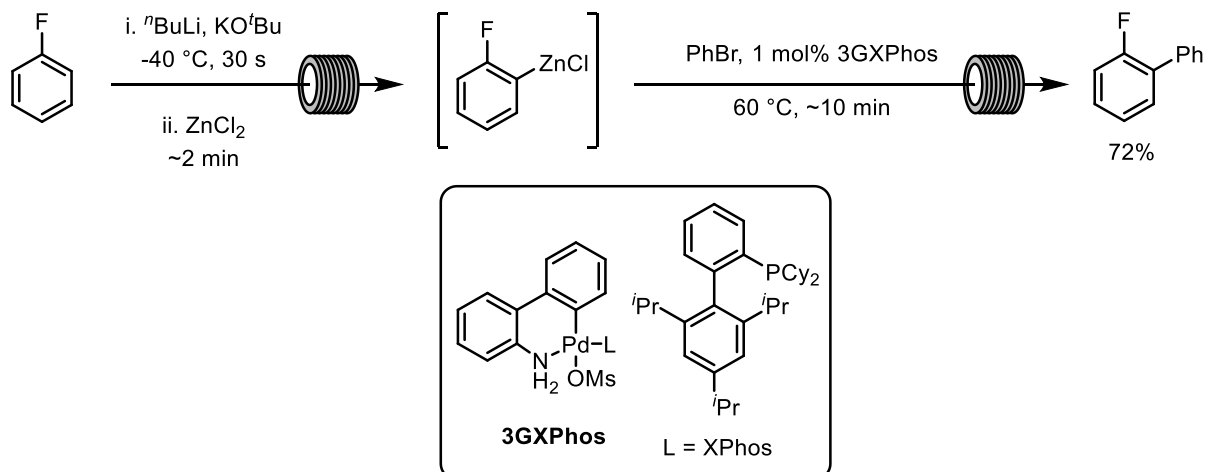
Using 0.25 mol% of Pd(PPh₃)₄ at 160 °C, made accessible in flow, an observed yield of up to 99% was reported for the Suzuki Coupling. Following scavenging of the Pd catalyst with a thiourea resin, the reaction products were then fed in to a second flow reactor, performing nitro group hydrogenation using a Pt/C catalyst.⁸⁸ This also demonstrates the appeal of multi-step syntheses, in flow.

Continuous flow approaches towards the NSAID Diflunisal⁸⁹ have also been applied, again this involved a Suzuki Coupling (Scheme 2.3.7).⁸⁴ Here, work from the Buchwald Group involved sequential lithiation-borylation of an aryl bromide in flow, before being telescoped in a sequence then involving a Suzuki coupling of the borylated product with a fluoroaryl substrate to produce the intermediate.⁹⁰



Scheme 2.3.7 three-step flow process involving lithiation-borylation, followed by a Suzuki coupling to furnish an intermediate in the synthesis of Diflunisal.⁹⁰

Further work from the Buchwald Group involved telescoped lithiation-zincation-Negishi Coupling for synthesis of the fluorinated core of pharmaceutical products Tedizolid and Brequinar (**Scheme 2.3.8**).⁹¹ In this process, the 2-fluoro lithiated aryl species were known to be unstable intermediates. Therefore, using flow reactors was useful as the reactive intermediate could be generated, before swiftly being flowed through to the next flow reactor where it would be consumed.^{4,91}

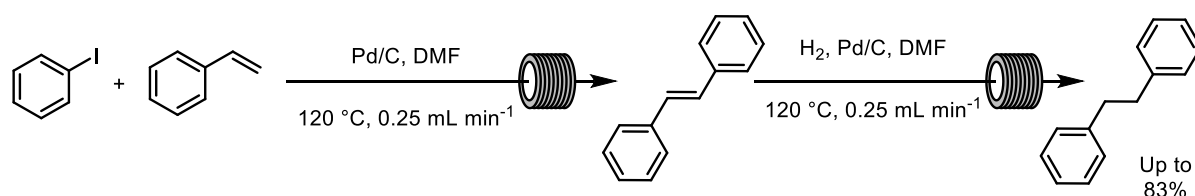


Scheme 2.3.8 multi-step flow synthesis of 2-fluorobiphenyl, the core of Brequinar and Tedizolid, involving formation of an aryl-zinc intermediate, with flow processing well-suited to this by allowing for rapid generation and consumption of the reactive species.⁹¹

These examples illustrate the interest in using flow reactors, attractive for manufacturing, for Pd-catalysed cross-coupling reactions.

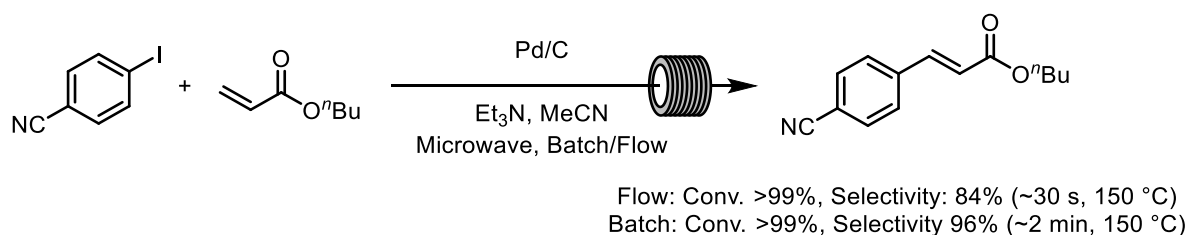
2.3.3 Further Examples of Continuous Flow Heck Reactions

The following examples highlight the interest in performing flow Heck Reactions, the subject of this Chapter. Many flow Heck Reactions involve heterogeneous Pd catalysts, and flow reactors can be suited to such heterogeneously catalysed reactions, using a packed-bed reactor which (provided leaching does not significantly occur) allows for alleviating the requirement for removal of the catalyst after processing.⁹² Examples of flow Heck Reactions using heterogeneous catalysis can involve the application of well-known heterogeneous Pd catalysts, such as Pd/C. This has been employed by Lapkin, Plucinski and co-workers, in the multi-step flow process involving firstly a Pd/C-catalysed Heck Reaction, followed by a Pd/C-catalysed hydrogenation to afford 1,2-diphenylethane (**Scheme 2.3.9**).⁹³ For the Heck Reaction step, the authors reported an observed yield of ~60%, though this was reduced to ~20% after 4 runs, using the same Pd/C catalyst repeatedly and an appreciable amount of leaching was observed. The outlet mixture from the Heck Reaction step was then introduced to H₂ gas and passed through a static mixer, before flowing into the second reactor containing Pd/C, where selectivities >80% were observed towards the desired reduced product. This therefore represents the advantages of simplified multi-step synthesis, using flow reactors.⁹³



Scheme 2.3.9 integrated Heck/hydrogenation continuous process towards 1,2-diphenylethanes.⁹³

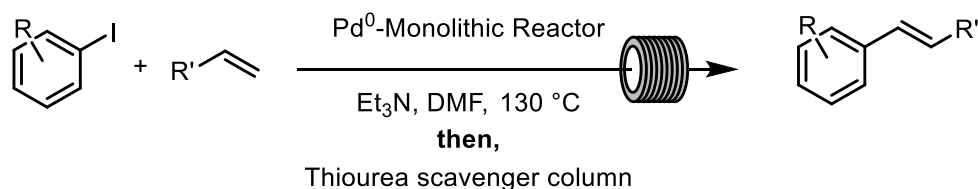
Heck Reactions using Pd/C in flow have also been reported by Kappe and co-workers, where microwave heating was used – particularly attractive due to the strong microwave absorption of Pd/C (**Scheme 2.3.10**).⁹⁴ Again, flow processing is appealing for scaling microwave-assisted syntheses.⁹⁵ Here, with microwave heating to 130-170 °C, the authors reported conversions up to >99%, with good selectivity towards the desired Heck product, in residence times as low as 30 s. Kappe and co-workers also performed complementary batch studies, which were actually observed to be more selective than their flow reactions.⁹⁶



Scheme 2.3.10 continuous flow Heck Reactions using Pd/C as a heterogeneous catalyst alongside microwave heating, observing good conversion/selectivity in short timescales, though greater selectivity was observed in comparable batch reactions.⁹⁶

Ley and co-workers disclosed the application of a monolithic cartridge functionalised with Pd-nanoparticles in a continuous flow Heck Reaction process (**Scheme 2.3.11**). Using an automated reactor system heated at 130 °C, the researchers reported good conversions and yields for a number of aryl iodides and alkenes, including alkenes tethered to heterocycles, though aryl bromides reacted less

efficiently. Furthermore, to circumvent issues with Pd leaching for heterogeneous catalysts, the work here involved integrating a thiourea scavenger column in the flow reactor system, to assist in removing residual Pd.⁹⁷ Again, this represents one of the possible benefits of flow chemistry for processing, with the removal of Pd species important in process chemistry involving *e.g.* pharmaceuticals.^{4,98}



Scheme 2.3.11 continuous flow Heck Reactions using Pd-nanoparticles immobilised on a monolithic reactor cartridge with inline Pd⁰ scavenging.⁹⁷

Other investigations have reported the use of immobilised Pd-particles or salts for Heck Reactions in continuous flow. For example, Evangelisti and co-workers addressed one of the issues that occurs with heterogeneous Pd-catalysis for coupling reactions, related to Pd leaching.⁹⁹ This is a difficult issue as it is believed that for heterogeneous catalysed coupling reactions, it is in fact homogeneous Pd species which are responsible for the catalytic activity¹⁰⁰ and so the Pd leaches from the surface, catalysed the desired process and then desirably redeposits, but also some will be lost and flow through with the reaction mixture. To address this, the researchers attempted to use poly(4-vinylpyridine) as a support for Pd-nanoparticles, as this polymer was known to be a good scavenger for Pd. The aim, therefore, was to recapture most of the Pd after leaching.⁹⁹ They were able to observe, for the Heck Reaction between iodobenzene and *n*-butyl acrylate, conversions of >90% over 14 runs at 125 °C, with Pd leaching being detected at a maximum of 8 ppm (on the first run) with leaching levels detected normally at <5 ppm for all subsequent runs, achieving acceptable levels for pharmaceutical standards (**Fig 2.3.5**).⁹⁸

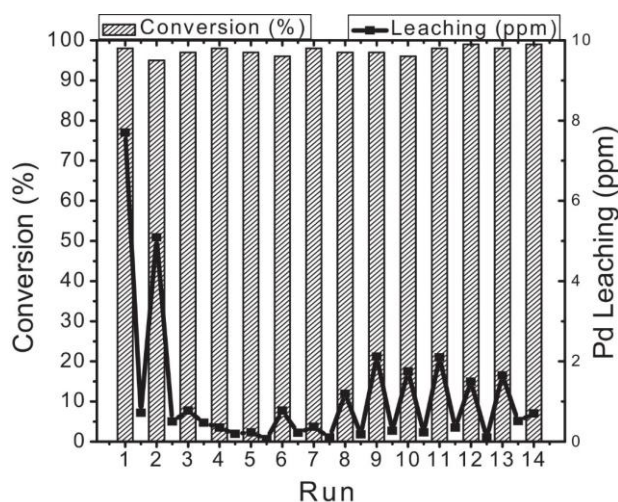


Fig 2.3.5 conversion and Pd-leaching observed by Evangelisti and co-workers for the Heck Reaction between iodobenzene and *n*-butyl acrylate using Pd-nanoparticles immobilised on poly(4-vinylpyridine), acting as a Pd scavenger as well as support. Reproduced with permission.⁹⁹

Similar works involving immobilised Pd salts have been reported, for example, the immobilisation of PdCl₂ via a 2-methylthiomethylpyridine ligand covalently attached to an organic polymer (via a phenol

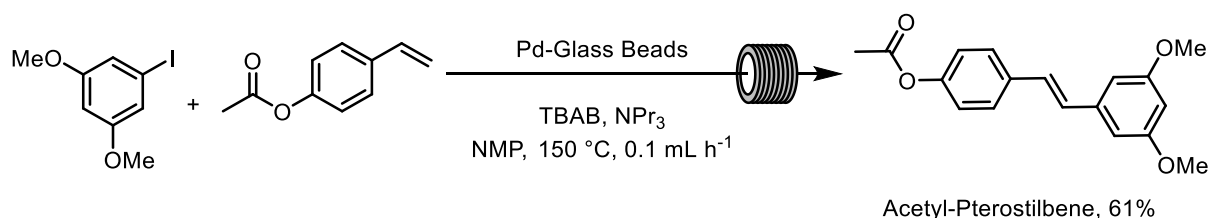
residue on the 2-methylthiomethylpyridine ligand). A 98% yield for the Heck Reaction of iodobenzene and *n*-butyl acrylate was observed, with a 39 min residence time at 120 °C.¹⁰¹ Kirschning and Kunz have also previously reported the use of a monolithic glass/polymer composite reactor, where palladium was immobilised *via* ion-exchange, with subsequent reduction used to afford the deposition of Pd-nanoparticles inside a flow reactor. The Heck Reaction between 4-iodoanisole and *iso*-butyl acrylate (as well as *e.g.* Sonogashira and Suzuki Reactions) was performed in the system, with full conversion observed in 30 min at 110 °C.¹⁰²

As well as conventional heterogeneous Pd catalysts (*e.g.*, Pd/C) and immobilised Pd salts/nanoparticles on solid supports, liquid/alternative supports have also been investigated in continuous Heck Reaction processing. Hessel, Noël and co-workers reported the use of a supported liquid phase catalyst for continuous flow Heck Reactions, which involves a stationary liquid film in which the catalyst is retained. They employed a polar phosphine ligand with Pd(OAc)₂, dissolved in ethylene glycol and then flushed the solution through a column containing molecular sieves to form the catalyst system in a flow-through column. Performing reactions between iodobenzene and *n*-butyl acrylate in the column at up to 230 °C resulted in the observation of yield up to 94% in a 26 min residence time.^{103,104}

Luis and colleagues reported the use of methyl-imidazole ionic liquids as immobilising units for anchoring Pd⁰ catalysts onto a monolithic polymer support. In their approach, supercritical-EtOH was applied as the reaction solvent, exploiting a number of potentially green methods (supercritical fluids, ionic liquids, flow processing, catalysis *etc.*).²¹ Using iodobenzene and methyl acrylate as coupling partners, yields of >80% was observed for the system at a 0.1 mL min⁻¹ flow rate, at 200 °C.¹⁰⁵

Also focusing on the use of alternative processing solvents for greener approaches, Styring and co-workers reported the application of supercritical-CO₂ for performing Heck Reactions in a continuous flow reactor. Using a Pd/SiO₂ heterogeneous catalyst, alongside DIPEA as a base with THF or methanol co-solvents, Styring and colleagues reported the Heck Reaction between 4-iodoanisole and methyl acrylate in both a continuous flow reactor, as well as a continuous stirred tank reactor.¹⁰⁶

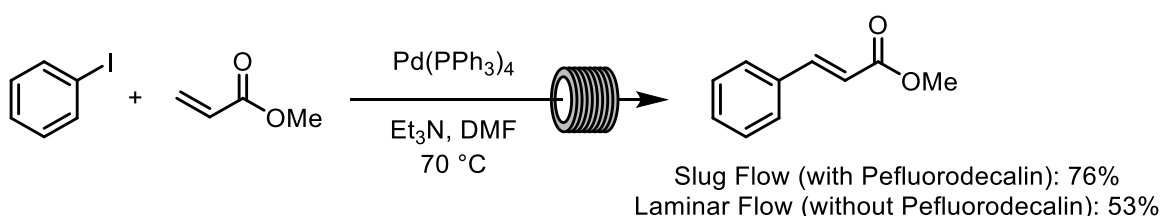
The targeted synthesis of interesting compounds *via* Heck Reactions in flow has also been performed. Laudadio, Evangelisti, Angelici and co-workers reported the synthesis of pterostilbene (a polyphenolic compound related to Resveratrol) using a continuous flow Heck Reaction (**Scheme 2.3.12**). Using a Pd catalyst immobilised on glass beads, at 135 °C, the authors observed conversions of around 80%, affording the desired pterostilbene following a deprotection step.¹⁰⁷



Scheme 2.3.12 continuous flow Heck Reaction employed in the synthesis of pterostilbene (following deprotection of acetyl-pterostilbene).¹⁰⁷

Despite heterogeneous catalysis offering, at face-value, the opportunity for simplified purification, issues with leaching can often negate this benefit.⁹² Moreover, some evidence suggests that the Heck Reactions (and similar reactions) may *rely* on leached species to promote the reaction, before (ideally) redepositing in heterogeneously catalysed reactions^{108–110}, meaning that leaching and redeposition becomes an aspect requiring further consideration when designing a flow reactor. As such, homogeneously catalysed Heck Reactions in flow have also attracted attention, much like in batch.

A model Heck Reaction (iodobenzene and methyl acrylate) was performed by Wirth and co-workers, using two flow processing conditions (**Scheme 2.3.13**).⁷⁷ The first involved laminar-flow conditions, where a 53% yield was observed. The second set of conditions employed a biphasic system, where the reaction solution was mixed with an immiscible fluorinated solvent, to generate segmented-flow conditions, resulting in an observed yield increase to 76%. This highlights the importance of process design in maximising the effect of a flow reactor. Being able to vary the flow regime can be considered a further benefit offered by flow reactors.⁷⁷



Scheme 2.3.13 model Heck Reaction between iodobenzene and methyl acrylate, applied by Wirth and co-workers in demonstrating the positive effect on yield of increased mixing in a biphasic flow system.⁷⁷

Researchers from Pfizer have also performed similar model Heck Reactions under segmented-flow conditions, at higher temperatures up to 200 °C, and were able to eliminate the necessity for an added ligand, with low loadings of Pd(OAc)₂ employed (0.05 mol%) sufficient for good yields of aryl iodides and butyl acrylate.⁷⁶

In the previously mentioned study from Kappe and co-workers, using Pd/C as a heterogeneous catalyst in flow alongside microwave heating, homogeneous Pd(OAc)₂, again in the absence of added ligands, was also used in flow reactions using microwave heating. They studied homogeneous catalysed systems due to noting the significant leaching of Pd/C in the heterogeneous system, leading to diminished catalytic activity. Kappe and colleagues reported an observed 99% conversion and 99% selectivity towards the Heck product of the reaction between 4-iodobenzonitrile and *n*-butyl acrylate, requiring a 10 min residence time at 170 °C.⁹⁶

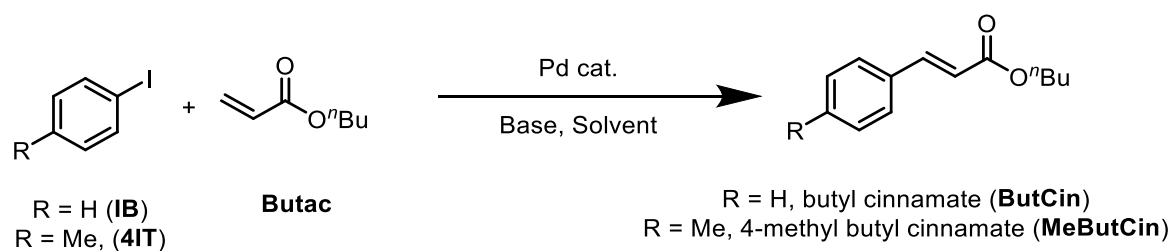
These examples therefore represent some of the benefits of continuous flow processing, for example, access to elevated temperature conditions and the possibility of streamlining reactions/processes. As has mentioned in the Strategy & General Aims Section, the work in this Chapter aims to build upon the area of Heck Reactions (and related reactions), in continuous flow processes.

2.4 Results & Discussion

2.4.1 Initial Investigations Using a Vapourtec Reactor

The preliminary objective was to obtain a system capable of performing Heck Reactions in flow. This was with the aim of further investigating the benefits of applying novel processing windows (high T/p) to the Heck Reaction, expanding upon previous literature. Furthermore, applying the reactor to variant Heck Reactions was also of interest (Chapters 3 and 4). Initially, a Vapourtec E-Series reactor was acquired. The aims of using this were, primarily, to determine whether the system was suitable for performing flow Heck Reactions and to assess the scope for using this for ongoing work. Using the Vapourtec system was also treated as a training exercise in performing thermal flow reactions and executing Pd-coupling reactions.

The reaction of *n*-butyl acrylate (**butac**) with either iodobenzene (**IB**) or 4-iodotoluene (**4IT**) was investigated (**Scheme 2.4.1**). The initial reactions involved Pd(OAc)₂ as the catalyst, without added ligands, as has been previously applied.⁷⁶ The expected products of these model reactions are cinnamate esters, butyl cinnamate (**ButCin**) and 4-methyl butyl cinnamate (**MeButCin**) for the reactions with **IB** and **4IT**, respectively. This reaction was chosen as such coupling partners are typical for model Heck Reactions, used to investigate flow methodologies previously.^{76,77,97,99,104,111}



Scheme 2.4.1 coupling of an aryl iodide with *n*-butyl acrylate, a typical model Heck Reaction.

Initial reactions were performed with a 10 min residence time and 5 mol% loading, at 140 °C (being the highest operational temperature in the Vapourtec reactor using MeCN as a solvent). However, under the conditions used, with Pd(OAc)₂ as the catalyst, precipitation of what appeared to be Pd⁰ was observed, which resulted in reactor blockage. A black coating which formed on the transparent reactor manifold tubing was removed with dilute nitric acid, and regular cleaning to ensure no Pd deposits were present on the internal walls of the reactor tubing was adopted. As such, reactions were repeated using lower loadings (0.1 mol% and 0.05 mol%), intending to prevent Pd precipitation. Similar conditions had been used in previously published literature, at 200 °C and 5 min reaction time.⁷⁶ As a lower temperature of 140 °C was being used here, an extended time of 10 min was applied.

Table 2.4.1 isolated yields for initial reactions between 4IT and butac.

Entry	Pd(OAc) ₂ Loading / mol%	MeButCin Isolated Yield / %
1	0.05	69
2	0.1	57
3	5	Failed

At the lower loadings, the reactions proceeded smoothly without blockage, though a small amount of presumably Pd black was observed at 0.1 mol%. The observations suggested that less palladium was leading to greater yields of product (Table 2.4.1, Entries 1 and 2), possibly because at 0.1 mol% loading, Pd⁰ appeared to precipitate (without causing blockage), which could have caused catalyst deactivation. At 0.05 mol% no Pd⁰ precipitation was apparent, hence the catalyst might have remained active over a longer period. Such observations, towards using so-called “homeopathic” Pd loadings (<0.1 mol% loading), have previously been observed by de Vries and co-workers.^{112–114} For avoiding precipitation, ligands can be employed, or the Jeffery conditions, using a quaternary ammonium salt to stabilise Pd⁰ and prevent precipitation.^{115–117} This indicated that the Vapourtec system was useful for performing such reactions, provided the conditions were suitable.

Moving on from this initial test two other ligated, preformed catalysts which were supplied by JM, were applied (Fig 2.4.1). These catalysts were based on Pd⁰ with a single XPhos ligand (Fig 2.4.1) which has been suggested to be a highly active catalyst for coupling reactions.^{118,119} This would allow for comparison against simple Pd(OAc)₂, without any added ligand – favourable due to being relatively cheap and not containing any phosphine ligands. The pre-formed catalysts might be expected to be more costly and so less appealing for process chemistry, however, the hypothesis would be that they might be more active and possibly avoid previously observed solubility issues.

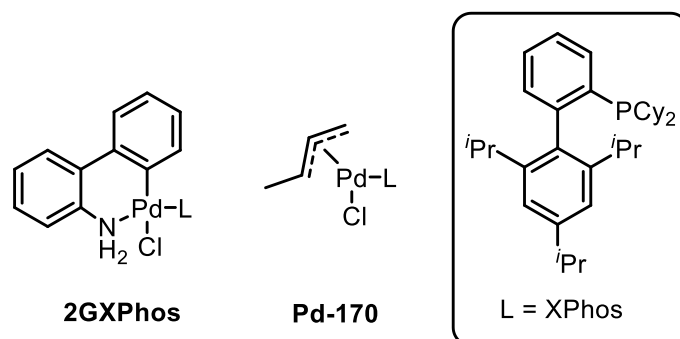
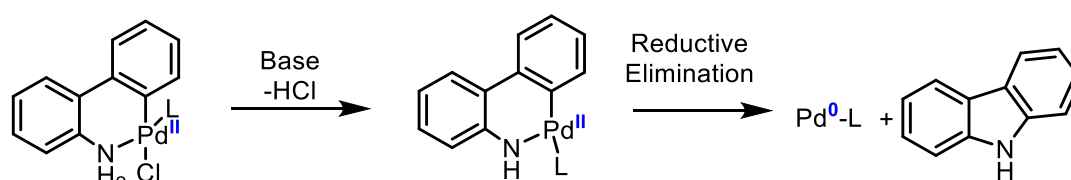


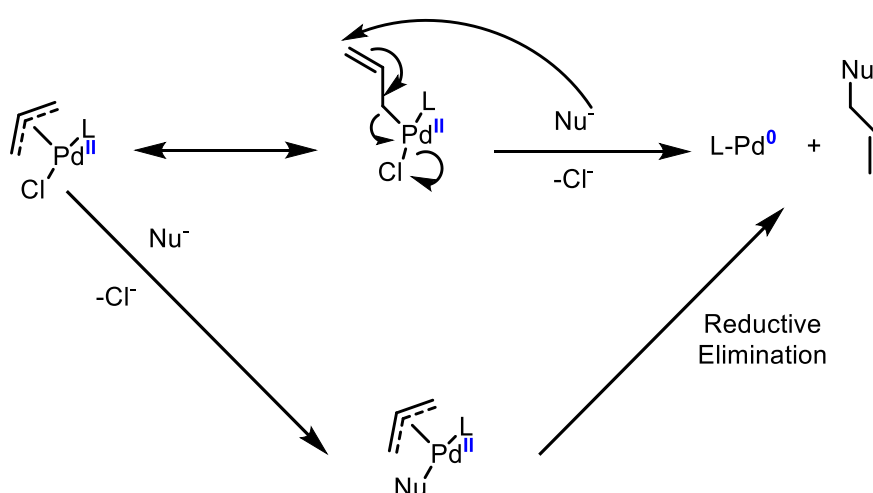
Fig 2.4.1 Pd-XPhos pre-catalysts supplied by JM, 2GXPhos is a well-established catalyst developed by the Buchwald Group, Pd-170 is an analogous pre-catalyst developed by collaborators at JM.

The two XPhos-based catalysts (and some of the other preformed catalysts provided, discussed later) undergo activation *in-situ* during the reaction (**Scheme 2.4.2** and **Scheme 2.4.3**), and the two selected here form the same active catalyst. 2GXPhos, amongst others in the Buchwald family of Pd catalysts, have been well established for performing typically difficult cross-coupling reactions.¹¹⁸ During the activation of 2GXPhos, however, the pre-catalyst undergoes the loss of a carbazole unit.¹²⁰ This has been noted to be undesirable due to some examples suggesting that the carbazole can inhibit reactions.¹²¹ Moreover, particularly considering industrial process synthesis, where larger amounts of catalyst would be required compared to a lab-scale reaction, the generation of carbazole, being toxic, would be undesirable. Due to these reasons, the Pd-170 catalyst, developed by JM, was designed to produce the same active catalyst as 2GXPhos, but instead involving loss of an innocuous leaving/activating group (by elimination of the crotyl ligand, **Scheme 2.4.3**).¹²¹ The mechanism for activation for the 2GXPhos catalyst (**Scheme 2.4.2**) involves deprotonation of the amine ligand, then reductive elimination of a carbazole unit, giving the active catalyst.¹²⁰



Scheme 2.4.2 mechanism of activation for the pre-catalyst 2GXPhos, $L = \text{XPhos}$.¹²⁰

The mechanism of activation for Pd-170 (**Scheme 2.4.3**) is suggested to follow one of two pathways. One involves the direct nucleophilic attack (possibly by an amine base in a Heck Reaction) on the crotyl ligand, leading to the elimination of an alkene and the displacement of a chloride anion. The other possibility involves firstly a substitution of the chloride ligand with a nucleophilic ligand (e.g. an amine base in a Heck reaction undergoes substitution with the chloride ligand), followed by subsequent reductive elimination of the nucleophile on the crotyl ligand.¹²¹



Scheme 2.4.3 possible activation pathways of the pre-catalyst Pd-170, $L = \text{XPhos}$.¹²¹

The three catalysts ($\text{Pd}(\text{OAc})_2$ and the XPhos-based catalysts) were then used for the reactions between **butac** with **IB** and **4IT**. Previously, 0.05 mol% $\text{Pd}(\text{OAc})_2$ was observed to give the highest yield and no Pd precipitation, so it was decided to use the same loading for the other catalysts.

Table 2.4.2 ^1H NMR yields of crude reaction mixtures from the Heck reactions of butyl acrylate with iodobenzene ($R=\text{H}$) and 4-iodotoluene ($R=\text{Me}$).

Entry	R	Catalyst	ButCin/MeButCin	IB/4IT
			^1H NMR Yield / %	^1H NMR Conversion / %
1		$\text{Pd}(\text{OAc})_2$	81 ± 1	82 ± 1
2	H	Pd-170	82 ± 4	85 ± 2
3		2GXPhos	80 ± 2	>99*
4		$\text{Pd}(\text{OAc})_2$	74 ± 6	78 ± 1
5	Me	Pd-170	91 ± 4	90 ± 1
6		2GXPhos	89 ± 3	88 ± 1

*Indicates no ArI detected in ^1H NMR spectrum of crude product mixture.

For reactions between **IB** and **butac** observed yields using all three catalysts were the same (Table 2.4.2, Entries 1-3). $\text{Pd}(\text{OAc})_2$ and Pd-170 were observed to give conversions of ~80–85%, whereas 2GXPhos appeared to give full conversion. However, due to **IB** being a liquid reagent, it could have been possible that **IB** was evaporated upon solvent removal (under gentle N_2 stream) prior to NMR spectroscopic yield analysis. This was identified as a negative aspect of using NMR spectroscopy for yield analysis, addressed later by employing GC analysis. For reactions between **4IT** and **butac**, yields of around 90% were seen for the catalysts Pd-170 and 2GXPhos. For $\text{Pd}(\text{OAc})_2$, a slightly lower yield of around 75% was observed (Table 2.4.2, Entries 4-6). Typically, Heck Reactions are favoured by an electron poor aryl halide, as oxidative addition (involving loss of electron density from the Pd centre) is accompanied by increased electron density on the arene, therefore electron-withdrawing aryl halides undergo this more efficiently.³⁷ Using Pd-170 or 2GXPhos however, observed yields were higher for **4IT**, a more electron rich aryl halide than **IB**. Notably, applying the pre-formed catalysts did not appear to give significantly higher yields than simple $\text{Pd}(\text{OAc})_2$.

This initial work appeared promising for using the Vapourtec. Heck Reactions had been performed, using different catalysts, managing to avoid blockages and good yields were obtained with low Pd loadings. Previous literature reports had also applied 0.05 mol% $\text{Pd}(\text{OAc})_2$ loadings but at 200 °C, achieving good yields (~80%) in 5 min residence times.⁷⁶ The Vapourtec therefore seemed to perform comparably to previous reports, here observing ~80% yields, also at 0.05 mol% $\text{Pd}(\text{OAc})_2$ loading, but in a 10 min residence time at 140 °C, being the highest temperature accessible using MeCN, due to the 10 bar backpressure limitation on the system. The maximum highest temperature achievable using the

system in the format available would have been 150 °C, so the maximum temperature using MeCN as solvent was not significantly below this threshold.

To further evaluate the system for ongoing work, a comparison of process parameters was made by performing the model reactions under a further range of conditions. The next reactions performed involved varying the temperature at a constant flow rate (0.2 mL min⁻¹, 10 min residence time). The aim was to determine how effective the benefits of using the Vapourtec at temperatures above solvent boiling points were on the Heck Reaction. That is, to determine whether access to superheated conditions (up to 140 °C, as in **Table 2.4.1** and **Table 2.4.2**) was providing any processing benefits (rate acceleration), or whether the same observations would be made at *e.g.*, 80 °C (close to the refluxing temperature of MeCN, easily attainable in batch).

For these next experiments the reaction involving **4IT** was chosen, using Pd(OAc)₂ as a catalyst. This decision was taken as **4IT**, being a solid, compared to **IB** being a liquid, would likely incur less issues with starting material evaporation when preparing samples for ¹H NMR spectroscopic yield analysis.

Table 2.4.3 ¹H NMR yields of the crude reaction mixture for the Heck Reaction between butyl acrylate and 4-iodotoluene, investigating the effect of temperatures accessible in the Vapourtec.

Entry	Temperature / °C	MeButCin ¹ H NMR Yield / %	4IT ¹ H NMR Conversion / %
1	140	74 ± 6	78 ± 1
2	110	16 ± 1	30 ± 1
3	80	4 ± 1	10 ± 4

The observed results suggested that increasing temperature from 80 to 110 °C, then significantly from 110 to 140 °C led to an increase in yield (**Table 2.4.3**). Temperatures of 110 and 140 °C, requiring a backpressure to prevent MeCN from boiling, are amenable flow processing (due to the small reactor volume, 2.0 mL here, only requiring a small total volume to be pressurised).^{4,5} As such, the advantages of using a flow system demonstrated a benefit towards the Heck Reaction processing.

Next, it was decided to evaluate the range of residence times available to be explored using the Vapourtec, and to determine whether at 140 °C, using 0.05 mol% Pd(OAc)₂ (**Table 2.4.2**, Entry 4, **Table 2.4.3**, Entry 1) the reaction could be pushed to complete conversion.

Table 2.4.4 ^1H NMR yields of the crude reaction mixture for the Heck reaction between 4-iodotoluene and butyl acrylate, investigating the effect of residence time in the Vapourtec.

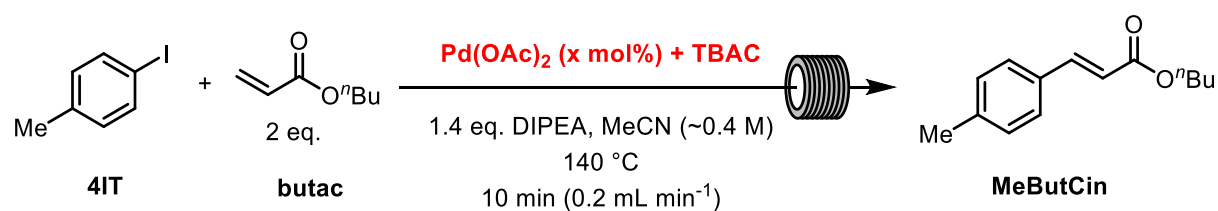
Entry	Residence Time / min	MeButCin ^1H NMR Yield / %	4IT ^1H NMR Conversion / %
1	2	37 ± 2	39 ± 3
2	5	54 ± 2	57 ± 1
3	10	80 ± 5	84 ± 1
4	15	83 ± 4	86 ± 1

As expected, a decrease in yield was observed when the residence time was decreased (*i.e.*, a faster flow rate was used). Upon increasing the reaction time from 10 to 15 min, the change in yield was small – only a slight increase was observed (**Table 2.4.4**). This was perhaps due to the observation that at slower flow rates (*e.g.*, 0.133 mL min⁻¹, required for 15 min residence time in a 2.0 mL reactor coil) the system would struggle to maintain the set backpressure, and the system pressure would fluctuate. This can be a known issue with certain types of pump, when operating at slow flow rates against backpressure.⁶ Due to this, the 15 min planned residence time (**Table 2.4.4**, Entry 4) might not have been what was expected, and if shorter than planned, this could explain the lower-than-expected observed yield. Increasing the residence time further using this system would therefore have been unfeasible at the temperature applied (140 °C). It should also be noted here that the reaction with a 10 min residence time (0.2 mL min⁻¹, 2.0 mL reactor manifold) was repeated, giving a similar yield to the previous experiment (74±6%, and 80±5%, compare **Table 2.4.2**, Entry 4 with **Table 2.4.4**, Entry 3), showing acceptable reproducibility using the Vapourtec reactor. This suggests, as with the expected benefits of flow chemistry,⁴ that good control over the reaction conditions was apparent.

The next experiments continued to investigate what conditions might achieve full conversion for the model Heck Reaction. So far, a further increase in temperature or extended residence time had been observed to not be feasible.

Therefore, it was considered that full conversion might be achieved by increasing the catalyst loading. However, issues with Pd⁰ precipitation were also anticipated due to previous observations (**Table 2.4.1**), using Pd(OAc)₂. Used extensively in previous literature, the addition of tetra-alkyl ammonium halide salts (Jeffery conditions) is known to assist in prevention of Pd⁰ precipitation, particularly with “ligandless” Pd catalysts – *ligandless* here, meaning generally that the catalyst is a simple Pd salt *e.g.* Pd(OAc)₂ or PdCl₂.^{115–117} Due to precipitates posing a major issue in flow due to blockages, it was decided to determine if Jeffery conditions would allow higher loadings to be more suited to flow processing. As such, reactions were run with the addition of 0.1 eq. tetrabutylammonium chloride (TBAC) at 0.05 mol% Pd(OAc)₂ (where no precipitate had been observed previously) and at 0.1 mol% loading of Pd(OAc)₂, where some precipitate had been observed previously (**Table 2.4.5**).

Table 2.4.5 ^1H NMR yields for the Heck reaction between 4-iodotoluene and butyl acrylate exploring the effect of a tetraalkylammonium salt on the reaction.



Entry	Pd(OAc) ₂ Loading / mol%	TBAC Loading* / mol%	MeButCin ¹ H NMR Yield / %	4IT ¹ H NMR Conversion / %
1	0.1	10	94 ± 4	96 ± 1
2	0.05	10	10 ± 1	16 ± 4
3 ^a	0.05	10	10 ± 2	19 ± 2
4	0.05	0	74 ± 6	78 ± 1
5 ^b	0.05	0	80 ± 5	84 ± 1
6 ^b	0.05	0	71 ± 2	71 ± 2

*TBAC equivalents relative to 4IT.

^aRepeat of Entry 2.

^bRepeat of Entry 4.

Increasing the loading to 0.1 mol% Pd(OAc)₂, which resulted in what appeared to be some Pd⁰ precipitate in the absence of TBAC (Table 2.4.1, Entry 2), resulted in no observed precipitate formation with added TBAC and an observed yield of 94% (Table 2.4.5, Entry 1). However, it was observed that, at 0.05 mol% Pd(OAc)₂, where a previous yield of around 80% had been observed without TBAC, the yield dropped to around 10% with TBAC addition (Table 2.4.5, compare Entries 2 and 3 with Entries 4-6). This was not investigated further but might be due to TBAC outcompeting the substrates for binding to Pd, so perhaps lower TBAC equivalents might have been effective.

The Vapourtec reactor had therefore been applied to the Heck Reaction, demonstrating the advantages of flow processing *e.g.*, access to superheated conditions for rate acceleration. Avoidance of precipitation issues and good yields were observed, even when using reasonably low loading of a “ligandless” catalyst (*i.e.* simple Pd salt with no added ligands), in short timescales. Due to the observed benefits of using the Vapourtec system, it was considered that for the ongoing work, access to a broader range of novel processing windows would be of interest, to determine whether the observed benefits could be expanded upon. To do so, a reactor system allowing access to higher temperatures, with great control over a range of pressures and with accurate pumping would be required.

2.4.2 Building a New Reactor to Enable Access to Novel Process Windows

To allow access to a wider range of novel processing windows, it was determined that a custom-built reactor should be constructed. Typically, homemade or “do-it-yourself” reactors offer a more flexible approach towards obtaining a flow system.⁶ Downsides include that such systems are not necessarily reproducible between labs.⁵² It was intended that the ongoing work was to involve high temperatures and high pressures, more easily/safely accessible by using flow reactors (with small heated and pressurised volumes).⁵ To access such conditions, considerations were made regarding design,

materials and equipment choice. It was also considered that the custom-built reactor should maintain the benefits of the Vapourtec reactor, such as simplicity of operation and design, with implemented safety features, and a small footprint.

To allow access to higher temperature (and pressure), tubing material choices considered were 316 stainless steel (316 SS) or Hastelloy. 316 SS is readily available, reasonably chemical/corrosion resistant and widely used^{4,54} and Hastelloy is a more corrosion-resistant alternative.⁴ Both would also allow access to higher temperatures and pressures than with most polymer tubing. It was considered that 316 SS would be suitable for the likely reaction conditions, so was selected as the tubing material for the pressurised and heated parts of the reactor. Tubing in the system where heat/pressure would not be applied was decided to be constructed out of a transparent polymer (*e.g.*, PTFE, FEP, PFA) to aid visibility of possible insoluble precipitates which could cause blockage. Below, some data are given comparing 316 SS stainless steel tubing with some polymer tubing, illustrating the considerations made in the decision making behind choosing SS tubing for the reactor.

Table 2.4.6 *pressure and temperature data quoted from manufactures, considered when choosing a material suitable for constructing a reactor to allow for higher temperature flow reactions to be performed.*

Material	Dimensions ^a	Source	Max. Temp. / °C	Max. Pressure / bar
316 SS*	1/8 " OD, 0.028 " WT	Swagelok	426	463
			315	491
			204	555
			93	578
			37	578
316 SS*	1/16 " OD, 0.020 " WT	Swagelok	426	653
			315	693
			204	783
			93	816
			37	816
PEEK	1/32 " OD, 0.020 " ID	Cole-Parmer ^b	100	344
PFA	1/16 " OD, 0.020 " ID	Cole-Parmer ^b	80	138

**For 316 SS, the maximum temp. and pressures are conditional i.e., maximum operational pressure varies with temperature of operation. The data given represent the maximum allowable working pressure at the temperature indicated, values calculated from the Swagelok Tubing Data Sheet, using the quoted maximum pressures and applying the temperature derating factors.*

^aOD = outer diameter, WT = wall thickness, ID = inner diameter.

^bvalues retrieved from Cole-Parmer website.

1/8 " OD SS tubing (**Table 2.4.6**) was selected for the heated part of the reactor, due to a reasonable length giving a desired reactor volume (3 mL, ~125 cm length). Other parts of the reactor which were pressurised (but not heated) involved 1/16 " OD SS tubing, to minimise the total system volume. Due to the lower pressure limitation of 1/8 " SS tubing, the maximum working pressures would be based off the values for tubing with these dimensions. Furthermore, with the eventual heaters chosen for the reactor, the temperature limit of which being 400 °C, the maximum pressure workable, at the maximum

allowable temperature (taken as the closest temperature *above* the actual value *i.e.*, 426 °C in **Table 2.4.6**) would be therefore 463 bar. This was far in excess of any backpressure required for experiments and, certain safety features were introduced to limit the maximum pressure.

To access high pressures (with now 316 SS being a suitable material selected to withstand them) and maintain efficient flow, it was considered that these requirements were similar to those for a HPLC system. Repurposing HPLC or GC equipment for constructing a flow reactor has been widely adopted in the flow community.⁵² As such, an old JASCO HPLC pump and BPR were repurposed for use in this reactor to allow for accessing high pressures (with the BPR) and pumping efficiently against them, using the HPLC pump.

It was decided that the reactor should be constructed as a tubular coiled reactor (**Fig 2.4.2**), that is, with the heated tubing being coiled around a small aluminium block (machined in-house), incorporating two Joule heaters. The coil design allows for a small footprint reactor, with efficient heat transfer both to and across the SS tubing. Alternatives included simply immersing a SS coil in a heated oil bath, however, using electrical Joule heaters was considered to likely allow for more convenient access to a wider range of temperatures. As mentioned, the heaters used in the reactor had an upper limit of 400 °C.

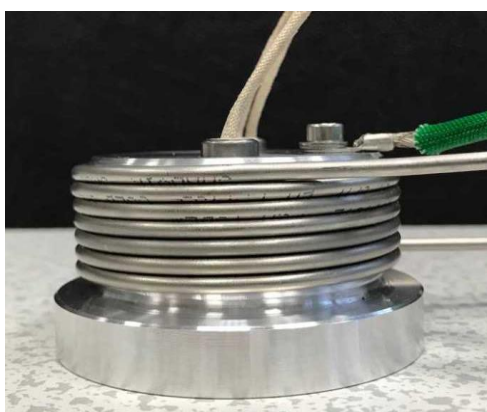


Fig 2.4.2 coiled 1/8 " (OD) SS tubing (3.0 mL internal volume, 125 cm length) around an aluminium heating block (~5 cm base diameter), with two Joule heaters inserted into central drilled cavities – forming the heated part of the reactor.

Considerations for the rest of the reactor system involved applying safety features to mitigate the risk/exposure to any hazard which may present itself due to the heated, pressurised system. Inherently, as one of the benefits of milli-scale flow reactors,⁴ the heated/pressurised volume was small and this itself could be considered the first safety feature. To the rest of the system, relevant monitors and trips were included, with detail in the Experimental Chapter.

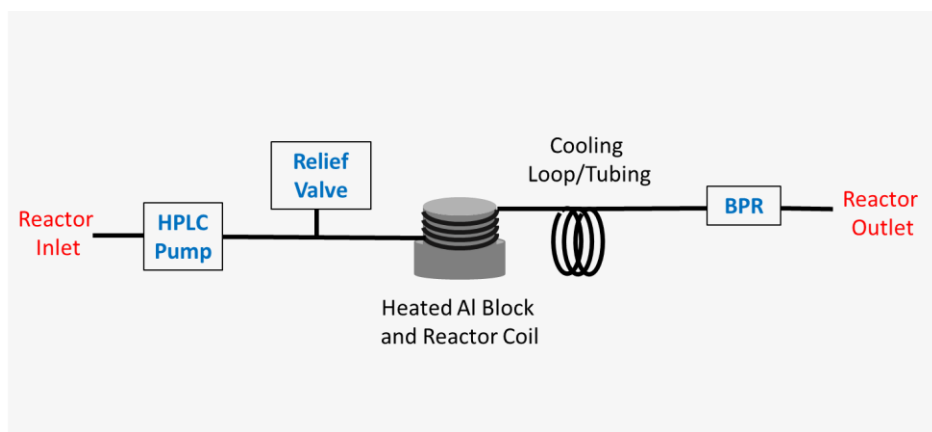


Fig 2.4.3 simplified cartoon diagram of the custom-built reactor, neglecting e.g., electrical connections and placement of thermocouples/pressure monitors. More detailed process diagrams can be found in the Experimental Chapter.

Further detail along with diagrams and images can be found in the Experimental Chapter. To summarise, a homemade flow reactor was built to safely and conveniently access high temperatures and pressures, for ongoing work with the aim of applying such conditions to Heck Reactions and (in later Chapters) related reactions.

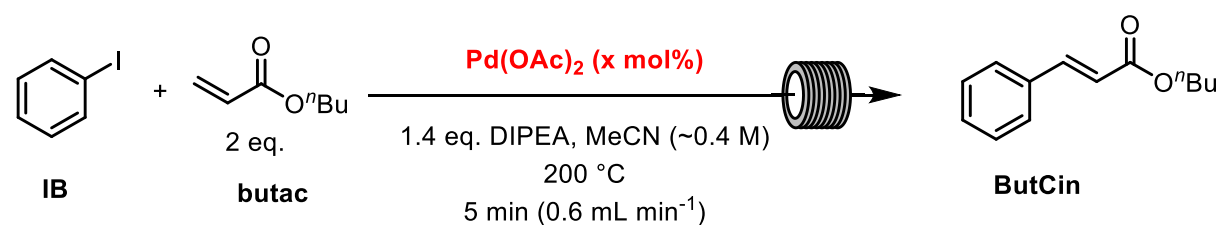
2.4.3 Applying the Custom-Built Reactor to Model Heck Reactions

The model Heck Reaction between **IB** and **butac** was studied in the custom-built reactor, as the same reaction has also been investigated before in flow in a number of studies.^{76,77,97,99,104,111} The aim of this was to determine the suitability of the newly built reactor for performing such reactions and to compare with e.g. a previous report from researchers at Pfizer, in which, temperatures were studied up to 200 °C, under segmented-flow conditions⁷⁶. This involved pumping a small slug of reaction mixture solution, followed by a small slug of immiscible solvent, as has also been investigated by Wirth and co-workers.⁷⁷ In the reactor built here, the intention was to run as a (presumably) laminar-flow tubular reactor, with a constant stream of reaction solution flowing through the reactor during operation (*i.e.* not pumping through alternating small slugs of reaction mixture and immiscible solvent). For segmented slug-flow conditions, the mixing/pumping system can lead to either segmented-flow or droplet flow (where a slug/droplet of reaction mixture is surrounded by the immiscible solvent acting as a carrier), which could lead to issues e.g. with heat transfer, or differing conditions between runs.⁶ Applying (presumably) laminar-flow was considered to be more reproducible and alleviate any possibilities with heat transfer for droplet flow conditions, particularly with the reactor being designed for efficient heat transfer. In the report from Pfizer, low loadings of 0.05 mol% Pd(OAc)₂ were able to be applied at 200 °C, observing good yields/conversions.⁷⁶ Other comparable works in flow which also involved the synthesis of similar products include the use of a 0.3% Pd/polymeric support catalyst, with conversions up to 99% achieved at 150 °C and a 0.025 mL min⁻¹ flow rate;⁹⁹ 99% conversion using a microwave heated flow reactor at 170 °C with a 0.01 mol% Pd(OAc)₂ loading and a 0.4 mL min⁻¹ flow rate;⁹⁶ Wirth and co-workers observed a 53% yield using 10 mol% Pd(PPh₃)₄ under laminar-flow conditions at 70 °C, increasing to 76% with segmented-flow conditions under otherwise analogous conditions;⁷⁷ and, a conversion of 94% was observed by Hessel and co-workers using a supported liquid phase Pd catalyst, at 230 °C and 26 min residence time.¹⁰⁴

Previously, **4IT** had been initially employed as the aromatic substrate and, due to it being solid, ^1H NMR spectroscopy was used to quantify yields and conversion. However, at this point, a GC method was developed to quantify the yields. This was preferred to NMR spectroscopic analysis as the samples could be taken directly from the reaction output stream with no further treatment (other than dilution) and so would likely be a more accurate approach. As such, **IB** was chosen as the ongoing model coupling partner, as an electron neutral aryl iodide. The initial aims of using this newly built reactor were to therefore determine firstly, if the homemade reactor could be applied to flow Heck Reactions, if so, whether the observed results were comparable against previous literature reports and to determine whether applying high temperatures under presumably laminar-flow conditions (rather than segmented-flow, which can lead to certain issues)⁶ could lead to further reductions in Pd loadings or other processing benefits.

A study was therefore conducted, using analogous conditions to those previously employed by the Pfizer researchers.⁷⁶

Table 2.4.7 differences in observed yields between work performed here, and previous work published by Pfizer, under segmented-flow conditions.



Entry	Loading / mol%	ButCin GC Yield (This Work) / %	Yield (Pfizer) ^{76*} / %
1	0.05	100 ± 1	85
2	0.01	95 ± 1	36
3	0.005	93	23

*Conducted on a 4-iodobenzonitrile substrate, for the same substrate, **IB**, an 83% yield was observed under conditions analogous to Entry 1.

At 200 °C, for this model reaction, the researchers at Pfizer reported a yield of around 80%, using 0.05 mol% Pd(OAc)₂ in a 5 min residence time.⁷⁶ However, the initial studies here gave observed yields >90% under the same conditions (**Table 2.4.7**, Entry 1), but also at lower loadings of 0.01 mol% and 0.005 mol% (**Table 2.4.7**, Entries 2 and 3).

Some controls were therefore conducted (**Table 2.4.8**). It was considered that (in poor experimental planning) as the 0.05 mol% loading reaction was conducted first, then 0.01 mol%, then 0.005 mol%, any Pd contaminant present from the higher loadings reaction might have resulted in higher-than-expected Pd loading for subsequent reactions. A “blank” reaction following this observation was performed at 200 °C *i.e.*, where no Pd was intentionally added to the reagent mixture, giving an observed yield of around 20% (**Table 2.4.8**, Entry 1). This indicated that possibly some Pd fouling might have been present within the reactor. The reactor was then cleaned using a small volume of diluted aqueous nitric acid, and the blank reaction was repeated. Again, the coupled product (**ButCin**) was observed in the GC analysis but at a lower yield of 11% (**Table 2.4.8**, Entry 2). After cleaning with

recirculating dilute aqueous nitric acid for ~2 hours, before neutralising/reconditioning, blank reactions were repeated and at 200 °C no product was observed (Table 2.4.8, Entry 3). A blank reaction at 250 °C was also performed and a small amount of product was observed to have formed (Table 2.4.8, Entry 4). However, it was considered that, due to the high temperature employed, and the nature of SS alloy, it could be possible that some catalysis due *e.g.*, to leaching of nickel from SS could have been responsible for this observation.

Table 2.4.8 observations from blank reactions (with no Pd added to reaction) on the **IB** + **butac** Heck Reaction, suggesting some Pd contamination in the reactor which was apparently removed upon flushing with diluted aqueous HNO₃.

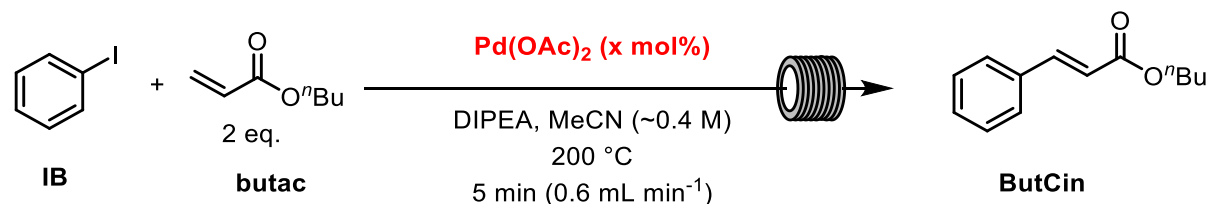
IB + **butac** $\xrightarrow[\text{5 min (0.6 mL min}^{-1}\text{)}]{\text{No added Pd, 1.4 eq. DIPEA, MeCN (~0.4 M), Temp. 200 }^\circ\text{C}}$ **ButCin**

Entry	Conditions	ButCin GC Peak Area	Corresponding ButCin GC Yield / %
1	Before Reactor Cleaning 200 °C	264,000	19
2	After First Clean 200 °C	129,000	11
3	After Second Clean 200 °C	Not observed	0
4	After Second Clean 250 °C	64,000	6

It was concluded from these preliminary tests that, at 200 and 250 °C, no appreciable product was formed without the intentional addition of Pd catalyst, but that after a few reactions, Pd contaminant could affect the observed result. Therefore, regular cleaning of the reactor (with aq. HNO₃) was adopted as standard procedure, when doing so, this was done using recirculating acid overnight to ensure good cleaning.

Following this, reactions were performed investigating catalyst loadings and the effect of temperatures >200 °C on the Heck Reaction. This was to determine, firstly, whether the results mentioned previously could be considered correct (*i.e.* the higher observed yields than the previous report from Pfizer)⁷⁶ and, following from this, whether temperatures above 200 °C, made easily accessible in flow, could offer processing benefits to the reaction. Reactions were performed at 200 °C, 5 min residence time and varied Pd(OAc)₂ loading, to compare against previous work from Pfizer⁷⁶ and to obtain a more reliable initial set of results.

Table 2.4.9 effect of Pd(OAc)₂ loading at 200 °C on the Heck Reaction of IB with butac.



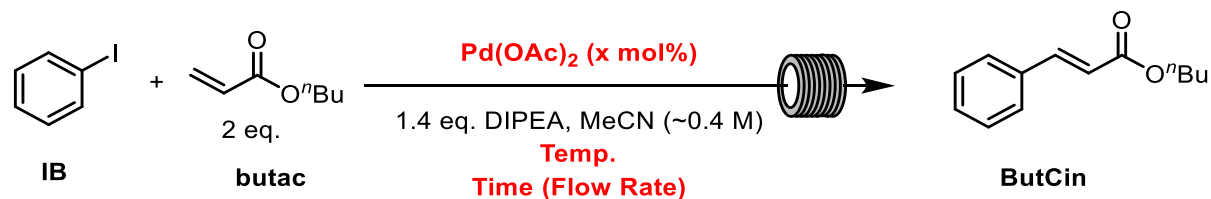
Entry	Loading / mol%	ButCin GC Yield / %	IB GC Conversion / %
1	0.005	68 ± 1	86 ± 1
2	0.001	17 ± 1	30 ± 5
3	0.0005	14 ± 1	19 ± 2

A yield of around 68% was observed at 200 °C with 0.005 mol% Pd(OAc)₂ loading (**Table 2.4.9**, Entry 1), compared to 93% observed previously (with Pd contamination) and a 23% reported yield from the Pfizer researchers, under comparable conditions (**Table 2.4.7**, Entry 3). As the blank reactions indicated no yield due to Pd contamination, this could not be associated with the yield being higher than that observed by the Pfizer researchers. Repeats were performed (analogous to **Table 2.4.9**, Entry 1) and were found to be in good agreement. Possible reasons for the difference may be related to the reactors and conditions used, for example, a commercially available reactor was used by the researchers from Pfizer, whereas the one used in this work could, perhaps, benefit from better heat transfer, due to *e.g.*, tubing material/dimension choices. Also, in the report from Pfizer, as previously mentioned, segmented-flow conditions were applied⁷⁶ and perhaps the flow conditions were not well suited to the reaction processing. This was a gratifying observation for use of the custom-built reactor, appearing to give greater yields (68% vs. 23%) relative to previously reported works under segmented-flow conditions.⁷⁶

With a suitable reactor at hand for exploring novel processing conditions, the following aim was to investigate whether higher temperatures could result in achieving good yield/conversion, at lower yet loadings. An objective was therefore set as to whether at the low loading of 0.0005 mol% (equivalent to 5 ppm, **Table 2.4.9**, Entry 3), full conversion and a good yield could be achieved. This was considered a good target as such a low loading of Pd(OAc)₂ would be desirable from a cost and sustainability perspective.^{112–114} Also, Heck Reactions are frequently employed in pharmaceutical manufacturing, however, due to Pd toxicity concerns, strict limits of <10 ppm Pd residue can be present in the final product.⁹⁸ Being able to perform a reaction in which the total amount of Pd used is already below this level could allow for benefits in process synthesis.

With the hypothesis that at elevated temperatures accessible in flow, reaction rates could be increased to allow for low Pd loadings, experiments were performed by conducting reactions at >200 °C.

Table 2.4.10 effect of temperatures >200 °C on the Heck reaction of **IB** with **butac**, showing how 5-10 ppm (0.0005-0.001 mol%) loadings can be applied under elevated temperatures.



Entry	Temperature / °C	Residence Time / min	Loading / mol%	ButCin GC Yield / %	IB GC Conversion / %
1		5	0.005	68 ± 1	86 ± 1
2	200	5	0.001	17 ± 1	30 ± 5
3		5	0.0005	14 ± 1	19 ± 2
4		5	0.005	94	>99*
5	225	5	0.001	42 ± 2	48 ± 2
6		5	0.0005	26 ± 1	32 ± 4
7		5	0.001	76 ± 1	80 ± 1
8		5	0.0005	53 ± 3	68 ± 1
9	250	10	0.001	87 ± 8	>99*
10		10	0.0005	86 ± 5	>99*
11		5	0.001	83 ± 2	92
12	270	5	0.0005	67 ± 2	78 ± 1
13	150	10	0.05	89 ± 2	>99*

*No **IB** was observed in the GC chromatogram of the crude reaction mixture.

The results supported the hypothesis that increased temperatures can increase the yield of the low loading Heck Reactions, in the custom-built flow reactor at >200 °C. For example, an increase in temperature from 200 to 225 °C gave an observed increase in yield from 68% to 94%, at a 0.005 mol% loading (**Table 2.4.10**, Entries 1 and 4). At lower loadings, almost full conversion of **IB** and 83% yield was observed when increasing the temperature to 270 °C at a loading of 0.001 mol% (10 ppm) (**Table 2.4.10**, Entry 11). At 0.0005 mol% (5 ppm), 67% yield was observed at 270 °C (**Table 2.4.10**, Entry 12). Increasing residence time from 5 min to 10 min resulted in full conversion and good yields of around 90% for both 10 ppm and 5 ppm loadings, at 250 °C (**Table 2.4.10**, Entries 9 and 10). As highlighted in **Fig 2.4.4**, it appeared that increased temperature resulted in increased yield, at all Pd loadings investigated.

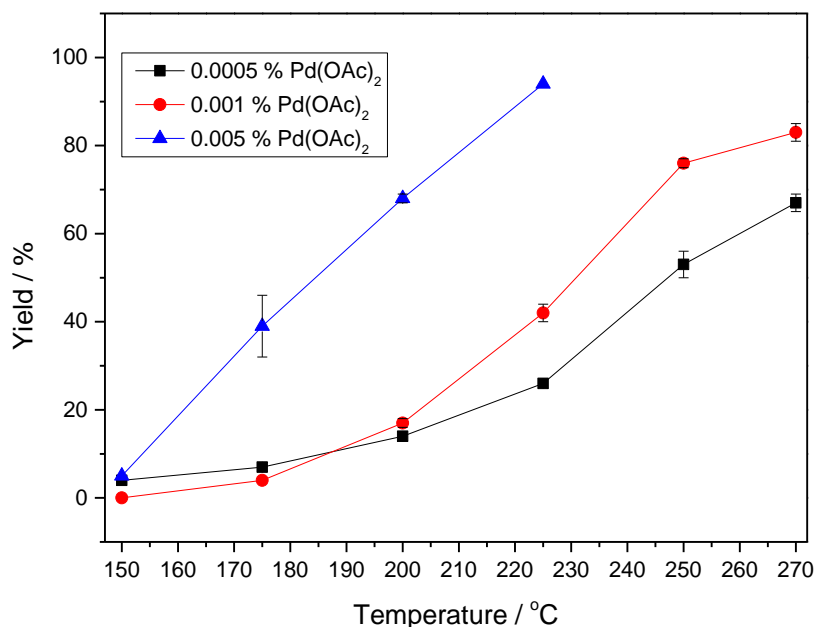
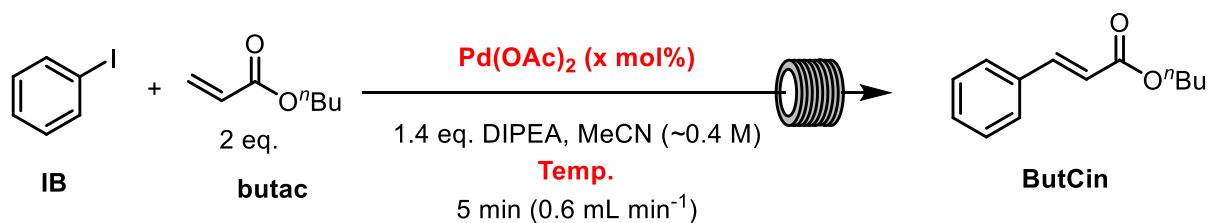


Fig 2.4.4 yield of **ButCin** at varied Pd(OAc)₂ loadings and temperatures, highlighting the increase in yield at increased temperatures. Lines are drawn to guide the eye.

It was then considered whether a further temperature increase *i.e.*, above 270 °C could have increased the conversion/yield further, following the trends of **Fig 2.4.4**. Such conditions had not been investigated previously due to being above the critical point of MeCN, so to remove any phase behaviour considerations from the interpretation of the previous results. It was now considered that investigating supercritical MeCN, or alternatively, other solvents with higher boiling points could be investigated. It was also considered that using an (in principle) more active catalyst might increase conversion/yield. For this, it was anticipated that, as short residence times were being used, possibly the catalysts could be stable to the extreme temperatures, over short timescales.

2.4.4 Catalyst Screen Involving Pre-Formed Pd Catalysts

The next investigations involved a catalyst screen, to determine whether a potentially more active catalyst could result in increased yields, *e.g.* in short residence times or with low catalyst loading. To test this, initially, the previously used catalysts (Pd-170 and 2GXPhos) in reactions in the Vapourtec, based on monoligated preformed Pd XPhos complexes, were again used (5 ppm loading) and applied over a 150-270 °C temperature range, with a 5 min residence time.

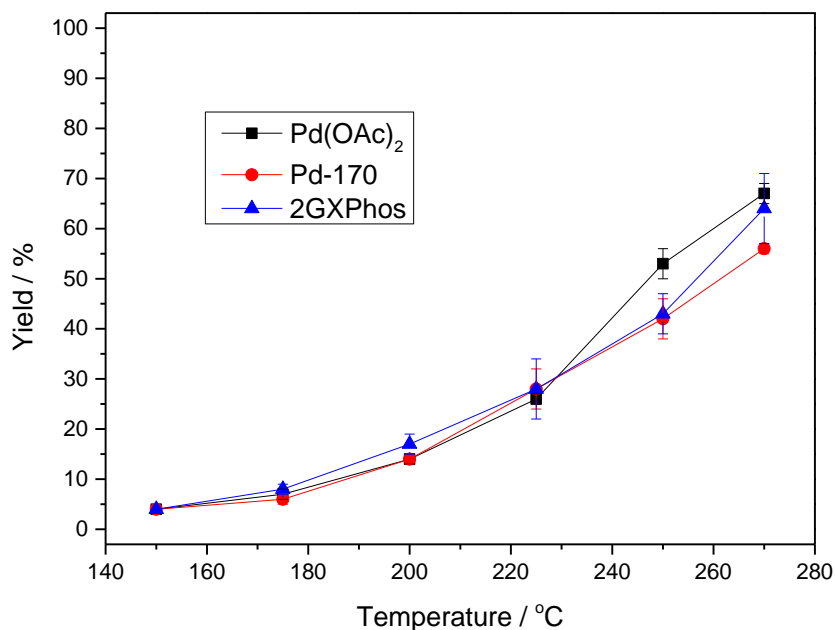
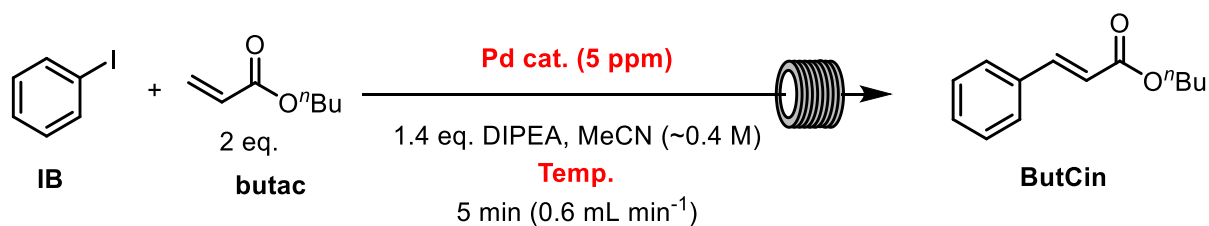


Fig 2.4.5 observed yields for an initial catalyst screen employing 5 ppm loading and 5 min residence time, showing no significant difference between using simple Pd(OAc)₂ or pre-formed XPhos based catalysts. Lines are drawn to guide the eye.

The observed yields using either the XPhos-based pre-formed catalysts or Pd(OAc)₂ were similar, with overlap of errors in yield (estimated from the difference between the average of triplicate measurements, and the single measurement furthest from the average) apparent for almost all sets of comparable conditions (**Fig 2.4.5**). As both preformed catalysts involved XPhos ligands, the next step taken was to expand the catalyst screen, using the other preformed catalysts supplied by JM, bearing other phosphine ligands. As well as being based upon other phosphine ligands, some of these catalysts also contained a variety of activating groups (**Fig 2.4.6**).

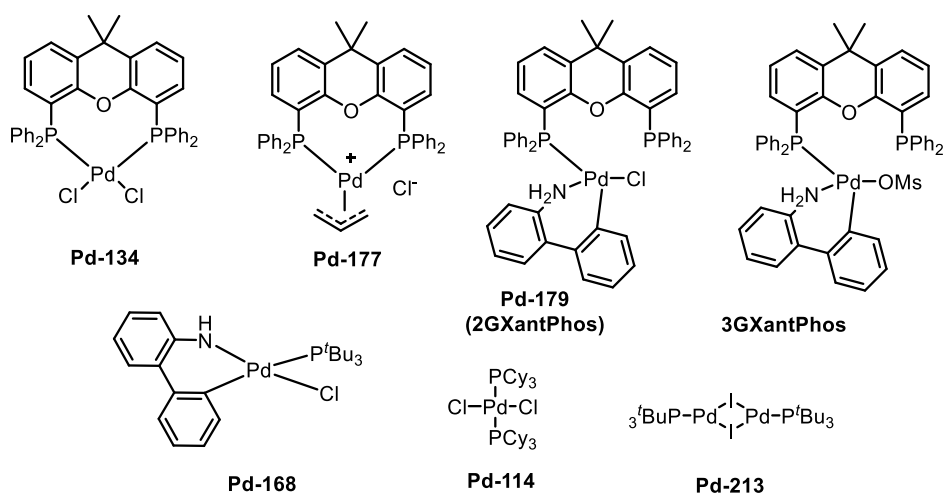


Fig 2.4.6 selection of Pd pre-formed catalysts screened in the high temperature flow reactor. Top row catalysts are based on XantPhos ligands with activating groups analogous to those shown in **Scheme 2.4.2** and **Scheme 2.4.3**, or simple chloride ligands. Bottom row catalysts are based on more simple phosphine ligands (P^tBu_3 , PCy_3) with an aminobiaryl activating group (Pd-168), chloride anions or a Pd^{II} bridged dimer, a speculated intermediate in the reduction of Pd^{II} halides by phosphine ligands.¹²²

These catalysts were then employed in a screen under a selection of conditions comparable to some of those previously employed *i.e.*, a range of temperatures at a 5 ppm loading and 5 min residence time.

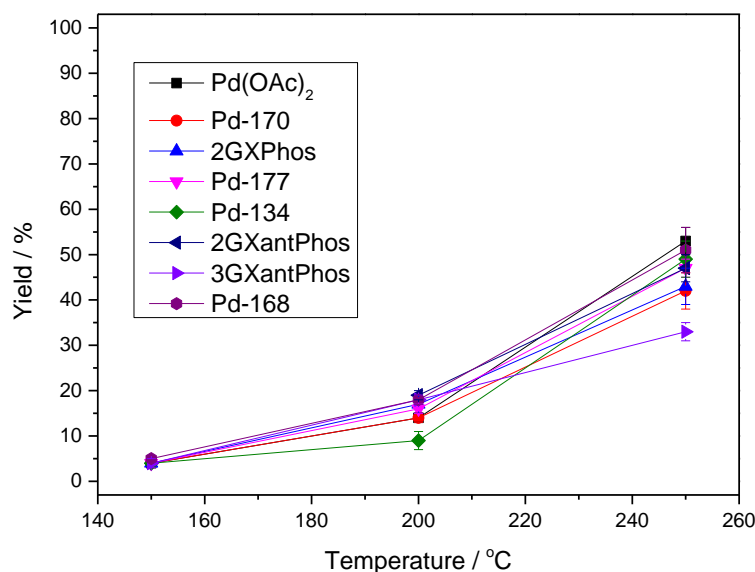
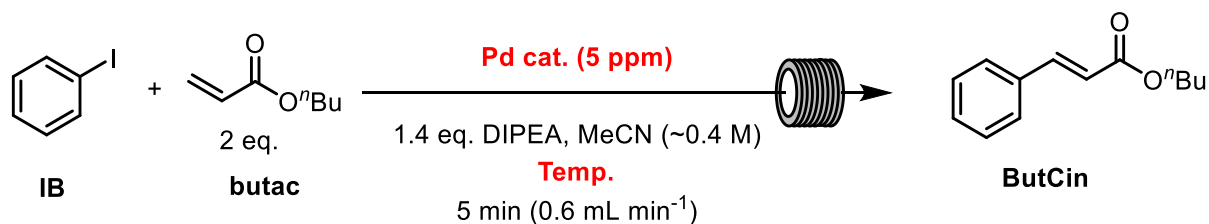


Fig 2.4.7 catalyst screen yields of **ButCin**, showing results comparable to using $\text{Pd}(\text{OAc})_2$. Catalysts Pd-213 and Pd-114 (**Fig 2.4.6**) were not soluble, so were not used. Lines are drawn to guide the eye.

Despite having screened a number of preformed catalysts across a wide temperature range, it was again observed that yields were similar to those observed with Pd(OAc)₂ (Fig 2.4.7). This would suggest that at ~150-200 °C, the catalysts were not active enough to promote reactions at such low loadings. At ~250 °C, the catalysts were perhaps not stable, even at short timescales. As the aims were to explore novel processing windows in flow, investigating lower temperatures (at higher loadings/longer timescales) for the preformed catalysts was not undertaken, especially because using a simple Pd(OAc)₂ catalyst was observed to benefit from increased temperatures in the flow reactor and using such a simple Pd catalyst offers benefits towards process chemistry.

2.4.5 Investigating >300 °C Reaction Conditions

The following hypothesis was to attempt reactions at >270 °C, as a positive temperature dependency on the yield had been established in conditions surveyed, so far. Temperatures >270 °C were not initially employed as MeCN has a critical temperature of 274 °C, therefore avoiding any influence on observed results due to phase behaviour. It was also considered that using an alternative, higher boiling point solvent could be attempted. The initial reactions to investigate this hypothesis used supercritical MeCN (sc-MeCN) as the solvent.

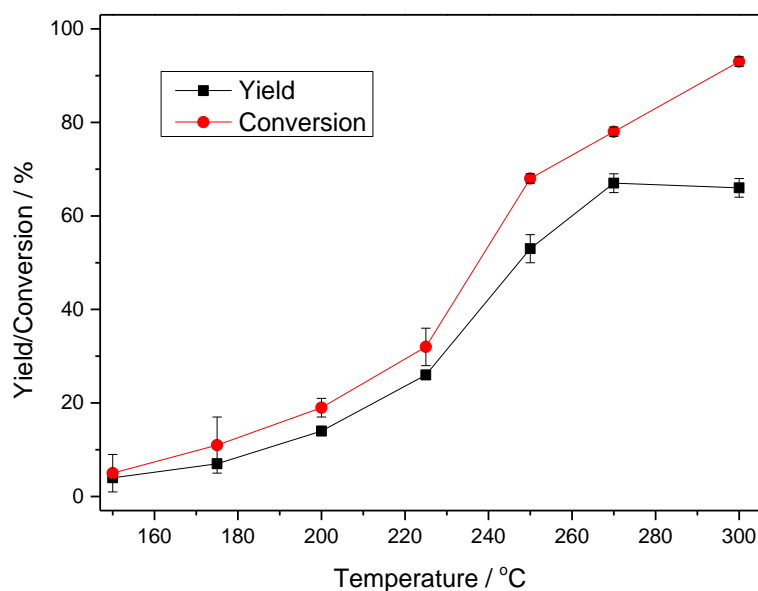
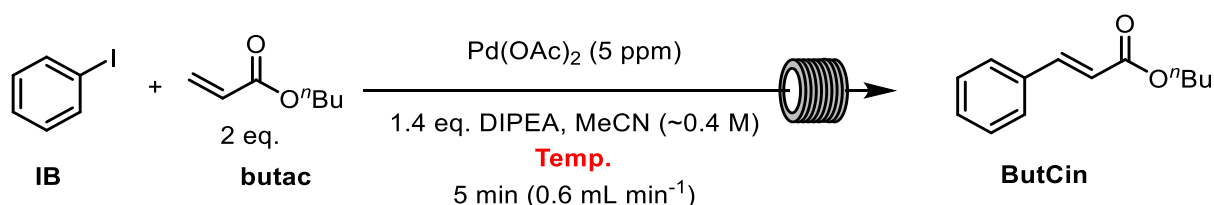


Fig 2.4.8 yield of ButCin at varied temperatures using a 5 ppm Pd(OAc)₂ loading, including sc-MeCN as a reaction medium at 300 °C, though no further increase in yield was observed on increasing temperature from 270 to 300 °C. Lines are drawn to guide the eye.

An initial reaction was conducted at 300 °C and 5 ppm Pd(OAc)₂ at a 5 min residence time. The conversion and yield of which are mapped in **Fig 2.4.8**, alongside previous results displayed in **Fig 2.4.4**. The conversion *did* increase with the increased temperature, as hypothesised, however, the yield observed at 300 °C was similar to that observed at 270 °C. It was considered that, due to the extreme temperature, perhaps the product or starting material was unstable and was decomposing to some extent, which could explain greater conversion, but yields remaining the same. No other major side-products were observable in the GC chromatogram used for quantification, so the issue was unlikely to be a change in selectivity. Another possibility could be that the more elevated temperatures were leading to polymerisation reactions, forming non-volatile species not detected in the GC chromatogram. Alternatively, as was previously speculated, a change in phase behaviour due to now using sc-MeCN could have resulted in changes to catalyst activity (perhaps encouraging aggregation and deactivation). Further tests involving processing of starting material or products in the absence of other reactants/reagents might allow for further insights towards this.

Next, it was decided to screen higher boiling solvents both below and above 270 °C, where conditions would not be supercritical. Also, it was hypothesised that if decomposition was occurring, it might be avoided at shorter residence times. It was speculated that, if decomposition could be avoided on rapid time scales (*e.g.*, <1 min), perhaps at >300 °C, good yields might still be observed. To begin testing these, experiments were firstly conducted at 300 °C in MeCN, at different residence times, using 5 or 1 ppm Pd(OAc)₂.

Table 2.4.11 yield of **ButCin** at varied residence times using 5 or 1 ppm Pd(OAc)₂ loadings, suggesting decomposition at 5 or 10 min residence times, but not at rapid 1 min residence times.

Entry	Loading / ppm	Time / min	ButCin GC Yield / %	IB GC Conversion / %
1		1	23*	27*
2	5	5	66 ± 2	93 ± 1
3		10	49 ± 4	92 ± 3
4		1	13 ± 1	14 ± 1
5	1	5	27 ± 1	48 ± 6
6		10	35 ± 3	71 ± 2

*Replicate samples were not taken so uncertainties were not estimated.

At both 5 ppm and 1 ppm Pd(OAc)₂ loadings, decomposition was not suggested at 300 °C temperatures at short 1 min residence times (**Table 2.4.11**, Entries 1 and 4). Decomposition was apparent (increased conversion, but decreased, or not significantly increased yield) when increasing residence times to 5 min, and even more strongly suggested at 10 min (**Table 2.4.11** compare Entry 1 with 2 and 3 and Entry 4 with 5 and 6). It was hypothesised that perhaps at these low ppm loadings and short 1 min residence times, yields/conversions might be increased at temperatures >300 °C, whilst avoiding the suggested

decomposition. However, the over-pressure sprung-relief valve which was in place did not allow for access to pressures >150 bar (130 bar had been used at 300 °C). As such, in MeCN and the pressure limited to 150 bar, it was not possible to operate at >300 °C. Due to this, it was decided to investigate the use of higher boiling, alternative solvents, for allowing processing at temperatures >300 °C.

2.4.6 Screening High Boiling Solvents as Potentially Greener Alternatives

A solvent screen was conducted at 250 °C, to determine any suitable solvents which could be used for such conditions, and those selected were as follows. Dimethylformamide (DMF) was chosen as this solvent is commonly used in Heck Reactions as a polar aprotic solvent, similar to MeCN, but with a higher boiling point. DMF, however, has several concerns from a Green Chemistry perspective.¹²³ Therefore, three other solvents were also selected. These solvents were chosen due to all being high boiling solvents and being polar aprotic (similar to those previously listed), however, for various reasons, are considered greener alternatives to solvents such as DMF. These solvents were γ -valerolactone (GVL), propylene carbonate (PC) and Cyrene.

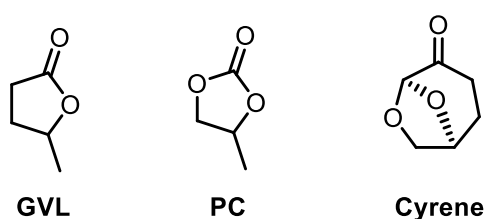
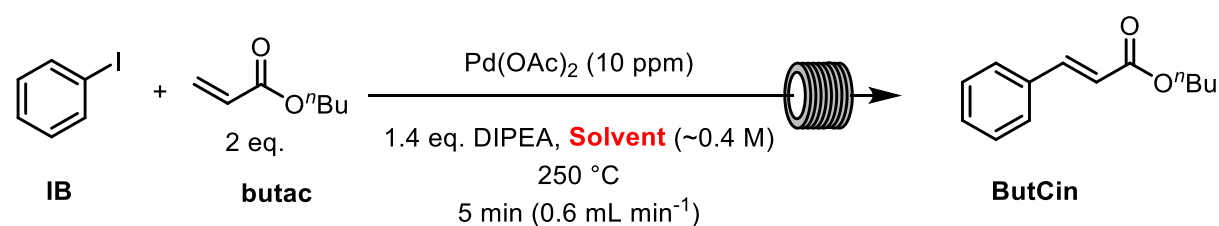


Fig 2.4.9 alternative, possibly greener solvents selected for screening in the flow Heck Reactions.

Reactions were conducted at 250 °C (70 bar pressure, as was used for MeCN at this temperature) with a 5 min residence time and a 10 ppm Pd(OAc)₂ for comparison with a previous reaction in MeCN.

Table 2.4.12 yield of **ButCin** at varied Pd(OAc)₂ loadings using a range of high boiling solvents.



Entry	Solvent	ButCin GC Yield / %	IB GC Conversion* / %
1	MeCN	76 ± 1	80 ± 1
2	DMF	26 ± 2	33 ± 2
3	Cyrene	18 ± 1	34 ± 1
4	Propylene Carbonate	47 ± 3	-
5	GVL	61 ± 3	77 ± 1

*For propylene carbonate, overlap with of the solvent signal with the starting material in GC analysis prevented conversion determination.

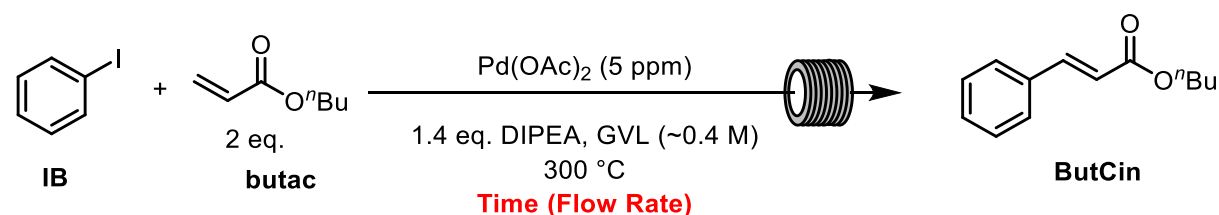
Under the conditions surveyed, MeCN was the solvent leading to the highest observed yield/conversion, notably higher than using PC, DMF or Cyrene (Table 2.4.12, Entries 1-5). For GVL

conversions were similar and yield slightly lower (**Table 2.4.12**, Entries 1 and 5). GVL was therefore selected as a potentially greener alternative, higher boiling solvent than MeCN.

2.4.7 Investigating GVL as a Green Reaction Solvent Enabling Access to Temperatures >300 °C

The aim was to determine whether GVL could be employed at $T > 300$ °C with the hypothesis that this might allow for high yields at low catalyst loadings and short residence times. Reactions were repeated at 300 °C, using GVL in place of MeCN, keeping other conditions (residence time, loading) the same as previously used with MeCN, for further comparison between the solvents.

Table 2.4.13 observed yield of *ButCin* using GVL as a greener solvent, again indicating apparent decomposition at a 5 min residence time but less significant at 1 min residence time, results in MeCN given for comparison.

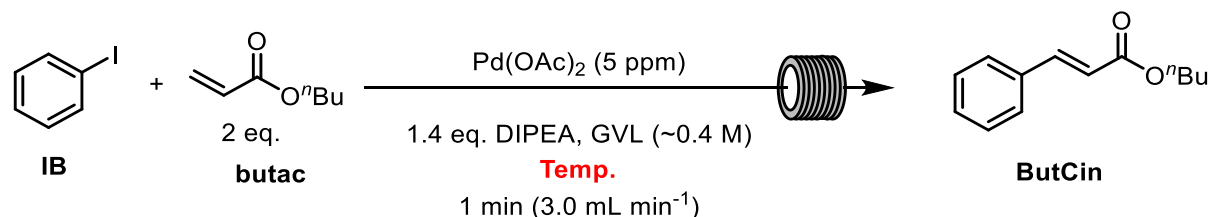


Entry	Solvent	Time / min	ButCin GC Yield / %	IB GC Conversion / %
1	MeCN	5	66 ± 2	93 ± 1
2		1	23*	27*
3	GVL	5	53 ± 6	95 ± 1
4		1	29 ± 1	37 ± 1

*Replicate samples were not taken so uncertainties were not estimated.

Observations were similar to when using MeCN as the reaction solvent. At 5 min residence time and 300 °C, product decomposition was suggested from the conversions approaching full, but the yields being relatively low (**Table 2.4.13**, Entries 1 and 3). However, at 1 min residence time, observed yield was expectedly lower than at 5 min, but selectivity towards the desired product was greater (**Table 2.4.13**, Entries 2 and 4). Therefore, following the previously outlined hypothesis that reactions at >300 °C might give increased yields, whilst maintaining a good selectivity at ~1 min residence times, the next step taken was to perform reactions in GVL at higher temperatures.

Table 2.4.14 yields and conversions in GVL solvent at >300 °C at a short 1 min residence time, illustrating how even at this short timescale, suspected decomposition was observed at temperatures required to give reasonable conversions.



Entry	Temperature / °C	ButCin GC Yield / %	IB GC Conversion / %
1	300	29 ± 1	37 ± 1
2	300 (Repeat)	26 ± 2	32 ± 2
3	325	28 ± 2	42 ± 2
4	350	25 ± 2	63 ± 2

The hypothesis was not supported by the observed results, because at both 325 °C and even more significantly at 350 °C, apparent degradation was observed, even at a short 1 min residence time (Table 2.4.14, Entries 3 and 4). This was suggested from the observations that conversion increased, but yield remained similar. This suggested that achieving good yields at short residence times with low loadings would likely not be feasible by increasing temperature, due to suspected thermal degradation. It might have been possible to observe good yield/conversion at ≥300 °C by using a residence time of *e.g.*, 1 min or less (to avoid decomposition), but at higher Pd(OAc)₂ loadings. However, as the aim of this work moved from the development of a flow reactor for processing of Heck Reactions, towards then aiming to reduce Pd loadings, this hypothesis was not explored further.

As such, it had been so far observed that using low Pd(OAc)₂ loadings *e.g.*, 5-10 ppm at temperatures of >250 °C could result in efficient processing of the Heck Reaction coupling partners. However, further decreasing loadings by applying temperatures >300 °C did not appear to warrant further investigation.

2.5 Conclusions & Further Work

Heck Reactions between IB and butac were performed using a homemade continuous flow reactor, enabling easy and safe access to high temperatures and pressures. Temperatures of >200 °C were investigated and it was observed that reactions could be carried out using extremely low loadings (down to 0.0005 mol%, 5 ppm) of Pd(OAc)₂ (without added ligands), whilst observing good yields and conversions. For example, 86% yield at 250 °C in 10 min residence time with 5 ppm Pd(OAc)₂, or, at 270 °C and 10 ppm Pd(OAc)₂, an 83% yield in 5 min residence time. At temperatures of 300 °C or above, decomposition appeared to occur unless very short residence times (1 min) were employed, in which case, low yields/conversions were observed (using ppm loadings). For example, ~25-20% yield in 1 min residence time, with 5 ppm Pd(OAc)₂, at 300 °C was observed (in GVL solvent).

In previous studies, it has been observed that temperatures up to 200 °C previously could allow for using Pd(OAc)₂ loadings down to 0.05 mol% in flow Heck Reactions.⁷⁶ Relative to this, a further 100-fold reduction in Pd(OAc)₂ loadings was apparent when processing the reactions at higher temperatures. Though, it should be noted that in the flow reactor used here, yields were notably higher under

analogous conditions to those previously reported, possibly due to more efficient heat transfer due to the flow regime applied.

Further work should involve extending and implementing such flow approaches towards commercial targets or more complex molecules. That is, as continuous flow technology is an attractive approach towards chemical manufacturing, the development of manufacturing processes involving such methodologies would be of interest to determine whether the benefits observed on model coupling partner systems can be extended to those with practical application. For the work performed specifically in this Chapter, it would be worthwhile to determine the temperature dependent nature of some of the species involved, whether reagents or catalysts, to determine whether decomposition was leading to low reaction yields at higher (>300 °C) temperatures. For the catalysts, this may lead to insights where temperature stable catalysts may be developed or applied in the reactions and, if the catalyst and ligands remain stable, may allow for further reductions in Pd demand for the reactions. For the reagents, if their temperature stabilities could be coupled with reactor engineering/modelling, it might allow for the more efficient design of processes avoiding such thermal decomposition.

Chapter 3

Flow Redox Relay Heck Reaction Towards a Pharmaceutical Intermediate

3.1 Abstract

In this Chapter, using the thermal flow reactor built and in Chapter 2 (detailed in the Experimental Chapter), the application to a Redox Relay Heck Reaction in the synthesis of a pharmaceutically relevant intermediate was performed. Having previously identified processing benefits such as reduction in catalyst loadings and short processing times using superheated conditions, easily accessed in the flow reactor, the aim was to determine whether similar benefits could also be applied towards a Redox Relay Heck Reaction. It was observed that the reaction, involving the coupling of 3-iodopyridine and 1,2-dihydroxy but-3-ene, could be performed in the flow reactor without experiencing any barriers to processing such as reactor blockage or overpressure. A short survey of catalysts, including simple Pd salts and preformed catalysts monoligated with an XPhos ligand, temperature and flow rate/residence time revealed that at 225 °C and a 15 min residence time, a good yield of 73% at >95% conversion could be observed, when using a so-called “*homeopathic*”^{112–114} loading of PdCl₂ (0.05 mol%, with no added ligands). At higher temperatures, decomposition appeared to predominate and at lower loadings, reactions were significantly slower. Compared to the previous disclosure of the reaction in batch, this would represent a notable reduction in reaction time (down from 3 h), reduction in Pd usage (0.1 mol% down to 0.05 mol%) and eliminating the need for using a ligand.¹²⁴ This therefore represents the benefits of using continuous flow methods in synthetic processing, applied to a contemporary Redox Relay Heck Reaction.

3.2 Strategy & General Aims

The remit of the work in Chapters 2-4 was to investigate C-C coupling reactions in thermal flow processes, beginning with simple C(sp²)-C(sp²) reactions (Chapter 2). The remit following the work on the traditional C(sp²)-C(sp²) coupling reaction was to perform more challenging C(sp²)-C(sp³) coupling reactions.

Having built and assessed the performance of a homemade tubular coil flow reactor for the Heck Reaction, the next logical step was to determine whether this apparatus could be extended to other Heck-type methodologies that feature in the literature. As such, the strategy adopted for the work in this (as well as largely for the following) Chapter was as follows:

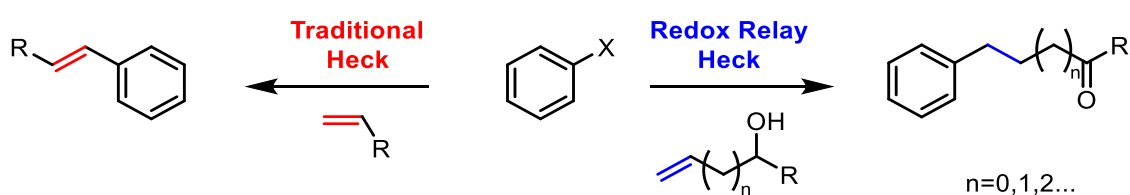
- To identify in the literature Heck-type reactions affording C(sp²)-C(sp³) coupled products.
- To determine whether the identified reactions may or may not be suitable for processing in the previously developed flow reactor in this work.
- To apply the previously built flow reactor to C(sp²)-C(sp³) Heck-type coupling reactions and to determine whether, as in Chapter 2, processing benefits could be shown towards the reactions of interest.

To summarise the initial outcome, two Heck-type reactions of interest were considered. These were Redox Relay Heck Reactions and Reductive Heck Reactions. Both of which are methodologies extending from the original Heck Reaction, as explored in Chapter 2. In this Chapter, a short project focussing on a Redox Relay Heck Reaction is described.

3.3 Introduction

3.3.1 Redox Relay Heck Reaction Basic Principles

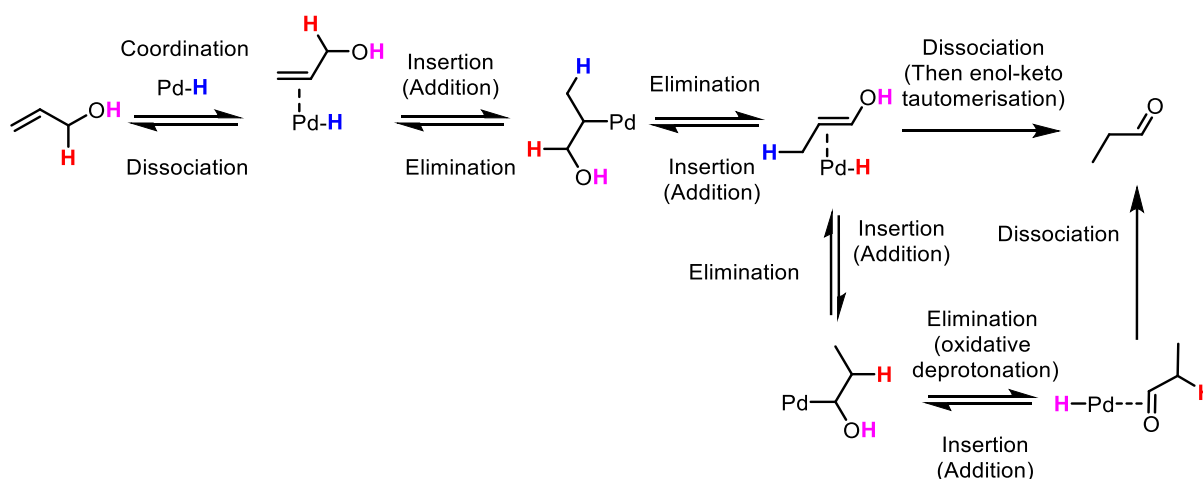
Redox Relay Heck Reactions (RRHRs) involve the reaction of an aryl halide, or *pseudo*-halide, with an alkenyl alcohol.¹²⁵ Unlike the traditional Heck Reaction (or Mizoroki-Heck Reaction), which mediates aryl alkenylation (*i.e.* resulting in a new C(sp²)-C(sp²) bond), the RRHR takes advantage of a remote thermodynamic sink (an OH group) to afford the outcome of aryl alkylation (*i.e.* resulting in a new C(sp²)-C(sp³) bond) alongside formation of a C=O unit (in place of the C-OH unit in the starting alkenyl alcohol), **Scheme 3.3.1**.^{125,126} The RRHR is therefore an attractive synthetic reaction, offering the ability to produce an alkylated aryl unit in a single step (which may otherwise require alkenylation followed by reduction), with a carbonyl unit present that can easily be subjected to further functionalisation.¹²⁵ As such, executing these reactions in flow, along with the relevant processing benefits, might lead to improvements in the reaction performance.



Scheme 3.3.1 general difference in outcomes of a traditional Heck Reaction and a RRHR.

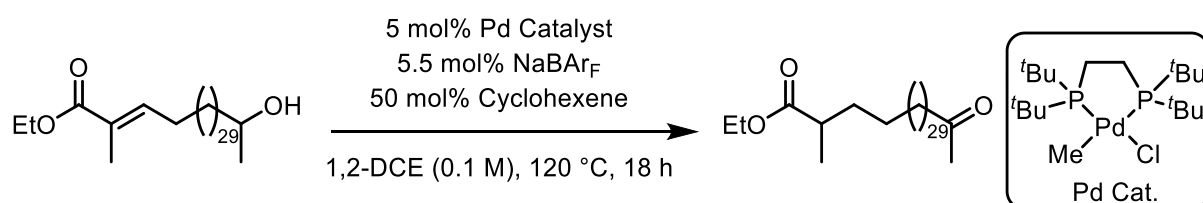
Redox relay refers to the *redox* process involved, reducing C=C to C-C, and oxidising C-OH to C=O, with *relay* referring to the transfer of this redox information between the functional groups, which can be separated by a single carbon unit (*i.e.* in an allylic alcohol), two carbon units (*i.e.* in a homoallylic alcohol), three carbon units (*i.e.* in a bis homoallylic alcohol), or even more.¹²⁶

Of relevance to the work in this Chapter is the RRHR involving allylic alcohols.^{124–128} In **Scheme 3.3.2**, it is illustrated how a “chain-walking” mechanism (sequential hydride addition-elimination steps, with Pd moving one carbon along after each pair of steps) can lead to the transfer of unsaturation from C=C to C=O in an allylic alcohol system.¹²⁹ In **Scheme 3.3.2**, two routes to furnishing the carbonyl product are shown. Firstly, after the first hydride insertion, an elimination step occurs, followed by another addition-elimination sequence (involving oxidative deprotonation, expanded on later), explaining one possible way in which the carbonyl is formed. An alternative involves dissociation of the enol intermediate and tautomerisation to the carbonyl product, also shown in **Scheme 3.3.2**.



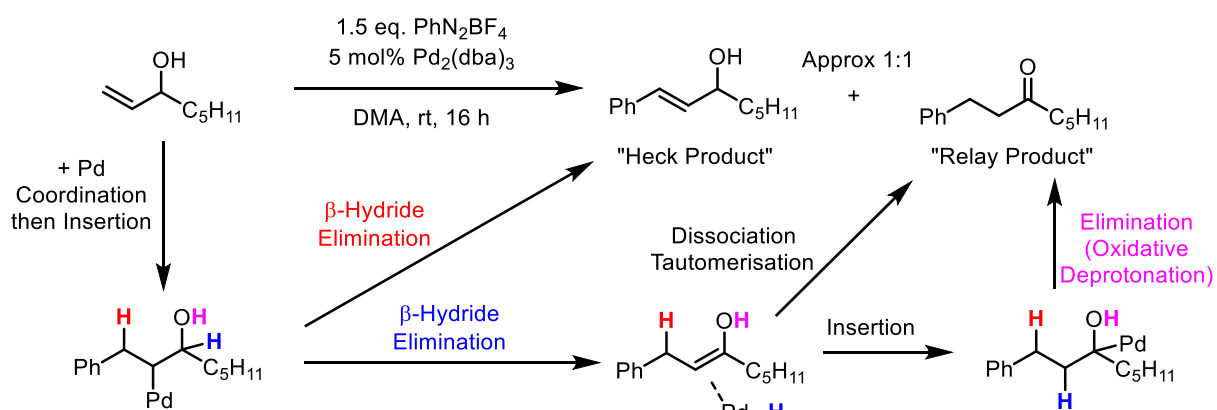
Scheme 3.3.2 chain-walking pathway, forming part of the mechanistic proposal for explaining the outcome of a RRHR. Pd in the scheme depicts a simplified nature of the coordinated Pd species, which in reality would have further coordination sites occupied.^{125,129}

In the RRHR of allylic alcohols, instead of a Pd-H species (**Scheme 3.3.2**), a Pd-Ar species would initially form and insert into the coordinated allylic alcohol. Certain mechanistic evidence and proposals however also support that this chain-walking (repeated addition-elimination) process occurs, and that the eventual formation of the C=O product occurs *via* an oxidative deprotonation involving the OH hydrogen,^{127,128,130,131} as opposed to the tautomerisation pathway, and these are discussed later in this Section. The insertion (addition) and elimination steps are reversible, likely going back and forth during the reaction until the carbonyl product is formed,^{130,131} at which point the stability of which (the thermodynamic sink) prevents reactions from reversing.^{125,126} Whilst again not in a RRHR (*i.e.* no arylation involved in the process) it has been demonstrated previously that a Pd-catalysed redox relay event can occur over a 30 carbon-chain alkenyl alcohol (**Scheme 3.3.3**).^{125,132}



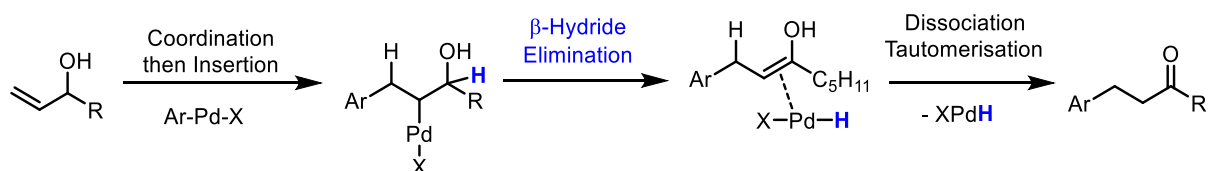
Scheme 3.3.3 chain-walking redox relay mechanism occurring over a 30 carbon unit chain alkenyl alcohol, outlining the possibility of synthetic utility for a RRHR, where it can be possible to achieve long range remote functionalisations.^{125,132}

The discovery of the RRHR can be attributed to work conducted by Heck and co-workers, shortly after their discovery of the Heck Reaction.^{127,128} The arylation of primary and secondary allylic alcohols was attempted, but instead of forming the expected Heck-type product, they instead observed the formation of 3-aryl aldehydes/ketones.^{127,128} Since the discovery of the reaction, further work has expanded the scope, particularly in a number of studies from Sigman and co-workers.^{126,130,131,133}



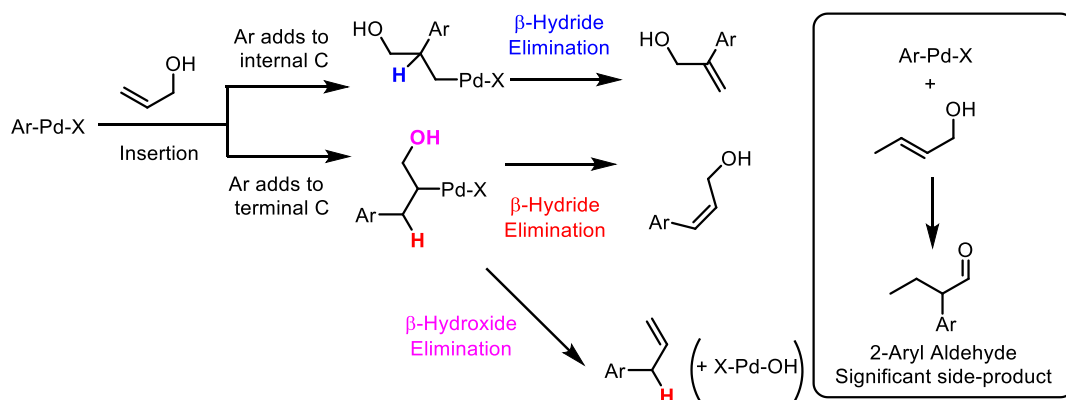
Scheme 3.3.4 early work from Sigman and co-workers performing a RRHR on an allylic alcohol, using an aryl diazonium salt (Redox Relay Matsuda-Heck Reaction). A product distribution was observed for the Heck product alongside what Sigman initially referred to here as the relay product in developing the term RRHR. Pd in the scheme depicts a simplified nature of the coordinated Pd species, which in reality would have further coordination sites occupied.¹²⁶

In early developments from Sigman, using aryl diazonium salts, moderate selectivity towards the desired relay product was observed. In **Scheme 3.3.4**, an example reaction of the Sigman Group's work using aryl diazonium salts is given, highlighting also how the traditional Heck product can form alongside the relay product. In **Scheme 3.3.4**, it is also shown how the two proposals to form the relay product occur specifically in a RRHR (*i.e.*, not as in **Scheme 3.3.2** earlier, where simple Pd-H species were used to demonstrate the principle). The following mechanism was proposed by Heck following the seminal investigations, whereby the reaction proceeded following a traditional Heck cycle, forming an enol product which would tautomerise to the observed Redox Relay Heck product.¹²⁷



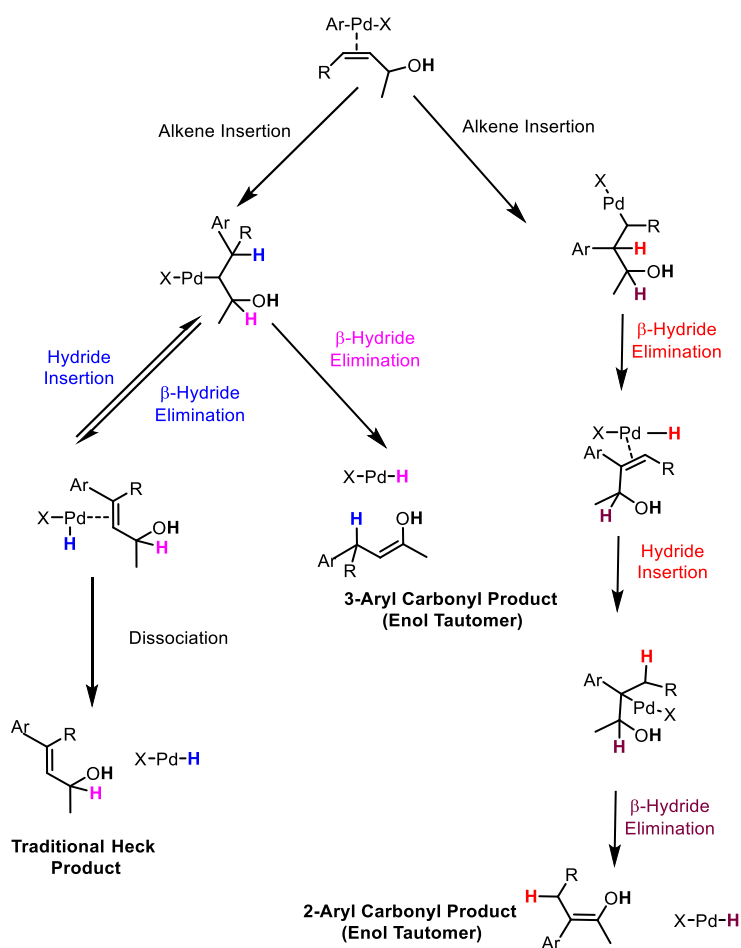
Scheme 3.3.5 early mechanistic proposal put forward by Heck, involving an analogous cycle to the Heck Reaction, but with β-hydride elimination occurring from an alternative site, so as to give an enol product as opposed to an alkenylated aryl product.¹²⁷

Heck proposed the expected side-products of this mechanism (**Scheme 3.3.6**), including the cinnamyl alcohol (*i.e.* traditional Heck product), a Heck-type product (*i.e.* retention of C-OH) where alkene insertion into the Pd-Ar unit proceeds *via* the Ar inserting into the internal olefinic C-atom (not the terminal olefinic C-atom), as well as a product formed by β-hydroxide elimination (an allylaromatic compound).¹²⁷ However, when using crotyl alcohol as the coupling partner, however, Heck also observed the formation of a 2-aryl aldehyde product.¹²⁷



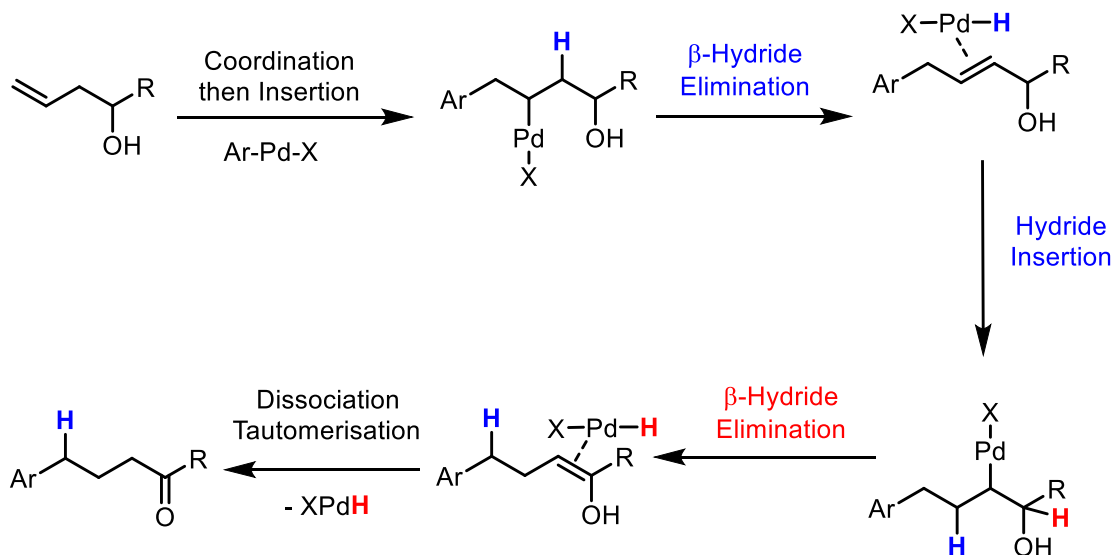
Scheme 3.3.6 possible side-products speculated by Heck to be observed should an analogous Heck Reaction mechanism be occurring and the observation of a 2-aryl aldehyde product (rather than an expected 3-aryl aldehyde product) when using crotyl alcohol, leading to the speculation of an addition-elimination sequence mechanism.¹²⁷

The observed formation of the 2-aryl carbonyl product led Heck to speculate on the possibility of a hydride elimination-addition mechanism (*i.e.* chain-walking mechanism).¹²⁷ Later, Heck and Melpolder proposed a series of mechanistic steps (**Scheme 3.3.7**) to explain the observed reaction outcome.¹²⁸



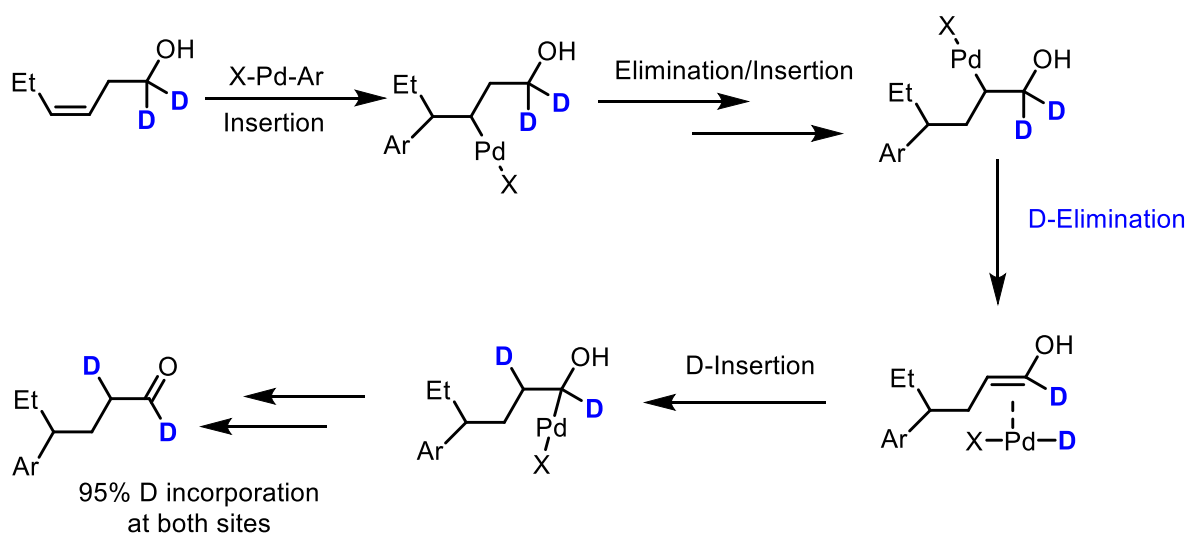
Scheme 3.3.7 mechanistic proposal from Heck and Melpolder to unify the observations made from their reactions of aryl halides and allylic alcohols. The formation of a 2-aryl carbonyl product supports the occurrence of chain-walking (via repeated addition-elimination sequences) in the system.¹²⁸

The mechanism proposed by Heck and Melpolder can be extended to longer chain alkenyl alcohols *e.g.* homoallylic alcohols,^{127,128} but require a further addition-elimination sequence to result in the redox relay (transfer of redox information) from the C=C to the eventual C=O (**Scheme 3.3.8**).



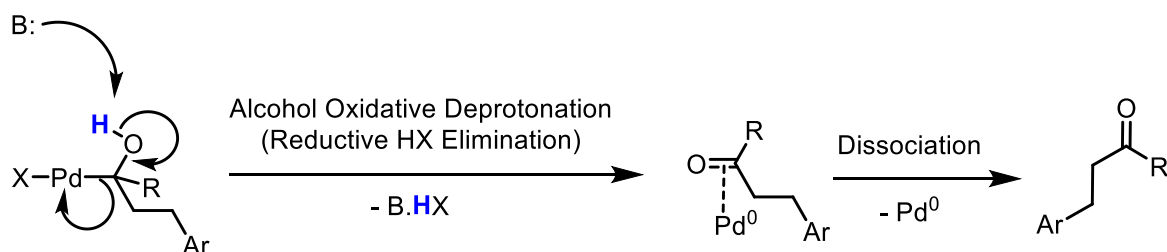
Scheme 3.3.8 plausible mechanism for the RRHR involving longer chain C=C and C-OH separation than in an allylic alcohol (here, shown using a homoallylic alcohol), based upon a hydride elimination-addition chain-walking mechanism.¹²⁵

There has also been speculation regarding the C=O formation step in the mechanism.^{130,131,134} Heck proposed β -hydride elimination to give an enol, dissociation from Pd and tautomerisation to the carbonyl product.^{127,128} However, should the enol intermediate remain coordinated to Pd, it can be imagined how a further hydride addition elimination sequence could occur (**Scheme 3.3.9**). Should this hydride re-addition occur, mechanistic proposals involving the elimination of the H present on OH could be speculated, as depicted in **Scheme 3.3.2** and **Scheme 3.3.4**, where oxidative deprotonation was noted as the final elimination step to form the C=O. Sigman and co-workers have investigated the mechanism of the carbonyl formation step *in-silico* and experimentally.^{130,131} Experimentally, using a homoallylic alcohol, the researchers used deuterium labelling studies that resulted in evidence supporting the occurrence of the extra addition-elimination sequence, involving the enol intermediate coordinated to Pd.



Scheme 3.3.9 deuterium labelling study performed by Sigman and co-workers showing that the major pathway of the RRHR involving a homoallylic alcohol resulted in deuterium being positioned at the carbonyl carbon and the carbonyl α -carbon, consistent with the mechanism depicted involving insertion of the enol intermediate, rather than dissociation of the enol intermediate followed by tautomerisation to the carbonyl. Should the tautomerisation mechanism occur, deuterium would not be present at the carbonyl α -carbon.^{130,131}

Sigman and co-workers labelling study supports the notion that tautomerisation (as depicted in **Scheme 3.3.8** and **Scheme 3.3.9** in mechanisms proposed by Heck) likely does *not* occur (or only to a limited extent).^{130,131} This would be consistent with a mechanistic proposal involving elimination of the H on the OH unit in the C=O forming step. In Sigman's studies, in which a conventional base was not added, they theoretically calculated that DMF, the reaction solvent that was being used, would be a strong enough base to deprotonate the hydroxyalkyl palladium intermediate, furnishing the desired aryl carbonyl product.^{130,131} As in reactions performed, for example, by Heck and Melpolder, an amine base (as often used in a conventional Heck Reaction) was also present, which could also be speculated to promote this step.^{127,128} This step has been alluded to in this Section in **Scheme 3.3.2** and in **Scheme 3.3.4** as oxidative deprotonation (referring to the alcohol oxidation in the step) and represents a plausible proposal for RRHRs.

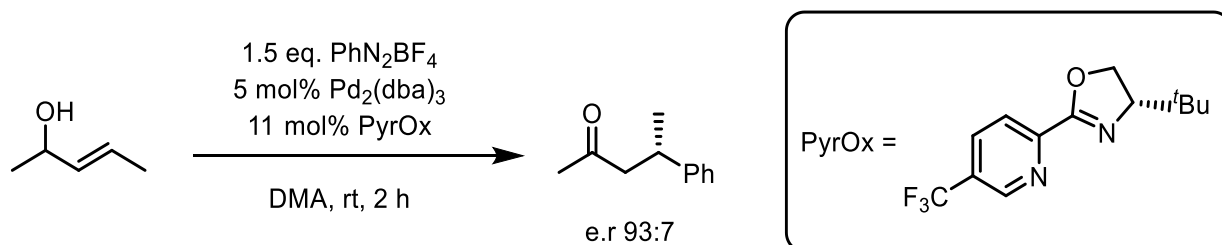


Scheme 3.3.10 oxidative alcohol deprotonation (reductive elimination at Pd) as a proposed step in forming the aryl carbonyl products in RRHRs.

3.3.2 Developments and Applications of Redox Relay Heck Reactions

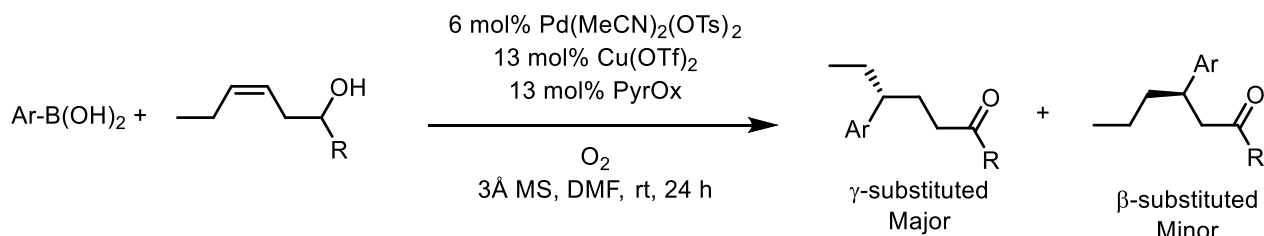
Developments from the Sigman Lab have included improving upon the regioselectivity of the reaction, conducting enantioselective RRHRs, extending the scope to include aryl diazonium coupling partners

as well as using aryl boronic acids as coupling partners in a combined Redox Relay/Oxidative Heck Reaction Process.^{126,130,131,133} Such developments are of interest as the RRHR can result in the formation of a carbonyl-containing product (subjectable to further functionalisation) alongside a remote stereocentre. For the enantioselective reactions, a chiral ligand would be required, often a pyridine-oxazoline (PyrOx) ligand, to impart the enantioselectivity (**Scheme 3.3.11**).^{125,126}



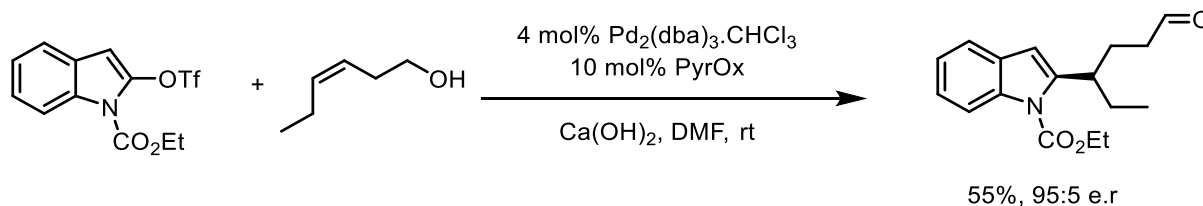
Scheme 3.3.11 application of a RRHR in an enantioselective synthesis using a PyrOx ligand, a further development from Sigman's seminal study.¹²⁶

As noted previously, developments from Sigman and co-workers have combined Oxidative Heck Reactions (which involve an aryl boronic acid and Pd^{II} catalyst, operating on a Pd^{II}/Pd^{IV} cycle as opposed to a Pd⁰/Pd^{II} cycle) along with enantioselective RRHR (**Scheme 3.3.12**).¹³³ Again, using a chiral PyrOx ligand, in the presence of a Cu co-catalyst and oxygen atmosphere, Sigman and colleagues demonstrated the formation of arylated carbonyl products from alkenyl alcohols and aryl boronic acids, with good enantioselectivities on C-atoms up to a 7 carbon chain length away from the newly formed C=O group.¹³³



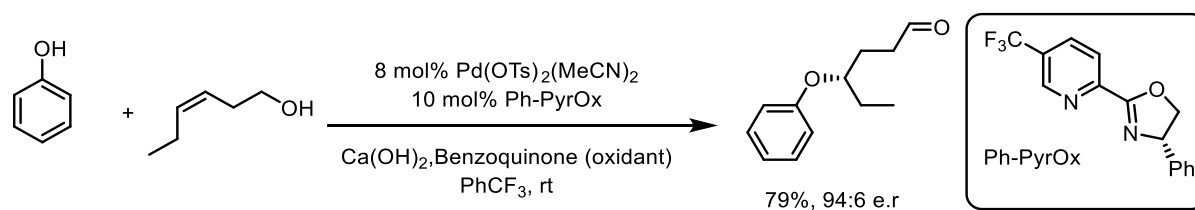
Scheme 3.3.12 an enantioselective, oxidative RRHR shown to operate via a chain-walking mechanism over a large number of C-atoms (i.e. not using an allylic alcohol for a RRHR) whilst also affording good enantioselectivities, and site selectivity towards the γ -aryl product.¹³³

Other developments within the scope of the RRHR have involved the employment of heterocyclic substrates in the reactions, e.g. indole triflates (**Scheme 3.3.13**) and chromenes.^{135,136}



Scheme 3.3.13 RRHR involving a heterocyclic indole triflate substrate in an enantioselective procedure.¹³⁵

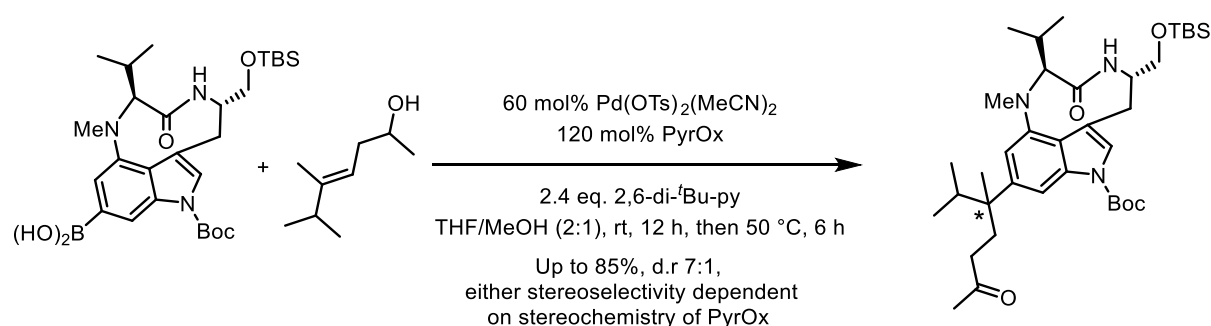
Other substrates that have been used in RRHRs include phenols as an O-nucleophile (**Scheme 3.3.14**), demonstrating how the methodology can also be used for formation of C-O bonds alongside a remote carbonyl.¹³⁷



Scheme 3.3.14 RRHR involving a phenol nucleophile for the enantioselective formation of C-O bonds with a remote carbonyl functionality.¹³⁷

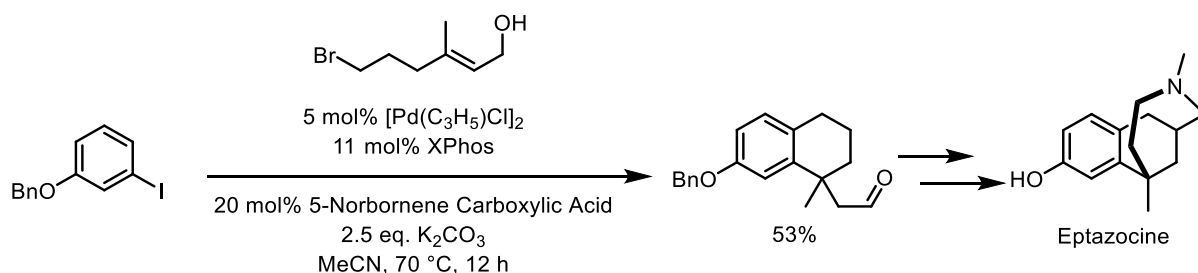
These examples highlight why RRHRs are of interest for synthetic chemistry. Due to such advantages including the versatile scope, opportunity for enantioselectivity and as the RRHR allows for the formation of a new single bond alongside a remote carbonyl functionality, the reaction has also attracted interest for synthesis of *e.g.*, drug molecules and natural products.

For example, Baran and co-workers employed an oxidative RRHR in the synthesis of natural products (-)-teleocidin B-1 to B-4 (**Scheme 3.3.15**). This involved coupling of a complex indole boronic acid with a homoallylic alcohol. The reaction however, did require an extremely high 60 mol% loading of Pd catalyst, with twice the amount of added PyrOx ligand to achieve reasonable to good yields.¹³⁸



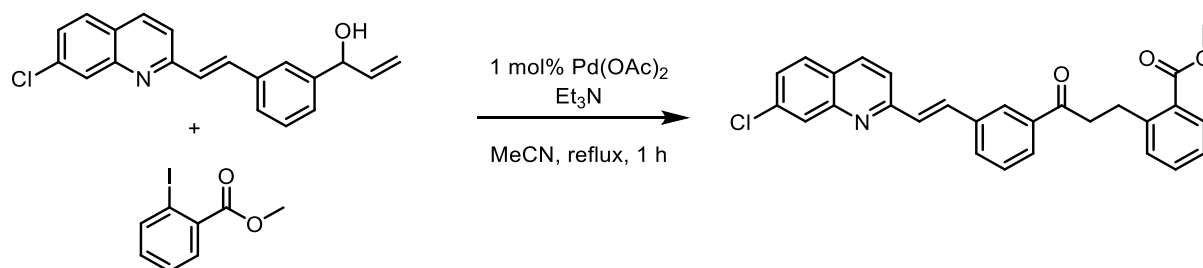
Scheme 3.3.15 RRHR employed in the synthesis of an intermediate in the total synthesis of (-)-teleocidin B-1 to B-4, reported by Baran and co-workers.¹³⁸

Zhou and co-workers reported the tandem Catellani RRHR in the total synthesis of natural product (±)-eptazocine (**Scheme 3.3.16**). The Catellani Reaction involves norbornene-mediated, Pd-catalysed C-H functionalisation at a position *ortho* to an aryl halide, followed by cross-coupling involving the halide, with the outcome of substitution at two adjacent aryl positions (substituting an H and a halide). For the RRHR-Catellani procedure, a brominated allylic alcohol was used as the reaction substrate (with an O-protected iodophenol).¹³⁹



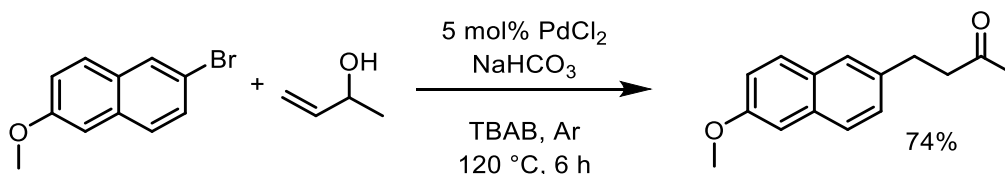
Scheme 3.3.16 tandem Catellani-RRHR employed in the preparation of an intermediate in the total synthesis of (\pm)-eptazocine by Zhou and co-workers.¹³⁹

The continuous flow synthesis of a pharmaceutical intermediate forms the interest of the work in this Chapter and the relevant target is discussed in the Results & Discussion Section. Due to the advantages offered from RRHRs, there are other existing processes where drug molecules/intermediates have been targeted. For example, an intermediate in the synthesis of anti-asthma drug Singulair has been prepared *via* RRHR methodology, involving coupling of an aryl iodide to an allylic alcohol (**Scheme 3.3.17**).¹⁴⁰



Scheme 3.3.17 synthesis of an intermediate towards pharmaceutical target Singulair, using RRHR.¹⁴⁰

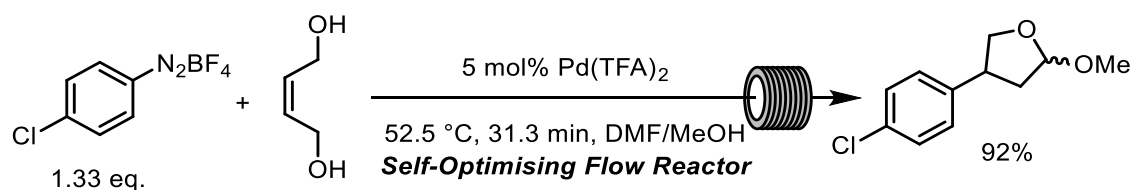
Other pharmaceutical targets prepared by RRHR approaches include Nabumetone, a non-steroidal anti-inflammatory drug (**Scheme 3.3.18**). This target contains a 3-naphtyl ketone structure so can be prepared conveniently *via* a RRHR using an allylic alcohol and a halogenated naphthalene. A reported synthesis Nabumetone using RRHR methodology involved the use of an ionic liquid (molten tetrabutylammonium bromide) as the reaction medium, which could be considered a green solvent, using PdCl_2 as a catalyst (with no added ligands).¹⁴¹



Scheme 3.3.18 RRHR in the synthesis of pharmaceutical target Nabumetone, in an ionic liquid solvent.¹⁴¹

An example of a Heck-Matsuda RRHR (involving an aryl diazonium salt) has been transferred to a continuous flow process (**Scheme 3.3.19**). This involved using a self-optimising flow reactor, which was demonstrated for optimisation of yield, process cost and productivity. The reaction investigated involved *cis*-2-buten-1,4-diol as the allylic alcohol coupling partner, resulting in subsequent cyclisation and then substitution by MeOH (used as part of a DMF/MeOH solvent system). The system used GC-

MS analysis for the optimisation.¹⁴² This reaction procedure was previously developed by the same researchers who then applied the self-optimising flow reactor to it.¹⁴³



Scheme 3.3.19 a continuous flow process for a Matsuda-RRHR, shown to give a yield of 92% under optimisation using an automated flow reactor.¹⁴²

This example of a continuous flow RRHR highlights the attractiveness of applying flow reactors for such Pd-catalysed processes. Furthermore, the benefits of flow reactors are illustrated, with careful control over reaction conditions achieved using flow chemistry, *via* efficient automated optimisation.

3.3.3 Summary

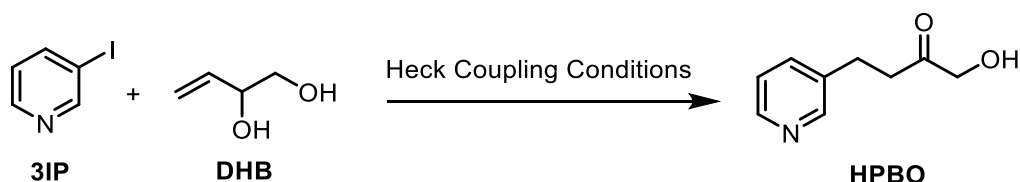
The RRHR represents an efficient process by which a new C(sp²)-C(sp³) bond can be produced in a single step, alongside the formation of a carbonyl that can readily be functionalised further and, under the right conditions, be performed enantioselectively and regioselectively, making this methodology appealing in synthesis.

In this Chapter, the RRHR of an iodo-heterocycle and an allylic diol has been investigated, in the synthesis of an intermediate in a pharmaceutical preparation. Details of the specific reaction are provided in the Results & Discussion Section of this Chapter. The aim of this was to build upon *e.g.*, the previous report from Felpin and co-workers, using a flow reactor to automate a RRHR process, with the focus here being on exploiting novel process windows for reaction benefits *e.g.*, short reaction times and low catalyst loadings.

3.4 Results & Discussion

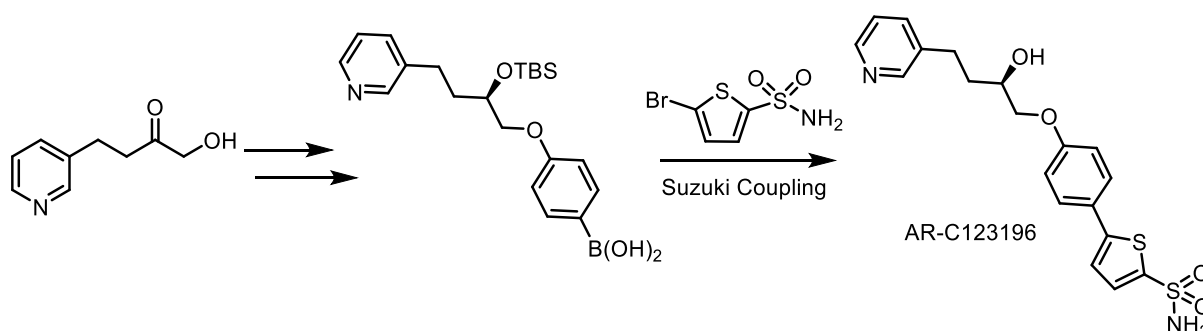
3.4.1 Redox Relay Heck Reaction in the Synthesis of a Pharmaceutical Intermediate

Whilst exploring the literature for suitable C(sp²)-C(sp³) coupling reactions for performing in the thermal tubular flow reactor used in Chapter 2 (detailed in Experimental Chapter), the application of a RRHR in the synthesis of a pharmaceutical intermediate was found.¹²⁴ This was considered an interesting target for investigating in flow, having not been undertaken previously and as continuous flow processing is attractive for chemical manufacturing. The identified reaction, published by researchers at AstraZeneca, involved the RRHR of a pyridine substrate (3-iodopyridine, **3IP**, was used in the work in this Chapter, though 3-bromopyridine was used in the initial publication) with an allyl alcohol, 1,2-dihydroxy but-3-ene (**DHB**), **Scheme 3.4.1**.¹²⁴ The product of the Heck coupling, 1-hydroxy-4-(3-pyridyl)butan-2-one (**HPBO**), was an important intermediate towards an anti-allergy drug target.¹²⁴ In the synthetic process, the next intermediate formed in the sequence involved a reduction of the ketone formed from the Heck Coupling stage. The same allylic alcohol starting material has also been used by researchers from Dow and GSK in batch, however, the traditional Heck product was the desired product here, and yields were generally quite low.¹⁴⁴



Scheme 3.4.1 application of a RRHR in the synthesis of a pharmaceutical intermediate.¹²⁴

Two papers were published from authors at AstraZeneca related to this process.^{124,145} The first of which involved the formation of the previously shown intermediate **HPBO**.¹²⁴ The second of which focused on using this intermediate in the formation of the final drug molecule, AR-C123196 (**Scheme 3.4.2**).¹⁴⁵ This target was produced using a second Pd-catalysed coupling reaction, a Suzuki Coupling, in a late-stage synthesis to give the final product.¹⁴⁵ Notably – using the RRHR allowed them to arrive at the diol intermediate after only two steps (RRHR then asymmetric reduction). In their two previous strategies for formation of the drug candidate it had taken 5 steps and 6 steps to prepare the diol intermediate.^{124,145} This highlights how using PGM catalysts can allow for reducing processing times and waste production, by circumventing the requirement for several other processing steps. The elegance of their process has been credited in a review on industrial applications of Pd-catalysed cross coupling reactions.¹⁴⁶



Scheme 3.4.2. late-stage Suzuki Coupling in a multi-step synthesis towards a pharmaceutical target involving a RRHR, Suzuki Coupling and a hydrogenation, all involving Pd-catalysis, furnishing the target pharmaceutical product after TBS protecting group removal.^{124,145}

With the reaction identified representing a contemporary Heck-type methodology (RRHR), resulting in the formation of a new C(sp²)-C(sp³) bond, it was considered that this was a suitable reaction for exploring the remit of C(sp²)-C(sp³) thermal coupling reactions, in flow, building from the work in Chapter 2. The optimisation here began using the same reactor as described previously, exploring temperatures >200 °C and low catalyst loadings of a number of Pd catalysts.

3.4.2 Continuous Flow Optimisation of a Redox Relay Heck Reaction

The initial aim was to determine whether the reaction could be performed using the homemade flow reactor. To begin, reactions using Pd(OAc)₂ at loadings between 0.005 mol% - 0.5 mol% (with respect to **3IP**) were carried out. The reactions were performed at 200 °C, with conditions applied informed by work in Chapter 2. In the original publication, optimised conditions involved toluene solvent, Pd(OAc)₂ or Pd₂dba₃ (0.1 mol%) with P(*o*-tolyl)₃ ligand in the presence of NBU₃, giving a 53% reported yield (20 g scale after purification), dropping to 33% at a 3 kg scale.¹²⁴ In this work, MeCN was employed as the reaction solvent, alongside DIPEA as base, without any added ligand (unless a preformed ligated catalyst

was used). As in Chapter 2, analogous conditions for a standard Heck Reaction were used and so it was expected that these would likely maintain solubility and be suited to flow processing, possibly unlike those from the previous publication.

Table 3.4.1. GC yields observed of product **HPBO** for the Heck reaction of **3IP** with **DHB**, showing an increase in both yield and conversion as the loading of $\text{Pd}(\text{OAc})_2$ was increased.

Entry	Pd(OAc) ₂ Loading / mol%	HPBO GC Yield / %	3IP GC Conversion / %
1	0.005	9 ± 1	17 ± 1
2	0.01	15 ± 1	48 ± 6
3	0.05	45 ± 5	61 ± 3
4	0.1*	50 ± 5	82 ± 1
5	0.5*	56 ± 1	94 ± 1

*0.1 and 0.5 mol% loadings also used 10 eq. (w.r.t. Pd) of tetrabutylammonium bromide (TBAB).

It was observed that higher loadings of $\text{Pd}(\text{OAc})_2$ led to greater conversions, and yield of desired product (**Table 3.4.1**). Importantly, no precipitate or blockage was observed, indicating that the reaction was suited to flow processing. This may perhaps be also assisted by the possibility for the pyridyl substrate to coordinate to the Pd-centre, which can inhibit rates, but may aid in preventing Pd-precipitation by stabilising Pd^0 intermediates.¹⁴⁷ The other side-products formed were likely homo-coupled products or isomers of **HPBO**, however, these side-products were not isolated.

Following this, a few other catalysts were screened (based simply on availability at the time of performing the reactions, Pd-170 and 2GXPhos, described in Chapter 2).

Table 3.4.2 GC yields observed of product **HPBO** from the Heck reaction of **3IP** and **DHB**, showing generally comparable conversions between the catalysts, but with the simpler Pd salt catalyst giving apparently greater selectivity towards the desired target.

$\text{3IP} + \text{DHB} \xrightarrow[\text{MeCN (0.48 M), 200 }^\circ\text{C, 10 min (0.3 mL min}^{-1}\text{)}]{\text{x mol\% Pd cat., 1.4 eq. DIPEA}}$

Entry	Catalyst	Loading / mol%	HPBO GC Yield / %	3IP GC Conversion / %	Selectivity Estimate ^a / %
1		0.005	9 ± 1	17 ± 1	53
2		0.01	15 ± 1	48 ± 6	31
3	Pd(OAc) ₂	0.05	45 ± 5	61 ± 3	74
4		0.1*	50 ± 5	82 ± 1	61
5		0.5*	56 ± 1	94 ± 1	59
6		0.005	7 ± 2	10 ± 4	70
7	PdCl ₂	0.05	45 ± 5	63 ± 1	71
8		0.5*	64 ± 7	89 ± 1	72
9		0.005	14 ± 2	29 ± 4	48
10	Pd-170	0.05	48 ± 5	74 ± 1	65
11		0.5	32 ± 2	>99 ^b	32
12		0.005	6 ± 1	19 ± 3	32
13	2GXPhos	0.05	47 ± 8	64 ± 3	73
14		0.5	45 ± 4	>99 ^b	45

*0.1 and 0.5 mol% loadings also used 10 eq. (w.r.t. Pd) of TBAB.

^aSelectivity estimate calculated from the ratio of product yield/limiting reagent conversion (expressed as a percentage), not accounting for the associated uncertainties, hence described as estimate.

^bNo **3IP** was observed in the GC chromatogram of the crude reaction mixture.

The two XPhos-based preformed catalysts could be considered to show greater conversions of starting material when comparing analogous conditions, in some cases (**Table 3.4.2**). However, a lower selectivity was also observed for the XPhos-based catalysts. Generally, observations were similar between comparable conditions for PdCl₂ and Pd(OAc)₂ (**Table 3.4.2**, Entries 1-8). From this screen, it was decided that PdCl₂ would be used for further optimisation, due to the consistently good selectivity, though, as noted in the tables, the selectivities quoted are described as estimates, due to the large effect that the uncertainties in the yields/conversions could have.

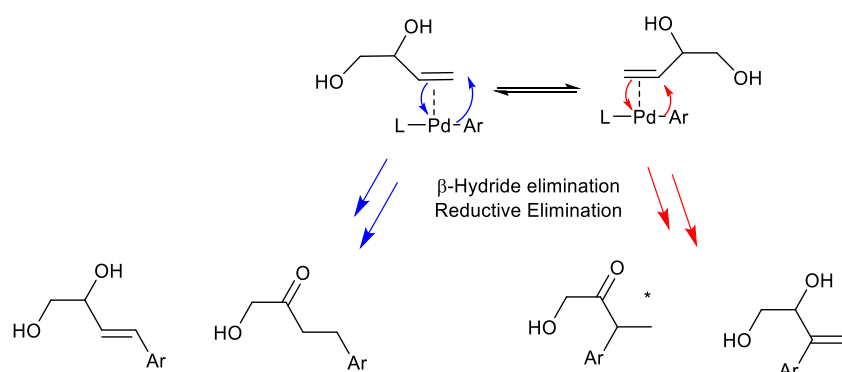
As well as **HPBO**, there are other products possible *e.g.*, as in **Scheme 3.3.6** and **Scheme 3.5.3**. For example, products with a C=C bond, more typical of a Heck Reaction, could be formed. Isomers of both this and **HPBO** could also be possible. In this work, no side-products of the reaction were isolated. However, the occurrence of side-products by relation to major peaks in the GC analyses of the product mixtures can allow for speculation and to determine relative changes in their appearance between different conditions. In the catalyst screen performed here, given below are some data relating to the

likely major side-products of the reaction (**Table 3.4.3**). It was observed in the GC chromatograms from various reaction that signals at 3.3 min, 8.0 min, 8.9 min and 9.2 min retention times were present (*c.f.* 9.8 min for **HPBO**), likely present due to the formation of side-products. The data given below relate to these signals and their intensity in the GC analyses from reactions with PdCl₂ and 2GXPhos catalysts from the above results (**Table 3.4.2**).

Table 3.4.3 GC responses (rounded to the nearest 100) for the likely major side-products of the reaction showing how, mostly, 2GXPhos results in greater amounts of certain side-products than PdCl₂ under comparable conditions.

Entry	Retention Time / min	0.05 mol% Loading			0.5 mol% Loading		
		PdCl ₂	2GXPhos	PdCl ₂ /2GXPhos	PdCl ₂	2GXPhos	PdCl ₂ /2GXPhos
1	3.3	102,600	163,300	0.63	184,600	353,800	0.52
2	8.0	57,000	62,700	0.91	155,200	199,900	0.78
3	8.9	137,600	143,400	0.96	222,300	192,500	1.15
4	9.2	9,200	13,400	0.69	70,100	280,900	0.25

Firstly, it was observed for the same catalyst at the two different loadings shown in **Table 3.4.3**, there was always more of each side-product observed at the higher loading. It was also observed that the data mostly suggests for 2GXPhos and PdCl₂ at the same loading, that 2GXPhos leads to a greater amount of side-product formation. Particularly, for the responses observed in the GC chromatograms at retention times of 3.3 min and 9.2 min, there are relatively much greater amounts of the side-products observed for 2GXPhos than for PdCl₂. This is perhaps due to an expected higher catalytic activity of the 2GXPhos catalyst. Moreover, it could be that the molecule responsible for the signal at 9.2 min may be formed favourably due to steric effects (**Scheme 3.4.3**). That is, the 2GXPhos catalyst provides a much more sterically hindered environment for the species coordinated to Pd. As such, this may favour certain orientations of the coupling partners when coordinated throughout certain parts of the catalytic cycle. Such effects can influence the selectivity of the Heck Reaction.⁸⁰ A possible proposal therefore, may be that the presence of the XPhos ligand favours the formation of a product where in the intermediate prior to insertion of the alkene, a certain orientation is favoured which causes the least steric hindrance. In the **Scheme 3.5.3** below, whilst a simplified analysis, the potential side-product formed from this reasoning is given. As stated, more work would be required to verify this claim but is a possible explanation as to why 2GXPhos would favour a certain side-product over a simpler PdCl₂ catalyst.



Scheme 3.4.3 possible product mixture, due to different orientations of the alkene prior to insertion. Where *L* is a bulky ligand e.g., XPhos, the red route may be favourable. Otherwise, the blue pathway might be favoured. *product was identified previously.¹²⁴

To exploit the benefits of flow reactors for the RRHR, it would be desirable to reduce the Pd loading. For instance, at a so-called “homeopathic”^{112–114} loading of 0.05 mol%, a yield of around 45% at around 63% conversion was observed. The hypothesis was e.g., at this loading, the conversion and yield could be increased by increasing the temperature. To test this hypothesis, reactions were carried out at different temperatures using a 0.05 mol% loading of PdCl₂ and 10 min residence time.

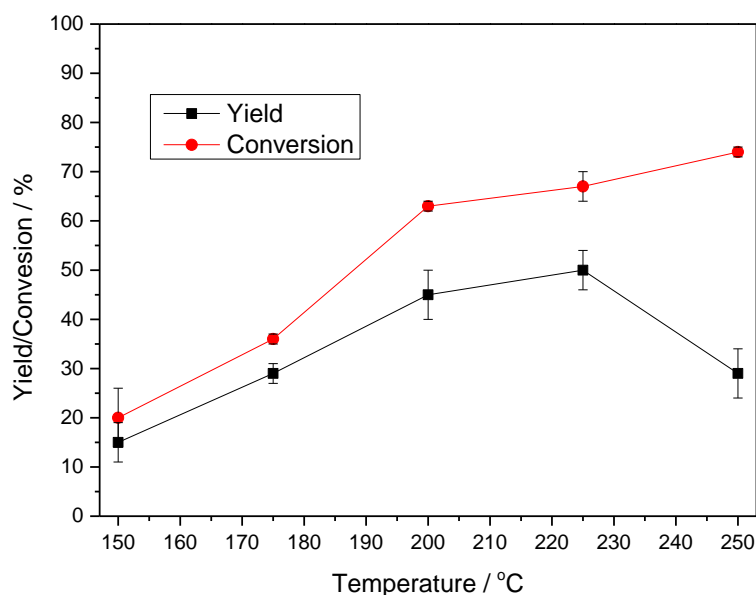
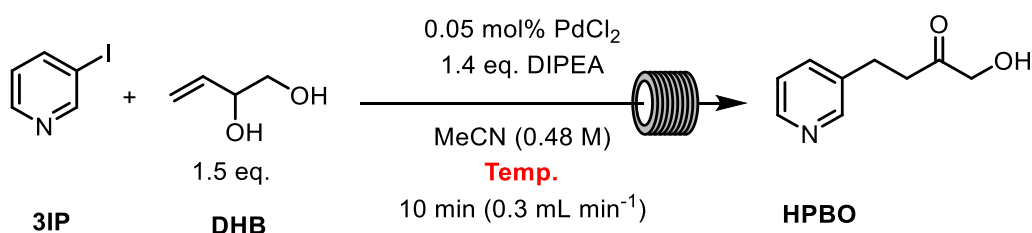


Fig 3.4.1 the effect of reaction temperature on the observed yield of *HPBO* from the Heck reaction between *3IP* and *DHB* showing how an increase in temperature increases the yield of *HPBO*, until 250 °C, where a decrease in yield was observed. Lines are drawn to guide the eye.

From 150–225 °C, an increase in conversion, and yield, with temperature was observed (**Fig 3.4.1**), showing a benefit of applying a flow reactor, as these temperatures for MeCN require the application of backpressure, easy to achieve in flow. However, above 225 °C, it was observed that, whilst conversion increased, the **HPBO** yield decreased. This was considered possibly due to thermal degradation of the product or starting materials. Again, the appearance of side-products from the GC analyses were considered (**Table 3.4.4**).

Table 3.4.4 GC responses (rounded to the nearest 100) of the probable side-products from reactions performed in MeCN with 0.05 mol% loading of PdCl₂, showing increased side-product formation as temperature increases, with a decrease in the response observed at 250 °C, supplementary to yield of desired product illustrated in **Fig 3.4.1**.

Entry	Retention Time / min	GC Peak Area				
		Temperature / °C				
		150	175	200	225	250
1	3.3	5,800	31,600	102,600	126,400	99,600
2	8.0	2,200	11,900	57,000	87,900	77,600
3	8.9	25,500	73,800	137,600	151,000	84,300
4	9.2	0	0	9,200	27,700	98,500

As with the desired product, the relative concentration of each species was observed to increase with increasing temperature from 150 °C to 225 °C. As was also observed for the desired product, it appeared that at 250 °C, the concentrations of the side-products were lower than at 225 °C. This observation would suggest that the lower yield of desired product was *not necessarily* a result of the typical side-reactions occurring *via* competing processes. These observations could perhaps suggest degradation/polymerisation of the products (or starting material), leading to lower observed concentrations.

Following this, it appeared that around 225 °C may be optimal for the reaction, on relatively short timescales (~10 min). With the aim of achieving full conversion of **3IP**, without loss of yield of the desired product, it was decided to investigate whether at slightly longer timescales at this temperature the yield could be increased along with conversion. As such, reactions were conducted at 225 °C, with an increased residence time of 15-20 min.

Table 3.4.5 effect of increased residence time on the Heck Reaction of **3IP** with **DHB**, showing almost full conversion of **3IP** after a 15 min residence time, with a yield of **HPBO** of around 73%.

$0.05 \text{ mol\% PdCl}_2$
 1.4 eq. DIPEA
 MeCN (0.48 M)
 $225 \text{ }^\circ\text{C}$

3IP + **DHB** (1.5 eq.) $\xrightarrow{\text{Time (Flow Rate)}}$ **HPBO**

Entry	Residence Time / min	HPBO GC Yield / %	3IP GC Conversion / %	Selectivity Estimate ^a / %
1	10	50 ± 4	67 ± 3	75
2	15	73 ± 2	96 ± 1	76
3	20	69 ± 9	97 ± 2	71

^aSelectivity estimate calculated from the ratio of product yield/limiting reagent conversion (expressed as a percentage), not accounting for the associated uncertainties, hence described as estimate.

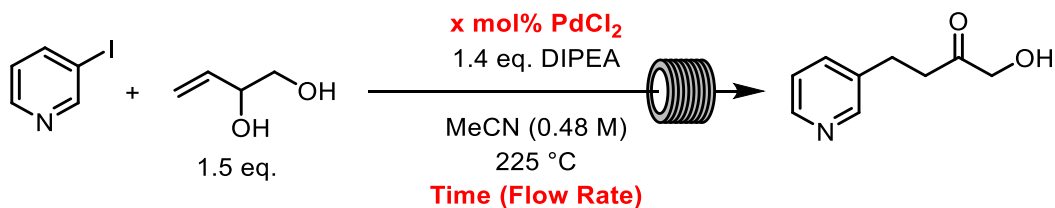
At both 15 min and 20 min planned residence times, yield of around 70% at >95% conversion was observed (**Table 3.4.5**). This suggested that indeed, flow reactors and the benefits they offer, could be demonstrated to the RRHR forming a pharmaceutical target. The apparent observations for the side-products were consistent with previous observations made. That is, for a PdCl₂ catalyst, the major side-products observed likely appeared at 3.3, 8.0, 8.9 and 9.2 min. It would be difficult to suggest which of these species would be the major side-product, without GC calibration. However, it could be speculated (**Table 3.4.6**) that, as was seen for the major desired product (**HPBO**), the relative concentrations of the side-products increase upon extending the residence time from 10 min to 15 min but remained reasonably similar from 15 min to 20 min (as full conversion was almost seen at both residence times).

Table 3.4.6 observed GC responses (rounded to the nearest 100) for the probable side-products, for reactions performed in MeCN, at 225 °C, with a 0.05 mol% PdCl₂ loading (supplementary to **Table 3.4.5**).

Entry	Retention Time / min	GC Peak Area		
		10 min	15 min	20 min
1	3.3	126,400	141,000	151,200
2	8.0	87,900	155,400	164,800
3	8.9	151,000	211,900	230,300
4	9.2	27,700	51,900	92,200

With good yield of **HPBO** observed at 225 °C, with a 0.05 mol% loading of simple PdCl₂, in a short 15 min residence time, the next step was to determine whether good yields could be obtained using a lower Pd loading. It was therefore decided to employ PdCl₂ loadings of 0.01 mol% and 0.005 mol%, representing a further 5-fold and 10-fold reduction in Pd loading, respectively, from the 0.05 mol% loading now optimised for in flow. The hypothesis was that extending the reaction time might allow for lower Pd loadings to be used. To test this, reactions were performed at 15-30 min residence times, at 225 °C and lower PdCl₂ loadings.

Table 3.4.7 effect of extended residence times on the yield of **HPBO** using lower loadings of Pd.



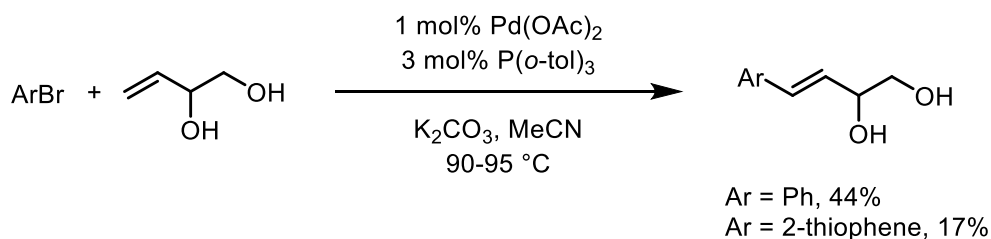
Entry	PdCl ₂ Loading / mol%	Residence Time / min	HPBO GC Yield / %	3IP GC Conversion / %	Selectivity Estimate ^a / %
1	0.05	15	73 ± 2	96 ± 1	76
2	0.01	15	27 ± 4	43 ± 3	63
3		30	38 ± 4	65 ± 1	58
4	0.005	15	15 ± 2	33 ± 9	45
5		30	25 ± 3	39 ± 1	64

^aSelectivity estimate calculated from the ratio of product yield/limiting reagent conversion (expressed as a percentage), not accounting for the associated uncertainties, hence described as estimate.

With lower Pd loadings, at residence times of 15 min show, as expected, a lower yield of desired product **HPBO** (Table 3.4.7, Entries 1, 2 and 4). Upon doubling the residence time to 30 min, the yields at the lower loadings of 0.01 mol% and 0.005 mol% were seen to increase, however, the yields observed were not as high as the 73% yield observed using a higher loading of 0.05 mol%. Moreover, selectivity towards the desired product appeared lower at reduced Pd loadings as well. Whilst this suggested it was not possible to achieve yields as observed for a 0.05 mol% loading at lower loadings and only a slightly longer residence time, the optimised conditions were taken as those where a 73% yield was observed, in a 15 min residence time at 225 °C, using 0.05 mol% PdCl₂.

3.5 Conclusions & Further Work

A flow process was developed for performing a RRHR in the synthesis of a pharmaceutical intermediate target, involving a challenging heterocyclic coupling partner (**3IP**) and **DHB**, an allylic alcohol. In the previous report disclosing the reaction, an isolated yield of 53% was observed, using 0.1 mol% Pd catalyst with P(*o*-tolyl)₃ as a ligand, in a batch process operating in refluxing toluene (95% conversion, 5:1 selectivity for the desired ketone product to the undesired traditional Heck Reaction diol product).¹²⁴ Here, a flow process in superheated (225 °C) MeCN (easily accessed in the flow reactor), allowed a low loading of PdCl₂ (0.05 mol%, a so-called “*homeopathic*”^{112–114} loading) without additional ligands to be employed, observing 73% yield and >95% conversion in only 15 min residence time. Notably, this work used 3-iodopyridine, as opposed to 3-bromopyridine as used in the original report and it should be expected that iodinated substrates may react quicker than the corresponding brominated substrates (which may be more attractive for a commercial process), however, the iodinated analogue was useful here in developing a flow process. The flow process developed here also represents processing benefits over a similar Heck Reaction, involving the same allylic diol substrate along with aryl bromides, developed by researchers at GSK and Dow (**Scheme 3.5.1**). The researchers intended to prepare the traditional Heck product, rather than the RRHR product, though yields were low when applying a heteroaromatic substrate (2-bromothiophene).¹⁴⁴ Compared to this work, the process developed here required lower Pd loading (0.05 mol% vs. 1 mol%) and also did not require the use of phosphine ligands, as was used in the previous report.¹⁴⁴



Scheme 3.5.1 a Heck Reaction involving the same allylic diol as used in this work, where the traditional Heck product was the desired target, with low observed yield when employing a heterocyclic substrate.¹⁴⁴

The flow process developed here also contributes towards applying flow reactors for Heck-type reactions. For instance, a self-optimising flow reactor was previously applied for a Matsuda-RRHR (and subsequent cyclisation/substitution, **Scheme 3.3.19**).¹⁴² This highlighted the benefits of flow reactors for integrating optimisation algorithms for automated synthesis. The authors were able to use the self-optimising reactor to achieve a yield of 92%.¹⁴² The work here highlights the use of flow reactors for controlling reaction conditions and extending access to novel processing windows (high temperature and pressure), and the advantages this can offer to such catalytic reactions.

As such, future work for this and related Heck-type Reactions in flow could involve performing the reactions on cheaper, more available halide/*pseudo*-halide substrates to further enhance the possibility of uptake of flow processing for such reactions. Of interest to this process as well, being part of a previously reported multi-step synthesis, would be the aim of investigating whether multiple synthetic reactions involving reactions such as this can be integrated into a telescoped process, representing a more efficient means of carrying out synthetic processes.

Chapter 4

Reductive Heck Reactions in Continuous Flow

4.1 Abstract

A Reductive Heck Reaction protocol involving aryl iodides and α,β -unsaturated ketones (enones)¹⁴⁸ was developed into a flow process, using a thermal tubular reactor, used in Chapters 2 and 3 (detailed in the Experimental Chapter). The approach used Pd(OAc)₂ (with no added ligands) in the presence of a tertiary amine and N-methyl-2-pyrrolidinone solvent. The aim was to determine whether process optimisation (*e.g.*, reaction times, selectivity, catalyst loadings *etc.*) could be performed in flow, and whether this offered any benefits when compared to a batch approach. In flow, it was observed that temperatures >200 °C resulted in low selectivity towards the desired product and that catalyst loadings <0.05 mol% also resulted in lower selectivity. For example, using 0.05 mol% Pd(OAc)₂ at 200 °C, in only 10 min residence time, a yield of 52% was observed, at 95% conversion. Then, it was observed that by employing an excess of *either* aryl iodide or enone starting material resulted in increased selectivity towards the desired reductively coupled product. Under the optimised flow conditions, a yield of ~75% at >95% conversion was observed, in only 10 min using a low 0.05 mol% Pd(OAc)₂ loading at 200 °C. Compared to the original publication in batch, loadings of 1-3 mol% Pd(OAc)₂ in 3-6 h reaction times were required to observe yields of ~75%,¹⁴⁸ whereas in flow, loadings of 0.05 mol% Pd(OAc)₂ in timescales of 10 min could be applied to observe the same reaction yield. It was also observed that one of the major side-products at elevated temperatures was the directly reduced enone starting material. As such, investigation of selective enone reduction using a Pd/tertiary amine system would represent an interesting avenue for further research as a means of performing homogeneous C=C reduction without needing to handle flammable H₂ gas, also with low Pd loading.

4.2 Strategy & General Aims

As previously described, the remit of this work generally involved developing Pd-catalysed C-C coupling reactions in flow. With the work in Chapter 2 being focused upon the traditional C(sp²)-C(sp²) Heck Coupling Reaction, it was logical to investigate whether the flow reactor constructed for the work in that Chapter could also be applied to the Reductive Heck Reaction, for the formation of new C(sp²)-C(sp³) bonds, using the work performed on the traditional Heck Reaction as a platform for doing so.

Therefore, with a reactor already in hand and an idea of related reaction conditions suited for processing such reactions, the strategy for this work involved the initial identification of Reductive Heck conditions suitable for flow processing. Following identifying suitable conditions, a survey of some conditions in batch was performed to understand what benefits may be achieved by alternatively using flow chemistry and to determine suitability for moving towards processing (and whether any modifications were required).

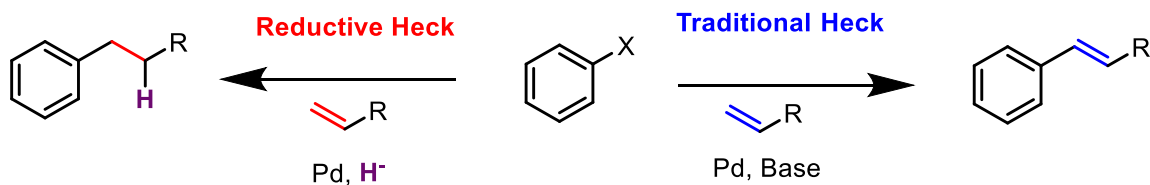
Following this, a survey of numerous conditions in the flow reactor were performed, to determine whether any processing benefits could be achieved by using a flow reactor and the ease of access to novel processing windows that using this allows.

4.3 Introduction

4.3.1 Traditional and Reductive Heck Reactions

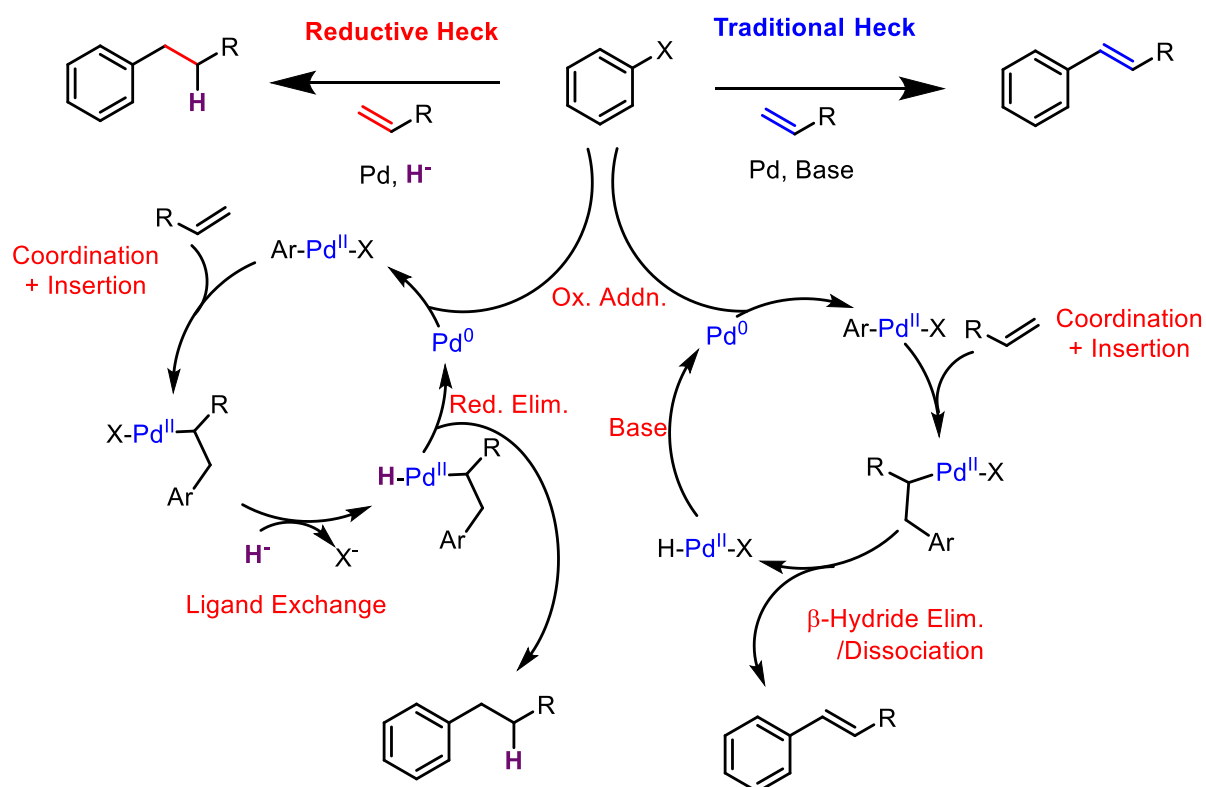
Like the traditional Heck Reaction, the Reductive Heck Reaction (RHR) involves the coupling of an alkene with an aryl halide, using Pd-catalysis. Whilst the traditional Heck Reaction outcome is olefination of

the aryl ring, the RHR outcome involves loss of the π -bond of the starting alkene after the coupling occurs, forming a new $C(sp^2)$ - $C(sp^3)$ bond between the aryl ring and the component which began as the alkene (**Scheme 4.3.1**). That is, whilst the traditional Heck Reaction is arylation of an alkene, the RHR is hydroarylation of an alkene.^{149,150}



Scheme 4.3.1 different products formed in traditional Heck and RHRs.

To achieve this outcome, often, a Heck Reaction is performed followed by hydrogenation of the $C=C$ bond, or other methods for example involving dual-catalysis.¹⁴⁹ In a RHR, the same outcome can be achieved in a single step. To do so, the reaction conditions divert from those of the traditional Heck Reaction so as to introduce a hydride source, altering the coupling mechanism (**Scheme 4.3.2**) so that where β -hydride elimination is expected in the traditional Heck Reaction mechanism (furnishing an alkene product), reductive elimination instead occurs, involving the alkene-inserted aryl ring and hydride as elimination partners (furnishing an alkyl product).^{149,150}



Scheme 4.3.2 variations in simplified catalytic cycles between traditional Heck Reactions and RHRs highlighting how a hydride source can influence formation of a reduced product.¹⁴⁹

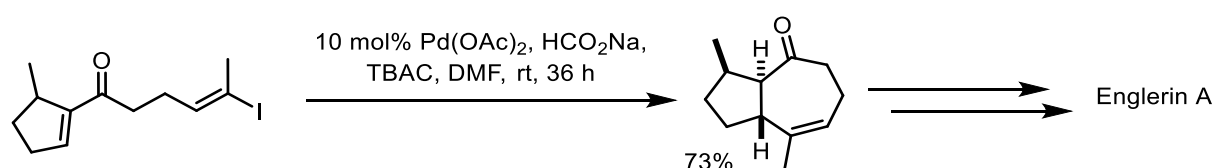
As such, the RHR is a useful component of the Synthetic Chemist's Toolkit for several reasons. For example, the reaction results in the formation of an aryl-alkyl linkage, which are typically difficult using *e.g.*, alkyl halides, whereas this procedure exploits alkenes as starting materials. Moreover, as

previously stated, compared to employing a Heck Reaction and subsequent hydrogenation protocol (using, often, two Pd-catalysed steps) this reaction achieves the same outcome in a single step and so has the potential to reduce the demand for precious metals in a synthetic procedure – particularly important considering multi-step synthetic processes *e.g.* for pharmaceutical manufacturing.^{149,150} Due to the utility of the RHR and the interest in applying it to natural product and pharmaceutical synthesis, developing a flow process for RHRs would be useful. Combining the advantages offered by flow processing (discussed in Chapter 1 and illustrated in Chapters 2 and 3) with the synthetic utility of the RHR might allow for attractive processes for chemical manufacturing to be developed.

4.3.2 Applications of Reductive Heck Reactions

Due to the benefits of the RHR, there has previously been interest in exploring the scope of the reaction, the conditions necessary for promoting the reaction and application in the synthesis of target natural products and pharmaceuticals.

For example, the RHR has been employed in a key cyclisation step en route to formation of the natural product Englerin A (**Scheme 4.3.3**). Here, a vinyl iodide was used in an intramolecular RHR with an enone for the formation of a 7-membered ring system. Sodium formate was used as the hydride source (as is commonly used, noted in Section 4.3.3), however, the reaction required a high 10 mol% Pd(OAc)₂ loading and prolonged 36 h reaction time to give a good 73% reported yield, at room temperature.¹⁵¹



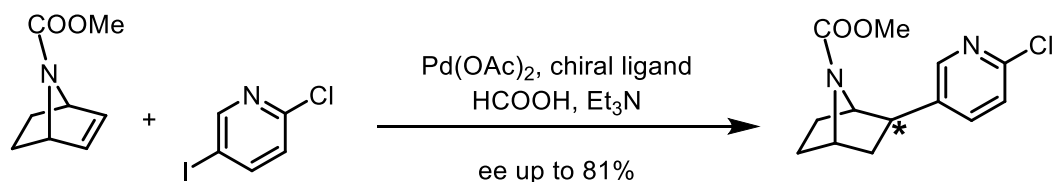
Scheme 4.3.3 application of a RHR in the total synthesis of natural product Englerin A.¹⁵¹

The RHR has been used in a number of total syntheses of Iboga Alkaloid natural products, which are promising targets in tackling drug addictions (**Scheme 4.3.4**).¹⁵² In two examples, sodium formate was applied as the hydride source with either Pd(PPh₃)₄ or Pd(OAc)₂ with PPh₃ added as a ligand. In the example using Pd(PPh₃)₄ along with a brominated indole substrate, reactions were complete in only 1 h with heating to 130 °C, though yields were modest (42% maximum).^{153–155}



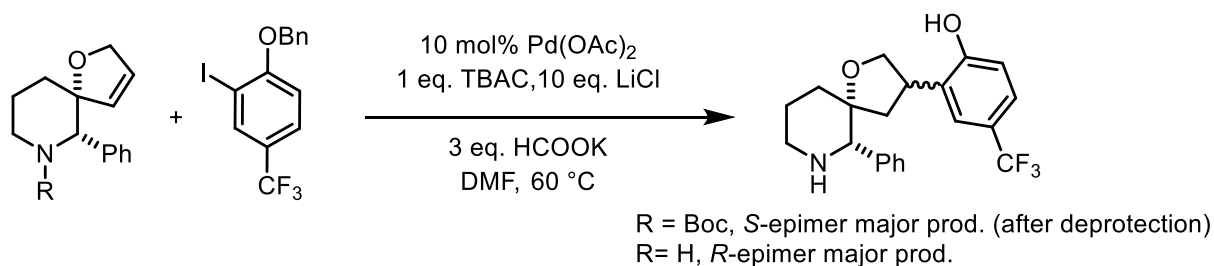
Scheme 4.3.4 the RHR in the synthesis of Iboga Alkaloids.^{153–155}

The RHR has also been applied in an intermolecular fashion for total synthesis (**Scheme 4.3.5**). For example, the reductive coupling of an N-heterocyclic alkene along with a halogenated pyridine was achieved in an enantioselective manner, by employing a chiral ligand, in the synthesis of Epibatidine by Kauffmann and co-workers.¹⁵⁶



Scheme 4.3.5 an enantioselective RHR in the synthesis of an intermediate towards Epibatidine.¹⁵⁶

Due to the expedient approach towards forming new C(sp²)-C(sp³) bonds, the RHR has not only found interest for natural product total syntheses (including targets with biologically active interest such as the Iboğa Alkaloids) but also in the synthetic processes towards pharmaceuticals.^{149,150} For example, NK₁ receptor antagonists are drug molecules with antidepressant and anti-anxiety properties and are also used to prevent nausea and vomiting in cancer patients undergoing chemotherapy.¹⁵⁷ Many of the structures of such drug molecules are rich in alky-aryl bonded units and as such, employing the RHR in the synthesis of such targets would be an effective approach, if applied correctly.¹⁵⁸ A late-stage (only followed by N- and O-deprotection steps) RHR was applied in the synthesis of one such NK₁ receptor antagonist (**Scheme 4.3.6**), reductively coupling a decorated aryl iodide with an O-heterocyclic alkene, using Pd(OAc)₂ as the catalyst and potassium formate as the hydride source.¹⁵⁸



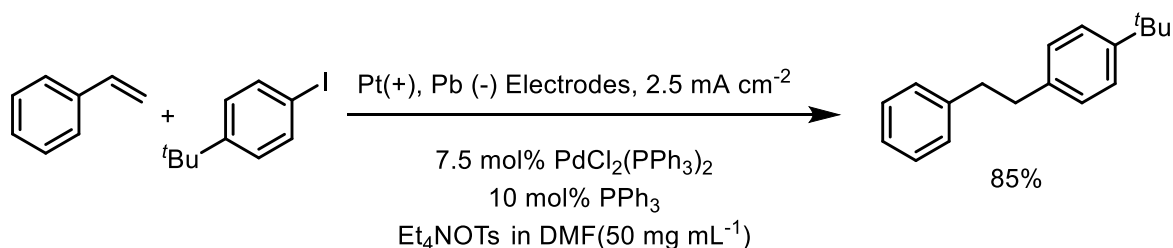
Scheme 4.3.6 a RHR employed as a late-stage step in the synthesis of an NK₁ receptor antagonist pharmaceutical target.¹⁵⁸

Examples such as these highlight the attractiveness of applying a RHR in the synthesis of complex and functional molecules. As well as the application to specific targets in multi-step syntheses such as those described previously, much research has been carried out in development of reaction conditions and scope of RHRs as the more broadly applicable the reaction conditions and scope can become, the more widely the methodology is likely to be adopted.

4.3.3 Conditions for Reductive Heck Reactions

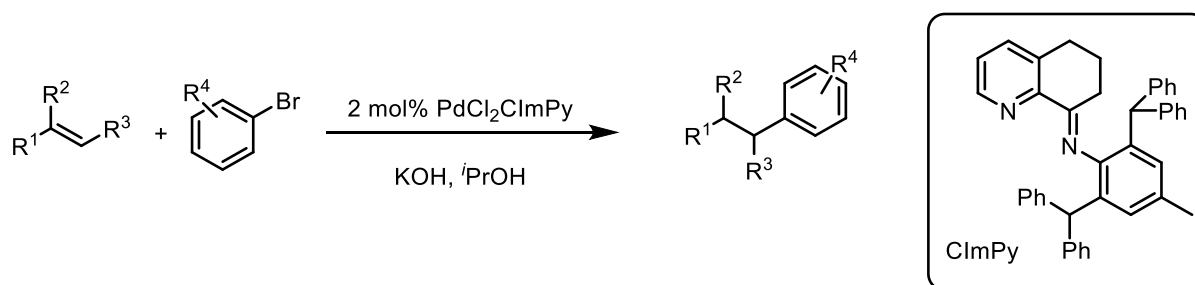
As in the previous examples given, a common adaptation to adjust traditional Heck Reaction conditions into RHR conditions is to introduce a formate salt as a hydride source.¹⁴⁹ The RHR can be considered a challenging reaction in that the formation of the Pd-hydride species and subsequent reductive elimination step (which furnishes the desired Reductive Heck product) must outcompete the β -hydride elimination which would produce the traditional Heck Reaction product. However, as noted in the Results & Discussion Section, the work here intended to *not* use formate salts for the flow RHRs to be developed (due to anticipated solubility issues). Alternative hydride sources also known to efficiently form Pd-hydride species were therefore sought, being used in RHRs as follows.

An electrochemical process, developed by Torii and co-workers (**Scheme 4.3.7**), demonstrated that RHRs of styrenes with aryl halides could be performed using a tetraalkyl ammonium salt as the electrolyte and source of hydride for reduction (due to the electrochemical processing conditions).¹⁵⁹



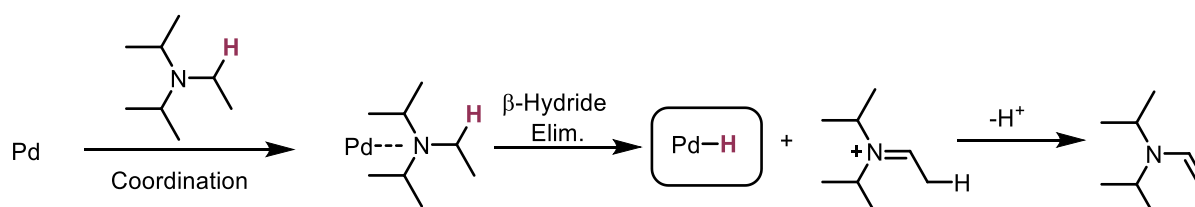
Scheme 4.3.7 electrochemical RHR developed by Torii and co-workers for coupling styrenes and aryl iodides, electrochemically generating hydrides from an alkylammonium salt.¹⁵⁹

Jin, Hu and colleagues demonstrated the use of *i*PrOH as a hydride source *via* β -hydride elimination in a transfer hydrogenation-type process (**Scheme 4.3.8**). They obtained yields ranging from poor to excellent for the methodology, but required relatively high loadings (2 mol%) of a bespoke bidentate imine catalyst to achieve these.¹⁶⁰



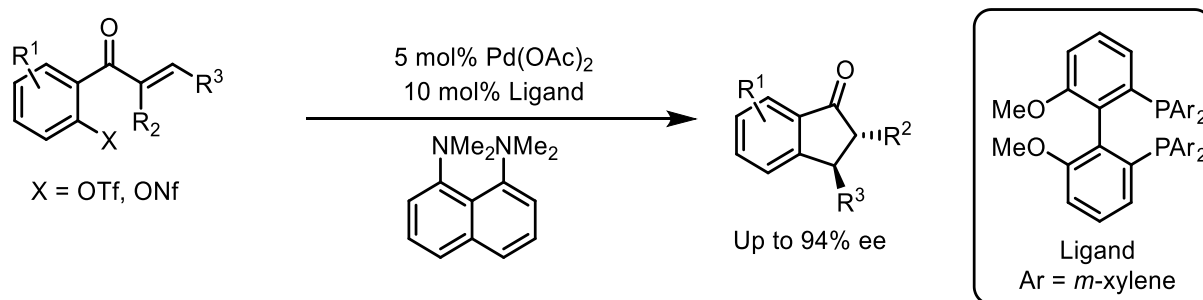
Scheme 4.3.8 RHR of aryl bromides and substituted alkenes using *i*PrOH as a hydride source.¹⁶⁰

RHRs have also been carried out using Michael acceptors (enones) as the alkene substrate, for example, in the synthesis of Englerin A (above).¹⁵¹ In that example, sodium formate was used as the hydride source. However, in other examples of RHRs of enones, tertiary amines have been used as a hydride source. This is likely to involve amine coordination, β -hydride elimination to form the hydride and an iminium by-product, followed by deprotonation of the iminium to form an enamine (**Scheme 4.3.9**).¹⁶¹



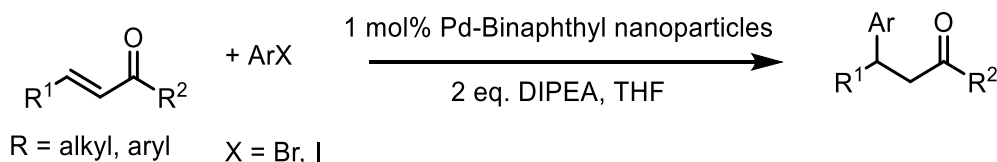
Scheme 4.3.9 plausible Pd-hydride generation from a Pd source and a tertiary amine (DIPEA).¹⁶¹

Such methodology has been applied in intramolecular (tethered enones) fashion to afford 3-arylindanone products (**Scheme 4.3.10**).^{162–164} These reactions resulted in good yields but required bespoke ligands when using a tertiary amine hydride donor.^{163,164}



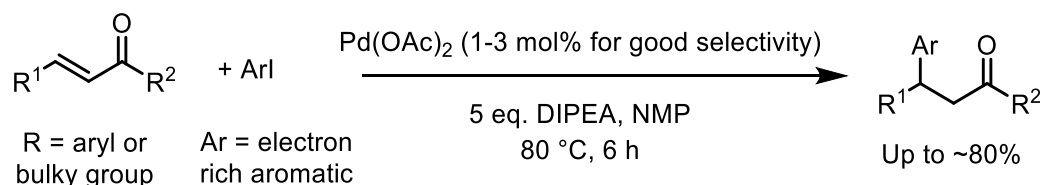
Scheme 4.3.10 intramolecular RHR of aryl halide tethered enones, resulting in the formation of 3-substituted indanones, using a tertiary amine as a hydride donor, reported by the Buchwald Group.¹⁶³

Further developments in using tertiary amines as a hydride source came from Sekar, Minnaard, de Vries and Reek. Sekar had previously observed that Pd-nanoparticles can be used for the RHR of aryl bromides and iodides with enones, in the presence of DIPEA and a Pd loading of 1 mol% (**Scheme 4.3.11**).¹⁶⁵ A similar methodology from Sekar was also used for the formation of indanones using a RHR approach catalysed by Pd-nanoparticles.¹⁶⁶



Scheme 4.3.11 Pd-nanoparticle-catalysed RHR of aryl halides and enones.¹⁶⁵

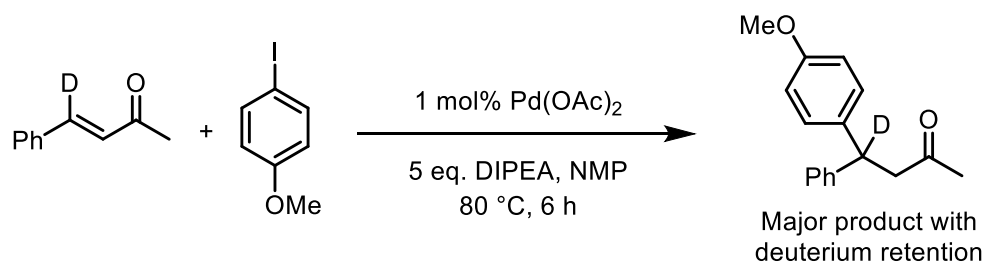
Minnaard, de Vries and Reek have also shown that N-heterocyclic carbene ligands can be used to promote RHRs involving enones (in the presence of NBU_3)^{167,168} but then simplifying this by serendipitously discovering that the combination of DIPEA and $\text{Pd}(\text{OAc})_2$ in NMP solvent could be used without the need for added ligands to promote the transformation (**Scheme 4.3.12**).¹⁴⁸ Other tertiary amine and solvent combinations were found to not work as effectively for the RHR of enones with aryl halides. Their NMP/DIPEA/ $\text{Pd}(\text{OAc})_2$ system worked well (good yield and selectivity) for enones with bulky aryl/alkyl groups and for both electron rich and neutral aryl halides. Selectivity and yields, however, decreased when using electron poor aryl halides and sterically unhindered enones.¹⁴⁸



Scheme 4.3.12 RHR of enones and electron rich/neutral aryl iodides with simple $\text{Pd}(\text{OAc})_2$, DIPEA as a hydride source and NMP solvent.¹⁴⁸

Deuterium labelling of the olefinic β -carbon showed that the position of the deuterium was retained during the reaction (**Scheme 4.3.13**),¹⁴⁸ implying a RHR mechanism occurs, as opposed to a tandem Heck Reaction followed by enone reduction (which would have resulted in loss of the β -deuterium in the postulated Heck Reaction step). The authors could use $\text{Pd}(\text{OAc})_2$ loadings down to 0.5 mol%,

observing only moderate yields of ~60%. Using a relatively high 1-3 mol% Pd(OAc)₂ loading, yields of up to around 75% could be reportedly observed.¹⁴⁸



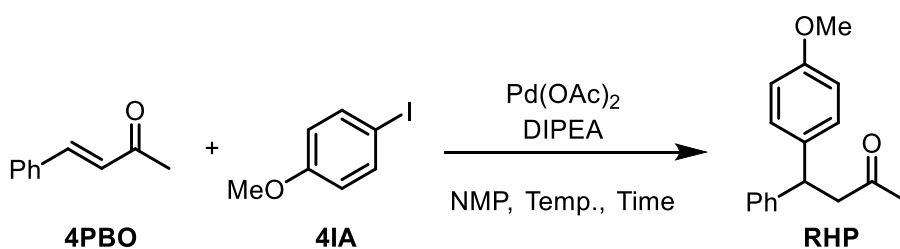
Scheme 4.3.13 deuterium labelling studies on the DIPEA/NMP/Pd(OAc)₂ RHR, indicating a genuine RHR mechanism as opposed to a traditional Heck Reaction (involving loss of deuterium) followed by sequential C=C reduction.¹⁴⁸

These examples further highlight the potential versatility and utility of RHRs for useful bond formations and served as a basis for selecting conditions for developing a flow process (discussed in Results & Discussion). As such, developing a flow process for a reaction with such utility could provide an efficient processing means possibly attractive for chemical manufacturing. In Chapters 2 and 3, it was observed that the flow reactor built could allow for significant reduction in Heck Reaction and Redox Relay Heck Reaction Pd loadings by convenient access to high temperatures. The aims of the work in this Chapter were therefore to investigate whether the application of flow chemistry to a RHR could result in processing benefits, including, whether novel processing windows accessible in flow could allow for a reduction in Pd demand, and acceleration of reaction rates.

4.4 Results & Discussion

4.4.1 Selection of an Appropriate Reductive Heck Reaction for Developing a Flow Process

The general RHR shown in **Scheme 4.3.12**, involving enone substrates with Pd(OAc)₂ catalyst and DIPEA as a hydride donor, was investigated in flow in the work carried out here. This was chosen because the reaction was reported to involve a homogeneous system using NMP/DIPEA/Pd(OAc)₂,¹⁴⁸ hence appearing suitable for developing into a flow process. Furthermore, the reaction conditions (being applied to enones) involved reaction coupling partners that have attracted an amount of interest in the previous literature, including in the total synthesis of Englerin A¹⁵¹ and in the synthesis of indanones.¹⁶²⁻¹⁶⁴ Hence, developing a flow process would represent a useful procedure possibly applicable to interesting targets. Moreover, aspects were identified which were considered improvable upon, in flow. For example, the relatively high (>1 mol%, **Scheme 4.3.12**) Pd loadings to achieve good yield/selectivity was considered something where possible improvements could be investigated in flow. It was decided to adopt the same model coupling partners as in the original publication (4-iodoanisole, **4IA**, and *trans*-4-Phenyl-3-buten-2-one, **4PBO**, **Scheme 4.4.1**).¹⁴⁸ From which, the expected products would be the Reductive Heck product (RHP, 4-(4-methoxyphenyl)-4-phenylbutan-2-one), the traditional Heck product (possibly two isomers) and possibly others such as homo-coupled **4IA**.



Scheme 4.4.1 reaction scheme for the previously reported RHR involving model substrates, used to develop a flow process in this work.¹⁴⁸

4.4.2 Initial Batch Reactions

The work began by attempting to replicate the literature reported observations¹⁴⁸ and to conduct a survey of conditions, in batch. The aim was to assess the suitability of the protocol towards flow processing.

Two reactions were initially conducted. These aimed to directly replicate what had been previously reported in the original paper, using a 0.5 mol% Pd(OAc)₂ loading, **4PBO** as the limiting reagent and 5 eq. DIPEA, in NMP solvent and heating at 80 °C for 17 h (similar to what was used in the paper).¹⁴⁸ One of these reactions was performed under inert conditions (using freeze-pump thaw techniques) as this was applied in the paper,¹⁴⁸ however, the other reaction was performed without deoxygenating, for comparison, as this was deemed to be more straightforward for processing using the flow reactor.

Table 4.4.1 comparison of degassed and non-degassed batch reaction processing conditions compared to previous literature reports, showing good reproducibility from the literature and suggesting further reactions without degassing would be suitable.

Entry	Source	Conditions	RHP Isolated Yield / %
1	This Work	Not Degassed	73
2	This Work	Degassed	68
3	Reek, Minnaard, de Vries <i>et al.</i> ¹⁴⁸	Degassed	61

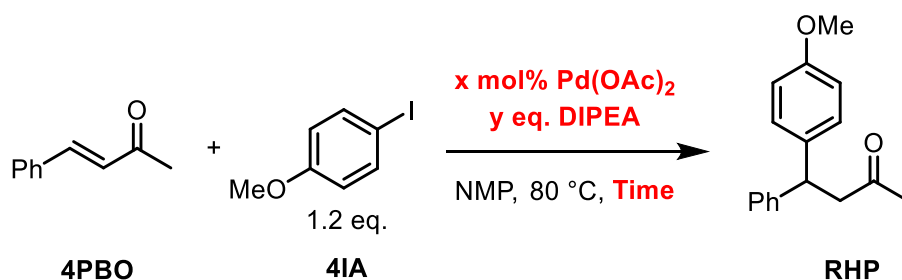
The reactions were conducted with good reproducibility from the literature, in slightly higher observed yield (**Table 4.4.1**, compare Entries 1 and 2 with 3). In both reactions there was no significant difference in isolated yield when degassing the reaction solution *via* freeze-pump-thaw, or when this was omitted (**Table 4.4.1**, Entries 1 and 2). Initial rates of each reaction also appeared similar (with new peaks prominent in crude GC samples after ~30 min). These observations suggested that performing the reactions without the need for strictly degassing the components would suffice. Moreover, no

precipitate was formed in either reaction, indicating that the reaction under such conditions would be, as suggested in the original publication,¹⁴⁸ suited to investigation in flow.

With previous observations in Chapters 2 and 3, an aim of using flow processing for the RHR was to reduce Pd catalyst loadings, as moving towards so-called “*homeopathic*” Pd loadings (*e.g.* <0.1 mol%) represents both an economic and sustainability advantage.^{112–114} However, there are implications for these RHRs at low loadings, with DIPEA used as a hydride donor.¹⁴⁸ In Chapter 2, investigating traditional Heck Reactions, DIPEA was also employed as a base, though standard Heck Reaction products are formed, rather than reduced products. Part of the reason for this change in selectivity of products formed could be due to the relative concentration of DIPEA. In traditional Heck Reactions, DIPEA is added as a stoichiometric base. In this RHR procedure, it is added in large excess, to encourage Pd-hydride formation (**Scheme 4.3.9**). Propensity of the respective substrates towards certain mechanistic processes used in each reaction may also influence selectivity. However, to favour Pd-hydride formation, an excess of amine additive is required and so at extremely low Pd loadings, the ratio of DIPEA/Pd will be extremely high. Whilst this may favour Pd-hydride formation, it can often also result in DIPEA coordination outcompeting coordination of the coupling partners, inhibiting the reaction.¹⁶⁹

With these points in mind, the initial batch survey conducted was to determine the impact of Pd loading, DIPEA equivalents and the ratio between the two components, upon the reaction, as this had not previously been investigated in the original publication. To test this, it was again decided to use a range of 0.5 mol% Pd(OAc)₂ (being the lowest loading used in the original publication) to 0.0005 mol% Pd(OAc)₂ (5 ppm – being a Pd loading used frequently in Chapter 2). At these loadings, different DIPEA equivalents were used (also varying the DIPEA/Pd ratio by doing so, at each loading). The temperature was fixed at 80 °C and NMP was used as the solvent.

Table 4.4.2 effect of Pd and DIPEA loading on the Reductive Heck enone reaction and how the ratio of the two impacts the observed reaction outcome showing how, under the conditions used, loadings of 0.05 mol% or lower were too slow to be useful and how at too high a DIPEA/Pd ratio, reaction rates were inhibited.



Entry	Pd(OAc) ₂	DIPEA	DIPEA/Pd Ratio	Time	RHP GC	4PBO GC
	Loading / mol%	Amount / eq.			Yield / %	Conversion / %
1		1	200	21 h	79	>99 ^a
2		2	400	21 h	81	>99 ^a
3	0.5	5	1000	21 h	81	>99 ^a
4		10	2000	21 h	86	99
5		25	5000	21 h	47	77
6	0.05	1-5*	2000 - 10,000*	24 h	Traces	
7	0.005	1-5*	20,000 - 100,000*	4 days	Traces	
8	0.0005	1-5*	200,000 - 1,000,000*	4 days	Traces	

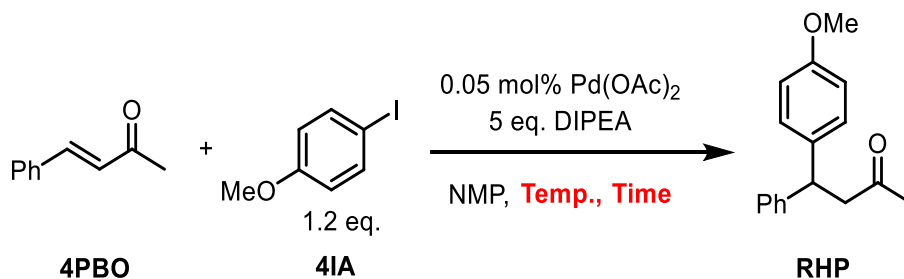
*Little difference in observations for results at these DIPEA loadings/DIPEA:Pd ratios.

^aNo **4PBO** observed in the GC chromatogram of the crude reaction mixture.

The observations largely confirmed what was to be expected. That is, at too high a DIPEA/Pd ratio, the reaction was inhibited presumably due to the substrates being outcompeted for binding to Pd (**Table 4.4.2**, compare Entries 1-4 with 5). It was also observed that under the conditions applied, reactions only resulted in observing traces of product using a lower Pd loading than 0.5 mol% (**Table 4.4.2**, Entries 6-8). This could be due to the higher DIPEA/Pd ratio, or simply due to using a lower amount of Pd.

With these observations in mind, the next step taken was to subject some of the lower Pd loading conditions to increased temperatures. The aim was to determine whether increased temperatures could increase the reaction rates. If so, this may serve as a good precedent for developing a flow process, as high temperature processing is much more achievable and efficient in flow. Reactions were performed, initially using a 0.05 mol% Pd(OAc)₂ loading and 5 eq. DIPEA at 100-200 °C, although, using an oil bath for heating, reaction timescales at 200 °C would be short (2 h at the longest were used).

Table 4.4.3 effect of temperature upon the batch RHR where it was observed that, under otherwise analogous conditions, an increase in temperature resulted in an increased reaction rate.



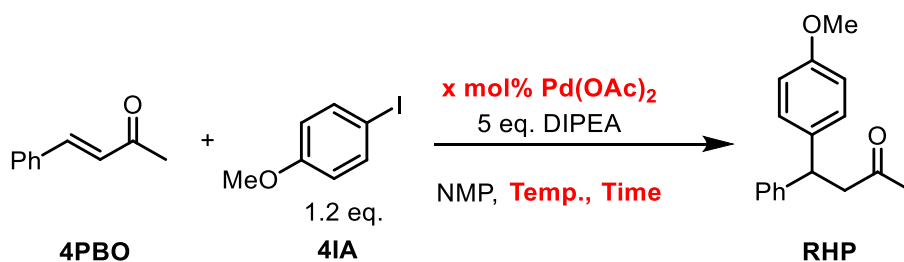
Entry	Temperature / °C	Time / h	RHP GC Yield / %	4PBO GC Conversion / %
1	80	24		Traces
2	100	19	29	48
3	150	19	74	>99*
4	150	1	52	72
5	200	1	64	93

*No **4PBO** observed in the GC chromatogram of the crude reaction mixture.

It was observed that at 100 °C and 0.05 mol% Pd(OAc)₂ loading, the reaction could be performed over a reasonably long timescale, observing a moderate yield, whereas, at 80 °C, only trace amounts of product were observed under comparable conditions (**Table 4.4.3**, Entries 1 and 2). This indicated that even at a slightly increased temperature, the reaction timescale could be notably shortened. After only 1 h at 150 °C, the observed yield was greater than that observed after 19 h at 100 °C (**Table 4.4.3**, Entries 2 and 4). This was promising for attempting to develop an improved process by using a flow reactor where more convenient access to such elevated temperatures would be possible.

It was decided next to determine whether lower yet catalyst loadings (0.005 mol% and 0.0005 mol%) could be employed to observe good yields, at these elevated temperatures, firstly in batch. At each loading, reactions were performed at 200 °C, using 5 eq. DIPEA.

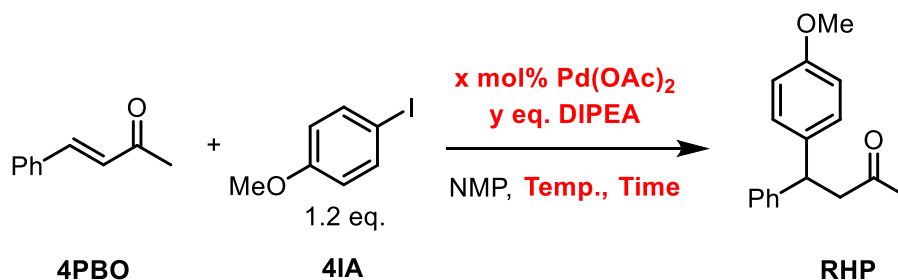
Table 4.4.4 screen of the effect on the RHR of applying low Pd loadings at elevated temperatures, in batch, where good conversions and moderate yields were observed in short timescales.



Entry	Pd(OAc) ₂ Loading / mol%	Temperature / °C	Time / h	RHP GC Yield / %	4PBO GC Conversion / %
1	0.05	150	1	52	72
2	0.05	200	1	64	93
3	0.005	200	2	53	96
4	0.0005	200	2	15	27

At a Pd(OAc)₂ loading of 0.005 mol%, good conversion, but moderate yield, was observed after 2 h heating at 200 °C (**Table 4.4.4**, Entry 3). Using a 0.0005 mol% loading, the reaction appeared to proceed much slower (**Table 4.4.4**, Entries 3 and 4). Also, at 0.005 mol% loadings, selectivity towards the desired product appeared to be diminished, compared to higher loadings used previously (**Table 4.4.4**, Entries 2 and 3 and **Table 4.4.2**, Entry 3). Considering this, the final investigation in batch intended to revisit the DIPEA/Pd ratio influence on the reaction, but at higher temperature. At 200 °C and the lowered Pd loadings of 0.005 mol% and 0.0005 mol%, reactions were conducted using 1 eq. and 2 eq. DIPEA, compared to using 5 eq. DIPEA in the previous reactions. The aim was to determine whether the increased temperature could lead to increased reaction rates under conditions where previously, only traces of products were observed at 80 °C.

Table 4.4.5 investigation of the relative amounts of Pd and DIPEA on the RHR outcome using low Pd loadings at elevated temperature. Moderate to good conversions could be obtained using 0.005 mol% or 0.0005 mol% Pd, but selectivity towards the desired product was reasonably low.



Entry	Temp. / °C	Pd(OAc) ₂ Loading / mol%	DIPEA Amount / eq.	Time / h	RHP GC Yield / %	4PBO GC Conversion / %	Selectivity / %
1	150	0.05	5	1	52	72	72
2	200	0.05	5	1	64	93	69
3	200	0.005	5	2	53	96	55
4	200	0.005	2	2	50	>99*	49
5	200	0.005	1	2	27	89	30
6	200	0.0005	5	2	15	27	56
7	200	0.0005	2	2	14	50	28
8	200	0.0005	1	2	6	32	19

*No 4PBO observed in the GC chromatogram of the crude reaction mixture.

Reactions possibly appeared to proceed faster (in terms of conversion) when using 2 eq. DIPEA than 5 eq., likely due to the decreased DIPEA/Pd ratio (Table 4.4.5, Entries 6 and 7). However, at these lower Pd loadings and reduced DIPEA equivalents, the selectivity towards the desired RHP was significantly reduced, compared to using a 0.05 mol% loading (Table 4.4.5, Entries 3-8). At this stage, side-products had not been identified, though this is discussed later in this Chapter.

With a survey of conditions in hand from these batch studies, it was considered that there was suitable precedent for developing a flow process for the reaction. This was based upon the observations that access to higher temperatures appeared to enhance reaction rates (although selectivity was reduced under certain conditions) and that the homogeneous reaction mixture was suitable for flow processing. It was therefore considered that a flow process, allowing convenient access to temperatures of 200 °C and above, could allow for fast reactions to be performed at possibly reduced Pd loading demands, in a safer and more efficient manner than using traditional batch approaches.

4.4.3 Initial Flow Temperature Dependence Investigation

Using the flow reactor built in this work (described in Chapter 2 and detailed in the Experimental Chapter), some initial investigations were performed, following the survey performed in batch and being informed by previous work conducted on the traditional Heck Reaction. Firstly, as a temperature dependence was determined in batch, it was decided that the scope of this temperature should be expanded by using the conveniently heated/pressurised flow reactor. Temperatures in the range of 200–300 °C were applied to determine whether a similar trend to that observed in batch (increasing

rate up to the maximum temperature studied, 200 °C) would also be observed in this range, in flow. Here, 2 eq. DIPEA was applied, as this had appeared to be beneficial (in terms of reaction rate, but perhaps detrimental in terms of selectivity) from the batch survey and a short 5 min residence time was used as it was hoped that this would make any significant changes in yield/conversion noticeable at different temperatures.

Table 4.4.6 initial screen of temperatures between 200-300 °C in the flow reactor highlighting how increased temperatures resulted in increased conversion, but generally poor yields were observed.

Reaction scheme showing the flow synthesis of RHP from 4PBO and 4IA. Reagents: 0.005 mol% Pd(OAc)₂, 2 eq. DIPEA. Solvent: NMP. Conditions: Temp. and Time (Flow Rate).

Entry	Temp. / °C	Residence Time / min	RHP GC Yield / %	4PBO GC Conversion / %	Selectivity Estimate ^a / %
1	200	5	2 ± 1	13 ± 4	15
2	250	5	11 ± 1	46 ± 4	24
3	250	10	16 ± 1	61 ± 1	26
4	250	20	26 ± 2	77 ± 7	34
5	250	30	28 ± 3	95 ± 1	29
6	275	5	8 ± 1	46 ± 1	17
7	275	10	16 ± 1	49 ± 1	33
8	300	5	10 ± 2	90 ± 1	11

^aSelectivity estimate calculated from the ratio of product yield/limiting reagent conversion (expressed as a percentage), not accounting for the associated uncertainties, hence described as estimate.

It was observed that at 200 °C, little product was observed in a 5 min residence time (Table 4.4.6, Entry 1). Upon increasing the temperature to 250 °C, a greater conversion and slightly higher yield was observed (Table 4.4.6, Entries 1 and 2). At 300 °C, almost full conversion was achieved but the observed yield was comparable to that observed at 250 °C (Table 4.4.6, Entries 2 and 8), indicating perhaps decomposition or the reaction favouring formation of a different product at 300 °C – with a notably larger peak detected at ~9.3 min in the GC chromatogram (the identity of which is discussed later). At 250 °C, conversions increased with temperature (Table 4.4.6, Entries 2-5) and could be pushed to near completion with a 30 min residence time, but only a low yield of desired RHP was observed (Table 4.4.6, Entry 5).

With the selectivity towards the desired RHP being low in these initial reactions, an investigation of the side-products being formed was undertaken.

As expected, the traditional Heck Reaction product was suggested by GC-MS to be being produced in the flow reactions as a side-product. From GC estimates (comparison of peak sizes, without having obtained a calibration plot), a similar amount of the traditional Heck product and RHP was formed in the previous flow reactions (similar GC response from the analysed samples). Small amounts of the

homo-coupled and dehalogenated **4IA** products were also formed. These were typically suggested from GC-MS, alongside GC samples of the commercially obtained suggested side-products matching with the retention times observed for the crude reaction mixtures. However, as mentioned previously an unassigned peak in the GC chromatograms had been identified at ~9.3 min. This peak, in all flow reactions so far, was similar in peak area to the desired **RHP** and so was considered to likely be being formed in a significant amount (though this could not be known for sure without obtaining a GC calibration).

4.4.4 Determining the Identity of an Unexpected Side-Product

The next step was therefore to determine the possible identity this unknown side-product to see if this could influence the strategy in going about improving reaction selectivity. It was confirmed that this was *not* the expected side-products of the reaction (noted previously) which are the homo-coupled aryl halide, traditional Heck products or dehalogenated aryl halide – all formed by known side-reactions. As **4PBO** and not **4IA** was the limiting reagent (the alkene, not the aryl halide) and the fact that the homo-coupled product and the dehalogenated product were not being formed in what appeared to be significant quantities, it was considered that the poor selectivity was due to formation of the traditional Heck product and a side-product being derived from **4PBO**.

GC/MS analysis was then carried out and a signal identified with a m/z of 2 greater than that of **4PBO** starting material was observed. This suggested that the **4PBO** was perhaps being directly reduced in the catalytic system (the addition of 2 H atoms across the C=C bond fitting with the observed mass). With some commercially supplied 4-phenylbutan-2-one at hand (the product of the supposed direct reduction of **4PBO** C=C bond), a retention time of ~9.3 min in the GC chromatogram was observed, *i.e.* the same retention time as the so far unidentified impurity. This therefore suggested that the identity of the side-product was 4-phenylbutan-2-one and hence that, under the subjected conditions, a significant amount of directly reduced enone was being produced.

This competing pathway was not commented on in the original publication and,¹⁴⁸ in the work performed here in batch (following a revisited analysis after identifying the nature of the side-product) was found to be formed only as a very minor side-product at 100 °C or less, but at higher temperatures was observed to have formed in a larger amount. To our knowledge, this would represent the first demonstration of a homogeneous Pd catalyst with an amine hydride donor being used for enone reduction in a transfer hydrogenation-type reaction, which appeared to be enabled at high temperature.

4.4.5 Attempts to Increase Reaction Selectivity

After identifying that the major side-products appearing to limit the selectivity were the traditional Heck Product and the direct enone reduction product, considerations were made as to how these could be avoided to favour formation of the desired **RHP**.

It was considered that to avoid formation of the traditional Heck product, using a greater amount of DIPEA might be beneficial, in principle, increasing the amount of Pd-hydride available to favour formation of **RHP** over the traditional Heck product. On the other hand, it was considered that using a lesser amount of DIPEA would be beneficial as this would result in less Pd-hydride available and hence disfavour the formation of the directly reduced enone. As such, these two hypotheses were

contradictory (at least, when considering changing the amount of DIPEA in isolation to changing any other reaction conditions). From previous batch reactions, it was also noted that the directly reduced enone was only formed at elevated temperatures. It was decided therefore to attempt to overcome the selectivity issues, by further investigating different combinations of added amounts of DIPEA, Pd loadings and different temperatures. The aim was to investigate how these would influence the reaction selectivity.

To investigate this, reactions were conducted with 0.005 mol% Pd(OAc)₂ (as initially used for the first flow reactions) using a 1 eq. added DIPEA, to compare to those with the same Pd loading but at a 2 eq. DIPEA loading (as in Table 4.4.6 and reproduced in Table 4.4.7, below).

Table 4.4.7 investigating lowered DIPEA loadings on the RHR outcome illustrating that yields/conversions were similar under comparable conditions when using either 1 or 2 eq. DIPEA.

Entry	DIPEA Loading / eq.	Temp. / °C	Residence Time / min	RHP GC Yield / %	4PBO GC Conversion / %	Selectivity Estimate ^a / %
1	1.2	250	20	26 ± 2	77 ± 7	34
2	2	250	30	28 ± 3	95 ± 1	29
3	2	200	30	31 ± 3	68 ± 3	46
4	1.2	250	20	21 ± 1	85 ± 1	25
5	1	250	30	26 ± 2	96 ± 1	27
6	2	200	30	22 ± 2	63 ± 3	35

^aSelectivity estimate calculated from the ratio of product yield/limiting reagent conversion (expressed as a percentage), not accounting for the associated uncertainties, hence described as estimate.

Using 0.005 mol% Pd(OAc)₂, at 250 °C, results were comparable when using 1 or 2 eq. DIPEA at 20 and 30 min residence times (Table 4.4.7, Entries 1, 2, 4 and 5). Using a 0.005 mol% Pd(OAc)₂ loading with 1 or 2 eq. DIPEA, but at 200 °C (Table 4.4.7, Entries 3 and 6) compared to 250 °C (Table 4.4.7, Entries 2 and 5), yields of RHP were similar, but conversions lower – indicating an improved selectivity at 200 °C. Furthermore, at 200 °C, the observed selectivity towards RHP was greater using 2 eq. DIPEA (Table 4.4.8 Entries 3 and 6). These observations would support using 200 °C (over 250 °C) and (at this temperature) using 2 eq. (over 1 eq.) DIPEA. Moreover, the ratio of the GC peak areas of the products suggest relatively lower amounts (when compared with the desired RHP) of reduced enone (RE) and homo-coupled product (HC) at 200 °C *c.f.* 250 °C (Table 4.4.8, compare Entries 1 and 2 with 3 and 4). These GC peak area ratios also suggested the formation of *more* standard Heck product (SH) at 200 °C with 1 eq. DIPEA (Table 4.4.8, compare Entries 1 and 2 with 3), but a lower amount of SH upon using 2 eq. DIPEA (Table 4.4.8, Entries 3 and 4).

Table 4.4.8 supplementary GC data to **Table 4.4.7** comparing relative ratios of GC peak areas, showing how at 250 °C with a 30 min residence time where conversion was >95%, more of the suspected direct enone reduction product was observed when using 1 eq. DIPEA. Entries in this table correspond to the Entries in **Table 4.4.7** where 30 min residence times were applied.

Entry	Temperature / °C	DIPEA Loading / eq.	RE/RHP*	SH/RHP*	HC/RHP*
1	250	1	0.90	0.58	0.02
2	250	2	0.70	0.58	0.06
3	200	1	0.49	0.93	0.003
4	200	2	0.32	0.63	0.003

***RE** = directly reduced enone product, **SH** = standard Heck product, **HC** = homo-coupled product. Ratios are ratios of the respective GC peak areas. Note that as GC response factors were not determined for the side-products, the ratio does **not** represent the relative molar amounts between products in any one reaction but allow for a comparison of amounts of side-products between reactions.

It therefore appeared that conducting reactions at 200 °C resulted in greater selectivity towards the desired **RHP**, perhaps by reducing the amount of **RE** which formed (**Table 4.4.8**). The next set of reactions also employed 200 °C as the reaction temperature in an attempt to increase selectivity. Using 2 eq. DIPEA appeared to possibly favour selectivity towards the desired reductively coupled product. For the next investigation, an increased (whilst still a so-called “homeopathic”^{112–114}) Pd(OAc)₂ loading of 0.05 mol% was employed, at 200 °C. Again, a 1 or 2 eq. addition of DIPEA was used for comparison. The hypothesis here was that increasing the Pd loading may have resulted in achieving good conversions in shorter timescales and to determine what the effect of increased Pd loading (and by extension a lower DIPEA/Pd ratio) would be on the reaction selectivity.

Table 4.4.9 investigation of the effect of employing higher (yet still low) 0.05 mol% Pd loadings on the outcome of the RHR, at shorter residence times, highlighting how good conversions could be observed in short processing times.

Entry	Pd(OAc) ₂ Loading / mol%	DIPEA Loading / eq.	Temp. / °C	Residence Time / min	RHP GC Yield / %	4PBO GC Conversion / %	Selectivity Estimate ^a / %
1	0.05	2	200	1	12 ± 1	29 ± 2	41
2	0.05	2	200	2.5	34 ± 2	65 ± 1	52
3	0.05	2	200	5	51 ± 1	84 ± 1	61
4	0.05	2	200	10	52 ± 2	95 ± 1	55
5	0.05	1	250	10	26 ± 1	99 ± 1	26
6	0.05	2	250	10	35 ± 1	96 ± 1	36
7	0.005	2	200	30	31 ± 3	68 ± 3	46
8	0.005	2	250	30	28 ± 3	95 ± 1	29

^aSelectivity estimate calculated from the ratio of product yield/limiting reagent conversion (expressed as a percentage), not accounting for the associated uncertainties, hence described as estimate.

Using a 0.05 mol% Pd(OAc)₂ loading, reactions were observed to have gone to almost completion in only a 10 min residence time, with a modest yield of around 52% using 2 eq. DIPEA (Table 4.4.9, Entry 4). Reactions were also performed at 250 °C, for comparison, and under analogous conditions (10 min, 0.05 mol% Pd, Table 4.4.9, Entry 6) a yield of only 35%, also at around full conversion, was observed, indicating the previously noted improved selectivity at lower temperature. At 200 °C and residence times <10 min, conversions were lower (Table 4.4.9, Entries 1-3). Compared to reactions at 0.005 mol% Pd loading (Table 4.4.7 and reiterated in Table 4.4.8, Entries 7 and 8), reactions with 0.05 mol% Pd loading occurred much quicker, perhaps with better selectivity with greater observed yields.

An analysis of further GC data (Table 4.4.10) suggests that the higher Pd loading resulted not only in quicker reaction times and higher yields but also suppressed formation of the undesired RE and SH products (Table 4.4.10, Entries 1 and 4). Analogous to findings shown in Table 4.4.8, it appeared that reactions at 200 °C (compared to 250 °C) also resulted in lesser formation of the undesired RE product and SH product (Table 4.4.10, Entries 1 and 2). Again, using 1 eq. DIPEA in place of 2 eq. DIPEA, here at 250 °C, a relatively greater amount of RE product apparently was being formed (Table 4.4.10, Entries 2 and 3). These observations would further suggest the application of lower temperature (200 °C) and higher amounts of DIPEA (at least 2 eq.) may be beneficial to the process.

Table 4.4.10 supplementary GC data to **Table 4.4.9** comparing relative ratios of GC peak areas, showing how 200 °C processing temperature appeared to suppress formation of the directly reduced enone product, with using 2 eq. DIPEA instead of 1 eq. DIPEA apparently also giving a similar observation. Entries 1-3 correspond to Entries 4, 6 and 5 in **Table 4.4.9**, respectively, and Entries 4 and 5 are reproduced from **Table 4.4.8**.

Entry	Pd(OAc) ₂ Loading / mol%	Temp. / °C	Residence Time / min	DIPEA Loading / eq.	RE/RHP	SH/RHP	HC/RHP
1	0.05	200	10	2	0.22	0.31	0.12
2	0.05	250	10	2	0.68	0.61	0.10
3	0.05	250	10	1	0.92	0.49	0.06
4	0.005	200	30	2	0.32	0.63	0.003
5	0.005	250	30	2	0.70	0.58	0.06

***RE** = directly reduced enone product, **SH** = standard Heck product, **HC** = homo-coupled product. Ratios are ratios of the respective GC peak areas. Note that as GC response factors were not determined for the side-products, the ratio does **not** represent the relative molar amounts between products in any one reaction but allow for a comparison of amounts of side-products between reactions.

To summarise the findings of the experiments described in **Table 4.4.7** to **Table 4.4.10**, a 0.05 mol% loading appeared to significantly reduce the required residence time from 30 min to 10 min and resulted in better reaction selectivity. Using 2 eq. DIPEA appeared to make the reaction more selective towards the desired **RHP**, perhaps by reducing the amount of undesired **RE** product forming. Reactions at 200 °C also appeared to be more selective towards the desired **RHP** than reactions at 250 °C. Despite these observations and achieving excellent conversion (>95%) in a short 10 min residence time at 200 °C in flow, a moderate yield of only around 50% still indicated selectivity issues for the process (**Table 4.4.9**, Entry 4). With the previous observations, however, a few further hypotheses were drawn.

It was considered that 200 °C was likely to be the optimal temperature for allowing enhanced reaction rates, but with the possibility of being able to improve reaction selectivity, as at temperatures greater than this, direct enone reduction appeared to occur efficiently. With the observation that 2 eq. DIPEA appeared beneficial over 1 eq. DIPEA, even unexpectedly appearing to inhibit direct enone reduction as was observed here, it was decided next to perform reactions using a greater amount of DIPEA in the flow reactor to determine whether this would further improve selectivity. In the original publication reporting this reaction, the authors used 5 eq. DIPEA but the lowest loading of Pd used was 0.5 mol%. Therefore, using a 10-fold reduction in Pd here, it was initially considered that 5 eq. DIPEA might have resulted in too high a DIPEA/Pd ratio for an efficient reaction (perhaps with DIPEA outcompeting the reaction substrates for Pd binding),¹⁶⁹ but based on previous experimental observations made here, it was considered this might not be the case. For the experiments to test whether a higher amount of DIPEA could improve the reaction selectivity, it was decided to (approximately) double the DIPEA loading from 2 eq. to 3.8 eq., as the volume used for this loading would correspond to 50% of the volume of NMP added.

To test this, reactions were conducted using a maximum residence time of 10 min, 3.8 eq. DIPEA and 0.05 mol% Pd(OAc)₂ loading.

Table 4.4.11 application of a higher (3.8 eq.) DIPEA loading to the RHR demonstrating an improved reaction selectivity towards the desired reductively coupled product.

Entry	DIPEA Loading / eq.	Residence Time / min	RHP GC Yield / %	4PBO GC Conversion / %	Selectivity Estimate ^a / %
1	2	5	51 ± 1	84 ± 1	61
2	2	10	52 ± 2	95 ± 1	55
3	3.8	5	58 ± 1	87 ± 1	67
4	3.8	10	61 ± 1	91 ± 1	67

^aSelectivity estimate calculated from the ratio of product yield/limiting reagent conversion (expressed as a percentage), not accounting for the associated uncertainties, hence described as estimate.

Using 3.8 eq. DIPEA at both 5 min and 10 min residence time, with conversions at around 90%, yields of around 60% were observed (Table 4.4.11, Entries 3 and 4). Whilst conversions were similar using either 2 eq. or 3.8 eq. DIPEA, yields were apparently slightly higher when using 3.8 eq. DIPEA (Table 4.4.11, compare Entries 1 with 3 and 2 with 4). As such, surveying the temperature, catalyst loading and added DIPEA amount in flow had now led to conditions where reasonable yields could be obtained, using so-called “homeopathic”^{112–114} Pd loadings (0.05 mol%). Compared to the initial publication, the lowest Pd(OAc)₂ loading used was 0.5 mol%, requiring a 12 h reaction time to achieve a yield of ~60%.¹⁴⁸ As such, using a flow reactor, a comparable yield could be obtained in a much shorter processing time with a 10-fold reduction in Pd demand.

In the original publication from de Vries, Reek and co-workers, their highest reported yield using Pd(OAc)₂ as the catalyst was around 75% and required a loading of 1-3 mol% to achieve this, in a 3-6 h reaction time. Yields of >80% were observed, but required N-heterocyclic carbene ligands.¹⁴⁸ With this, the next steps taken were to determine whether further adaptations to the process might result in a further improved selectivity, with the aim of achieving yields of desired RHP of ~75% or greater to determine whether any further benefits of performing the reaction in flow could be shown.

It was considered that, as the modest yields obtained were apparently due to competing reaction pathways, using either of the starting substrates in a slightly larger excess might have resulted in observing better yield/selectivity towards the desired RHP. This was hypothesised to “allow” for sacrificial competing reactions leading to the observed side-products, whilst still leaving excess material present for the desired Reductive Heck pathway. This was investigated using a 2 eq. excess of either starting material, and reactions repeated under analogous conditions to those used previously (0.05 mol% Pd(OAc)₂, 5 min residence time, 3.8 eq. DIPEA at 200 °C).

Table 4.4.12 final optimisation reactions using an excess of either coupling partner, showing how an excess of either resulted in good yields of >70%.

Entry	4PBO Eq.	4IA Eq.	Time / min	RHP GC Yield / %	Lim. Reagent Conversion / %	Selectivity Estimate ^a / %	RE/RHP ^b	SH/RHP ^b	HC/RHP ^b
1	1	1.2	5	58 ± 1	87 ± 1	67	0.22	0.30	0.16
2	1	1.2	10	61 ± 1	91 ± 1	67	0.21	0.32	0.11
3	1	2	5	75 ± 3	95 ± 1	79	0.18	0.31	0.06
4	1	2	10	73 ± 1	98 ± 1	74	0.17	0.30	0.13
5	2	1	5	71 ± 3	92 ± 1	77	0.30	0.39	0.003
6	2	1	10	70 ± 2	90 ± 2	78	0.33	0.40	0.003

^aSelectivity estimate calculated from the ratio of product yield/limiting reagent conversion (expressed as a percentage), not accounting for the associated uncertainties, hence described as estimate.

^bRatios are those of the respective GC peak areas. Note that as GC response factors were not determined for the side-products, the ratio does **not** represent the relative molar amounts between products in any one reaction but allow for a comparison of amounts of side-products between reactions.

Upon adding **4IA** in 2 eq. rather than 1.2 eq. (previously employed), a notable increase in reaction yield was observed (Table 4.4.12, Entries 1-4). Whereas a maximum yield of ~60% (Table 4.4.11) had so far been observed in the work performed here (similar to the yield observed in the original report at the lowest applied Pd loading),¹⁴⁸ a yield of ~75% was observed here when adding a further excess of **4IA** (Table 4.4.12, Entries 3 and 4). When reactions were performed using **4IA** as the limiting reagent along with 2 eq. of **4PBO**, selectivity towards the desired **RHP** was also observed to increase with yields of around 70% being observed (Table 4.4.12, Entries 5 and 6).

Here, the ratios of the GC FID responses for the major side-products against those of the desired **RHP** were compared. Note that these ratios do not provide *quantitative* insights into the reaction outcomes as no calibration for the side-products was performed. However, the ratios do allow for a comparison of *relative amounts* of side-products being formed under different conditions. For example, on increasing the **4IA** excess to 2 equivalents, it was observed that the *relative ratio* of directly reduced **4PBO** (**RE**) to desired **RHP** *decreased* upon adding further excess of **4IA** and the *relative ratio* of traditional Heck Reaction product to desired **RHP** remained the same. Therefore, it could be reasoned that the addition of further excess of **4IA** resulted in suppression of **4PBO** reduction, resulting in an observed greater selectivity towards the desired **RHP**. Upon changing **4IA** to become the limiting reagent with 2 equivalents of **4PBO**, a negligible amount of homocoupling was observed to occur. The *relative ratio* of **4PBO** reduction product and traditional Heck Reaction product were both observed to

increase, however, here the **4PBO** reduction would not influence the maximum obtainable yield of desired **RHP** (unless the direct reduction was efficient enough to consume **4PBO** to the point that it became the limiting reagent).

With this, the observations had demonstrated the optimisation of a flow RHR process, whereby good yield of ~75% was observed at >95% conversion. High temperature (200 °C) was applied easily with the use of a flow reactor, allowing for using a very low 0.05 mol% loading of simple Pd(OAc)₂, to achieve these results in short reaction timescales (5-10 min). These findings represent further developments in improving RHR processes, specifically for the methodology adapted here involving RHRs of enones, initially described by Reek, de Vries, Minnaard and co-workers.¹⁴⁸

4.5 Conclusions & Further Work

A procedure for homogeneous RHRs was identified and developed into a flow process for the construction of C(sp²)-C(sp³) bonds. The transfer to a flow process was straightforward due to the homogeneous mixture.¹⁴⁸ Despite this, realising the associated benefits initially targeted from exploiting flow processing were not as straightforward. The aim was to determine whether novel processing windows (high temperature and pressure) accessible in flow could allow for benefits to the reaction procedure, such as accelerated rates and a reduction in Pd requirement. Under a number of the conditions surveyed in flow, however, poor reaction selectivity was observed, with notable amounts of traditional Heck Reaction products forming, as well as observing direct reduction of the enone starting material, presumably by the Pd(OAc)₂/DIPEA reductive system – in what, to our knowledge, constitutes identification of a new reaction pathway.

Selectivity issues were able to be overcome by optimising temperature, Pd loading and added amount of DIPEA. Optimal conditions allowed for a so-called “*homeopathic*”^{112–114} Pd loading of 0.05 mol% (10-fold less than the lowest loading used in the initial publication)¹⁴⁸ to be applied, along with 3.8 eq. DIPEA as the hydride donor whilst observing good yields. Processing temperature was found to be key, for example, in **Table 4.4.9**, a ~30% yield was observed at 250 °C and a ~50% yield was observed at 200 °C, at similar conversion (90%), employing 2 eq. DIPEA. Yields were able to be improved upon from this observed ~50% yield at 200 °C, by (as mentioned) employing 3.8 eq. of DIPEA in the reaction, alongside an excess of *either* coupling partner, with observed yields of >70% at >90% conversion (**Table 4.4.12**). As such, a flow process operating efficiently in short timescales with good selectivity for the desired reductively coupled product was developed.

For further work, an investigation into RHRs beyond that of just enones with aryl halides in flow would be interesting, as there are a number of ways to achieve Reductive Heck conditions. This may broaden the scope of performing such reactions for the formation of new C(sp²)-C(sp³) bonds in continuous flow and allow for such methodologies to be exploited in the synthesis of *e.g.*, natural products or pharmaceuticals. Furthermore, whilst it has been demonstrated here that Pd loadings can be significantly reduced by exploiting high temperatures in flow, perhaps other RHR conditions may be more amenable to even higher temperature processing (whilst avoiding *e.g.*, enone reduction as observed using this methodology), allowing for further reductions in Pd demands.

Furthermore, an exploration of the Pd(OAc)₂/DIPEA high temperature system for a means of enone C=C reduction warrants further investigation to determine whether this can constitute an efficient synthetic methodology.

Photocatalysed C-O Coupling Reactions

Flow Ir/Ni and Ir/Cu Reaction Processes

Chapter 5

Photocatalysed C-O Bond Synthesis in Continuous Flow:
Ir/Ni-Catalysed C-O Coupling

5.1 Abstract

An Ir/Ni dual catalytic approach to alkyl-aryl etherification, previously reported by MacMillan and co-workers,¹⁷⁰ was adapted and developed into a flow process. With K₂CO₃ as a base (insoluble in the MeCN reaction solvent) and quinuclidine, presumed by the authors to be a reductive quencher, the reaction was not initially suited towards processing in flow, due to the heterogeneous conditions. Therefore, a screen of organic bases was conducted in batch and *N,N,N',N'*-tetramethyl guanidine was found to give good yields in short timescales, whilst remaining soluble throughout the reaction. Moreover, this appeared suitable to replace both K₂CO₃ as a base *and* quinuclidine as an electron donor (presuming a reductive quenching cycle of the Ir photocatalyst). Yields were observed to reach ~80% in only 2 h, using this adapted methodology (with a similar performance under comparable conditions for the procedure described by MacMillan *et al.*).¹⁷⁰ Having developed reaction conditions suited to flow processing, a simple flow photoreactor was constructed, based upon an FEP coil design, making use of in-house built blue LEDs (410 nm, coined “Lightsabre”, described in the Experimental Chapter). This was applied to investigate whether the possible benefits of flow photochemistry (*e.g.*, improved light penetration, heat transfer, *etc.*) could result in an improved process for the Ir/Ni-catalysed C-O coupling. Using the reactor, it was observed that (relative to the initial publication) Ir loadings could be decreased by 10-fold (1 mol% to 0.1 mol%), Ni loadings decreased by 5-fold (5 mol% to 1 mol%), and solvent requirement decreased by 2-fold or 4-fold whilst observing good yields (>90%) in short residence times (up to 10 min). Scale-up was demonstrated *via* a numbering-up approach (2 identical FEP coils wrapped around one Lightsabre) and *via* a dimensioning approach (using an FEP coil with doubled dimensions relative to the originally employed coil). In doing so, productivities of a model coupling product were observed to approach 200 g day⁻¹.

5.2 Strategy & General Aims

The remit for the work presented in Chapters 5-7 was to combine Ir or Ru photocatalytic approaches towards C-O bond forming reactions with continuous flow technologies. Hence, within the remit of the entire work of this Thesis, the work presented was to involve PGM catalysis in organic synthesis, here, using photochemistry, with flow reactors. Therefore, the broad aims of the work in this Chapter focus on the development and assessment of continuous flow processes for photocatalytic C-O bond forming reactions. Specifically, some of the key aims involved were as follows:

- To identify relevant reactions suitable for development or adaptation into a continuous flow process.
- To develop conditions from the identified reactions amenable to flow processing.
- To determine whether flow technology could possibly allow for scalable processing.
- To determine whether continuous flow technology can lead to processing benefits *e.g.*, decreasing reaction time, lowering of catalyst loading, improved productivity.

With the above aims in mind, the following strategy was adopted for the work in this Chapter.

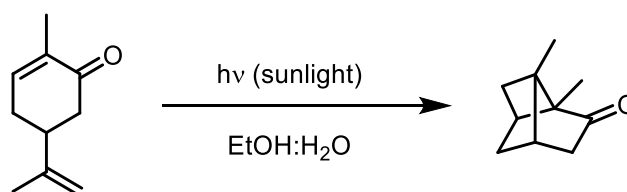
- To perform a screen of conditions in batch for an identified Ir/Ni-catalysed C-O coupling reaction to determine whether the reaction could be performed homogeneously.
- To acquire/construct a suitable reactor for performing continuous flow photoreactions.

- To use the reactor to determine whether flow chemistry could offer advantages such as short reaction times and reduced catalyst loadings.
- To determine whether the flow process developed, and any associated benefits, appeared scalable.

5.3 Introduction

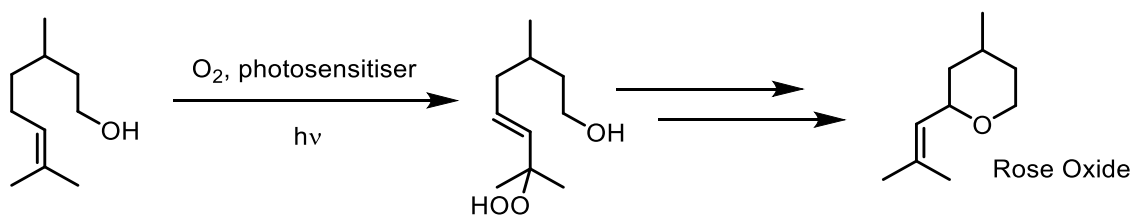
5.3.1 Photochemistry and Photoredox Catalysis

Photochemistry concerns the interaction of light with matter and the chemical changes which follow, with “light” usually referring to the visible and ultraviolet (UV) regions of the electromagnetic (EM) spectrum.^{12,171} Synthetic photochemistry represents the application of photochemistry toward organic molecules. The origins of which can be traced to Ciamician and Silber who were working at the University of Bologna. They demonstrated, for example, the isomerisation of carvone to carvonecamphor under solar irradiation (**Scheme 5.3.1**).¹⁷²



Scheme 5.3.1 solar photochemical [2+2] intramolecular isomerisation of carvone to carvonecamphor, as observed by Ciamician and Silber.¹⁷²

Recognising the possible benefits of organic photochemistry, Ciamician’s vision of “forests of glass tubes” for the future factories of chemical manufacturing emerged.¹⁷³ Photochemistry has become recognised as a powerful strategy in synthetic chemistry. For example, towards Ciamician’s vision, the photo-oxidation of citronellol (**Scheme 5.3.2**), has been used as a step in the synthesis of rose oxide - a commercial fragrance.¹⁷⁴



Scheme 5.3.2 photo-oxidation of citronellol, in the synthesis of a fragrant molecule, rose oxide.¹⁷⁴

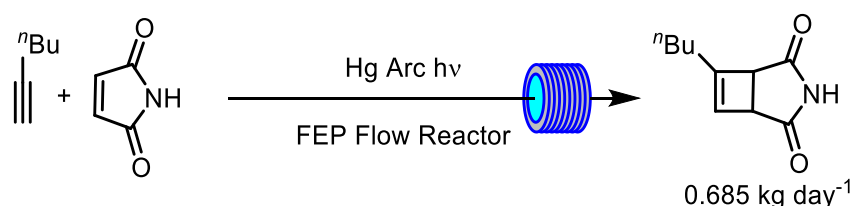
Synthetic photochemistry is attractive for chemical processing, meeting some of the principles of Green Chemistry. For example, photochemistry can prevent waste (with photons being a “traceless” reagent), and photocatalysis can employ catalytic reagents under mild reaction conditions.^{11,12,171,175,176} However, there are issues with scale-up in batch, relating to light penetration,^{10,11} shown by the Beer-Lambert Law.

$$A = \epsilon Cl$$

Eqn 5.1 the Beer-Lambert Law for determining the light absorbance of a substrate as a function of its concentration, A = absorbance ($\log_{10}(I_0/I_T)$), ϵ = molar extinction coefficient, C = concentration of solute and l = path length of irradiation. In the equation for absorbance, I_0 = intensity of incident light, I_T = intensity of transmitted light.¹⁷¹

A large-scale batch solution presents an extremely long path length, meaning that, in the Beer-Lambert equation (**Eqn 5.1**), absorbance will be very high because l is very long, leading to inefficient irradiation.¹⁰ Flow reactors offer certain benefits for enabling synthetic photochemistry. Primarily, the issue which arises due to the Beer-Lambert Law is alleviated as narrow-channel tubing can be used in a flow reactor. Moreover, due to the continual pumping of reagents through the reactor, flow chemistry lends itself well to reactions with low concentrations as they can be processed quickly. Also, issues related to over-irradiation in photochemical reactions can be somewhat avoided, due to the products leaving the reactor after their formation.¹⁰

Interest in applying flow reactors to organic photochemistry followed the development of the Booker-Milburn continuous flow Fluorinated Ethylene-Propylene (FEP) UV photochemistry reactor.¹⁷⁷ This was demonstrated on [2+2] cycloaddition reactions, involving a Hg UV lamp placed within an immersion well (to allow cooling), with FEP tubing wrapped around the immersion well and a pump to flow reagent solution around the tubing. This was also shown to be scalable, producing 0.685 kg day⁻¹ of a cycloadduct of maleimide and 1-hexyne (**Scheme 5.3.3**).¹⁷⁷



Scheme 5.3.3 photochemical [2+2] cycloaddition reaction performed in a continuous flow FEP tubing reactor, allowing for high productivities to be realised.¹⁷⁷

5.3.2 Photoredox Catalysis

An important area of organic photochemistry exploiting visible light is photoredox catalysis, pioneered by Yoon, Stephenson and MacMillan. This exploits that a species in an electronically excited state is both a better oxidant (itself more likely to be reduced, accepting an electron) *and* a better reductant (itself more likely to be oxidised, losing an electron).¹⁷⁸ Often, Ru- or Ir-polypyridyl complexes are used as photocatalysts, although complexes based on other transition metals or organic photocatalysts are available.¹⁷⁸⁻¹⁸⁰

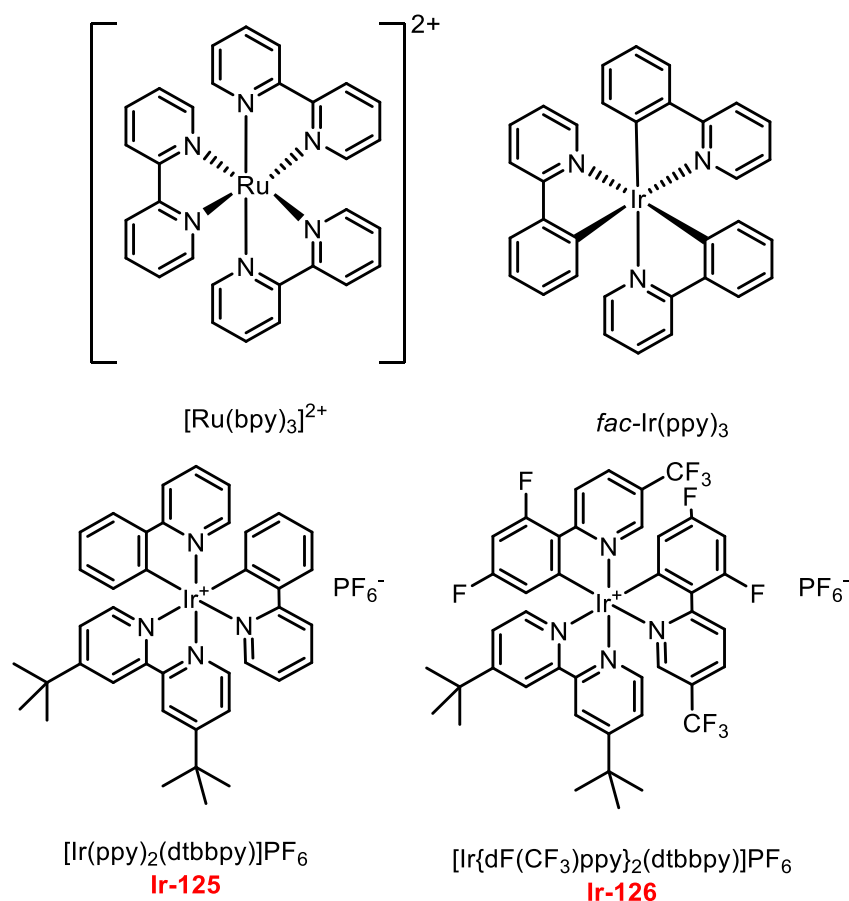


Fig 5.3.1 structures of two prototypical Ru/Ir-polypyridyl photoredox catalysts and Ir-125 and Ir-126, the catalysts used in this work.

[Ru(bpy)₃]²⁺ and [Ir(ppy)₃]³⁺ are commonly used metal-polypyridyl photocatalysts, Ir-125 and Ir-126 were the photocatalysts of interest in this Chapter and Chapters 6 and 7 (**Fig 5.3.1**). Metal-polypyridyls are typically useful for a number of reasons.^{178–180} Firstly, the π* (mainly ligand-centred molecular orbital) level is observed to have an energy *in between* those of the (mainly metal centred) t_{2g} and e_g d-orbital levels (**Fig 5.3.2**).¹⁷⁹ As such, upon photoexcitation, an electron is transferred from the lower energy d-orbitals, to the π* level in a metal-to-ligand charge transfer (MLCT) transition.^{178–181} Due to the presence of heavy metals in the complexes, spin-orbit coupling is typically efficient and, whilst the singlet MLCT (¹MLCT) state forms initially, this quickly undergoes intersystem crossing (ISC) to the triplet MLCT state (³MLCT) (**Fig 5.3.2**).^{182,183} The ³MLCT state is relatively long-lived,^{178–180} and is a better oxidant/reductant than the ground state complex, so has a tendency to accept or lose an electron (in turn, generating another highly oxidising/reducing complex).¹⁷⁸ For example, if a photoexcited Ir^{III*} species undergoes reductive quenching to Ir^{II}, the Ir^{II} species will typically be a strong reductant – itself being oxidised back to Ir^{III}. Also, the MLCT state also involves a spatial separation of the electron from the metal centre.¹⁸⁴ This, along with the long-lived nature of the ³MLCT state means that the strongly oxidising/reducing photocatalysts can exist for long enough to encounter other species in solution, thereby allowing for electron transfers to occur between them.¹⁷⁹

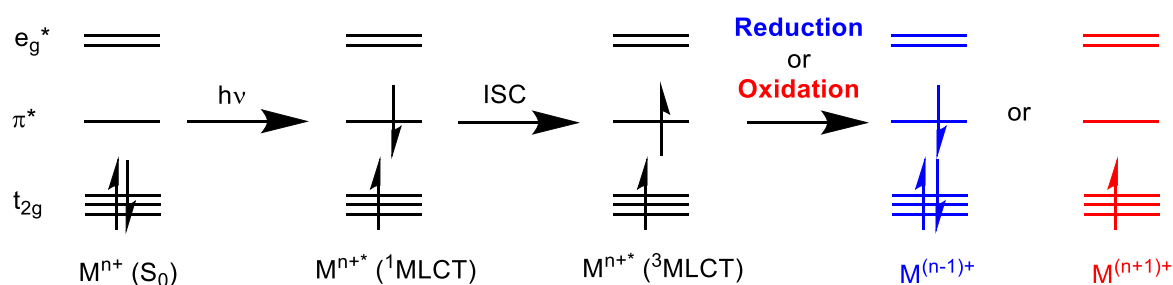


Fig 5.3.2 simplified depiction of the absorption of light (followed by rapid intersystem crossing) in a Ru/Ir-polypyridyl photocatalyst, followed by the possibility of either reduction or oxidation of the photoexcited catalyst.

Should the $^3\text{MLCT}$ state complex encounter and undergo an electron transfer with another species in solution, the excited complex will be reductively quenched (the excited photocatalyst is reduced) or oxidatively quenched (the excited photocatalyst is oxidised), **Fig 5.3.3**.¹⁷⁹ This typically generates a highly reactive radical species from the quenching substrate, which facilitates further reactivity. Importantly, requiring only visible light and usually under ambient conditions, a very mild way to impart high reactivity is afforded by this approach.^{178–181} Common reductive quenchers are amines and common oxidative quenchers include dinitro-/dicyano-benzenes, aryldiazonium salts, viologens and polyhalomethanes.¹⁷⁹

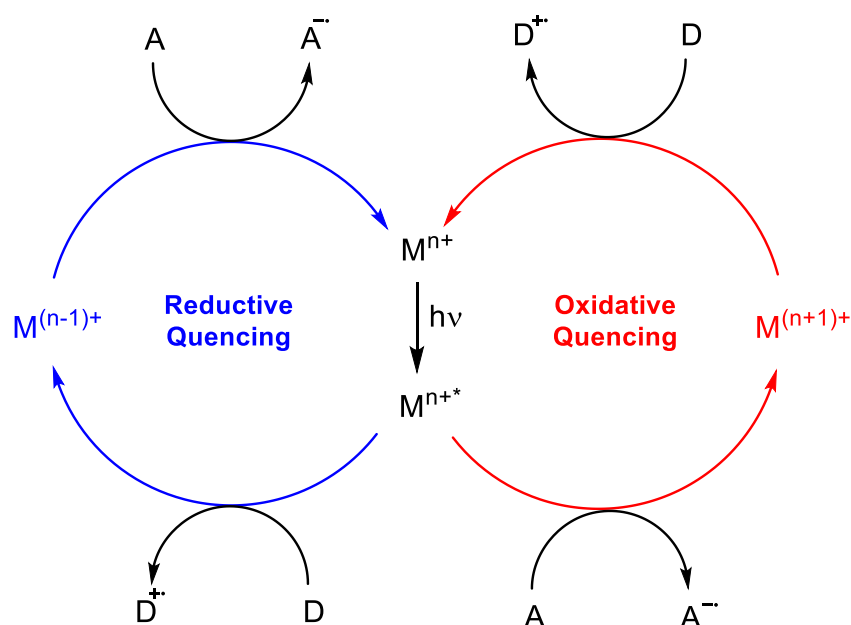


Fig 5.3.3 a generic cycle illustrating the two means by which Ru/Ir-polypyridyl complexes can promote photoredox reactions. A = electron acceptor, D = electron donor.

For photoredox catalysts (based on Ru/Ir-polypyridyls), it is possible to tune the catalytic activity by changing the metal centre, or the ligands.^{180,184} Typically, the optoelectronic properties are important *i.e.* absorption wavelength and redox potentials.¹⁸⁴ For *ground state* Ru^{II}/Ir^{III}-polypyridyls (both d^6), it can be considered that the oxidation is a metal-centred oxidation, and the reduction is a ligand centred reduction.¹⁸⁰ Therefore, a stronger electron donating ligand makes the oxidation more favourable, whereas a stronger electron withdrawing ligand makes the oxidation less favourable (due to the

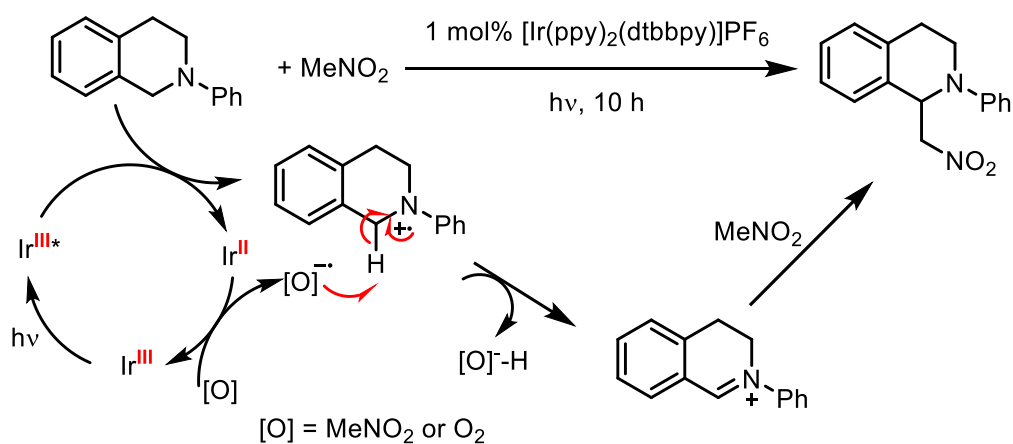
electron density on the metal).¹⁸⁰ Considering the reduction potential *e.g.* Ru^{III}/Ru^{II}, a *more positive reduction potential* means that *reduction is more favourable* (conversely, a less positive reduction potential means that the reverse oxidation process of the reduction being considered is more favourable). For [Ru(bpy)₃]²⁺, the Ru^{III}/Ru^{II} reduction potential is 1.26 V (though this can vary based on solvent, reference electrode *etc.*).¹⁸⁰ For Ru(bpy)(pz)₂, where pz is an electron donating anionic pyrazolo ligand, the Ru^{III}/Ru^{II} reduction potential is 0.30 V *i.e.* less positive (meaning the Ru^{II}/Ru^{III} *oxidation* is more favourable) than for the corresponding reduction potential for [Ru(bpy)₃]²⁺.¹⁸⁰ For [Ru(bpz)₃]²⁺, where bpz is a strongly π-accepting bipyrazine ligand, the Ru^{III}/Ru^{II} reduction potential is 1.86 V *i.e.* more positive (meaning the Ru^{III}/Ru^{II} *reduction* is more favourable) than for the corresponding reduction potential for [Ru(bpy)₃]²⁺.¹⁸⁰

Comparing Ir- and Ru-polypyridyl complexes, which are typically d⁶ octahedral complexes of Ir^{III} or Ru^{II}, Ir^{III} complexes (being 3+ at the Ir centre) are less electron dense, hence more difficult to oxidise than corresponding Ru^{II} (being 2+ at the Ru centre and hence more electron dense) complexes.¹⁸⁴ For example, [Ru(bpy)₃]²⁺ (in MeOH, vs. SCE) has a Ru^{III}/Ru^{II} reduction potential of 1.31 V, whereas [Ir(bpy)₃]³⁺, under analogous conditions, has an Ir^{III}/Ir^{II} reduction potential of 1.93 V *i.e.* more positive than that of the corresponding Ru complex, hence the Ir^{III}/Ir^{II} reduction is more favourable, and Ru(II)/Ru(III) oxidation is more favourable.¹⁸⁴ Such reduction potentials for the ground states can be measured experimentally, for excited states, these are typically calculated from the ground state reduction potential as well as spectroscopic data (the zero-zero excitation energy E_{0,0}, which is the energy difference between the ³MLCT excited state and ground state, estimated from the emission maximum).^{180,184} Whilst the ground state considerations are therefore helpful in considering excited state redox properties, adjusting ligands/metal centres in such complexes will also necessarily influence the spectroscopic properties. Typically, Ir complexes experience smaller Stokes shifts than Ru complexes (*i.e.* Ir complexes have a larger E_{0,0}) and this usually makes corresponding Ir complexes both stronger reductants and oxidants than Ru complexes, often favourable for photoredox reactions.^{180,184}

Following photoexcitation of the catalyst to the ³MLCT state, the complex can undergo electron transfer (as mentioned), or energy transfer *via* Dexter transfer (through bonds, considered as two simultaneous electron transfers between an energy donor and energy acceptor, requiring orbital overlap *i.e.* a short-range process).¹⁸⁴ Alternatively, Förster energy transfer can achieve the same outcome (through space, *via* a non-radiative coupling between transition moment dipoles of the energy donor and acceptor, requiring overlap of donor emission spectrum and acceptor absorption spectrum, operable over longer distances).¹⁸⁴ Such processes have useful applications in synthetic chemistry but, for true photoredox reactions, electron transfer occurs to quench the excited photocatalyst. Dexter energy transfer, involving a two-electron transfer, has a much greater distance dependency than single electron transfer. However, as single electron transfer leads to new charge distributions/geometries in products, there is an associated reorganisation energy for the molecule and the associated solvent.¹⁸⁴

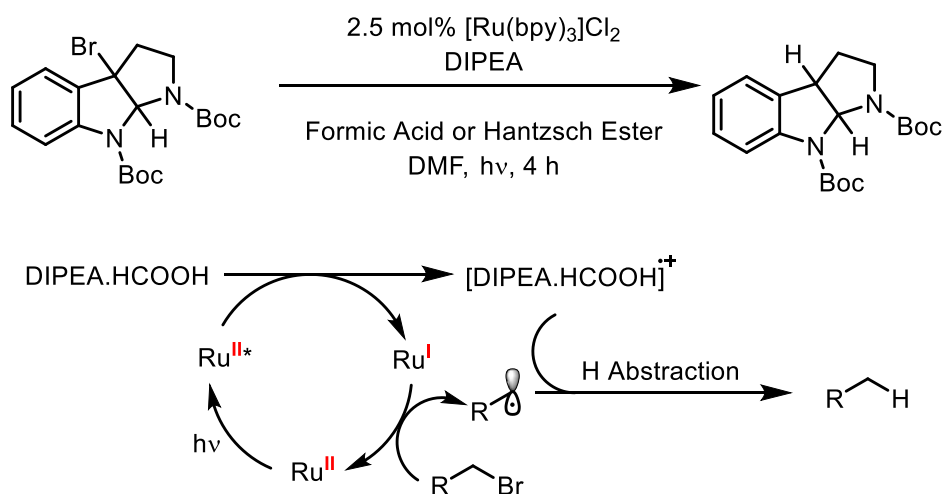
Typical electron donors (therefore participating in a reductive quenching cycle) are amines, whereby upon donating an electron to the ³MLCT state complex, an amine radical cation forms.¹⁸⁵ The amine can simply be a sacrificial donor not engaged further, or can itself be a reaction substrate. For example, the amine radical cation can engage in back electron transfer (reforming the original amine), hydrogen transfer (generating an electrophilic iminium ion which can be attacked by a nucleophile, *via* loss of a H-atom), deprotonation (to give an α-amino radical which is nucleophilic so can attack *e.g.*, an electron

deficient alkene, or, lose an electron to form an iminium ion) or C-C cleavage, if a C-C bond is present in the α -position to the N-atom, generating an alkyl radical and iminium ion.¹⁸⁵ Such reactivity has been exploited, for example, by Stephenson in an aza-Henry Reaction (**Scheme 5.3.4**).¹⁸⁶



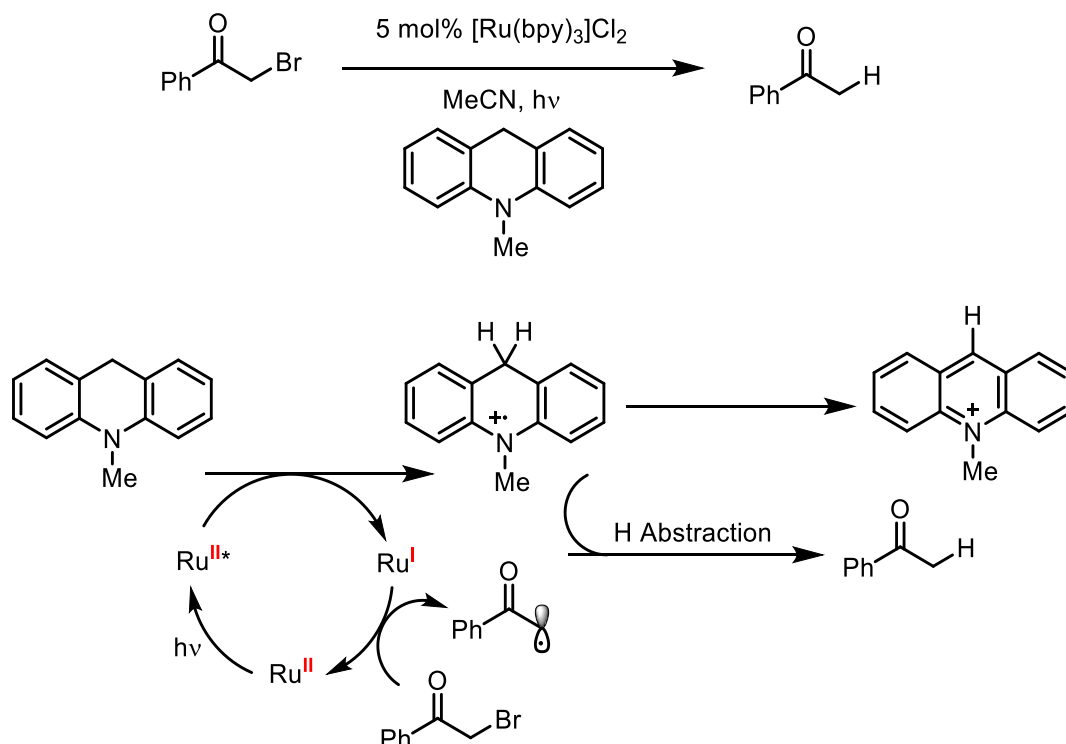
Scheme 5.3.4 aza-Henry reaction developed by Stephenson and co-workers and mechanistic proposal involving amine oxidation and iminium formation via H-atom abstraction.¹⁸⁶

Other photoredox reactions that have been developed include reductive dehalogenation reactions, where a C-X bond is reduced to a C-H bond. An example from the Stephenson Group of reductive dehalogenation (**Scheme 5.3.5**) was developed for the replacement of toxic organotin reagents with photoredox catalysts and was found to be useful for the dehalogenation of C-Br and C-Cl units. In this example, an amine was also used and was proposed to act as an electron donor for the photocatalyst and a H-atom source.¹⁸⁷



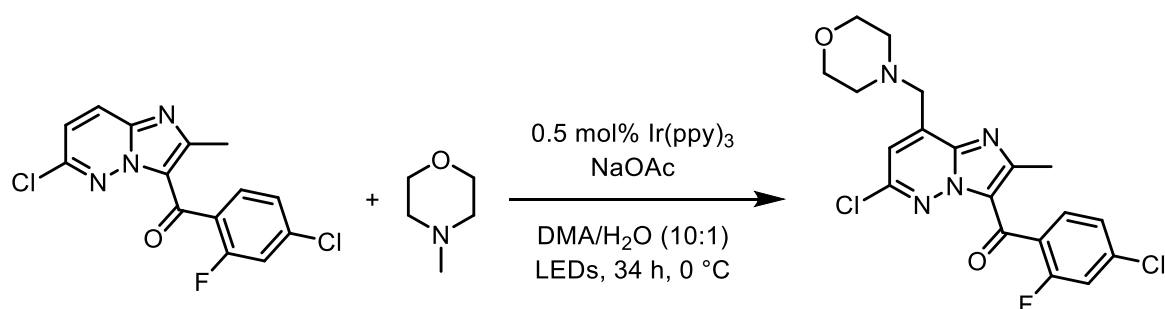
Scheme 5.3.5 reductive dehalogenation and proposed mechanism using photoredox catalysis, developed by Stephenson and co-workers.¹⁸⁷

In an early example of the use of photoredox catalysis, Fukuzumi demonstrated a similar approach for the reductive dehalogenation of phenacyl bromides (**Scheme 5.3.6**).¹⁸⁸



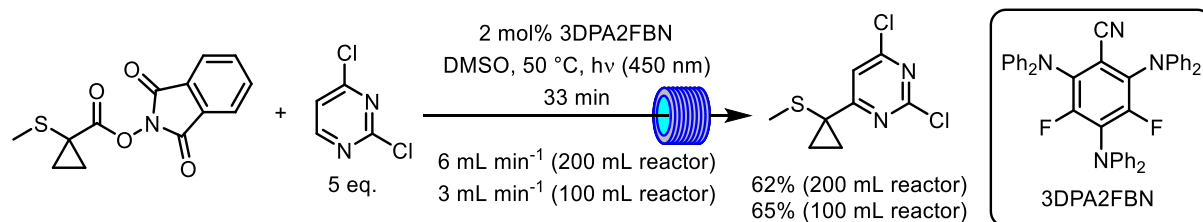
Scheme 5.3.6 reductive dehalogenation of phenacyl bromides developed by Fukuzumi.¹⁸⁸

Photoredox reactions have also been applied to pharmaceutical preparation, due to the attractiveness for applying in synthetic process chemistry. An example from the Stephenson Group, in collaboration with Eli Lilly, demonstrated the preparation of an intermediate en route to a pharmaceutical intermediate. They employed photoredox catalysis for the coupling of N-methyl morpholine with a pyridazine, involving an α -amino C-H arylation reaction with $\text{Ir}(\text{ppy})_3$ as the photoredox catalyst (**Scheme 5.3.7**).¹⁸⁹



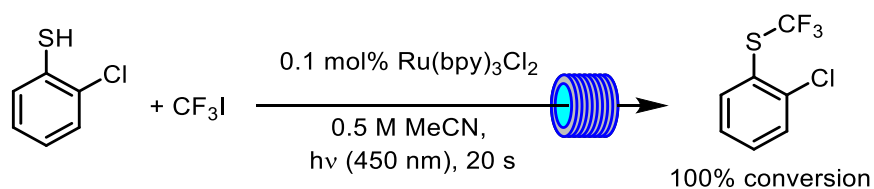
Scheme 5.3.7 a photoredox catalysis approach towards the preparation of a synthetically important intermediate as demonstrated by Stephenson in collaboration with Eli Lilly.¹⁸⁹

Continuous flow approaches towards pharmaceutical target molecules have also been reported. For example, a flow photoredox Minisci Reaction (radical substitution of an aromatic compound) for the synthesis of Ceralasertib was disclosed by researchers from AstraZeneca and Asymchem (**Scheme 5.3.8**).¹⁹⁰ This was used to decarboxylatively couple a redox-active N-hydroxy phthalimide ester (discussed in Chapter 6) to a dichloropyrimidine and, using a flow reactor, they were able to observe yields of up to ~60%. The authors anticipated that, in a larger volume reactor, productivities of around 6.6 kg day^{-1} might be achieved.¹⁹⁰



Scheme 5.3.8 continuous flow photoredox Minisci Reaction for the synthesis of Ceralasertib, a cancer treatment.¹⁹⁰

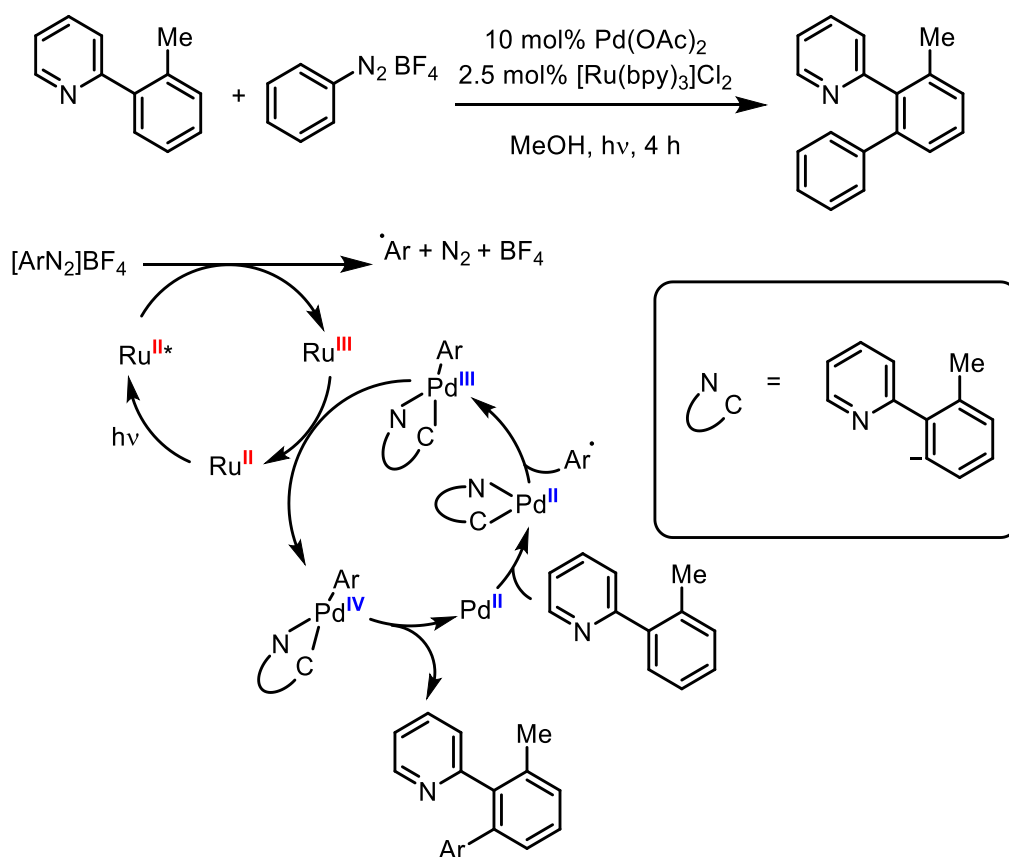
Researchers from AbbVie and Asymchem have also reported the development of a scalable flow photoredox process for trifluoromethylation of a thiophenol (**Scheme 5.3.9**).¹⁹¹ Using 450 nm LEDs as a light source in a plug-flow reactor (as well as demonstrating the use of a laser-irradiated continuously stirred tank reactor), the authors reported full conversion in only 20 s irradiation. They also reported the scale-up of the process, producing >500 kg of the desired intermediate.¹⁹¹



Scheme 5.3.9 scalable continuous trifluoromethylation of a thiophenol, producing >500 kg product.¹⁹¹

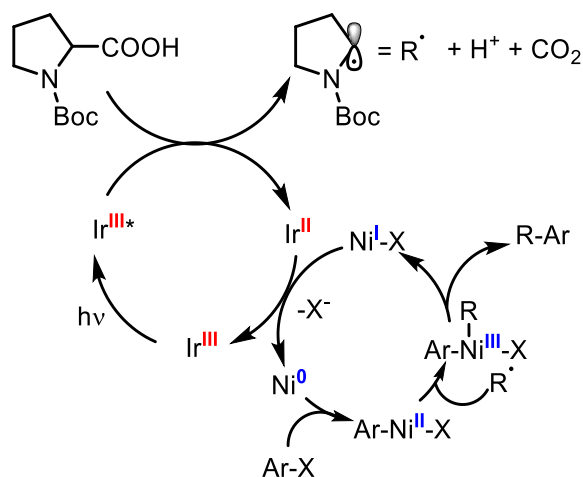
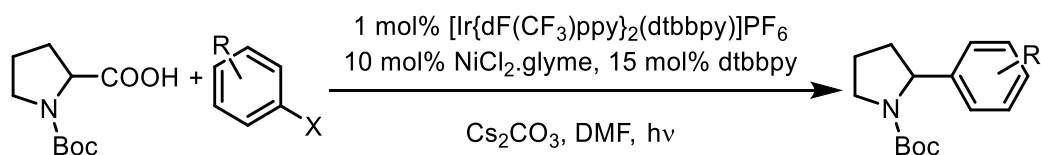
5.3.3 Dual Metallaphotoredox Catalysis

One area of photoredox catalysis that has attracted much interest is dual metallaphotoredox catalysis,¹⁷⁸ where a photoredox catalyst is employed alongside another transition metal catalyst. This is central to the work in Chapters 5-7. Conventionally, organometallic-mediated coupling reactions involve two-electron redox events in the catalytic cycles. Single electron transfer events, facilitated by photoredox catalysis, allow for otherwise elusive pathways to occur using organometallic catalysts.¹⁷⁸ This can involve a direct single electron transfer between the two catalytic species, oxidative/reductive generation of a radical coupling partner by the photocatalyst that can then be intercepted by the organometallic catalyst, or, by oxidative/reductive generation of a radical species by the photocatalyst which then undergoes a single electron transfer with the organometallic catalyst.¹⁷⁸ An early example was developed by Sanford and co-workers, for C-H arylation (**Scheme 5.3.10**). This approach used dual photoredox/Pd-catalysis, for coupling an aryl diazonium salt (as a proposed radical precursor) with an arene functionalised with a directing group.¹⁹²



Scheme 5.3.10 dual Ru/Pd metallaphotoredox procedure for directed C-H arylation developed by Sanford and co-workers.¹⁹²

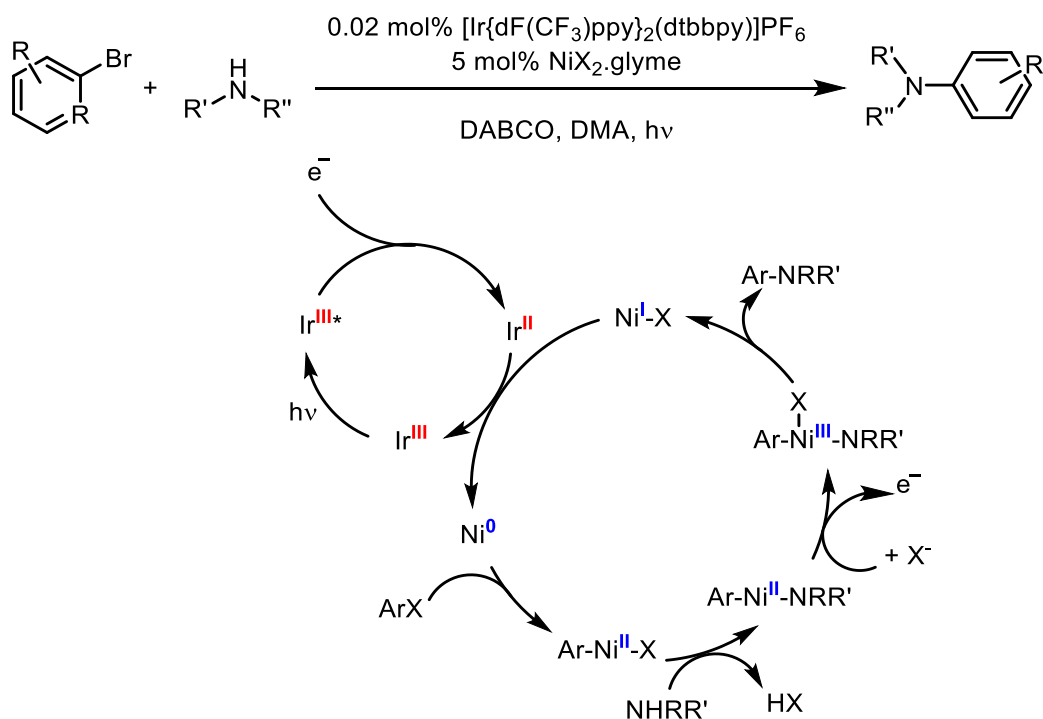
Dual Ir/Ni-catalysis has been found to be particularly useful, due to the propensity of Ni to undergo single electron transfers.¹⁹³ MacMillan and Doyle developed approaches to C-C coupling using this approach, *via* a carboxylic acid radical precursor or tertiary amine radical precursor (**Scheme 5.3.11**). The mechanistic proposal involved reductive quenching (Ir^{III}/Ir^{II}) of the Ir photocatalyst by the electron donor radical precursors to generate a C-radical. The Ni catalyst was proposed to undergo a conventional Ni⁰/Ni^{II} oxidative addition with an aryl bromide, before interception of the C-radical to give a Ni^{III} species, observed to then undergo Ni^{III}/Ni^I reductive elimination, furnishing the C-C coupled product. Following this, reduction of Ni^I back to Ni⁰ by the Ir^{II} intermediate (regenerating Ir^{III}) was proposed.¹⁹⁴



Scheme 5.3.11 procedure and mechanistic proposal for a dual Ir/Ni metallaphotoredox C-C coupling reaction using carboxylic acids as radical precursors, developed by Doyle and MacMillan.¹⁹⁴

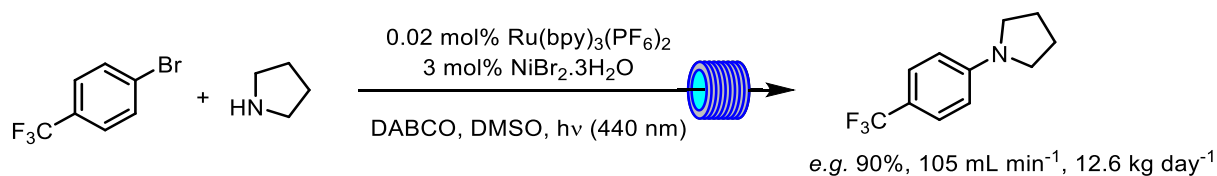
Such C-C couplings have been extended to involve enantioselective variants, as well as the incorporation of other radical precursors, for example, trifluoroborate salts and aryl bromides, facilitated by silyl radical activation.¹⁷⁸

Other developments involving Ir/Ni metallaphotoredox catalysis led to C-X coupling reactions. For example MacMillan has also developed a C-O coupling protocol¹⁷⁰ (the focus of this Chapter) as well as a C-N coupling protocol in collaboration with Buchwald and Merck (**Scheme 5.3.12**).¹⁷⁸



Scheme 5.3.12 dual metallaphotoredox Ir/Ni arene amination protocol developed by MacMillan, Buchwald and Merck and mechanistic proposal highlighting the modulation of the Ni oxidation state by the photoredox catalyst.¹⁹⁵

Notably, a similar C-N Ir/Ni-catalysed photoredox reaction has been reported by researchers at Merck to be scaled-up, using a flow reactor (**Scheme 5.3.13**).¹⁹⁶ Reaction productivities of 12.6 kg day⁻¹ were observed (at 90% yield) and up to 43.4 kg day⁻¹, but at a reduced 42% yield for the C-N coupling. This was achieved using a large-scale flow reactor employing 30 x 100 W LEDs in a large volume (up to 725 mL) tubular reactor.¹⁹⁶



Scheme 5.3.13 continuous flow process developed for large-scale aryl amination using Ir/Ni metallaphotoredox catalysis.¹⁹⁶

5.3.4 C-O Bond Forming Reactions in Organic Synthesis

As noted, an Ir/Ni C-O coupling reaction reported by MacMillan forms the central theme of this Chapter. C-O bonds are found in ethers, common structural motifs in a number of important commercial chemicals (**Fig 5.3.4**).¹⁹⁷ Other C-O bonds are found in alcohols, esters, acetals and hemi-acetals (amongst others),¹⁹⁸ but it is etherification reactions which are of interest here. Particularly, due to the prevalence in important commercial chemicals, C-O bond formation in the preparation of alkyl-aryl ethers is of primary interest to the work presented in this Chapter.

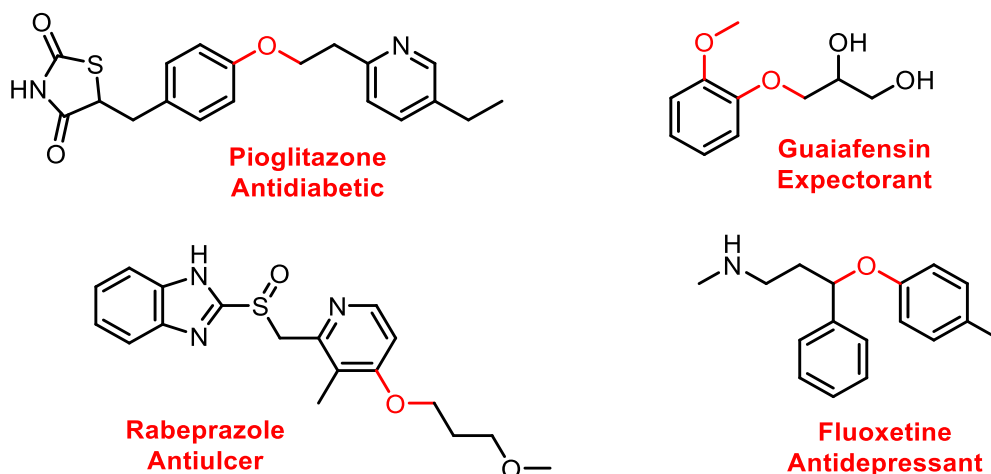


Fig 5.3.4 some pharmaceuticals containing alkyl-aryl ether units (red).

5.3.4.1 Bimolecular Alcohol Dehydration

This is perhaps the simplest approach for ether formation. An alcohol is heated in the presence of sulfuric acid, resulting in alcohol acidification followed by displacement by a second alcohol molecule to furnish the ether product (Scheme 5.3.14).¹⁹⁹

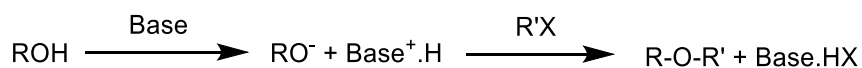


Scheme 5.3.14 general scheme for an acid-catalysed bimolecular alcohol dehydration to furnish simple symmetrical ethers.

This approach is limited to homo-etherification of small primary alcohols (to give symmetric ethers) and competes with elimination reactions (*i.e.*, alkene formation). For secondary and tertiary alcohols, elimination predominates. As such, this is a limited synthetic method. If unsymmetrical ethers are attempted to be synthesised (*i.e.* from two different alcohols) a product mixture will be obtained of the desired unsymmetrical ether, and the two symmetrical ethers of each individual alcohol.¹⁹⁹

5.3.4.2 Williamson Ether Synthesis

The Williamson Ether Synthesis (Scheme 5.3.15) involves a simple S_N2 mechanism.¹⁹⁸ This typically involves heating an alcohol (and base to generate an alkoxide nucleophile) and alkylating agent (such as a halide or *pseudo*-halide) at reflux.¹⁹⁹ Therefore, this is a simple approach towards ether formation.



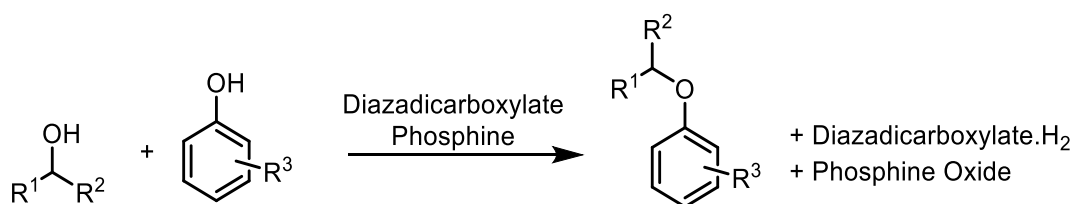
Scheme 5.3.15 general scheme for a Williamson Ether Synthesis.

The Williamson Synthesis is therefore a widely used approach, however, it is not without drawbacks. For example, base-catalysed elimination reactions often compete and for phenol etherification reactions, C-alkylation competes with O-alkylation after the phenoxide anion has formed. Base-catalysed elimination predominates for tertiary alkylating agents and is highly competitive with

secondary alkylating agents but S_N2 predominates for primary alkylating agents.^{198,199} Therefore, despite the simplicity, the Williamson Ether Synthesis is not always a suitable approach.

5.3.4.3 Mitsunobu Reaction

The Mitsunobu Reaction (**Scheme 5.3.16**) is a versatile reaction that can be used for the formation of products other than just ethers.^{199,200} It involves a dehydrative coupling of an alcohol with a reasonably acidic pronucleophile (*i.e.* becomes the nucleophile after deprotonation, such as a carboxylic acid or imine). To obtain an alkyl-aryl ether product, a phenol would be used as the nucleophile. To achieve this coupling, the Mitsunobu Reaction employs an azodicarboxylate (oxidant) and a phosphine (reductant), requiring mild conditions.²⁰⁰

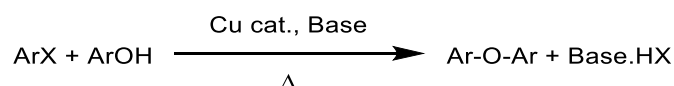


Scheme 5.3.16 general scheme for a Mitsunobu Reaction for preparing alkyl-aryl ethers.

The mechanism is relatively complex and can lead to complications in practical preparations of the reaction. Another major drawback of the Mitsunobu approach for ether synthesis (and in general) is the waste generated from the phosphine and azodicarboxylate coupling system.²⁰⁰ However, work for example from Denton and co-workers has looked towards developing a catalytic Mitsunobu Reaction, generating less waste, which could alleviate the drawback associated with the stoichiometric waste.²⁰¹

5.3.4.4 Ullmann Reaction

The Ullmann Reaction (**Scheme 5.3.17**) is a Cu-catalysed approach with two variants. The classic Ullmann Reaction can be used for the homo-coupling of aryl halides (producing a biaryl) using Cu-catalysis (or Pd or Ni).²⁰² The variant of this reaction of interest here is an Ullmann Reaction where a nucleophile and base are also employed along with the aryl halide and Cu catalyst. A phenol can be employed as the nucleophilic coupling partner in this variant and the Ullmann Reaction can therefore be used for production of biaryl ethers.^{199,203}



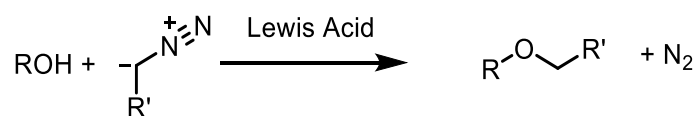
Scheme 5.3.17 general scheme for an Ullmann Coupling for synthesising diaryl ethers.

Issues with the Ullmann approach to biaryl ethers include harsh reaction conditions and that the effectiveness of the Cu catalyst is often highly dependent on the nature of the substrates, solvents and bases selected, *i.e.* the approach is not very general.^{199,203}

5.3.4.5 Diazoalkane Reagents

Diazoalkane reagents (*e.g.*, diazomethane) can be protonated by acidic reagents. For example, a carboxylic acid will protonate diazomethane to give a carboxylate anion and diazonium cation. Following this, transfer of the methyl group from the diazonium to the carboxylate anion affords a

methyl ester and N₂.²⁰⁴ A similar approach using an alcohol or phenol in place of a carboxylic acid leads to etherification (**Scheme 5.3.18**), however, a Lewis Acid catalyst (*e.g.* BF₃.OEt₂) is required to make the alcohol sufficiently acidic that it can protonate a diazoalkane.^{205,206}



Scheme 5.3.18 *general scheme for short chain diazoalkane etherification reactions.*

A major drawback of this approach is that diazoalkane reagents are explosive, particularly diazomethane. Specialised lab equipment and techniques are required for small scale experiments and scale-up of such dangerous conditions are undesirable and problematic. Furthermore, the approach is only useful for short chain primary and unhindered secondary diazoalkane reagents, limiting the synthetic utility.^{205,206}

5.3.4.6 Buchwald-Hartwig C-O Coupling Reaction

The classical Buchwald-Hartwig reaction involves the Pd-catalysed reaction between an aryl halide and an amine, for the amination of arenes in a C-N coupling reaction. The C-O coupling variant (**Scheme 5.3.19**) of this reaction employs an alcohol in place of the amine for the preparation of alkyl-aryl ethers.^{197,207–209}



Scheme 5.3.19 *general scheme for the C-O variant of the Buchwald-Hartwig Coupling Reaction.*

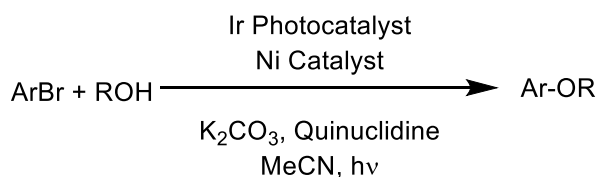
As a general approach, this reaction is very broad in scope and can be used for coupling aryl halides to primary,^{197,208} secondary,²⁰⁹ tertiary alcohols²¹⁰ and phenols.²¹¹ However, this broad scope is a result of extensive ligand developments for the Pd catalysts. For any particular transformation, therefore, there typically is required extensive development and screening of conditions, with many catalysts failing where they could have been expected to run smoothly.^{197,209} Along with this, a strong base (typically NaO^tBu) is required for the reaction, limiting substrate scope or enforcing the need for protecting groups in certain syntheses.²¹⁰ The reaction typically is much more efficient for activated (electron poor) aryl halides than it is for unactivated counterparts.^{197,209}

5.3.5 Photocatalytic Developments in C-O Bond Forming Alky-Aryl Etherification Reactions

A number of approaches to C-O bond formation exist, but not without their drawbacks. These drawbacks range from significant (*e.g.* explosive reagents²⁰⁶) to problematic (*e.g.* time and labour-intensive work required to determine suitable conditions, such as in the Buchwald-Hartwig approach^{197,209}). Other drawbacks of certain reactions would imply that the specific methodology may not be at all suitable for providing the desired target (*e.g.* Williamson Synthesis where a tertiary alkylating agent is necessitated^{198,199}).

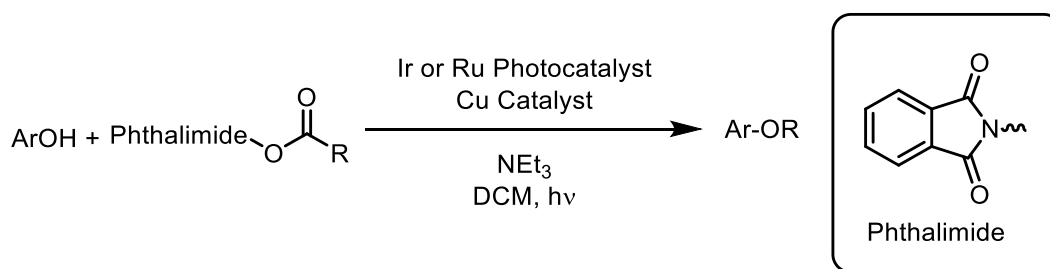
As photochemistry and photoredox catalysis has attracted much attention in the field of organic synthesis,^{178,212} it is unsurprising that some attention has been turned to photochemical alkyl-aryl etherification reactions.

In a seminal work from the MacMillan Group, coupling of aryl bromides with primary and secondary alcohols to give alkyl-aryl ethers (or water to give phenols) was accomplished using a dual-catalytic approach.¹⁷⁰ An Ir photocatalyst was used alongside a Ni co-catalyst (metallaphotoredox catalysis), where the authors proposed that the Ir photocatalyst undergoes electron transfer with the Ni co-catalyst in a photoredox mechanism (with an amine to mediate the electron transfer).¹⁷⁰ This work was of particular interest as traditionally, Ni-catalysis for such reactions is difficult due to a thermodynamically unfavourable reductive elimination from Ni^{II} to Ni⁰, required to furnish the alkyl-aryl ether product.^{170,213} In the presence of light and Ir photocatalyst, it could be possible that an electron transfer to give Ni^{III} could occur, whereby the reductive elimination (now from Ni^{III} to Ni^I) to give the alkyl-aryl ether product becomes thermodynamically favourable and can therefore allow the reaction to occur.¹⁷⁰ A plausible alternative pathway could involve energy transfer from the excited state Ir photocatalyst to the Ni intermediate, facilitating reductive elimination from the Ni^{II} intermediate by providing the energy from the excited state photocatalyst, with various other speculative pathways also feasible.^{214–217} Good functional group compatibility was demonstrated as well as the application to pharmaceutical-related products (N-protected fluoxetine), in good yield (82%).¹⁷⁰ The approach involved [Ir{dF(CF₃)ppy}₂(dtbbpy)]PF₆ (Ir-126) as the photocatalyst, NiCl₂.glyme with di-tert-butyl-2,2'-dipyridyl (dtbbpy) as a ligand with K₂CO₃ as a stoichiometric base and quinuclidine as an amine additive, in MeCN solvent (**Scheme 5.3.20**).¹⁷⁰



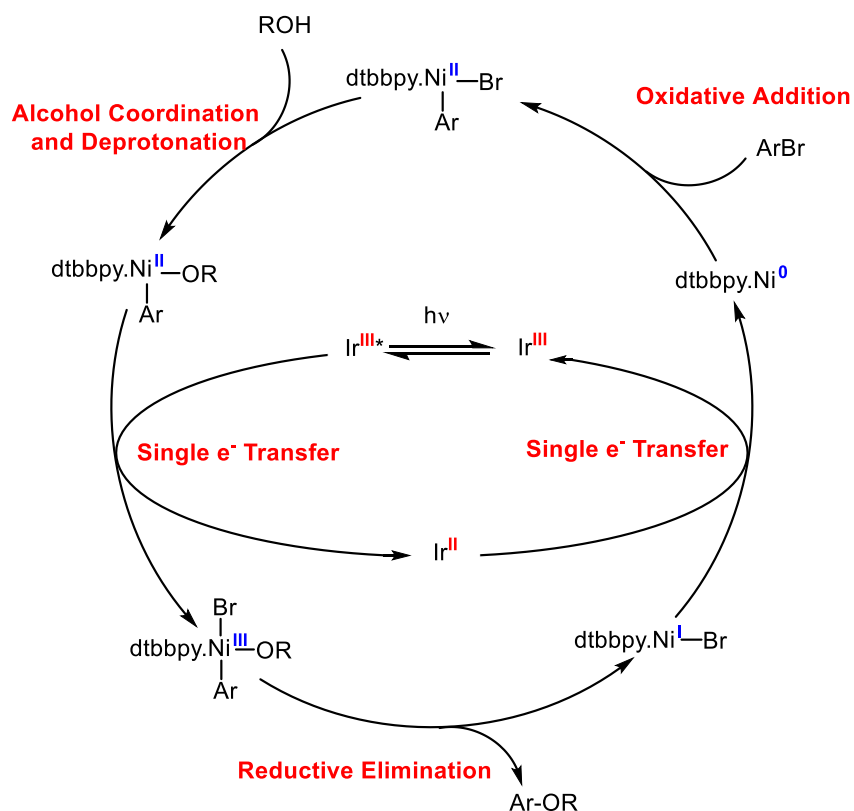
Scheme 5.3.20 dual Ir/Ni approach for alkyl-aryl ether formation developed by MacMillan and co-workers.¹⁷⁰

Another dual metallaphotocatalytic approach towards alkyl-aryl ether synthesis has been developed by Xile Hu and co-workers.²¹⁸ Their reaction considered the opposite retrosynthetic C-O bond disconnection to that of the MacMillan Group. That is, for the reaction developed by MacMillan and co-workers, the alkyl-aryl ether products relates to the starting materials *via* a disconnection between the O-atom and the C-atom of the aryl ring.¹⁷⁰ In the reaction developed by the Hu Group, the product relates to the starting materials *via* a disconnection between the O-atom and the alkyl chain.²¹⁸ To achieve this, they developed a decarboxylative approach (using N-hydroxy phthalimide esters, NHPI-esters, redox-active ester of the alkyl carboxylic acid) using phenols as starting materials with Ir/Ru-photocatalysis with a Cu co-catalyst (**Scheme 5.3.21**).²¹⁸ This reaction is the feature of Chapter 6 and is discussed further there.



Scheme 5.3.21 dual Ir or Ru with Cu approach for alkyl-aryl ether formation via decarboxylative coupling of a carboxylic acid derivative and a phenol.²¹⁸

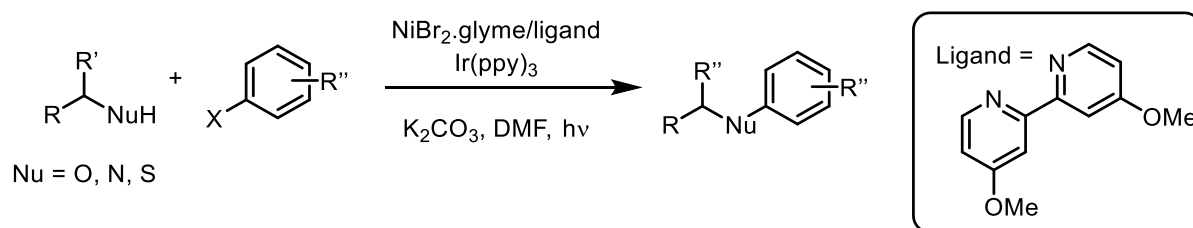
As with the MacMillan Group's approach, the mechanism is proposed to involve photoredox catalysis *i.e.* transfer of an electron from the photocatalyst.²¹⁸ The likely mechanisms differ slightly however, in that the Ir/Ni approach is suggested to involve electron transfer with the Ni co-catalyst, mediating the Ni oxidation state between Ni^{II} and Ni^{III} (**Scheme 5.3.22**), the dual Cu-photocatalytic approach (employing a redox-active ester) can be considered to generate an alkyl radical *via* electron transfer to the redox-active ester, furnishing the radical *via* N-O bond homolysis followed by decarboxylation.^{170,214,215,218} This radical could then be proposed to coordinate to the Cu^I photocatalyst, where a coupling catalytic cycle occurs.²¹⁸ Note – the mechanistic detail of such reactions is considered in more detail in Chapter 7 where the aims of the work within the Chapter were concerned with mechanistic studies of such reactions.



Scheme 5.3.22 possible cycle for photocatalysed alkyl-aryl ether syntheses proposed by MacMillan.¹⁷⁰

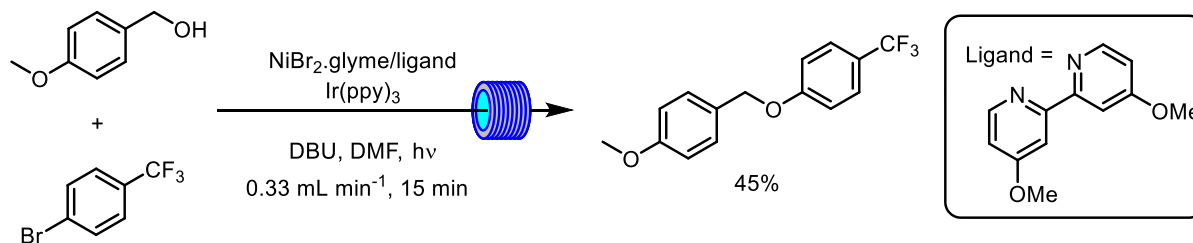
In a further development, Johannes and Escobar demonstrated a similar dual Ni-photocatalytic approach for the reaction of aryl halides (including chlorides and iodides as well as bromides) with

alcohols, as well as a variety of other nucleophiles including amines and thiols.²¹⁹ The authors used NiBr₂.glyme as a catalyst (as opposed to the NiCl₂ analogue used by MacMillan and co-workers) and Ir(ppy)₃ as a photocatalyst, in DMF solvent (**Scheme 5.3.23**).²¹⁹



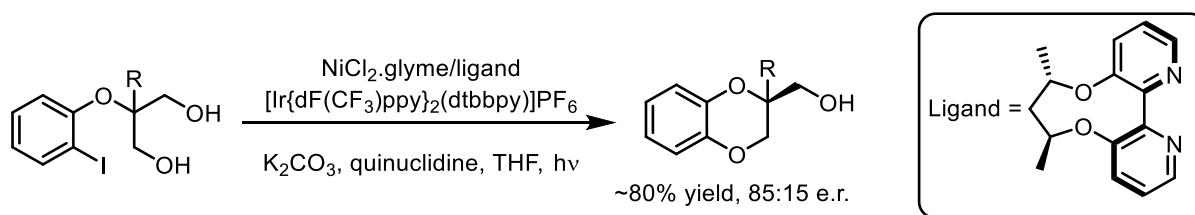
Scheme 5.3.23 unified methodology developed by Johannes and Escobar for the cross-coupling of aryl halides (X=I, Br, Cl) with various heteroatom nucleophiles.²¹⁹

The authors attempted a small number of conditions in a commercially available flow photochemical reactor (**Scheme 5.3.24**).²¹⁹ Despite their efforts, Johannes and Escobar noted the limitations of this reactor for their purposes, being prevented from accessing flow rates they desired for their reactions by the equipment used.²¹⁹ Furthermore, in the conditions they employed (where they replaced the insoluble K₂CO₃ with DBU as the base) the authors noted a drop in yield from 77% to 45%, when transferring to a flow process.²¹⁹ The authors themselves concluded that whilst they were able to scale-up somewhat their reaction, proper flow apparatus for demonstrating scale would be required to demonstrate the scope of such reactions and this Chapter explores, in greater depth, the possible advantages of performing scalable reactions in flow, for such chemistry.



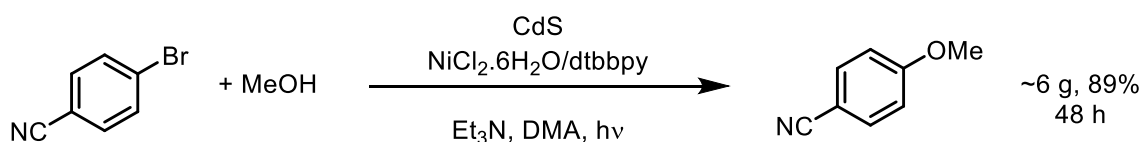
Scheme 5.3.24 flow approach to C-O coupling using Johannes and Escobar's methodology.²¹⁹

Wen-Jing Xiao and colleagues reported an elegant strategy for the enantioselective synthesis of chiral 1,4-benzodioxanes in another procedure adapted from that in the seminal work of MacMillan.²²⁰ Many such products display important biological activity and are motifs found in natural products and drugs. The Xiao Group adapted the MacMillan Ir/Ni reaction by using an axially chiral bipyridine ligand for Ni and THF as the solvent, with 2-(*o*-halophenoxy)-propane-1,3-diols as the reaction substrate (**Scheme 5.3.25**).²²⁰ Their approach was noted to give good yields, usually around 80%, for a variety of substrates, with enantiomeric ratios quoted typically around 85:15.²²⁰ Their work can be considered an example of how metallaphotoredox catalysis attracts interest for making synthetically useful products. Again, to achieve useful amounts, demonstrating scalability and any other processing benefits (as in this Thesis) would be of interest and could be achieved in flow.



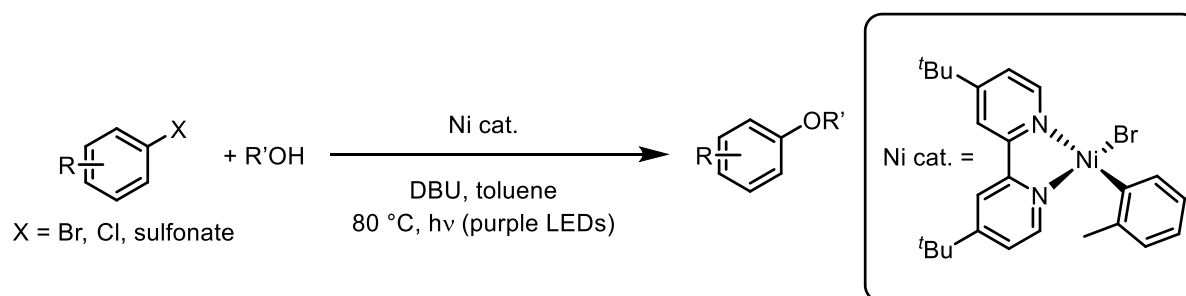
Scheme 5.3.25 *enantioselective procedure for the synthesis of 1,4-benzodioxanes, reported by the Wen-Jing Xiao Group.*²²⁰

Further reports from Wen-Jing Xiao and co-workers have focused on further modifications to the MacMillan C-O coupling reaction. The Xiao Group merged CdS visible light catalysis with Ni-catalysis to achieve a heterogeneously photocatalysed process.²²¹ $\text{NiCl}_2\cdot 6\text{H}_2\text{O}$ was used as the Ni catalyst in DMA solvent (**Scheme 5.3.26**).²²¹ The system was used for C-O coupling of aryl bromides with alcohols or water and also for C-N coupling with amines.^{219,221} Furthermore, this approach apparently eliminated the need for a ligand on the Ni catalyst, in some instances (whereas a bipyridine ligand, usually dtbbpy, has typically been used). Irradiation times of up to 48 h were required however, on a ~6 g scale in this batch process.²²¹



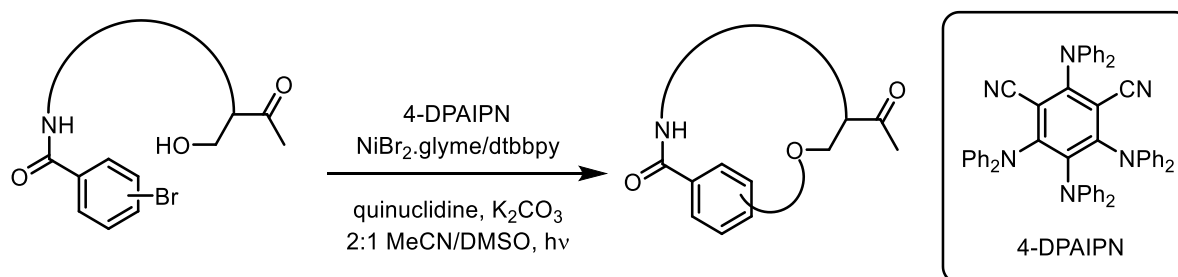
Scheme 5.3.26 *a heterogeneously photocatalysed reaction, scaled somewhat in batch, adopting methodology developed by Wen-Jing Xiao using CdS as a heterogeneous photocatalyst.*²²¹

The MacMillan style C-O coupling reaction has also been reported to occur *in the absence* of an Ir photocatalyst.^{222,223} Here, a Ni-arene catalyst has been synthesised and reported to, upon irradiation specifically with purple light (~390 nm), lead to C-O coupling between aryl halides (and *pseudo*-halides) and alcohols (**Scheme 5.3.27**).^{222,223} Light of any other wavelength was found to be much less effective. Aryl chlorides could be coupled, but many examples required 15 mol% catalyst loading, compared with 5 mol% for most aryl bromides/sulfonates.^{222,223} The authors proposed that irradiation at the required wavelength resulted in homolysis of the Ni-C bond between Ni and the arene ligand to generate a Ni^{I} species (with supporting evidence from EPR experiments). Upon oxidative addition of an aryl halide a Ni^{III} species would be produced, able to then undergo favourable reductive elimination (after alcohol coordination/deprotonation) to give an alkyl-aryl ether and return the Ni^{I} species, though continuous irradiation was required, possibly due to comproportionation of Ni^{I} and Ni^{III} species to give Ni^{II} species, requiring light to constantly regenerate the active $\text{Ni}^{\text{I}}/\text{Ni}^{\text{III}}$ cycle.^{222,223}



Scheme 5.3.27 Ir-free Ni photocatalytic approach towards alkyl-aryl ether formation exploiting specific wavelength purple light to generate catalytically active Niⁱ species.^{222,223}

Furthermore, dicyanobenzene-based organic photocatalysts have also been reported to be useful for C-O bond formation reactions.^{224,225} 4-DPAIPN and Ni dual-catalysis has been exploited by researchers at Merck for C-O coupling in peptides (**Scheme 5.3.28**).²²⁴ Using conditions analogous to those in the original work from MacMillan, the authors here were able to perform intermolecular C-O bond formation reactions, as well as intramolecular macrocyclization reactions on peptides.²²⁴



Scheme 5.3.28 organophotocatalytic adaptation of MacMillan's initial dual catalytic C-O coupling reaction, exploited for the macrocyclization of peptides by researchers at Merck.²²⁴

5.4 Results & Discussion

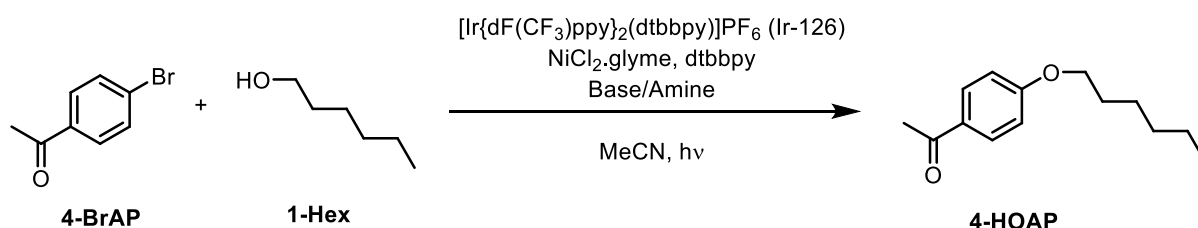
5.4.1 Determination of a Suitable Reaction to Investigate in Flow

The aim of the work in this Chapter was to develop a continuous flow process for a photocatalysed C-O bond forming reaction. As per the remit of this work, the primary aim was to determine whether performing such reactions using Ru/Ir photocatalysts, in continuous flow, could offer processing benefits towards such reactions and a means of scalability (which often pervades photochemical methodologies in batch).⁹⁻¹¹ Possible benefits targeted were faster processing times, greater energy efficiency (*via* improved photon capture), reduction in catalyst loadings *etc.* and the reasons for these aims were that conventional approaches to C-O bond forming reactions (often using thermal catalytic approaches) usually have several downfalls. These include long processing times, expensive catalyst systems, low functional group tolerance, amongst others (as discussed in the Introduction).

The two main candidates selected involved dual-catalytic systems, described previously in the Introduction.^{170,218} One of these candidates used Ir/Ni-catalysis to couple an aryl bromide with an alcohol (**Scheme 5.3.20**) to form alkyl-aryl ethers, commonly encountered in pharmaceuticals.¹⁷⁰ This was considered suitable due to previously published work demonstrating that the reaction occurs with good yields for a variety of alcohol and arene coupling partners, in batch.¹⁷⁰ Therefore, performing the reaction in flow may lead to a broadly applicable, scalable process. The second candidate identified was

a decarboxylative coupling of phenols with NHPI-esters, reported by Xile Hu and co-workers, described in the Introduction (**Scheme 5.3.21**).²¹⁸ This involved an Ir/Cu catalytic system, furnishing alkyl-aryl ethers and was also observed to be applicable for a range of substrates.²¹⁸

The MacMillan Coupling Reaction was investigated first, as the focus of this Chapter. To study this reaction, the same model substrates as used in the original MacMillan publication were used (**Scheme 5.4.1**). These were 4-bromoacetophenone (**4-BrAP**) and 1-hexanol (**1-Hex**), which couple to give product 4-hexyloxyacetophenone (**4-HOAP**), with Ir-126, $[\text{Ir}\{\text{dF}(\text{CF}_3)\text{ppy}\}_2(\text{dtbbpy})]\text{PF}_6$, as the photocatalyst - selected for ease of comparison to previously published work.¹⁷⁰ The reaction involving NHPI-esters and phenols as coupling partners was investigated in Chapter 6.



Scheme 5.4.1 representative reaction scheme for the model MacMillan Coupling Reaction conditions used in previously published work and in this work.¹⁷⁰

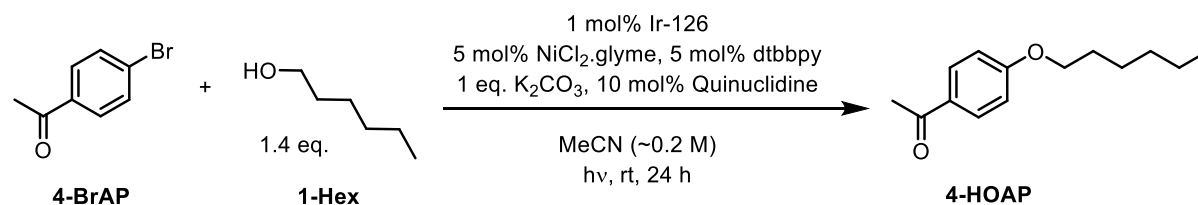
5.4.2 Initial Investigations in Batch to Determine Conditions Suited to Flow Processing

5.4.2.1 Literature Reproduction

The first problem was to develop conditions suitable for performing the reaction in flow. This was required because the reaction employed K_2CO_3 as an insoluble base in MeCN solvent (**Scheme 5.4.1**), which would result in blockages.¹⁷⁰ In batch, performing the reaction as a slurry would not be a problem (with sufficient mixing). Therefore, the first objective was to identify and screen conditions where insolubilities/precipitates were not present, before conducting investigations in flow.

This began by repeating previously reported conditions from MacMillan and co-workers to isolate the reaction product and determine whether their observations could be replicated using the apparatus available here. The MacMillan Group reported the use of (mainly) “blue LEDs” for their work, as well as using a 4 W fluorescent tube (white) light source with no significant difference in their reported yields between using the blue or white light sources.¹⁷⁰ Available for this work was a small scale, 3.5 W (at 1 A current) blue LED, with an emission maximum at 457 nm (see Experimental Chapter). This was used to replicate the previous literature, being deemed likely similar to the “blue LEDs”¹⁷⁰ used by the MacMillan Group.

Table 5.4.1 comparison of model MacMillan Coupling Reaction performed in this work using a 3.5 W 457 nm LED with the same reaction performed in previously published work.



Entry	Light Source	4-HOAP Yield / %	4-BrAP Conversion / %
1 (This Work)	3.5 W Blue LEDs (457 nm)	78 (Isolated)	>99*
2 (MacMillan) ¹⁷⁰	"Blue LEDs"	91	>99
3 (MacMillan) ¹⁷⁰	26 W Compact Fluorescent Lamp	86	>99

*No recovered 4-BrAP and not detected in ¹H NMR spectrum of crude reaction mixture.

As expected, K₂CO₃ was insoluble at the start of the reaction, and remained undissolved throughout. An isolated yield of 78% was observed, without recovery of any starting material (slightly lower to that reported by the MacMillan Group, **Table 5.4.1**). As such, it was confirmed that this set of conditions would *not* be readily suited for investigation in flow, due to the presence of insoluble species throughout the reaction process.

It was therefore determined that a screen of conditions in batch, to find conditions suited to flow processing, should be undertaken. It was noted that using the previously mentioned small scale 3.5 W blue LED would be inefficient for conducting a survey of numerous conditions as this could be used only for irradiating one reaction vessel at a time. Also available was a slightly larger white LED block (with 5 x 12 W white LED strips, see Experimental Chapter). This was suitable to possibly irradiate up to 4 reaction vessels on the scale being performed in this screen. To confirm this (and to confirm whether this light source worked for the reaction) four reactions using the original MacMillan conditions were performed at once. This was to determine whether irradiation across the LED block could be considered uniform enough for running four simultaneous reactions in a screen of conditions.

Table 5.4.2 comparison of 4 simultaneous model MacMillan Coupling Reactions, run using a white LED block illustrating a reasonable agreement in results for each position of irradiation across the block, Entries 4-7 (and comparison against other light sources from this work and previously published work, Entries 1-3).

Entry	Light Source	4-HOAP Isolated Yield / %	4-BrAP Conversion / %
1 (This Work)	3.5 W Blue LEDs (457 nm)	78	>99*
2 (MacMillan) ¹⁷⁰	"Blue LEDs"	91	>99
3 (MacMillan) ¹⁷⁰	26 W Compact Fluorescent Lamp	86	>99
4 (This Work)	Position 1 : 5 x 12 W White LEDs ^a	74	>99*
5 (This Work)	Position 2 : 5 x 12 W White LEDs ^a	71	>99*
6 (This Work)	Position 3 : 5 x 12 W White LEDs ^a	63	>99*
7 (This Work)	Position 4 : 5 x 12 W White LEDs ^a	67	>99*

*No recovered **4-BrAP**, or not detected in ¹H NMR spectrum of crude reaction mixture.

^aPositions 1 and 4 correspond to the edge of the LED block, positions 2 and 3 correspond to the centre of the LED block (see **Exp. Fig 9**).

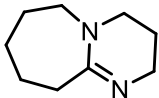
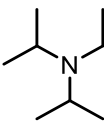
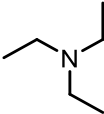
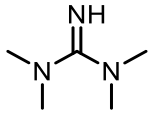
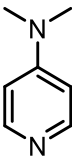
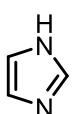
It was observed that across the 4 positions, observed yields were similar (all between 63% to 74%) and no starting material was recovered from any reaction (**Table 5.4.2** Entries 4-7). These were considered similar enough for employing the white LED block for a survey of conditions.

5.4.2.2 Screening of Organic Bases Towards Developing Homogeneous Conditions

It was decided that a base screen should be carried out to identify conditions suitable to flow processing (*i.e.*, homogeneous). As K₂CO₃ is a weak mineral base, it was considered that many organic bases (such as amines) might have been suitable replacements. The base in the reaction would presumably deprotonate the alcohol (or Ni-coordinated alcohol) to form a Ni-alkoxide intermediate, speculated to be present in the catalytic cycle (**Scheme 5.3.22**).¹⁷⁰ A mechanism whereby an O-centred radical forms *via* H-atom transfer with an oxidised amine could also be speculated, not requiring formal deprotonation.²¹⁶ MacMillan and co-workers also postulated that quinuclidine (an amine) acted as an "electron-shuttle", mediating Ni oxidation states after reductively quenching the Ir photocatalyst, also observing no reaction in the absence of quinuclidine.¹⁷⁰ As such, it was considered that should an alternative amine base be found, this might also be able to replace quinuclidine as a reductive quencher.

For this screen, 11 bases (**Table 5.4.3**) were initially selected to replace K₂CO₃ (listed further in this Section). These were based upon the criteria of having a basicity similar to K₂CO₃ and possibly being more soluble in MeCN (along with their respective salts).

Table 5.4.3 bases selected for a solvent screen to determine conditions amenable to flow processing.

Base	Structure	pKa*
1,8-Diazabicyclo[5.4.0]undec-7-ene DBU		12
1,4-Diazabicyclo[2.2.2]octane DABCO		8.82
Diisopropylethylamine DIPEA		10.75 ^a
Triethylamine TEA		10.75
Quinuclidine		11.0
1,1,3,3-Tetramethylguanidine TMG		13.6
Pyridine		5.2
4-Dimethylaminopyridine DMAP		9.2
Imidazole		6.95
Tetramethyl ammonium hydroxide pentahydrate TMAOH	NMe ₄ ⁺ OH ⁻ .5H ₂ O	NA (15.7) ^b
Tetrabutyl ammonium hydroxide 30-hydrate TBAOH	NBu ₄ ⁺ OH ⁻ .30H ₂ O	NA (15.7) ^b

*pKa of conjugate acid in H₂O, taken directly from the Ripin and Evans pKa table, unless noted.

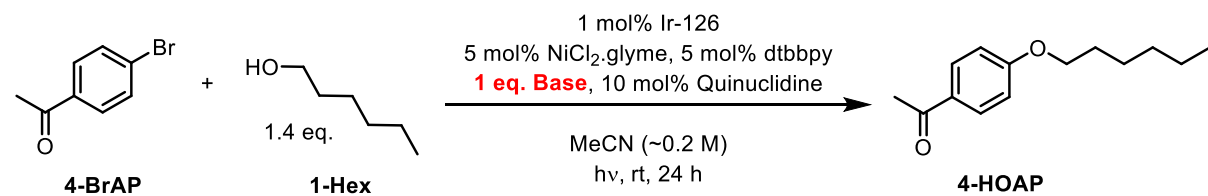
^apKa of conjugate acid in H₂O, taken from Perrin, *Dissociation constants of organic bases in aqueous solutions*, Butterworths, London, 1965.

^bNot found, 15.7 is pKa of conjugate acid of OH⁻ (i.e. H₂O), taken from the Ripin and Evans pKa table.

In a previous report from Nocera,²¹⁵ where a homogeneous starting solution was required for spectroscopic studies, the authors noted that using 1.1 eq. quinuclidine (in place of 1 eq. K₂CO₃ + 0.1

eq. quinuclidine) gave a homogeneous solution suitable to their studies. Hence, this was considered a promising starting point without significant deviation from the previously reported conditions.

Table 5.4.4 outcome of a screen of bases used for the model MacMillan Coupling Reaction indicating homogeneity of the reaction starting/product mixture and yield observations.



Entry	Base	Homogeneous Starting Solution	Homogeneous Product Solution	¹ H NMR Spectroscopic Observations of Crude Reaction Mixture	4-HOAP Yield* / %
1	DBU	✓	✓	Product and SM present.	7 ^a
2	TMG	✓	✓	Product present, no SM remains.	58
3	Quinuclidine	✓	✗	Product present, no SM remains.	59
4	DIPEA	✓	✓	Product and SM present.	9
5	TEA	✓	✓	Product and SM present.	15 ^a
6	TMAOH	✗	✗	Complex mixture. No product or SM noticeable.	-
7	TBAOH	✗	✗	Complex mixture. No product and trace of SM noticeable.	-
8	Pyridine	✓	✓	Product and SM present.	7
9	DMAP	✗	✓	SM present and small traces of product noticeable.	2
10	Imidazole	✗	✗	SM remains, no noticeable product or other products.	-
11	DABCO	✓	✗	Product and SM present.	39

*Isolated yield, unless otherwise noted.

^aEstimated yield, where product and SM co-eluted in chromatography, ratio of signals in ¹H NMR spectrum were used to estimate a yield from the mass of co-eluted mixture.

Unfortunately, using quinuclidine (Table 5.4.4, Entry 3), despite giving a homogeneous starting solution, led to a precipitate forming during the reaction. Therefore, whilst allowing for a suitable spectroscopic study, this would not allow for a reliable synthetic procedure in flow.

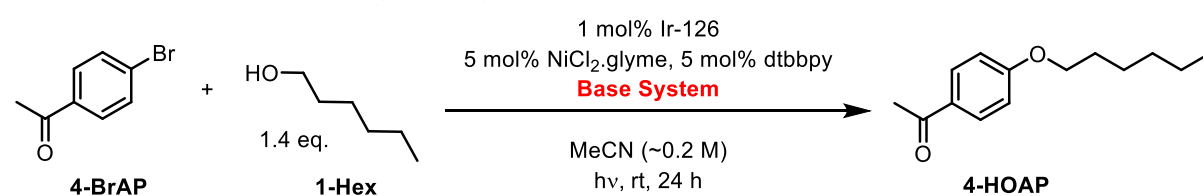
Of the 11 bases screened however, all apart from imidazole, DMAP and the tetraalkyl ammonium hydroxide salts (**Table 5.4.4**, Entries 6, 7, 9 and 10) were soluble in the starting solution. For DMAP, however, the precipitate appeared to vanish over the course of the reaction. Quinuclidine and DABCO (**Table 5.4.4**, Entries 3 and 11), whilst dissolving in the starting solution, formed a precipitate during the reaction. DBU, TMG, DIPEA, TEA and pyridine were observed to be fully dissolved at the start and end of the reaction (**Table 5.4.4**, Entries 1, 2, 4, 5 and 8). DBU had previously been employed for flow processing of a similar reaction, developed by Johannes and Escobar²¹⁹ (detailed in the Introduction) so has been identified for suitability towards continuous reactions, however here (and in the report from Johannes and Escobar), reduced yields were observed when using this.²¹⁹ When the tetraalkyl ammonium hydroxide salts were used, no product was detected in the ¹H NMR spectrum of the crude reaction mixture (appearing as a complex mixture without identifiable peaks for the desired product). No product was observed when imidazole was employed as the base and when DMAP was used, only a trace amount of desired product was identified in the ¹H NMR spectrum of the crude reaction mixture. When using TEA, DIPEA, DABCO or pyridine, product peaks were identified in the ¹H NMR spectrum of the crude reaction mixture but signals due to the starting aryl bromide were also noticeable, indicating that the reaction had not gone to full conversion, even after 24 h. When using TMG or quinuclidine, it was observed that **4-HOAP** was present in the ¹H NMR spectrum of the crude reaction mixture, whilst also showing no trace of **4-BrAP** starting material. These observations are summarised in **Table 5.4.4** above. Overall, TMG and quinuclidine appeared to give similar observations to what was seen here using the original MacMillan (K₂CO₃ + quinuclidine) conditions¹⁷⁰ *i.e.* full conversion of starting material and good **4-HOAP** yield. Of these two amine species, only TMG maintained homogeneity throughout the reaction.

It was therefore concluded that TMG was a candidate for replacing K₂CO₃ in the reaction mixture, for development towards a flow process. A semi-continuous approach, for example, using the PhotoVap reactor, was considered as an alternative for solid-handling reaction conditions.²²⁶ To determine whether to proceed with a semi-continuous or a fully continuous flow approach, it was considered that a further examination of the reaction mixtures would be required. For example, the reactions so far had been conducted over a 24 h timescale but revealed no insight as to how quickly full conversion was reached. For example, if the reaction with K₂CO₃/quinuclidine reached completion after <10 h, but with TMG reached completion after the full 24 h, continuing with a semi-continuous, solid-handling approach might have been more appropriate. Furthermore, as the previous screen had simply swapped out 1 eq. K₂CO₃ for 1 eq. organic base (each accompanied with an extra 0.1 eq. quinuclidine), it was considered that further simplification *i.e.*, replacing the K₂CO₃ + quinuclidine system with just a single organic base may have been beneficial.

Therefore, the next objective was to determine whether the reactions could be performed using a homogeneous one-component system (in terms of base/quencher). For this, the following bases were examined: quinuclidine (for comparison), TMG (being the most promising base giving full conversion without precipitation forming), TEA and DIPEA (as the other bases which proceeded without precipitate formation, although they did not go to completion after 24 h) as well as DABCO (which previously gave good yield, but a small amount of precipitate formed). TEA and DIPEA were selected in the (albeit unlikely) case that they appeared more efficient in the absence of quinuclidine. DABCO resulted in a small amount of precipitate forming previously, but it was considered this may have been a precipitate

due to the presence of quinuclidine and so was worth investigating whether no precipitate formed in the absence of quinuclidine.

Table 5.4.5 yields and qualitative evaluation of whether reactions had proceeded to completion for model MacMillan Coupling Reactions where the originally reported K_2CO_3 + quinuclidine system was investigated to be replaced with a simpler, one component base system, possibly amenable to a flow process – showing that replacing the K_2CO_3 + quinuclidine system with TMG alone allowed for a homogeneous process, with similar observed yields.



Entry	Base System	1H NMR Spectroscopic Observations of Crude Reaction Mixture	4-HOAP Yield* / %
1	1 eq. K_2CO_3 + 0.1 eq. quinuclidine	No SM remains.	69 ± 6^a
2	1.1 eq. quinuclidine	No SM remains.	59
3	1 eq. TMG + 0.1 eq. quinuclidine	No SM remains.	58
4	1.1 eq. TMG	No SM remains.	61
5	1 eq. DABCO + 0.1 eq. quinuclidine	Product and SM present.	39
6	1.1 eq. DABCO	Product and SM present.	53
7	1 eq. TEA + 0.1 eq. quinuclidine	Product and SM present.	15^b
8	1.1 eq. TEA	Product and SM present.	9
9	1 eq. DIPEA + 0.1 eq. quinuclidine	Product and SM present.	9
10	1.1 eq. DIPEA	Product and SM present.	24^b

*Isolated yield, unless otherwise noted.

^aAverage of 4 isolated yields from **Table 5.4.2**, Entries 4-7.

^bEstimated yield, where product and SM co-eluted in chromatography, ratio of signals in 1H NMR spectrum were used to estimate a yield from the mass of co-eluted mixture.

It was observed that all reactions performed here gave the same qualitative observations as in the previous screen *i.e.*, TMG, TEA and DIPEA were used without forming any precipitate. For TMG, no **4-BrAP** was present in the 1H NMR spectrum of the crude reaction mixture, for DIPEA and TEA, product signals were observed in the 1H NMR spectrum of the crude reaction mixture, along with signals due to remaining starting material, indicating the reaction had not gone to completion again. For the reaction using DABCO, some product was observed in the 1H NMR spectrum of the crude reaction mixture, however, a precipitate again formed during the reaction.

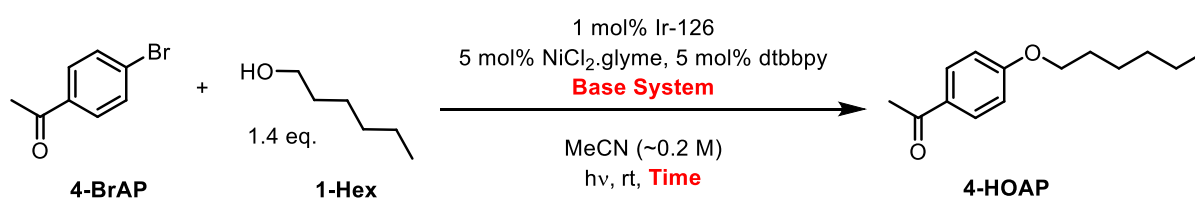
From these observations, it was considered that DIPEA and TEA could be ruled out for further investigation due to appearing to give rates much slower than K_2CO_3 /quinuclidine/TMG/DABCO, despite not forming precipitate. DABCO was also ruled out for further investigation as the previous investigation confirmed the precipitate formation to be a result of employing DABCO, not due to the quinuclidine present in the first run (*c.f.* reaction with DABCO + quinuclidine with just DABCO).

Therefore, the candidates for continued investigation were K_2CO_3 + quinuclidine, quinuclidine alone as well as TMG with or without quinuclidine. These combinations resulted in similar observations after 24 h, with the conditions requiring K_2CO_3 or quinuclidine alone possibly suited to a semi-continuous process and the conditions using TMG possibly suited to a fully continuous process.

5.4.2.3 Comparative Assessment of Newly Developed Conditions with Existing Conditions

Prior to determining whether to proceed with a semi-continuous or fully continuous flow approach, it was decided to investigate (roughly) the relative rates of the reactions over shorter timescales. This was to be attempted by monitoring the reaction progress using GC at certain time intervals, rather than isolating products after 24 h irradiation. Furthermore, using a total of 1 eq. base rather than a total of 1.1 eq. base was to be investigated – again for simplifying conditions and assessing the rate under these conditions.

The following conditions were considered to test the previously mentioned hypothesis: 1 eq. each of TMG, quinuclidine and K_2CO_3 (to determine the comparative rate compared to using 1.1 eq. of each, or 1 eq. + 0.1 eq. quinuclidine); 1.1 eq. of TMG and quinuclidine (to assess if the slight excess offers a significant enhancement of the rate or whether the starting mixture can be simplified to just 1 eq. of a single component); 1 eq. K_2CO_3 or TMG + 0.1 eq. quinuclidine (to assess whether the presence of quinuclidine offers a rate enhancement when using either of these bases). From previous reports, it was considered unlikely for K_2CO_3 alone to result in any product formation,¹⁷⁰ but was attempted here as a control and to support/refute previous reports.



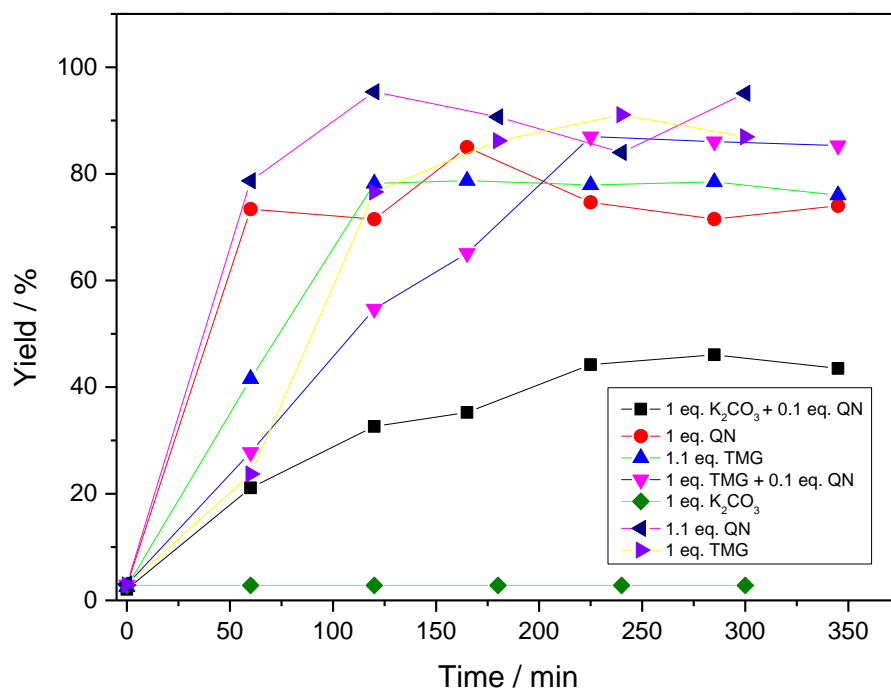


Fig 5.4.1 observed GC yields at certain time intervals for the batch MacMillan C-O coupling reaction with a variety of base systems suggesting that the developed homogeneous systems appeared to give greater yield at shorter timescales than the originally reported K_2CO_3 + quinuclidine system, and how no reaction occurred in the absence of an amine. Error bars omitted as replicate samples were not taken as the study was intended to provide a rough insight to how the newly developed conditions compared against previously reported literature conditions. Lines drawn to guide the eye.

It was observed that no reaction occurred in the presence of K_2CO_3 alone. The reaction using K_2CO_3 and quinuclidine (*i.e.* the original MacMillan conditions¹⁷⁰) was observed to give the slowest apparent rate of the remaining 6 conditions. For the remaining conditions using TMG, quinuclidine, or mixtures thereof, generally observed yields were >50% after around 2 h. The reaction using 1 eq. TMG with 0.1 eq. quinuclidine, appeared slightly slower than reactions using just quinuclidine or just TMG (after 2 h). It was also observed that the initial rates using just quinuclidine appeared faster than the initial rates using just TMG. Rates also appeared similar when using either 1 or 1.1 eq. TMG (or 1 or 1.1 eq. quinuclidine). These experiments were designed to advise and compare conditions for ongoing work and should *not* be considered a meticulous examination of the rates of each condition. The observation that using TMG alone (or quinuclidine alone) appeared apparently beneficial when compared with using a K_2CO_3 system or a TMG/quinuclidine mixed system was therefore the key observation here. This suggested that it could be worthwhile to develop a flow approach using TMG, as opposed to a semi-continuous slurry approach using K_2CO_3 or quinuclidine alone.

The observed results presented in **Fig 5.4.1** were obtained in experiments run in parallel using the white LED block (discussed previously). In the original report from MacMillan and co-workers, blue LEDs were used for batch irradiation and the authors reported a comparison with a 26 W white light source as well where, over the timescales they studied, no major discrepancy was apparent.¹⁷⁰ Available for this work,

alongside the 5 x 12 W white LED block used was also the previously described smaller 3.5 W blue LED (457 nm). Previously, this work had compared the two LED light sources for reactions following conditions analogous to those reported by MacMillan and over a 24 h period, no significant difference was observed in terms of the yield of desired product. However, the results in **Fig 5.4.1** suggested that time periods much shorter than 24 h are suitable for the conditions surveyed whilst still leading to good yields and conversions (full conversion and yield ~80% or higher in some instances). Again, these were using a white LED source, therefore, it was considered at this stage that, using TMG as a base, a comparison with the previously used 3.5 W blue LED would be useful.

Table 5.4.6 comparison of yield and conversion over time between using a white and blue LED source (of differing powers) for the newly developed homogeneous reaction conditions using 1.1 eq. TMG in place of 1 eq. K_2CO_3 and 0.1 eq. quinuclidine, illustrating how the significantly more powerful white LED block appeared to give much shorter reaction times for the conditions.

Entry	Light Source	Time / min	4-HOAP GC Yield / %	4-BrAP GC Conversion / %
1		60	42	61
2	White	120	78	94
3		345	76	95
4		60	15	21
5	Blue	180	22	29
6		24 h	42	53

The observations in **Table 5.4.6** appeared to show that the more powerful white LED block light source resulted in quicker reaction times. This was considered likely due to the significantly higher power of the white LED block (5 x 12 W strips *c.f.* 1 x 3.5 W blue LED).

5.4.2.4 Photocatalyst Screen

It was also considered that a screen of photocatalysts should be performed. Of relevance to this project due to interest of collaborators at JM were other polypyridyl complexes of Ru or Ir, typically used for photocatalysis. Those of which were supplied for the project were $[Ru(bpy)_3]Cl_2$, $[Ru(bpy)_3](PF_6)_2$, $Ir(ppy)_3$ and $[Ir(ppy)_2dtbbpy]PF_6$ (Ir-125). This was considered a worthwhile screen as the speculated mechanism involves electron transfer between the photocatalyst and amine base. In the original work from the MacMillan Group, quinuclidine was used as the amine,¹⁷⁰ but was found here to be potentially problematic for a flow process. Changing the amine to TMG, determined to be the most promising in this study, could therefore have an effect on the electron transfer process¹⁷⁰, or possible H-atom transfer process with the alcohol.²¹⁶ Different photocatalysts have different redox potentials (though this is not the only factor in determining whether a photocatalyst will be effective, solubility, lifetime and other parameters are also important) and therefore it was considered that this screen of available, widely used photocatalysts should be conducted to determine if any perform better than Ir-126 which had been used so far. Again, the larger white LED block was used.

Table 5.4.7 observed yields from a screen of commonly used PGM-based photocatalysts showing Ir-125 to give similar, slightly higher results to Ir-126 on a 2 h timescale (c.f. **Table 5.4.6**, Entry 2).

Entry	Photocatalyst	Time / min	4-HOAP GC Yield / %	4-BrAP GC Conversion / %
1	[Ru(bpy) ₃]Cl ₂	120	11	16
2	[Ru(bpy) ₃]PF ₆	120	16	26
3	Ir-125	120	87	>99*
4	Ir(ppy) ₃	120	6	20
5		24 h	63	90

*No 4-BrAP was observed in the GC chromatogram of the crude reaction mixture.

In this study, it was observed that the Ru-based photocatalysts and Ir(ppy)₃ appeared to give much slower rates than previously used Ir-126 (c.f. **Table 5.4.7** and **Table 5.4.6**). Ir-125, the non-fluorinated analogue of Ir-126, appeared to give slightly greater yields on a 120 min timescale than Ir-126. The results could be considered likely to be within error as these experiments were not duplicated, nor were multiple samples taken as these studied were intended as guides. For ongoing work, involving establishing conditions in flow, it was decided to maintain using Ir-126 to allow for closer comparison with previously reported literature from MacMillan and co-workers.

5.4.2.5 Control Reactions for the Newly Developed Conditions

As a final investigation in batch before transferring the developed conditions to flow, it was deemed important to perform appropriate control reactions. So far, in **Fig 5.5.1** it was observed that in the presence of a base (K₂CO₃) without any amine present, no product was observed, which itself can be considered as a control, highlighting the need for an amine. To test the requirement for the other conditions, which have been developed here, a series of control experiments were conducted in the presence/absence of one of the catalysts, with/without the presence of a light source, and with/without heat being applied. The aim was to show that all components were necessary for an efficient reaction and to determine whether the reaction was indeed photochemical or was merely promoted thermally by heat generated by a light source.

Table 5.4.8 control reactions performed showing how in the absence of any catalyst or light leads to low observed yields after extended timescales.

Entry	Conditions	4-HOAP GC Yield	
		(3 h) / %	(72 h) / %
1	All components present, no heat, dark.	4	5
2	All components present, heated at 60 °C, dark.	0	0
3	No Ir cat., light.	3	3
4	No Ni cat., light.	4	4
5	No Ir cat., heated at 60 °C, dark.	4	7
6	No Ni cat., heated at 60 °C, dark.	4	8
7	No Ni or Ir cat., light.	0	4
8	No Ni or Ir cat. heated at 60 °C, dark.	0	6

The observed results (**Table 5.4.8**) provide support for the claim that the developed conditions mainly required photochemical activation (little product observed when light was omitted, even when heated). Furthermore, the omission of either catalyst also resulted in very low observed yields even after 72 h irradiation, providing support that the system indeed functions *via* dual-catalysis and not *via* sole Ni-catalysis, as has been reported for some other Ni catalysts.^{222,223}

To conclude this work in batch, to investigate the possible benefits of performing a MacMillan Reaction continuously, it was initially required to develop conditions amenable to flow. TMG was found to be an effective base/reductive quencher, for the reaction, maintaining homogeneity throughout. This was also shown to give reaction rates slightly greater than the previously reported conditions using K₂CO₃/quinuclidine. As such, using TMG was selected for developing a flow process.

5.4.3 Construction of a Flow Reactor for Investigating Continuous MacMillan C-O Coupling

With a new set of conditions developed amenable to flow processing, the next objective was to obtain a suitable flow reactor. It was decided to construct a flow reactor for this purpose and the intent was for this to be a simple reactor with a small overall volume (to avoid wasting large amounts of expensive Ir photocatalyst). Importantly, a system allowing for temperature control over the reaction solution was desired. For the batch reactions, no heating/cooling of the reaction solution was applied, other than that generated by the light source. As the reaction involves dual-catalysis, it was considered that the ability to efficiently heat (as well as irradiate) the reaction solution may result in increased rates, with the hypothesis that heating could lead to increased rate of the Ni catalytic cycle and possible reduction in Ni catalyst loadings.

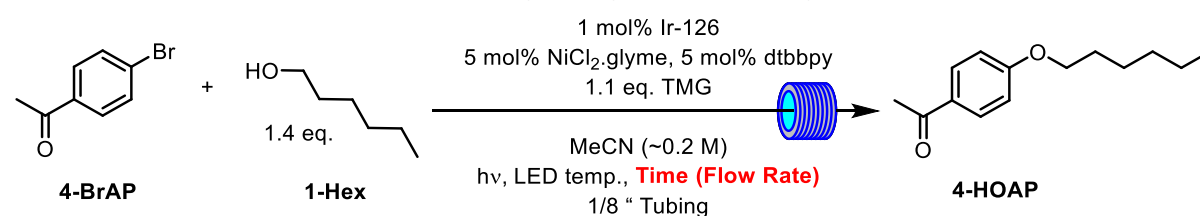
To achieve this, a simple solution based upon a Booker-Milburn FEP coil flow reactor was considered.¹⁷⁷ The reactor design involves a jacketed pyrex tube, made in-house. The inner jacket of the tube was designed to house the Lightsabre LEDs, described in the Experimental Chapter, but in summary was a

~410 nm blue LED source. Transparent FEP tubing was coiled around the exterior of the tube, forming the irradiated reactor coil. The central jacket was connected to a recirculating chiller/heater, to allow for temperature control over the reactions. A number of different FEP coils were used in this work for various optimisation/scale-up experiments (details in the Experimental Chapter and choice of tubing for experiments is described where necessary). To complete the system, a peristaltic pump was used, as a pressurised system was not required, and a three-way valve was joined to the pump, which was connected to two tubing lengths to allow for filling two separate vessels (one with neat solvent, one with reagent solution). Full details and diagrams can be found in the Experimental Chapter.

5.4.4 Initial MacMillan C-O Bond Formations in Flow

Now equipped with suitable reaction conditions and a suitable reactor, it was possible to develop a C-O coupling flow process. Initial flow reactions were intended to determine the timescales required for performing a reaction in the Lightsabre flow reactor, prior to any further optimisation. To investigate this, the same conditions as used in batch were employed and several flow rates applied. At this stage, the only suitable FEP tubing available for the reactor was 1/8 " OD FEP tubing (FEP coils used are detailed in the Experimental Chapter). To not use excessive amounts of costly Ir catalyst, it was desired to keep the volume of irradiated tubing small for these initial reactions. Unfortunately, using a short 97 cm length of this tubing gave a larger than desired irradiated volume of 6 mL, whilst the tubing coil covered only a very small section of the emissive area of the Lightsabre *i.e.*, leading to much of the emitted light not being incident upon the reaction mixture. This initial set-up was therefore far from optimal and only intended for a "look-see" style experiment.

Table 5.4.9 yield of **4-HOAP** from the preliminary flow reactions in a crude, non-optimal FEP coil reactor using the Lightsabre LED strips.



Entry	Residence Time / min	4-HOAP GC Yield / %	4-BrAP GC Conversion / %
1	30	88 ± 1	>99*
2	15	85 ± 1	>99*
3	5	55 ± 3	71 ± 3

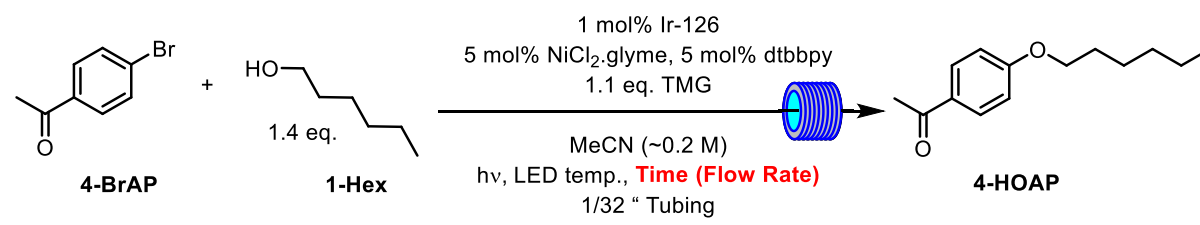
*No **4-BrAP** was observed in the GC chromatogram of the crude reaction mixture.

Even with this crude flow set-up, very short residence times could be employed, with good and yields observed (**Table 5.4.9**). Moreover, the reactions ran without issue *i.e.*, no precipitation or blockages, indicating the newly developed conditions were suited to flow processing.

The next consideration was that the reaction residence time might be shortened using narrower FEP tubing, better suited to capturing light from the Lightsabre LED. Therefore, 1/32 " ID FEP tubing was obtained. A 25 ft length gave a total internal volume of 3.7 mL and spanned a much greater section of

the length of the Lightsabre LED strips once coiled around the jacketed tube. This still did not cover the entire length, however, but was an improvement upon the previously used tubing.

Table 5.4.10 yield of **4-HOAP** using the same flow reactor set-up as in **Table 5.4.9** but with a longer length of narrower channel FEP tubing.



Entry	Residence Time / min	4-HOAP GC Yield / %	4-BrAP GC Conversion / %
1	10	97 ± 3	>99*
2	5	85 ± 4	90 ± 3
3	2.5	69 ± 3	71 ± 6
4	1	33 ± 1	39 ± 2

*No **4-BrAP** was observed in the GC chromatogram of the crude reaction mixture.

Here, promising observations for performing the reaction in flow were also observed (**Table 5.4.10**). With 1/8 " FEP tubing, a yield of around 55% was observed in a 5 min residence time, whereas with 1/32 " FEP tubing, an 85% yield was observed for the same residence time (**Table 5.4.10**, Entry 2 *c.f.* **Table 5.4.9**, Entry 3). The results, therefore, were generally supportive of the hypothesis that using a longer length of narrower tubing could lead to improved yields, presumably due to greater light capture.

Using the set-up with the 1/32 " FEP coil, there was an irradiated volume of 3.7 mL, compared to a very similar reaction volume for the previous batch reactions (~4.2 mL). For these similar volumes, it was apparent that using the flow FEP coil system provided observed benefits in terms of processing times, with observed yields after 5 min being comparable to observed yields after a few h for the batch reactions under analogous conditions (compare results in **Table 5.4.9** with results in **Table 5.4.6**). Using this set-up (with 1/32 " FEP tubing) was considered suitable for ongoing optimisation reactions, with benefits over batch processing already apparent.

5.4.5 Considerations for Optimisation of MacMillan Coupling Conditions in Flow

For further optimisation in flow, a few considerations were made. For example, it was considered how to improve the processing aspects *e.g.*, whether the productivity of the reaction could be improved and whether Ir or Ni catalyst loadings could be reduced. These considerations included the application of heat to the reaction (which the jacketed tube had been designed to allow for). Being dual-catalytic, it was considered that the Ni catalytic cycle may operate as a conventional Pd-type cross-coupling cycle and that therefore by heating the reaction, the rate of this would be enhanced, giving a more productive reaction, or allowing for use of less Ni catalyst.

As with many photochemical processes, temperature would likely have little implication for the photophysics of the Ir photocatalyst.¹⁷⁶ However, it was further considered that due to efficient

irradiation in the narrow flow channels that the Ir concentration could be increased. This would be desirable by reducing the solvent amount, which, in turn, could lead to a more productive reaction, with a greener footprint for solvent demand. It was also planned at this stage to investigate whether lower Ir photocatalyst loadings could be used whilst maintaining good yields and conversions, possibly compensated for by the previously mentioned decrease in solvent usage.

5.4.6 Investigating Temperature Dependence of MacMillan C-O Coupling in Flow

The next step taken was to investigate the temperature dependence of the reaction. The hypothesis was that the Ni catalytic cycle might have an increased rate at higher temperature. Reactions were conducted keeping all conditions the same as previous (tubing diameter, length and reaction stoichiometries) but with a cooled/heated fluid flowing through the jacket of the tube which the FEP tubing was coiled around. A fixed residence time of 1 min was applied, as previously (**Table 5.4.10**, Entry 4), a yield of ~30% and conversion ~40% was observed under analogous conditions, without the presence of heating/cooling fluid. It was therefore considered that any changes when heating/cooling fluid was applied would be noticeable, relative to this data point.

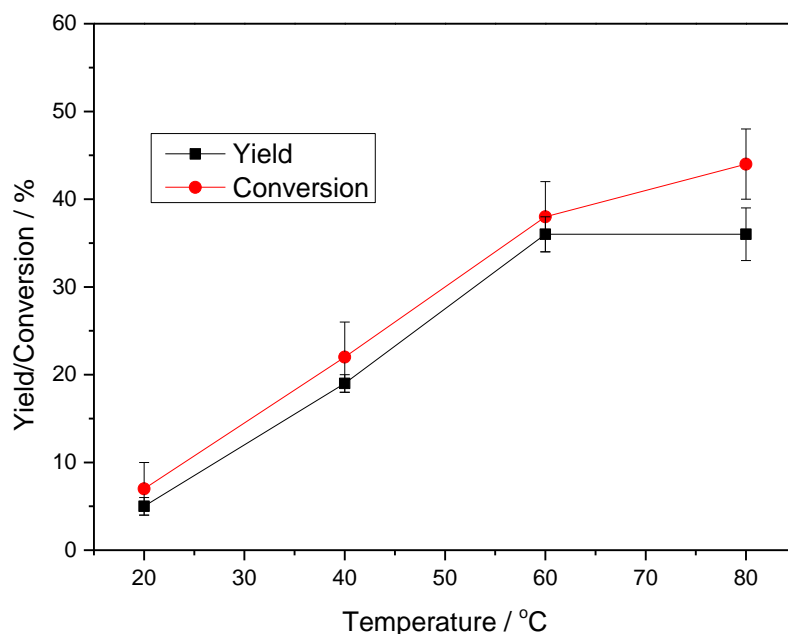
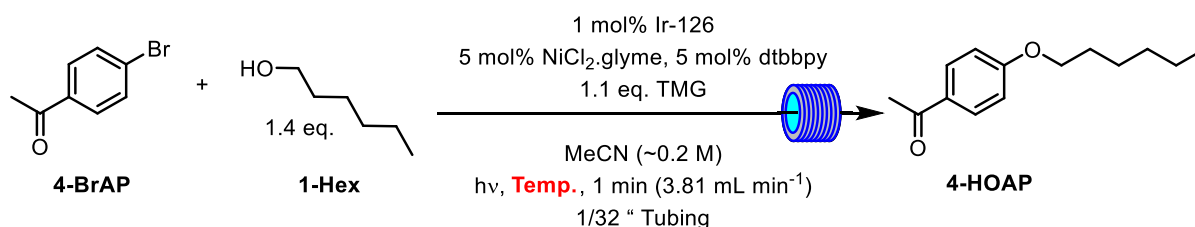


Fig 5.4.6 observed GC yields and conversions for a study into the temperature dependency of the adapted MacMillan C-O coupling reaction in flow displaying yields increasing with temperature up to 60 °C. Lines are drawn to guide the eye.

In this study (Fig 5.4.6), it was observed that at 20 °C and 40 °C, yields were lower when compared with reactions without the presence of heating/cooling fluid. At 20 °C, only trace amount of product was observed. At 60 °C, observed yields were comparable to reactions without the presence of heating/cooling fluid – this would likely be a rough indicator of the temperature the reaction reaches due to the LEDs acting as a heat source. Indeed, temperatures surrounding the FEP coil were measured to be ~60-70 °C when the Lightsabre was turned on. At 80 °C, the observed yield was similar to that observed at 60 °C. At this stage, therefore, a temperature dependence was suggested between 20–60 °C, with product yield increasing with temperature, but no further increase was observed between 60–80 °C. It should be noted that, due to using MeCN solvent, 80 °C was a limiting temperature at this point (without requiring applying backpressure to the system which was not possible at this stage).

A further investigation into the temperature relationship in the 60–80 °C temperature region was therefore undertaken. It was considered that, due to the short residence time applied that perhaps the heat transfer to the reagent solution was not optimal and that longer residence times should be applied to determine whether an increase in temperature to 80 °C could be observed at a longer residence time. Reactions were therefore carried out under analogous conditions but at 2.5 and 5 min.

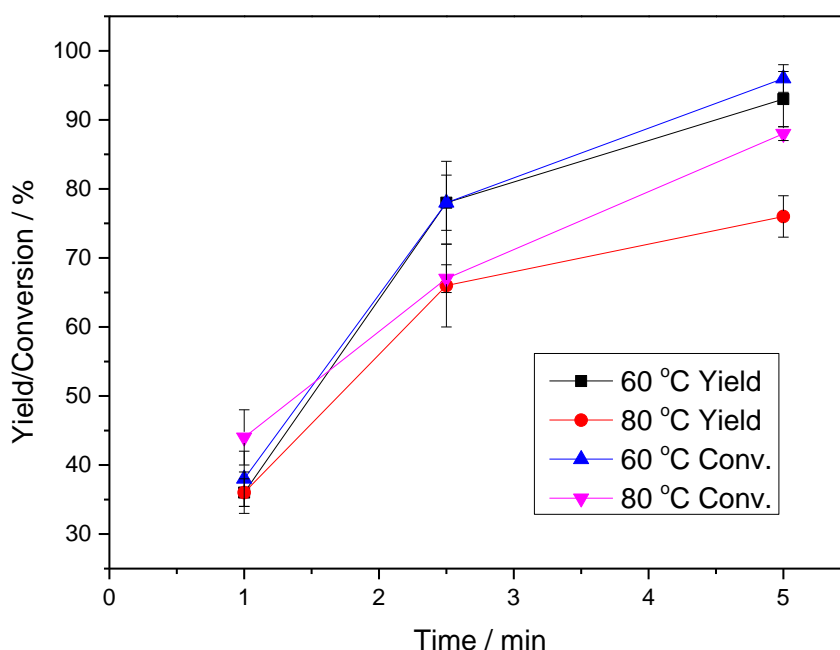
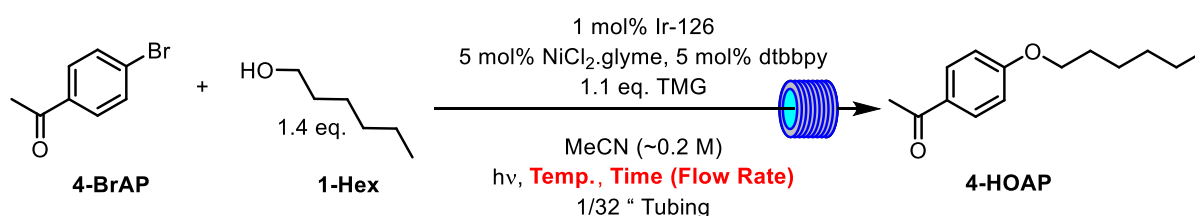
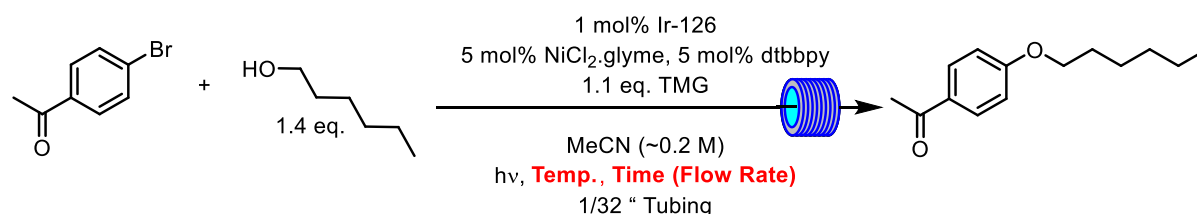


Fig 5.4.7 comparison of 4-HOAP GC yields at 80 °C and 60 °C at different residence times illustrating how reactions at 60 °C appeared to give slightly higher but comparable observed yields to those at 80 °C. Lines are drawn to guide the eye.

It was observed that at increased residence times of 2.5 min and 5 min, yields of **4-HOAP** were lower at 80 °C than they were at 60 °C (again with yields at 60 °C being similar at 2.5 min and 5 min to the yields observed without applying heating/cooling fluid). It was also noticed that at 80 °C, a black precipitate was present in the reaction product outlet stream. It was speculated that this might have been Ni⁰ precipitation, possibly with the elevated temperature leading to ligand dissociation. The results observed at different temperatures are summarised in **Table 5.4.11**, below.

Table 5.4.11 summary of results for a temperature study in continuous flow using the 1/32 " FEP coil flow reactor.



Entry	Temperature / °C	Residence Time / min	4-HOAP GC Yield / %	4-BrAP GC Conversion / %
1	Not Used	1	33 ± 1	39 ± 2
2	Not Used	2.5	69 ± 3	71 ± 6
3	Not Used	5	85 ± 4	90 ± 3
4	20	1	5 ± 1	7 ± 3
5	40	1	19 ± 1	22 ± 4
6	60	1	36 ± 2	38 ± 4
7	60	2.5	78 ± 6	78 ± 4
8	60	5	93 ± 4	96 ± 2
9	80	1	36 ± 3	44 ± 4
10	80	2.5	67 ± 6	67 ± 2
11	80	5	76 ± 3	88 ± 1

The results observed so far suggested that running reactions without applying any heating/cooling would be sufficient for the current conditions, due to the heat generated by the light source. Therefore, the next step taken was to investigate if the Ir and Ni catalyst loadings could be lowered, whilst still maintaining good yields in short timescales.

5.4.7 An Assessment of Reactor Fouling and Control Experiments

Importantly, after performing the reactions summarised in **Table 5.4.11**, alongside observing a black precipitate during the reaction, a small amount of black precipitate deposited on the inner wall of the reactor coil tubing was also noticed. This was only observable (by eye) at a small section where the reaction solution would first enter the irradiated coil *i.e.*, it did not appear to have deposited across the whole length of the tubing (**Fig 5.4.8**).

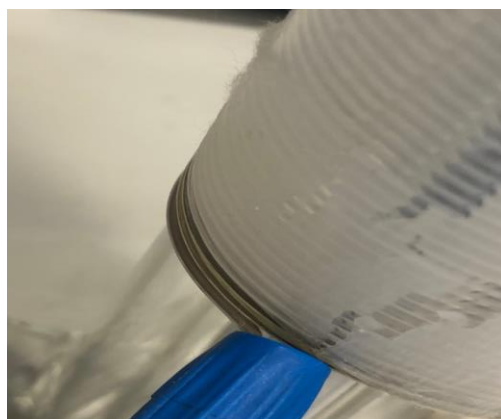


Fig 5.4.8 black precipitate deposited on the internal wall of the inlet part of the reactor coil FEP tubing, assumed to be an Ir or Ni species.

It was assumed that this deposit was due to the aggregation and subsequent precipitation and deposition of Ir or Ni. Therefore, it was considered important to run blank reactions (no intentionally added catalyst) in the presence of the deposit. Three reactions were considered necessary. The first being a reaction with neither catalyst present to determine whether any yield/conversion is observed. Then, one reaction in the absence of the Ir catalyst and another in the absence of the Ni catalyst were to be attempted to determine which, if any, present in the black deposit was responsible for any observed yield/conversion. The aim, therefore, was to determine whether the black deposit resulted in any observed catalytic activity *i.e.*, would any **4-HOAP** product be formed, or would any significant conversion of starting aryl bromide be observed, in the absence of either added catalyst?

The runs in the absence of either catalyst as previously noted were conducted employing a 2.5 min residence time, without any heating fluid applied. This could have been expected to give a yield of up to ~70% following observations in **Table 5.4.11** so this was chosen as the processing conditions as any effect of remaining catalyst should have been noticeable.

Table 5.4.12 observations from GC analysis of some control reaction conditions in the absence of one or both catalysts in a “dirty” reactor, with black deposit present.



Entry	Catalyst Presence	4-BrAP Starting Conc. / M	4-BrAP Crude Product Conc. / M	4-HOAP GC Yield / %
1	None	0.21 ± 0.01 ^a	0.21 ± 0.01 ^a	Not observed
2	No Ir, 5 mol% Ni	0.23 ^b	0.21 ^c	1
3	No Ni, 1 mol% Ir	0.23 ^b	0.22 ^c	<1

^aConc. determined experimentally via triplicate GC measurements (deviation from the average used to estimate uncertainty).

^bConc. calculated from a measured volume of starting solution (4.4 mL) and amount of **4-BrAP** (1.0 mmol) – other concentrations were determined experimentally via GC.

^cConc. determined experimentally via single GC measurement (uncertainty therefore not estimated).

It was observed that in the absence of both catalysts, no product signals were present in the GC analysis and no conversion of starting material was detected (**Table 5.4.12**, Entry 1). In the presence of just Ir or Ni catalyst, both runs led to trace amounts of product being observed in the GC analysis (**Table 5.4.12**, Entries 2 and 3). Some conversion of starting material for both was also observed, however, this was in part attributable to a small volume of starting material solution (~4 mL, to conserve costly catalyst) being used, so some dilution effects (due to neat solvent being pumped prior to and after the reaction mixture solution) would likely have been somewhat responsible for this. Where a large volume (~16 mL, without any costly catalyst to conserve) solution was used with no catalysts present, no conversion was noticed and dilution effects would be much less significant (although no product was detected in this run, either). These observations suggested that the black deposit likely had no/minimal effect on the reaction outcome. Only trace amounts of product were observed in the absence of either catalyst, in agreement with the observations in **Table 5.4.8** for control reactions in batch. Some starting material conversion was observed, though some of which may be attributable to dilution effects. Furthermore, along with observed results in **Table 5.4.8**, the results here provide further support that the conditions developed in this work necessitate the presence of both catalysts for an efficient reaction, in both flow and batch systems.

Despite the observed fouling not appearing to influence the reaction outcome, it was determined that attempts should be made to remove the deposit, in case larger amounts would affect, e.g. light penetration. This was attempted by flushing with a dilute solution of aqueous HNO₃ as this was known to be compatible (even at very high concentrations) with FEP and related fluoropolymer tubing. The images below show time-lapse photography of the fouled tubing being flushed with dilute aqueous

HNO₃. Over a few minutes (which the photos were acquired over), the black deposit can be seen to dissolve completely (by eye).



Fig 5.4.9 time-lapse photographs of the reactor coil FEP tubing being flushed with dilute aq. HNO₃ showing the removal of the black deposit over the course of a few minutes (time progressing from left to right).

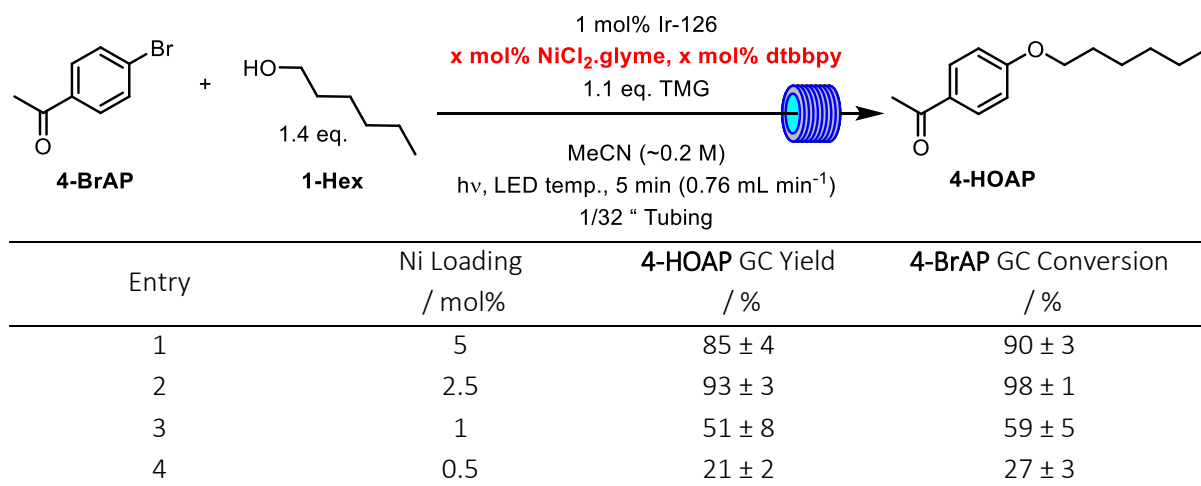
Due to these observations, it was decided to flush the reactor with dilute HNO₃, whenever a deposit appeared visible on the inner wall of the tubing.

5.4.8 Investigations into Reduced Ir and Ni Catalyst Loadings in Continuous Flow

So far, it has been observed that running MacMillan C-O coupling reactions in flow had allowed for a notable increase in productivity *i.e.*, the flow reactor used had given good observed yields in very short timescales. The ongoing aim would be to further optimise reaction processing parameters, using the flow reactor as an enabling tool to do so.

Due to efficient light penetration in flow, improved mixing and other related benefits, it was decided to investigate whether the flow reactor could allow for reactions with reduced catalyst loadings. Experiments to investigate this involved fixing the loading of one organometallic catalyst, whilst varying the loading of the other catalyst (then repeating for the other catalyst). Again, for these experiments, the previously used FEP coil reactor was used, with 1/32" FEP tubing. For the first set of experiments, the loading of the Ir photocatalyst was fixed at 1 mol% (as was used in the previous experiments) and the loading of the Ni catalyst was varied.

Table 5.4.13 yield of **4-HOAP** observed at different $\text{NiCl}_2\cdot\text{glyme}/\text{dtbbpy}$ catalyst loadings illustrating how using the FEP flow reactor allowed for a 2-fold reduction in loading without decreasing yield/conversion. Lower Ni loadings were observed to lead to lower yields and conversions. Conditions other than Ni loading were the same as previous flow reactions using the methodology developed in this work (at the LED temperature).

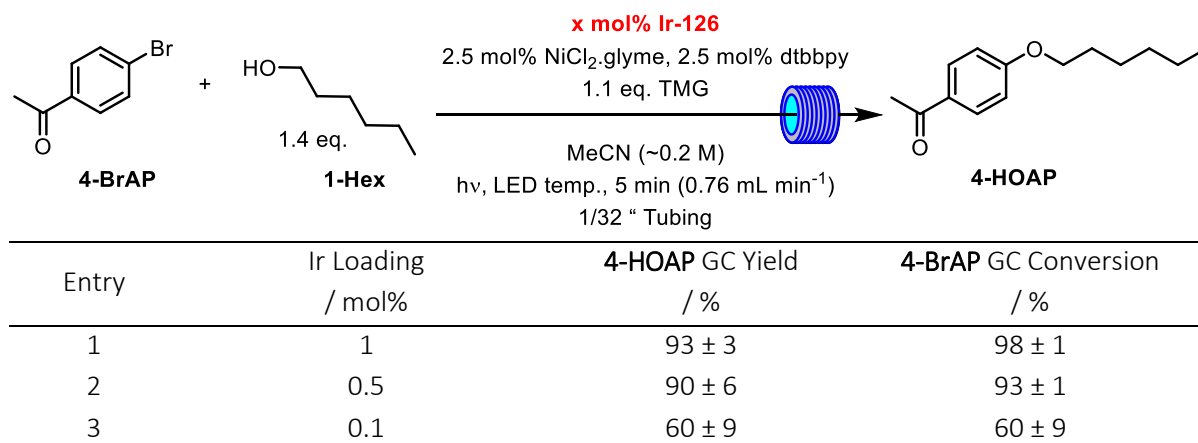


Here, it was observed that at a loading of 2.5 mol% of Ni catalyst, the yields seen were comparable to those from previous experiments using twice the amount of Ni catalyst (5 mol% loading), with 1 mol% Ir photocatalyst loading (Table 5.4.13, Entries 1 and 2). This indicated that a 50% reduction in requirement of Ni catalyst, whilst observing good yields in short timescales.

Following this, the next investigation was to determine the effect of reduced Ir photocatalyst loadings. Again, to examine this, it was decided to employ a fixed Ni catalyst loading and vary the Ir catalyst loading. From the previous observations, a fixed Ni catalyst loading of 2.5 mol% was used as the results were comparable to using a 5 mol% loading (as was used for previous experiments in batch and initial flow reactions).

Table 5.4.14 yield of **4-HOAP** observed at different Ir-126 photocatalyst loadings illustrating how using the FEP flow reactor allowed for a 2-fold reduction in Ir loading without decreasing yield/conversion.

Lower Ni loadings were observed to lead to lower yields and conversions. Conditions other than catalyst loadings were the same as previous flow reactions using the methodology developed in this work (at the LED temperature).



Here, it was also observed that the Ir photocatalyst loading could be halved (from 1 mol% to 0.5 mol%) and, with a 2.5 mol% Ni catalyst loading, a good yield was observed whilst maintaining a short residence time of 5 min (**Table 5.4.14**, Entries 1 and 2). Observations such as these highlight the benefits of employing flow reactors for photochemical reactions. At this stage, the lowest loadings of catalysts employed were 0.1 mol% for Ir photocatalyst (a 10-fold reduction from the original publication) and 1 mol% for the Ni catalyst (a 5-fold reduction from the original publication). 0.1 mol% Ir photocatalyst loading was employed with a 2.5 mol% Ni catalyst loading (**Table 5.4.14**, Entry 3) and 1 mol% Ni catalyst loading was employed with a 1 mol% Ir photocatalyst loading (**Table 5.4.13**, Entry 3). The observed yields for these conditions were reasonable, at around 50% for each.

A follow up experiment was planned, combining *both* of these lowest loadings used, together *i.e.*, 0.1 mol% Ir loading and 1 mol% Ni loading. It was to be expected that lowering to these loadings would give a decreased observed yield of product. However, the ongoing aim was to determine what yield this would give and to determine whether good productivities (*i.e.*, good yields in short timescales) could be observed using such low loadings, as this would represent a significant improvement in the processing of the reaction.

Table 5.4.15 summary of yield of **4-HOAP** under reduced catalyst loadings compared to the methodology developed for a flow process in this work, initially based on the MacMillan C-O coupling reaction



Entry	Ir Loading / mol%	Ni Loading / mol%	4-HOAP GC Yield / %	4-BrAP GC Conversion / %
1	1	5	85 ± 4	90 ± 3
2	1	0.5	21 ± 2	27 ± 3
3	1	1	51 ± 8	59 ± 5
4	1	2.5	93 ± 3	98 ± 1
5	0.5	2.5	90 ± 6	93 ± 1
6	0.1	2.5	60 ± 9	60 ± 9
7	0.1	1	26 ± 2	29 ± 1

The experiment was conducted using these conditions and as expected, a reasonably low yield was observed, relative to the observed yields from other conditions employed in this screen of catalyst loadings (**Table 5.4.15**). As mentioned, the ongoing aim was to determine whether these low loadings could be employed, whilst maintaining good yields in short timescales.

5.4.9 Concentration Dependence Investigations

With the aim of employing significantly reduced catalyst loadings (0.1 mol% Ir, 1 mol% Ni), alongside short reaction residence times whilst observing good yield, the next steps taken were to study concentration dependence of the reaction. The scientific hypothesis was that, by increasing the concentration of the starting material mixture, aspects such as light penetration would be improved (due to the narrow path length tubing being used, 1/32" FEP). Furthermore, increased concentration would also represent a process improvement in minimising solvent usage.

Experiments were planned to test this hypothesis where the relative amounts of reagents increased by two, four and six-fold (relative to the amounts used in previous experiments) and the relative solvent volume kept constant. Reactions were conducted under conditions otherwise analogous to those conducted previously, employing a 0.1 mol% Ir catalyst loading and a 1 mol% Ni catalyst loading.

Table 5.4.16 yield of **4-HOAP** at a range of **4-BrAP** starting material concentrations highlighting how increased concentration resulted in an increase in yield when approximately doubling/quadrupling the concentration from ~0.2 to ~0.4 M or 0.8 M, but a decrease in observed yield/conversion upon increasing to ~1.1 M.

Entry	Conc. / M	Residence Time / min	4-HOAP GC Yield / %	4-BrAP GC Conversion / %
1	0.23	5	26 ± 2	29 ± 1
2	0.43	5	63 ± 4	65 ± 1
3	0.47	10	96 ± 1	97 ± 1
4	0.85	10	84 ± 2	85 ± 1
5	1.14	10	33 ± 2	46 ± 3

It was observed that upon increasing the concentration (~0.2 M to ~0.43-0.85 M), an increase in yield/conversion was apparent (Table 5.4.16, Entries 1-4). A significant decrease upon increasing to >1 M was observed (Table 5.4.16, Entry 5). This could be explained by an initial increase in light capture by the photocatalyst, but then further increasing the concentration perhaps leading to light saturation.

It was concluded from this that a concentration of ~0.5-0.8 M would likely be optimal, presumably because of efficient light capture in the flow reactor. This would also allow for using a reduced amount of solvent compared to the original publication from the MacMillan Group, representing a further improvement for performing the C-O coupling process in flow.

5.4.10 Investigation of the Process Productivity and Scalability

So far, an optimisation of a variety of conditions for the reaction, including time/flow rate, temperature, concentration and catalyst loadings had been conducted, in flow. This had resulted in observing processing benefits and the final aim of the optimisation was to determine whether the process-improved conditions (lower catalyst loadings, reduced solvent requirement, short processing time, etc.) could be translated to high productivities, and whether this appeared scalable.

Two approaches were made towards investigating this. Firstly, a numbering-up (in-series) approach was conducted, where two FEP reactor coils (each identical to the 1/32 " ID FEP coil used previously) were connected, in series, coiled around the Lightsabre LEDs. This would essentially give an effectively doubled irradiated volume compared to the initial single FEP coil. The second approach was based on a scale-up dimensioning approach, where a 1/16 " ID FEP coil was used (of the same length as the previous, single 1/32 " ID FEP coil). This would result in a 4-fold increase in reactor volume compared to the initial single 1/32 " coil. However, in doing so, factors such as heat transfer (with the 1/16 " tubing also having a thicker wall) and light penetration (through a larger solution effective path length and possibly also due to the thicker walls) would not be expected to be identical between the coils of different dimensions.

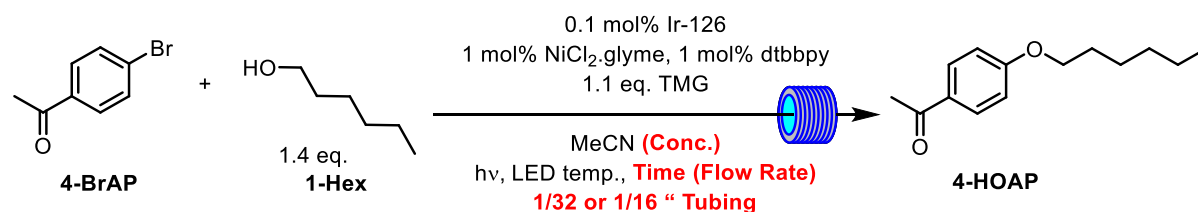
The consideration was that, with each of the previously described approaches leading to a larger irradiated volume, a faster flow rate would be required to maintain a given residence time. Therefore, if yield/conversion observations were similar at a given residence time, the productivity of the reaction (amount of product formed per unit time) would increase. By either approach, this would demonstrate scalability of the developed process. Though, for any specific application, likely a more well-engineered reactor would be used, which would benefit from modelling, particularly if pursuing a dimensioning style approach to scale-up.



Fig 5.4.10 the original single 1/32 " ID FEP coil, far right, the double coiled tubing, far left, and the larger dimension 1/16 " ID FEP coil, centre right, positioned next to the Lightsabre LED, centre left, to illustrate the difference in the coils span across the emission source.

To determine the maximum productivity for the reaction under the process improved optimised conditions, concentrations of ~0.4–0.8 M were applied, and reactions processed in the larger volume FEP coils under otherwise analogous conditions to previously conducted experiments.

Table 5.4.17 yield and productivity of **4-HOAP** in scale-up experiments, highlighting how the concentration, reactor size, catalyst loadings and flow rate can be adjusted to achieve productivities approaching 200 g day⁻¹.



Entry	Reactor Volume* / mL	Conc. / M	Time / min	Flow Rate / mL min ⁻¹	4-HOAP GC Yield / %	4-BrAP GC Conversion / %	Productivity / g day ⁻¹
1	3.8	0.23	5	0.76	26 ± 2	29 ± 1	14.3
2 ^a	3.8	0.22	5	0.76	90 ± 6	93 ± 1	48.6
3	3.8	0.43	5	0.76	63 ± 4	65 ± 1	64.5
4	3.8	0.47	10	0.38	96 ± 1	97 ± 1	54.4
5	3.8	0.85	10	0.38	84 ± 2	85 ± 1	85.9
6	7.6	0.85	10	0.76	89 ± 3	99 ± 1	183.6
7 ^a	7.6	0.45	5	1.52	80 ± 2	91 ± 1	174.4
8	15.2	0.47	10	1.52	85 ± 4	92 ± 2	193.7

^a0.5 mol% Ir-126 and 2.5 mol% NiCl₂.glyme/dtbbpy was used.

*3.8 mL reactor used 1 x 1/32 " ID FEP coil, 7.6 mL used 2 x 1/32 " ID FEP coils, 15.2 mL used 1 x 1/16 " ID FEP coil – details in Experimental Chapter.

The developed flow process was scalable *via* a numbering-up style approach (using two coils of 3.8 mL each to give a total volume of 7.6 mL, **Table 5.4.17**, Entries 6 and 7) and, somewhat, using a dimensioning approach (using a larger diameter 1/16 " FEP coil, **Table 5.4.17**, Entry 8). The dimensioning approach was only somewhat successful because, at the higher concentration of 0.85 M, precipitation (presumably of a **TMG** salt) and blockage occurred. This could possibly be due to the slightly larger tubing dimensions favouring crystallisation, though this was not investigated further. As such, a reduction in concentration was required, essentially resulting in the faster flow rate applied (due to maintaining a given residence time in a larger volume coil) being offset by the requirement for a lower concentration, in terms of achieving higher productivity (**Table 5.4.17**, Entries 5 and 8). This would highlight the importance of engineering-based modelling, when adopting an increased dimensions approach towards scalability, which could further assist in optimisation of the conditions in the design of a larger-scale flow reactor.

The numbering-up approach, however, was observed to result in good yields and conversions at higher concentrations and lowered catalyst loadings (**Table 5.4.17**, Entries 5 and 6). As such, a productive, scalable flow process was demonstrated, whereby notably reduced solvent demand, catalyst loadings and processing times (relative to the initial publication from MacMillan *et al.*¹⁷⁰) was realised, highlighting the benefits of applying flow chemistry to photochemical reactions.

5.5 Conclusions & Further Work

A dual metallaphotoredox catalysed C-O coupling reaction, initially reported by the MacMillan Group,¹⁷⁰ has been adapted and developed into a flow process. This involved replacing the base/electron shuttle system of quinuclidine and K_2CO_3 (as used in the original publication) with **TMG**, as this was found to give a homogeneous reaction mixture, suited to flow processing. After identifying these conditions, an optimisation was performed in a FEP coil flow reactor, using in-house built Lightsabre LEDs (~410 nm). It was demonstrated that performing the reactions in flow could allow a reduction in catalyst loadings (a 10-fold decrease in Ir loading and 5-fold decrease in Ni loading, relative to the initial publication)¹⁷⁰ whilst being applied towards scalable, productive processing. Performing the reactions in flow also allowed for reduction in solvent demand (~2 to 4-fold based upon the initial publication)¹⁷⁰ and a significant decrease in reaction timescale (from 24 h in the original publication,¹⁷⁰ or a few hours as measured in batch reactions in this work, to minutes). This allowed for extrapolated productivities equivalent to ~200 g day⁻¹ (at yields/conversions ~90% upwards) to be observed, illustrating the benefits of continuous flow photochemistry.

There are several avenues for further work. For example, whilst productivity for the process has been demonstrated to be good and scalability can easily be achieved by “numbering-up” flow reactors, a more thorough approach towards reactor design/engineering might result in further benefits towards performing these reactions in flow. For example, a reactor system incorporating a light source with a tuneable wavelength might allow for more efficient photon capture, if a better spectral overlap could be achieved. This, in turn, might allow a further reduction in catalyst loading or shortened reaction times. To complement this, engineering-based modelling of the photoreactors is likely to contribute towards enhanced scale-up.

Furthermore, it has been demonstrated here that this reaction (and possibly similar reactions) displays a temperature dependence. Presumably, this is due to rate enhancement of the Ni catalytic cycle. This suggests that a flow reactor designed for performing high temperature photochemistry may lead to improvements in processing aspects, such as further reduced Ni catalyst demand or shortened reaction times. Whilst temperature control was possible to a limited extent in these experiments, the reactor was not suited to being pressurised (which can be easily achieved in flow, using the right equipment). Therefore, a photoreactor allowing for superheated conditions may be of interest for studying this, and similar metallaphotoredox reactions.

Furthermore, the application of this methodology in a targeted process for the synthesis of a compound of interest (such as a pharmaceutical target or intermediate) may represent the applicability of performing the reactions in flow in a commercial/manufacturing related setting. Ultimately, the goal of performing research in this area (*i.e.*, continuous flow synthesis) is to determine whether process improvements (such as those discovered here) can translate to real world, tangible benefits, and implementing a process such as this into such a system, if successful, would represent a notable benefit.

Chapter 6

Photocatalysed C-O Bond Formation in Continuous Flow:
Ir/Cu-Catalysed C-O Coupling

6.1 Abstract

A flow process for C-O coupling to form alkyl-aryl ethers was developed from a previously published methodology²¹⁸ employing a redox-active *N*-hydroxyphthalimide ester and a phenol, alongside dual Ir/Cu metallaphotoredox catalysis. Being homogeneous, the approach was straightforwardly transferred to a flow process using the same reactor as in Chapter 5 (detailed in the Experimental Chapter).

Process development and optimisations were performed using guaiacol and a cyclohexyl carboxylic acid redox-active ester as coupling partners. Using DCM as a reaction solvent, temperature control over the reactions was implemented to prevent solvent boiling and initial reactions were conducted analogous to the literature conditions²¹⁸ (20 mol% CuCl, 1 mol% Ir-125, 2 eq. Et₃N, ~0.1 M). This led to good observed yields of around 60%, in residence times as short as 2.5 min at 5-20 °C. Subsequent optimisation of catalyst loadings led to the observation that halving both CuCl and Ir-125 loadings (to 10 mol% and 0.5 mol%, respectively) resulted in only a slight reduction in observed yield. Using a lower amount of added Et₃N (1 eq. instead of 2 eq.) appeared to result in improved reaction yields and selectivity, with ~95% yields observed at 5 and 20 °C, in only 2.5 min, using 10 mol% CuCl, 0.5 mol% Ir-125 and 1 eq. Et₃N. These conditions were shown to be suited to a scalable flow process, with observed productivities of up to ~80 g day⁻¹.

Therefore, using the flow reactor, catalyst loadings and processing times were able to be notably reduced for the Ir/Cu-catalysed etherification of the model coupling partners, compared to batch reactions in the previous publications, and good projected productivities observed for a small-footprint reactor, following optimisation.

6.2 Strategy & General Aims

In Chapter 5, the Strategy for developing continuous flow photocatalysed C-O bond forming processes was presented and two reactions were identified as promising for development into a flow process. The first reaction was investigated in Chapter 5 and was focused on developing/adapting conditions previously reported by MacMillan and co-workers,¹⁷⁰ into a continuous process. The second reaction identified involved a decarboxylative approach to the formation of alkyl-aryl ethers, developed by Xile Hu and co-workers.²¹⁸ The decarboxylative approach was investigated in this Chapter, and the reaction stems from the opposite retrosynthetic disconnection of an alkyl-aryl ether to that for the Ir/Ni approach in Chapter 5. As such, a flow process for both approaches would give complementary routes towards alkyl-aryl ethers, in flow.

The broad aims of this Chapter are to investigate whether a second continuous process for photocatalytic C-O bond formation reactions can be developed, by building upon this methodology. If such a process can be developed as part of this work, the aims would then be to optimise the process for factors such as productivity, catalyst loadings *etc.*, much the same as in Chapter 5, to determine whether a developed flow process could allow for processing benefits of the decarboxylative coupling reaction.

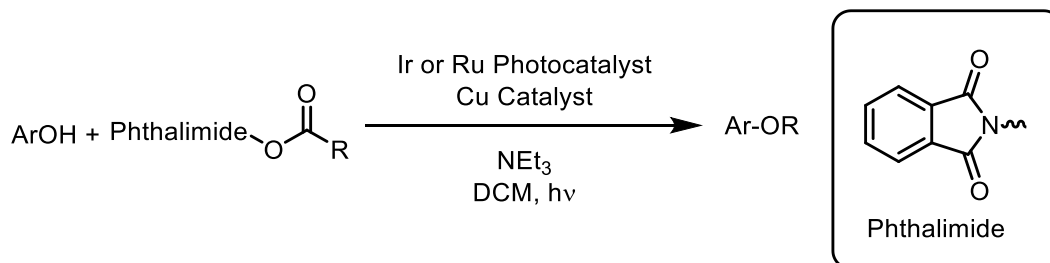
To achieve these aims, the following strategy was taken:

- To determine whether the conditions, as reported in the original publication, could be suited to flow processing.
- To develop conditions suited to flow processing if the original conditions were not identified to be suitable.
- To develop/optimize a flow process using the Booker-Milburn style FEP coil flow reactor, developed as part of the work in Chapter 5.
- To compare flow processes developed from the MacMillan and Xile Hu methodology for processing aspects such as productivity (*i.e.*, yield/time) and catalyst loading.

6.3 Introduction

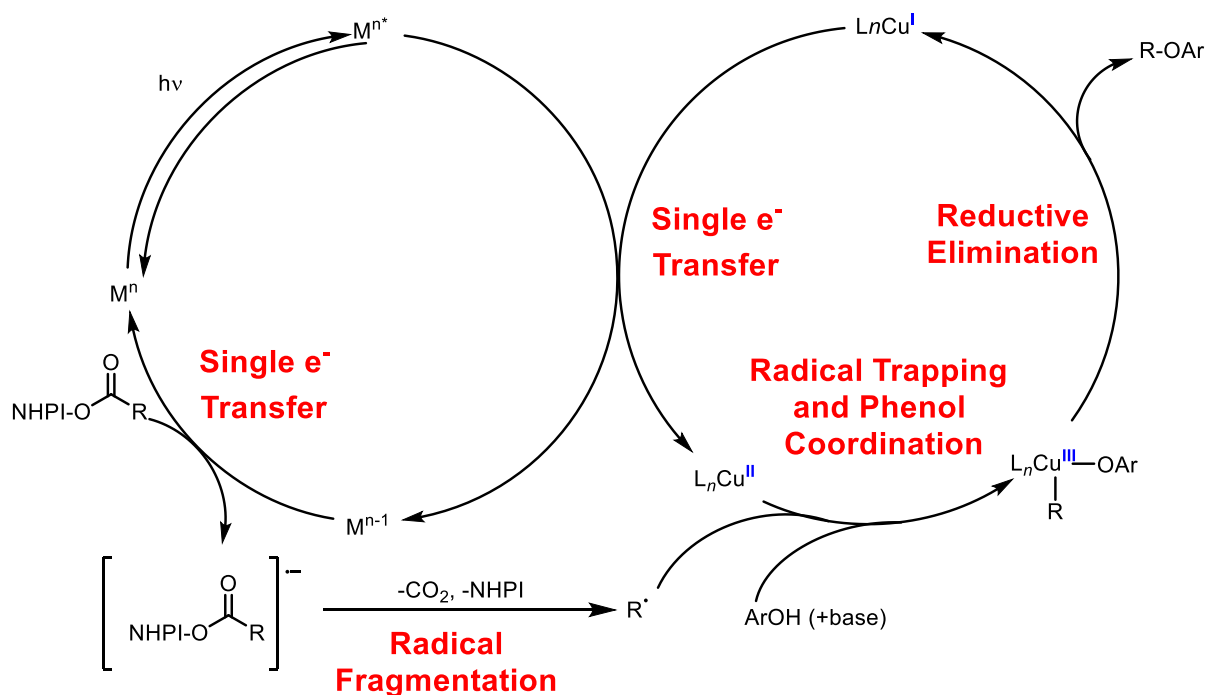
6.3.1 Decarboxylative Metallaphotoredox C-O Coupling Reaction

In Chapter 5, a continuous flow process for a Ir/Ni photocatalytic approach to prepare alkyl-aryl ethers was developed. This hinged upon a reaction from a disconnection between the O-atom and the aryl group in the alkyl-aryl ether linkage, from a procedure originally reported by MacMillan and co-workers.¹⁷⁰ The alternate disconnection for forming such a bond (*i.e.* that between the O-atom and the alkyl group in the alkyl-aryl ether linkage) also furnishes synthons that can be, and have been, considered previously for a photocatalytic approach for alkyl-aryl ether formation, in a procedure reported by the Xile Hu Group (**Scheme 6.3.1**).²¹⁸ This approach employs a redox-active N-hydroxyphthalimido (NHPI) ester of a carboxylic acid, for a decarboxylative approach towards forming alkyl-aryl ethers.²¹⁸



Scheme 6.3.1 general scheme for the decarboxylative, photocatalysed C-O bond formation reaction, developed by Xile Hu and co-workers.²¹⁸

To achieve the transformation, the authors employed a Ru/Cu or Ir/Cu dual-catalytic system. The mechanism for the reaction has been proposed to occur *via* the connected cycles shown in **Scheme 6.3.2**.²¹⁸



Scheme 6.3.2 a general mechanism for the dual-catalytic Ir/Ru with Cu decarboxylative coupling reaction, affording alkyl-aryl ethers.²¹⁸

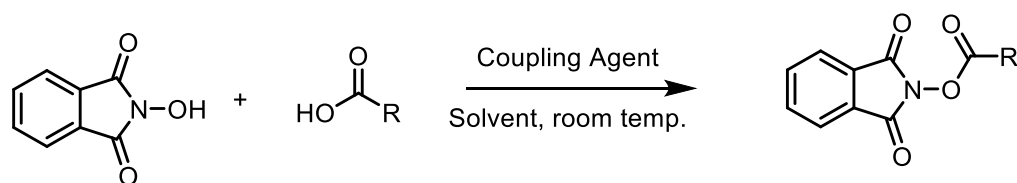
The authors made the following observations in support of this mechanistic proposal. Fluorescence quenching experiments were conducted, and they reported that quenching was *only* observed when the photocatalyst ($[\text{Ir}(\text{dtbbpy})(\text{ppy})_2](\text{PF}_6)$, Ir-125) was in the presence of Cu catalyst (they used $\text{Cu}(\text{MeCN})_4\text{PF}_6$ for these experiments) *and* Et_3N . This would suggest that the photocatalyst was interacting only with a $\text{Cu}^{\text{I}}\text{-NEt}_3$ complex (*i.e.* where $\text{L} = \text{NEt}_3$ and $\text{M}^{\text{n}*} = \text{Ir}^{\text{III}*}$ in **Scheme 6.3.2**).²¹⁸ Undergoing a single electron transfer to the Cu^{I} complex would furnish a Cu^{II} intermediate and an Ir^{II} species. NHPI-esters (with a reduction potential of ~ 1.3 V vs. SCE) could then be reduced by the Ir^{II} species (with an $\text{Ir}^{\text{III}}/\text{Ir}^{\text{II}}$ reduction potential of ~ 1.5 V vs. SCE, more negative than that of the NHPI-ester).²¹⁸ This would generate an alkyl radical, with the loss of CO_2 (**Scheme 6.3.4**). This radical was proposed to then be trapped by the Cu^{II} intermediate (formed by single electron transfer from Cu^{I} to $\text{Ir}^{\text{III}*}$), generating a Cu^{III} intermediate which could then furnish the product and the Cu^{I} intermediate by reductive elimination.²¹⁸ Furthermore, in the presence of TEMPO, the authors reportedly observed trapping of the proposed alkyl radical, supporting somewhat the suggestion of its existence in the mechanism.²¹⁸

Another plausible mechanism could be proposed for this reaction. Differing to that shown in **Scheme 6.3.2**. The photoexcited $\text{Ir}^{\text{III}*}$ could reduce the NHPI-ester, giving an Ir^{IV} species. This Ir^{IV} species could then be reduced by a Cu^{I} species, returning Ir^{III} and generating a Cu^{II} intermediate. The evidence reported by Xile Hu and co-workers however does not support this, as they did not determine any fluorescence quenching of the $\text{Ir}^{\text{III}*}$ by the NHPI-ester.²¹⁸

6.3.2 Redox-Active NHPI-Esters

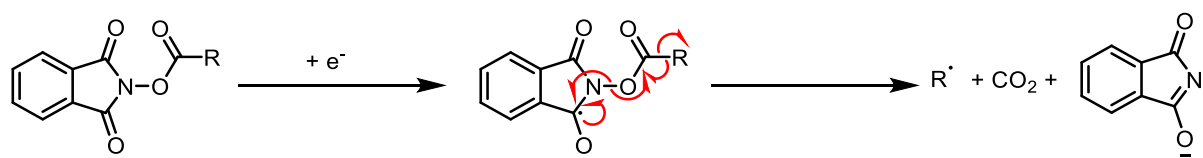
The redox-active nature of NHPI-esters appears crucial to the reaction (by providing an alkyl radical).²¹⁸ These esters are readily formed by coupling of a carboxylic acid and N-hydroxy phthalimide (**Scheme**

6.3.3, using dicyclohexyl carbodiimide and DMAP as coupling agents in this work). NHPI-esters are usually bench-stable so can be useful in synthetic transformations.²²⁷



Scheme 6.3.3 general synthesis of redox-active NHPI-esters using a dialkylcarbodiimide and DMAP as the coupling agents, typically in DCM solvent, generating a dialkyl urea as a stoichiometric by-product in an approach frequently used, for example by Baran.²²⁸

NHPI-esters can be reduced in a single electron transfer and, when doing so, form a carboxyl radical which collapses to give CO₂, the phthalimidyl anion and an alkyl radical (**Scheme 6.3.4**).^{218,227} This is the property which makes these useful for photoredox chemistry, though it is also possible for NHPI-esters to be reduced in non-photo-initiated manners *e.g.* by a transition metal or electrochemically.²²⁷ Therefore, NHPI-esters are important precursors to alkyl radicals, which can then be trapped by various acceptors, in useful synthetic transformations.²²⁷



Scheme 6.3.4 representative pathway for radical generation from redox-active NHPI-esters, where the electron can be provided chemically, photochemically, or electrochemically.²²⁷

6.3.3 Issues with Cu-Catalysis in Synthesis

Xile Hu and co-workers used a Cu^I source to trap the alkyl radical, generated from the redox-active NHPI-ester.²¹⁸ Cu, being an earth-abundant metal, has attracted interest for replacing *e.g.* Pd in coupling reactions due to potential economic and environmental benefits.²²⁹ However, oxidative addition of aryl halides (as typically used in a coupling reaction) to Cu^I is slower than for Pd (and Ni).²³⁰ Reductive elimination on the other hand, from Cu^{III} to Cu^I can be extremely facile, hence Cu can be useful for such reactions, should the issue with slow oxidative addition be resolved (**Fig 6.3.1**).²³⁰

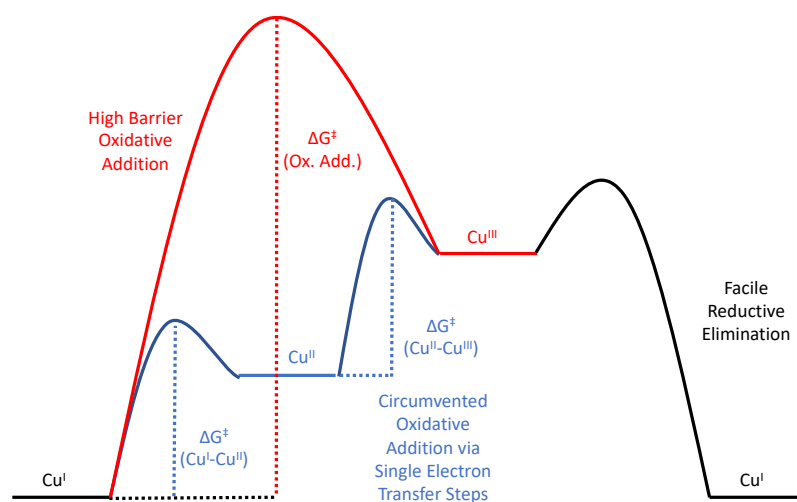


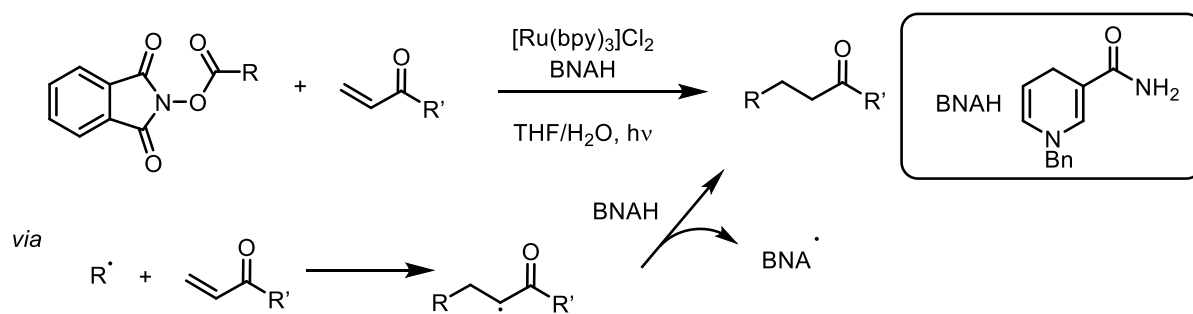
Fig 6.3.1 representation of difficult and facile transformations associated with Cu-catalysis in synthetic chemistry, ΔG^\ddagger represents the free energy change of activation for each respective process.²³⁰

Hu and colleagues addressed the oxidative addition issue to Cu^I,²¹⁸ exploiting that aryl radicals can be readily captured by Cu^{II} species.^{231,232} Therefore, formation of a Cu^{II} species from Cu^I, followed by radical addition to Cu^{II}, giving a Cu^{III} species essentially circumvents the requirement for a direct oxidative addition, whilst affording a Cu^{III}-alkyl species. This can then undergo facile reductive elimination back to Cu^I. In this decarboxylative C-O coupling, single electron transfers *via* photoredox catalysis are used to form a Cu^{II} species *and* to provide an alkyl radical then able to participate in the reaction after capture by Cu^{II}.²¹⁸

6.3.4 Works Exploiting Redox-Active NHPI-Esters

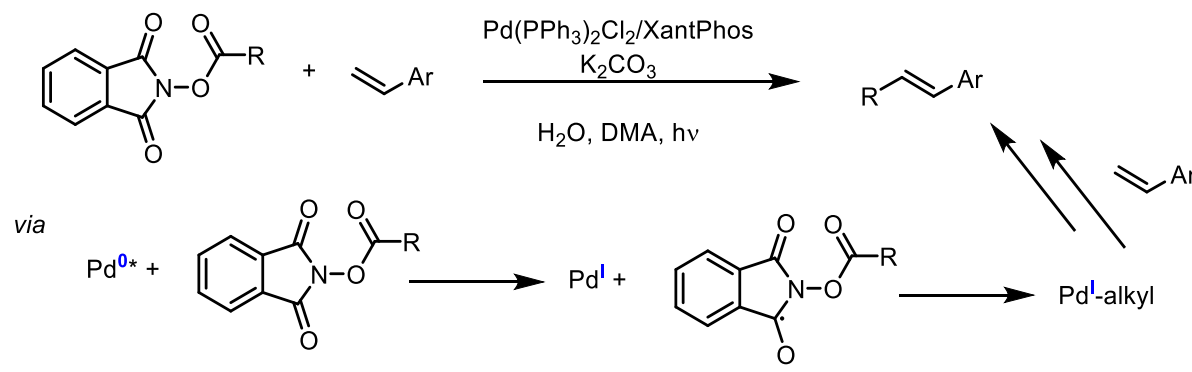
The reaction developed by the Hu Group therefore exploits radical generation from NHPI-esters, and the facile reductive elimination of Cu^{III}, whilst circumventing the requirement for formal oxidative addition to Cu^I.²¹⁸ Previous works have also exploited similar phenomena (though not necessarily together).

Redox-active NHPI-esters have been exploited in C-C and C-X coupling reactions.²²⁷ In an early report using NHPI-esters (and photoredox catalysis), Okada and co-workers demonstrated that irradiation of an NHPI-ester, in the presence of [Ru(bpy)₃]Cl₂, was observed to lead to a reductive Michael addition reaction (in the presence of a hydrogen donor), achieving the formation of a new C-C bond (**Scheme 6.3.5**).²³³ The authors proposed a similar photochemical mechanism to that from Xile Hu in the reaction of interest here. That is, where Ru(II)* undergoes single electron transfer with BNAH forming the reduced Ru(I), that then can reduce the NHPI-ester to form the radical anion and subsequently an alkyl radical *via* decarboxylation. This photoinduced decarboxylation mechanism has also been previously investigated by the Okada Group.²³⁴



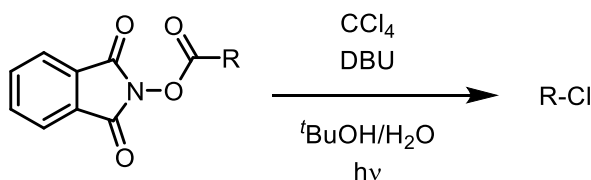
Scheme 6.3.5 radical Michael addition, generating alkyl radicals photochemically from NHPI-esters.²³³

C-C coupling exploiting NHPI-esters has also been shown for decarboxylative Heck-Type Reactions (**Scheme 6.3.6**).²³⁵ The authors proposed that the radical would be generated from the NHPI-ester accepting an electron from the excited state Pd catalyst (forming a Pd^I species). They then propose the radical to be captured by the Pd^I species, giving a Pd^{II} species from which reductive elimination could occur to give olefination of the NHPI-ester alkyl group (with loss of CO₂ and N-hydroxy phthalimidyl anion).²³⁵



Scheme 6.3.6 photoinduced Heck-type Reactions, generating radicals from NHPI-esters.²³⁵

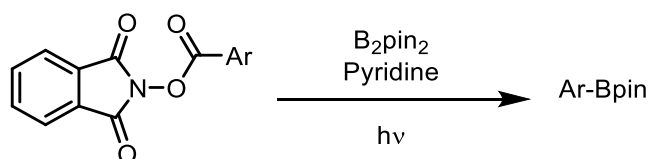
As well as for C-C bond formation reactions, NHPI-esters have also been exploited for C-X bond formation reactions. In a seminal work, Okada and co-workers reported the generation of alkyl radicals from an NHPI-ester *via* direct irradiation using UV irradiation, and that the alkyl radicals can react with CCl₄ to form C-Cl bonds (**Scheme 6.3.7**).²³⁶



Scheme 6.3.7 C-Cl bond formation from NHPI-esters and CCl₄.²³⁶

Also, a number of strategies for achieving photodecarboxylative borylation from NHPI-esters have been reported.²²⁷ One example was reported by Glorius and co-workers (**Scheme 6.3.8**).²³⁷ The authors proposed that direct excitation of the aryl NHPI-ester resulted in single electron transfer from a pyridine-activated diboron complex, generating the aryl radical following decarboxylation. Boron

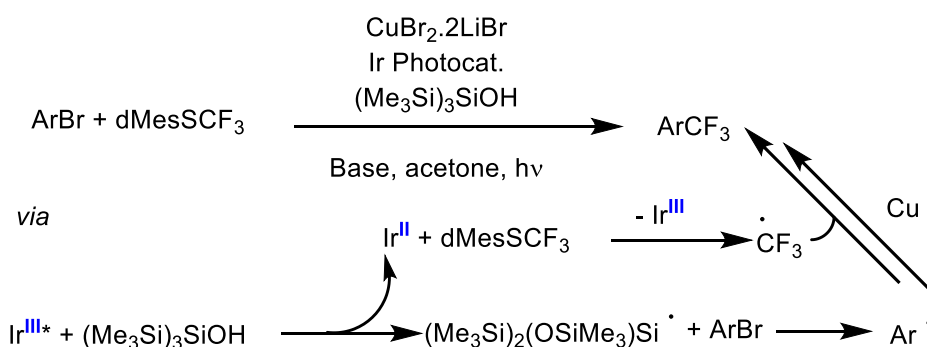
transfer from a pyridine (or phthalimidyl) boron complex to the aryl radical was then proposed to complete the transformation.²³⁷



Scheme 6.3.8 decarboxylative borylation of aryl radicals, generated from NHPI-esters.²³⁷

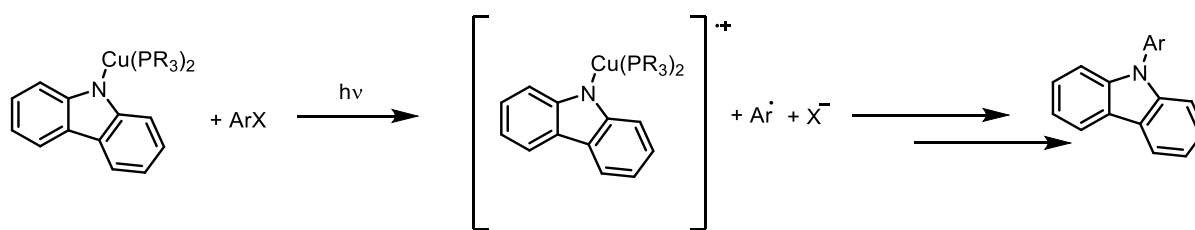
6.3.5 Other Works Circumventing Cu-Catalysis Issues

The MacMillan Group have also investigated the previously mentioned issue in Cu-catalysis using photochemistry, for trifluoromethylation of aryl bromides. To get around the need for oxidative addition to Cu^{I} and instead follow a radical capture pathway, MacMillan and co-workers reportedly generated aryl radicals *via* silyl radical halogen abstraction (**Scheme 6.3.9**).²³⁰ A trifluoromethyl radical was proposed to be generated *via* single electron transfer from the reduced form *i.e.* Ir^{II} form, of the Ir^{III} photocatalyst they employed. This reduced form itself was generated from the photoexcited $\text{Ir}^{\text{III}*}$ first accepting an electron from (*i.e.* being reduced by) the silyl radical precursor which, in turn, generated the aryl radical. Therefore, the authors achieved the generation of two radicals, the aryl radical and the trifluoromethyl radical. Each of these could then be captured by a Cu^{I} catalyst, giving a Cu^{III} species (after capture of both radicals), with subsequent facile reductive elimination giving the trifluoromethylated arene and returning a Cu^{I} species.²³⁰



Scheme 6.3.9 photocatalytic trifluoromethylation of aryl bromides reported by MacMillan, addressing the issue with unfavourable oxidative addition to Cu^{I} .²³⁰

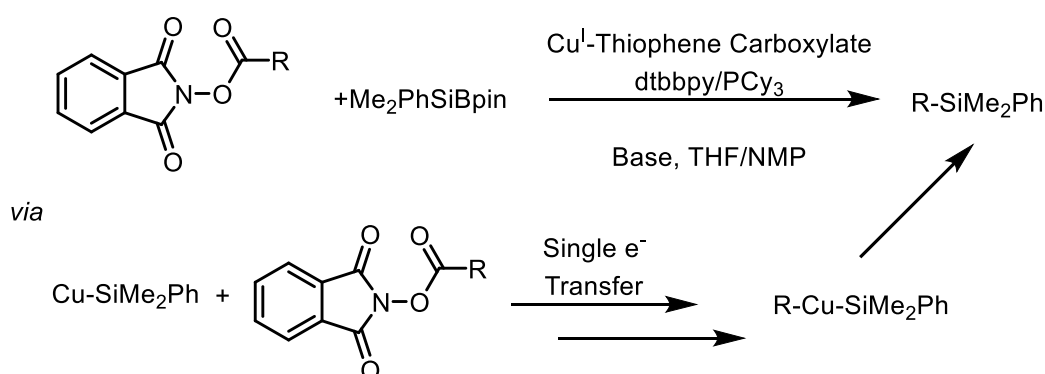
Ullmann Coupling chemistry was introduced in Chapter 5 for C-C coupling (forming biaryls), with a variant of interest for C-O coupling, forming biaryl ethers.^{199,202,203} Another variant on this reaction exists, for C-N coupling, forming aryl amines. Ullmann reaction conditions, using Cu-catalysis, typically require extremely harsh conditions and high Cu loadings.²³² Peters, Fu and co-workers reported a photoinduced Cu-catalysed C-N coupling Ullmann Reaction between an aryl halide and amine (**Scheme 6.3.10**), with EPR spectroscopic evidence to support the occurrence of a radical pathway, circumventing the need for the aryl halide to undergo oxidative addition to Cu. The authors exploited a photoactive Cu-carbazole complex to achieve this.²³²



Scheme 6.3.10 photoinduced Ullmann C-N Coupling exploiting a photoactive Cu catalyst.²³²

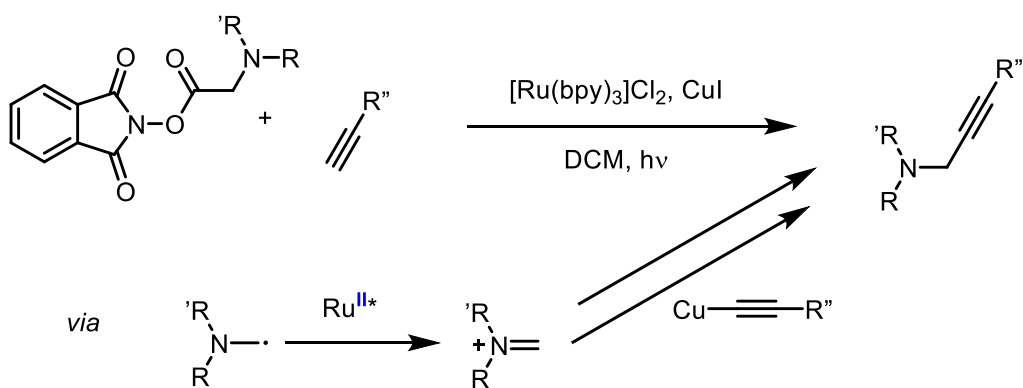
6.3.6 Other Works Circumventing Cu-Catalysis Issues with Redox-Active NHPI-Esters

Oestreich and co-workers combined the previously discussed NHPI-ester radical generation, with Cu-catalysis, as a way to circumvent Cu oxidative addition problems, for C-Si bond formation (**Scheme 6.3.11**).²³⁸ Differing from the approach reported by Xile Hu and co-workers is that Oestreich did not exploit photocatalysis to generate radicals in their work.²³⁸ A Si-B species was used as the Si source, which, when activated by a base was proposed to generate a Si nucleophile.²³⁸ With quantum mechanical calculations used to predict a possible mechanism, the authors then suggested that this Si species was captured by a Cu^I catalyst, with the resulting Cu-Si species then able to undergo a single electron transfer, reducing the NHPI-ester. The subsequent decarboxylative collapse, generating the alkyl radical able to then be captured by the Cu intermediate, forming a species then able to furnish the C-Si coupled product, regenerating the Cu^I species.²³⁸



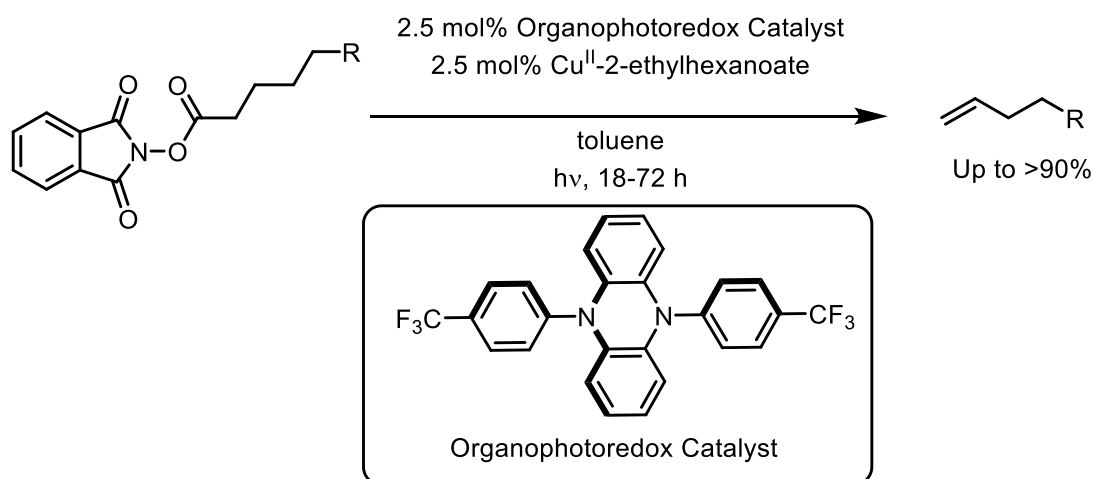
Scheme 6.3.11 C-Si coupling exploiting radical generation via Cu-catalysis, in the absence of light.²³⁸

The merger of photocatalysis/Cu-catalysis, exploiting radicals generated from NHPI-esters, has been reported by Fu and co-workers, for alkylation of amino acid derived NHPI-esters (**Scheme 6.3.12**).²³⁹ The phthalimidyl anion generated as a result of the NHPI-ester fragmentation was suggested to abstract a proton from the alkyne, and an iodide from the CuI starting catalyst the authors used (forming iodide and phthalimide). This resulted in the formation of a Cu^I-alkyl species, then able to undergo reaction with an iminium ion (formed from electron transfer with the photocatalyst), generating the final alkynylated amino acid product.²³⁹



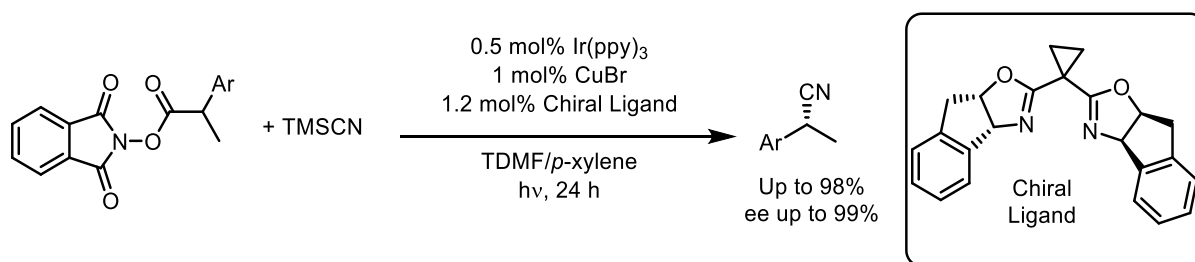
Scheme 6.3.12 amino acid derivative alkylation exploiting Cu and photocatalysis.²³⁹

The Glorius Group have reported organophotoredox/Cu-catalysed olefination, using NHPI-esters (**Scheme 6.3.13**).²⁴⁰ Good yields were achieved for a various NHPI-esters, including those prepared from bio-derived carboxylic acids. A Cu^{II} catalyst was used, and mechanistic studies suggested that the organic photocatalyst undergoes oxidative quenching by the NHPI-ester. The generated alkyl radical was then proposed to be trapped by the Cu^{II} catalyst, generating a Cu^{III} species which eliminates the olefin product, forming a Cu^I species which can regenerate the Cu^{II} catalyst *via* another single electron transfer event.²⁴⁰



Scheme 6.3.13 organophotoredox/Cu-catalysed olefination using NHPI-esters and Cu-catalysis.²⁴⁰

Furthermore, the Liu Group have previously observed that photoredox and Cu-catalysis can be applied for cyanation, generating alkyl nitriles enantioselectively (**Scheme 6.3.14**).²⁴¹ High yields and good enantioselectivities were observed using this approach, under mild conditions, with trimethylsilyl cyanide (TMSCN) as the cyanide source and the reaction was scaled to ~30 g. Fluorescence quenching suggested the NHPI-ester to be the major quenching species (perhaps suggesting an oxidative quenching pathway, forming the radical anion of the NHPI-ester). Furthermore, when TEMPO was added to the reaction mixture, the benzylic radical was trapped, again suggesting decarboxylation of the NHPI-ester to generate the alkyl radical.²⁴¹

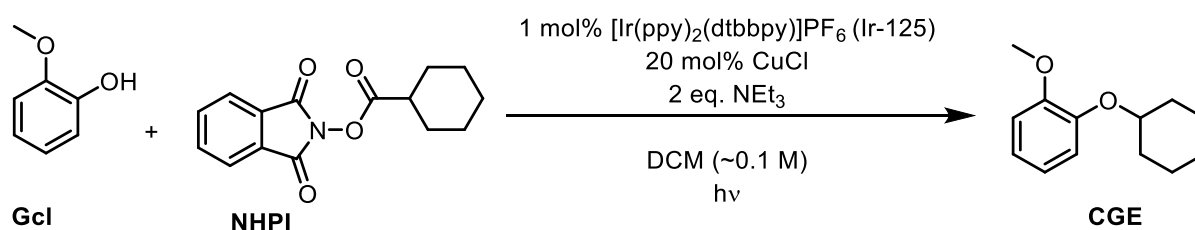


Scheme 6.3.14 *enantioselective cyanation using dual photoredox and Cu-catalysis.*²⁴¹

6.4 Results & Discussion

6.4.1 Initial Reactions in Batch

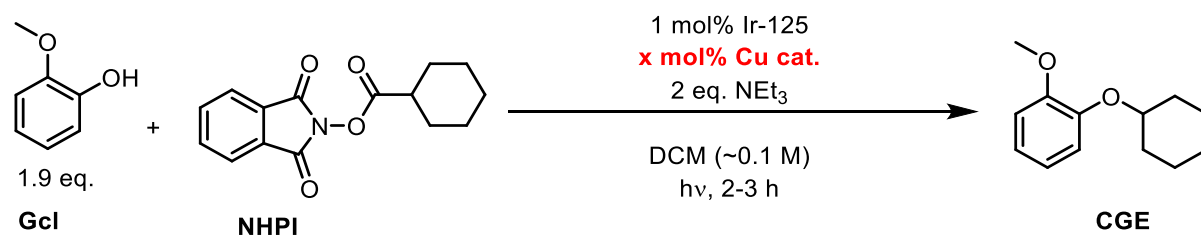
With the aim of developing a flow process for the Ir/Cu dual-catalysed reaction, the first step was to repeat work from the original publication. To develop a flow process, the reaction should be homogeneous throughout, otherwise blockages and reaction failure can occur. Therefore, the initial objective involved repeating the reaction to assess the viability for the development of a flow process.



Scheme 6.4.1 *initial conditions chosen from the literature to begin an assessment of developing a flow process for the coupling method developed by Xile Hu.*²¹⁸

The set of conditions chosen from the original paper involved a Cu^I catalyst with Ir-125 photocatalyst ([Ir(ppy)₂(dtbbpy)]PF₆) to facilitate the reaction between cyclohexyl carboxylic acid NHPI-ester (1,3-dioxoisindolin-2-yl cyclohexanecarboxylate, **NHPI**) and guaiacol (**Gcl**), in the presence of Et₃N, in DCM (Scheme 6.4.1). The authors reported a cyclohexyl-guaiacol ether (1-(cyclohexyloxy)-2-methoxybenzene, **CGE**) yield of between 60-80% under such conditions.²¹⁸

Table 6.4.1 yield of CGE comparing work performed here, with that reported in the literature, showing a discrepancy between the observations.



Entry	Source	Cu Catalyst (Loading, mol%)	CGE Yield / %
1	Xile Hu ²¹⁸	CuCl (20)	62
2	Xile Hu ²¹⁸	Cu(OTf).benzene (10)	82
3	This Work	CuCl (27)	29 ^a
4	This Work	CuCl (20)	65 ^b
5	This Work	Cu(OTf).benzene (20)	75 ^b
6	This Work	Cu(OTf).4(MeCN) (20)	68 ^b

Work conducted here used either a 3.5 W blue (457 nm) LED or 5 x 12 W white LEDs, work from Xile Hu and co-workers used 40 W blue LEDs.

^aIsolated yield for this work after 18 h, GC yield from the work by Xile Hu, after 20 h.²¹⁸

^bGC yield after 2 h.

Observed GC yields were similar here to those reported by the Hu Group (Table 6.4.1, compare Entry 1 with 4 and Entry 2 with 5). Notably, the isolated yield performed in this work was much lower than the GC yields, speculated to perhaps be due to poor isolation procedure, or over-irradiation (18 h irradiation prior to isolation *c.f.* 2 h for GC yield, and no starting material was observed in the crude ¹H NMR spectrum for the mixture prior to isolation). To briefly investigate the reaction timescale, some NMR spectroscopic studies on crude reaction mixtures were performed.

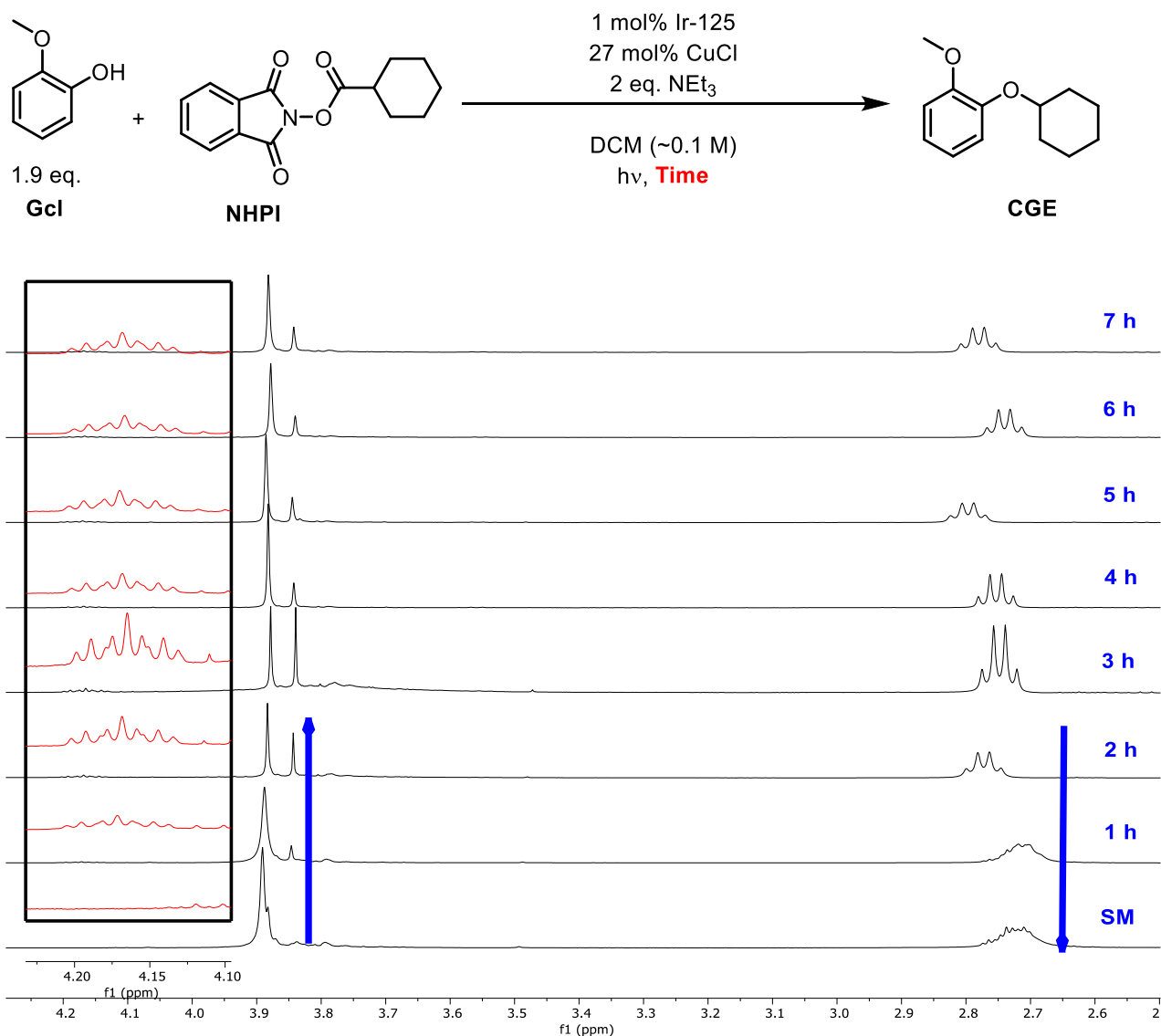


Fig 6.4.1 ¹H NMR spectra taken from crude samples of the decarboxylative C-O coupling reaction at specified time intervals. The signal around 2.7 ppm represents **NHPI** starting material (overlapped with a quartet due to Et₃N) – after 2 h, the Et₃N signal appears well resolved, suggesting full consumption of **NHPI**. The signal around 3.85 ppm (and expansion around 4.15 ppm) are due to **CGE** product, which can be seen to grow in after 1 h irradiation. The signal at around 3.9 ppm is due to **Gcl** starting material (in excess so would likely not be fully consumed). See the Experimental Chapter/Appendix for NMR spectra of pure samples.

The ¹H NMR spectra collected appeared to show that full conversion was attained in ~2 h, due to the disappearance of a peak (overlapped with an Et₃N peak) at around 2.7 ppm (**Fig 6.4.1**). Signals due to product protons were apparent at ~3.85 ppm and 4.15 ppm, observed to grow in (no added standard so not measured quantitatively). It should also be noted that the signal at ~3.9 ppm was representative of the **Gcl** starting material and whilst, observationally, the relative sizes of the product peak (3.85 ppm) and the **Gcl** peak (3.9 ppm) appears to reach a maximum ratio (product/**Gcl**) after 3 h before dropping off, this is not likely a useful analytical interpretation. This is due to the instability of Cu^I-alkoxide/phenoxide complexes upon exposure to air,²⁴² which would form between the CuCl catalyst

and guaiacol, and was rapidly observed to turn brown upon exposure to the atmosphere outside of the inert reaction vessel.

Importantly, the conditions were amenable to flow processing *i.e.*, no solids were observed. Cu(OTf) catalysts appeared to give slightly better yield (both here and in the previous report from Xile Hu),²¹⁸ however the decision was taken to use CuCl in ongoing work for flow process optimisation, due to economic and availability considerations.

6.4.2 Initial Development of Flow Processing Conditions – Residence Time and Temperature

To develop a flow process, the initial objective was to directly transfer the previously employed batch conditions, into flow, using the FEP coil reactor (used in Chapter 5, detailed in the Experimental Chapter). For the batch reactions, a fan was used to cool the reaction mixture to prevent boiling of DCM solvent. However, as the flow reactor used was designed to allow for heating/cooling, this was employed to ensure DCM did not boil off (knowing that the temperature surrounding the LEDs in the flow reactor had been measured to reach up to 70 °C, Chapter 5). All other conditions were analogous to those in batch previously with a 20 mol% CuCl loading, 1 mol% Ir-125 loading using 2 eq. Et₃N as a base/additive and DCM solvent (~0.1 M). Various residence times were explored to determine an idea of working conditions, in the flow reactor.

Table 6.4.2 effect of temperature and residence time on the decarboxylative dual catalytic etherification showing how reactions appear to proceed faster at 20 °C and that reasonable yields could be observed in residence times as low as 1-2.5 min.

Entry	Temperature / °C	Residence Time / min	CGE GC Yield / %
1	5	10	57 ± 5
2	5	5	60 ± 1
3	5	2.5	57 ± 1
4*	5	1	30 ± 5
5*	5	1	33 ± 1
6	10	1	33 ± 5
7	20	1	63 ± 2

*Repeated conditions.

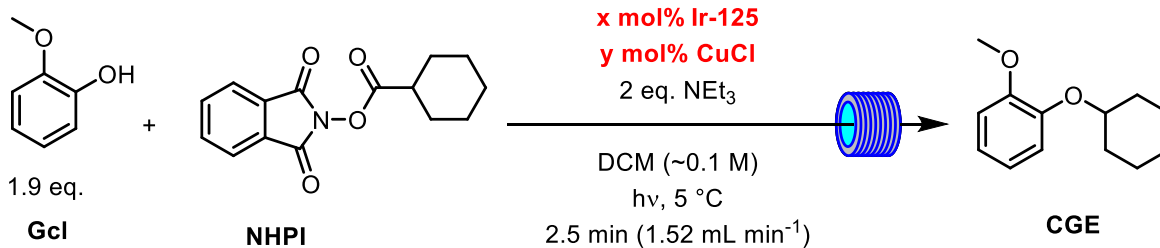
Initially, reactions were cooled to 5 °C to prevent DCM boiling. At a 1 min residence time, a yield of ~30% was observed, whereas, at residence times of 2.5 min or longer, maximum yields of ~60% were observed in all cases (Table 6.4.2, Entries 1-5). Reactions were also conducted at 10 °C and 20 °C and at 5 and 10 °C observed yields were comparable (Table 6.4.2, Entries 4-6). However, at 20 °C, a notably higher yield was observed (Table 6.4.2, Entries 4-7). It was decided to employ 5 and 20 °C for ongoing

reactions, to determine whether notable differences were still obtained under conditions to be attempted in the subsequent optimisation. Having observed good yields in short timescales, it was decided next to determine whether any further benefits of flow processing could be attained, following an optimisation.

6.4.3 Catalyst Loading Screen

It was decided to investigate whether the loadings of both catalysts could be decreased, representing an improvement in the sustainability of the process. The residence time was fixed at 2.5 min where (Table 6.4.3, Entry 1), the maximum yield had previously been observed using the initial catalyst loadings. This was chosen as it was expected that decreasing the catalyst loadings would result in a decreased yield, so a reduction in yield was expected to be observable. Experiments were conducted where, firstly, the Cu loading was reduced at a fixed Ir loading, then, the Ir loading was reduced at a fixed Cu loading.

Table 6.4.3 observed GC yields at different Cu and Ir catalyst loadings illustrating that both loadings could be halved with only a slight reduction in observed yields, though further reductions of either catalyst resulted in lower observed yields.



Entry	CuCl Loading / mol%	Ir-125 Loading / mol%	CGE GC Yield / %
1*	20	1	57 ± 1
2	10	1	24 ± 2
3	5	1	15 ± 1
4	10	0.5	43 ± 1
5	10	0.1	24 ± 3
6	10	0.05	13 ± 1
7	10	0.025	12 ± 1

*Reproduced from Table 6.4.2, Entry 3.

Upon lowering the CuCl loading at a fixed 1 mol% Ir-125 loading, it was observed that the yield decreased (Table 6.4.3, Entries 1-3). Then, fixing the CuCl loading at 10 mol% and varying the Ir-125 loading, it was noted that the observed yield *increased* with an initial decrease to 0.5 mol% Ir-125 (Table 6.4.3, Entries 2 and 4). Further decreases in Ir-125 loading resulted in a notable decrease in observed yield. These observations could perhaps be explained by noting the relative concentrations of Ir:Cu, whereby 10 mol% CuCl and 0.5 mol% Ir-125 (Table 6.4.3, Entry 4) and 20 mol% CuCl and 1 mol% Ir-125 (Table 6.4.3, Entry 1) returned the highest observed yields, both having the same Ir:Cu ratio. Dedicated spectroscopic investigations would likely be required to confirm this hypothesis.

It was therefore observed that the Cu loading could be halved (from 20 mol% to 10 mol%) and the Ir loading also reduced by half (from 1 mol% to 0.5 mol%) observing only a slight decrease in observed yield. In addition, a 10 mol% Cu loading with an Ir loading decreased by 10-fold (from 1 mol% to 0.1 mol%) resulted in the observed yield only approximately halving (~25%) yield. These catalyst loadings were selected for ongoing optimisations.

6.4.4 Optimising Amine Additive Equivalents

As noted by Xile Hu *et al.*, the reaction yield can be influenced by the amount of Et₃N added, and that a decrease in amount of added Et₃N could result in an increase in reaction yield.²¹⁸ This could be due to several reasons. For example, a higher concentration of Et₃N might outcompete reaction substrates for binding to the Cu catalyst, or a higher concentration of amine could lead to quenching of the excited state photocatalyst. Therefore, experiments were conducted using lower Et₃N amounts. The role of Et₃N in the reaction could simply be to deprotonate the phenol starting material (or the phenol after coordination to Cu) to give a Cu-alkoxide intermediate. The Et₃N however may also act as an electron donor (accepting an electron from the photoexcited Ir-125) and be involved in the catalytic electron transfer cycle. Considering that *at least 1 equivalent* (relative to the limiting reagent, here, the NHPI-ester) would be necessary (to ensure deprotonation of the phenol starting material), it was set out to determine whether decreasing the amount of Et₃N could result in improved reaction yield. The aim was to determine whether the observed yields could be increased using a reduced Ir-125 loading (0.1 mol% and 0.5 mol%) and a halved loading of CuCl (10 mol%), by studying the effect of the amount of amine added. As previously, a 2.5 min residence time was used, and reactions were conducted at 5 and 20 °C.

Table 6.4.4 observed yields of the etherification product with different Et₃N equivalents, highlighting how 1 eq. amine appeared to give greater observed yields and that, with a 0.5 mol% Ir loading, excellent yields were observed.

Entry	Temperature / °C	Ir-125 Loading / mol%	Et ₃ N Loading / eq.	CGE GC Yield / %
1*	5	0.1	2	24 ± 2
2	5	0.1	1.5	35 ± 5
3	5	0.1	1	38 ± 3
4	5	0.1	0.5	26 ± 1
5	5	0.5	1	96 ± 6
6	20	0.5	1	97 ± 3

*Repeat of **Table 6.4.3**, Entry 5.

At 0.1 mol% Ir loading, decreasing the amount of Et₃N from 2 eq. to 1.5 or 1 eq. (relative to the NHPI-ester) resulted in an increase in the observed yield, from ~25% to ~35% (**Table 6.4.4**, Entries 1-3). Using a 0.5 mol% Ir loading with 1 eq. Et₃N gave observed yields of ~95%, at both 5 and 20 °C, representing

the highest observed yields so far and, notably, higher than the ~60% yields observed in **Table 6.4.2**, which appeared to be the maximum observable yield previously (though corresponding conversions were not determined). This suggests that the lower Et₃N loading also favoured production of the desired alkyl-aryl ether, possibly due to altering which quenching pathways were favoured. Again, further mechanistic investigation would be required for this.

6.4.5 Optimising Concentration

So far, the reaction had been investigated for the effect of time, temperature, catalyst loadings and amine loadings in a flow process. The aim was to determine whether a scalable, productive process could be developed for the Ir/Cu-photocatalysed C-O coupling. It was decided next to investigate the effect of concentration on the reaction. The hypothesis here was that if the concentration could be increased, the process would benefit from a reduction in solvent requirement, increased productivity (due to increased throughput) and possibly, increased light absorption leading to more efficient reactions. To investigate this hypothesis, at a fixed 2.5 min, at 5 °C or 20 °C, using a 10 mol% CuCl loading and 0.1 mol% or 0.5 mol% Ir-125 loading with 1 eq. Et₃N, the reaction was studied in the flow reactor at concentrations >0.1 M (as was previously employed).

Table 6.4.5 effect of concentration on the metallaphotoredox decarboxylative etherification showing how increased concentrations (>0.1 M) resulted in lower yields.

Entry	Ir-125 Loading / mol%	Temperature / °C	Concentration / M	CGE GC Yield / %
1*	0.1	5	0.1	38 ± 3
2	0.1	5	0.19	13 ± 1
3	0.1	5	0.43	4 ± 1
4	0.5	5	0.14	59 ± 4
5	0.5	5	0.18	31 ± 1
6	0.5	20	0.14	79 ± 6
7	0.5	20	0.18	26 ± 1

*Reproduced from **Table 6.4.4**, Entry 3.

It was observed that an increased concentration resulted in a marked decrease in yield. With a 0.1 mol% Ir loading, upon approximately doubling the reaction concentration, the observed yield reduced to less than half, and significantly reduced at ~0.4 M (**Table 6.4.5**, Entries 1-3). With a 0.5 mol% Ir-125 loading, observed yields were unsurprisingly higher than using a 0.1 mol% loading though, again, increasing the concentration resulted in decreased observed yields (**Table 6.4.5**, Entries 4-7). Therefore, it was decided to conduct the remaining optimisation using a 0.1 M concentration.

6.4.6 Catalyst Screen

For the final optimisation of reaction conditions, it was decided to perform a catalyst screen (involving CuCl and the previously used Cu^I catalysts in **Table 6.4.1**). This was to determine whether either of the Cu-triflate catalysts might have given excellent yields (as in **Table 6.4.4**, Entries 5 and 6), but perhaps in shorter timescales. To investigate this, reactions were performed at shorter residence times (faster flow rates) for the CuCl catalyst (as used previously) to determine the observed yields. Then, at the same residence times, reactions were conducted using the Cu^I-triflate catalysts, to determine whether they gave higher observed yields under comparable conditions.

Table 6.4.6 decarboxylative etherification reactions at 1.25-2.5 min residence times with different Cu^I catalysts, illustrating how shorter residence times resulted in lower observed yields and that CuCl appeared to give higher observed yields under analogous conditions than Cu-triflate catalysts.

Reaction scheme showing the decarboxylative etherification of GcI and NHPI to form CGE. Conditions: 0.5 mol% Ir-125, 10 mol% Cu Cat., 1 eq. NEt₃, DCM (~0.1 M), hv, Temp., Time (Flow Rate).

Entry	Temp. / °C	Flow Rate / mL min ⁻¹	Residence Time / min	Cu Cat.	CGE GC	NHPI GC
					Yield / %	Conversion / %
1*	5	1.52	2.50	CuCl	88 ± 4	88 ± 1
2	5	2.28	1.67	CuCl	50	51
3	5	3.04	1.25	CuCl	41	45
4	5	2.28	1.67	Cu(OTf).4(MeCN)	47 ± 1	62 ± 6
5	20	2.28	1.67	Cu(OTf).4(MeCN)	61 ± 3	69 ± 1
6	5	2.28	1.67	Cu(OTf).benzene	21 ± 1	-
7	20	2.28	1.67	Cu(OTf).benzene	33 ± 5	-

*Repeat of **Table 6.4.4**, Entry 5.

It was observed that the Cu(OTf) acetonitrile adduct gave similar observed yield, but at higher conversion, under comparable conditions to CuCl (**Table 6.4.6**, Entries 2 and 4), whereas the benzene adduct, under comparable conditions, resulted in lower observed yields than CuCl, used in the previous optimisations (**Table 6.4.6**, Entries 2 and 6). As such, the optimised conditions from the screens performed appeared to be 0.5 mol% Ir-125, 10 mol% CuCl, 1 eq. Et₃N (all 2-fold reductions from the original publication) in a short 2.5 min residence time at either 20 °C or 5 °C. These conditions were therefore used ongoing, to determine whether scalability and good productivities could be demonstrated. Using CuCl in place of a Cu(OTf) catalyst would also be a more economic choice.

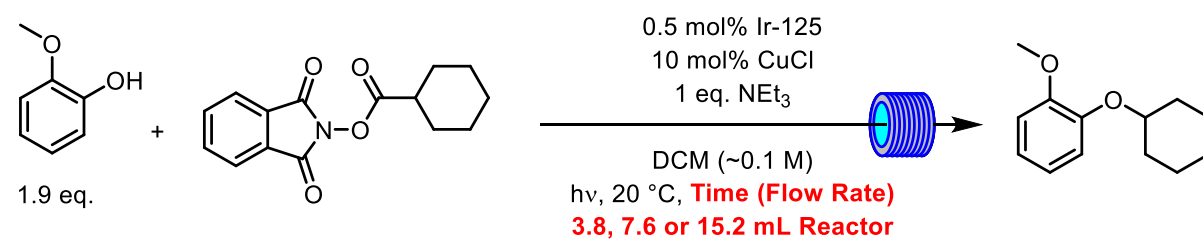
6.4.7 Assessment of the Reaction Scalability and Productivity

So far, a flow process had been developed by implementing the FEP coil flow reactor to the previously developed Ir/Cu dual catalytic methodology. In a short 2.5 min residence time, the maximum reaction yield could be obtained, using conditions only slightly adapted from those previously reported in the literature, but requiring lowered catalyst loadings and amine additive. This highlights the benefit of

using flow reactors for photochemistry, with efficient light penetration leading to rapid reaction timescales.

To finalise the development, determining whether the improved conditions in flow (in terms of reduced catalyst and additive amounts) could be employed for a scalable/productive process. Both an in-series numbering-up or dimensioning approach to scale-up using the FEP coil reactor was to be attempted to determine whether this could increase reaction productivity, by using faster flow rates. These reactor coils were previously described in Chapter 5 (detailed in the Experimental Chapter) and were again applied in this work to determine whether the developed process lent itself towards simple and efficient scale-up, or, whether scale-up of the process would require an approach involving more sophisticated reactor engineering. Furthermore, reaction conversions were also investigated here to determine the selectivity of the reaction, as this had previously been neglected during the survey of conditions, with reaction yield being used to assess the efficiency of the process.

Table 6.4.7 scalability/productivity assessment for the optimised conditions using the Lightsabre FEP flow reactor with a single 1/32 " ID coil (3.8 mL), or two in-series numbered-up 1/32 " ID coils (7.6 mL) or a single 1/16 " ID coil (15.2 mL), illustrating an increase in observed productivity upon reactor scale-up.



Entry	Reactor Volume / mL	Residence Time / min (Flow Rate / mL min ⁻¹)	CGE GC Yield / %	NHPI GC Conversion / %	Productivity / g day ⁻¹
1*	3.8	2.5 (1.52)	97 ± 3	-	44
2	7.6	2.5 (3.04)	62 ± 3	65 ± 3	53
3	7.6	3.0 (2.53)	73 ± 3	85 ± 1	50
4	7.6	4.0 (1.90)	94 ± 5	99 ± 1	49
5	15.2	2.5 (6.08)	51 ± 3	56 ± 5	87
6	15.2	4.0 (3.80)	71 ± 1	98 ± 1	77

*Repeat of **Table 6.4.4**, Entry 6.

Employing a scale-out approach (with two identical 1/32 " ID FEP coils in series, 7.6 mL volume), a slight increase in reaction residence time from 2.5 min to 4.0 min was required to observe similar yields, resulting only in a moderate increase in reaction productivity to ~50 g day⁻¹. Using a dimensioning approach to scale-up (using a 1/16 " ID coil rather than a 1/32 " ID coil of the same length) also required a 4.0 min residence time to achieve good conversion, therefore also resulting in a more notable increase in reaction productivity to ~80 g day⁻¹. As such, these observations demonstrate that the flow process developed could be applied to scalable synthesis, with good projected productivity for a small-footprint flow reactor.

Moreover, compared to the Ir/Ni approach for which a flow process was developed and optimisation performed in Chapter 5, projected reaction productivities were observed to be up to $\sim 200 \text{ g day}^{-1}$, whilst also using a lower Ir loading (0.1 mol% *c.f.* 0.5 mol% in this Chapter). As such, for the processes developed here, the Ir/Ni system appeared more efficient, for the respective model substrates. However, with both systems displaying good yields and productivity *etc.* and showing that processing in flow can be beneficial over a traditional batch approach, applying either Ir/Cu or Ir/Ni approaches appear promising and whichever approach is better for a certain target may depend on the substrates required, for a specific target.

6.5 Conclusions & Further Work

A continuous flow process for the previously reported Ir/Cu dual-catalysed decarboxylative alkyl-aryl etherification reaction was developed *via* optimisation using a FEP photochemical flow reactor. The methodology, using Ir-photocatalysis and Cu-catalysis to furnish an alkyl-aryl ether *via* decarboxylative reduction of an NHPI-ester alongside a phenol coupling partner, in the presence of an amine, was able to benefit from several processing advantages from using a flow reactor. For example, relative to the initial publication in batch,²¹⁸ both the Ir and Cu loadings were able to be halved, representing a more sustainable process likely due to efficient light penetration in flow reactors. Furthermore, the reaction was able to be optimised further by using a lower amount of Et₃N. Using a temperature-controlled reactor to prevent DCM boiling, reactions were found to proceed efficiently in the range of 5–20 °C, appearing to occur faster at 20 °C, in most cases.

With these benefits, short processing times were able to be used (~ 2.5 –4 min), compared to several hours in batch from the previous report²¹⁸ (as well as investigations in this work). Again, this highlights the benefits of applying flow reactors for photochemical synthesis. With this, good reaction productivities were observed, up to $\sim 80 \text{ g day}^{-1}$, using a reactor with only a small-footprint.

Further work should involve determining the scope of the process *i.e.*, whether other redox-active esters or phenols can also be employed, with similar benefits. As well as this, simplifying the process to use a starting material other than NHPI-esters would be beneficial in developing a reaction/process with better atom economy and less processing steps. For example, should a photocatalyst or otherwise which could allow for direct decarboxylation from a carboxylic acid be employed in the reaction then the synthesis of the NHPI-ester and the waste generated both in this synthesis and in the use of the NHPI-ester in the etherification would be mitigated. Also considering the ‘greenness’ of the process, performing the reaction in an alternative solvent to DCM would be desirable. Such considerations therefore represent performing further work into improving the sustainability metrics of the process. Furthermore, Cu-based photocatalysts have also found use in visible light photocatalysis²⁴³ and therefore it could be worthwhile to determine whether a sole Cu catalyst could be employed in the process.

Chapter 7

Investigating the Dual Ir/Ni Etherification Mechanism with
Time-Resolved Infrared Spectroscopy

7.1 Abstract

Time-resolved infrared (TRIR) spectroscopy was used to investigate the mechanism of the MacMillan C-O coupling reaction, forming alkyl-aryl ethers using dual Ni-catalysis and Ir-photocatalysis. Lifetime quenching was observed for excited state Ir-126 in the presence of any of quinuclidine, TMG, NiCl₂.glyme/dtbbpy. No obvious new transient bands were detected, and the ground state Ir-126 fully recovered, apart from when quinuclidine or TMG were present. This suggests quenching occurring *via* an energy transfer pathway for the Ni^{II} catalyst. Complementary spectroelectrochemical measurements suggested that reductive quenching pathways were occurring for quinuclidine and TMG, with a transient signal assigned to the quinuclidine radical cation observed, as well as bleach signals indicating consumption of TMG, as well as a tentative assignment of the reduced Ir^{II} species. Notably, for TMG, quenching was more efficient at 60 °C than at 20 °C, also supported by synthetic observations in Chapter 5. In the presence of all components of the reaction mixture, another tentative assignment was made of a persistent transient band, to be a Ni^I species, formed *via* reduction of the Ni^{II} species added to the mixture. With these observations, and previous synthetic experimental observations (*e.g.*, the fact that no reaction occurred in the absence of quinuclidine or TMG, Chapter 5), a partial mechanistic proposal was conceived. This involved the reductive quenching of Ir^{III*} by quinuclidine/TMG to give Ir^{II} and an amine radical cation. Subsequent reduction of Ni^{II} to Ni^I, presumably by Ir^{II} (reforming Ir^{III}), would give an intermediate which could be postulated to undergo a self-sustained Ni^I/Ni^{III} cycle, in agreement with previous observations reported elsewhere.²¹⁵ Further work, however, would be required to support the tentative assignments (*e.g.* from concentration dependence studies, complementary computational calculations, *etc.*) to reinforce this partial mechanistic proposal. Furthermore, insights into the Ni catalytic cycle might be investigated by the synthesis of proposed intermediates and using TRIR spectroscopy to determine the behaviour of such species following irradiation. With revealing further detail, it would also be interesting to determine the kinetics of steps in the mechanism, and *e.g.*, their temperature dependency, as this might allow for informing optimisation of synthetic processes.

7.2 Strategy & General Aims

This Chapter aimed to investigate the mechanism of the Ir/Ni dual photocatalytic approach for C-O bond formation. These mechanistic investigations used ultrafast time-resolved infrared spectroscopy for studying the processes following photoexcitation.

The purpose of these investigations is ultimately to provide information for the optimisation of synthetic approaches to the reaction of interest. The reaction, in Chapter 5, has been performed in a continuous flow photochemical reactor. The overarching aim would be to determine whether the data from such spectroscopic investigations can allow for improved processing benefits of photocatalytic C-O (and related) bond forming reactions, or the development of new similar reactions, by acquiring an improved mechanistic understanding.

The following general strategies were adopted for the spectroscopic investigations to try and address these aims:

- To use TRIR spectroscopy for characterising the excited state photocatalyst used in the reaction.

- To use TRIR spectroscopy to understand the effect of the reactants, co-catalysts and additives on the photocatalyst, following photoexcitation.
- To use spectroelectrochemistry experiments to determine the spectroscopic features of the redox-active species and to correlate these with observations in the TRIR spectra.
- To combine the above points to give proposals towards mechanistic steps.

7.3 Introduction

7.3.1 Time-Resolved Spectroscopy for Mechanistic Investigation

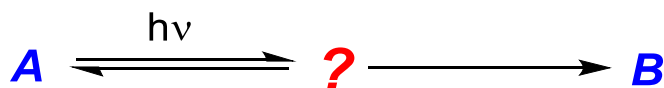
Mechanistic understanding is important for optimising or developing reactions.^{244,245} This involves identifying possible intermediate formation in the mechanistic pathway (**Scheme 7.3.1**). Following a scientific philosophy, determining a *true* mechanism is elusive *i.e.*, experimental observations might allow for eliminating one or more possibilities, towards arriving at a satisfactory understanding of the process of interest, but a full picture can never truly be obtained. Numerous approaches exist for investigating mechanisms such as *in situ* monitoring, isotopic labelling, preformation of proposed intermediates, intermediate trapping and so on.²⁴⁵ In many cases, intermediates are short-lived species and so only ever exist in extremely low concentration at any given moment in the reaction. If trapping of such an intermediate is not possible, it can often be difficult to characterise the proposed/possible intermediate.²⁴⁵



Scheme 7.3.1 *intermediate species formed in the reaction of A → B, understanding what these are and how they form allow for further synthetic advances to be made.*

Time-resolved spectroscopy is a useful approach for possible identification of intermediates involved in ultrafast dynamic processes, in a photochemical reaction pathway.^{246,247} The approach is a “pump-probe” technique.²⁴⁸ This is that a pulse of radiation of a certain wavelength is used to “pump” the species under investigation, *i.e.* to excite the species. A second pulse of a different wavelength (or numerous wavelengths) follows – this is the “probe” signal.²⁴⁸ Due to the extremely fast velocity of radiation, the delay in time which the probe signal arrives at the investigated sample after the pump signal can be very precisely controlled at extremely short timescales, by allowing the pump and probe signal to follow different paths from the source to the sample. In time-resolved infrared (TRIR) spectroscopy, the pump signal is a UV (or visible) beam, and the probe signal is an IR beam. As such, the technique allows for determining the vibrational spectrum of an excited species (or other species formed following photoexcitation), at a chosen ultrafast time-delay after excitation, hence allowing for investigating ultrafast processes following photoexcitation.

As time-resolved spectroscopy can be used to determine the species formed shortly after irradiation of a chromophore (usually at a ps or ns timescale), it can be exploited for identifying short-lived excited states and intermediate species in a photochemical reaction (**Scheme 7.3.2**).²⁴⁸ For example, metal-polypyridyl complexes, commonly used in photoredox catalysis and used in the reaction in Chapter 5 (and in this Chapter) have been investigated previously using time-resolved spectroscopy,²⁴⁹ lending the technique towards mechanistic investigations for photocatalytic reactions.



Scheme 7.3.2 *time-resolved spectroscopy can be used for identifying intermediate species in photochemical reactions.*

Specific detail of the TRIR system used in this work is presented in the Experimental Chapter. In general a TRIR set-up is as follows (**Fig 7.3.1**).²⁵⁰ A seed laser (often Ti:sapphire), generates a pulse that is then split into two optically coupled pump (UV) and probe (broadband or tuneable IR) pulses.²⁵⁰ Each pulse can then pass to *e.g.* an optical parametric amplifier (OPA) to generate the required wavelengths for the pump and probe pulses.²⁵⁰ An optical delay line (typically motorised) is then present along the path of either of the two pulses, to give relative time-delays between each pulse. In a dispersion spectrometer set-up, the pump pulse is filtered out after passing through the sample whereas the probe pulse is fed through to the spectrometer set-up, and the *difference spectra* are acquired.²⁵⁰

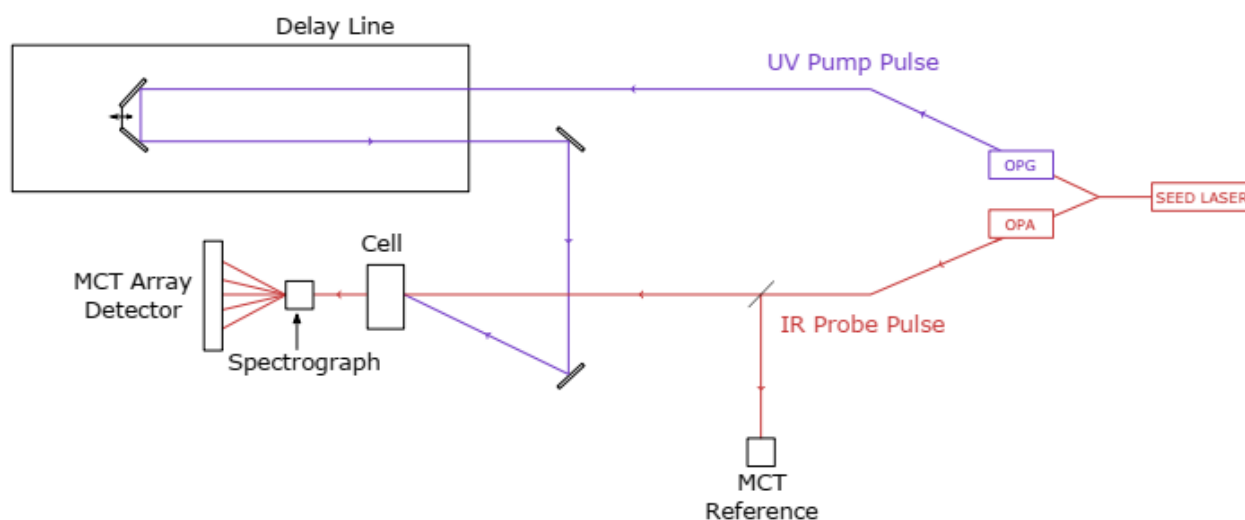


Fig 7.3.1 *an example TRIR spectroscopy set-up. OPG = optical parametric generator, OPA = optical parametric amplifier, MCT = mercury cadmium telluride. Reproduced with permission from Katherine Reynolds' PhD Thesis.²⁵¹*

As TRIR provides difference spectra (*i.e.* subtracts the ground state IR spectrum of the sample from the spectrum at ultra-fast timescales),^{250,252} the spectra obtained show both positive and negative peaks (some example spectra are given later in this section). As such, negative (bleach) peaks correspond to species consumed following photoexcitation (such as ground state species with an IR response in the region being studied). Positive (transient) peaks, on the other hand, correspond to the transient species present (such as photoexcited species, or those which form following photoexcitation).²⁵⁰ Over time, the bleached peaks might grow back in, indicative of *e.g.* the ground state species recovering from the excited state species. If the bleached peaks grow all the way back (giving a change in absorbance of 0 at a particular time-delay), then the ground state species will have fully recovered, in the timescale investigated.²⁵⁰ If they partially grow back (or not at all), there may be some longer-lived species present, or, the excited species might have reacted to give a further species which does not decay back to the ground state.²⁵⁰ Likewise, for the positive signals, if these represent transient species which decay back fully to the ground state in the timescale investigated, the change in absorbance will become 0. If

not, this could be indicative of longer-lived species.²⁵⁰ As such, TRIR spectroscopy can provide insights into the intrinsic vibrational frequencies of the species present in a sample of interest, by tuning time-delays between pump and probe pulse on ultra-fast scales, from analysing the transient features/changes in the IR spectra acquired.^{252–254}

7.3.2 Time-Resolved Infrared Investigations Related to Photoredox Catalysis

It is the aim of the work presented in this Chapter to investigate the mechanism of the MacMillan C-O coupling reaction, using an Ir-polypyridyl photocatalyst, by employing TRIR spectroscopy, which can be used to observe the species which form upon irradiation of such complexes.^{248,253} Upon irradiation, such complexes undergo excitation to the first singlet excited state, typically a ¹MLCT (metal-to-ligand-charge-transfer) state. This is enabled by the low lying LUMO (mainly ligand centred π^*) residing in between the energy levels of the HOMO (mainly metal centred t_{2g} character) and the e_g d-orbitals.^{178–181,253,254} Enabled by the presence of heavy metal atoms leading to efficient spin-orbit coupling, this ¹MLCT state rapidly (usually ps timescale) undergoes intersystem crossing to the lowest energy triplet state (³MLCT).^{182,183} This excitation process can be conceptualised as an oxidation at the metal centre and coincident reduction of the polypyridyl ligand.²⁵³ Due to the formation of the ³MLCT state, the excited state complex typically has a lifetime on the order of ns- μ s due to (relatively) slower relaxation from the triplet to the singlet ground state.^{178–180} As such, the processes occurring on the ps- μ s timescale (Fig 7.3.2) can be investigated using TRIR spectroscopy.^{250,253} Further detail regarding photophysics/photochemistry of such complexes can be found in Chapter 5.

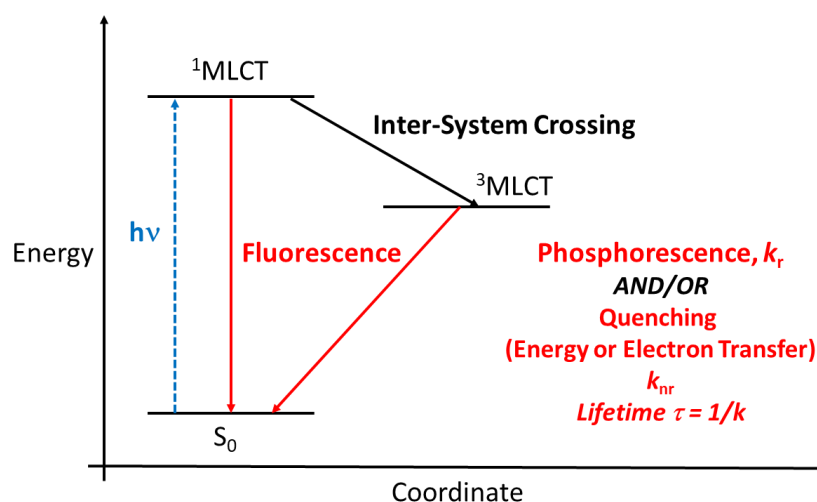


Fig 7.3.2 a simplified Jablonski diagram indicating processes of interest using TRIR spectroscopy.²⁵⁵ For the investigations in this Chapter, the processes occurring on the ns- μ s timescale were of interest, involving the ³MLCT excited state, its lifetime (τ , the reciprocal rate constant, time taken for the concentration to decay to 37% its value) and the resultant species forming.²⁵⁵

It has been well documented that the excited states of metal complexes, such as $[\text{Ru}(\text{bpy})_3]^{2+}$, can be studied using techniques such as TRIR spectroscopy (Fig 7.3.3).²⁴⁹ That is, for example, triplet excited state lifetimes of such metal complexes is typically on the μ s–ns timescale²⁵⁶ and with appropriate laser set-ups, experiments can be performed using the pump-probe technique with the “probe” following the “pump” pulses at time intervals on these scales.^{250,252,253} Singlet excited states are often on the ps timescale,²⁵⁶ which can also be investigated, with an appropriate set-up. In general, due to the absence

of reporter ligands *e.g.* containing carbonyl groups, metal-polypyridyls (such as $[\text{Ru}(\text{bpy})_3]^{2+}$) TRIR experiments are executed in the fingerprint region ($\sim <1500 \text{ cm}^{-1}$).²⁵⁷ In this region, one might expect to observe vibrational modes due to ring stretches (*e.g.* C=C, C-N) as transient excited state signals, or as bleach signals due to the ground state complex.

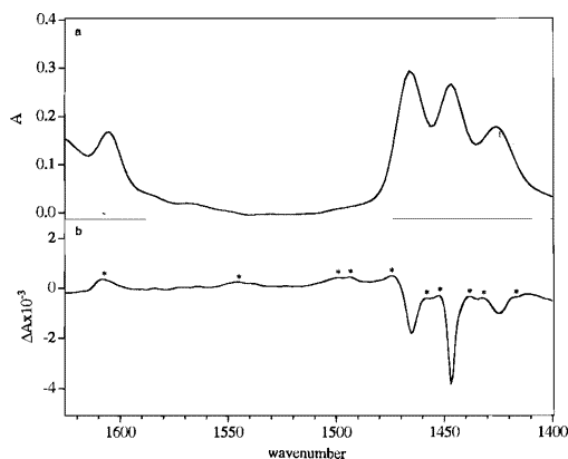


Fig 7.3.3 the first TRIR spectrum acquired for $[\text{Ru}(\text{bpy})_3]^{2+}$ by Meyer and co-workers on around 100 ns timescale (b), with the ground state FTIR above (a) matching with observed bleach signals.²⁴⁹ Reproduced with permission from K. M. Omberg, J. R. Schoonover, J. A. Treadway, R. M. Leasure, R. Brian Dyer and T. J. Meyer, *J. Am. Chem. Soc.*, 1997, **119**, 7013–7018. Copyright (1997) American Chemical Society.

Two of the prototypical Ir-based photocatalysts are $\text{Ir}(\text{ppy})_3$ and $[\text{Ir}(\text{dtbbpy})(\text{ppy})_2]^+$ (Ir-125), related to the catalyst used in this work (Ir-126, $[\text{Ir}\{\text{dF}(\text{CF}_3)\text{ppy}\}_2(\text{dtbbpy})]^+$ which possesses two fluorinated ppy ligands, and a dtbbpy ligand). In a report from Castellano, Bernhard and co-workers, the TRIR spectra of Ir catalysts closely related to Ir-125 and Ir-126 were collected (**Fig 7.3.4**).²⁵⁸ In place of the *t*-butyl groups present on the dtbbpy ligands, two ester functionalities were present (deeb ligand, 4,4'-diethylester-2,2'-bipyridine), and a range of fluorination patterns were used. That is, $[\text{Ir}(\text{ppy})_2(\text{deeb})]^+$ was used as the parent complex and $[\text{Ir}\{\text{dF}(\text{CF}_3)\text{ppy}\}_2(\text{deeb})]^+$ (along with another fluorinated analogue) was also investigated, constituting the deeb analogues of Ir-125 and Ir-126, respectively, with deeb serving as a reporter ligand due to the C=O stretch. Qualitative observations of the TRIR spectra were very similar in each case (**Fig 7.3.4**, with the carbonyl features at $\sim 1700 \text{ cm}^{-1}$ not undergoing significantly different red shifts in any of the excited complexes). This led the authors to conclude that the nature of the excited state in each complex is similar, with supporting DFT calculations assigning these to be mixed MLCT/LLCT (ligand-to-ligand charge transfer) states (*i.e.* not ligand or metal-centred).²⁵⁸ The authors also note that the C=O stretch in each excited state complex was notably red-shifted compared with the ground state C=O stretch, by $\sim 35 \text{ cm}^{-1}$ (**Fig 7.3.4**), indicating a reduction in C=O bond order, suggesting an Ir-deeb MLCT state (as MLCT leads to a formal reduction of deeb by increasing electron density in the deeb π^* -orbital).²⁵⁸ Furthermore, whilst more difficult to interpret, the fingerprint region stretches (assigned to ring stretches on deeb and the ppy ligands by Castellano, Bernhard and co-workers)²⁵⁸ were also shifted to lower wavenumbers in the excited state relative to the ground state (**Fig 7.3.4**), further suggesting the occurrence of deeb reduction (associated with an MLCT excited state). The observation that all of the ring stretches (associated with both deeb and ppy ligands) were red-shifted led the researchers to conclude that the ppy ligands (or fluorinated analogues) were also

undergoing reduction upon excitation, hence the mixed MLCT/LLCT excited state character, a more accurate depiction of what is typically often simply regarded to as the MLCT (or $^3\text{MLCT}$) excited state.²⁵⁸

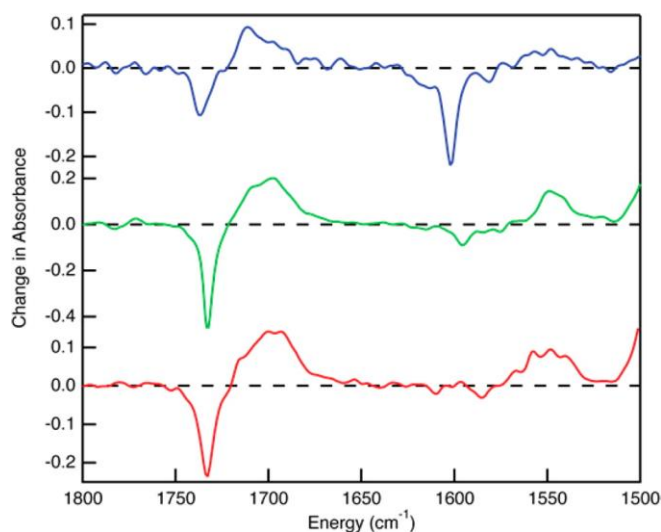
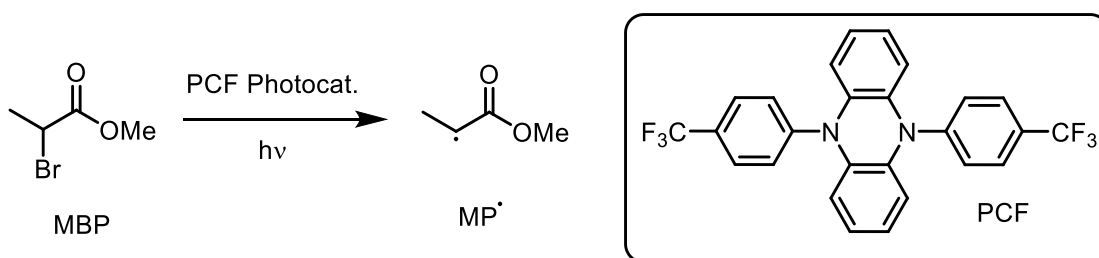


Fig 7.3.4 TRIR spectra of $[\text{Ir}(\text{ppy})_2(\text{deeb})]^+$ (red), $[\text{Ir}(\text{F-mpy})_2(\text{deeb})]^+$ (green) and $[\text{Ir}(\text{dF}(\text{CF}_3)\text{ppy})_2(\text{deeb})]^+$ (blue), in the carbonyl and fingerprint regions, 20 ns after photoexcitation. This shows a red-shift in the carbonyl band ($\sim 1700\text{-}1750\text{ cm}^{-1}$) and the ring stretching bands ($\sim 1600\text{ cm}^{-1}$) indicating the formation of a mixed MLCT/LLCT excited state, with the red-shift indicating a reduction in bond order due to increased electron density in the π^* -orbitals upon photoexcitation.²⁵⁸ Reproduced with permission from Chirdon, D. N., McCusker, C. E., Castellano, F. N., Bernhard, S., *Inorg. Chem.*, 2013, **52**(15), 8795-8804. Copyright 2013 American Chemical Society.

TRIR can therefore identify features of excited state complexes, used as photocatalysts.²⁵³ By extension, TRIR might be used here to identify what happens to excited photocatalysts, in the presence of reaction substrates.^{245,247,255} For example, an interaction between an excited state photocatalyst and a substrate might reduce the lifetime of the excited state photocatalyst *via* electron transfer or energy transfer quenching. TRIR spectroscopy could be used to measure excited state lifetimes (from the decay kinetics of excited state transient peaks or from the recovery of ground state bleach signals). Hence, TRIR spectroscopy could be used to determine what species can act as excited state quenchers, and possibly how they do this. TRIR investigations could also inform upon the nature of the resultant transient species or intermediates, particularly using complementary techniques, such as spectroelectrochemistry.

The Orr-Ewing Group have previously used TRIR and transient absorption (TA – time-resolved spectroscopy with a UV/vis pulse and UV/vis probe) spectroscopy to investigate the mechanism of a proposed photoredox-catalysed reaction.²⁴⁶ This involved an atom-transfer radical polymerisation reaction (**Scheme 7.3.3**), with methylbromopropionate (MBP) as a radical initiator (radical generated *via* photoredox catalysis), and an organic photocatalyst (PCF).^{246,247}



Scheme 7.3.3 atom-transfer radical polymerisation initiation step, via photoredox radical generation from MBP, using an organic photocatalyst (PCF), investigated by Orr-Ewing and co-workers using TRIR and TA spectroscopy.²⁴⁶

Their TRIR experiments (**Fig 7.3.5**) suggested that electron transfer did indeed occur, from the PCF singlet excited state (whereas this would be expected to occur from a triplet excited state for a Ru/Ir catalyst) and that this was responsible for the formation of a methylpropionate radical (MP•, resulting in the PCF radical cation).²⁴⁶ The authors made this conclusion from the TRIR spectra as it was observed that in the absence of MBP, a bleach signal (due to the PCF ground state) was observed, accompanied by a transient band, assigned to the PCF singlet excited state (**Fig 7.3.5 A**). In the presence of MBP, singlet excited state PCF was also identified, but this was observed to decay to a new transient band, with the coincident formation of a second new transient band (assigned to the PCF radical cation and MP radical, respectively (**Fig 7.3.5 B**)).²⁴⁶

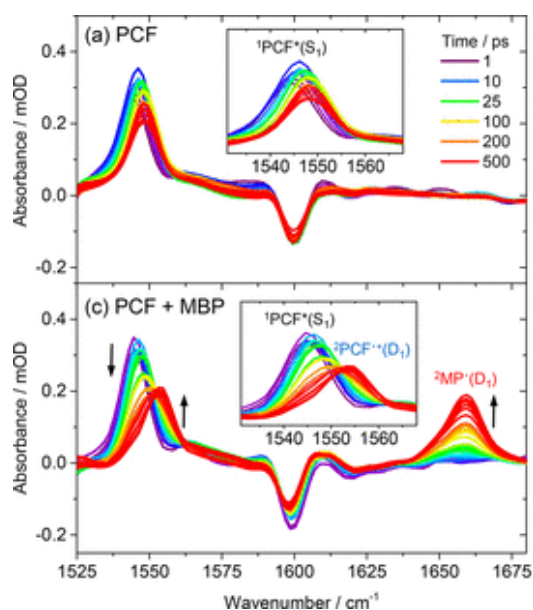
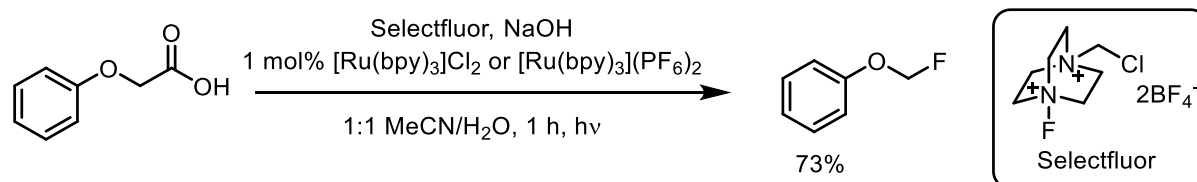


Fig 7.3.5 TRIR spectra of the PCF organic photocatalyst in the (a) absence of MBP, showing the singlet excited state PCF, and (b) presence of MBP, showing formation of a PCF radical cation and a methylpropionate radical.²⁴⁶ Reproduced with permission from D. Koyama, H. J. A. Dale and A. J. Orr-Ewing, *J. Am. Chem. Soc.*, 2018, **140**, 1285–1293. Copyright (2018) American Chemical Society.

Paquin, Sammis and co-workers reported the development of a decarboxylative C-F bond forming photocatalytic reaction, using $[\text{Ru}(\text{bpy})_3]^{2+}$ as the photocatalyst and Selectfluor as the fluorine source (**Scheme 7.3.4**).²⁵⁹ Observing the necessity of both the photocatalyst and light, the authors proposed three possible mechanistic pathways based on either an oxidative quenching, reductive quenching or energy transfer pathway *i.e.* it was possibly considered to be a photoredox reaction (*via* oxidative or

reductive quenching), but an energy transfer photocatalytic mechanism was also plausible. The oxidative quenching proposal involved oxidation by Selectfluor, the reductive quenching proposal involved reduction from the phenoxyacetic acid substrate and the energy transfer proposal involved transfer of energy to the phenoxyacetic acid substrate, facilitating decarboxylation.²⁵⁹



Scheme 7.3.4 decarboxylative C-F bond forming reaction using $[Ru(bpy)_3]^{2+}$ as a photocatalyst, investigated by Paquin, Sammis and co-workers using TA spectroscopy.²⁵⁹

The authors used TA spectroscopy to investigate, which, if any, of their proposals could be supported by the direct observation of intermediates using this technique (**Fig 7.3.6**). To investigate this, they acquired the TA spectra of the photocatalyst alone, the photocatalyst in the presence of Selectfluor and the photocatalyst in the presence of the phenoxyacetic acid substrate.²⁵⁹ For the catalyst alone, formation of the expected 3MLCT state was observed. When phenoxyacetic acid was added to the photocatalyst, an identical set of TA spectra were acquired – suggesting no interaction (*i.e.*, offering no support for the reductive quenching proposal *or* the energy transfer proposal as no interaction with phenoxy acetic acid was observed). When Selectfluor was added to the photocatalyst, a new transient band was apparent after around 2 μs , indicating an interaction between the excited state photocatalyst and Selectfluor.²⁵⁹ Therefore, the observations made by Paquin, Sammis *et al.* would offer some support for their oxidative quenching pathway proposal.

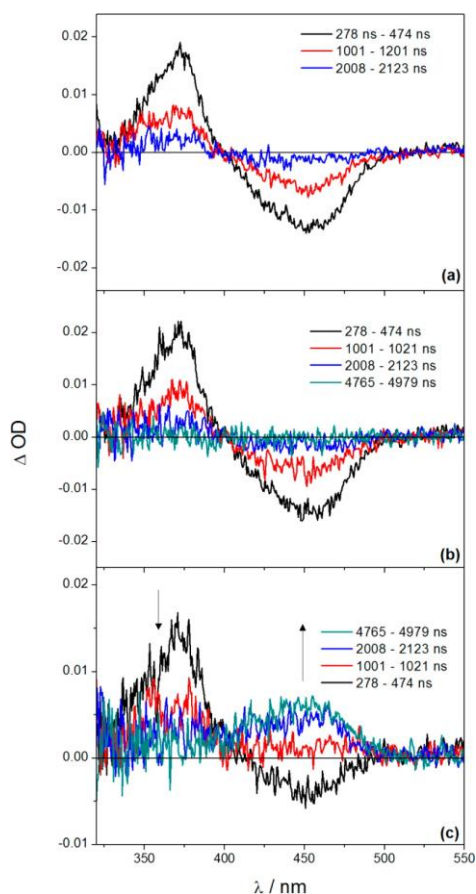
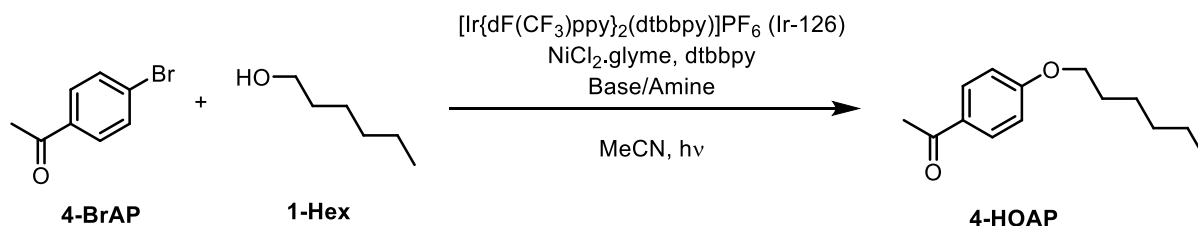


Fig 7.3.6 TA spectra acquired by Paquin, Sammis and co-workers for their $[Ru(bpy)_3](PF_6)_2$ photocatalyst alone (a), the photocatalyst in the presence of phenoxyacetic acid (b) – showing no interaction, and the photocatalyst in the presence of Selectfluor (c) showing the growth of a new transient species.²⁵⁹ Reproduced with permission from M. Rueda-Becerril, O. Mahé, M. Drouin, M. B. Majewski, J. G. West, M. O. Wolf, G. M. Sammis and J. F. Paquin, *J. Am. Chem. Soc.*, 2014, **136**, 2637–2641. Copyright (2014) American Chemical Society.

Similarly, TA spectroscopy has also been used to investigate the mechanism of a photoredox reaction for the anti-Markovnikov selective alkene hydrofunctionalisation, using organic photocatalysts, by Nicewicz and co-workers.²⁶⁰ These examples serve to highlight how TRIR and other ultrafast spectroscopic techniques (*e.g.* TA) can be useful for photocatalysed reactions.

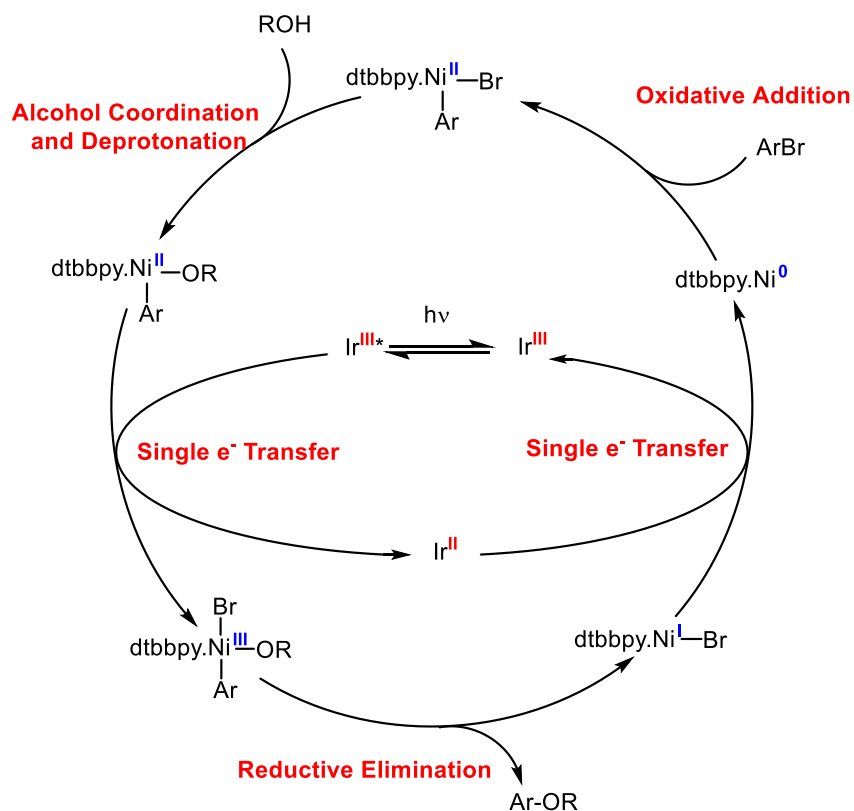
7.3.3 Mechanistic Proposals for the MacMillan C-O Coupling Reaction

As noted in the Strategy Section, the work in this Chapter aimed to investigate the mechanism of a dual Ir/Ni photocatalysed C-O coupling, previously reported by MacMillan¹⁷⁰ and which was the subject of Chapter 5, for developing a flow process. As reported by MacMillan, the C-O coupling reaction involves an aryl bromide, coupled with an alcohol, to furnish an alkyl-aryl ether in the presence of an Ir photocatalyst, a Ni catalyst with a base and/or an amine. MacMillan and co-workers initially reported the use of quinuclidine as an amine additive and K_2CO_3 as a stoichiometric base.¹⁷⁰ The work in Chapter 5 employed *N,N,N',N'*-tetramethyl guanidine (TMG) as a stoichiometric amine/base and it was also observed here, and reported elsewhere,^{170,215} that quinuclidine can be used as a stoichiometric amine/base allowing for removal of K_2CO_3 .



Scheme 7.3.5 MacMillan C-O coupling reaction.¹⁷⁰

MacMillan and co-workers proposed a dual-catalytic cycle in their original report, based upon electron transfer phenomena (Scheme 7.3.6). Their proposal was that the photoexcited Ir catalyst, Ir^{III*}, undergoes reductive quenching by a Ni^{II} proposed intermediate.¹⁷⁰ The Ni catalytic cycle they proposed was mainly reminiscent of a traditional cross-coupling cycle *i.e.* involving oxidative addition, followed by alcohol deprotonation/coordination and reductive elimination to furnish the alkyl-aryl ether product (and a subsequent electron transfer to regenerate Ni⁰ and the ground state Ir catalyst). The difference between the Ni cycle and a conventional cross-coupling cycle being, as indicated previously, the involvement of reductive quenching.¹⁷⁰ The authors noted that Ni^{II}/Ni⁰ reductive elimination (to furnish a C-O bond) had previously been suggested to be energetically unfavourable, whereas Ni^{III}/Ni^I reductive elimination had been suggested to be favourable.²¹³ As such, they proposed the reductive quenching to give a Ni^{III} intermediate as a key mechanistic step. They also observed that the reaction did not proceed well in the absence of quinuclidine *i.e.*, in the presence of K₂CO₃ alone (the same observations were made in Chapter 5), the authors speculated that quinuclidine acted as an “electron shuttle”. That is, that the reductive quenching of Ir by a Ni^{II} intermediate (Scheme 7.3.6) was suggested to be mediated by a quinuclidine species and not occurring directly between the Ir and Ni species.¹⁷⁰



Scheme 7.3.6 *mechanistic proposal published alongside the initial report of the development of the MacMillan C-O coupling reaction.*¹⁷⁰

Whilst the proposal from MacMillan and co-workers appears plausible for producing the observed products, a few immediate questions could be raised and a few of these have been the subject of further investigation, including from MacMillan and co-workers.^{214,261} Some of these questions surrounding the mechanism are briefly summarised below.

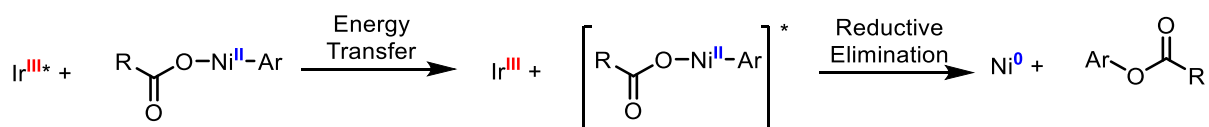
- **Does quinuclidine act as a base and/or a quencher?** Does this mediate electron transfer *and* act as a base (a base would appear necessary for deprotonating the alcohol to give an alkoxide to then coordinate to Ni, or, to deprotonate the alcohol *after* coordination to Ni to give the Ni-alkoxide).
- **Does electron transfer necessarily occur?** That is, is Ni^{III}-Ni^I reductive elimination of absolute importance for obtaining the reaction products, or could an alternative involve *energy transfer* to a Ni intermediate, providing the energy required to undergo Ni^{II}-Ni⁰ reductive elimination.
- **Could an oxidative quenching process be occurring?** That is, a NiCl₂ species is added to the reaction starting mixture. However, beginning a catalytic cycle from Ni⁰ would be likely required for a traditional cross-coupling style cycle. Could Ni⁰ form from oxidative quenching, giving Ni^I with loss of one chloride, which upon alcohol coordination, allows quinuclidine to act as base, pulling off HCl from the resultant catalytic intermediate (a proton from the coordinated alcohol and a chloride ligand from Ni). This would likely *not involve* electron transfers with quinuclidine (as this would be expected to quench *via* reductive quenching not oxidative).
- **Could a quinuclidine radical cation act, if formed by reductive quenching, undergo H-atom transfer (HAT) with the alcohol?** That is, could a quinuclidine radical cation act as a radical generator, rather than as a mediator between Ir and Ni, whereby the resultant radicals facilitate the possible oxidation state modulation of Ni?
- **What Ni species (if any) are involved in electron/energy transfer steps?** That is, does oxidative addition and/or alcohol/alkoxide coordination occur prior to electron transfer (if this is occurring)?
- **Is there a self-sustained Ni^I/Ni^{III} cycle?** That is, (if occurring) does a photoredox electron transfer event form Ni^I from a Ni^{II} precursor, and then a Ni^I/Ni^{III} cycle operate, or (again, if occurring) is a photoredox electron transfer event required in every cycle turnover?

The points above intend to highlight how, even for a plausible mechanism with an amount of supporting evidence, numerous suggestions can be made which could also be plausible. It could also be plausible that the product of the reaction can be formed by numerous mechanisms. Furthermore, it could be possible that these mechanisms occur at different extents under different conditions. The aim of this Chapter is to investigate mechanistic aspects of the MacMillan C-O coupling, using TRIR spectroscopy.

7.3.4 Previous Investigations of Mechanisms for the MacMillan C-O Coupling Reaction

Previous investigations were reported by the MacMillan Group in collaboration with the Scholes Group.^{214,261} In this work, they used representative substrates from a C-O coupling reaction where the product would be an alkyl-aryl *ester* using a *carboxylic acid* (Scheme 7.3.7) rather than an alkyl-aryl ether, using an alcohol, as used in the work in this Thesis.²⁶¹ In the initial report from the MacMillan Group on the synthesis, the authors concluded that an energy transfer mechanism was operative from

the following observations. A variety of Ir photocatalysts were synthesised with varied ³MLCT state energies. Catalysts with a ³MLCT energy below a certain threshold were observed to give no conversion.²⁶¹ Furthermore, the catalysts also showed that the yield of the product was correlated *oppositely* to the oxidising potential of the catalyst *i.e.* the more strongly oxidising catalysts (more capable of being reduced, whilst in turn oxidising Ni^{II}-Ni^{III}) were shown to give lower yields – the opposite of what would have been expected if a mechanism such as in **Scheme 7.3.6** was operative.²⁶¹ Moreover, the authors also pre-formed a proposed intermediate (a Ni^{II} carboxylate) and showed that irradiation in the presence of an Ir photocatalyst resulted in reductive elimination furnishing the reaction product (though this could still be considered possible *via* a direct electron transfer process, rather than amine mediated) – importantly, this did not occur in the absence of light though, lending support to the idea that some form of activation is required to make the reductive elimination step become a facile process.²⁶¹ In a follow-up study in collaboration with Scholes, the authors used TA spectroscopy.²¹⁴ Both this and the synthetic study used Ir(ppy)₃ as a catalyst and ^tBuⁱPrNH as an amine. In their TA experiments *no Ir^{III}* quenching due to the amine was observed.*²¹⁴ Highly efficient quenching by a pre-formed Ni^{II}-Ar-acetate proposed intermediate, however, was observed.²¹⁴ This therefore exemplifies the way in which time-resolved spectroscopy can be used to begin to determine mechanistic features. Using spectroelectrochemistry as a complement, the authors did not observe the presence of Ir or Ni species other than Ir^{III} or Ni^{II}, supporting the claim of energy transfer rather than electron transfer leading to the furnished product.²¹⁴



Scheme 7.3.7 part of a mechanistic proposal for alkyl-aryl ester formation involving energy transfer, not electron transfer, from Ir^{III}* to an Ni^{II} intermediate, with supporting evidence from TA spectroscopy indicating a direct interaction between Ir^{III}* and no direct interaction between Ir^{III}* and ^tBuⁱPrNH – a possible reductant.^{214,261}

Based on these mechanistic suggestions from MacMillan and Scholes on the esterification reaction, it could be plausible therefore, that an energy transfer, rather than electron transfer mechanism, could be proposed for the etherification reaction. Other works have investigated which mechanism could be operative in the etherification reaction, of interest to work in this Thesis.

In a study from the Nocera Group, the MacMillan etherification reaction was investigated using TA spectroscopy.²¹⁵ The reaction starting materials in this work were the same model species used in the synthetic work in this Thesis apart from using methanol as the alcohol instead of 1-hexanol. That is, they employed 4-bromoacetophenone as the aryl bromide, methanol as the alcohol, [Ir{dF(CF₃)ppy}₂(dtbbpy)]PF₆ (Ir-126) as the photocatalyst and quinuclidine as a stoichiometric amine additive (due to K₂CO₃, insoluble in MeCN, being unsuitable for spectroscopic measurements).²¹⁵ In contrast to observations reported from MacMillan and Scholes on the esterification reaction, the authors noted that the amine they employed (quinuclidine) was the predominant quencher of their Ir^{III}* species.^{214,215,261}

At this stage, from these observations alone it can be noted therefore that whether quenching is observed from the photocatalyst by an amine depends on the specific identities of the photocatalyst

and the amine. That is, using $\text{Ir}(\text{ppy})_3$ and ${}^t\text{Bu}^i\text{PrNH}$ *did not* lead to observed quenching²¹⁴ whereas using $[\text{Ir}\{\text{dF}(\text{CF}_3)\text{ppy}\}_2(\text{dtbbpy})]\text{PF}_6$ and quinuclidine *did* lead to observed quenching in these two studies.²¹⁵ This could be due to differing reduction potentials, which itself could suggest that electron *or* energy transfer mechanisms may be predominant, depending possibly upon the selection of such components. In the study from Nocera and co-workers, quenching of $\text{Ir}^{\text{III}*}$ *was observed* from the Ni^{II} catalyst (here, the authors used the catalyst as entered into the reaction mixture *i.e.*, $\text{NiCl}_2\cdot\text{dtbbpy}$ as opposed to a pre-formed proposed intermediate as MacMillan, Scholes and co-workers opted for). However, the quenching was much less efficient compared to quenching from quinuclidine.²¹⁵ This observation could suggest that the interaction between the photocatalyst and quinuclidine is the major mechanistic step. However, further evidence than simple quenching studies are required for fuller mechanistic details.²⁵⁵

Nocera and co-workers attempted to deconvolute their TA spectra to attempt to identify the transient species (Fig 7.3.6). The authors proposed the formation of a quinuclidine radical cation, with a feature in their subtracted TA spectra being similar to a computed spectrum of a quinuclidine radical cation dimer.²¹⁵ To obtain their subtracted spectra, the authors performed spectroelectrochemical experiments on the Ir complex and subtracted this from the acquired TA spectra.²¹⁵ This observation would support the occurrence of a mechanism involving reductive quenching by quinuclidine, however, a more direct observation of the suggested radical cation would further strengthen this claim.

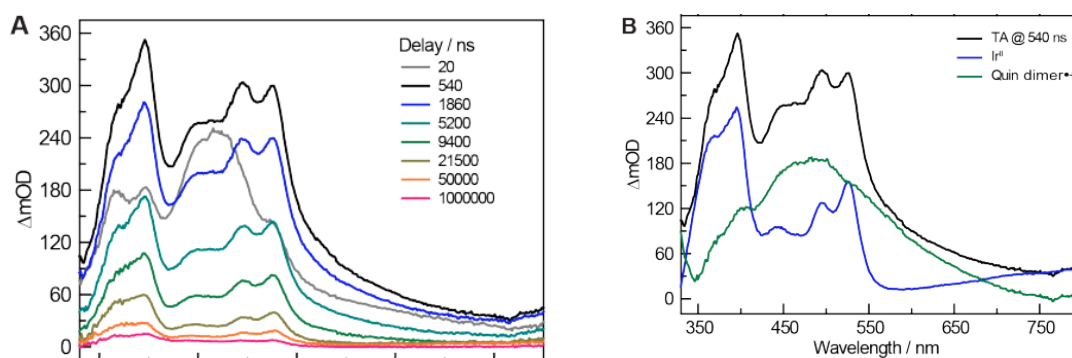
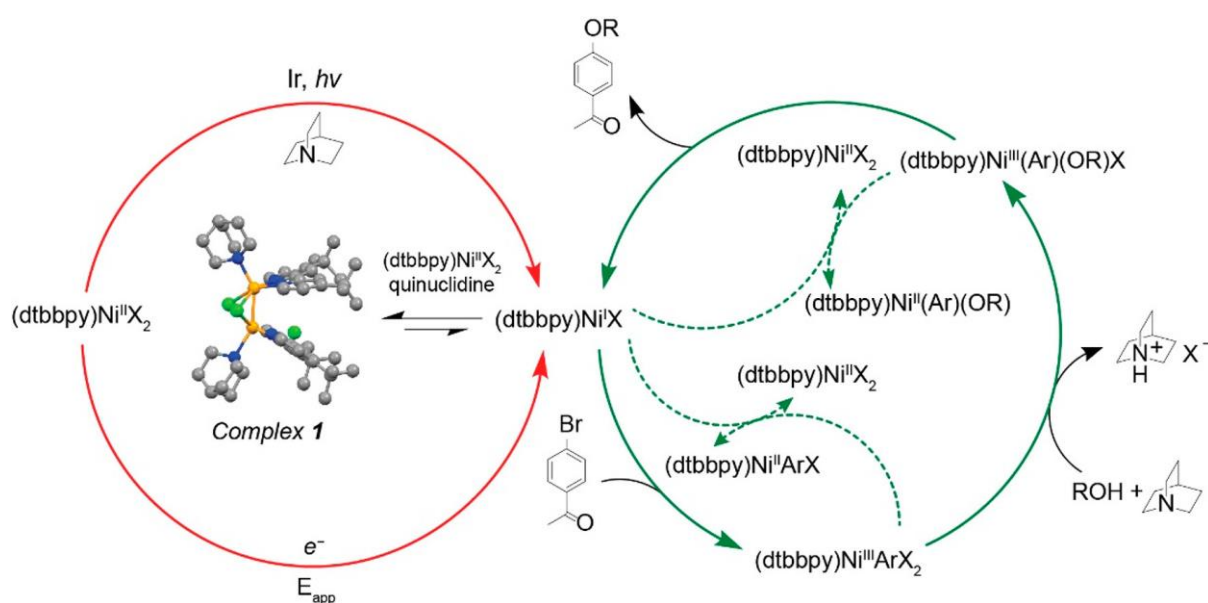


Fig 7.3.6 TA spectra acquired by Nocera and co-workers for an Ir^{III} photocatalyst, in the presence of quinuclidine (left), with a deconvolution (right) assisted by spectroelectrochemistry measurements and computational calculations suggesting the presence of a quinuclidine radical cation dimer – offering support for reductive quenching by quinuclidine.²¹⁵ Reproduced with permission from R. Sun, Y. Qin, S. Rucolo, C. Schnedermann, C. Costentin and D. G. Nocera, *J. Am. Chem. Soc.*, 2019, **141**, 89–93. Copyright (2019) American Chemical Society.

Another observation from Nocera and co-workers was that the Ni catalytic cycle may be self-sustained,²¹⁵ *i.e.* not every cycle involving the Ni catalyst requires a photon for turnover. Their evidence to support was as follows. Firstly, a quantum yield of >1 was measured indicating multiple catalytic cycles could turnover to generate the product from just a single photon.²¹⁵ Furthermore, using electrochemical apparatus, a Faradaic yield of >1 was observed for the Ni-catalysed reaction *i.e.* just a single electron transfer could facilitate the turnover of multiple catalytic cycles.²¹⁵ This would suggest a self-sustained Ni catalytic cycle. This could raise the following question: in the photochemical synthesis, could a flash of light be used to initiate the reaction, then turned off and the reaction would still occur? Evidence elsewhere, however, has suggested this to not be a useful means of performing the reaction.^{222,223} Nocera and co-workers made another observation to support a hypothesis as to why this

might be the case. In their TA experiments, over the course of a few hundred μs , they identified a new species forming in their transient spectra and subsequently isolated a bimetallic Ni intermediate and characterised this crystallographically.²¹⁵ When subjected to the reaction conditions, this was shown to give suppressed reactivity. They proposed that the bimetallic intermediate they identified was a result of comproportionation of Ni^{I} and Ni^{III} species in the suspected self-sustained catalytic cycle, giving the Ni^{II} bimetallic intermediate, resulting in catalyst deactivation.²¹⁵ The authors proposed therefore, that redox steps (*i.e.* from the continued irradiation) was necessary to break up the Ni^{II} bimetallic intermediate, regenerating active Ni^{I} species. This would explain quantum/faradaic yields >1 and also explain the necessity for sustained irradiation.²¹⁵ They used these observations for a mechanistic proposal (Scheme 7.3.8).



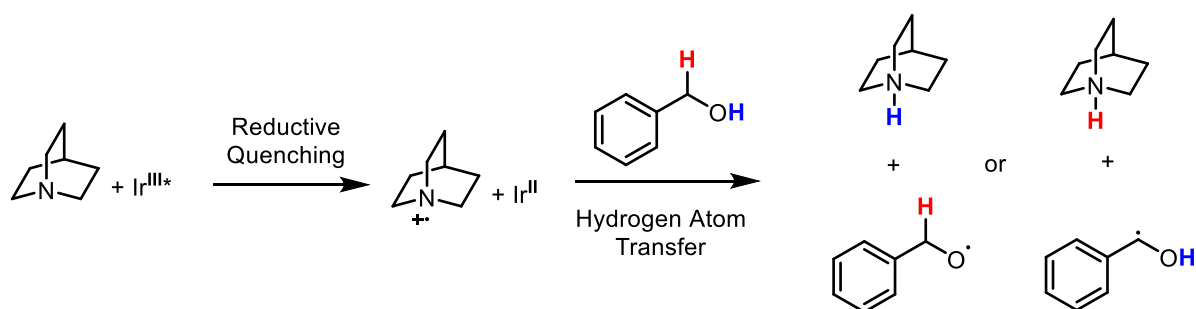
Scheme 7.3.8 proposed catalytic cycle from Nocera and co-workers highlighting their identification of a dimeric Ni complex, their observation a self-sustained $\text{Ni}^{\text{I}}/\text{Ni}^{\text{III}}$ cycle, the possibility of direct electrochemical activation and noting the importance of quinuclidine as an electron transfer agent as suggested by their TA experiments.²¹⁵ Reproduced with permission from R. Sun, Y. Qin, S. Rucolo, C. Schnedermann, C. Costentin and D. G. Nocera, *J. Am. Chem. Soc.*, 2019, **141**, 89–93. Copyright (2019) American Chemical Society.

Despite the interesting findings from Nocera and co-workers, there are further mechanistic aspects which further studies *e.g.*, using TRIR spectroscopy may inform, or provide further support for, alongside this.

Work related to this reaction has also been carried out from a theoretical perspective. Zhong-Min Su, Wei Guan and co-workers investigated, computationally, the role of quinuclidine in the reaction.²¹⁶ The authors cited the possibility of quinuclidine acting as a base, HAT agent or electron shuttle as some of the ambiguities surrounding its use.²¹⁶ It should be noted that multiple pathways may well exist and to some extent all of these *may* occur in a real synthesis.

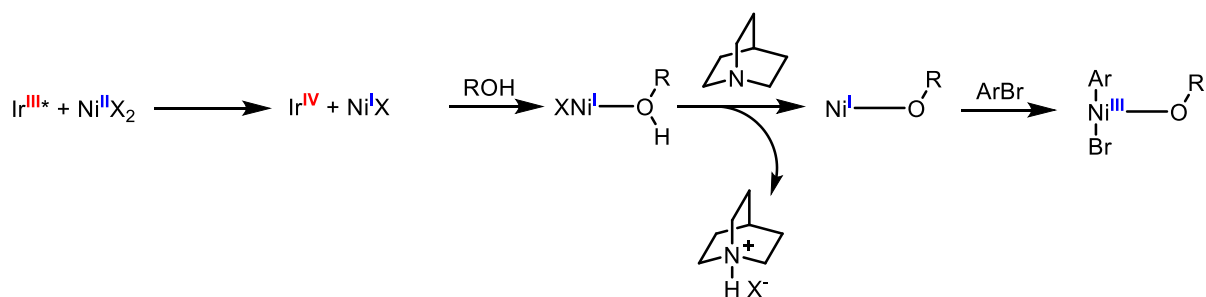
Investigating a reductive quenching proposal, where $\text{Ir}^{\text{III}*}$ is reduced to Ir^{II} by quinuclidine, forming a quinuclidine radical cation, the authors used computational methods to model HAT processes involving

the quinuclidine radical cation.²¹⁶ Two reasonable suggestions were considered. That the quinuclidine radical cation could undergo HAT generating an O-centred radical (*via* HAT of the hydroxyl hydrogen on the alcohol, for which they modelled using benzyl alcohol) or alternatively, the quinuclidine radical cation could undergo HAT generating a C-centred radical (*via* HAT of the benzylic hydrogen), **Scheme 7.3.9**.²¹⁶ Due to the stability of benzylic radicals, as would be expected, their calculations suggested a more stable C-centred radical than the O-centred radical. What is more, the activation energy for the formation of the C-centred radical was notably lower than the activation energy for the formation of the O-centred radical.²¹⁶ Their proposal for this mechanism would then likely involve radical trapping *via* the Ni catalyst where the radical capture processes would modulate the Ni oxidation state. However, with their calculations suggesting more favourable production of a C-centred radical, it would be expected that at least some C-C coupled product as opposed to C-O coupled product would be formed, and this has not been suggested experimentally. This would suggest a HAT mechanism to not be operative, however, under real experimental conditions using substrates where the C-centred radical may not be as stable as a benzylic radical, it may not be totally unexpected for a O-centred radical to form in such a case and possibly be responsible for (maybe some) product formation.²¹⁶



Scheme 7.3.9 *H-atom transfer mechanistic possibilities investigated as part of a theoretical study from Zhong-Min Su, Wei Guan and co-workers.*²¹⁶

Zhong-Min Su, Wei Guan and co-workers then theoretically investigated the possibility of a mechanism based upon oxidative quenching, whereby Ir^{III}* oxidised to Ir^{IV} whilst reducing Ni^{II} to Ni^I, **Scheme 7.3.10**.²¹⁶ In their investigations, NiCl₂.dtbbpy was probed as the Ni^{II} source, as was used experimentally in the work in this Thesis and elsewhere. Generating a Ni^ICl.dtbbpy intermediate, their proposal then involved coordination of benzyl alcohol and coordination of quinuclidine to the hydroxyl proton. Removal of this proton by quinuclidine was proposed to give a Ni^I-alkoxide species capable of undergoing oxidative addition of the aryl bromide then reductive elimination to furnish the product and a Ni^I-bromide.²¹⁶ Oxidation by the previously generated Ir^{IV} species was proposed to return the Ni^{II} and Ir^{III} species, closing the two cycles. Their calculations suggested this pathway to be favourable over either of the previously described pathways initiated by reductive quenching. However, the study only represents a comparison between two possibilities where others, such as those described previously *e.g.* involving reductive quenching but not necessarily HAT may be operative.²¹⁶



Scheme 7.3.10 part of a mechanistic proposal involving oxidative quenching of Ir photocatalyst eventually forming a proposed crucial Ni^{III} intermediate required for reductive elimination. Subsequent oxidation of the resultant Ni^I species was proposed to reform Ir^{III} and Ni^{II}, connecting a catalytic cycle. This mechanism was investigated theoretically by Zhong-Min Su, Wei Guan and co-workers where they reported their findings to show the mechanism feasible.²¹⁶

7.3.5 Summary

An overview has been given as to how time-resolved spectroscopy can be used as a tool for determining features of ultrafast processes occurring in *e.g.*, metal complexes typically used in photocatalysis. The MacMillan C-O coupling reaction is one such reaction involving metal complex photocatalysts. For such reactions, there typically exists a number of plausible catalytic pathways and key to further advances and developments may come from a thorough understanding of what mechanisms operate.

For the MacMillan C-O coupling reaction, several mechanistic studies have been undertaken, some of which exploit TA spectroscopy. It is hypothesised here that using TRIR spectroscopy along with complementary techniques may allow for *direct observation* of intermediate species forming after photoexcitation of an Ir^{III} photocatalyst and possibly support/refute previously made observations using other techniques. The ongoing aim in this work, therefore, is to determine which steps appear to be occurring to further support a mechanistic proposal, using TRIR spectroscopy.

7.4 Results & Discussion

7.4.1 Assigning the Excited State Photocatalyst

The initial aim was to observe the spectroscopic features of the ground and electronically excited state of the Ir photocatalyst used for the model MacMillan C-O coupling reaction (**Fig 7.4.1**). This photocatalyst was [Ir{dF(CF₃)ppy}₂(dtbbpy)]PF₆ (Ir-126), as used in the original publication as well as in Chapter 5.

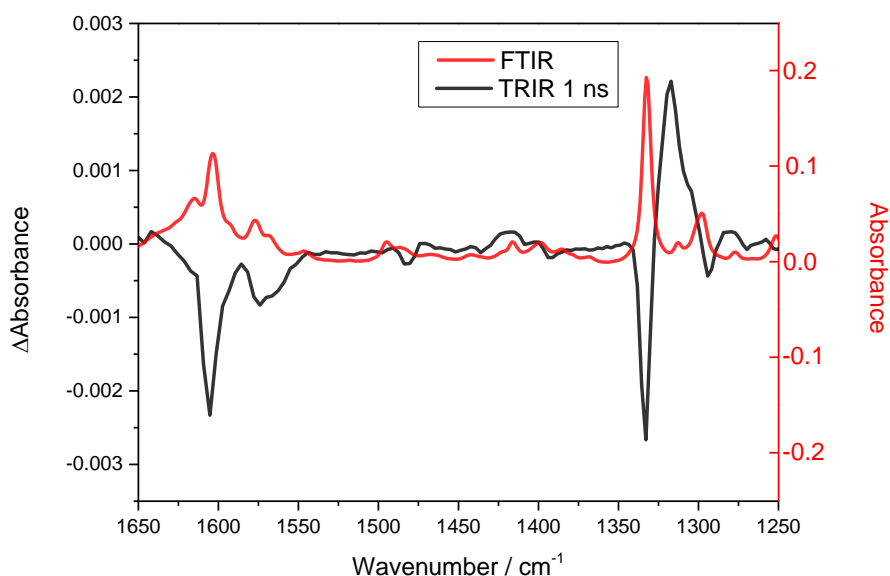


Fig 7.4.1 FTIR (red) and TRIR spectrum (black) obtained 1 ns following irradiation (355 nm) of Ir-126 in CD₃CN (1 mM TRIR, 2 mM FTIR). The parent bands are bleached, and new transient bands are seen at ~1315 cm⁻¹, and a less intense feature at ~1410 cm⁻¹.

These transient bands were assigned to the ³MLCT state of Ir-126. For the TRIR investigations, measurements were made from around the fingerprint region (~1200-1700 cm⁻¹), as no conventional spectroscopic reporting groups (*e.g.*, carbonyls) were present on the photocatalyst. Hence, for the measurements, low Ir-126 concentrations (~1 mM) were used, as the compound is a very strong UV absorber (as to not saturate light attenuation) but this necessarily resulted in weak changes in IR absorbance in the fingerprint region (due to no strong IR reporter groups being present).

Tentative assignments of the observed bands in the ground state FTIR spectrum (**Fig 7.4.1**) could be that the band at ~1330 cm⁻¹ is due to a C-N stretch (on one of the aromatic amine ligands) and the band(s) at ~1600 cm⁻¹ is due to a C-F stretch (on the fluorinated ppy ligands) or possibly C=C stretches, in either ligand (assignments made alongside the Merck IR Spectrum Table). With that, in the TRIR spectra (**Fig 7.4.1** and **Fig 7.4.2**), the transient band at ~1420 cm⁻¹ might be assigned as the corresponding C-N stretch possibly observed for the ground state, in the excited state, with a shift approximately 10 cm⁻¹ lower in energy. This shift in energy could be consistent with the excited state (³MLCT – which could be thought of as an oxidation of the Ir centre and a reduction of a ligand) as this adds an electron to a pyridyl ligand π*-orbital, hence expected to decrease the bond order, resulting in a shift to lower IR stretching frequencies. As mentioned, these suggestions are tentative and would require further work for confident assignments. The observations were, however, consistent with observations made by Castellano, Bernhard and co-workers, on related Ir-complexes.²⁵⁸ Furthermore, in the spectra acquired by Castellano, Bernhard and colleagues (**Fig 7.3.4**), a pronounced bleach signal was observed at around 1600 cm⁻¹ for their complex containing a CF₃ group,²⁵⁸ which might support that the bleaches observed in this work (**Fig 7.4.1** and **Fig 7.4.2**) were due to a C-F stretch, though further work would be required.

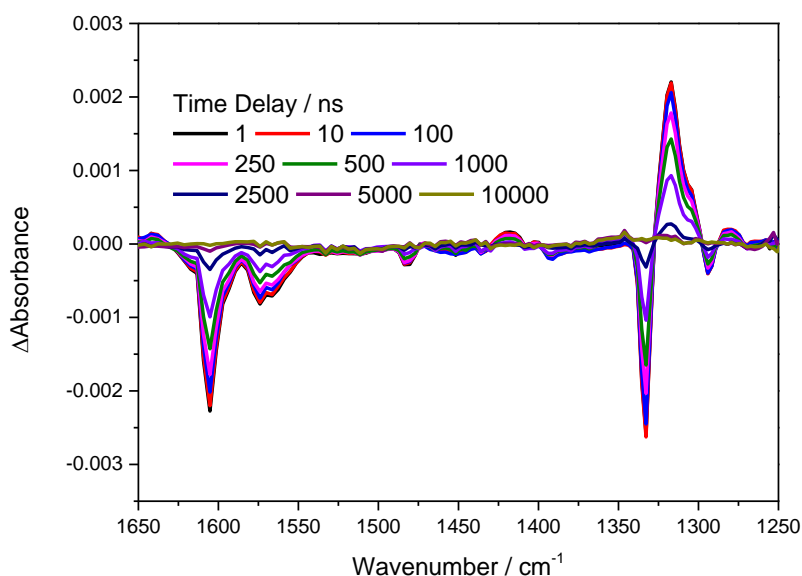


Fig 7.4.2 superimposed TRIR spectra of Ir-126 following irradiation (355 nm), in CD_3CN (1 mM). The transient bands are not stable and decay at the same rate as the parent bands are reformed (single point kinetics below in **Fig 7.4.3**).

A selection of the collected TRIR spectra can be seen in **Fig 7.4.2**, superimposed as to illustrate the growth of transient bands (*i.e.*, the features due to the excited state) and their subsequent decay (due to relaxation back to the ground state), alongside the appearance of bleach signals (due to the ground state Ir-126) and their subsequent recovery to the baseline (indicating full recovery of the ground state species). It should again be noted at this stage that bleach signals appear due to the transient spectra *y*-axis showing the *change in absorbance*, relative to the IR spectrum of the parent, ground state molecule.²⁵⁰

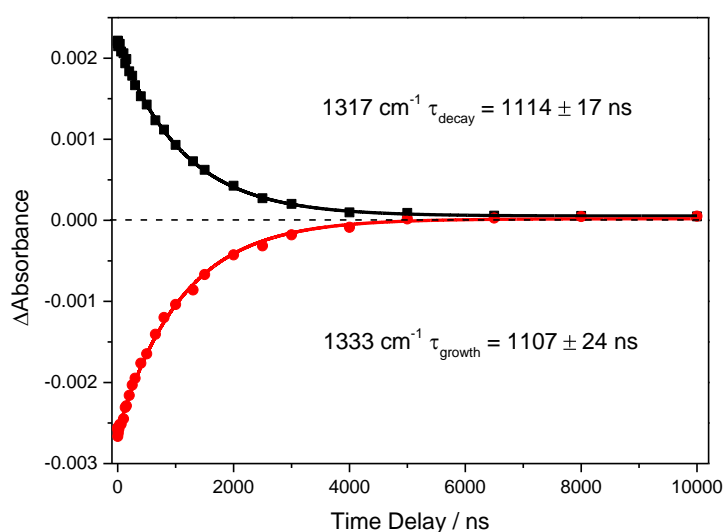


Fig 7.4.3 single point kinetic plots used to determine Ir-126 lifetime, corresponding to the spectra in **Fig.4.2**, fitted to a monoexponential growth/decay.

From single-point kinetic plots, the decay/growth kinetics were acquired from exponential fittings and used to evaluate the lifetime (τ) of the excited state Ir-126. For the photocatalyst, the transient signal (1317 cm^{-1}) was observed to decay and the bleach signal (1333 cm^{-1}) was observed to recover with the same lifetime, $\sim 1.1\ \mu\text{s}$ in deoxygenated CD_3CN . This would be consistent with lifetimes of other similar Ir-polypyridyl complexes, typically in the range of 100's ns to μs .

Having acquired the IR signature for the Ir-126 photocatalyst, the following investigations were to determine how the photocatalyst interacted with other species from the reaction mixture. Note that, prior to each subsequent experiment, the Ir-126 TRIR spectra were collected again, so that subsequent measurements (containing reaction substrates or reagents) could be referenced against the exact photocatalyst solution the reagents were added to. This was to account for any changes in lifetime due to *e.g.*, concentration fluctuations or oxygen content (the samples were deoxygenated using freeze-pump-thaw techniques and deoxygenated again following the addition of further substrates/reagents).

7.4.2 Investigations with Quinuclidine as a Reaction Additive

Following the original report from MacMillan¹⁷⁰ and other mechanistic studies such as from Nocera,²¹⁵ the initial investigations here were performed using quinuclidine as the amine additive, in the presence of Ir-126 photocatalyst (as opposed to TMG as the amine additive, as used in Chapter 5, which was employed later). The first experiments planned were to investigate whether any evidence to support electron/energy transfer processes between the Ir-126 photocatalyst and quinuclidine or the Ni co-catalyst could be observed. This was to explore whether the reaction mechanism involves Ni oxidation state modulation (to give favourable reductive elimination from Ni^{III}), and if so, whether this was occurring *via* direct electron transfer between Ir and Ni, or by an initial single electron transfer involving quinuclidine to facilitate the electron transfer steps.

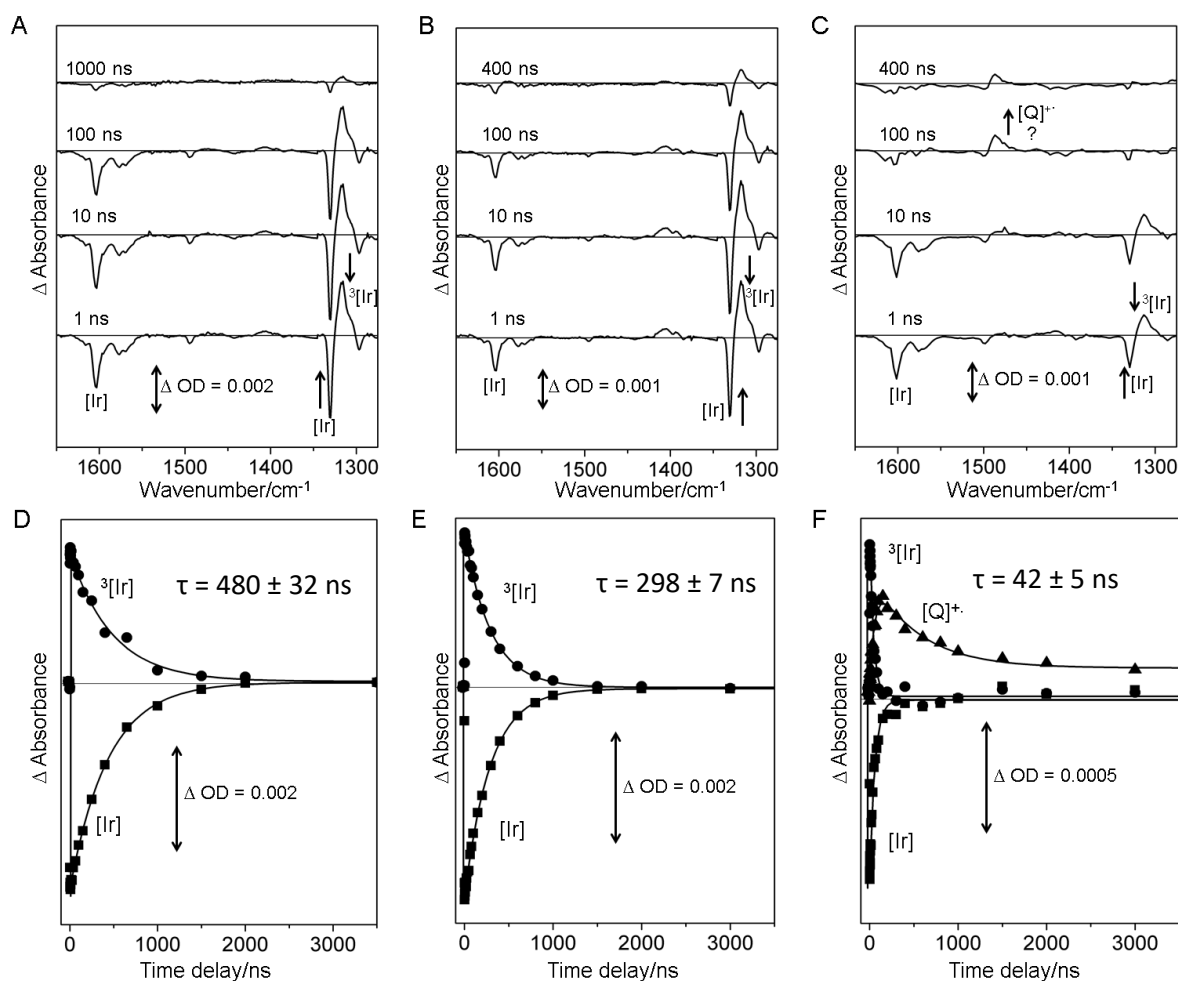


Fig 7.4.4 TRIR spectra (above) and single-point kinetic traces (below) for Ir-126 (A and D), Ir-126 + NiCl₂.glyme/dtbbpy (B and E) and Ir-126 + quinuclidine (C and F), following irradiation (355 nm), in CD₃CN (1 mM Ir-126, 5 mM NiCl₂.glyme/dtbbpy, 10 mM quinuclidine). Lifetimes are for Ir-126*.

As highlighted in **Fig 7.4.4**, the TRIR spectra of Ir-126 alone (A) and Ir-126 along with NiCl₂.glyme/dtbbpy (B) are, qualitatively, similar. In the presence of Ni^{II} however, the lifetime of the excited state photocatalyst was measured to be much shorter than in the absence of Ni^{II}, indicating that quenching is occurring (**Table 7.4.1**, at the end of this Sub-Section). The spectroelectrochemistry measurements (see Appendix) for Ir^{IV} and Ni^{III} (present if oxidative or reductive quenching by Ni^{II} was occurring, respectively) both showed a pronounced band at ~1365 cm⁻¹, which was not observed in the TRIR spectra, suggesting no direct electron transfer quenching by Ni^{II}. As such, an energy transfer quenching mechanism occurring could be suggested from these observations. From spectra B in **Fig 7.4.4**, a weakly intense feature at ~1400 cm⁻¹ is apparent, which could perhaps be due to excited state Ni^{II} formed by an energy transfer quenching pathway, though this would be speculative.

Comparing the TRIR spectra of Ir-126 alone (**Fig 7.4.4 A**) and Ir-126 along with quinuclidine (**Fig 7.4.4 C**), a new transient band at 1486 cm⁻¹ appears to grow in and was observed to be a relatively persistent species with a lifetime of ~5 μs (**Fig 7.4.4 F** and **Table 7.4.1**). A much shorter excited state lifetime of Ir-126 was also observed (**Table 7.4.1**). Spectroelectrochemistry measurements for quinuclidine (see Appendix, held at an oxidising potential to form the radical cation) showed a feature at 1470 cm⁻¹, in a

similar region to that observed in the TRIR. This could suggest that the quinuclidine radical cation was formed upon irradiation of Ir-126, *via* reductive quenching. Furthermore, alongside the long-lived species (presumed to be the quinuclidine radical cation) the bleach signal at 1330 cm^{-1} (due to the Ir ground state) was observed not to return to the baseline (*i.e.*, full recovery of the Ir-126 ground state was not apparent) at the same timescale in which the excited state Ir-126 had fully decayed. This would suggest that *not all* Ir^{III*} returned to the ground state and that some was converted to a longer-lived species. This could also be consistent with a reductive quenching pathway, if Ir^{II} was to be the longer-lived species, formed from Ir^{III*}. The lifetime data are summarised below in **Table 7.4.1**, noting significant excited state quenching in the presence of quinuclidine.

Following this, TRIR spectra were measured for Ir-126 in the presence of both reaction substrates and quinuclidine, as well as all reaction components (4-bromoacetophenone, 1-hexanol, NiCl₂.glyme/dtbbpy and quinuclidine). This was to determine any interactions between either the excited state photocatalyst or the suggested quinuclidine radical cation with any of the components of the reaction mixture.

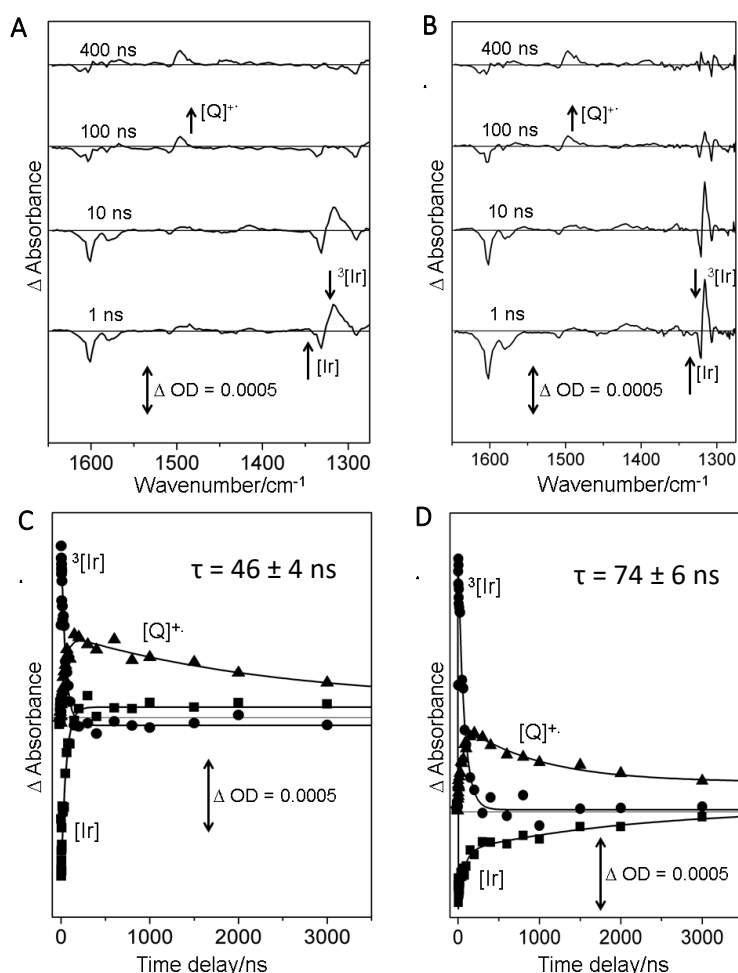


Fig 7.4.5 TRIR spectra (above) and single-point kinetic traces (below) for Ir-126 + quinuclidine + 4-bromoacetophenone + 1-hexanol (A and C) and Ir-126 + NiCl₂.glyme/dtbbpy + quinuclidine + 4-bromoacetophenone + 1-hexanol quinuclidine (B and D), following irradiation (355 nm), in CD₃CN (1 mM Ir-126, 10 mM 4-bromoacetophenone, 10 mM quinuclidine, 10 mM 1-hexanol, 5 mM NiCl₂.glyme/dtbbpy). Lifetimes are for Ir-126*.

When the reaction substrates were added alongside quinuclidine, but no Ni catalyst (**Fig 7.4.5 A**), the qualitative and quantitative (lifetime, **Table 7.4.1**) features of the TRIR spectra were similar to those of the mixture containing Ir-126 and quinuclidine alone (**Fig 7.4.4 C**). That is, a long-lived species with a feature at $\sim 1490\text{ cm}^{-1}$ was observed (assigned to the quinuclidine radical cation) and the ground state Ir-126 bleach signal did not return to the baseline at the same rate as the decay of the $\text{Ir}^{\text{III}*}$ transient signal. When the mixture containing all the reaction components was irradiated (**Fig 7.4.5 B**), again, the TRIR spectra collected were similar to those of Ir-126 and quinuclidine, alone (**Fig 7.4.4 C**). These observations might suggest that in the reaction mixture, the predominating mechanistic step following irradiation is the reductive quenching of Ir-126 by quinuclidine.

Reductive quenching should result in the formation of Ir^{II} , which could be responsible for the Ir^{III} bleach not fully recovering. Spectroelectrochemical measurements (see Appendix) showed a feature for the quinuclidine radical cation in a similar region to a feature for Ni^{I} , so could be overlapped. Mechanistic proposals following this could be the reduction of Ni^{II} to Ni^{I} (*e.g.*, *via* Ir^{II} acting as a reductant, itself oxidising back to ground state Ir^{III} accompanied by bleach recovery in the TRIR spectra). Alternatively, the oxidation of Ni^{I} to Ni^{II} (*e.g.*, *via* the quinuclidine radical cation acting as an oxidant, itself reducing back to quinuclidine) could be suggested.

For the spectroelectrochemical measurements for the Ni complex (see Appendix), $\text{NiCl}_2\cdot\text{glyme}$ along with an equimolar amount of dtbbpy were added and mixed until dissolution and formation of a blue colour was observed, indicative of dtbbpy coordination by displacing the glyme ligand. Spectroelectrochemical measurements were not made in the presence of 4-bromoacetophenone or 1-hexanol. In an actual reaction mixture, many different Ni^{I} , Ni^{II} or Ni^{III} species might be present at any given point, due to oxidative addition, ligand displacements *etc.* forming other intermediate complexes. As such, in the presence of the reaction substrates, time-resolved and spectroelectrochemical measurements were performed to act as a guide though isolation of proposed intermediates could be necessary to unravel a more thorough mechanistic picture.

In the TRIR spectra containing all components of the reaction mixture (**Fig 7.4.5 C** or **Fig 7.4.6** for an expansion), a weak feature at $\sim 1352\text{ cm}^{-1}$ was observed (and measured to reach a maximum then begin to decay after around 20 ns). Ir^{IV} and Ni^{III} measurements from spectroelectrochemistry were observed to give pronounced signals in a similar region $\sim 1365\text{ cm}^{-1}$ (see Appendix). The previously proposed reductive quenching (*via* quinuclidine) to give an Ir^{II} species would mean it unlikely to subsequently form an Ir^{IV} species (unless present from a competing mechanistic pathway). If the observed signal was due to Ni^{III} , this would be consistent with a quinuclidine radical cation forming (*via* reductive quenching, $\text{Ir}^{\text{III}*} \rightarrow \text{Ir}^{\text{II}}$) and then going on to oxidise the Ni catalyst ($\text{Ni}^{\text{II}} \rightarrow \text{Ni}^{\text{III}}$), regenerating quinuclidine in the process. At this stage, however, with the collected data it would be tentative to suggest this, particularly given the short delay at which the signal appears to decay.

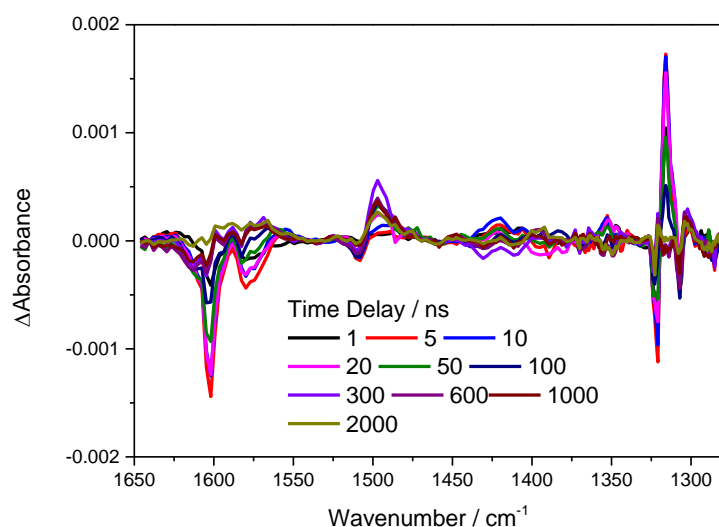


Fig 7.4.6 collection of TRIR spectra for a solution containing all components of the reaction mixture, following irradiation (355 nm), in CD_3CN (1 mM Ir-126, 5 mM $NiCl_2 \cdot glyme/dtbbpy$, 10 mM quinuclidine, 10 mM 4-bromoacetophenone, 10 mM 1-hexanol).

At this stage, TRIR observations alongside spectroelectrochemical measurements had suggested that, following photoexcitation of the Ir-126 photocatalyst, a reductive quenching mechanism was operating, forming a quinuclidine radical cation (assigned to a new transient band $\sim 1490\text{ cm}^{-1}$) and, presumably, an Ir^{II} species. An Ir^{II} species was not confidently observed spectroscopically, although not observing full recovery of the Ir^{III} ground state bleach signal suggested the formation of another species from Ir^{III*} other than just relaxation back to Ir^{III} . This would support the existence of an electron transfer *i.e.* true photoredox mechanism for the Ir/Ni-catalysed etherification, particularly as this proposed reductive quenching pathway appeared to be the dominant mechanism, consistent with reports from Nocera and co-workers.²¹⁵ Scientifically, however, such observations cannot preclude the possibility that, for example, reductive quenching by quinuclidine occurs, but, *e.g.* an energy transfer pathway may still result in product formation (even if the pathway occurs to a much smaller extent).

Table 7.4.1 lifetime data for Ir-126 (and assigned quinuclidine radical cation where relevant) showing significant lifetime quenching in the presence of quinuclidine.

Entry	Components	Lifetime* / ns
1	Ir-126	480 ± 32*
2	Ir-126 + NiCl ₂ .glyme/dtbbpy	298 ± 7
3	Ir-126 + quinuclidine	42 ± 5 66 ± 5 (τ ₁) and 4.7 ± 0.1 μs (τ ₂) for transient at 1486 cm ⁻¹
4	Ir-126 + quinuclidine + 4-bromoacetophenone + 1-hexanol	46 ± 4 2.7 ± 0.2 μs for transient at 1486 cm ⁻¹
5	Ir-126 + quinuclidine + NiCl ₂ .glyme/dtbbpy + 4-bromoacetophenone + 1-hexanol	74 ± 6 2.7 ± 0.2 μs for transient at 1486 cm ⁻¹

*From decay of signal ~1315 cm⁻¹. Lifetime of parent solution was lower than in that observed in **Fig 7.4.3**, possibly due to fluctuations in oxygen content. Repeats would be required for detailed kinetic analysis but not conducted here as experiments provided desired qualitative observations.

7.4.3 Investigations with TMG as a Reaction Additive

Ongoing investigations were performed using TMG as a reaction additive, as used for the reactions described in Chapter 5. The initial investigations here were to determine whether similar observations could be made for using TMG in place of quinuclidine.

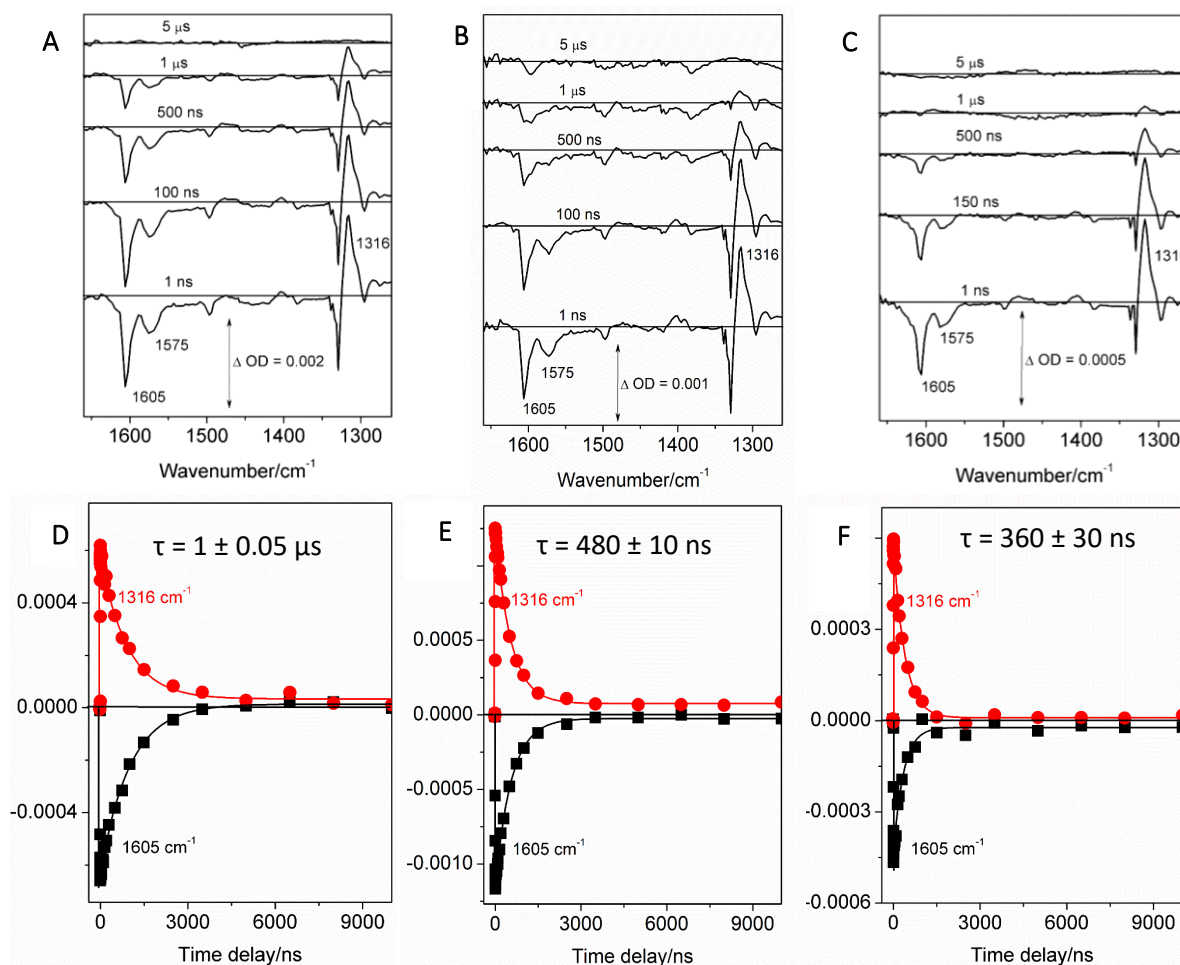


Fig 7.4.7 TRIR spectra (above) and single-point kinetic traces (below) for Ir-126 (A and D), Ir-126 + TMG (B and E) and Ir-126 + NiCl₂.glyme/dtbbpy (C and F), all at 20 °C, following irradiation (355 nm) in CD₃CN (1 mM Ir-126, 10 mM TMG, 5 mM NiCl₂.glyme/dtbbpy). Lifetimes from decay of signal ~1316 cm⁻¹.

Comparing **Fig 7.4.7** (A and C) with **Fig 7.4.4** (A and B) the qualitative observations from the TRIR spectra appear the same for both Ir-126 alone, and Ir-126 along with NiCl₂.glyme/dtbbpy. The TRIR spectra for Ir-126 + TMG (**Fig 7.4.7** B) shows (at 1 ns and 100 ns) a weak transient band appearing at just above 1400 cm⁻¹, which could be attributed to the TMG radical cation (from reductive quenching by TMG), where spectroelectrochemical measurements suggesting a band at 1415 cm⁻¹ present for oxidised TMG (see Appendix). Moreover, a bleach signal at slightly below 1400 cm⁻¹ was observed in the TRIR spectra and was also observed in the spectroelectrochemical measurements (see Appendix), which could therefore suggest the loss of TMG following irradiation, possibly *via* reductive quenching. Again, quenching of the excited state by NiCl₂.glyme/dtbbpy was suggested from lifetime analyses, though no new transient bands might suggest energy transfer as the quenching mechanism. A reduced lifetime of excited state Ir-126 was also observed in the presence of TMG, which could further support (alongside the bleach signal and weak transient band) the occurrence of reductive quenching by TMG. Lifetime data are summarised in **Table 7.4.2** at the end of this Sub-Section.

Following this, spectra were then recorded for Ir-126 in the presence of both Ni catalyst and TMG and in the presence of all reaction substrates. This was to determine any features suggesting a primary quenching pathway or the occurrence of new transients.

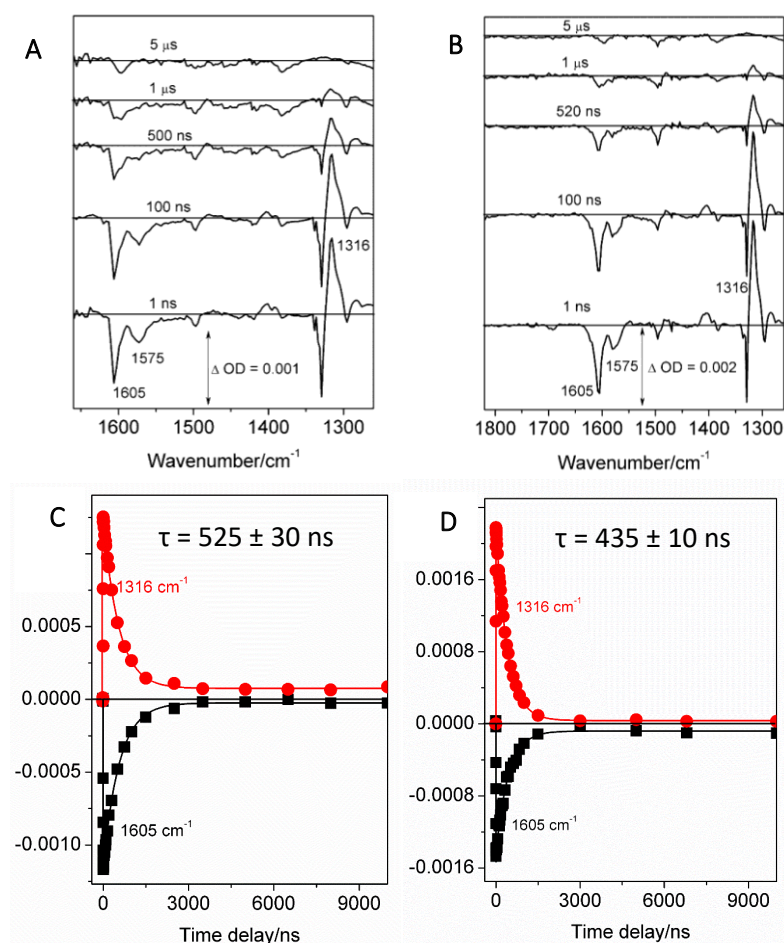


Fig 7.4.8 TRIR spectra (above) and single-point kinetic traces (below) for Ir-126 + TMG + NiCl₂.glyme/dtbbpy (A and C), Ir-126 + TMG + NiCl₂.glyme/dtbbpy + 4-bromoacetophenone + 1-hexanol (B and D), both at 20 °C, following irradiation (355 nm) in CD₃CN (1 mM Ir-126, 10 mM TMG, 5 mM NiCl₂.glyme/dtbbpy, 10 mM 4-bromoacetophenone, 10 mM 1-hexanol). Lifetimes from decay of signal ~1316 cm⁻¹.

The observations from the recorded spectra of Ir-126 in the presence of just TMG (**Fig 7.4.7 B**) and in the presence of TMG + NiCl₂.glyme/dtbbpy (**Fig 7.4.8 A**) appear similar, with a persistent bleach signal present, tentatively attributed to being due to loss of TMG (*via* oxidation to the radical cation). The measured lifetime of the excited photocatalyst was longer in the presence of both TMG + NiCl₂.glyme/dtbbpy, than it was for the excited photocatalyst with either component separately (compare **Fig 7.4.8 C** with **Fig 7.4.7 D** and **E**, repeated measurement would be required here), though, apparent quenching of the Ir-126 excited state was suggested in all cases. Observationally, TRIR spectra appear similar for Ir-126 + TMG + NiCl₂.glyme/dtbbpy and for the same components alongside the reaction substrates (**Fig.4.8 A** and **B**), however the excited state lifetime was unsurprisingly analysed to be slightly shorter in the presence of the substrates alongside TMG and the Ni catalyst.

With the data collected so far using TMG in the mixture (**Fig 7.4.7** and **Fig 7.4.8**), some of the observations supported the occurrence of an electron transfer step (*i.e.*, reductive quenching by TMG). However, the signals ($\sim 1415\text{ cm}^{-1}$ transient and $\sim 1400\text{ cm}^{-1}$ bleach) were of relatively weak intensity. It was considered that (as discussed in Chapter 5) due to the temperature dependence of the reaction, whereby for the system in flow using TMG, very slow rates were apparent at $20\text{ }^{\circ}\text{C}$, that running higher temperature TRIR experiments might allow for stronger intensity signals to be observed, should the thermal energy contribute towards the proposed reductive quenching. As such, measurements were repeated at $60\text{ }^{\circ}\text{C}$, around the temperature that the LEDs in the flow reactor reached in the synthetic work (Chapter 5).

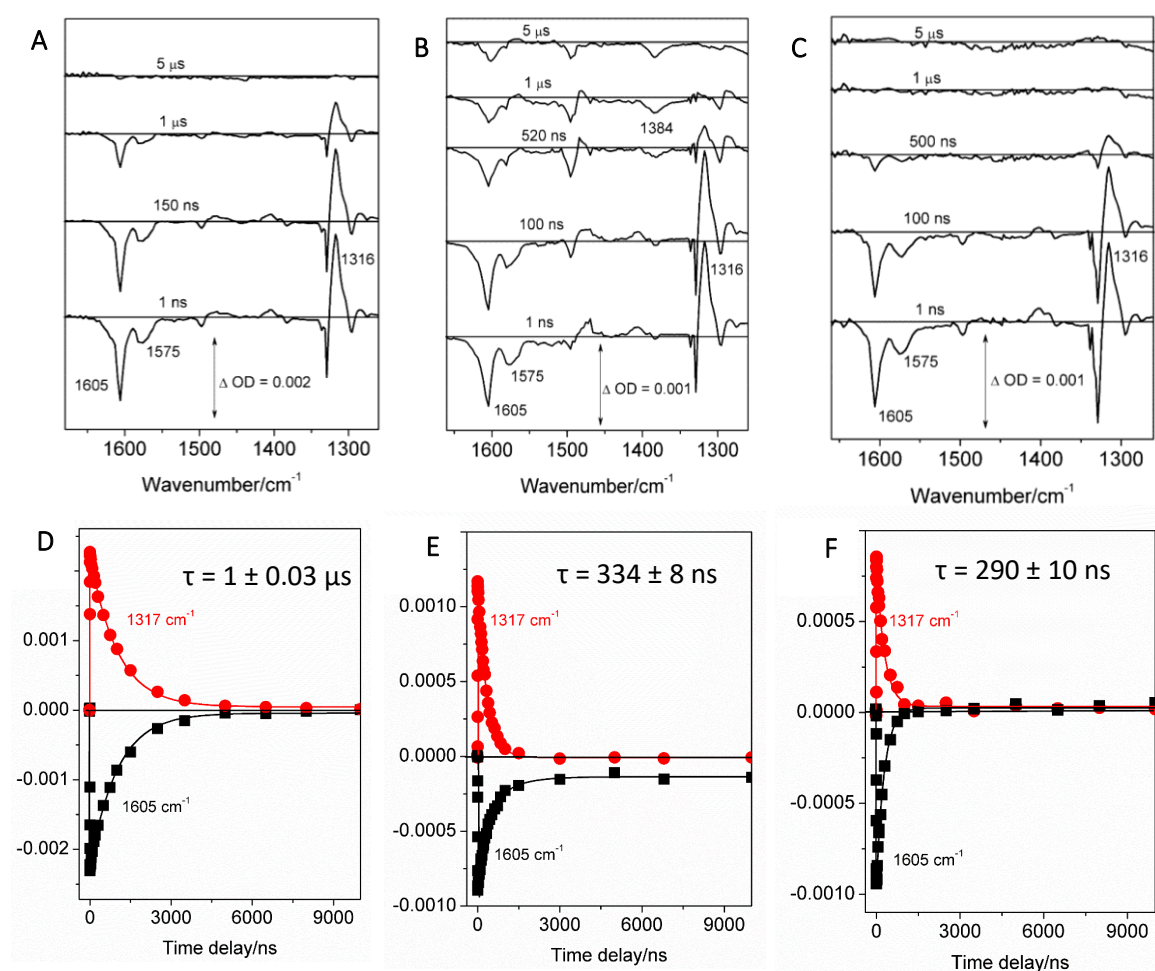


Fig 7.4.9 TRIR spectra (above) and single-point kinetic traces (below) for Ir-126 (A and D), Ir-126 + TMG (B and E) and Ir-126 + NiCl₂.glyme/dtbbpy (C and F), all at $60\text{ }^{\circ}\text{C}$, following irradiation (355 nm) in CD_3CN (1 mM Ir-126 , 10 mM TMG , $5\text{ mM NiCl}_2\text{.glyme/dtbbpy}$). Lifetimes from decay of signal $\sim 1317\text{ cm}^{-1}$.

For Ir-126 along with *either* TMG or NiCl₂.glyme/dtbbpy, an increased quenching rate was observed at $60\text{ }^{\circ}\text{C}$ relative to $20\text{ }^{\circ}\text{C}$ (compare **Fig 7.4.9 E and F** with **Fig 7.4.7 E and F**), possibly due to more frequent molecular collisions at the higher temperature. For the $60\text{ }^{\circ}\text{C}$ spectra with Ir-126 and TMG, the bleach signals (previously suggested to possibly be due to TMG consumption, accompanied by radical cation formation) appeared more prominent than at $20\text{ }^{\circ}\text{C}$ (compare **Fig 7.4.7 B** and **Fig 7.4.9 B**). Furthermore,

at 60 °C (Fig 7.4.9 B), the recovery of the bleach signal at 1605 cm⁻¹ does not appear to make a full recovery to the baseline, indicating that much of the Ir-126 did not return to the ground state following photoexcitation. This therefore might suggest that reductive quenching was occurring and hence some Ir^{II} did not recover to the ground state Ir^{III} on the timescales investigated.

Next, the measurements were repeated at 60 °C with Ir-126 alongside both TMG and the Ni catalyst and as well as containing all components of the reaction mixture.

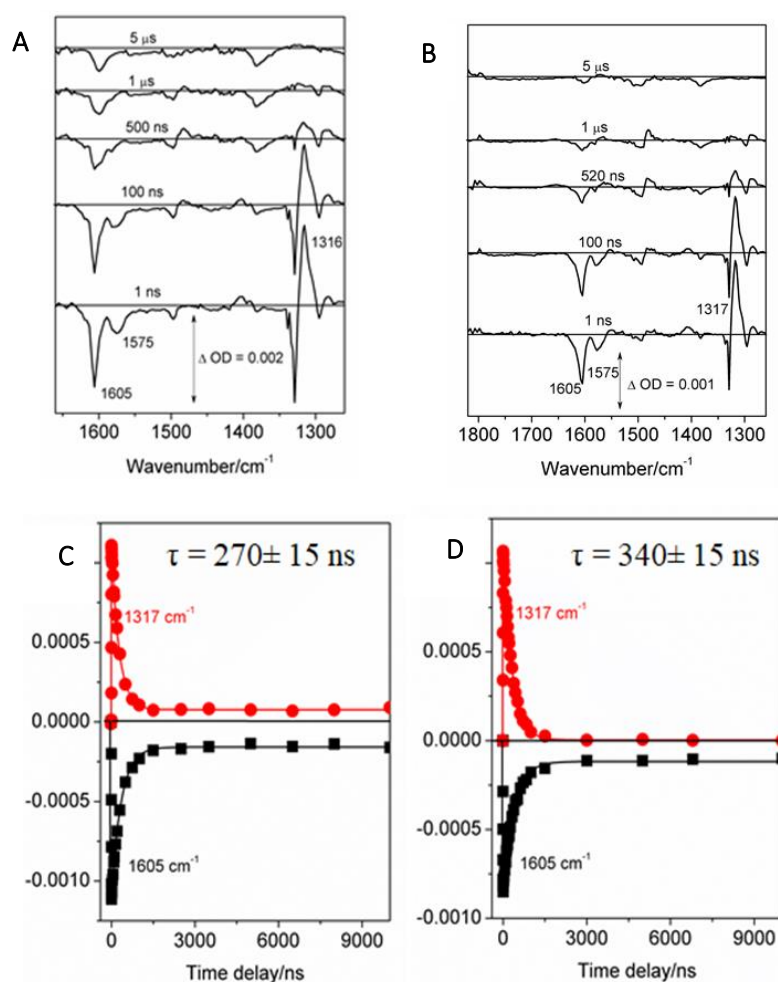


Fig 7.4.10 TRIR spectra (above) and single-point kinetic traces (below) for Ir-126 + TMG + NiCl₂.glyme/dtbbpy (A and C), Ir-126 + TMG + NiCl₂.glyme/dtbbpy + 4-bromoacetophenone + 1-hexanol (B and D), both at 60 °C, following irradiation (355 nm) in CD₃CN (1 mM Ir-126, 10 mM TMG, 5 mM NiCl₂.glyme/dtbbpy, 10 mM 4-bromoacetophenone, 10 mM 1-hexanol). Lifetimes from decay of signal ~1317 cm⁻¹.

Again, the bleach signal due to ground state Ir-126 was observed to not fully recover (Fig 7.4.10). This might indicate reductive quenching giving a longer-lived Ir^{II} species. Moreover, the lifetime of excited state Ir-126 was notably quenched compared with no additives present (Fig 7.4.9 D and Fig 7.4.10 C and D). Qualitative features of the TRIR spectra (Fig 7.4.10 A and B) were similar and both were similar to the TRIR spectra of Ir-126 along with just TMG (Fig 7.4.9 B). This could suggest that in the presence of

all reaction components (on the timescales investigated) the interaction between Ir-126 and TMG is the major pathway (tentatively suggested to be reductive quenching).

Overall, following the tentative assignments previously discussed, the following observations were made in relation to quenching (Table 7.4.2). At 60 °C and 20 °C, Ir-126 lifetimes were the same (Table 7.4.2, Entry 1). Quenching was observed to occur at a faster rate at 60 °C than at 20 °C, for all mixtures investigated (Table 7.4.2, Entries 2-5), perhaps due to increased molecular motions. At both temperatures, NiCl₂.glyme/dtbbpy appeared a more efficient quencher than TMG (Table 7.4.2, Entries 2 and 3, with Ni catalyst leading to a greater reduction in lifetime, despite being at half the concentration of TMG), though whether the proposed energy transfer quenching occurring with the Ni catalyst leads to a reaction occurring remains open. Furthermore, in an actual reaction, the relative concentration of TMG would be much higher than used here, likely making TMG become the most efficient quencher. This is because quenching rate constants are a function of concentration. Due to the stronger signals observed at 60 °C (perhaps due to the more efficient quenching), lifetimes for tentatively assigned Ir^{II} could be determined and was present when TMG was a component in the sample. Often in the presence of TMG, the bleach recovery was better fitted to a bi-exponential with one shorter-lifetime component and one longer-lifetime component. This could be representative of not all Ir^{III*} recovering to the Ir^{III} ground state, perhaps due to Ir^{II} formation.

Table 7.4.2 lifetime data (from decay of signal ~1315 cm⁻¹) for Ir-126 showing significant lifetime quenching in the presence of TMG and other reaction components. Ni = NiCl₂.glyme/dtbbpy, substrates = 4-bromoacetophenone + 1-hexanol. Bleach recovery of signal ~1330 cm⁻¹. Ir^{II} assigned tentatively to signal ~1475 cm⁻¹, discussed below.

Entry	Components	20 °C Lifetimes	60 °C Lifetimes
1	Ir-126	Ir ^{III*} 1 ± 0.05 μs	Ir ^{III*} 1 ± 0.03 μs
2	Ir-126 + TMG	Ir ^{III*} 480 ± 15 ns Bleach Recovery: 355 ± 50 ns (τ ₁ , 80%), 800 ± 100 ns (τ ₂ , 20%)	Ir ^{III*} 334 ± 8 ns Bleach Recovery: 345 ± 25 ns (τ ₁ , 80%), 950 ± 100 ns (τ ₂ , 20%) Ir ^{II} 2.3 μs
3	Ir-126 + Ni	Ir ^{III*} 360 ± 30 ns	Ir ^{III*} 290 ± 10 ns Ir ^{III*} 270 ± 15 ns
4	Ir-126 + TMG + Ni	Ir ^{III*} 525 ± 30 ns Bleach Recovery: 570 ± 10 ns	Bleach Recovery: 290 ± 30 ns (τ ₁ , 80%), 925 ± 100 ns (τ ₂ , 20%). Ir ^{II} 660 ns Ir ^{III*} 340 ± 15 ns
5	Ir-126 + TMG + Ni + substrates	Ir ^{III*} 435 ± 10 ns	Bleach Recovery: 330 ± 30 ns (τ ₁ , 80%), 980 ± 120 ns (τ ₂ , 20%) Ir ^{II} 1.6 μs.

In Fig 7.4.11, some possible correlations between signals in selected TRIR spectra and spectroelectrochemical spectra are shown, demonstrating the thought process behind interpreting the acquired data, leading to some mechanistic insights.

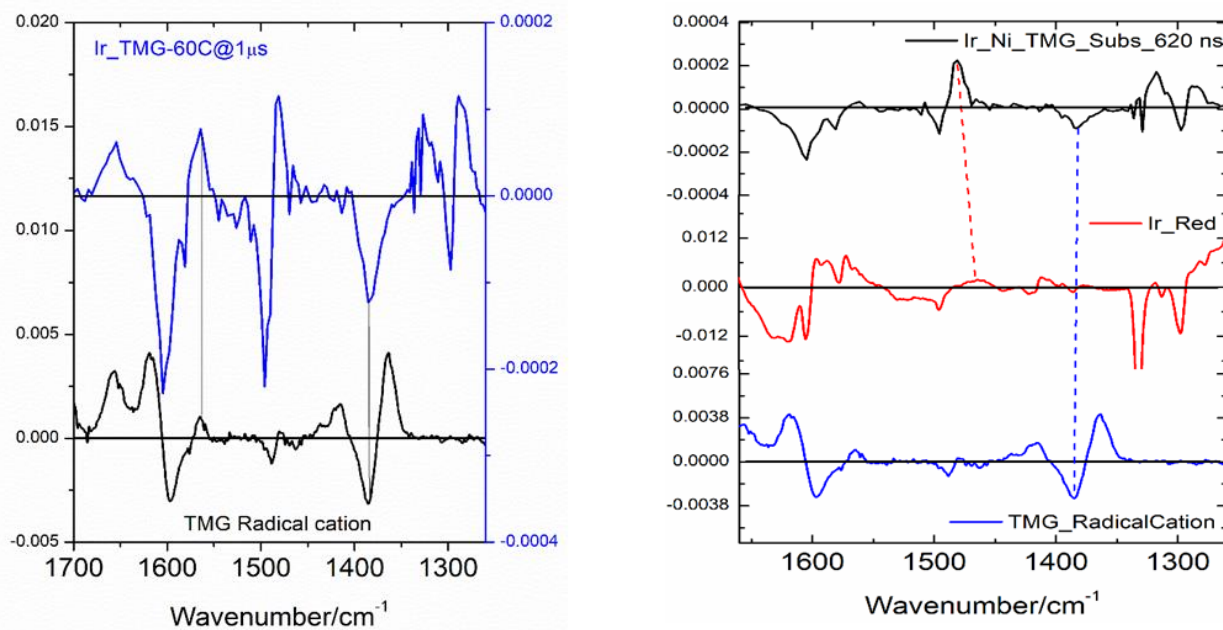


Fig 7.4.11 stacked TRIR spectrum at 1 μ s for Ir-126 + TMG alongside a spectroelectrochemical spectrum of suspected TMG radical cation (left) and stacked TRIR spectrum at 620 ns for Ir-126 + TMG + NiCl_2 .glyme/dtbbpy + 4-bromoacetophenone + 1-hexanol alongside spectroelectrochemical spectra of suspected Ir^{II} species and TMG radical cation (right).

Bleach signals in the spectroelectrochemical measurements of the suspected TMG radical cation align to bleach signals in the TRIR spectrum. Therefore, the TRIR spectra suggest the consumption of TMG following irradiation in only the presence of Ir-126 and TMG itself. Furthermore, weak bands at $\sim 1650 \text{ cm}^{-1}$ were observed in both the TRIR spectra (of Ir-126 and TMG) and the spectroelectrochemical spectrum (of TMG), which could also suggest formation of the TMG radical cation following irradiation. Analysis of the TRIR spectrum at 620 ns of the solution containing all reaction components displays similar bleach signals, attributed to consumption of TMG, likely by reductive quenching. Furthermore, a transient signal was observed at $\sim 1475 \text{ cm}^{-1}$ (observed with Ir-126 along with TMG alone, and all other mixtures with TMG present, **Fig 7.4.9-Fig 7.4.11**). Initially, this signal was possibly thought to be due to TMG radical cation, however, after acquiring and comparing TRIR spectra to spectroelectrochemical spectra, this feature was tentatively assigned to be due to Ir^{II} , possibly also supporting reductive quenching by TMG.

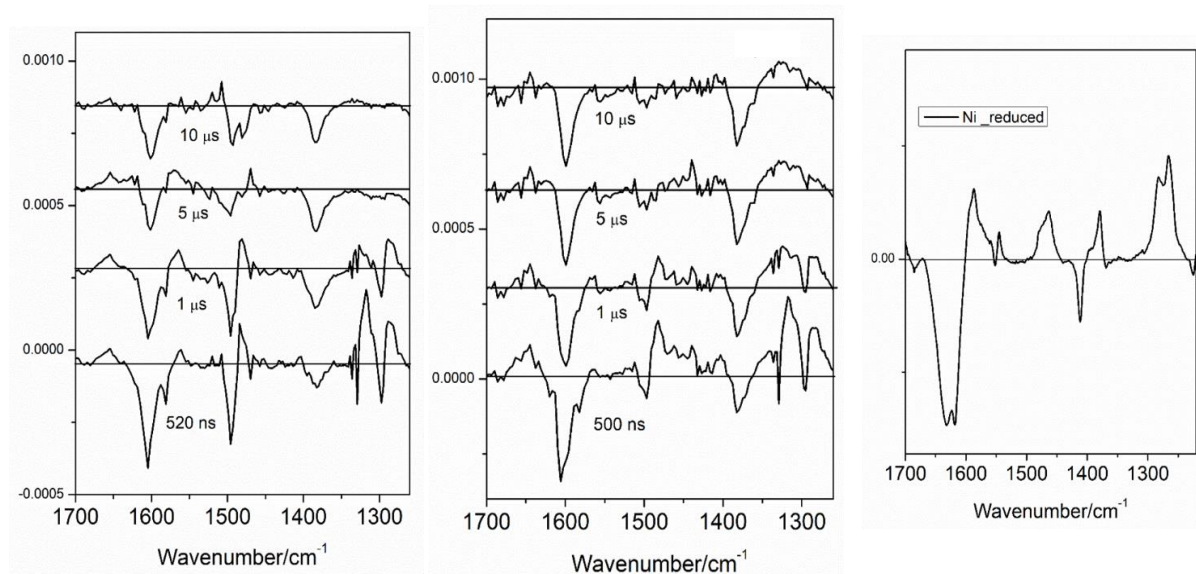


Fig 7.4.12 TRIR spectra of Ir-126 + TMG (left), Ir-126 + TMG + NiCl₂.glyme (middle) and suspected Ni^I species spectroelectrochemical spectrum (right).

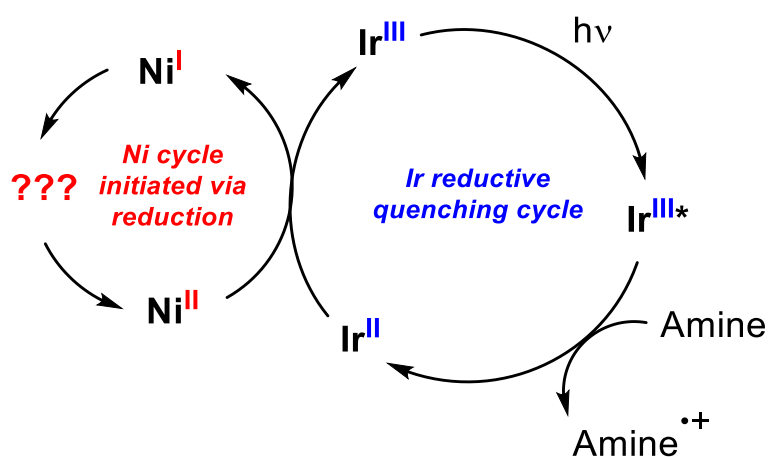
The spectroelectrochemical spectrum for NiCl₂.glyme/dtbbpy (held at the first reducing potential) displayed a band at around 1300 and 1450 cm⁻¹ (**Fig 7.4.12**). In the TRIR spectra of Ir-126 + TMG + NiCl₂.glyme, a persistent feature (still present at 10 μs alongside the TMG bleach signals) was also observed in a similar region, which was not observed at similar timescales in the absence of the Ni catalyst. Tentatively, this could possibly suggest the formation of a Ni^I species. This would require further studies to support/refute this suggestion, however, it could be considered that following Ir-126 reductive quenching (by TMG, possibly supported by observations here), the Ir^{II} species then could be oxidised by a Ni^{II} species, regenerating Ir^{III} and forming Ni^I.

7.4.4 TMG and Quinuclidine Comparison

Comparing **Table 7.4.1** and **Table 7.4.2**, a few comparisons are worth noting. Firstly, it is acknowledged that the lifetime of Ir-126 alone was approximately half the usual measured value for experiments with quinuclidine (summarised in **Table 7.4.1**). This is possibly due to differences in deoxygenation as the other measured lifetimes were consistently around 1 μs. However, comparing the relative quenching rates between TMG and quinuclidine, quinuclidine appears a more efficient quencher than TMG, which could also be consistent with observations in Chapter 5, where quinuclidine resulted in slightly faster reaction rates than TMG (in batch). For example, TMG resulted in Ir^{III}* lifetime reduction by ~half at 20 °C and by ~two-thirds at 60 °C (**Table 7.4.2**). Quinuclidine resulted in Ir^{III}* lifetime reduction by ~10-fold, at room temperature (**Table 7.4.1**). Furthermore, when using quinuclidine, quinuclidine was a more efficient quencher than the Ni-catalyst (at the applied concentrations), however, it appeared with TMG that the Ni-catalyst was a more efficient quencher (at the applied concentrations). However, qualitative features between TRIR spectra were similar for the mixture containing Ir-126 + TMG and the mixture containing Ir-126 + TMG + Ni-catalyst, which might indicate that the interaction with TMG is the dominant process which might lead to product formation. Moreover, as the relative concentration of TMG was much lower than what would be applied in a synthesis, TMG would likely become the most efficient quencher, at these higher concentrations.

7.4.5 Mechanistic Proposal

Based on the previously outlined observations, with tentative assignments of signals in the TRIR spectra, the following partial mechanistic proposal was suggested (**Scheme 7.4.1**). It should be noted that further work would be required to further support this proposal, with the work discussed previously aiding in the assistance of further experiments to unravel mechanistic details and kinetic data.



Scheme 7.4.1 a proposed partial mechanistic cycle for the Ir/Ni dual-catalysed etherification. Possible aspects of the Ni catalytic cycle were given in **Scheme 7.3.6** and **Scheme 7.3.8**, for example, involving oxidative addition of an aryl halide and subsequent alkoxide substitution to give a Ni^{III} species that could undergo reductive elimination to furnish the alkyl-aryl ether product.

The proposal is consistent with the assumed observations. These are the reductive quenching of Ir-126 by either quinuclidine or by TMG, to give Ir^{II} following photoexcitation. With the tentative observation of a Ni^I species, this could be proposed to form *via* reduction from the resultant Ir^{II} species, in turn, regenerating Ir^{III} and forming the Ni^I species. From the TRIR investigations, no observations were made relating to the Ni coupling cycle. This has been previously proposed to operate *via* a Ni^I/Ni^{III} cycle, and further work using TRIR spectroscopy could provide evidence for this. As such, from the observations here it could still be speculated as to whether the Ni coupling cycle involves a self-sustained Ni^I/Ni^{III} cycle, as previously suggested elsewhere. Or for example, whether a Ni⁰ species forms, which requires reoxidation to Ni^I to maintain catalytic turnover (this could be achieved, for example, by oxidation from the amine radical cation), points for further work are discussed in the following section.

7.5 Conclusions & Further Work

Mechanistic investigations into the Ir/Ni dual photocatalysed C-O coupling reaction were conducted, using TRIR spectroscopy. Support for the reductive quenching of Ir-126 by either quinuclidine or TMG was observed. Bleached signals of Ir-126 not making a full baseline recovery in the presence of either, as well as spectroelectrochemical supporting measurements suggesting the occurrence of a quinuclidine radical cation and the consumption of TMG following irradiation supported this claim. Furthermore, in the presence of other reaction components, similar observations were made, possibly indicating that this pathway predominates in the reaction mixture. Tentative TRIR spectral assignments possibly suggest the presence of an Ir^{II} species (formed *via* reductive quenching) as well as a Ni^I species (formed *via* reduction of the Ni^{II} pre-catalyst). Therefore, as in **Scheme 7.4.1**, a mechanistic proposal involving reductive quenching, followed by Ni^{II} reduction by Ir^{II} would be plausible. Furthermore, a temperature dependence for electron transfer was suggested when using TMG as the quencher, with measurements at 60 °C appearing to lead to more efficient quenching, perhaps due to increased frequency of molecular collisions.

Several avenues for further work could allow for the mechanistic proposal to be expanded upon, and perhaps allow for developing insights into the optimisation of synthetic procedures.

Firstly, as was mentioned, some of the spectral assignments are tentative and require further work for giving further confidence to the assignments. To do so, performing experiments at a variety of concentrations of the species of interest could allow for strengthening the assignments made. For example, if a larger concentration of TMG was used, it might be possible to see more intense transient bands possibly due to the proposed TMG radical cation. The same considerations might apply to the Ir-126 photocatalyst where (with carefully considered tuning of the experimental set-up) a higher concentration might allow for a stronger signal for what has been suggested to be an Ir^{II} species observed. This same feature, however, might also become more intense with a greater concentration of quencher (TMG or quinuclidine). Moreover, concentration dependent measurements for various quenchers would allow for establishing reliable rate constants for quenching processes. These could then be compared *e.g.*, at different temperatures and such insights might allow for finetuning of synthetic processes, by revealing further kinetic aspects of the reaction.

It would also be interesting to determine whether insights into the Ni catalytic cycle could be determined spectroscopically. In these experiments, there were no obvious observations of possible Ni intermediates (other than possibly the reduction to Ni^I). As such, numerous questions could be investigated. Due to the rapid timescales of TRIR spectroscopy and the (likely) low concentration of any intermediates present, experiments to investigate this might have to be carefully planned. For example, it could be possible to synthesis suspected intermediates in the catalytic cycle, such as performing oxidative addition of an aryl halide (*e.g.*, 4-bromoacetophenone) and isolating (if possible) the resultant Ni complex. This could be useful as, in the synthesis, it could be that the oxidative addition to Ni occurs prior to the involvement of electron transfer steps (depending on what the mechanism is in reality). Moreover, Ni-alkoxide intermediates could also be proposed and these could be formed by conventional deprotonation (*e.g.*, of 1-hexanol) and substitution of a chloride ligand, or perhaps also by a radical pathway. That is, the synthesis of speculated Ni intermediates (rather than just the NiCl₂.glyme/dtbbpy catalyst precursor) may allow for further aspects to be investigated.

Chapter 8

Summary

In Chapter 1, the background to the project, the aims and the strategy to investigate these aims were outlined. The overarching theme was to develop flow syntheses/processes for PGM catalysed coupling reactions. The aims of the work presented can be summarised as follows:

Thermal Palladium-Catalysed C-C Coupling Reactions:

1. To determine a suitable area of thermal Pd cross-coupling catalysis to investigate for C(sp²)-C(sp²) and C(sp²)-C(sp³) bond formation.
2. To obtain a suitable flow reactor for performing the previously mentioned reactions, in flow.
3. To determine whether flow syntheses can be developed and whether the unique advantages offered by flow chemistry can impart processing benefits.

These aims have been investigated and can be summarised as follows:

1. Heck-type Reactions were identified as suitable candidates, with precedent for performing conventional Heck Reactions in flow for C(sp²)-C(sp²) coupling existing, with room for further exploration of novel processing windows, accessible in flow. Furthermore, variant reactions such as the Reductive Heck Reaction and the Redox Relay Heck Reaction were identified as natural progressions for being able to perform C(sp²)-C(sp³) coupling in flow, under similar conditions.
2. After first using a commercially available flow reactor, it was decided to construct a homemade flow reactor. This allowed for surveying a wider novel processing window range, to achieve the aim of determining whether these unique features to flow chemistry can lead to processing benefits for Heck-type Reactions.
3. It was determined that under extreme temperature conditions in the flow reactor, processing benefits towards the Heck-type reactions were observed. For example, the standard Heck Reaction was conducted at ppm loadings, whilst observing good yield/conversion in short timescales. Similarly, reduced loadings for Redox Relay and Reductive Heck Reactions could be observed, due to elevated temperatures in flow, compared to previous batch reports. Being able to perform such coupling reactions efficiently, involving challenging bond formations, in a flow process highlights the benefits of performing reactions in flow and offers a scalable approach, with enhanced sustainability aspects.

Photochemical Iridium-Catalysed C-O Coupling Reactions:

1. To determine a suitable area of Ir/Ru-photocatalysis for the formation of C-O bonds, with the possibility of transfer to flow processing.
2. To obtain a suitable reactor for performing the reactions in flow.
3. To determine whether flow processes could be developed for the reactions of interest and whether improved light penetration in flow could lead to processing benefits.
4. To use time-resolved infrared spectroscopy as an approach to investigating photocatalytic mechanisms.

These aims were investigated and can be summarised as follows:

1. Dual Ir metallaphotoredox catalysis was identified as an area which could be used for preparing alkyl-aryl ethers, *via* either retrosynthetic disconnection of the ether bond. One such approach used Ir/Ni-catalysis and the alternative used Ir/Cu-catalysis.
2. A flow reactor based on a well-documented FEP coil design was constructed for the development of flow processes and was suitable for the Ir/Cu system (as previously had been reported) and suitable for the Ir/Ni system after adapting conditions *via* batch screening (to give homogeneous conditions).
3. The reactor was applied for both C-O bond forming reactions. For both, notable reductions in processing times were observed in flow (from hours in batch to minutes in flow). Furthermore, reductions in catalyst loadings, solvent demand, *etc.* were also observed, following flow optimisation.
4. Time-resolved infrared spectroscopy was applied for mechanistic investigations of the Ir/Ni C-O bond formation reaction, with previous literature speculating on the nature of the catalysis (*e.g.*, whether this involves energy or electron transfer). The investigations suggested that electron transfer processes were indeed occurring and that amine radical cations were formed in a reductive quenching pathway, following irradiation of the photocatalyst. Reduced Ni species were also possibly observed, which could suggest reduction of Ni^{II} by Ir^{II} (formed after reductive quenching). These experiments highlight the utility of using time-resolved infrared spectroscopy as a method for photocatalytic mechanism investigations and add further insights into the mechanism of metallaphotoredox reactions.

As such, the outlined aims were achieved and in doing so, it was generally suggested that the application of flow reactors to PGM catalysed reactions involving either thermal or photochemical activation can lead to processing benefits (reduced reaction times, reduced catalyst loadings). Therefore, it could be concluded that flow processes for such reactions allows for the development of scalable, efficient and more sustainable reactions involved in important bond formations to the synthetic and process community.

In general, this work could be furthered by applying the developed conditions towards targets of interest (perhaps in a streamlined, multi-step flow process), expanding the scope of the processes and applying engineering-based reactor/reaction modelling for scale-up of the processes. These would be useful as, ultimately, the application of flow chemistry is of interest to chemical manufacturing processes and further work in these areas could result in the appeal/likelihood of being implemented in a manufacturing process to deliver *e.g.*, pharmaceuticals or agrochemicals.

References

- 1 W. P. Griffith, *Johnson Matthey Technol. Rev.*, 2017, **61**, 257–261.
- 2 P. B. Kettler, *Org. Process Res. Dev.*, 2003, **7**, 342–354.
- 3 L. B. Hunt and F. M. Lever, *Platin. Met. Rev.*, 1969, **13**, 126–138.
- 4 M. B. Plutschack, B. Pieber, K. Gilmore and P. H. Seeberger, *Chem. Rev.*, 2017, **117**, 11796–11893.
- 5 V. Hessel, D. Kralisch, N. Kockmann, T. Noël and Q. Wang, *ChemSusChem*, 2013, **6**, 746–789.
- 6 J. H. Bannock, S. H. Krishnadasan, Martin Heeney and J. C. de Mello, *Mater. Horizons*, 2014, **1**, 373–378.
- 7 K. Geyer, J. D. C. Codée and P. H. Seeberger, *Chem. - A Eur. J.*, 2006, **12**, 8434–8442.
- 8 S. Lee and G. Robinson, *Process Development Fine Chemicals from Grams to Kilograms*, Oxford University Press, Oxford, 1st edn., 1995.
- 9 L. D. Elliott, J. P. Knowles, P. J. Koovits, K. G. Maskill, M. J. Ralph, G. Lejeune, L. J. Edwards, R. I. Robinson, I. R. Clemens, B. Cox, D. D. Pascoe, G. Koch, M. Eberle, M. B. Berry and K. I. Booker-Milburn, *Chem. - A Eur. J.*, 2014, **20**, 15226–15232.
- 10 J. P. Knowles, L. D. Elliott and K. I. Booker-Milburn, *Beilstein J. Org. Chem.*, 2012, **8**, 2025–2052.
- 11 D. Cambié, C. Bottecchia, N. J. W. Straathof, V. Hessel and T. Noël, *Chem. Rev.*, 2016, **116**, 10276–10341.
- 12 P. Klan and J. Wirz, *Photochemistry of Organic Compounds: From Concepts to Practice*, Wiley, Chichester, West Sussex, 1st edn., 2009.
- 13 B. König, *European J. Org. Chem.*, 2017, **2017**, 1979–1981.
- 14 K. C. Nicolaou, *Proc. R. Soc. A Math. Phys. Eng. Sci.*, 2014, **470**, 1–17.
- 15 P. Ball, *Nature*, 2015, **528**, 327–329.
- 16 United States Patent Office, 644077, 1900.
- 17 S. V. Ley and I. R. Baxendale, *Chem. Rec.*, 2002, **2**, 377–388.
- 18 K. C. Nicolaou, E. J. Sorensen and N. Winssinger, *J. Chem. Educ.*, 1998, **75**, 1225–1258.
- 19 S. L. Lee, T. F. O'Connor, X. Yang, C. N. Cruz, S. Chatterjee, R. D. Madurawe, C. M. V. Moore, L. X. Yu and J. Woodcock, *J. Pharm. Innov. 2015 103*, 2015, **10**, 191–199.
- 20 P. T. Anastas and J. C. Warner, *Green Chemistry: Theory and Practice*, Oxford University Press, New York, 1st edn., 1998.
- 21 M. Lancaster, *Green Chemistry An Introductory Text*, Royal Society of Chemistry, Cambridge, 3rd edn., 2016.
- 22 US Environmental Protection Agency, Green Chem.
- 23 S. L. Y. Tang, R. L. Smith and M. Poliakoff, *Green Chem.*, 2005, **7**, 761.
- 24 T. Newhouse, P. S. Baran and R. W. Hoffmann, *Chem. Soc. Rev.*, 2009, **38**, 3010–3021.
- 25 B. M. Trost, *Science*, 1991, **254**, 1471–1477.
- 26 P. A. Wender, V. A. Verma, T. J. Paxton and T. H. Pillow, *Acc. Chem. Res.*, 2008, **41**, 40–49.
- 27 N. Z. Burns, P. S. Baran and R. W. Hoffmann, *Angew. Chemie Int. Ed.*, 2009, **48**, 2854–2867.
- 28 R. A. Sheldon, *Green Chem.*, 2007, **9**, 1273–1283.
- 29 J. B. Hendrickson, *J. Am. Chem. Soc.*, 2002, **97**, 5784–5800.
- 30 T. Gaich and P. S. Baran, *J. Org. Chem.*, 2010, **75**, 4657–4673.
- 31 M. Poliakoff, P. Licence and M. W. George, *Angew. Chemie Int. Ed.*, 2018, **57**, 12590–12591.
- 32 J. Clark, R. Sheldon, C. Raston, M. Poliakoff and W. Leitner, *Green Chem.*, 2013, **16**, 18–23.
- 33 B. C. Gates, *Catalytic Chemistry*, John Wiley & Sons, Ltd., New York, 1st edn., 1992.
- 34 C. E. Housecroft and A. G. Sharpe, *Inorganic Chemistry*, Pearson, Harlow, Essex, England, 4th edn., 2012.
- 35 S. K. Ritter, *Chem. Eng. News*, 2013, **91**, 46–47.
- 36 B. C. Garrett, *Theor. Chem. Acc.*, 2000, **103**, 200–204.
- 37 A. de Meijere and F. Diederich, *Metal Catalyzed Cross-Coupling Reactions*, Wiley-VCH Verlag,

- Weinheim, 1st edn., 2004.
- 38 M. Boudart, A. Aldag, J. E. Benson, N. A. Dougharty and C. Girvin Harkins, *J. Catal.*, 1966, **6**, 92–99.
- 39 S. Kozuch and J. M. L. Martin, *ACS Catal.*, 2012, **2**, 2787–2794.
- 40 J. N. Armor, *Catal. Today*, 2011, **163**, 3–9.
- 41 J. Wisniak, *Educ. Química*, 2010, **21**, 60–69.
- 42 G. W. Parshall, *Homogeneous Catalysis*, John Wiley & Sons, Ltd., New York, 1st edn., 1980.
- 43 C. C. C. Johansson Seechurn, M. O. Kitching, T. J. Colacot and V. Snieckus, *Angew. Chemie Int. Ed.*, 2012, **51**, 5062–5085.
- 44 R. Jira, *Angew. Chemie Int. Ed.*, 2009, **48**, 9034–9037.
- 45 M. A. Murphy, *Found. Chem.*, 2018, **20**, 121–165.
- 46 X. Liu and L. Dai, *Nat. Rev. Mater.*, 2016, **1**, 16064.
- 47 C. K. Chua and M. Pumera, *Chem. - A Eur. J.*, 2015, **21**, 12550–12562.
- 48 C. C. C. Johansson Seechurn, A. J. DeAngelis and T. J. Colacot, in *New Trends in Cross-Coupling: Theory and Applications*, ed. T. J. Colacot, Royal Society of Chemistry, London, 1st edn., 2015, pp. 1–19.
- 49 T. J. Colacot, *Platin. Met. Rev.*, 2011, **55**, 84–90.
- 50 G. Jas and A. Kirschning, *Chem. - A Eur. J.*, 2003, **9**, 5708–5723.
- 51 D. Webb and T. F. Jamison, *Chem. Sci.*, 2010, **1**, 675–680.
- 52 T. Glasnov, in *Continuous-Flow Chemistry in the Research Laboratory*, Springer International Publishing, Cham, 2016, pp. 7–20.
- 53 Mara Guidi, P. H. Seeberger and Kerry Gilmore, *Chem. Soc. Rev.*, 2020, **49**, 8910–8932.
- 54 J. Britton and T. F. Jamison, *Nat. Protoc. 2017 1211*, 2017, **12**, 2423–2446.
- 55 A. Ghanem, T. Lemenand, D. Della Valle and H. Peerhossaini, *Chem. Eng. Res. Des.*, 2014, **92**, 205–228.
- 56 D. S. Lee, Z. Amara, C. A. Clark, Z. Xu, B. Kakimpa, H. P. Morvan, S. J. Pickering, M. Poliakoff and M. W. George, *Org. Process Res. Dev.*, 2017, **21**, 1042–1050.
- 57 D. S. Lee, M. Sharabi, R. Jefferson-Loveday, S. J. Pickering, M. Poliakoff and M. W. George, *Org. Process Res. Dev.*, 2020, **24**, 201–206.
- 58 J. G. Sczechowski, C. A. Koval and R. D. Noble, *Chem. Eng. Sci.*, 1995, **50**, 3163–3173.
- 59 P. Oxley, C. Brechtelsbauer, F. Ricard, N. Lewis and C. Ramshaw, *Ind. Eng. Chem. Res.*, 2000, **39**, 2175–2182.
- 60 S. D. Pask, O. Nuyken and Z. Cai, *Polym. Chem.*, 2012, **3**, 2698–2707.
- 61 S. R. L. Gobert, S. Kuhn, L. Braeken and L. C. J. Thomassen, *Org. Process Res. Dev.*, 2017, **21**, 531–542.
- 62 R. E. Martin, *Science*, 2016, **352**, 44–45.
- 63 Z. Dong, Z. Wen, F. Zhao, S. Kuhn and T. Noël, *Chem. Eng. Sci. X*, 2021, **10**, 100097.
- 64 L. Vaccaro, D. Lanari, A. Marrocchi and G. Strappaveccia, *Green Chem.*, 2014, **16**, 3680–3704.
- 65 T. Noël and S. L. Buchwald, *Chem. Soc. Rev.*, 2011, **40**, 5010–5029.
- 66 I. Rossetti and M. Compagnoni, *Chem. Eng. J.*, 2016, **296**, 56–70.
- 67 J. Britton and C. L. Raston, *Chem. Soc. Rev.*, 2017, **46**, 1250–1271.
- 68 J. Li, H. Šimek, D. Ilioa, N. Jung, S. Bräse, H. Zappe, R. Dittmeyer and B. P. Ladewig, *React. Chem. Eng.*, 2021, **6**, 1497–1507.
- 69 C. A. Shukla and A. A. Kulkarni, *Beilstein J. Org. Chem.*, 2017, **13**, 960–987.
- 70 M. Baumann, T. S. Moody, M. Smyth and S. Wharry, *Org. Process Res. Dev.*, 2020, **24**, 1802–1813.
- 71 M. Baumann and I. R. Baxendale, *Beilstein J. Org. Chem.*, 2015, **11**, 1194–1219.
- 72 N. S. Marzijarani, D. R. Snead, J. P. McMullen, F. Lévesque, M. Weisel, R. J. Varsolona, Y. Lam, Z. Liu and J. R. Naber, *Org. Process Res. Dev.*, 2019, **23**, 1522–1528.
- 73 A. V. Silamkoti, P. W. Allan, A. E. A. Hassan, A. T. Fowler, E. J. Sorscher, W. B. Parker and J. A. Secrist, *Nucleosides. Nucleotides Nucleic Acids*, 2005, **24**, 881–885.

- 74 J. P. McMullen, C. H. Marton, B. D. Sherry, G. Spencer, J. Kukura and N. S. Eyke, *Org. Process Res. Dev.*, 2018, **22**, 1208–1213.
- 75 T. L. LaPorte, M. Hamedi, J. S. DePue, L. Shen, D. Watson and D. Hsieh, *Org. Process Res. Dev.*, 2008, **12**, 956–966.
- 76 P. Cyr, S. T. Deng, J. M. Hawkins and K. E. Price, *Org. Lett.*, 2013, **15**, 4342–4345.
- 77 B. Ahmed-Omer, D. A. Barrow and T. Wirth, *Tetrahedron Lett.*, 2009, **50**, 3352–3355.
- 78 G. Strappaveccia, E. Ismalaj, C. Petrucci, D. Lanari, A. Marrocchi, M. Drees, A. Facchetti and L. Vaccaro, *Green Chem.*, 2014, **17**, 365–372.
- 79 D. Fodor, T. Kégl, J. M. Tukacs, A. K. Horváth and L. T. Mika, *ACS Sustain. Chem. Eng.*, 2020, **8**, 9926–9936.
- 80 E. Negishi, *Handbook of Organopalladium Chemistry for Organic Synthesis*, John Wiley & Sons, Ltd, New York, 1st edn., 2002.
- 81 K. Kohler, K. Wussow and A. S. Wirth, in *Palladium-Catalyzed Coupling Reactions*, ed. A. Molnar, Wiley-VCH Verlag, Weinheim, 1st edn., 2013, pp. 1–31.
- 82 H. L. Parker, J. Sherwood, A. J. Hunt and J. H. Clark, *ACS Sustain. Chem. Eng.*, 2014, **2**, 1739–1742.
- 83 H. Zeng, Z. Qiu, A. Domínguez-Huerta, Z. Hearne, Z. Chen and C.-J. Li, *ACS Catal.*, 2017, **7**, 510–519.
- 84 M. Picquet, *Platin. Met. Rev.*, 2013, **57**, 272–280.
- 85 T. Noël and V. Hessel, in *New Trends in Cross-Coupling: Theory and Applications*, ed. T. J. Colacot, Royal Society of Chemistry, London, 1st edn., 2015.
- 86 B. S. Flowers and R. L. Hartman, *Challenges*, 2012, **3**, 1–18.
- 87 L. Degennaro, C. Carlucci, S. De Angelis and R. Luisi, *J. Flow Chem. 2016 63*, 2016, **6**, 136–166.
- 88 T. N. Glasnov and C. O. Kappe, *Adv. Synth. Catal.*, 2010, **352**, 3089–3097.
- 89 R. N. Brogden, R. C. Heel, G. E. Pakes, T. M. Speight and G. S. Avery, *Drugs*, 1980, **19**, 84–106.
- 90 W. Shu, L. Pellegatti, M. A. Oberli and S. L. Buchwald, *Angew. Chemie Int. Ed.*, 2011, **50**, 10665–10669.
- 91 S. Roesner and S. L. Buchwald, *Angew. Chemie Int. Ed.*, 2016, **55**, 10463–10467.
- 92 R. Ciriminna, M. Pagliaro and R. Luque, *Green Energy Environ.*, 2021, **6**, 161–166.
- 93 X. Fan, M. G. Manchon, K. Wilson, S. Tennison, A. Kozynchenko, A. A. Lapkin and P. K. Plucinski, *J. Catal.*, 2009, **267**, 114–120.
- 94 E. Cini, E. Petricci and M. Taddei, *Catal. 2017, Vol. 7, Page 89*, 2017, **7**, 89.
- 95 I. Baxendale, J. Hayward and S. Ley, *Comb. Chem. High Throughput Screen.*, 2007, **10**, 802–836.
- 96 T. N. Glasnov, S. Findenig and C. O. Kappe, *Chem. – A Eur. J.*, 2009, **15**, 1001–1010.
- 97 N. Nikbin, M. Ladlow and S. V. Ley, *Org. Process Res. Dev.*, 2007, **11**, 458–462.
- 98 M. M. Reddy, K. H. Reddy and M. U. Reddy, *Pharm. Regul. Aff.*, 2016, **5**, 1–8.
- 99 R. P. Jumde, M. Marelli, N. Scotti, A. Mandoli, R. Psaro and C. Evangelisti, *J. Mol. Catal. A Chem.*, 2016, **414**, 55–61.
- 100 N. T. S. Phan, M. Van Der Sluys and C. W. Jones, *Adv. Synth. Catal.*, 2006, **348**, 609–679.
- 101 R. C. Jones, A. J. Canty, J. A. Deverell, M. G. Gardiner, R. M. Guijt, T. Rodemann, J. A. Smith and V. A. Tolhurst, *Tetrahedron*, 2009, **65**, 7474–7481.
- 102 W. Solodenko, H. Wen, S. Leue, F. Stuhlmann, G. Sourkouni-Argirusi, G. Jas, H. Schönfeld, U. Kunz and A. Kirschning, *European J. Org. Chem.*, 2004, **2004**, 3601–3610.
- 103 S. C. Stouten, Q. Wang, T. Noël and V. Hessel, *Tetrahedron Lett.*, 2013, **54**, 2194–2198.
- 104 S. C. Stouten, T. Noël, Q. Wang and V. Hessel, *Chem. Eng. J.*, 2015, **279**, 143–148.
- 105 N. Karbass, V. Sans, E. Garcia-Verdugo, M. I. Burguete and S. V. Luis, *Chem. Commun.*, 2006, **29**, 3095–3097.
- 106 N. T. S. Phan and P. Styring, *Green Chem.*, 2008, **10**, 1055.
- 107 G. Laudadio, G. Fusini, G. Casotti, C. Evangelisti, G. Angelici and A. Carpita, *J. Flow Chem. 2019 92*, 2019, **9**, 133–143.
- 108 A. Biffis, M. Zecca and M. Basato, *Eur. J. Inorg. Chem.*, 2001, **5**, 1131–1133.

- 109 A. Biffis, M. Zecca and M. Basato, *J. Mol. Catal. A Chem.*, 2001, **173**, 249–274.
- 110 A. Biffis, P. Centomo, A. Del Zotto and M. Zecca, *Chem. Rev.*, 2018, **118**, 2249–2295.
- 111 Y. Monguchi, T. Ichikawa, T. Yamada, Y. Sawama and H. Sajiki, *Chem. Rec.*, 2019, **19**, 3–14.
- 112 A. H. M. de Vries, J. M. C. A. Mulders, J. H. M. Mommers, H. J. W. Henderickx and J. G. de Vries, *Org. Lett.*, 2003, **5**, 3285–3288.
- 113 A. Alimardanov, L. Schmieder-van de Vondervoort, A. H. M. de Vries and J. G. de Vries, *Adv. Synth. Catal.*, 2004, **346**, 1812–1817.
- 114 I. P. Beletskaya and A. V. Cheprakov, *Chem. Rev.*, 2000, **100**, 3009–3066.
- 115 T. Jeffery, *Tetrahedron Lett.*, 1994, **35**, 3051–3054.
- 116 K. C. Nicolaou, P. G. Bulger and D. Sarlah, *Angew. Chem. Int. Ed*, 2005, **44**, 4442–4489.
- 117 B. P. Carrow and J. F. Hartwig, *J. Am. Chem. Soc.*, 2010, **132**, 79–81.
- 118 T. Kinzel, Y. Zhang and S. L. Buchwald, *J. Am. Chem. Soc.*, 2010, **132**, 14073–14075.
- 119 T. Noël and A. J. Musacchio, *Org. Lett.*, 2011, **13**, 5180–5183.
- 120 A. Bruneau, M. Roche, M. Alami and S. Messaoudi, *ACS Catal.*, 2015, **5**, 1386–1396.
- 121 C. C. C. Johansson Seechurn, S. L. Parisel and T. J. Colacot, *J. Org. Chem.*, 2011, **76**, 7918–7932.
- 122 C. C. C. J. Seechurn, T. Sperger, T. G. Scrase, F. Schoenebeck and T. J. Colacot, *J. Am. Chem. Soc.*, 2017, **139**, 5194–5200.
- 123 R. K. Henderson, C. Jiménez-González, D. J. C. Constable, S. R. Alston, G. G. A. Inglis, G. Fisher, J. Sherwood, S. P. Binks and A. D. Curzons, *Green Chem.*, 2011, **13**, 854–862.
- 124 D. Ainge and L.-M. Vaz, *Org. Process Res. Dev.*, 2002, **6**, 811–813.
- 125 H. E. Bonfield, D. Valette, D. M. Lindsay and M. Reid, *Chem. – A Eur. J.*, 2021, **27**, 158–174.
- 126 E. W. Werner, T.-S. Mei, A. J. Burckle and M. S. Sigman, *Science*, 2012, **338**, 1455.
- 127 R. F. Heck, *J. Am. Chem. Soc.*, 1968, **90**, 5526–5531.
- 128 J. B. Melpolder and R. F. Heck, *J. Org. Chem.*, 1976, **41**, 265–272.
- 129 R. Uma, C. Crévisy and R. Grée, *Chem. Rev.*, 2002, **103**, 27–51.
- 130 L. Xu, M. J. Hilton, X. Zhang, P.-O. Norrby, Y.-D. Wu, M. S. Sigman and O. Wiest, *J. Am. Chem. Soc.*, 2014, **136**, 1960–1967.
- 131 M. J. Hilton, L.-P. Xu, P.-O. Norrby, Y.-D. Wu, O. Wiest and M. S. Sigman, *J. Org. Chem.*, 2014, **79**, 11841–11850.
- 132 L. Lin, C. Romano and C. Mazet, *J. Am. Chem. Soc.*, 2016, **138**, 10344–10350.
- 133 T.-S. Mei, E. W. Werner, A. J. Burckle and M. S. Sigman, *J. Am. Chem. Soc.*, 2013, **135**, 6830–6833.
- 134 Y. Dang, S. Qu, Z.-X. Wang and X. Wang, *J. Am. Chem. Soc.*, 2014, **136**, 986–998.
- 135 N. J. Race, Q. Yuan and M. S. Sigman, *Chem. – A Eur. J.*, 2019, **25**, 512–515.
- 136 Z.-Z. Jiang, A. Gao, H. Li, D. Chen, C.-H. Ding, B. Xu and X.-L. Hou, *Chem. – An Asian J.*, 2017, **12**, 3119–3122.
- 137 N. J. Race, C. S. Schwalm, T. Nakamuro and M. S. Sigman, *J. Am. Chem. Soc.*, 2016, **138**, 15881–15884.
- 138 H. Nakamura, K. Yasui, Y. Kanda and P. S. Baran, *J. Am. Chem. Soc.*, 2019, **141**, 1494–1497.
- 139 Z. S. Liu, G. Qian, Q. Gao, P. Wang, H. G. Cheng, Y. Hua and Q. Zhou, *Tetrahedron*, 2019, **75**, 1774–1780.
- 140 J. G. De Vries, *Can. J. Chem.*, 2001, **79**, 1086–1092.
- 141 S. Bouquillon, B. Ganchegui, B. Estrine, F. Hénin and J. Muzart, *J. Organomet. Chem.*, 2001, **634**, 153–156.
- 142 D. Cortés-Borda, K. V. Kutonova, C. Jamet, M. E. Trusova, F. Zammattio, C. Truchet, M. Rodriguez-Zubiri and F.-X. Felpin, *Org. Process Res. Dev.*, 2016, **20**, 1979–1987.
- 143 W. Khodja, A. Leclair, J. Rull-Barrull, F. Zammattio, K. V. Kutonova, M. E. Trusova, F.-X. Felpin and M. Rodriguez-Zubiri, *New J. Chem.*, 2016, **40**, 8855–8862.
- 144 N. Cheeseman, M. Fox, M. Jackson, I. C. Lennon and G. Meek, *Proc. Natl. Acad. Sci. U. S. A.*, 2004, **101**, 5396.
- 145 G. L. Allsop, A. J. Cole, M. E. Giles, E. Merifield, A. J. Noble, M. A. Pritchett, L. A. Purdie and J. T.

- Singleton, *Org. Process Res. Dev.*, 2009, **13**, 751–759.
- 146 C. Torborg and M. Beller, *Adv. Synth. Catal.*, 2009, **351**, 3027–3043.
- 147 V. F. Slagt, A. H. M. de Vries, J. G. de Vries and R. M. Kellogg, *Org. Process Res. Dev.*, 2010, **14**, 30–47.
- 148 S. Mannathan, S. Raoufmoghaddam, J. N. H. Reek, J. G. de Vries and A. J. Minnaard, *ChemCatChem*, 2015, **7**, 3923–3927.
- 149 L. J. Oxtoby, J. A. Gurak, Jr., S. R. Wisniewski, M. D. Eastgate and K. M. Engle, *Trends Chem.*, 2019, **1**, 572.
- 150 T. Ghosh, *ChemistrySelect*, 2019, **4**, 4747–4755.
- 151 P. Gao and S. P. Cook, *Org. Lett.*, 2012, **14**, 3340–3343.
- 152 M. IM and G. SD, *Pharmacol. Biochem. Behav.*, 2003, **75**, 607–618.
- 153 G. K. Jana and S. Sinha, *Tetrahedron*, 2012, **68**, 7155–7165.
- 154 G. K. Jana and S. Sinha, *Tetrahedron Lett.*, 2012, **53**, 1671–1674.
- 155 A. C. Kruegel, S. Rakshit, X. Li and D. Sames, *J. Org. Chem.*, 2015, **80**, 2062–2071.
- 156 J. C. Namyslo and D. E. Kaufmann, *Synlett*, 1999, **6**, 804–806.
- 157 F. Aziz, *Ann. Palliat. Med.*, 2012, **1**, 130–136.
- 158 J. J. Kulagowski, N. R. Curtis, C. J. Swain and B. J. Williams, *Org. Lett.*, 2001, **3**, 667–670.
- 159 S. Torii, H. Tanaka and K. Morisaki, *Chem. Lett.*, 2006, **14**, 1353–1354.
- 160 L. Jin, J. Qian, N. Sun, B. Hu, Z. Shen and X. Hu, *Chem. Commun.*, 2018, **54**, 5752–5755.
- 161 S. Murahashi, T. Hirano and T. Yano, *J. Am. Chem. Soc.*, 2002, **100**, 348–350.
- 162 G. Yue, K. Lei, H. Hirao and J. S. Zhou, *Angew. Chem. Int. Ed. Engl.*, 2015, **54**, 6531–6535.
- 163 A. Minatti, X. Zheng and S. L. Buchwald, *J. Org. Chem.*, 2007, **72**, 9253–9258.
- 164 S. Mannathan, S. Raoufmoghaddam, J. N. H. Reek, J. G. de Vries and A. J. Minnaard, *ChemCatChem*, 2017, **9**, 551–554.
- 165 N. Parveen, R. Saha and G. Sekar, *Adv. Synth. Catal.*, 2017, **359**, 3741–3751.
- 166 N. Parveen and G. Sekar, *Adv. Synth. Catal.*, 2019, **361**, 4581–4595.
- 167 S. Raoufmoghaddam, S. Mannathan, A. J. Minnaard, J. G. de Vries and J. N. H. Reek, *Chem. – A Eur. J.*, 2015, **21**, 18811–18820.
- 168 A. L. Gottumukkala, J. G. de Vries and A. J. Minnaard, *Chem. – A Eur. J.*, 2011, **17**, 3091–3095.
- 169 J. A. Mueller, C. P. Goller and M. S. Sigman, *J. Am. Chem. Soc.*, 2004, **126**, 9724–9734.
- 170 J. A. Terrett, J. D. Cuthbertson, V. W. Shurtleff and D. W. C. MacMillan, *Nature*, 2015, **524**, 330–334.
- 171 C. E. Wayne and R. P. Wayne, *Photochemistry*, Oxford University Press, Oxford, 1st edn., 1996.
- 172 M. Oelgemöller, *Chem. Rev.*, 2016, **116**, 9664–9682.
- 173 G. Ciamician, *Science*, 1912, **36**, 385–394.
- 174 N. Monnerie and J. Ortner, *J. Sol. Energy Eng.*, 2001, **123**, 171–174.
- 175 A. B. Beeler, *Chem. Rev.*, 2016, **116**, 9629–9630.
- 176 A. Albini and M. Fagnoni, *Handbook of Synthetic Photochemistry*, Wiley-VCH Verlag, Weinheim, 1st edn., 2010.
- 177 B. D. A. Hook, W. Dohle, P. R. Hirst, M. Pickworth, M. B. Berry and K. I. Booker-Milburn, *J. Org. Chem.*, 2005, **70**, 7558–7564.
- 178 M. H. Shaw, J. Twilton and D. W. C. MacMillan, *J. Org. Chem.*, 2016, **81**, 6898–6926.
- 179 C. K. Prier, D. A. Rankic and D. W. C. MacMillan, *Chem. Rev.*, 2013, **113**, 5322–5363.
- 180 J. W. Tucker and C. R. J. Stephenson, *J. Org. Chem.*, 2012, **77**, 1617–1622.
- 181 J. M. R. Narayanam and C. R. J. Stephenson, *Chem. Soc. Rev.*, 2011, **40**, 102–113.
- 182 M. Chergui, *Acc. Chem. Res.*, 2015, **48**, 801–808.
- 183 C. M. Marian, *Annu. Rev. Phys. Chem.*, 2021, **72**, 617–640.
- 184 D. M. Arias-Rotondo and J. K. McCusker, *Chem. Soc. Rev.*, 2016, **45**, 5803–5820.
- 185 J. Hu, J. Wang, T. H. Nguyen and N. Zheng, *Beilstein J. Org. Chem.* 9234, 2013, **9**, 1977–2001.
- 186 A. G. Condie, J. C. González-Gómez and C. R. J. Stephenson, *J. Am. Chem. Soc.*, 2010, **132**, 1464–1465.

- 187 J. M. R. Narayanam, J. W. Tucker and C. R. J. Stephenson, *J. Am. Chem. Soc.*, 2009, **131**, 8756–8757.
- 188 S. Fukuzumi, S. Mochizuki and T. Tanaka, *J. Phys. Chem.*, 2002, **94**, 722–726.
- 189 J. J. Douglas, K. P. Cole and C. R. J. Stephenson, *J. Org. Chem.*, 2014, **79**, 11631–11643.
- 190 M. A. Graham, G. Noonan, J. H. Cherryman, J. J. Douglas, M. Gonzalez, L. V. Jackson, K. Leslie, Z. Liu, D. McKinney, R. H. Munday, C. D. Parsons, D. T. E. Whittaker, E. Zhang and J. Zhang, *Org. Process Res. Dev.*, 2020, **25**, 57–67.
- 191 K. Harper, T. Grieme, T. Towne, D. Mack, M. Diwan, Y.-Y. Ku, J. Griffin, R. Miller, E. Zhang, Z. Liu, S. Zheng, N. Zhang, S. Grangula, J. Yuan, P. Huang and J. Gage, *ChemRxiv*, 2021, Pre-print, not peer-reviewed.
- 192 D. Kalyani, K. B. McMurtrey, S. R. Neufeldt and M. S. Sanford, *J. Am. Chem. Soc.*, 2011, **133**, 18566–18569.
- 193 Yong-Yuan Gui, Liang Sun, Zhi-Peng Lu and Da-Gang Yu, *Org. Chem. Front.*, 2016, **3**, 522–526.
- 194 Z. Zuo, D. T. Ahneman, L. Chu, J. A. Terrett, A. G. Doyle and D. W. C. MacMillan, *Science*, 2014, **345**, 437–440.
- 195 E. B. Corcoran, M. T. Pirnot, S. Lin, S. D. Dreher, D. A. DiRocco, I. W. Davies, S. L. Buchwald and D. W. C. MacMillan, *Science*, 2016, **353**, 279–283.
- 196 F. Lévesque, M. J. Di Maso, K. Narsimhan, M. K. Wismer and J. R. Naber, *Org. Process Res. Dev.*, 2020, **24**, 2935–2940.
- 197 H. Zhang, P. Ruiz-Castillo and S. L. Buchwald, *Org. Lett.*, 2018, **20**, 1580–1583.
- 198 J. Clayden, N. Greeves and S. Warren, *Organic Chemistry*, Oxford University Press, Oxford, 2nd ed., 2012.
- 199 S. Mandal, S. Mandal, S. K. Ghosh, P. Sar, A. Ghosh, R. Saha and B. Saha, *RSC Adv.*, 2016, **6**, 69605–69614.
- 200 T. Y. S. But and P. H. Toy, *Chem. – An Asian J.*, 2007, **2**, 1340–1355.
- 201 R. H. Beddoe, H. F. Sneddon and R. M. Denton, *Org. Biomol. Chem.*, 2018, **16**, 7774–7781.
- 202 P. E. Fanta, *Chem. Rev.*, 1946, **38**, 139–196.
- 203 R. Giri, A. Brusoe, K. Troshin, J. Y. Wang, M. Font and J. F. Hartwig, *J. Am. Chem. Soc.*, 2018, **140**, 793–806.
- 204 R. R. Schmidt and W. Frick, *Tetrahedron*, 1988, **44**, 7163–7169.
- 205 C. Chavis, F. Dumont, R. H. Wightman, J. C. Ziegler and J. L. Imbach, *J. Org. Chem.*, 1982, **47**, 202–206.
- 206 M. Neeman, M. C. Caserio, J. D. Roberts and W. S. Johnson, *Tetrahedron*, 1959, **6**, 36–47.
- 207 X. Wu, B. P. Fors and S. L. Buchwald, *Angew. Chemie - Int. Ed.*, 2011, **50**, 9943–9947.
- 208 C. W. Cheung and S. L. Buchwald, *Org. Lett.*, 2013, **15**, 3998–4001.
- 209 H. Zhang, P. Ruiz-Castillo, A. W. Schuppe and S. L. Buchwald, *Org. Lett.*, 2020, **22**, 5369–5374.
- 210 M. Watanabe, M. Nishiyama and Y. Koie, *Tetrahedron Lett.*, 1999, **40**, 8837–8840.
- 211 C. H. Burgos, T. E. Barder, X. Huang and S. L. Buchwald, *Angew. Chemie - Int. Ed.*, 2006, **45**, 4321–4326.
- 212 M. Reckenthäler and A. G. Griesbeck, *Adv. Synth. Catal.*, 2013, **355**, 2727–2744.
- 213 R. Han and G. L. Hillhouse, *J. Am. Chem. Soc.*, 1997, **119**, 8135–8136.
- 214 L. Tian, N. A. Till, B. Kudisch, D. W. C. MacMillan and G. D. Scholes, *J. Am. Chem. Soc.*, 2020, **142**, 4555–4559.
- 215 R. Sun, Y. Qin, S. Ruccolo, C. Schnedermann, C. Costentin and D. G. Nocera, *J. Am. Chem. Soc.*, 2019, **141**, 89–93.
- 216 B. Zhu, L. K. Yan, Y. Geng, H. Ren, W. Guan and Z. M. Su, *Chem. Commun.*, 2018, **54**, 5968–5971.
- 217 P. Ma, S. Wang and H. Chen, *ACS Catal.*, 2020, **10**, 1–6.
- 218 R. Mao, J. Balon and X. Hu, *Angew. Chemie Int. Ed.*, 2018, **57**, 13624–13628.
- 219 R. A. Escobar and J. W. Johannes, *Chem. – A Eur. J.*, 2020, **26**, 5168–5173.
- 220 Q. Q. Zhou, F. D. Lu, D. Liu, L. Q. Lu and W. J. Xiao, *Org. Chem. Front.*, 2018, **5**, 3098–3102.
- 221 Y. Y. Liu, D. Liang, L. Q. Lu and W. J. Xiao, *Chem. Commun.*, 2019, **55**, 4853–4856.

- 222 C. Xiao and W. J. Xiao, *Chinese J. Org. Chem.*, 2020, **40**, 3004–3006.
- 223 L. Yang, H. Lu, C. Lai, G. Li, W. Zhang, R. Cao, F. Liu, C. Wang, J. Xiao and D. Xue, *Angew. Chemie Int. Ed.*, 2020, **59**, 12714–12719.
- 224 H. Lee, N. C. Boyer, Q. Deng, H. Y. Kim, T. K. Sawyer and N. Sciammetta, *Chem. Sci.*, 2019, **10**, 5073–5078.
- 225 S. S. Shah, M. Shee, A. K. Singh, A. Paul and N. D. P. Singh, *J. Org. Chem.*, 2020, **85**, 3426–3439.
- 226 C. A. Clark, D. S. Lee, S. J. Pickering, M. Poliakoff and M. W. George, *Org. Process Res. Dev.*, 2016, **20**, 1792–1798.
- 227 S. Murarka, *Adv. Synth. Catal.*, 2018, **360**, 1735–1753.
- 228 F. Toriyama, J. Cornella, L. Wimmer, T. G. Chen, D. D. Dixon, G. Creech and P. S. Baran, *J. Am. Chem. Soc.*, 2016, **138**, 11132–11135.
- 229 S. R. Chemler, *Beilstein J. Org. Chem.*, 2015, **11**, 2252–2253.
- 230 C. Le, T. Q. Chen, T. Liang, P. Zhang and D. W. C. MacMillan, *Science*, 2018, **360**, 1010–1014.
- 231 M. W. Johnson, K. I. Hannoun, Y. Tan, G. C. Fu and J. C. Peters, *Chem. Sci.*, 2016, **7**, 4091–4100.
- 232 S. E. Creutz, K. J. Lotito, G. C. Fu and J. C. Peters, *Science*, 2012, **338**, 647–651.
- 233 K. Okada, K. Okamoto, N. Morita, K. Okubo and M. Oda, *J. Am. Chem. Soc.*, 1991, **113**, 9401–9402.
- 234 K. Okada, K. Okamoto and M. Oda, *J. Am. Chem. Soc.*, 2002, **110**, 8736–8738.
- 235 G. Z. Wang, R. Shang and Y. Fu, *Org. Lett.*, 2018, **20**, 888–891.
- 236 K. Okada, K. Okamoto and M. Oda, *J. Chem. Soc. Chem. Commun.*, 1989, 1636–1637.
- 237 L. Candish, M. Teders and F. Glorius, *J. Am. Chem. Soc.*, 2017, **139**, 7440–7443.
- 238 W. Xue and M. Oestreich, *Angew. Chemie Int. Ed.*, 2017, **56**, 11649–11652.
- 239 H. Zhang, P. Zhang, M. Jiang, H. Yang and H. Fu, *Org. Lett.*, 2017, **19**, 1016–1019.
- 240 A. Tlahuext-Aca, L. Candish, R. A. Garza-Sanchez and F. Glorius, *ACS Catal.*, 2018, **8**, 1715–1719.
- 241 D. Wang, N. Zhu, P. Chen, Z. Lin and G. Liu, *J. Am. Chem. Soc.*, 2017, **139**, 15632–15635.
- 242 G. M. Whitesides, J. S. Sadowski and J. Lilburn, *J. Am. Chem. Soc.*, 1974, **96**, 2829–2835.
- 243 A. Hossain, A. Bhattacharyya and O. Reiser, *Science*, 2019, **364**, 1–11.
- 244 M. Marchini, G. Bergamini, P. G. Cozzi, P. Ceroni and V. Balzani, *Angew. Chemie Int. Ed.*, 2017, **56**, 12820–12821.
- 245 L. Buzzetti, G. E. M. Crisenza and P. Melchiorre, *Angew. Chemie Int. Ed.*, 2019, **58**, 3730–3747.
- 246 D. Koyama, H. J. A. Dale and A. J. Orr-Ewing, *J. Am. Chem. Soc.*, 2018, **140**, 1285–1293.
- 247 A. J. Orr-Ewing, *Struct. Dyn.*, 2019, **6**, 010901.
- 248 F. E. Lytle, R. M. Parrish and W. T. Barnes, *Appl. Spectrosc.*, 1985, **39**, 444–451.
- 249 K. M. Omberg, J. R. Schoonover, J. A. Treadway, R. M. Leasure, R. Brian Dyer and T. J. Meyer, *J. Am. Chem. Soc.*, 1997, **119**, 7013–7018.
- 250 V. Kumar, S. Schlüker and E. Hasselbrink, in *Molecular and Laser Spectroscopy*, eds. V. P. Gupta and Y. Ozaki, Elsevier, Amsterdam, Oxford, Cambridge, 2nd edn., 2020.
- 251 K. Reynolds PhD Thesis, University of Nottingham, 2019.
- 252 Y. Paz, *J. Phys. Condens. Matter*, 2019, **31**, 1–22.
- 253 M. W. George and J. J. Turner, *Coord. Chem. Rev.*, 1998, **177**, 201–217.
- 254 P. C. Ford, J. S. Bridgewater and B. Lee, *Photochem. Photobiol.*, 1997, **65**, 57–64.
- 255 N. Kandoth, J. Pérez Hernández, E. Palomares and J. Lloret-Fillol, *Sustain. Energy Fuels*, 2021, **5**, 638–665.
- 256 T. J. Meyer, *Pure Appl. Chem.*, 1986, **58**, 1–193.
- 257 J. R. Schoonover and G. F. Strouse, *Chem. Rev.*, 1998, **98**, 1335–1356.
- 258 D. N. Chirdon, C. E. McCusker, F. N. Castellano and S. Bernhard, *Inorg. Chem.*, 2013, **52**, 8795–8804.
- 259 M. Rueda-Becerril, O. Mahé, M. Drouin, M. B. Majewski, J. G. West, M. O. Wolf, G. M. Sammis and J. F. Paquin, *J. Am. Chem. Soc.*, 2014, **136**, 2637–2641.
- 260 N. A. Romero and D. A. Nicewicz, *J. Am. Chem. Soc.*, 2014, **136**, 17024–17035.
- 261 E. R. Welin, C. Le, D. M. Arias-Rotondo, J. K. McCusker and D. W. C. MacMillan, *Science*, 2017,

- 355, 380–385.
- 262 W. L. . Armarego and D. D. Perrin, *Purification of Laboratory Chemicals*, Butterworth Heinemann, Oxford, 4th edn., 1996.
- 263 N. Zhang, D. J. Hoffman, N. Gutsche, J. Gupta and V. Percec, *J. Org. Chem.*, 2012, **77**, 5956–5964.
- 264 S. Engl and O. Reiser, *European J. Org. Chem.*, 2020, **2020**, 1523–1533.

Experimental

Exp.1 General Experimental Detail

Reagents/catalysts/solvents *etc.* were generally purchased from commercial suppliers (including Fluorochem, Sigma/Merck, Acros, Fisher, Honeywell, Strem) and mainly used as received. CuCl (used in Chapter 6) was purified using a known approach before use, involving dissolution in conc. HCl, before precipitation by addition of water.²⁶² PGM (Ir and Pd) catalysts were supplied by JM (apart from PdCl₂ used mostly in Chapter 3), and were used as received. NHPI-ester starting material (Chapter 6) was synthesised in this work (details later in the Experimental Chapter). Stainless steel tubing was purchased from Swagelok (supplied by Sandvik) and stainless steel fittings, connections and sprung-relief valves were purchased from Swagelok. FEP tubing was purchased from Cole-Parmer (used in the photochemical flow reactor), and plastic fittings/connections were purchased from commercial sources (Gilson, Omni-Fit). Tubing materials were cut to size and fabricated into reactors as part of this work or machined in-house.

NMR spectra were recorded on a 400 MHz (¹H) and 100 MHz (¹³C) Bruker instrument. Mass spec. were recorded using a Bruker MicroTOF instrument. IR spectra were recorded using a Bruker Alpha-p instrument, with an ATR attachment (Chapter 3), or a Thermo Nicolet 6700 FT-IR instrument (Chapter 7). Automatic column chromatography was performed using a Teledyne ISCO CombiFlash Rf + system, using UV detection. GC analyses were carried out using a Shimadzu GC-2014 system. This was equipped with either a 30 m length, 0.25 mm diameter Supelco SPB-170 column (0.25 μm particles, fused silica with polycyanopropylphenyl/polydimethylsiloxane bonded phase – intermediate polarity, Chapters 2-4 and some of Chapter 5) or, a 30 m length, 0.25 mm diameter Supelco Equity-1701 column (0.25 μm particles, fused silica with polycyanopropylphenyl/polydimethylsiloxane bonded phase – intermediate polarity, Chapter 6 and some of Chapter 5). All GC methods used flame ionisation detection, 300 °C, with H₂ (generated using a Dornick Hunter water electrolyser) and compressed air for generating the flame. He was used as the carrier gas. Specific method details are given in the Appendix.

Yields/conversions were evaluated by isolation, ¹H NMR spectroscopy, or GC, with details given in the Appendix. When ¹H NMR spectroscopy was used for yield quantification, samples were taken from the crude reaction product, and the solvent removed under a gentle N₂ stream. 1,4-dinitrobenzene was then added as an external standard and the mixture diluted in deuterated solvent. When GC was used for yield quantification, samples were typically taken from the flow reactor outlet stream (or removed from a batch vessel) and diluted before analysing with a suitable GC method (details in the Appendix). GC Yields were calculated using a calibration plot approach (details in the Appendix) and were calculated from replicate (usually triplicate) samples from crude product mixtures, with the quoted yield being the average of the replicates. Uncertainties were estimated from the discrepancy between the average, and the measurement furthest away from the average. Conversions were determined from the ratio of the GC peak area of the limiting reagent in the crude product mixture against the (average) peak area of the limiting reagent in starting material samples (again usually triplicate). Specific details are given in the Appendix. Where selectivity towards the desired product was estimated, this was calculated from the ratio of the product yield to the limiting reagent conversion (expressed as a percentage), and this was stated as an *estimate* as the yield and conversions used were the averages

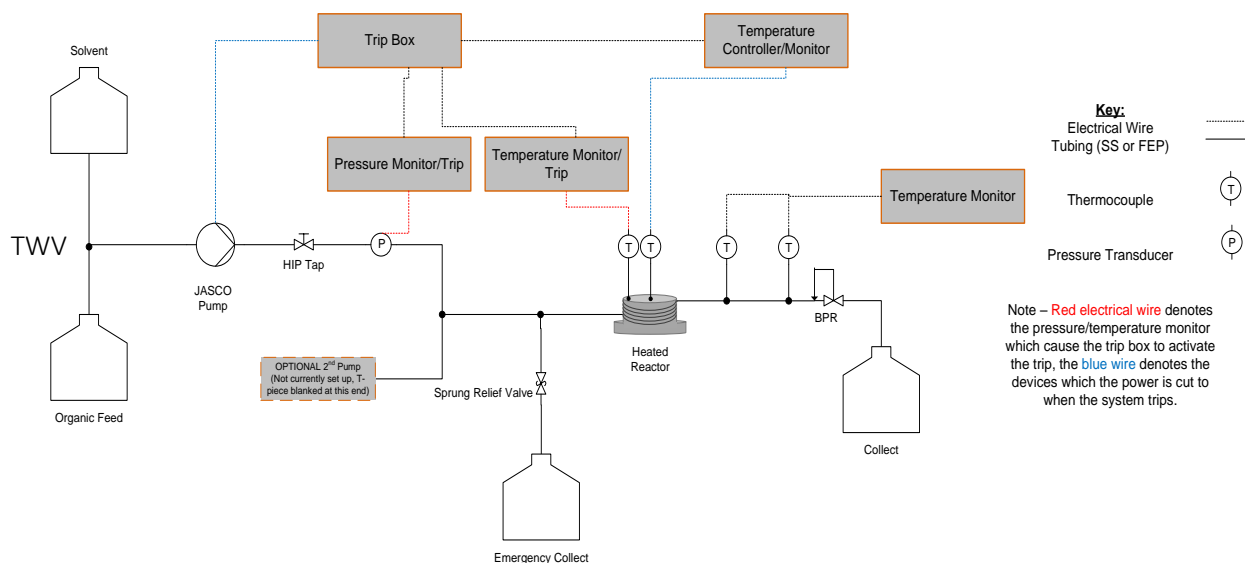
from the replicate samples (therefore not accounting for the uncertainty when calculating the selectivity).

Exp.2 Flow Reactors

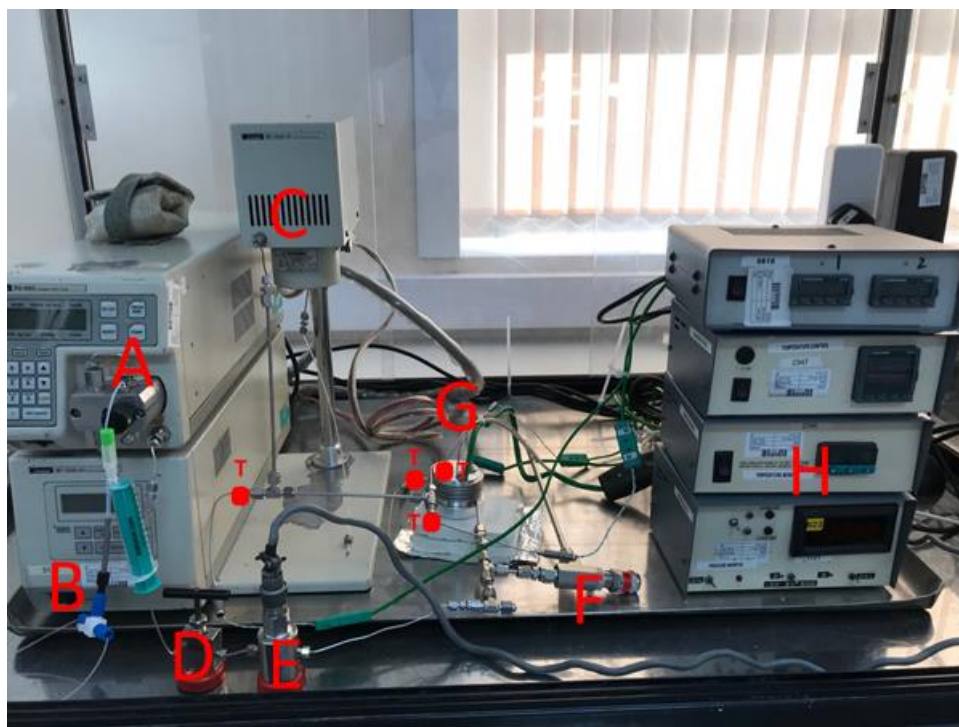
Exp.2.1 Thermal Tubular Flow Reactor

The reactor is based on stainless steel tubing (316 SS), purchased from Sandvik and fittings were purchased from Swagelok for the assembly of the parts of the reactor based upon this tubing. A diagram and photograph of the system can be seen below.

Two lengths of 1/16 " OD FEP or PTFE tubing were connected to opposite ends of a PTFE three-way valve (Omni-Fit). The third connection point of the three-way valve was connected to the pump-head inlet of a JASCO PU-980 HPLC pump. The outlet of the pump-head was joined, *via* a length of 1/16 " OD SS tubing, to a HIP tap (to allow for closing the pump to the system). The other end of this tap was joined *via* another length of 1/16 " OD SS tubing to a pressure transducer, for monitoring the system pressure whilst in operation (the transducer, in turn, was connected to an electronic display). The other end of this transducer was connected to a T-piece *via* 1/16 " OD SS tubing. One end of this T-piece was joined to a Swagelok sprung-relief valve rated at ~150 bar to ensure the release of pressure in the event of any serious blockages. The other end of this T-piece connected to, *via* a length of 1/8 " OD SS tubing, a 1/8 " – 1/8 " SS tubing union and the other end of this union joined to the 1/8 " OD SS tubing coil used to form the heated reactor coil. This tubing forming the heated reactor coil was 125 cm in length as to give a heated volume of 3.0 mL (calculation detailed below). The tubing was coiled around an in-house machined aluminium block. The top of the block had drilled through two holes to house two cartridge Joule heaters (purchased from RS Components). Along with this, two smaller holes were drilled to house thermocouples. One of the thermocouples was used as a control for the cartridge heaters (placed in the centre of the heated block) and the other thermocouple was used to monitor the temperature at the edge of the box, next to where the heated tubing was positioned. The outlet at the top of the heated tubing coil was connected *via* a 1/8 " – 1/8 " SS tubing union to a T-piece. One end of this T-piece was connected to a thermocouple for monitoring the outlet temperature of the reaction mixture when in a flowing stream. The other end of this T-piece was connected to a further length of 1/8 " tubing (where which the outlet stream was allowed to cool). This tubing was joined to another T-piece which was connected to a second thermocouple (to ensure sufficient cooling of the reaction stream upon flowing out of the heated reactor coil and along this length of tubing). The other end of this T-piece was joined to (*via* a reducing union) a length of 1/16 " OD SS tubing, connected to a JASCO BPR. *Via* a final length of 1/16 " FEP or PTFE tubing, the outlet stream to the reactor system was formed.



Exp. Fig 1 rig diagram for the high temperature/pressure continuous flow reactor system designed and constructed in this work.



Exp. Fig 2 photograph of the high temperature flow reactor, highlighting: A – Pump, B – BPR interface, C – BPR, D – HIP tap, E – Pressure transducer, F – Sprung relief valve, G – Heated reactor, H – Pressure and temperature monitors. Thermocouple locations indicated with red dots and a red T.

The heated reactor coil was constructed from a 125 cm length of 1/8 " SS Swagelok tubing. The details below were used to determine an internal volume of 3.0 mL.

1/8 " SS tubing: OD = 1/8 " , wall thickness (WT) = 0.028 " .

Therefore, ID = 1/8 " – 2 x (0.028 ") = 0.069"

0.069 " x 2.54 cm " ⁻¹ = 0.175 cm

Therefore, radius of tubing inner = 0.175 cm / 2 = 0.0875 cm

Therefore, in **each centimetre** of tubing, volume of tubing is...

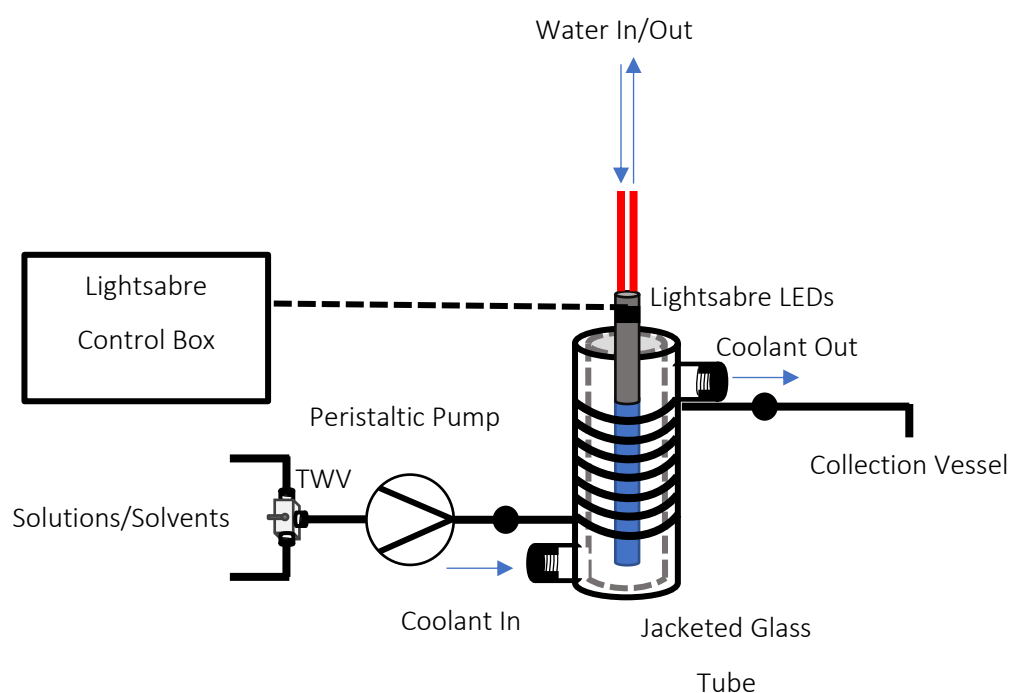
$$\pi \times (0.0875 \text{ cm})^2 \times 1 \text{ cm} = 0.024 \text{ cm}^3 = 0.024 \text{ mL}$$

Therefore, in 125 cm, $125 \text{ cm} \times 0.024 \text{ mLcm}^{-1} = 3.0 \text{ mL}$.

The total system volume was determined experimentally to be ~4.0 mL. See Exp.2.2. regarding the photochemical flow reactor for a diagrammatic representation of similar calculations, for a flow reactor built for processing photochemical reactions.

Exp.2.2 Photochemical FEP Coil Flow Reactor

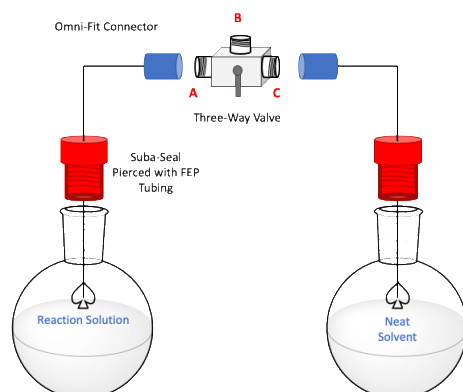
The continuous flow reactors used in this work were built as part of the project and were based upon a Booker-Milburn FEP coil continuous flow reactor.¹⁷⁷



Exp. Fig 3 reactor diagram of the photochemical FEP flow reactor built for performing continuous flow Ir/Ni C-O coupling reactions. Solid black line (-) denotes FEP tubing, dashed black line (---) denotes electrical wiring, TWV = three-way valve.

Two lengths of 1/32 " ID FEP tubing were pierced through two separate suba-seals. To the opposite end of the suba-seal "stopper side" was connected two Omni-Fit plastic connectors, held in place with a plastic ferrule. Each of these connectors was used to join the tubing lengths to an Omni-Fit three-way valve (TWV). This was intended to allow for attachment of two round bottomed flasks (to the suba-seals) with the ability to close the three way-valve to the third outlet, allowing for each flask to be handled without exposure to the surrounding atmosphere (intended as a mechanism to allow for degassing of the two flasks using a freeze-pump-thaw method and then being able to subsequently attach the three-way valve to the rest of the reactor system without exposing the degassed contents to the air). The third outlet of the three-way valve could then be connected to peristaltic pump-head PTFE tubing (Masterflex, 2 mm ID, 4 mm OD, 38 cm length), using an Omni-Fit plastic connector. This

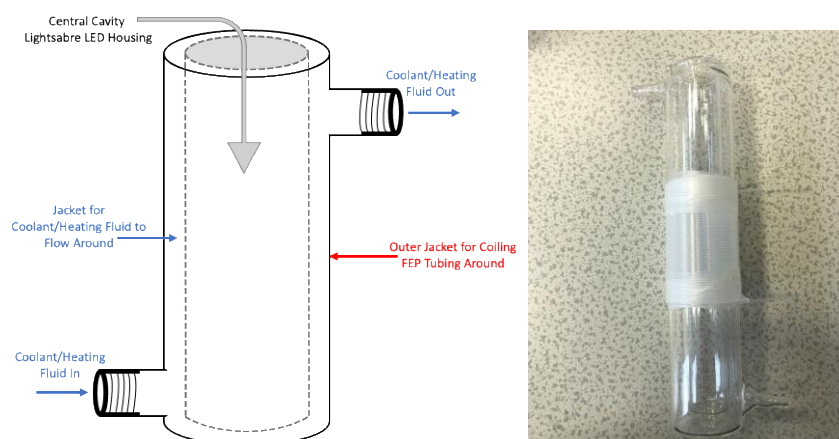
tubing was used with a Masterflex L/S 77390-00 (Cole-Parmer) peristaltic pump and the tubing was inserted into the pump-head of the pump.



Exp. Fig 4 three-way valve device constructed to allow for degassing (via freeze-pump-thaw) a reaction mixture and neat reaction solvent. The TWV can be closed to position **B** to prevent exposure to the surroundings. The flasks could then be degassed via piercing the suba-seals with a needle connected to a Schlenk line. Following degassing, position **B** could then be connected to the rest of the flow reactor system and the TWV opened to position **C** to allow degassed solvent to purge the reactor prior to opening position **A** to begin flowing the reaction mixture.

To the outlet end of the peristaltic pump tubing was another Omni-Fit plastic connector. This connected the pump-head tubing to the irradiated reactor coil which was either a length of 1/8, 1/16 or 1/32 " FEP tubing (details below). This tubing was coiled around a jacketed pyrex tube (described below) and at the other end, was joined (again using Omni-Fit plastic connectors and appropriate seals/ferrules) to a short (~30 cm) length of 1/32 " ID FEP tubing, forming the reactor outlet.

The jacketed tube was made in-house by the glassblowing workshop at the University of Nottingham. The FEP reactor coil was wrapped around this, and it was designed to meet a small number of criteria. These were to appropriately house the Lightsabre LED light source identified for use in the system, to allow for the tubing to be coiled around the outside of the tube with a coil diameter as small as could conveniently be produced by the workshop and to allow for a range of temperatures to be applied to the reactor coil. The idea with the small diameter was that the smaller the diameter of the coil, the greater the length of the coil produced would be for tubing of a given length – desired in the project as a small volume reactor coil, whilst capturing all emitted light from the source was desired.



Exp. Fig 5 diagram (left) of the jacketed tube forming the central part of the reactor system and a photograph (right) with an example tubing coil wrapped around the outer jacket.

Lightsabre LEDs were used as the emission source in this flow reactor. For the work in this project, a blue Lightsabre was used with an emission maximum at around 410 nm (measured as part of this work). A full description of this is given in Section 4.5. For their relevance to the reactor, the Lightsabre was housed within the central cavity of the jacketed tube. Water cooling was attached to inlet and outlet tubes at the top of the light source to ensure the LEDs did not get too hot whilst operating. When turned on, the emission of the Lightsabre LEDs would therefore fall upon the FEP reactor coil, wrapped around the outer jacket of the tube.

The inner jacket of the tube was connected to a recirculating chiller/heater (where required) *via* an inlet at the bottom and an outlet at the top. When used, the recirculating chiller/heater was a VWR-1162A recirculating chiller with the pump speed set to high and a thermocouple inserted into the cooling/heating bath to ensure the temperature was at the desired value. The coolant fluid was always 50/50 H₂O:ethylene glycol, or H₂O. This was used to allow for a range of temperatures to be studied whilst maintaining transparency to visible light as, when coolant was present, the emission from the Lightsabre would necessarily have to penetrate through the fluid to irradiate the reactor coil containing the reaction mixture, due to the design of the jacketed tube.



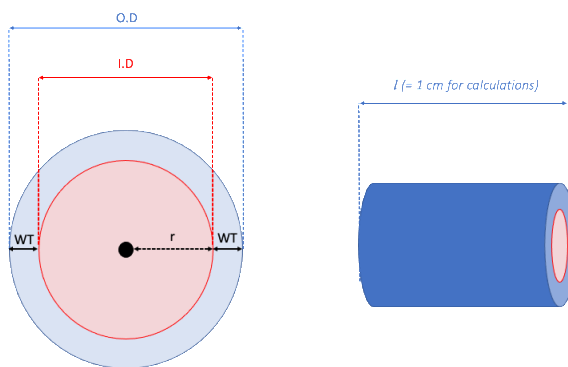
Exp. Fig 6 photograph of a small footprint completed reactor system containing all possible components used (i.e., including connected recirculating chiller/heater which was not always present).

The total internal volume of the tubing in the reactor system (in the initial format Tubing 1 in table below) was determined to be 7.0 mL. 5.0 mL of this volume was constituting the irradiated reactor coil and the remaining 2.0 mL constituting the tubing in the remaining parts of the reactor system (*i.e.*, the inlet tubings to the pump, the pump-head tubing and the reactor outlet stream tubing). This was determined by first calibrating the pump to an accurate flow rate, then, flowing through IPA at a known flow rate and recording the time taken for the system to fill up right to the end, whilst separately timing the time taken for the IPA to fill the reactor coil part of the system. From the known flow rate and these two times, it was possible to calculate the volume of IPA both in the entire system and in just the reactor coil. To double check the calculation, the IPA used was filled to 10 mL in a measuring cylinder and 3 mL of IPA remained in the cylinder after filling the system – further indicating a 7.0 mL volume of IPA being required to fill the system. This was repeated several times at different flow rates to ensure accurate results. In much of the work, the reactor was not used in this initial format, with the change being made only to the reactor coil *i.e.*, using an FEP coil of different dimensions. Therefore, the remaining parts of the system would remain at a volume of 2.0 mL as previously calculated. When tubing was changed, the expected internal volume of the tubing was calculated as follows:

$$V = \pi r^2 l$$

Exp. Eqn 1 calculation for the volume (V) of a cylinder where r is the cylinder cross-sectional radius and l is the length of the cylinder. For the reactor tubing, r corresponds to the internal tubing radius.

The tubing used for the reactor coil can be treated as a cylinder, following **Exp. Eqn 1**, above. Here, this equation was used to calculate the volume *per cm* of tubing of a given specification *i.e.*, to calculate V where $l = 1$ cm. When this is known, the total internal volume of the tubing can be calculated by multiplying V (per cm) by the length of tubing used (in cm).



Exp. Fig 7 schematic diagram of tubing used for constructing the reactor, treated as cylinder, showing the cross-section (left) and how the cross-section relates to a piece of tubing of given length, l . Here, OD is the tubing outer diameter, ID is the inner diameter, WT is the wall thickness and r is the radius (half of the ID) used to calculate the volume of tubing.

To calculate the internal volume of the tubing, the radius (r) required is the internal radius *i.e.*, half of the ID of the tubing. In some instances, the OD for the tubing is given and not the ID . In this case, the WT must be known or measured (using electronic callipers) to calculate the ID , **Exp. Eqn 2** below shows this calculation.

$$ID = OD - (2 \times WT)$$

Exp. Eqn 2 calculation for determining the ID of a piece of tubing where the dimensions are not fully specified – this can be manipulated for determining any of the three parameters.

With all dimensions known or measured, the volume per cm of tubing can be calculated.

$$V \text{ (per cm)} = \pi r^2 \times 1 \text{ cm}$$

Exp. Eqn 3 an adaptation of **Exp. Eqn 1** to determine the volume of a 1 cm long piece of tubing *i.e.*, the volume per cm of tubing.

Then, from **Exp. Eqn 3**, the volume per cm can then simply be multiplied by the length of tubing (in cm) to be used to form a reactor coil to determine the internal volume of the tubing *i.e.*, the volume of material to be irradiated at any one time.

$$V \text{ (reactor coil internal)} = V \text{ (per cm)} \times l \text{ (length to be used in cm)}$$

Exp. Eqn 4 calculation for determining the internal volume of tubing from the volume per cm of tubing.

To be sure of the calculation, whenever new tubing was used, the previously noted process was conducted again *i.e.*, using a known flow rate and timing how long the reactor coil tubing would take to fill up and calculating the internal volume of the reactor tubing from this. In all cases, no discrepancy was noted between what was measured by this test and what was calculated from the specifications quoted by the manufacturers (Cole Parmer). The specifications of each piece of tubing used in this work as a reactor coil are given below.

Exp. Table 1 dimensions and specifications of tubing used as a reactor coil in this work containing the required information to calculate an internal volume of the reactor coil tubing.

Tubing	ID / " (mm)	OD / " (mm)	Wall Thickness / " (mm)	Length / cm	Vol. Per cm / mL	Total Vol / mL
1 (1/8 ")	0.111 (2.8)	1/8 (3.2)	0.007 (0.18)	81	0.062	5.0
2 (1/8 ")		As above		97	0.062	6.0
3 (1/32 ")	1/32 (0.79)	1/16 (1.59)	1/64 (0.40)	762	0.005	3.8
4 (1/32 ")*		As above		1524	0.005	7.6
5 (1/16 ")	1/16 (1.59)	1/8 (3.2)	1/32 (0.79)	762	0.020	15.2

*Tubing 4 consisted of 2 identical lengths of Tubing 3 joined together with an Omni-Fit connector and each coiled around the jacketed tube in the reactor system.

It should be noted that Tubing 1 in **Exp. Table 1** was never used for performing a reaction in the work described in this Thesis, it was simply used only for volume determination.

Exp.3 Light Sources

Exp.3.1 Variable Colour LED Block

This light source was used for some batch screening/optimisation reactions and involves a single LZ7-04M100 LED (supplier LED Engin), mounted on an in-house built fan-cooled block. This light source was

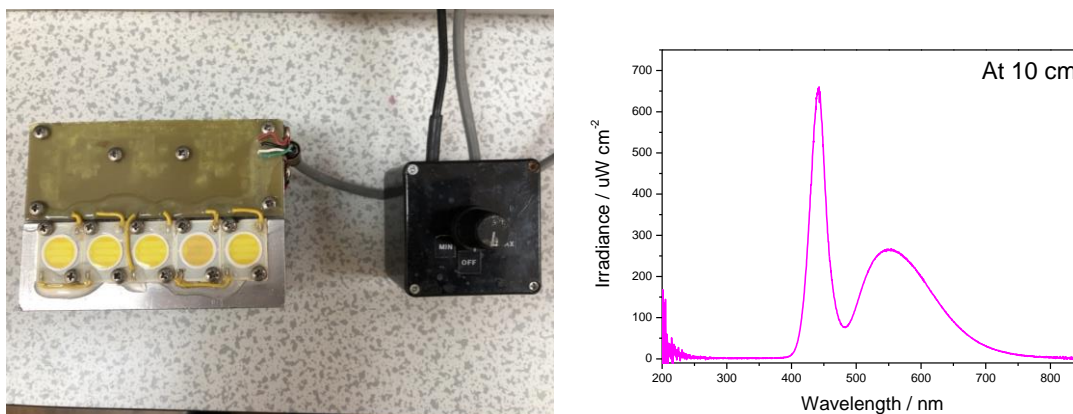
operated using an in-house built control box. The source contains 7 different coloured LEDs, specified as being red, green, blue, amber, cyan, violet and white (all other 6 colours at once), with the control box allowing for selecting between all 7 of the available colours. For the work performed here, only the “blue” LED was used. The manufacturers quote an emission maximum of 453 nm for this channel, at 700 mA current (which was not experimentally determined in this work). For the blue LED of this source, a maximum current rating of 1000 mA was reported by the manufacturers, and this was used as the operating current in all experiments performed here, set using the control box. At this operating current, the power output (as displayed on the control box) was 3.5-3.6 W, in every instance this source was used. The LED source mounted on the fan-cooled block and the control box are pictured, below.



Exp. Fig 8 multi-colour LED source mounted on a fan-cooled block (right), used for experiments with “blue” light irradiation and control box for operation (left).

Exp.3.2 White LED Block

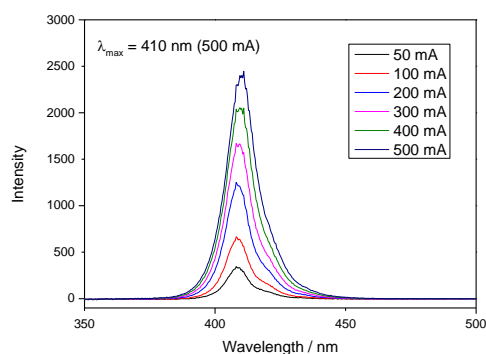
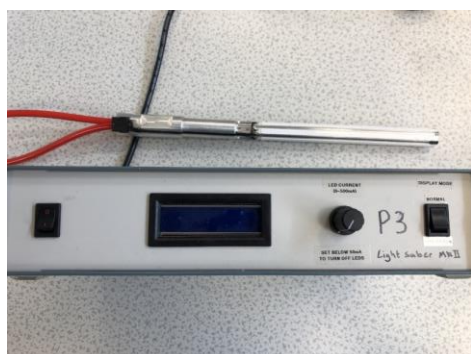
In other batch screening/optimisation reactions, a white LED source was used. The source here involved 5 x 12 W white Citizen LEDs, mounted on an in-house built fan cooled block. An in-house built control unit was also used for this, though this did not have an interface/display unlike the control box used for the variable colour LED source. The control unit for this white LED source was operated by turning on (by setting the control unit above minimum intensity) and adjusting the control unit up to maximum intensity. For all experiments, the control unit was set to maximum intensity to best replicated conditions between experiments. Emission spectra were measured previously (provided by D. S. Lee) and determined that the white source was comprised of one sharp emission band centred at 445 nm and one broad emission band centred at 557 nm with the irradiance measured to be (when operating at maximum intensity, from 10 cm distance) $656.39 \mu\text{Wcm}^{-2}$ (445 nm) and $259.69 \mu\text{Wcm}^{-2}$ (557 nm), again, measured previously with information provided by D. S. Lee. The white LED block and control unit are pictured, below.



Exp. Fig 9 white LED source (5 x 12 W) mounted on a fan-cooled block and control unit (left) and emission spectrum at maximum output power (right).

Exp.3.3 Lightsabre LEDs

The “Lightsabre” LED source involves 6 blue LED strips, mounted on a water-cooled hollow metal tube, with attachments for connecting water cooling and an electrical connection to the in-house built control box/power source. The LED manufacturer quote an emission wavelength of 425 nm, however, in this work, an emission maximum of ~410 nm was measured experimentally over the range of power (current) outputs available using the in-house built control box. The manufacturer also quote an output power of up to 20 W and operating voltage of 48 V. The in-house built control box operates using a driver supplied by Mean Well, operating within 48 V and 3.2 A, giving a maximum power output of 153.6 W (used to power not only the 6 LED strips but also the control box itself). The control box also involves a display/interface, which can be used to display the current being drawn across each of the 6 LED strips. The control box is used to turn on the LEDs by setting the current above 0 A, up to a maximum of 500 mA (per LED strip). For all the experiments performed, this was set to the maximum value of 500 mA (the set and actual current values were also displayed on the control box interface during operation). As such, it would be possible to estimate an LED power output, if the input voltage from the driver unit was to be known, however, for purposes here, the power output was assumed to be *less than* 144 W. This value is obtained by assuming (or determining from the interface) that, if each of the 6 LED strips draws 500 mA (0.5 A) current and is operating at the maximum voltage of 48 V, using $P = I_1V_1+I_2V_2...+I_6V_6$ (where $I_x = 0.5$ A and $V_x = 48$ V for all x , then 144 W would be obtained (where P is power, I is current, V is voltage). The Lightsabre LED source, control box and emission spectrum (obtained previously) are shown below.



Exp. Fig 10 Lightsabre LED source used in the continuous flow reactor in this work and control unit (left) and output emission spectrum.

Exp.4 TRIR Experimental Detail

Exp.4.1 General Detail

All spectroscopy samples were prepared in a Harrick cell “flow-pot” system, where the material could be constantly being pumped through the CaF₂ windows of the Harrick cell, allowing for avoiding degradation of the sample. 390 μm PTFE spacers between the windows were used in all cases here (determining the path length). All solutions were made up in CD₃CN solvent, purchased from either Fluorochem, or Merck. Mixtures were degassed (deoxygenated) *via* 3 freeze-pump-thaw cycles, using the Harrick cell flow system, with freezing *via* immersion in liquid N₂, pumping *via* high vacuum (<0.5 mbar) using a Schlenk line, then thawing to room temperature and purging with Ar. For TRIR experiments where the temperature was controlled, a temperature controllable Harrick cell (connected to a recirculating heater/chiller) was used, and the “flow-pot” system was also immersed in a heated/cooled bath, set to the desired temperature.

Exp.4.2 Detail of the Time-Resolved Infrared Spectroscopy Equipment

Note – all TRIR measurements were performed by trained laser operators Surajit Kayal and Xue-Zhong Sun. Experiments were planned and spectroscopy samples prepared by Toby Waldron Clarke and Rodolfo Teixeira. Detail given here has been reproduced (with permission) from a document belonging to Xue-Zhong Sun, with only minor stylistic modifications.

The TRIR system used is based on a pump-probe method. 800 nm laser pulses (100 fs) are generated with a commercial Ti:sapphire oscillator (MaiTai)/regenerative amplifier system (Spitfire Pro) (Spectra Physics, USA). The pulse energy is over 2 mJ at a repetition rate of 1 kHz. This 800 nm laser beam is divided into two parts with approximately equal energy. One part pumps either a TP-1 harmonic generator (TimePlate Tripler, Minioptic Technology, Inc) to generate UV pulses (400 nm, or 267 nm) or a TOPAS-C OPA (Light Conversion, Lithuania) to produce tunable UV-Vis-NIR pulses (300 nm - NIR) for pumping. Another part pumps the second TOPAS-C OPA with a DFG (Difference Frequency Generator) unit to produce tunable mid-IR pulses (2.5-10 μm) with duration of ~90 fs as a probe beam. The spectral bandwidth of the IR pulse is around 180 cm⁻¹, and the pulse energy is around 200 μJ at 2000 cm⁻¹. The pump and probe beams are synchronised and the time difference between them can be controlled with an optical delay line.

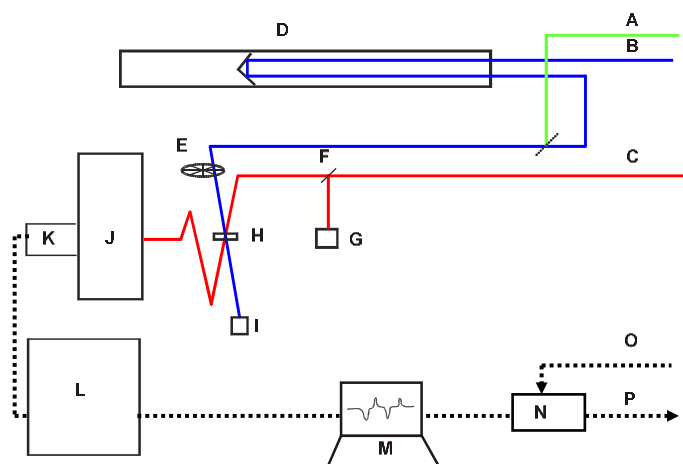
The optical arrangement of the TRIR system is shown below (**Exp. Fig 11**). The IR beam passes through a Ge beam splitter so half of the IR beam is reflected onto a single element MCT detector (Kolmar Technology) to serve as a reference and another half, passing through the Ge beam splitter is focused and overlaps with the pump beam at the sample position to probe the change introduced by the excitation. The UV-Vis pump pulse is optically delayed (up to 3 ns) by a 1 m translation stage (LMA Actuator, Aerotech, USA), and focused onto the sample with a quartz lens. The polarization of the pump pulse is set at the magic angle (54.7 °) relative to the probe pulse to recover the isotropic absorption spectrum. For a measurement with a longer time-delay, a Q-switched Nd:YVO laser (ACE-25QSPXHP/MOPA, Advanced Optical Technology, UK) is employed as a pump source which is synchronised to the Spitfire Pro amplifier. The delay between ns pump and fs probe pulses varies from 0.5 ns to 100 μs with a pulse generator (DG535, Stanford Research System).

The broadband transmitted IR probe beam is dispersed with a spectrograph and detected with a N₂(l)-cooled HgCdTe linear array detector (Infrared Associates, USA) which consists of 128 elements (1 mm high, 0.25 mm wide) with the typical peak detectivity, $D^* = 3 \times 10^{10} \text{ cm Hz}^{1/2} \text{ W}^{-1}$ at 1 kHz. The array detector is mounted in the focal plane of a 250 mm IR spectrograph (DK240, Spectra Product, USA). The spectral resolution at 2000 cm⁻¹ is about 4 cm⁻¹ with a 150 g/mm grating and 2 cm⁻¹ with a 300 gmm⁻¹ grating. The spectrograph is calibrated with the IR bands of the parent molecule or a standard polystyrene film in the spectral region investigated. The signals from the array detector elements and the single element detector are amplified with a 144-channel amplifier and digitized by 16-bit analogue-to-digital converters (IR-0144, Infrared Systems Development Corporation, USA). The optical chopper synchronized with the laser running at half the repetition frequency blocks one pulse (pump off) and passes one pulse (pump on) continuously.

The pulse energy of pump beam varies from 2 to 6 μJ while that of the IR probe beam is around 1 μJ. All beams are focused and spatially overlapped in the sample which is held in a Harrick cell with 2 mm thick CaF₂ windows separated by PTFE spacers (390 μm spacers were used in the work in this Thesis). The path length and concentrations of the samples are adjusted to give an optical density less than 0.7 in the spectral region for both pump and probe. At the focus, the pump beam size (~500 μm diameter) is larger than the probe spot (~200 μm diameter) to ensure spatially uniform photoexcitation across the spatial area of the probe pulse. The Harrick solution cell is mounted on a motorized cell mount, which moves the cell in x and y dimensions rapidly and continuously in a plane perpendicular to the beam direction, so laser pulses illuminate different portions of the sample each time and overheating and degrading induced by laser can be minimised.

The change in the IR absorbance ΔA is calculated from the ratio between the pump-on and pump-off transmittance. The signal of the single element detector is served as reference to normalize the shot to shot fluctuation. So ΔA is calculated with the following equation, where I is IR intensity:

$$\Delta A = -\log \left[\frac{I_{pump-on}^{array}}{I_{pump-off}^{array}} \times \left(\frac{I_{pump-off}^{single}}{I_{pump-on}^{single}} \right) \right]$$



Exp. Fig 11 schematic diagram of the optical layout of ps-Nottingham TRIR system. A: ns pump beam; B: ps pump beam; C: IR probe beam; D: optical delay line; E: Optical chopper; F: Germanium beam splitter; G: Single element MCT detector; H: Sample; I: Silicon detector; J: Spectrograph; K: 128-element MCT array detector; L: IR-144 multi-channel preamplifier and digitiser; M: Computer; N: Pulse generator; O: Trigger signal from ps-Laser; P: Trigger signal to ns Laser.

Exp.4.3 Data Processing, Analysis and Fitting

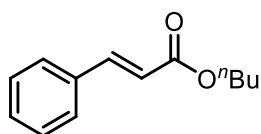
Laser experiments were conducted by Surajit Kayal or Xue-Zhong Sun using the set-up described in Exp.4.2. The raw spectral data was processed by Surajit Kayal using LabView and OriginPro. Further analyses were then conducted in some instances, using OriginPro, for example, single-point kinetic lifetimes were obtained by manually determining the maxima (or minima) of transients (or bleaches) and their decay (or growth) kinetics were fitted to (usually) a monoexponential, using OriginPro.

Exp.5 Characterisation/Isolation Data for Compounds Synthesised

Spectra are included in the Appendix.

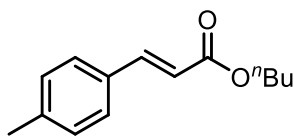
Exp.5.1 Chapter 2

Butyl Cinnamate (ButCin)



This product was formed from the Heck Reaction between iodobenzene with ⁿbutyl acrylate. From multiple reactions, the crude product mixtures were collected and combined. The solvent was then removed under reduced pressure, giving the crude product as a yellowish white powder. Following this, 2-3 spatulas of silica gel were added to the crude product, and the mixture dissolved in ~30 mL DCM. The solvent was again removed under reduced pressure, giving the crude product dry-loaded on to silica. This was then purified using automatic column chromatography, with cyclohexane:EtOAc as the eluent (gradient from 100% cyclohexane – 6:4 cyclohexane/EtOAc, over 15 min). The solvent was then removed from the fractions containing the product, affording the purified product, butyl cinnamate, as a clear, colourless oil. *R*_f 0.33; (¹H, 400 MHz, CDCl₃) 7.68 (d, 16 Hz, **1H**), 7.53 (m, **2H**), 7.39 (m, **3H**), 6.44 (d, 16 Hz, **1H**), 4.22 (t, 8 Hz, **2H**), 1.70 (m, **2H**), 1.44 (m, **2H**), 0.97 (t, 8 Hz, **3H**); (¹³C, 100 MHz, CDCl₃) 167.3 (COOR), 144.7 (sp² C), 134.6 (sp² C), 130.4 (sp² C), 129.0 (sp² C), 128.2 (sp² C), 118.5 (sp² C), 64.6 (CH₂COOR), 30.9 (CH₂CH₂COOR), 19.4 (sp³ C) 13.9 (sp³ C). Data consistent with previous reports.⁷⁶

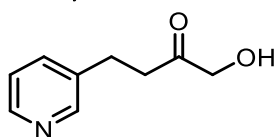
4-Methyl Butyl Cinnamate (MeButCin)



This product was formed from the Heck Reaction between 4-iodotoluene and *n*-butyl acrylate. From multiple reactions the crude product mixtures were collected and combined. The solvent was then removed under reduced pressure, giving the crude product as an orangey brown oil. To the crude product, 2-3 spatulas of silica gel was added, and the mixture then dissolved in ~30 mL DCM. The solvent was then removed under reduced pressure, giving the crude product dry loaded on to silica. This was then purified using automatic column chromatography, with cyclohexane:EtOAc as the eluent (gradient from 100% cyclohexane – 6:4 cyclohexane/EtOAc, over 15 min). The solvent was then removed from the fractions containing the product, affording the purified product, 4-methyl butyl cinnamate, as a clear, colourless oil. R_f 0.59; (^1H , 400 MHz, CD_3CN) 7.63 (d, 16 Hz, **1H**), 7.51 (d, 8 Hz, **2H**), 7.23 (d, 8 Hz, **2H**), 6.45 (d, 16 Hz, **1H**), 4.16 (t, 8 Hz, **2H**), 2.35 (s, **3H**), 1.65 (m, **2H**), 1.42 (m, **2H**), 0.95 (t, 8 Hz, **3H**); (^{13}C , 100 MHz, CDCl_3) 167.8 (COOR), 145.0 (sp^2 C), 141.1 (sp^2 C), 132.2 (sp^2 C), 130.1 (sp^2 C), 128.5 (sp^2 C), 117.7 (sp^2 C), 64.8 (CH_2COOR), 31.3 ($\text{CH}_2\text{CH}_2\text{COOR}$), 21.9 (sp^3 C), 19.7 (sp^3 C) 14.2 (sp^3 C). Data consistent with previous reports.⁷⁶

Exp.5.2 Chapter 3

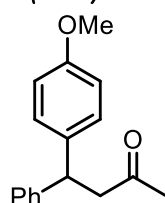
1-hydroxy-4-(3-pyridyl)butan-2-one (HPBO)



The product mixture of several reactions were combined, and the solvent removed under reduced pressure. Following this, the crude product, a brown oil, was dissolved in DCM (~20 mL) and silica gel was added to this until all the brown oil appeared to be adsorbed. The solvent was again removed under reduced pressure, affording the crude product dry loaded on to silica. Using automatic column chromatography, the mixture was then purified. Firstly, an eluent of 99:1 DCM:MeOH was used, followed by a second column using an eluent of 9:1 EtOAc:cyclohexane. The product was then collected, and the solvent removed under reduced pressure to afford the purified product as a pale yellow, clear oil. R_f 0.24 (99:1 DCM/MeOH); (^1H , 400 MHz, CDCl_3) 8.45 (m, **2H**), 7.51 (dt, 8 Hz, 4 Hz, **1H**), 7.21 (dd, 8 Hz, 5 Hz, **1H**), 4.21 (s, **2H**), 2.97 (t, 8 Hz, **2H**), 2.75 (t, 8 Hz, **2H**), (^{13}C , 100 MHz, CDCl_3) 208.3 (C=O), 149.9 (Ar CH), 148.0 (Ar CH), 136.1 (Ar C-C), 135.8 (Ar CH), 123.6 (Ar CH), 68.5 (CH_2), 39.5 (CH_2), 26.6 (CH_2); ν_{max} / cm^{-1} 3183 (OH), 2664 (CH), 1712 (C=O), 1577 (C=C, Ar), 1422 (CH bend), 1062 (OH); m/z 277.1 (100%, MH^+). Data consistent with previous reports.¹²⁴

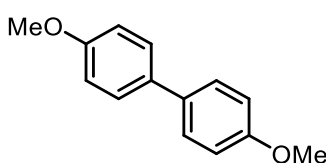
Exp.5.3 Chapter 4

4-(4-methoxyphenyl)-4-phenylbutan-2-one (RHP)



This product was formed from the Reductive Heck Reaction between 4-iodoanisole and 4-phenyl-3-buten-2-one. This was isolated from batch reactions for determination of isolated yields, and from combined crude product mixtures of multiple flow reactions. The crude product was diluted in diethyl ether and filtered through a ~1 cm silica plug and washed with further diethyl ether. Silica gel was then added to the filtrate and the solvent removed under reduced pressure. The dry loaded crude product was then purified using automatic column chromatography (95:5 pentane/EtOAc). Removal of the solvent under reduced pressure gave the title compound, as a straw coloured solid. (^1H , 400 MHz, CDCl_3) 7.33-7.17 (m, **7H**), 6.86 (d, 8.8 Hz, **2H**), 4.58 (t, 7.7 Hz, **1H**), 3.81 (s, **3H**), 3.19 (d, 7.5 Hz, **2H**), 2.12 (s, **3H**); (^{13}C , 100 MHz, CDCl_3) δ_{ppm} = 207.2, 158.2, 144.4, 136.1, 128.8, 128.7, 127.7, 126.5, 114.1, 55.4, 55.1, 45.4, 30.8. Data consistent with previous reports.¹⁴⁸

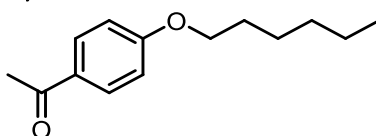
4,4'-dimethoxy-1,1'-biphenyl (HC)



This side-product was isolated as a separate fraction following the procedure outlined for 4-(4-methoxyphenyl)-4-phenylbutan-2-one (**RHP**), as a straw coloured solid. Yield not determined. (^1H , 400 MHz, CDCl_3) 7.48 (d, 8.7 Hz, **4H**), 6.96 (d, 8.7 Hz, **4H**), 3.84 (2, **6H**). Data consistent with previous reports.²⁶³

Exp.5.4 Chapter 5

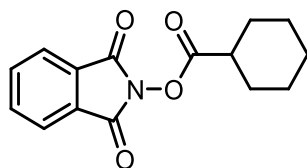
4-hexyloxy acetophenone (4-HOAP)



This product was that formed by the model reaction of 4-bromoacetophenone with 1-hexanol, as was studied in the original publication from MacMillan.¹⁷⁰ In some instances, **4-HOAP** was isolated and characterised as necessary to obtain an isolated yield. In other instances, **4-HOAP** was not isolated as GC was used for yield quantification. In such cases, the crude reaction mixtures of multiple experiments were combined and concentrated and purified product was obtained following the same purification procedure as for when isolating for yield determination. This procedure involved work-up and column chromatography, with specific details being given in the relevant Experimental Procedures. In general, crude mixtures were dissolved in EtOAc, washed with brine (this step was sometimes missed out) and concentrated on a rotary evaporator. Addition of a small amount of DCM and silica gel, followed by removal of solvent on a rotary evaporator afforded the crude product dry loaded on silica This would then be purified using automatic column chromatography (EtOAc with pentane or a hexane solvent) to afford the product as a yellow oil. Again, specific isolation details are given where necessary throughout the Experimental Chapter. (^1H , 400 MHz, CDCl_3) δ_{ppm} = 7.92 (d, 8.9 Hz, **2H**), 6.92 (d, 8.9 Hz, **2H**), 4.02 (t, 6.0 Hz, **2H**), 2.55 (s, **3H**), 1.84-1.76 (m, **2H**), 1.50-1.43 (m, **2H**), 1.36-1.233 (m, **4H**) 0.91 (t, 5.9 Hz, **3H**); (^{13}C , 100 MHz, CDCl_3) δ_{ppm} = 197.0, 163.3, 130.7, 130.3, 114.3, 68.4, 31.7, 29.2, 26.5, 25.8, 22.7, 14.2. Data consistent with previous reports.¹⁷⁰

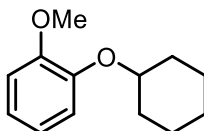
Exp.5.5 Chapter 6

1,3-dioxoisindolin-2-yl cyclohexanecarboxylate (NHPI-Ester)



Synthesis and isolation details are given in the Experimental Synthesis Procedures Section, below. (^1H , 400 MHz, CDCl_3) $\delta_{\text{ppm}} = 7.88$ (dd, 5.5 Hz, 3.1 Hz, **2H**), 7.78 (dd, 5.5 Hz, 3.1 Hz, **2H**), 2.73 (tt, 10.9 Hz, 3.6 Hz, **1H**), 2.11-2.08 (m, **2H**), 1.86-1.81 (m, **2H**), 1.67 (t, 10.2 Hz, **3H**), 1.42-1.29 (m, **3H**); (^{13}C , 100 MHz, CDCl_3) $\delta_{\text{ppm}} = 172.0, 162.2, 134.8, 129.2, 124.0, 40.6, 28.9, 25.8, 25.2$. Data consistent with previous reports.²⁶⁴

1-(cyclohexyloxy)-2-methoxybenzene, Cyclohexyl-Guaiacol Ether (CGE)



This product was formed from the model reaction between the cyclohexylcarboxylic acid NHPI-ester and guaiacol, as used by Xile Hu and co-workers.²¹⁸ Specific isolation details are given in the Experimental Procedures Section, and product was isolated either from batch reactions (for isolated yields) or, from the combined crude mixtures of multiple flow reactions. For isolation, the crude product mixture was diluted in EtOAc and washed with brine. The brine extractions were combined and washed with EtOAc. The organic extractions were then combined and dried over MgSO_4 before removing the solvent under reduced pressure. To the dried mixture, silica gel was added until the all the crude mixture appeared to be adsorbed and then DCM was added. The solvent was then again removed under reduced pressure to furnish the crude material dry loaded on silica This was then purified using automatic column chromatography with a Redisep R_f Gold column and an eluent of 95:5 pentane:EtOAc. Fractions were combined and the solvent removed to afford the desired product as a clear, colourless oil. (^1H , 400 MHz, CDCl_3) $\delta_{\text{ppm}} = 6.94$ -6.85 (m, **4H**), 4.18 (tt, 9.6 Hz, 3.8 Hz, **1H**), 3.85 (s, **3H**), 2.07-2.01 (m, **2H**), 1.86-1.79 (m, **2H**), 1.61-1.51 (m, **3H**), 1.42-1.19 (m, **3H**); (^{13}C , 100 MHz, CDCl_3) $\delta_{\text{ppm}} = 150.8, 147.4, 121.5, 120.9, 116.8, 112.4, 56.1, 32.3, 25.8, 24.3$. Data consistent with previous reports.²¹⁸

Exp.6 Experimental Synthesis Procedures

Exp.6.1 Chapter 2

Exp.6.1.1 Procedure for Reactions in the Vapourtec Reactor

Exp.6.1.1.1 Procedure for Reactions Between Iodobenzene and Butyl Acrylate (Table 2.4.2)

Iodobenzene (0.46 g, 2.3 mmol) was dissolved in 3 mL MeCN to give a clear solution. To this, 0.7 mL of butyl acrylate (4.7 mmol, 2 eq.) and 0.6 mL DIPEA (3.2 mmol, 1.4 eq.) was added. 1 mL of a catalyst stock MeCN solution was then added, with a concentration of catalyst such as to give a loading of 0.05 mol% (*w.r.t.* ArI, stock solution details given below), giving a pale yellow, clear solution of total volume ~5.5 mL (details tabulated below).

Reactions were then run following the procedure detailed in the Standard Operating Procedure. The reactor was flushed with MeCN at 5 mL min⁻¹ for at least 10 min. The flow was then set to 0.2 mL min⁻¹, required for a 10 min residence time in the 2 mL heated reactor. The system pressure was then set, using the manual BPR, to ≥ 6.3 bar. Once the pressure had stabilised, the reactor was heated to 140 °C.

After the conditions were stable, the prepared reaction solution was pumped through the reactor. An orange solution would be observed to form within the heated part of the reactor. When the reagent solution had been fully pumped into the system, the inlet to the pump was switched to neat MeCN. After ~30 min (corresponding to 6 mL total volume being pumped after beginning the reaction, inclusive of the neat MeCN inside the system prior to pumping through the reactant solution), triplicate samples of the crude product mixture were taken. From each, an aliquot of between 0.1-0.2 mL was taken (and the exact volume recorded). From each aliquot, the solvent was removed using a gentle N₂ stream. To the dried samples of crude product, 1,4-dinitrobenzene was added (≤ 15 mg), and the mass noted. The samples were then dissolved in CDCl₃ and submitted for ¹H NMR spectroscopic analysis for yield quantification.

Stock Solution Concentrations:

The molecular weights of the catalysts used were 224.5 gmol⁻¹ (Pd(OAc)₂), 673.70 gmol⁻¹ (Pd-170) and 858.90 gmol⁻¹ (2GXPhos). In these experiments, a loading of 0.05 mol% (*w.r.t.* ArI) was employed. 2.3 mmol of ArI was used in the experiments, therefore requiring 0.00115 mmol of catalyst. A stock solution of each catalyst was prepared, such that 1 mL of the stock solution could be added to the reagent mixture to give the desired loading. That is, to give a 0.00115 mol mL⁻¹ concentration of the catalyst. This value, in mg mL⁻¹, is given below for each catalyst used. Note that details of the catalysts used are detailed in the discussion section of this report.

Catalyst	Conc. / mg mL ⁻¹
Pd(OAc) ₂	0.26
Pd-170	0.77
2GXPhos	0.99

Catalyst	¹ H NMR Yield / %
Pd(OAc) ₂	81
Pd-170	82
2GXPhos	80

Exp.6.1.1.2 Procedure for Reactions Between 4-iodotoluene and Butyl Acrylate (Tables 2.4.1–2.4.6) Reactions in Table 2.4.1 using 0.1 mol% Pd(OAc)₂:

4-Iodotoluene (1.008 g, 4.6 mmol) was dissolved in 7 mL MeCN. To this, 1.2 mL diisopropyl ethylamine (DIPEA, 0.89 g, 6.9 mmol, 1.5 eq.) was added, along with 1.3 mL butyl acrylate (9mmol, 2 eq.). To this was added 1 mL of a 1 mg mL⁻¹ stock solution of Pd(OAc)₂ in MeCN was added (1 mg, 0.0045 mmol, 0.1 mol% loading *w.r.t.* ArI), giving a pale yellow, clear solution. This was then sparged under a balloon pressure of N₂.

Reaction was then run by following the Standard Operating Procedure for the Vapourtec reactor. The system was flushed with MeCN under a balloon pressure of N₂ for 5 min at 5 mL min⁻¹. Then, the flow

rate was set to 0.2 mL min⁻¹ (to give a 10 min residence time in the 2 mL heated reactor), before setting the backpressure using the manual BPR to >6.3 bar. Once the pressure had stabilised, the temperature was set to 140 °C and the conditions allowed to equilibrate. Once the conditions were stable, the flow was swapped from neat MeCN to the reagent solution. For this reaction, fluid was pumped for 2 h and the entire volume collected in this time, with the pump inlet being switched to neat MeCN after the flask of reagent solution ran dry. The solution turned orange in the heated reactor, and small amounts of black precipitate were observed, but no issue involving blockage occurred.

After collection of all the material, the solvent was removed using a rotary evaporator. The crude product was then dissolved in dichloromethane (DCM) and a small amount of silica gel added, before the solvent was again removed using a rotary evaporator. Following this, the crude mixture was purified using column chromatography (silica, 95:5 cyclohexane:EtOAc). The product was collected, and the solvent removed using a rotary evaporator, affording 4-methyl butyl cinnamate as a clear, colourless oil (0.57 g, 2.6 mmol, 57%).

Reactions in Table 2.4.1 using 0.05 mol% Pd(OAc)₂:

The procedure was repeated as above, except with different amounts of starting materials. In this reaction 0.503 g 4-iodotoluene was used (2.3 mmol), 0.6 mL DIPEA (3.5 mmol, 1.5 eq.), 0.65 mL butyl acrylate (4.5 mmol, 2 eq.). These materials were dissolved in 3 mL MeCN, and the addition of 1 mL of 0.26 mg mL⁻¹ Pd(OAc)₂ in MeCN stock solution was added (0.26 mg, 0.00115 mmol, 0.05 mol% loading). Procedure for the reaction was repeated, collecting all reaction mixture for 1.5 hr. Following the same purification procedure, 0.35 g of product was isolated (1.6 mmol, 69%).

Reactions in Table 2.4.2 Entries 4-6:

4-iodotoluene (0.5 g, 2.3 mmol) was dissolved in 3 mL MeCN to give a clear solution. To this, 0.7 mL of butyl acrylate (4.7 mmol, 2 eq.) and 0.6 mL DIPEA (3.2 mmol, 1.4 eq.) was added. 1 mL of a catalyst stock solution in MeCN was then added, with a concentration of catalyst such as to give a loading of 0.05 mol% (*w.r.t.* ArI, stock solution details given below), giving a pale yellow, clear solution of total volume ~5.5 mL (details tabulated below).

Reactions were then run following the procedure detailed in the Standard Operating Procedure. The reactor was flushed with MeCN at 5 mL min⁻¹ for at least 10 min. The flow was then set to 0.2 mL min⁻¹, required for a 10 min residence time in the 2 mL heated reactor. The system pressure was then set, using the manual BPR, to ≥6.3 bar. Once the pressure had stabilised, the reactor was heated to 140 °C and allowed to equilibrate.

After the conditions were stable, the prepared reaction solution was pumped through the reactor. An orange solution would be observed to form within the heated part of the reactor. When the reagent solution had been fully pumped into the system, the inlet to the pump was switched to neat MeCN. After ~30 min (corresponding to 6 mL total volume being pumped after beginning the reaction, inclusive of the pure solvent filling the Vapourtec system prior to the reaction mixture entering the system), triplicate samples of the crude product mixture were taken. From each, an aliquot of between 0.1-0.2 mL was taken (and the exact volume recorded). From each aliquot, the solvent was removed using a gentle N₂ stream. To the dried samples of crude product, 1,4-dinitrobenzene was added (≤15 mg), and

the mass noted. The samples were then dissolved in CDCl₃ and submitted for ¹H NMR analysis for yield quantification.

Mass 4-Iodotoluene / g	Moles 4-Iodotoluene / mmol	Total Vol. / mL	Conc. / M	Catalyst	¹ H NMR Yield / %
0.4920	2.3	5.6	0.41	Pd(OAc) ₂	74
0.5044	2.3	5.6	0.41	Pd-170	91
0.4973	2.3	5.6	0.41	2GXPhos	89

Catalyst	Conc. / mg mL ⁻¹
Pd(OAc) ₂	0.26
Pd-170	0.77
2GXPhos	0.99

Reactions in Table 2.4.3:

4-Iodotoluene (0.5 g, 2.3 mmol) was dissolved in 3 mL MeCN, to give a clear, colourless solution. To this, was added 0.7 mL of butyl acrylate (4.7 mmol, 2 eq.) and 0.6 mL DIPEA (3.2 mmol, 1.4 eq.). 1 mL of a 0.26 mg mL⁻¹ stock solution of Pd(OAc)₂ in MeCN was then added (0.26 mg Pd(OAc)₂, 0.0012 mmol, 0.05 mol% loading). This gave a pale yellow, clear solution of volume 5.6 mL, which was sparged with N₂ under a balloon pressure.

Reactions were then run according to the Vapourtec Standard Operating Procedure. The reactor system was flushed with neat MeCN, under balloon pressure of N₂, at 5 mL min⁻¹ for at least 5 min. The flow rate was then set to 0.2 mL min⁻¹. The temperature was then set to the desired value (see details in table below) and the manual BPR was adjusted to maintain the minimum pressure required to prevent solvent boiling (see details in table below).

After conditions had equilibrated, the flow was swapped from neat MeCN, to the reagent solution. A pale orange solution would form in the heated part of the reactor. After 30 min (the time required to pump 6 mL of fluid at this flow rate), triplicate samples were taken of the crude reaction product mixture. An aliquot of between 0.2-0.4 mL of each sample was then taken and the volume recorded. From these aliquots, the solvent was removed under a gentle N₂ stream. Following this, around 10 mg 1,4-dinitrobenzene was added to each of the dried aliquots (and the exact mass of 1,4-dinitrobenzene noted). This was then dissolved in CDCl₃ and submitted for ¹H NMR spectroscopic analysis, for yield quantification.

Mass 4-Iodotoluene / g	Moles 4-Iodotoluene / mmol	Total Vol. / mL	Conc. / M	Time / min	Temp. / °C	Backpressure / bar	¹ H NMR Yield / %
0.4920	2.3	5.6	0.41	10	140	>6.3	74
0.5012	2.3	5.6	0.41	10	110	>2.7	16
0.5049	2.3	5.6	0.41	10	80	1	4

Reactions in Table 2.4.4:

4-Iodotoluene (0.5 g, 2.3 mmol) was dissolved in 3 mL MeCN, to give a clear, colourless solution. To this, was added 0.7 mL of butyl acrylate (4.7 mmol, 2 eq.) and 0.6 mL DIPEA (3.2 mmol, 1.4 eq.). 1 mL of a 0.26 mg mL⁻¹ stock solution of Pd(OAc)₂ in MeCN was then added (0.26 mg Pd(OAc)₂, 0.0012 mmol, 0.05 mol% loading). This gave a pale yellow, clear solution of volume between 5.4-5.6 mL (indicated in table below), which was sparged with N₂ under a balloon pressure.

Reactions were then run according to the Vapourtec Standard Operating Procedure. The reactor system was flushed with neat MeCN, under balloon pressure of N₂, at 5 mL min⁻¹ for at least 5 min. The flow rate was then set to the value required for the desired reactor residence time, see the table below. The temperature was then set to 140 °C and the manual BPR was adjusted to maintain a backpressure ≥ 6.3 bar to prevent MeCN boiling.

After conditions had equilibrated, the flow was swapped from neat MeCN, to the reagent solution. A pale orange solution would form in the heated part of the reactor. After the time required to pump 6 mL of fluid had passed, triplicate samples were taken of the crude reaction product mixture. An aliquot of between 0.1-0.3 mL of each sample was then taken and the volume recorded. From these aliquots, the solvent was removed under a gentle N₂ stream. Following this, around 10 mg 1,4-dinitrobenzene was added to each of the dried aliquots and the mass noted. This was then dissolved in CDCl₃ and submitted for ¹H NMR spectroscopic analysis, for yield quantification.

Mass 4-iodotoluene / g	Moles 4-iodotoluene / mmol	Total Vol. / mL	Conc. / M	Time / min	Flow Rate / mL min ⁻¹	Time to Sample / min	Temp. / °C	¹ H NMR Yield / %
0.5079	2.3	5.6	0.41	2	1	6	140	37
0.4990	2.3	5.6	0.41	5	0.4	15	140	54
0.5031	2.3	5.4	0.43	10	0.2	30	140	80
0.4999	2.3	5.6	0.41	15	0.13	46	140	83

Reactions in Table 2.4.5:

4-Iodotoluene (0.5 g, 2.3 mmol) was dissolved in 3 mL MeCN*, to give a clear, colourless solution. To this, was added 0.7 mL of butyl acrylate (4.7 mmol, 2 eq.) and 0.6 mL DIPEA (3.2 mmol, 1.4 eq.). 1 mL* of a 0.26 mg mL⁻¹ stock solution of Pd(OAc)₂ in MeCN was then added (0.26 mg Pd(OAc)₂, 0.0012 mmol, 0.05 mol% loading). Where indicated in the table below, tetrabutyl ammonium chloride was also then added to the solution (0.064 g, 0.23 mmol, 0.1 eq. *w.r.t.* 4-iodotoluene). This gave a pale yellow, clear solution of volume between 5.4 - 5.8 mL (indicated in table below), which was sparged with N₂ under a balloon pressure.

*Where a 0.1 mol% loading was used, 4-iodotoluene was dissolved in 2 mL MeCN, and 2 mL of 0.26 mg mL⁻¹ Pd(OAc)₂ in MeCN was added.

Reactions were then run according to the Vapourtec Standard Operating Procedure. The reactor system was flushed with neat MeCN, under balloon pressure of N₂, at 5 mL min⁻¹ for at least 5 min. The flow rate was then set to 0.2 mL min⁻¹, required for a 10 min residence time in the heated reactor. The

temperature was then set to 140 °C and the manual BPR was adjusted to maintain a backpressure ≥ 6.3 bar to prevent MeCN boiling.

After conditions had equilibrated, the flow was swapped from neat MeCN, to the reagent solution. A pale orange solution would form in the heated part of the reactor. After the time required to pump 6 mL of fluid had passed, triplicate samples were taken of the crude reaction product mixture. An aliquot of between 0.1-0.2 mL of each sample was then taken and the volume recorded. From these aliquots, the solvent was removed under a gentle N₂ stream. Following this, around 10 mg 1,4-dinitrobenzene was added to each of the dried aliquots (and the exact mass of 1,4-dinitrobenzene added noted). This was then dissolved in CDCl₃ and submitted for ¹H NMR spectroscopic analysis, for yield quantification.

Mass 4-Iodotoluene / g	Moles 4-Iodotoluene / mmol	Mass TBAC / mg	Total Vol. / mL	Conc. / M	Loading / mol%	Time / min	Temp. / °C	¹ H NMR Yield / %
0.5025	2.3	65	5.8	0.40	0.1	10	140	94
0.5027	2.3	64	5.6	0.41	0.05	10	140	10
0.4983	2.3	64	5.6	0.41	0.05	10	140	10
0.4920	2.3	0	5.6	0.41	0.05	10	140	74
0.5031	2.3	0	5.4	0.43	0.05	10	140	80
0.5035	2.3	0	5.6	0.41	0.05	10	140	71

Exp.6.1.2 Procedure for Reactions in the Custom-Built Flow Reactor

Exp.6.1.2.1 Procedure for Reactions in Table 2.4.7

n-butyl acrylate (0.44 g, 3.4 mmol) was dissolved in 3 mL MeCN, giving a clear, colourless solution. To this solution, iodobenzene (0.47 g, 2.3 mmol) was added, followed by diisopropyl ethylamine (0.6 mL, 0.45 g, 3.4 mmol), with the solution remaining clear and colourless. To this, 1.0 mL of a Pd(OAc)₂ in MeCN stock solution was added, as detailed in the table below, to give the desired catalyst loading for each reaction performed. This resulted in a clear, colourless solution, which was sparged with N₂ under a balloon pressure.

Pd(OAc) ₂ Loading / %	Concentration of Pd(OAc) ₂ in MeCN Stock / mg mL ⁻¹
0.05	0.26
0.01	0.05
0.005	0.026

Reactions were then run according to the Standard Operating Procedure for the High Temperature Flow Reactor. The reactor was flushed with the reaction solvent (MeCN), under a balloon pressure of N₂, at around 5 mL min⁻¹ for at least 5 min. The flow was then set to 0.6 mL min⁻¹, required for a 5 min planned residence time. The backpressure regulator was set to 40 bar. After stabilisation of the system pressure, the heated reactor temperature was set to the 200 °C and allowed to heat up.

After equilibration of the system conditions, using the three-way valve in the system (see reactor details in Exp.2.1), the flow was switched from pumping neat MeCN, to the previously prepared reagent

solution. After a yellowish orange colour was observed in the reactor outlet stream, indicating the reaction mixture was flowing out of the system, ~1.5 mL of reaction mixture was collected and discarded. Following this, 3 samples of volume approximately 0.5 mL were taken. From each of the triplicate samples, a 0.1 mL aliquot was taken. Each aliquot was then diluted in MeOH (1 mL), to prepare the sample for yield analysis *via* GC.

Intended Pd(OAc) ₂ Loading / %	GC Yield / %
0.05	100
0.01	95
0.005	93

Exp.6.1.2.2 Procedure for Reactions in Table 2.4.8

n-butyl acrylate (0.44 g, 3.4 mmol) was dissolved in 4 mL MeCN, giving a clear, colourless solution. To this solution, iodobenzene (0.47 g, 2.3 mmol) was added, followed by diisopropyl ethylamine (0.6 mL, 0.45 g, 3.4 mmol), with the solution remaining clear and colourless. This resulted in a clear, colourless solution, which was sparged with N₂ under a balloon pressure.

Reactions were then run according to the Standard Operating Procedure for the High Temperature Flow Reactor. The reactor was flushed with the reaction solvent (MeCN), under a balloon pressure of N₂, at around 5 mL min⁻¹ for at least 5 min. The flow was then set to 0.6 mL min⁻¹, required for a 5 min planned residence time. The backpressure regulator was set to the required value to prevent solvent boiling at the intended temperature. After stabilisation of the system pressure, the heated reactor temperature was set to the desired temperature, and allowed to heat up, see below for temperature and pressure details.

After equilibration of the system conditions, using the three-way valve in the system (see reactor details in Exp.2.1), the flow was switched from pumping neat MeCN, to the previously prepared reagent solution. A timer was started and the time for approximately 1.5 reactor system volumes to pump through was allowed to pass. Then, 3 samples of volume approximately 0.5 mL were taken. From each of the triplicate samples, a 0.1 mL aliquot was taken. Each aliquot was then diluted in MeOH (1 mL), to prepare the sample for yield analysis *via* GC. This procedure was repeated for reactions at different temperatures before and after cleaning of the reactor with the procedure for this found in the S.O.P in the Appendix.

Temp. / °C	Backpressure / bar
200	40
250	70

Exp.6.1.2.3 Procedure for Reactions in Table 2.4.9 and Table 2.4.10/Fig 2.4.4

n-butyl acrylate (0.44 g, 3.4 mmol) was dissolved in 3 mL MeCN, giving a clear, colourless solution. To this solution, iodobenzene (0.47 g, 2.3 mmol) was added, followed by diisopropyl ethylamine (0.6 mL, 0.45 g, 3.4 mmol), with the solution remaining clear and colourless. To this, 1.0 mL of a Pd(OAc)₂ in

MeCN stock solution was added, as detailed in the table below, to give the desired catalyst loading. This resulted in a clear, colourless solution, which was sparged with N₂ under a balloon pressure.

Pd(OAc) ₂ Loading / %	Concentration of Pd(OAc) ₂ in MeCN Stock / mg mL ⁻¹
0.05	0.26
0.005	0.026
0.001	0.005
0.0005	0.005*

*0.5 mL of the stock solution was added, and 3.5 mL of MeCN was used to dissolve the reagents.

Reactions were run according to the Standard Operating Procedure for the High Temperature Flow Reactor. The reactor was flushed with the reaction solvent (MeCN), under a balloon pressure of N₂, at around 5 mL min⁻¹ for at least 5 min. The flow was then set to 0.6 mL min⁻¹, required for a 5 min planned residence time (or 0.3 mL min⁻¹ for a 10 min planned residence time). The backpressure regulator was set to the value required to prevent solvent vaporisation at the temperature to be used. After stabilisation of the system pressure, the heated reactor temperature was set to the desired value and allowed to heat up. See the table below regarding backpressures and temperatures set.

Temp. / °C	Backpressure / bar
150	20
200	40
225	50
250	70
270	100

After equilibration of the system conditions, using the three-way valve in the system (see reactor details in Exp.2.1), the flow was switched from pumping neat MeCN, to the previously prepared reagent solution. After a yellowish orange colour was observed in the reactor outlet stream, indicating the reaction mixture was flowing out of the system, ~1.5 mL of reaction mixture was collected and discarded. Following this, 3 samples of volume approximately 0.5 mL were taken. From each of the triplicate samples, a 0.1 mL aliquot was taken. Each aliquot was then diluted in MeOH (1 mL), to prepare the sample for yield analysis *via* GC.

Temp. / °C	Loading / %	GC Yield / %
150	0.0005	4
	0.001	Not Detected
	0.005	5
175	0.0005	7
	0.001	4
	0.005	39
200	0.005	68
	0.001	17
	0.0005	14
225	0.005	94
	0.001	42
	0.0005	26
250	0.001	76
	0.0005	53
250 (10 min)	0.001	87
	0.005	86
270	0.001	83
	0.0005	67
150 (10 min)	0.05	89

Exp.6.1.2.4 Procedure for Reactions in Fig 2.4.5

n-butyl acrylate (0.44 g, 3.4 mmol) was dissolved in 3 mL MeCN, giving a clear, colourless solution. To this solution, iodobenzene (0.47 g, 2.3 mmol) was added, followed by diisopropyl ethylamine (0.6 mL, 0.45 g, 3.4 mmol), with the solution remaining clear and colourless. To this, 1.0 mL of a Pd catalyst in MeCN stock solution was added, as detailed in the table below, to give a 0.0005 mol% (5 ppm) loading. This resulted in a clear, colourless solution, which was sparged with N₂ under a balloon pressure.

Catalyst	Molecular Weight / g mol ⁻¹	Stock Solution Conc. / mg mL ⁻¹
Pd-170	673.7	0.0077
2GXPhos	858.9 (THF adduct)	0.0099

Reactions were run according to the Standard Operating Procedure for the High Temperature Flow Reactor. The reactor was flushed with the reaction solvent (MeCN), under a balloon pressure of N₂, at around 5 mL min⁻¹ for at least 5 min. The flow was then set to 0.6 mL min⁻¹, required for a 5 min planned residence time. The backpressure regulator was set to the value required to prevent solvent vaporisation at the temperature to be used. After stabilisation of the system pressure, the heated reactor temperature was set to the desired value and allowed to heat up. See the table below regarding backpressures and temperatures set.

Temp. / °C	Backpressure / bar
150	20
175	30
200	40
225	50
250	70
270	100

After equilibration of the system conditions, using the three-way valve in the system (see reactor details in Exp.2.1), the flow was switched from pumping neat MeCN, to the previously prepared reagent solution. After a yellowish orange colour was observed in the reactor outlet stream, indicating the reaction mixture was flowing out of the system, ~1.5 mL of reaction mixture was collected and discarded. Following this, 3 samples of volume approximately 0.5 mL were taken. From each of the triplicate samples, a 0.1 mL aliquot was taken. Each aliquot was then diluted in MeOH (1 mL), to prepare the sample for yield analysis *via* GC.

Catalyst	Temp. / °C	GC Yield / %
Pd-170	150	4
	175	6
	200	14
	225	28
	250	42
	270	56
2GXPhos	150	4
	175	8
	200	17
	225	28
	250	43
	270	64

Exp.6.1.2.5 Procedure for Reactions in Fig 2.4.7

n-butyl acrylate (0.44 g, 3.4 mmol) was dissolved in 3 mL MeCN, giving a clear, colourless solution. To this solution, iodobenzene (0.47 g, 2.3 mmol) was added, followed by diisopropyl ethylamine (0.6 mL, 0.45 g, 3.4 mmol), with the solution remaining clear and colourless. To this, 1.0 mL of a Pd catalyst in MeCN stock solution was added, as detailed in the table below, to give a 0.0005 mol% (5 ppm) loading. This resulted in a clear, colourless solution, which was sparged with N₂ under a balloon pressure.

Catalyst	Molecular Weight / gmol ⁻¹	Stock Solution Conc. / mg mL ⁻¹
Pd-168	512.4	0.0059
Pd-134	755.95	0.0087
Pd-177	761.6	0.0088
Pd-179	888.7	0.0102
3GXantPhos	948.35	0.0109

Reactions were the run according to the Standard Operating Procedure for the High Temperature Flow Reactor. The reactor was flushed with the reaction solvent (MeCN), under a balloon pressure of N₂, at around 5 mL min⁻¹ for at least 5 min. The flow was then set to 0.6 mL min⁻¹, required for a 5 min planned residence time. The backpressure regulator was set to the value required to prevent solvent vaporisation at the temperature to be used. After stabilisation of the system pressure, the heated reactor temperature was set to the desired value and allowed to heat up. See the table below regarding backpressures and temperatures set.

Temp. / °C	Backpressure / bar
150	20
200	40
250	70

After equilibration of the system conditions, using the three-way valve in the system (see reactor details in Exp.2.1), the flow was switched from pumping neat MeCN, to the previously prepared reagent solution. After a yellowish orange colour was observed in the reactor outlet stream, indicating the reaction mixture was flowing out of the system, ~1.5 mL of reaction mixture was collected and discarded. Following this, 3 samples of volume approximately 0.5 mL were taken. From each of the triplicate samples, a 0.1 mL aliquot was taken. Each aliquot was then diluted in MeOH (1 mL), to prepare the sample for yield analysis *via* GC.

Catalyst	Temp. / °C	GC Yield / %
Pd-168	150	5
	200	18
	250	51
Pd-134	150	4
	200	9
	250	49
Pd-177	150	4
	200	16
	250	47
Pd-179	200	19
	250	47
3GXantPhos	150	4
	200	18
	250	33
Pd-114 ^a	200	5
Pd-213 ^a	200	12

^aResults not included in **Fig 7** as catalyst observed to be insoluble in reaction media so was not pursued further.

Exp.6.1.2.6 Procedure for Reactions in Fig 2.4.8

n-butyl acrylate (0.44 g, 3.4 mmol) was dissolved in 3.5 mL MeCN, giving a clear, colourless solution. To this solution, iodobenzene (0.47 g, 2.3 mmol) was added, followed by diisopropyl ethylamine (0.6 mL, 0.45 g, 3.4 mmol), with the solution remaining clear and colourless. To this, 0.5 mL of a 0.005 mg mL⁻¹ Pd(OAc)₂ in MeCN stock solution was added, to give a 0.0005 mol% (5 ppm) loading. This resulted in a clear, colourless solution, which was sparged with N₂ under a balloon pressure.

Reactions were then run according to the Standard Operating Procedure for the High Temperature Flow Reactor. The reactor was flushed with the reaction solvent (MeCN), under a balloon pressure of N₂, at around 5 mL min⁻¹ for at least 5 min. The flow was then set to the desired flow rate for the planned residence time (0.6 mL min⁻¹ for 5 min, 0.3 mL min⁻¹ for 10 min). The backpressure regulator was set to 130 bar required to prevent solvent vaporisation at 300 °C. After stabilisation of the system pressure, the heated reactor temperature was set to the 300 °C and allowed to heat up.

After equilibration of the system conditions, using the three-way valve in the system (see reactor details in Exp.2.1), the flow was switched from pumping neat MeCN, to the previously prepared reagent solution. After a yellowish orange colour was observed in the reactor outlet stream, indicating the reaction mixture was flowing out of the system, ~1.5 mL of reaction mixture was collected and discarded. Following this, 3 samples of volume approximately 0.5 mL were taken. From each of the triplicate samples, a 0.1 mL aliquot was taken. Each aliquot was then diluted in MeOH (1 mL), to prepare the sample for yield analysis *via* GC.

Residence Time / min	GC Yield / %
5	66
10	49*

*Not included in Fig 2.4.8 but is presented in Table 2.4.11.

Exp.6.1.2.7 Procedure for Reactions in Table 2.4.11 Entries 1 and 4-6

Results presented in Entries 2 and 3 are covered in the procedures above.

n-butyl acrylate (0.44 g, 3.4 mmol) was dissolved in 3.5 mL MeCN, giving a clear, colourless solution. To this solution, iodobenzene (0.47 g, 2.3 mmol) was added, followed by diisopropyl ethylamine (0.6 mL, 0.45 g, 3.4 mmol), with the solution remaining clear and colourless. To this, 0.5 mL of a 0.005 mg mL⁻¹ Pd(OAc)₂ in MeCN stock solution was added, to give a 0.0005 mol% (5 ppm) loading (or, 3.9 mL MeCN was used to dissolve the reagents, followed by addition of 0.1 mL of the Pd(OAc)₂ stock solution to give a 1 ppm loading). This resulted in a clear, colourless solution, which was sparged with N₂ under a balloon pressure.

Reactions were then run according to the Standard Operating Procedure for the High Temperature Flow Reactor. The reactor was flushed with the reaction solvent (MeCN), under a balloon pressure of N₂, at around 5 mL min⁻¹ for at least 5 min. The flow was then set to the desired flow rate for the planned residence time (3.0 mL min⁻¹ for 1 min, 0.6 mL min⁻¹ for 5 min, 0.3 mL min⁻¹ for 10 min). The backpressure regulator was set to 130 bar required to prevent solvent vaporisation at 300 °C. After stabilisation of the system pressure, the heated reactor temperature was set to the 300 °C and allowed to heat up.

After equilibration of the system conditions, using the three-way valve in the system (see reactor details in Exp.2.1), the flow was switched from pumping neat MeCN, to the previously prepared reagent solution. After a yellowish orange colour was observed in the reactor outlet stream, indicating the reaction mixture was flowing out of the system, ~1.5 mL of reaction mixture was collected and discarded. Following this, 3 samples of volume approximately 0.5 mL were taken. From each of the triplicate samples, a 0.1 mL aliquot was taken. Each aliquot was then diluted in MeOH (1 mL), to prepare the sample for yield analysis *via* GC.

Pd(OAc) ₂ Loading / ppm	Residence Time / min	GC Yield / %
5	1	23
5	5	66*
5	10	49*
1	1	13
1	5	27
1	10	35

*Experimental procedure also detailed in Exp.6.1.2.6, above.

Exp.6.1.2.8 Procedure for Reactions in Table 2.4.12 Entries 2-5

Results presented in Entries 1 are covered in the procedures above. *n*-butyl acrylate (0.44 g, 3.4 mmol) was dissolved in 3.0 mL of the relevant solvent, giving a clear, colourless solution. To this solution, iodobenzene (0.47 g, 2.3 mmol) was added, followed by diisopropyl ethylamine (0.6 mL, 0.45 g, 3.4 mmol), with the solution remaining clear and colourless. To this was added 1.0 mL of a 0.005 mg mL⁻¹ Pd(OAc)₂ stock solution to give a 10 ppm loading. This resulted in a clear, colourless solution, which was sparged with N₂ under a balloon pressure.

Reactions were then run according to the Standard Operating Procedure for the High Temperature Flow Reactor. The reactor was flushed with DMF, under a balloon pressure of N₂, at around 5 mL min⁻¹ for at least 5 min. The flow was then set to 0.6 mL min⁻¹ for the planned residence time of 5 min. The backpressure regulator was set to 70 bar required to prevent solvent vaporisation at 250 °C (this was the same backpressure used for the lower boiling MeCN used previously, as phase behaviour data was not readily available for all solvents). After stabilisation of the system pressure, the heated reactor temperature was set to 250 °C and allowed to heat up.

After equilibration of the system conditions, using the three-way valve in the system (see reactor details in Exp.2.1), the flow was switched from pumping neat DMF, to the previously prepared reagent solution. After a yellowish orange colour was observed in the reactor outlet stream, indicating the reaction mixture was flowing out of the system, ~1.5 mL of reaction mixture was collected and discarded. Following this, 3 samples of volume approximately 0.5 mL were taken. From each of the triplicate samples, a 0.1 mL aliquot was taken. Each aliquot was then diluted in MeOH (1 mL), to prepare the sample for yield analysis *via* GC.

Solvent	Pd(OAc) ₂ Loading / ppm	GC Yield / %
DMF	10	26
Cyrene	10	18
Propylene Carbonate	10	47
GVL	10	61

Exp.6.1.2.9 Procedure for Reactions in Table 2.4.13 Entries 3 and 4

Results presented in Entries 1 and 2 are covered in the procedures above. *n*-butyl acrylate (0.44 g, 3.4 mmol) was dissolved in 3.5 mL GVL, giving a clear, colourless solution. To this solution, iodobenzene (0.47 g, 2.3 mmol) was added, followed by diisopropyl ethylamine (0.6 mL, 0.45 g, 3.4 mmol), with the solution remaining clear and colourless. To this, 0.5 mL of a 0.005 mg mL⁻¹ Pd(OAc)₂ in GVL stock solution was added, to give a 0.0005 mol% (5 ppm) loading. This resulted in a clear, colourless solution, which was sparged with N₂ under a balloon pressure.

Reactions were then run according to the Standard Operating Procedure for the High Temperature Flow Reactor. The reactor was flushed with GVL, under a balloon pressure of N₂, at around 5 mL min⁻¹ for at least 5 min. The flow was then set to 0.6 mL min⁻¹ for the planned residence time of 5 min (or 3.0 mL min⁻¹ for 1 min residence time). The backpressure regulator was set to 130 bar required to prevent solvent vaporisation at 300 °C (this was the same backpressure used for the lower boiling MeCN used

previously, as phase behaviour data was not readily available for GVL). After stabilisation of the system pressure, the heated reactor temperature was set to 300 °C and allowed to heat up.

After equilibration of the system conditions, using the three-way valve in the system (see reactor details in Exp.2.1), the flow was switched from pumping neat GVL, to the previously prepared reagent solution. After a yellowish orange colour was observed in the reactor outlet stream, indicating the reaction mixture was flowing out of the system, ~1.5 mL of reaction mixture was collected and discarded. Following this, 3 samples of volume approximately 0.5 mL were taken. From each of the triplicate samples, a 0.1 mL aliquot was taken. Each aliquot was then diluted in MeOH (1 mL), to prepare the sample for yield analysis *via* GC.

Time / min	GC Yield / %
5	53
1	29

Exp.6.1.2.10 Procedure for Reactions in Table 2.4.14 Entries 2 and 4

Procedure for Entry 1 is covered by procedures above. *n*-butyl acrylate (0.44 g, 3.4 mmol) was dissolved in 3.5 mL GVL, giving a clear, colourless solution. To this solution, iodobenzene (0.47 g, 2.3 mmol) was added, followed by diisopropyl ethylamine (0.6 mL, 0.45 g, 3.4 mmol), with the solution remaining clear and colourless. To this, 0.5 mL of a 0.005 mg mL⁻¹ Pd(OAc)₂ in GVL stock solution was added, to give a 0.0005 mol% (5 ppm) loading. This resulted in a clear, colourless solution, which was sparged with N₂ under a balloon pressure.

Reactions were then run according to the Standard Operating Procedure for the High Temperature Flow Reactor. The reactor was flushed with GVL, under a balloon pressure of N₂, at around 5 mL min⁻¹ for at least 5 min. The flow was then set to 0.6 mL min⁻¹ for the planned residence time of 5 min (or 3.0 mL min⁻¹ for 1 min residence time). The backpressure regulator was set to the pressure required to prevent solvent vaporisation at the appropriate temperature. After stabilisation of the system pressure, the heated reactor temperature was set to the desired value and allowed to heat up.

Temperature / °C	Backpressure* / bar
300	130
325	130
350	130

**130 bar was used in all cases – this was the pressure required to prevent MeCN boiling at 300 °C and was observed to be suitable to prevent GVL boiling, without readily available phase behaviour data.*

After equilibration of the system conditions, using the three-way valve in the system (see reactor details in Exp.2.1), the flow was switched from pumping neat GVL, to the previously prepared reagent solution. After a yellowish orange colour was observed in the reactor outlet stream, indicating the reaction mixture was flowing out of the system, ~1.5 mL of reaction mixture was collected and discarded. Following this, 3 samples of volume approximately 0.5 mL were taken. From each of the triplicate

samples, a 0.1 mL aliquot was taken. Each aliquot was then diluted in MeOH (1 mL), to prepare the sample for yield analysis *via* GC.

Temperature / °C	GC Yield / %
300	26
325	28
350	25

Exp.6.2 Chapter 3

Exp.6.2.1 Procedure for Reactions in Table 3.4.1

1,2-Dihydroxy but-3-ene (0.60 g, 6.9 mmol) was dissolved in 6 mL MeCN, giving a cloudy solution. The solution was then agitated with a vortex mixer until appeared homogeneous, before filtering through a 0.4 μm PTFE syringe filter into 3-Iodopyridine (0.94 g, 4.6 mmol), giving a clear solution. To this, was added 1.1 mL diisopropyl ethylamine (0.82 g, 6.3 mmol), followed by 2 mL of a Pd(OAc)₂ in MeCN stock solution of concentration required to give desired catalyst loading (see table below). The resultant pale yellow, clear solution was then sparged with N₂ under balloon pressure.

Reactions were then run according to the Standard Operating Procedure for the High Temperature Flow Reactor. The reactor was flushed with the reaction solvent (MeCN), under a balloon pressure of N₂, at around 5 mL min⁻¹ for at least 5 min. The flow was then set to 0.3 mL min⁻¹ (required for a 10 min residence time) and the backpressure regulator was set to 40 bar. After stabilisation of the system pressure, the heated reactor temperature was set to 200 °C and allowed to heat up.

After equilibration of the system conditions, using the three-way valve in the system (see reactor details in Exp.2.1), the flow was switched from pumping neat MeCN, to the previously prepared reagent solution. After ~20 min after beginning pumping the reagents, a colour change in the reactions outlet would be seen, going from clear/colourless, to an orangey brown colour, indicating the reaction mixture was flowing out of the system. After ~25 min triplicate samples were taken, each for around 1 min (therefore discarding the first 1.5 mL of reaction mixture exiting the system – 0.3 mL min⁻¹ x 5 min = 1.5 mL, allowing to negate any dilution effects). From each of the triplicate samples, a 0.1 mL aliquot was taken. Each aliquot was then diluted in MeOH (1 mL), to prepare the sample for yield analysis *via* GC.

Loading / mol%	GC Yield / %
0.005	9
0.01	15
0.05	45
0.1	50
0.5	56

*Associated uncertainties listed in main body tables.

Desired Pd(OAc) ₂ Loading / mol%	Conc. Of Stock Solution / mg mL ⁻¹
0.005	0.026
0.01	0.052
0.05	0.26
0.1 ^a	0.52
0.5 ^a	*

*For this loading, a stock solution wasn't used – the 1,2-dihydroxy but-3-ene was dissolved in 8 mL MeCN, the rest of the procedure as above was followed, but 5 mg of Pd(OAc)₂ was added directly to the mixture, rather than using a stock solution.

^aTBAB (10 eq. *w.r.t.* Pd) was added when these loadings were applied, for 0.5 mol% loading, 74 mg TBAB was added, for 0.1 mol% loading, 15 mg TBAB was added.

Exp.6.2.2 Procedure for Reactions in Table 3.4.2 Entries 6-14

Entries 1-5 are covered by procedures above. 1,2-Dihydroxy but-3-ene (0.60 g, 6.9 mmol) was dissolved in 6 mL MeCN, giving a cloudy solution. The solution was then vortexed until appeared homogeneous, before filtering through a 0.4 μm PTFE syringe filter into 3-Iodopyridine (0.94 g, 4.6 mmol), giving a clear solution. To this, was added 1.1 mL diisopropyl ethylamine (0.82 g, 6.3 mmol), followed by 2 mL of a Pd catalyst in MeCN stock solution, of concentration required to give desired catalyst loading (see table below for details of catalyst stock solution). The resultant pale yellow, clear solution was then sparged with N₂ under balloon pressure.

Reactions were the run according to the Standard Operating Procedure for the High Temperature Flow Reactor. The reactor was flushed with the reaction solvent (MeCN), under a balloon pressure of N₂, at around 5 mL min⁻¹ for at least 5 min. The flow was then set to 0.3 mL min⁻¹ (required for a 10 min residence time) and the backpressure regulator was set to 40 bar. After stabilisation of the system pressure, the heated reactor temperature was set to 200 °C and allowed to heat up.

After equilibration of the system conditions, using the three-way valve in the system (see reactor details in Exp.2.1), the flow was switched from pumping neat MeCN, to the previously prepared reagent solution. After ~20 min after beginning pumping the reagents, a colour change in the reactions outlet would be seen, going from clear/colourless, to an orangey brown colour, indicating the reaction mixture was flowing out of the system. After ~25 min triplicate samples were taken, each for around 1 min (therefore discarding the first 1.5 mL of reaction mixture exiting the system – 0.3 mL min⁻¹ x 5 min = 1.5 mL, allowing to negate any dilution effects). From each of the triplicate samples, a 0.1 mL aliquot was taken. Each aliquot was then diluted in MeOH (1 mL), to prepare the sample for yield analysis *via* GC.

Catalyst	Loading / mol%	GC Yield / %
Pd-170	0.005	14
	0.05	48
	0.5	32
2GXPhos	0.005	6
	0.05	47
	0.5	45
PdCl ₂	0.005	7
	0.05	45
	0.5	64

Catalyst	Desired Loading / mol%	Conc. of Stock Solution / mg mL ⁻¹
Pd-170	0.005	0.08
	0.05	0.78
	0.5	*1
2GXPhos	0.005	0.10
	0.05	1.00
	0.5	*2
PdCl ₂	0.005	0.02
	0.05	0.21
	0.5	*3

¹ 16 mg of Pd-170 was added directly to the starting solution, with 8 mL of MeCN instead of 6 mL being used to dissolve the reagents.

² 20 mg of 2GXPhos was added directly to the starting solution, with 8 mL of MeCN instead of 6 mL being used to dissolve the reagents.

³ 4 mL of a 1 mg mL⁻¹ stock solution was used, with the reagents being dissolved in an initial 4 mL of MeCN. Also, 10 eq. TBAB (*w.r.t.* Pd), 74 mg, was added.

Exp.6.2.3 Procedure for Reactions in Fig 3.4.1 150, 175, 225 and 250 °C

The data point at 200 °C is covered in procedures above and is reiterated here. 1,2-Dihydroxy but-3-ene (0.60 g, 6.9 mmol) was dissolved in 7 mL MeCN, giving a cloudy solution. The solution was then vortexed until appeared homogeneous, before filtering through a 0.4 µm PTFE syringe filter into 3-Iodopyridine (0.94 g, 4.6 mmol), giving a clear solution. To this, was added 1.1 mL diisopropyl ethylamine (0.82 g, 6.3 mmol), followed by 1 mL of a 0.4 mg mL⁻¹ PdCl₂ in MeCN stock solution. The resultant pale yellow, clear solution was then sparged with N₂ under balloon pressure.

Reactions were the run according to the Standard Operating Procedure for the High Temperature Flow Reactor. The reactor was flushed with the reaction solvent (MeCN), under a balloon pressure of N₂, at around 5 mL min⁻¹ for at least 5 min. The flow was then set to 0.3 mL min⁻¹ (required for a 10 min residence time) and the backpressure regulator was set to the pressure required to prevent MeCN boiling at the temperature intended to be used. After stabilisation of the system pressure, the heated

reactor temperature was set to the desired temperature and allowed to heat up. See table below for details of pressures applied at each temperature.

Reaction Temperature / °C	Backpressure Applied / bar
150	20
175	25
200	40
225	50
250	70

After equilibration of the system conditions, using the three-way valve in the system (see reactor details in Exp.2.1), the flow was switched from pumping neat MeCN, to the previously prepared reagent solution. After ~20 min after beginning pumping the reagents, a colour change in the reactions outlet would be seen, going from clear/colourless, to an orangey brown colour, indicating the reaction mixture was flowing out of the system. After ~25 min triplicate samples were taken, each for around 1 min (therefore discarding the first 1.5 mL of reaction mixture exiting the system – $0.3 \text{ mL min}^{-1} \times 5 \text{ min} = 1.5 \text{ mL}$, allowing to negate any dilution effects). From each of the triplicate samples, a 0.1 mL aliquot was taken. Each aliquot was then diluted in MeOH (1 mL), to prepare the sample for yield analysis *via* GC.

Reaction Temperature / °C	GC Yield / %
150	15
175	29
200	45
225	50
250	29

Exp.6.2.4 Procedure for Reactions in Table 3.4.5 Entries 2-3

Procedure for Entry 1 is covered in procedures above and is reiterated here. 1,2-Dihydroxy but-3-ene (0.60 g, 6.9 mmol) was dissolved in 7 mL MeCN, giving a cloudy solution. The solution was then vortexed until appeared homogeneous, before filtering through a 0.4 μm PTFE syringe filter into 3-Iodopyridine (0.94 g, 4.6 mmol), giving a clear solution. To this, was added 1.1 mL diisopropyl ethylamine (0.82 g, 6.3 mmol), followed by 1 mL of a 0.4 mg mL^{-1} PdCl_2 in MeCN stock solution. The resultant pale yellow, clear solution was then sparged with N_2 under balloon pressure.

Reactions were the run according to the Standard Operating Procedure for the High Temperature Flow Reactor. The reactor was flushed with the reaction solvent (MeCN), under a balloon pressure of N_2 , at around 5 mL min^{-1} for at least 5 min. The flow was then set to the value required for the desired residence time, see table below. The backpressure regulator was set to 50 bar, after stabilisation of the system pressure, the heated reactor temperature was set to 225 °C and allowed to heat up.

Flow Rate / mL min ⁻¹	Residence Time / min
0.3	10
0.2	15
0.15	20

After equilibration of the system conditions, using the three-way valve in the system (see reactor details in Exp.2.1), the flow was switched from pumping neat MeCN, to the previously prepared reagent solution. After an orangey brown colour was observed in the reactor outlet stream, indicating the reaction mixture was flowing out of the system, ~1.5 mL of reaction mixture was collected and discarded. Following this, 3 samples of volume approximately 0.5 mL were taken. From each of the triplicate samples, a 0.1 mL aliquot was taken. Each aliquot was then diluted in MeOH (1 mL), to prepare the sample for yield analysis *via* GC.

Flow Rate / mL min ⁻¹	Residence Time / min	GC Yield / %
0.3	10	50
0.2	15	73
0.15	20	69

Exp.6.2.5 Procedure for Reactions in Table 3.4.7 Entries 2-5

Procedure for Entry 1 is covered in procedures above and is reiterated here. 1,2-Dihydroxy but-3-ene (0.30 g, 3.4 mmol) was dissolved in 3 mL MeCN, giving a cloudy solution. The solution was then vortexed until appeared homogeneous, before filtering through a 0.4 µm PTFE syringe filter into 3-Iodopyridine (0.47 g, 2.3 mmol), giving a clear solution. To this, was added 0.6 mL diisopropyl ethylamine (0.45 g, 3.4 mmol), followed by an amount of PdCl₂ in MeCN stock solution, required to give the desired catalyst loading. The resultant pale yellow, clear solution was then sparged with N₂ under balloon pressure.

Reactions were the run according to the Standard Operating Procedure for the High Temperature Flow Reactor. The reactor was flushed with the reaction solvent (MeCN), under a balloon pressure of N₂, at around 5 mL min⁻¹ for at least 5 min. The flow was then set to the value required for the desired residence time, see table below. The backpressure regulator was set to 50 bar, then, after stabilisation of the system pressure to the value set, the heated reactor temperature was set to 225 °C and allowed to heat up.

After equilibration of the system conditions, using the three-way valve in the system (see reactor details in Exp.2.1), the flow was switched from pumping neat MeCN, to the previously prepared reagent solution. After an orangey brown colour was observed in the reactor outlet stream, indicating the reaction mixture was flowing out of the system, ~1.5 mL of reaction mixture was collected and discarded. Following this, 3 samples of volume approximately 0.5 mL were taken. From each of the triplicate samples, a 0.1 mL aliquot was taken. Each aliquot was then diluted in MeOH (1 mL), to prepare the sample for yield analysis *via* GC.

PdCl ₂ Loading / mol%	Residence Time / min	Flow Rate / mL min ⁻¹	GC Yield / %
0.05	15	0.20	73
0.01	15	0.20	27
0.01	30	0.10	38
0.005	15	0.20	15
0.005	30	0.10	25

Exp.6.3 Chapter 4

Exp.6.3.1 General Experimental Procedure for Batch Reductive Heck Reactions

To a suitable glass vial, the required amount of 4-iodoanisole, *trans*-4-phenyl-3-buten-2-one and Pd(OAc)₂ (if required amount was readily measurable on an analytical balance) were added. To this a measured volume of a stock solution of Pd(OAc)₂ in NMP was added (if required amount was not readily measurable on an analytical balance). DIPEA was then added to give the required equivalents and the mixture then dissolved in the required amount of NMP. If needed, this was sonicated to dissolve all solid components, resulting in a transparent pale yellow, homogeneous solution.

A sample of the starting solution was then removed for GC analysis and the remaining reaction mixture was stoppered with a suba-seal and immersed in a preheated oil bath set to the required temperature. Reaction vessels were removed briefly from the oil bath at intervals required for sampling for GC analysis, before being replaced in the oil bath. After the required time had passed, the reaction vessels were removed from the oil bath, the heat turned off and then either analysed *via* GC or worked-up for purification.

Purification involved addition of diethyl ether, filtration of insoluble precipitates formed upon addition of diethyl ether before purification with automatic column chromatography (95:5 pentane/EtOAc).

Exp.6.3.2 General Experimental Procedure for Flow Reductive Heck Reactions

Flow reactions were conducted using the tubular thermal flow reactor (Exp.2.1.), in accordance with the Standard Operating Procedure (see Appendix).

To a round bottomed flask, the required amount of aryl halide, enone and Pd(OAc)₂ (if required amount was readily measurable on an analytical balance) were added. To this a measured volume of a stock solution of Pd(OAc)₂ in NMP was added (if required amount was not readily measurable on an analytical balance). DIPEA was then added to give the required equivalents and the mixture then dissolved in the required amount of NMP. If needed, this was sonicated to dissolve all solid components, resulting in a transparent pale yellow, homogeneous solution.

The reaction mixture(s) was then transferred to a measuring cylinder for volume determination, before removal of samples for GC analysis and then transferred back to the round bottom flask. The inlet to the pump on the reactor system was then immersed in the reaction solution on one side of the switchable three-way valve to the pump. According to the Standard Operating Procedure, the other inlet to the three-way valve was immersed in neat NMP (the reaction solvent used in all cases) and used to flush out the reactor, before setting the required conditions for the experiments to be conducted

(flow rate, then pressure, then temperature) – whilst ensuring all safety and leak checks were performed in the process. After equilibrating at the required conditions, the three-way valve was then switched to the reaction solution to begin processing the mixture. Samples to monitor the reaction progression by GC were removed after 15 mL sample (~3 system volumes) had been passed through the reactor. At which point, the next set of conditions were set for the next experiment, or the system was shut-down according to the Standard Operating Procedure. If more than one set of conditions were being performed, the previous procedure of allowing 15 mL solution to pass was repeated until finished. At which point, the system would then be shut-down according to the Standard Operating Procedure. In this work, no more than 3 reactions were performed without employing the cleaning/reconditioning procedure, where the system would be flushed with IPA or MeOH, then H₂O then with recirculating dilute aqueous HNO₃ overnight, before reconditioning with aqueous NaOH and returning to neutrality with H₂O.

Exp.6.3.3 Procedure for Reactions in Table 4.4.1 Entries 1 and 2

Result presented in Entry 3 was reproduced from the literature. To two separate Schlenk tubes, the required amount of 4-iodoanisole and *trans*-4-phenyl-3-buten-2-one (detailed below) were added. To this, 0.5 mL of a 2.4 mg mL⁻¹ stock solution of Pd(OAc)₂ in NMP was added (1.2 mg, 0.0053 mmol, 0.5 mol%). DIPEA (1.0 mL, 0.724 g, 5.6 mmol, 5 eq.) was then added and the mixture then dissolved in 1.0 mL NMP, giving a homogeneous, clear yellow solution. One of the Schlenk tubes (for degassed conditions) was then frozen in liquid N₂, put under a high vacuum (<0.3 mbar) on a Schlenk line, then allowed to thaw gradually to room temperature before being purged with Ar. This procedure was repeated a further two times. The other Schlenk tube (for non-degassed conditions) was not subjected to this procedure.

A sample of each starting solution was then removed for GC analysis before immersing each vessel in a preheated oil bath set to 80 °C (the degassed Schlenk tube was equipped with an Ar balloon for the duration of the reaction). Each vessel was quickly observed to turn a deep red colour. Reaction vessels were removed briefly from the oil bath at intervals required for sampling for GC analysis, before being replaced in the oil bath. After 17 h, the reaction vessels were removed from the oil bath and the heat turned off.

20 mL of diethyl ether was added to each tube and the contents of each were then filtered through a ~1 cm silica plug and washed with ~200 ml total diethyl ether in a number of separate washings. A few spatulas of silica gel were then added to the filtrate and then the solvent was removed from the filtrate under reduced pressure before purification with automatic column chromatography (95:5 pentane/EtOAc). Removal of solvent afforded the reductively coupled product as a yellow oil (yields detailed below).

Conditions	Amount Enone	Amount 4-Iodoanisole	Isolated Yield
Degassed	0.1628 g, 1.11 mmol	0.3079 g, 1.32 mmol, 1.2 eq.	0.1912 g, 0.75 mmol, 68%.
Not Degassed	0.1648 g, 1.13 mmol	0.3087 g, 1.32 mmol, 1.2 eq.	0.2121 g, 0.83 mmol, 73%

Exp.6.3.4 Procedure for Reactions in Table 4.4.2

To separate Schlenk tubes, 4-iodoanisole (0.309 g, 1.32 mmol, 1.2 eq.) and *trans*-4-phenyl-3-buten-2-one (0.161 g, 1.10 mmol) were added. To this, the required amount of a stock solution of Pd(OAc)₂ in NMP was added (amounts detailed below). DIPEA (amounts details below) was then added to the give the required equivalents and the mixture then dissolved in the required amount of NMP to take the total volume of NMP added to 1.5 mL (amounts detailed below), giving a homogeneous, clear yellow solution.

Desired Pd Loading / mol%	Pd Stock Added	NMP Added for Make Up to 1.5 mL / mL
0.5	1.2 mg mL ⁻¹ , 1.0 mL (1.2 mg, 0.0053 mmol, 0.5 mol%)	0.5
0.05	1.2 mg mL ⁻¹ , 0.1 mL (0.12 mg, 0.00053 mmol, 0.05 mol%)	1.4
0.005	0.012 mg mL ⁻¹ , 1.0 mL (0.012 mg, 0.000053 mmol, 0.005 mol%)	0.5
0.0005	0.012 mg mL ⁻¹ , 0.1 mL (0.0012 mg, 0.0000053 mmol, 0.0005 mol%)	1.4

Desired DIPEA Loading / eq.	Amount DIPEA Added
1	0.2 mL, 0.14 g, 1.1 mmol
2	0.4 mL, 0.29 g, 2.2 mmol
5	1.0 mL, 0.72 g, 5.6 mmol
10	2.0 mL, 1.45 g, 11.2 mmol
25	5.0 mL, 3.62 g, 28.0 mmol

A sample of each starting solution was then removed for GC analysis before immersing each vessel in a preheated oil bath set to 80 °C. Solutions containing 1 or 2 eq. DIPEA and a 0.5 mol% Pd(OAc)₂ loading turned red immediately, with 5 eq. DIPEA and 0.5 mol% Pd(OAc)₂ loading turned red shortly after. The other mixtures turned shades of red/orange/brown after stirring overnight. Reaction vessels were removed briefly from the oil bath at intervals required for sampling for GC analysis, before being replaced in the oil bath. After 21 h to 4 days, the reaction vessels were removed from the oil bath and the heat turned off. Samples were again removed for GC analysis, used to calculate yield and conversion (using calibration plot for determining the concentration of reductively coupled product to do so). Concentrations for the starting material (used in yield calculations) were determined from the mass of *trans*-4-phenyl-3-buten-2-one added (0.161 g, 1.10 mmol in all cases) and the total volume of liquids added (NMP, 1.5 mL in all cases, and DIPEA, varied between experiments) *e.g.* where a 5 eq. loading of DIPEA was used, the volume added was 1.0 mL, therefore the total volume was assumed to be 1.5 mL + 1.0 mL = 2.5 mL, where 1.10 mmol of *trans*-4-phenyl-3-buten-2-one were used, the concentration would therefore be calculated as 1.10 mmol / 2.5 mL = 0.44 M. Yields were then calculated by dividing the determined GC concentration of reductively coupled product by the calculated *trans*-4-phenyl-3-buten-2-one concentration.

Pd(OAc) ₂ Loading / mol%	DIPEA Loading / eq.	Time	GC Yield / %
0.5	1	21 h	79
0.5	2	21 h	81
0.5	5	21 h	81
0.5	10	21 h	86
0.5	25	21 h	47
0.0005-0.05	1-5	1-4 days	Traces

Exp.6.3.5 Procedure for Reactions in Table 4.4.3 Entries 2-5

Experimental procedure for result presented in Entry 1 was covered in procedures above. To separate Schlenk tubes, 4-iodoanisole (0.310 g, 1.32 mmol, 1.2 eq.) and *trans*-4-phenyl-3-buten-2-one (0.160 g, 1.09 mmol) were added. To this, 0.1 mL of a 1.2 mg mL⁻¹ stock solution of Pd(OAc)₂ in NMP was added (0.12 mg, 0.00053 mmol, 0.05 mol%). DIPEA (1.0 mL, 0.72 g, 5.6 mmol, 5 eq.) was then added and the mixture then dissolved in an additional 1.4 mL NMP to take the total volume of NMP added to 1.5 mL, giving a homogeneous, clear yellow solution.

A sample of each starting solution was then removed for GC analysis before immersing each vessel in a preheated oil bath set to 100, 150 or 200 °C. Reaction vessels were removed briefly from the oil bath at intervals required for sampling for GC analysis, before being replaced in the oil bath. After 19 h, the reaction vessels were removed from the oil bath and the heat turned off. Samples were again removed for GC analysis, used to calculate yield and conversion (using calibration plot for determining the concentration of reductively coupled product to do so). Concentrations for the starting material (used in yield calculations) were determined from the mass of *trans*-4-phenyl-3-buten-2-one added (0.16 g, 1.09 mmol in all cases) and the total volume of liquids added (1.5 mL NMP and 1.0 mL DIPEA, therefore 2.5 mL total, in all cases), giving a calculated concentration of 1.09 mmol / 2.5 mL = 0.44 M for each reaction mixture. Yields were then calculated by dividing the determined GC concentration of reductively coupled product by the calculated *trans*-4-phenyl-3-buten-2-one concentration.

Temperature / °C	Time / h	GC Yield / %
100	19	29
150	19	74
150	1	52
200	1	64

Exp.6.3.6 Procedure for Reactions in Table 4.4.4 Entries 3-4

Experimental procedures for results presented in Entries 1 and 2 were covered in procedures above. To separate Schlenk tubes, 4-iodoanisole (0.310 g, 1.32 mmol, 1.2 eq.) and *trans*-4-phenyl-3-buten-2-one (0.160 g, 1.09 mmol) were added. To this, the required amount of a 0.012 mg mL⁻¹ stock solution of Pd(OAc)₂ in NMP was added (amounts detailed below). DIPEA (1.0 mL, 0.72 g, 5.6 mmol, 5 eq.) was then added and the mixture then dissolved in the required amount of NMP to take the total volume of NMP added to 1.5 mL (detailed below), giving a homogeneous, clear yellow solution.

Desired Pd Loading /mol%	Pd Stock Added	NMP Added for Make Up to 1.5 mL / mL
0.005	0.012 mg mL ⁻¹ , 1.0 mL (0.012 mg, 0.000053 mmol, 0.005 mol%)	0.5
0.0005	0.012 mg mL ⁻¹ , 0.1 mL (0.0012 mg, 0.0000053 mmol, 0.0005 mol%)	1.4

A sample of each starting solution was then removed for GC analysis before immersing each vessel in a preheated oil bath set to 200 °C. After 2 h, the reaction vessels were removed from the oil bath and the heat turned off. Samples were again removed for GC analysis, used to calculate yield and conversion (using calibration plot for determining the concentration of reductively coupled product to do so). Concentrations for the starting material (used in yield calculations) were determined from the mass of *trans*-4-phenyl-3-buten-2-one added (0.16 g, 1.09 mmol in all cases) and the total volume of liquids added (1.5 mL NMP and 1.0 mL DIPEA, therefore 2.5 mL total, in all cases), giving a calculated concentration of 1.09 mmol / 2.5 mL = 0.44 M for each reaction mixture. Yields were then calculated by dividing the determined GC concentration of reductively coupled product by the calculated *trans*-4-phenyl-3-buten-2-one concentration.

Pd(OAc) ₂ Loading / mol%	GC Yield after 2 h / %
0.005	53
0.0005	15

Exp.6.3.7 Procedure for Reactions in Table 4.4.5 Entries 4, 5, 7 and 8

Experimental procedures for results presented in Entries 1-3 and 6 were covered in procedures above. To separate Schlenk tubes, 4-iodoanisole (0.310 g, 1.32 mmol, 1.2 eq.) and *trans*-4-phenyl-3-buten-2-one (0.160 g, 1.09 mmol) were added. To this, the required amount of a 0.012 mg mL⁻¹ stock solution of Pd(OAc)₂ in NMP was added (amounts detailed below). DIPEA (amounts detailed below) was then added, and the mixture then dissolved in the required amount of NMP to take the total volume of NMP added to 1.5 mL (detailed below), giving a homogeneous, clear yellow solution.

Desired Pd Loading / mol%	Pd Stock Added	NMP Added for Make Up to 1.5 mL / mL
0.005	0.012 mg mL ⁻¹ , 1.0 mL (0.012 mg, 0.000053 mmol, 0.005 mol%)	0.5
0.0005	0.012 mg mL ⁻¹ , 0.1 mL (0.0012 mg, 0.0000053 mmol, 0.0005 mol%)	1.4

Desired DIPEA Loading / eq.	Amount DIPEA Added
1	0.2 mL, 0.14 g, 1.1 mmol
2	0.4 mL, 0.29 g, 2.2 mmol

A sample of each starting solution was then removed for GC analysis before immersing each vessel in a preheated oil bath set to 200 °C. After 2 h, the reaction vessels were removed from the oil bath and the heat turned off. Samples were again removed for GC analysis, used to calculate yield and conversion (using calibration plot for determining the concentration of reductively coupled product to do so). Concentrations for the starting material (used in yield calculations) were determined from the mass of *trans*-4-phenyl-3-buten-2-one added (0.16 g, 1.09 mmol in all cases) and the total volume of liquids added (1.5 mL NMP and 0.2 or 0.4 mL DIPEA, therefore 1.7 or 1.9 mL total), giving a calculated concentration of 1.09 mmol / 1.7 mL = 0.64 M or 1.09 mmol / 1.9 mL = 0.57 M for the reaction mixtures. Yields were then calculated by dividing the determined GC concentration of reductively coupled product by the calculated *trans*-4-phenyl-3-buten-2-one concentration.

Pd(OAc) ₂ Loading / mol%	DIPEA Loading / eq.	GC Yield after 2 h / %
0.005	1	27
0.005	2	50
0.0005	1	6
0.0005	2	14

Exp.6.3.8 Procedure for Reactions in Table 4.4.6

To three separate round bottomed flasks, the required amount of *trans*-4-phenyl-3-buten-2-one and 4-iodoanisole were added (detailed below). To this, 1.0 mL of a 0.3 mg mL⁻¹ stock solution of Pd(OAc)₂ in NMP was added (0.3 mg, 0.0013 mmol, 0.005 mol%). DIPEA (9.6 mL, 6.95 g, 53.8 mmol) was then added to give the required equivalents and the mixture then dissolved in an extra 35.0 mL NMP*. If needed, this was sonicated to dissolve all solid components, resulting in a transparent pale yellow, homogeneous solution.

Solution	Amount <i>trans</i> -4-phenyl-3-buten-2-one	Amount 4-iodoanisole	Total volume / mL	Concentration <i>trans</i> -4-phenyl-3-buten-2-one / M
A	3.7894 g, 25.9 mmol	7.4284 g, 31.7 mmol, 1.2 eq.	47.0	0.55*
B	3.8384 g, 26.3 mmol	7.4242 g, 31.7 mmol, 1.2 eq.	54.0	0.49
C	3.8333 g, 26.2 mmol	7.4012 g, 31.6 mmol, 1.2 eq.	53.0	0.49

*29.0 mL instead of 35.0 mL NMP was added to the mixture giving a higher than planned concentration.

Reactions were then carried out according to Exp.6.3.2., and the procedure was repeated for each reaction mixture solution, until all reactions in the experiment were completed. Concentrations for the starting material (used in yield calculations) were determined from the mass of *trans*-4-phenyl-3-buten-2-one added and the total volume of the reaction solution (measured with a measuring cylinder, detailed above). Yields were then calculated by dividing the determined GC concentration of reductively coupled product by the calculated *trans*-4-phenyl-3-buten-2-one concentration.

Temperature / °C	Pressure / bar	Solution	Time / min	Flow Rate / mL min ⁻¹	GC Yield / %
200	5	A	5	0.6	2
250	15	A	5	0.6	11
250	15	B	10	0.3	16
250	15	C	20	0.15	26
250	15	C	30	0.1	28
275	50	B	5	0.6	8
275	50	B	10	0.3	16
300	50	A	5	0.6	10

Exp.6.3.9 Procedure for Reactions in Table 4.4.7 Entries 3-6

Procedures for Entries 1 and 2 are covered in procedures above. To three separate round bottomed flasks, the required amount of *trans*-4-phenyl-3-buten-2-one and 4-iodoanisole were added (detailed below). To this, a stock solution of 0.3 mg mL⁻¹ Pd(OAc)₂ in NMP was added (detailed below). DIPEA (detailed below) was then added to give the required equivalents and the mixture then dissolved in an extra amount of neat NMP to give the required volume (detailed below). If needed, this was sonicated to dissolve all solid components, resulting in a transparent pale yellow, homogeneous solution.

Solution	Amount <i>trans</i> -4-phenyl-3-buten-2-one	Amount 4-iodoanisole	Amount Pd Stock	Amount DIPEA	Amount Neat NMP / mL	Total volume / mL	Concentration <i>trans</i> -4-phenyl-3-buten-2-one / M
A	2.5211 g, 17.2 mmol	4.9313 g, 21.1 mmol, 1.2 eq.	0.67 mL, 0.20 mg, 0.0009 mmol, 0.005 mol%	3.2 mL, 2.32 g, 18.0 mmol, 1 eq.	23.0	32.0	0.54
B	1.9115 g, 13.1 mmol	3.7080 g, 15.8 mmol, 1.2 eq.	0.5 mL, 0.15 mg, 0.0007 mmol, 0.005 mol%	2.4 mL, 1.74 g, 13.5 mmol, 1 eq.	17.5	24.5	0.53
C	1.9093 g, 13.1 mmol	3.7114 g, 15.9 mmol, 1.2 eq.	0.5 mL, 0.15 mg, 0.0007 mmol, 0.005 mol%	4.8 mL, 3.48 g, 26.9 mmol, 2 eq.	17.5	26.5	0.49

Reactions were then carried out according to Exp.6.3.2., and the procedure was repeated for each reaction mixture solution, until all reactions in the experiment were completed. Concentrations for the starting material (used in yield calculations) were determined from the mass of *trans*-4-phenyl-3-buten-

2-one added and the total volume of the reaction solution (measured with a measuring cylinder, detailed above). Yields were then calculated by dividing the determined GC concentration of reductively coupled product by the calculated *trans*-4-phenyl-3-buten-2-one concentration.

Temperature / °C	DIPEA Amount / eq.	Pressure / bar	Solution	Time / min	Flow Rate / mL min ⁻¹	GC Yield / %
200	2	5	C	30	0.1	31
250	1	15	A	20	0.15	21
250	1	15	A	30	0.1	26
200	1	5	B	30	0.1	22

Exp.6.3.10 Procedure for Reactions in Table 4.4.9 Entries 1-6

Procedures for Entries 7 and 8 are covered in procedures above. To three separate round bottomed flasks, the required amount of *trans*-4-phenyl-3-buten-2-one and 4-iodoanisole were added (detailed below). To this, a stock solution of 0.3 mg mL⁻¹ Pd(OAc)₂ in NMP was added (detailed below) or was weighed out directly and added. DIPEA (detailed below) was then added to give the required equivalents and the mixture then dissolved in an extra amount of neat NMP to give the required volume (detailed below). If needed, this was sonicated to dissolve all solid components, resulting in a transparent pale yellow, homogeneous solution.

Solution	Amount <i>trans</i> -4-phenyl-3-buten-2-one	Amount 4-iodoanisole	Amount Pd	Amount DIPEA	Amount Neat NMP / mL	Total volume / mL	Concentration <i>trans</i> -4-phenyl-3-buten-2-one / M
A	3.8120 g, 26.1 mmol	7.4075 g, 31.7 mmol, 1.2 eq.	3.0 mg Pd(OAc) ₂ , 0.013 mmol, 0.05 mol%	9.6 mL, 6.95 g, 53.8 mmol, 2 eq.	36.0	53.0	0.49
B	1.9105 g, 13.1 mmol	3.7098 g, 15.9 mmol, 1.2 eq.	5.0 mL, 1.5 mg, 0.007 mmol, 0.05 mol%	2.4 mL, 1.74 g, 13.5 mmol, 1 eq.	13.0	24.5	0.53
C	1.9098 g, 13.1 mmol	3.7075 g, 15.8 mmol, 1.2 eq.	5.0 mL, 1.5 mg, 0.007 mmol, 0.05 mol%	4.8 mL, 3.48 g, 26.9 mmol, 2 eq.	13.0	27.0	0.49

Reactions were then carried out according to Exp.6.3.2., and the procedure was repeated for each reaction mixture solution, until all reactions in the experiment were completed. Concentrations for the starting material (used in yield calculations) were determined from the mass of *trans*-4-phenyl-3-buten-

2-one added and the total volume of the reaction solution (measured with a measuring cylinder, detailed above). Yields were then calculated by dividing the determined GC concentration of reductively coupled product by the calculated *trans*-4-phenyl-3-buten-2-one concentration.

Temperature / °C	DIPEA Amount / eq.	Pressure / bar	Solution	Time / min	Flow Rate / mL min ⁻¹	GC Yield / %
200	2	5	A	1	3.0	12
200	2	5	A	2.5	1.2	34
200	2	5	A	5	0.6	51
200	2	5	A	10	0.3	52
250	1	15	B	10	0.3	26
250	2	15	C	10	0.3	35

Exp.6.3.11 Procedure for Reactions in Table 4.4.11 Entries 3 and 4

Procedures for Entries 1 and 2 are covered in procedures above. To a round bottomed flask, *trans*-4-phenyl-3-buten-2-one (3.8310 g, 26.2 mmol) and 4-iodoanisole (7.4142 g, 31.7 mmol, 1.2 eq.) were added. To this, Pd(OAc)₂ (3.0 mg, 0.013 mmol, 0.05 mol%). DIPEA (18.0 mL, 13.03 g, 100.8 mmol, 3.8 eq.) was then added and dissolved in 36.0 mL NMP, giving a total volume of 64.0 mL (0.41 M *w.r.t.* *trans*-4-phenyl-3-buten-2-one). If needed, this was sonicated to dissolve all solid components, resulting in a transparent pale yellow, homogeneous solution.

Reactions were then carried out according to Exp.6.3.2., and the procedure was repeated for each set of conditions, until all reactions in the experiment were completed. Concentrations for the starting material (used in yield calculations) were determined from the mass of *trans*-4-phenyl-3-buten-2-one added and the total volume of the reaction solution (measured with a measuring cylinder, detailed above). Yields were then calculated by dividing the determined GC concentration of reductively coupled product by the calculated *trans*-4-phenyl-3-buten-2-one concentration.

Temperature / °C	Pressure / bar	Time / min	Flow Rate / mL min ⁻¹	GC Yield / %
200	5	5	0.6	58
200	5	10	0.3	61

Exp.6.3.12 Procedure for Reactions in Table 4.4.12 Entries 2-6

Procedures for Entries 1 and 2 are covered in procedures above. To two separate round bottomed flasks, the required amount of *trans*-4-phenyl-3-buten-2-one and 4-iodoanisole were added (detailed below). To this, Pd(OAc)₂ (3.0 mg, 0.013 mmol, 0.05 mol%) was added. DIPEA (18.0 mL, 13.03 g, 100.8 mmol, 3.8 eq.) was then added and dissolved in 36.0 mL NMP. If needed, this was sonicated to dissolve all solid components, resulting in a transparent pale yellow, homogeneous solution.

Solution	Amount <i>trans</i> -4-phenyl-3-buten-2-one	Amount 4-iodoanisole	Total volume / mL	Concentration (Limiting Reagent) / M
A	3.8203 g, 26.1 mmol	12.1968 g, 52.1 mmol, 2 eq.	65.0	0.40 M (<i>trans</i> -4-phenyl-3-buten-2-one)
B	7.5950 g, 52.0 mmol, 2 eq.	6.0792 g, 26.0 mmol	64.0	0.41 M (4-iodoanisole)

Reactions were then carried out according to Exp.6.3.2., and the procedure was repeated for each reaction mixture solution, until all reactions in the experiment were completed. Concentrations for the starting material (used in yield calculations) were determined from the mass of *trans*-4-phenyl-3-buten-2-one added and the total volume of the reaction solution (measured with a measuring cylinder, detailed above). Yields were then calculated by dividing the determined GC concentration of reductively coupled product by the calculated *trans*-4-phenyl-3-buten-2-one concentration.

Temperature / °C	Pressure / bar	Solution	Time / min	Flow Rate / mL min ⁻¹	GC Yield / %
200	5	A	5	0.6	75
200	5	A	10	0.3	73
200	5	B	5	0.6	71
200	5	B	10	0.3	70

Exp.6.4 Chapter 5

Exp.6.4.1 General Experimental Procedure for Batch MacMillan C-O Coupling Reactions

To a suitable vessel, 4-bromoacetophenone and [Ir{dF(CF₃)ppy}₂(dtbbpy)]PF₆ were added and dissolved in MeCN, to give a yellow homogeneous solution. To a separate vial was added NiCl₂.glyme and dtbbpy which was then dissolved in MeCN, forming a solution initially orange, which turned blue with agitation with a vortex mixer.

The reaction vessel was charged with a magnetic stirrer and the base/amine added. The Ir photocatalyst and 4-bromoacetophenone was added to the reaction vessel, followed by the Ni containing solution, to give solutions of usually a yellowish green colour (which might or might not have been homogeneous, depending on the amine/base system used). This was then stoppered with a suba-seal and sealed with parafilm. Following this, the vessel was immersed in liquid N₂ until full solidification of the mixture occurred and then put under a high vacuum on a Schlenk line (to a pressure of at least 0.4 mbar) for around 5 min. After this, the vessel was filled with Ar and thawed. To the reaction vessel was then added the required amount of 1-hexanol and, after this, a further two repeats of the freeze-pump-thaw cycle were applied.

Reactions were then executed with the following general procedure. The reaction vessel was then clamped in position above a stirrer plate 1 cm from the light source to be used. The mixture was then stirred, and the light source turned on, with aluminium foil positioned around the set-up as a shield for the intense light. The mixture was then left for the required amount of time before sampling or isolation. Where samples were taken, the light source was turned down to its lowest intensity, a N₂/Ar

balloon inserted through the suba-seal, and samples taken with a syringe following air-sensitive protocols, before turning the light source back up to maximum intensity and continuing irradiation, until the final sample was taken, at which point the light source was turned off.

Where products were isolated, 10 mL EtOAc was added, along with 10 mL H₂O. The organic layers were separated, and the aqueous layers were washed with a further 2 x 10 mL EtOAc. The organic extracts from each vessel were combined and washed with 10 mL brine. The solvent from the organic washings was then removed on a rotary evaporator to give a green oil (along with some solid). To this, ~30 mL DCM and silica gel were added until the crude product appeared adsorbed, before removal of DCM on a rotary evaporator to give the crude product dry loaded on silica. The dry loaded crude product was then purified using automatic column chromatography (95:5 cyclohexane/EtOAc, 4 g or 12 g Redisep R_f Gold column, 15 mL min⁻¹, 10 min). The solvent was then removed from the eluent on a rotary evaporator to give the desired product, 4-hexyloxy acetophenone, as a yellow oil (yield for each vessel in table below). Characterisation data as in Exp.5 and Appendix.

Where GC samples were taken, the light source was turned off, or down to the lowest intensity. An Ar or N₂ balloon was inserted through the suba-seal on the reaction vessels and a 0.1 mL sample from each vessel was taken. This sample was dissolved in 1.0 mL MeOH and used for GC analysis for determination of approximate yield and conversion at the relevant time interval. Following sample removal from all vessels being irradiated at one time, the Ar or N₂ balloon was removed, and the light source turned back up to full intensity. This was repeated for each time interval samples were taken at, until the experiment was terminated by turning off the light source.

Exp.6.4.2 General Experimental Procedure for Flow MacMillan C-O Coupling Reactions

To a round bottomed flask, aryl halide, *N,N,N',N'*-tetramethyl guanidine and [Ir{dF(CF₃)ppy}₂(dtbbpy)]PF₆ were added and dissolved in MeCN, to give a yellow homogeneous solution. To a separate vial was added NiCl₂.glyme and dtbbpy which was then dissolved in the required MeCN, forming a solution initially orange, which was then agitated using a vortex mixer (until a homogeneous blue solution was formed). Addition of the blue Ni-containing solution to the yellow Ir-containing solution resulted in a green, homogeneous solution.

The flask was then stoppered with a suba-seal, pierced with FEP tubing connected to a three-way valve. The three-way valve was shut to one outlet and to the third connection point was another length of FEP tubing pierced through a suba-seal. This suba-seal was used to stopper a second round bottomed flask containing ~50 mL of neat MeCN. This tubing/three-way valve system was used for allowing degassing of the contents of the flask and then enabling attachment to the reactor system, without exposing the solution to the air. Further details of this can be seen in Exp.2.2.

Following this, each flask was immersed in liquid N₂ until full solidification of the mixture occurred and then put under a high vacuum on a Schlenk line (to a pressure of at least 0.4 mbar) for around 5 min. After this, each flask was filled with Ar and thawed. To the reaction mixture flask was then added the required amount of the relevant alcohol and, after this, a further two repeats of the freeze-pump-thaw cycle were applied to each flask. Samples of the starting solution after addition of alcohol were taken to enable conversion quantification using a GC approach.

The flasks were then connected *via* the three-way valve to the flow reactor system, up-stream of the peristaltic pump. The reactions were then performed following a Standard Operating Procedure. The three-way valve was first opened to the degassed MeCN, and this was flowed around the reactor system until around at least 2 system volumes of solvent had passed through. Checks for leaks in the system were made whilst doing so and, if leak free, the pump was then stopped, and the irradiated coil and jacketed tube shrouded with foil to prevent stray light. If required, a recirculating chiller/heater was connected to the inlet and outlet of the jacketed tube, turned on and allowed to reach the desired temperature. Following shrouding and temperature equilibration (where required), the Lightsabre LEDs were connected to a cold tap for cooling and turned on. The three-way valve was then opened to the reaction starting mixture and the pump started at the desired flow rate. A timer was started, and the reaction solution was pumped around the irradiated coil for the time taken for approximately 2 system volumes to pass through the reactor system. After this time, replicate samples were taken from the crude product outlet stream, each sample being taken a short time apart (to identify whether equilibration had not occurred, which would be suggested by subsequent samples giving observed yields significantly increasing with time).

An aliquot from each sample would then be taken and diluted in MeOH for yield/conversion quantification using GC analysis. At most substrate concentrations, this would involve a 0.1 mL aliquot being diluted in a further 1 mL MeOH. For higher substrate concentrations, this would be diluted up to the same total volume by a further factor of 2, 4 or 6 (*e.g.*, 50 μ L aliquot along with 1050 μ L MeOH to give a further 2-fold dilution, maintaining 1.1 mL total volume) using appropriate and calibrated auto-pipetting techniques.

Where relevant, products were isolated following work-up and automatic column chromatography, with the specific details given in the relevant sections.

If multiple flow rates were being investigated using the same starting material mixture, following sampling, the flow rate would be set to the next desired flow rate. The three-way valve would then be switched to degassed MeCN for a few minutes, before switching back to the starting material mixture and restarting the timer. The procedure for timing and sampling would then be repeated, as necessary. Following acquisition of the last samples, the three-way valve would then be switched to degassed MeCN. The Lightsabre LEDs would then be turned off (and cooled with water for a further few minutes before closing the tap) along with the recirculating chiller/heater (if used). The foil shrouding would then be removed, and the reactor allowed to flush with MeCN until all green reaction mixture was no longer visible. The suba-seal and tubing previously connecting the reaction mixture round bottomed flask to the three-way valve would then be removed from the flask and immersed in neat MeCN so that the system was thoroughly flushed through with MeCN. After this, the inlet tubings to the pump would be removed from the solvent and each allowed to flush through with air until the system emptied of solvent. The irradiated reactor coil would then be inspected for fouling. If a visible black coating on the entrance to the irradiate coil was noticed, the system would then be flushed through with \sim 100 mL H₂O before flushing through a small volume (\sim 20 – 30 mL) of aq. HNO₃ (diluted to \sim 30%). The black coating would noticeably disappear from the tubing, at which point, the system would be flushed through with 1 M aq. NaOH (\sim 100 mL) before flushing with H₂O until the aqueous outlet appeared neutral by indicator paper. Note that “dirty-blank” reactions had been conducted in absence of added catalysts

(one or both) and suggested that even in the presence of fouling, no product was formed in the absence of either catalyst, however, the cleaning procedure was adopted as to use conditions as reproducible as possible and avoid build-up of black coating significant enough to interfere with the incident light.

Exp.6.4.3 Procedure for Reactions in Table 5.4.1

Data presented in Entries 2 and 3 were taken from the literature for comparison. Reaction solutions were prepared according to Exp.6.4.1 with 4-bromoacetophenone (0.1987 g, 1.0 mmol), [Ir{dF(CF₃)ppy}₂(dtbbpy)]PF₆ (0.0108 g, 0.01 mmol, 1 mol%), quinuclidine (0.0108 g, 0.1 mmol, 0.1 eq.) and K₂CO₃ (0.1387 g, 1.0 mmol, 1 eq.) in MeCN (2.0 mL). Separately, NiCl₂.glyme (0.0114 g, 0.05 mmol, 5 mol%) and dtbbpy (0.0137 g, 0.05 mmol, 5 mol%) in MeCN (2.0 mL) was prepared, and the two mixtures combined. The mixture was then degassed according to Exp.6.4.1, with addition of 1-hexanol (0.2 mL, 0.16 g, 1.6 mmol, 1.6 eq.).

Reactions were then performed according to Exp.6.4.1. After 24 h irradiation, samples were taken for ¹H NMR spectroscopic analysis of the crude reaction mixture, and product then isolated according to Exp.6.4.1 (0.1709 g, 0.78 mmol, 78%). Characterisation data as in Exp.5 and Appendix.

Exp.6.4.4 Procedure for Reactions in Table 5.4.2 Entries 4-7

Procedure for Entry 1 is covered by procedures above. Data presented in Entries 2 and 3 were taken from the literature for comparison.

Reaction solutions were prepared according to Exp.6.4.1 with 4-bromoacetophenone (0.7962 g, 4.0 mmol), [Ir{dF(CF₃)ppy}₂(dtbbpy)]PF₆ (0.0441 g, 0.04 mmol) and quinuclidine (0.0447 g, 0.4 mmol) in MeCN (8.0 mL). Separately, NiCl₂.glyme (0.0434 g, 0.2 mmol) and dtbbpy (0.0530 g, 0.2 mmol) in MeCN (8.0 mL) was prepared. 2.0 mL of each solution was then added to a vessel containing K₂CO₃, and mixtures degassed according to Exp.6.4.1, with addition of 1-hexanol (0.2 mL, 0.16 g, 1.6 mmol, 1.6 eq.) to each.

Reactions were then performed according to Exp.6.4.1. After 24 h irradiation, samples were taken for crude ¹H NMR spectroscopic analysis, and product isolated according to Exp.6.4.1. Characterisation data as in Exp.5 and Appendix.

Reaction Vessel	Amount K ₂ CO ₃	Isolated Yield
1	0.1376 g, 1 mmol, 1 eq.	0.1629 g, 0.74 mmol, 74%
2	0.1375 g, 1 mmol, 1 eq.	0.1554 g, 0.71 mmol, 71%
3	0.1383 g, 1 mmol, 1 eq.	0.1386 g, 0.63 mmol, 63%
4	0.1375 g, 1 mmol, 1 eq.	0.1465 g, 0.67 mmol, 67%

Exp.6.4.5 Procedure for Reactions in Table 5.4.4

Reaction solutions were prepared according to Exp.6.4.1 with 4-bromoacetophenone, [Ir{dF(CF₃)ppy}₂(dtbbpy)]PF₆, and quinuclidine in MeCN (amounts detailed below). Separately, NiCl₂.glyme and dtbbpy in MeCN was prepared (amounts detailed below). 2.0 mL each solution was then added to a vessel containing the base (detailed below) and mixtures degassed according to Exp.6.4.1, with addition of 1-hexanol (0.2 mL, 0.16 g, 1.6 mmol, 1.6 eq.) to each.

Reactions were then performed according to Exp.6.4.1. After 24 h irradiation, samples were taken for ^1H NMR spectroscopic analysis of the crude reaction mixture, and product then isolated according to Exp.6.4.1. Characterisation data as in Exp.5 and Appendix.

Reaction Vessel	Amount Base	Amount Product
1	DBU, 0.1541 g, 1 mmol, 1 eq.	0.0160 g, 0.07 mmol, 7%.
2	TMG, 0.1141 g, 1 mmol, 1 eq.	0.1280 g, 0.58 mmol, 58%.
3	Quinuclidine, 0.1076 g, 1 mmol, 1 eq.	0.1298 g, 0.59 mmol, 59%.
4	DIPEA, 0.1262 g, 1 mmol, 1 eq.	0.0191 g, 0.09 mmol, 9%.
5	TEA, 0.1081 g, 1 mmol, 1 eq.	0.033 g, 0.15 mmol, 15%.*
6	TMAOH, 0.1797 g, 1 mmol, 1 eq.	Not observed/isolated.
7	TBAOH, 0.8009 g, 1 mmol, 1 eq.	Not observed/isolated.
8	Pyridine, 0.0794 g, 1 mmol, 1 eq.	0.0152 g, 0.07 mmol, 7%.
9	DMAP, 0.1226 g, 1 mmol, 1 eq.	0.0051 g, 0.02 mmol, 2%.
10	Imidazole, 0.0677 g, 1 mmol, 1 eq.	Not observed/isolated.
11	DABCO, 0.1124 g, 1 mmol, 1 eq.	0.0851 g, 0.39 mmol, 39%.

*Amount of product was estimated from ^1H NMR spectrum of impure product obtained after work-up and isolation.

For the starting solutions, to reaction vessels 1-4 was added 2.0 mL of each of the following solutions:

- 4-Bromoacetophenone (0.7933 g, 4.0 mmol), $[\text{Ir}\{\text{dF}(\text{CF}_3)\text{ppy}\}_2(\text{dtbbpy})]\text{PF}_6$ (0.0448 g, 0.04 mmol) and quinuclidine (0.0451 g, 0.4 mmol), in 8.0 mL MeCN.
- $\text{NiCl}_2\cdot\text{glyme}$ (0.0434 g, 0.2 mmol) and dtbbpy (0.0528 g, 0.2 mmol), in 8.0 mL MeCN.

To reaction vessels 5-7 was added 2.0 mL of each of the following solutions:

- 4-Bromoacetophenone (0.5957 g, 3.0 mmol), $[\text{Ir}\{\text{dF}(\text{CF}_3)\text{ppy}\}_2(\text{dtbbpy})]\text{PF}_6$ (0.0334 g, 0.03 mmol) and quinuclidine (0.0332 g, 0.3 mmol), in 6.0 mL MeCN.
- $\text{NiCl}_2\cdot\text{glyme}$ (0.0329 g, 0.15 mmol) and dtbbpy (0.0406 g, 0.15 mmol), in 6.0 mL MeCN.

To reaction vessels 8-11 was added 2.0 mL of each of the following solutions:

- 4-Bromoacetophenone (0.7962 g, 4.0 mmol), $[\text{Ir}\{\text{dF}(\text{CF}_3)\text{ppy}\}_2(\text{dtbbpy})]\text{PF}_6$ (0.0451 g, 0.04 mmol) and quinuclidine (0.0438 g, 0.4 mmol), in 8.0 mL MeCN.
- $\text{NiCl}_2\cdot\text{glyme}$ (0.0437 g, 0.2 mmol) and dtbbpy (0.0540 g, 0.2 mmol), in 8.0 mL MeCN.

Exp.6.4.6 Procedure for Reactions in Table 5.4.5 Entries 4, 6, 8 and 10

Procedures for Entries 1-3, 5 and 7 are covered by procedures above. Reaction solutions were prepared according to Exp.6.4.1. with 4-bromoacetophenone (0.7960 g, 4.0 mmol) and $[\text{Ir}\{\text{dF}(\text{CF}_3)\text{ppy}\}_2(\text{dtbbpy})]\text{PF}_6$ (0.0453 g, 0.04 mmol) in MeCN (8.0 mL). Separately, $\text{NiCl}_2\cdot\text{glyme}$ (0.0444 g, 0.2 mmol) and dtbbpy (0.0534 g, 0.2 mmol) in MeCN (8.0 mL) was prepared. 2.0 mL of each solution was added to a vessel containing the base and mixtures degassed according to Exp.6.4.1, with addition of 1-hexanol (0.2 mL, 0.16 g, 1.6 mmol, 1.6 eq.) to each.

Reactions were then performed according to Exp.6.4.1. After 24 h irradiation, samples were taken for ^1H NMR spectroscopic analysis of the crude reaction mixture, and product then isolated according to Exp.6.4.1. Characterisation data as in Exp.5 and Appendix.

Reaction Vessel	Amount Base	Amount Product
1	TMG, 0.1292 g, 1.1 mmol, 1.1 eq.	0.1337 g, 0.61 mmol, 61%
2	TEA, 0.1113 g, 1.1 mmol, 1.1 eq.	0.0197 g, 0.09 mmol, 9%
3	DABCO, 0.1232 g, 1.1 mmol, 1.1 eq.	0.1162 g, 0.53 mmol, 53%
4	DIPEA, 0.1448 g, 1.1 mmol, 1.1 eq.	0.052 g, 0.24 mmol, 24%*

*Amount of product was estimated from ^1H NMR spectrum of impure product obtained after work-up and isolation.

Exp.6.4.7 Procedure for Reactions in Approximate Kinetic Studies Presented in Fig 5.4.1

Reaction solutions were prepared according to Exp.6.4.1 with 4-bromoacetophenone and $[\text{Ir}\{\text{dF}(\text{CF}_3)\text{ppy}\}_2(\text{dtbbpy})]\text{PF}_6$ in MeCN (amounts detailed below). Separately, $\text{NiCl}_2\cdot\text{glyme}$ and dtbbpy in MeCN was prepared (amounts detailed below). 2.0 mL of each solution was added to each of the reaction vessels containing the base and mixtures degassed according to Exp.6.4.1, with addition of 1-hexanol (0.2 mL, 0.16 g, 1.6 mmol, 1.6 eq.) to each.

Reactions were then performed according to Exp.6.4.1. After certain time intervals, GC samples were taken according to Exp.6.4.1.

Reaction Vessel	Amount Base	Amount Quinuclidine
1	K_2CO_3 , 0.1381 g, 1 mmol, 1 eq.	0.0113 g, 0.1 mmol, 0.1 eq.
2	Quinuclidine, 0.1166 g, 1 mmol, 1 eq.	
3	TMG, 0.1285 g, 1.1 mmol, 1.1 eq.	Not added.
4	TMG, 0.1190 g, 1 mmol, 1 eq.	0.0112 g, 0.1 mmol, 0.1 eq.
5	K_2CO_3 , 0.1378 g, 1 mmol, 1 eq.	Not added.
6	Quinuclidine, 0.1222 g, 1.1 mmol, 1.1 eq.	
7	TMG, 0.1148 g, 1 mmol, 1 eq.	Not added.

Note – yields for each vessel at each timescale are presented graphically in the Results & Discussion Section.

For the starting solutions, to reaction vessels 1-4 was added 2.0 mL of each of the following solutions:

- 4-Bromoacetophenone (0.7961 g, 4.0 mmol) and $[\text{Ir}\{\text{dF}(\text{CF}_3)\text{ppy}\}_2(\text{dtbbpy})]\text{PF}_6$ (0.0447 g, 0.04 mmol) in 8.0 mL MeCN.
- $\text{NiCl}_2\cdot\text{glyme}$ (0.0436 g, 0.2 mmol) and dtbbpy (0.0536 g, 0.2 mmol), in 8.0 mL MeCN.

To reaction vessels 5-7 was added 2.0 mL of each of the following solutions:

- 4-Bromoacetophenone (0.5974 g, 3.0 mmol) and $[\text{Ir}\{\text{dF}(\text{CF}_3)\text{ppy}\}_2(\text{dtbbpy})]\text{PF}_6$ (0.0337 g, 0.03 mmol) in 6.0 mL MeCN.
- $\text{NiCl}_2\cdot\text{glyme}$ (0.0326 g, 0.15 mmol) and dtbbpy (0.0403 g, 0.15 mmol), in 6.0 mL MeCN.

Exp.6.4.8 Procedure for Reactions in Table 5.4.6 Entries 4-6

Procedures for Entries 1-3 are covered by procedures above. Reaction solutions were prepared according to Exp.6.4.1 with *N,N,N',N'*-tetramethyl guanidine (0.1231 g, 1.1 mmol), 4-bromoacetophenone (0.1986 g, 1.0 mmol) and [Ir{dF(CF₃)ppy}₂(dtbbpy)]PF₆ (0.0114 g, 0.01 mmol, 1 mol%). Separately, NiCl₂.glyme (0.0109 g, 0.05 mmol, 5 mol%) and dtbbpy (0.0134 g, 0.05 mmol, 5 mol%) in MeCN (4.0 mL) was prepared. The two mixtures were combined and degassed according to Exp.6.4.1, with addition of 1-hexanol (0.2 mL, 0.16 g, 1.6 mmol, 1.6 eq.).

Reactions were then performed according to Exp.6.4.1. After certain time intervals, GC samples were taken according to Exp.6.4.1.

Light Source	Time	GC Yield / %
Blue	60 min	15
Blue	180 min	22
Blue	24 h	42

Exp.6.4.9 Procedure for Reactions in Table 5.4.7

Reaction solutions were prepared according to Exp.6.4.1 with 4-bromoacetophenone (0.7940 g, 4.0 mmol) and *N,N,N',N'*-tetramethyl guanidine (0.4570 g, 4.0 mmol) in 8.0 mL MeCN. Separately, NiCl₂.glyme (0.0438 g, 0.2 mmol) and dtbbpy (0.0539 g, 0.2 mmol) in 8.0 mL MeCN was prepared. 2.0 mL of each solution was added to each reaction vessel containing the photocatalyst (amounts detailed below). The mixtures were then degassed according to Exp.6.4.1, with addition of 1-hexanol (0.2 mL, 0.16 g, 1.6 mmol).

Reactions were then performed according to Exp.6.4.1. After certain time intervals, GC samples were taken according to Exp.6.4.1.

Reaction Vessel	Amount Photocatalyst	Observation of Starting Solution	GC Yield after 2 h / %
1	[Ru(bpy) ₃]Cl ₂ .6H ₂ O (0.0073 g, 0.01 mmol)	Homogeneous, orange.	11
2	[Ru(bpy) ₃]PF ₆ (0.0085 g, 0.01 mmol)	Homogeneous, orange.	16
3	[Ir(ppy) ₂ (dtbbpy)]PF ₆ (0.0091 g, 0.01 mmol)	Homogeneous, greenish yellow.	87
4	Ir(ppy) ₃ (0.0062 g, 0.01 mmol)	Yellow soln. + solids	6

Note – yields were also determined at other timescales, as presented in Table 5.4.7.

Exp.6.4.10 Procedure for Reactions in Table 5.4.8

Stock solution 1 was prepared by adding *N,N,N',N'*-tetramethyl guanidine (0.6372 g, 5.5 mmol), 4-bromoacetophenone (0.9963 g, 5.0 mmol) and [Ir{dF(CF₃)ppy}₂(dtbbpy)]PF₆ (0.0558 g, 0.05 mmol) to a vial and dissolving in 10.0 mL MeCN, giving a yellow solution. Stock solution 2 was prepared by adding NiCl₂.glyme (0.0436 g, 0.2 mmol) and dtbbpy (0.0537 g, 0.2 mmol) to a vial and

dissolving in 8.0 mL MeCN. This was vortexed until it became a homogeneous blue solution. Stock solution 3 was prepared by adding *N,N,N',N'*-tetramethyl guanidine (0.5025 g, 4.4 mmol), 4-bromoacetophenone (0.7962 g, 4.0 mmol) to a vial and dissolving in 8.0 mL MeCN to give a colourless solution. Appropriate combinations of the above stock solutions (with additional MeCN where necessary) were made to give the desired starting solutions for control reactions. The combinations are detailed in the table below.

Reaction Vessel*	Vol. Stock Solution 1 / ml	Vol. Stock Solution 2 / ml	Vol. Stock Solution 3 / ml	Vol. Neat MeCN / mL
1	2.0	2.0	0	0
2	2.0	2.0	0	0
3	0	2.0	2.0	0
4	2.0	0	0	2.0
5	0	2.0	2.0	0
6	1.0	0	0	1.0
7	0	0	2.0	2.0
8	0	0	2.0	2.0

*Reaction vessel number corresponds to Entry number in **Table 5.4.8**. See results presented in **Table 5.4.8** for yields after 3h and 72 h and for a description of conditions the above solution combinations resulted in.

Mixtures were then degassed according to Exp.6.4.1, with addition of 1-hexanol (0.2 mL, 0.16 g, 1.6 mmol) (mixtures 1-5 and 7-8) or (0.1 mL, 0.08 g, 0.8 mmol) (mixture 6).

Reaction vessel 1 was then wrapped in foil and stirred in a dark vented box. Reaction vessels 2, 5, 6 and 8 were immersed in an oil bath and stirred at 60 °C, with the entire set-up shrouded loosely in foil and placed in a fumehood with the light off. Reaction vessels 3, 4 and 7 were then placed 1 cm away from a fan cooled white LED block (5 x 12 W LED strips) and clamped above a stirrer plate, with the position of each vessel relative to the light source noted. The mixtures were then stirred, and the apparatus shrouded in aluminium foil before turning on the light source.

At certain time intervals, samples were taken for GC analysis. Negligible GC yields were observed in all cases.

Exp.6.4.11 Procedure for Reactions in Table 5.4.9

Reaction solutions were prepared according to Exp.6.4.2 with *N,N,N',N'*-tetramethyl guanidine (1.5944 g, 13.8 mmol), 4-bromoacetophenone (2.4867 g, 12.5 mmol) and [Ir{dF(CF₃)ppy}₂(dtbbpy)]PF₆ (0.1402 g, 0.13 mmol) in 40 mL MeCN. Separately, NiCl₂.glyme (0.1382 g, 0.63 mmol) and dtbbpy (0.1667 g, 0.62 mmol) in MeCN (10.0 mL) was prepared, and the two solutions combined. The mixtures, along with a flask containing neat MeCN, were then degassed according to Exp.6.4.2, with addition of 1-hexanol (2.4 mL, 2.0 g, 19.6 mmol), followed by sample removal for GC analysis.

The mixture was then connected back to the pump-head inlet of the reactor system, with a 1/8 " FEP tubing reactor coil in place around the flow reactor jacketed tube, giving a reactor irradiated volume of 6 mL and total system volume of 8 mL (Tubing 2 in **Exp. Table 1**).

The reactions were then performed according to Exp.6.4.2, with the required flow rate. Samples were taken according to Exp.6.4.2 and then the flow rate was then set to the next desired value (detailed below), until all experiments were completed, then the system shut-down according to Exp.6.4.2.

Residence Time / min	Flow Rate / mL min ⁻¹	GC Yield / %
30	0.2	88
15	0.4	85
5	1.2	55

Exp.6.4.12 Procedure for Reactions in Table 5.4.10

Reaction solutions were prepared according to Exp.6.4.2 with *N,N,N',N'*-tetramethyl guanidine (1.7869 g, 15.5 mmol), 4-bromoacetophenone (2.7849 g, 14.0 mmol) and [Ir{dF(CF₃)ppy}₂(dtbbpy)]PF₆ (0.1577 g, 0.14 mmol) in 28 mL MeCN. Separately, NiCl₂.glyme (0.1533 g, 0.7 mmol) and dtbbpy (0.1884 g, 0.7 mmol) in MeCN (28 mL) was prepared, and the two solutions were combined. The mixtures, along with a flask containing neat MeCN, were then degassed according to Exp.6.4.2, with addition of 1-hexanol (2.8 mL, 2.3 g, 22.5 mmol), followed by sample removal for GC analysis.

The mixture was then connected back to the pump-head inlet of the reactor system, with a 1/32 " FEP tubing reactor coil in place around the flow reactor jacketed tube, giving a reactor irradiated volume of 3.8 mL and total system volume of 5.8 mL (Tubing 3 in **Exp. Table 1**).

The reactions were then performed according to Exp.6.4.2, with the required flow rate. Samples were taken according to Exp.6.4.2 and then the flow rate was then set to the next desired value (detailed below), until all experiments were completed, then the system shut-down according to Exp.6.4.2.

Residence Time / min	Flow Rate / mL min ⁻¹	GC Yield / %
10	0.38	97
5	0.76	85
2.5	1.52	69
1	3.80	33

Exp.6.4.13 Procedure for Reactions in Table 5.4.11 Entries 4-11 (and Fig 5.4.6 and 5.4.7)

Procedures for Entries 1-3 are covered by procedures above. Reaction solutions were prepared according to Exp.6.4.2 with *N,N,N',N'*-tetramethyl guanidine, 4-bromoacetophenone and [Ir{dF(CF₃)ppy}₂(dtbbpy)]PF₆ in MeCN (amounts detailed below). Separately, NiCl₂.glyme and dtbbpy in MeCN was prepared (amounts detailed below) and the two solutions were combined. The mixtures, along with a flask containing neat MeCN, were then degassed according to Exp.6.4.2, with addition of 1-hexanol (amounts detailed below), followed by sample removal for GC analysis.

The device was then connected back to the pump-head inlet of the reactor system, with a 1/32 " FEP tubing reactor coil in place around the flow reactor jacketed tube, giving a reactor irradiated volume of 3.8 mL and total system volume of 5.8 mL (Tubing 3 in **Exp. Table 1**). A recirculating chiller/heater was connected to the inlet and outlet of the jacketed tube and was set to the first desired temperature.

The reactions were then performed according to Exp.6.4.2, with the required flow rate and temperature. Samples were taken according to Exp.6.4.2 and then the flow rate was then set to the next desired value (detailed below), until all experiments were completed, then the system shut-down according to Exp.6.4.2.

The Entries 4-11 in **Table 5.4.11** are based on results where two different stock solutions were made. For Entries 4-7, 9 the following amounts were used:

- TMG (2.0224 g, 17.6 mmol), 4-bromoacetophenone (3.1776 g, 16.0 mmol), Ir-126 (0.1787 g, 0.16 mmol), dissolved in 35 mL MeCN.
- NiCl₂.glyme (0.1751 g, 0.8 mmol), dtbbpy (0.2141 g, 0.8 mmol), dissolved in 25 mL MeCN.
- 3.2 mL 1-hexanol was added (2.6 g, 25.4 mmol).

For Entries 8, 10-11, the following amounts were used:

- TMG (1.0145 g, 8.8 mmol), 4-bromoacetophenone (1.5920 g, 8.0 mmol), Ir-126 (0.0900 g, 0.08 mmol), dissolved in 16 mL MeCN.
- NiCl₂.glyme (0.0882 g, 0.4 mmol), dtbbpy (0.1067 g, 0.4 mmol), dissolved in 16 mL MeCN.
- 1.6 mL 1-hexanol was added (1.3 g, 12.8 mmol).

Temp. / °C	Residence Time / min	Flow Rate / mL min ⁻¹	GC Yield / %
20	1	3.80	5
40	1	3.80	19
60	1	3.80	36
60	2.5	1.52	78
60	5	0.76	93
80	1	3.80	36
80	2.5	1.52	67
80	5	0.76	76

Exp.6.4.14 Procedure for Reactions in Table 5.4.12

Reaction solutions were prepared according to Exp.6.4.2 with amounts of reagents detailed below. The mixtures were then degassed according to Exp.6.4.2 and 1-hexanol added as detailed below.

The device was then connected back to the pump-head inlet of the reactor system, with a 1/32 " FEP tubing reactor coil in place around the flow reactor jacketed tube, giving a reactor irradiated volume of 3.8 mL and total system volume of 5.8 mL (Tubing 3 in **Exp. Table 1**).

Reactions were then performed according to Exp.6.4.2 at the required flow rate. Samples were taken according to Exp.6.4.2 and then the process repeated for each solution, until all experiments were completed, then the system shut-down according to Exp.6.4.2.

For Entry 1 (no catalyst), the following amounts were used:

- TMG (0.5119 g, 4.4 mmol), 4-bromoacetophenone (0.7957 g, 4.0 mmol), 1-hexanol (0.8 mL, 0.66 g, 6.5 mmol), dissolved in 16 mL MeCN, conc. of 4-bromoacetophenone 0.21 M determined by GC analysis with a calibration plot.

For Entry 2 (no Ir photocatalyst), the following amounts were used:

- TMG (0.1327 g, 1.2 mmol), 4-bromoacetophenone (0.2007 g, 1.0 mmol), dissolved in 2 mL MeCN.
- NiCl₂.glyme (0.0115 g, 0.05 mmol), dtbbpy (0.0133 g, 0.05 mmol), dissolved in 2 mL MeCN.
- 0.2 mL 1-hexanol was added (0.16 g, 1.6 mmol), after the first degas cycle.
- A 4-bromoacetophenone concentration of 0.23 M in the starting solution was determined as the total volume of the solution prior to 1-hexanol addition was 4.2 mL, after addition of 0.2 mL 1-hexanol, this total volume was assumed to be 4.4 mL.

For Entry 3 (no Ni catalyst), the following amounts were used:

- TMG (0.1272 g, 1.1 mmol), 4-bromoacetophenone (0.2006 g, 1.0 mmol), Ir-126 (0.0133 g, 0.01 mmol), 1-hexanol (0.2 mL, 0.16 g, 1.6 mmol), dissolved in 4 mL MeCN.
- The volume was measured to be 4.4 mL, used to calculate a 4-bromoacetophenone concentration of 0.23 M in the starting solution.

Note – where no Ni catalyst was added, 1-hexanol was added prior to degas (as addition after the first degas cycle was precautionary in case of Ni-alkoxide instability). When no Ni was present, the alkoxide formation leading to the precaution would not be present.

Catalyst Presence	4-BrAP conc. Before Processing / M	4-BrAP conc. After Processing / M	GC Yield / %
None	0.21	0.21	0
No Ir	0.23	0.21	Traces
No Ni	0.23	0.22	Traces

Exp.6.4.15 Procedure for Reactions in Table 5.4.13 Entries 2-4

Procedure for Entry 1 is covered by procedures above. Reaction solutions were prepared according to Exp.6.4.2 with amounts detailed below and the mixtures were degassed according to Exp.6.4.2 with addition of 1-hexanol (0.8 mL, 0.66 g, 6.5 mmol) followed by sample removal for GC analysis.

The mixture was then connected back to the pump-head inlet of the reactor system, with a 1/32 " FEP tubing reactor coil in place around the flow reactor jacketed tube, giving a reactor irradiated volume of 3.8 mL and total system volume of 5.8 mL (Tubing 3 in **Exp. Table 1**).

Reactions were then performed according to Exp.6.4.2 at 0.76 mL min⁻¹, required for a 5 min residence time. Samples were taken according to Exp.6.4.2 and then the process repeated for each solution, until all experiments were completed, then the system shut-down according to Exp.6.4.2.

The reaction mixture giving a 0.5 mol% Ni loading used the following amounts:

- TMG (0.5127 g, 4.5 mmol), 4-bromoacetophenone (0.7961 g, 4.0 mmol), Ir-126 (0.0448 g, 0.04 mmol), dissolved in 8 mL MeCN.
- NiCl₂.glyme (0.0043 g, 0.02 mmol), dtbbpy (0.0054 g, 0.02 mmol), dissolved in 8 mL MeCN.

The reaction mixture giving a 1 mol% Ni loading used the following amounts:

- TMG (0.5094 g, 4.4 mmol), 4-bromoacetophenone (0.7967 g, 4.0 mmol), Ir-126 (0.0452 g, 0.04 mmol), dissolved in 8 mL MeCN.
- NiCl₂.glyme (0.0086 g, 0.04 mmol), dtbbpy (0.0106 g, 0.04 mmol), dissolved in 8 mL MeCN.

The reaction mixture giving a 2.5 mol% Ni loading used the following amounts:

- TMG (0.5109 g, 4.4 mmol), 4-bromoacetophenone (0.7951 g, 4.0 mmol), Ir-126 (0.0447 g, 0.04 mmol), dissolved in 8 mL MeCN.
- NiCl₂.glyme (0.0219 g, 0.1 mmol), dtbbpy (0.0266 g, 0.1 mmol), dissolved in 8 mL MeCN.

Ni Loading / mol%	GC Yield / %
2.5	93
1	51
0.5	21

Exp.6.4.16 Procedure for Reactions in Table 5.4.14 Entries 2-3

Procedure for Entry 1 is covered by procedures above. Reaction solutions were prepared according to Exp.6.4.2 with *N,N,N',N'*-tetramethyl guanidine, 4-bromoacetophenone and [Ir{dF(CF₃)ppy}₂(dtbbpy)]PF₆ in 8 mL MeCN (amounts detailed below). Separately, NiCl₂.glyme (0.0444 g, 0.2 mmol) and dtbbpy (0.0534 g, 0.2 mmol) in 16 mL MeCN was prepared as a stock solution for both experiments. 8 mL of the Ni-containing solution was then added to each of the two solutions containing the 4-bromoacetophenone, Ir photocatalyst and tetramethylguanidine. The mixtures, along with a flask containing neat MeCN, were then degassed according to Exp.6.4.2, with addition of 1-hexanol (0.8 mL, 0.66 g, 6.5 mmol), followed by sample removal for GC analysis.

The device was then connected back to the pump-head inlet of the reactor system, with a 1/32 " FEP tubing reactor coil in place around the flow reactor jacketed tube, giving a reactor irradiated volume of 3.8 mL and total system volume of 5.8 mL (Tubing 3 in **Exp. Table 1**).

Reactions were then performed according to Exp.6.4.2 at 0.76 mL min⁻¹, required for a 5 min residence time. Samples were taken according to Exp.6.4.2 and then the process repeated for each solution, until all experiments were completed, then the system shut-down according to Exp.6.4.2.

The reaction mixture giving a 0.1 mol% Ir loading used the following amounts, prior to addition of the previously described Ni stock solution:

- TMG (0.5072 g, 4.4 mmol), 4-bromoacetophenone (0.7953 g, 4.0 mmol), Ir-126 (0.0045 g, 0.004 mmol), dissolved in 8 mL MeCN.

The reaction mixture giving a 0.5 mol% Ir loading used the following amounts, prior to addition of the previously described Ni stock solution:

- TMG (0.5062 g, 4.4 mmol), 4-bromoacetophenone (0.7954 g, 4.0 mmol), Ir-126 (0.0225 g, 0.02 mmol), dissolved in 8 mL MeCN.

Ir Loading / mol%	GC Yield / %
0.1	60
0.5	90

Exp.6.4.17 Procedure for Reactions in Table 4.15 Entry 7

Procedures for Entries 1-6 are covered by procedures above. Reaction solutions were prepared according to Exp.6.4.2 with *N,N,N',N'*-tetramethyl guanidine (0.5036 g, 4.4 mmol), 4-bromoacetophenone (0.7961 g, 4.0 mmol) and [Ir{dF(CF₃)ppy}₂(dtbbpy)]PF₆ (0.0045 g, 0.004 mmol) in 8 mL MeCN. Separately, NiCl₂.glyme (0.0087 g, 0.04 mmol) and dtbbpy (0.0109 g, 0.04 mmol) were added followed by addition of 8 mL MeCN and the solutions were combined and degassed according to Exp.6.4.2 with addition of 1-hexanol (0.8 mL, 0.66 g, 6.5 mmol), followed by sample removal for GC analysis.

The device was then connected back to the pump-head inlet of the reactor system, with a 1/32 " FEP tubing reactor coil in place around the flow reactor jacketed tube, giving a reactor irradiated volume of 3.8 mL and total system volume of 5.8 mL (Tubing 3 in **Exp. Table 1**).

Reactions were then performed according to Exp.6.4.2 at 0.76 mL min⁻¹, required for a 5 min residence time. Samples were taken according to Exp.6.4.2 then the system shut-down according to Exp.6.4.2, with an observed GC yield of 26%.

Exp.6.4.18 Procedure for Reactions in Table 5.4.16 Entries 2-5

Procedure for Entry 1 is covered by procedures above. Reaction solutions were prepared according to Exp.6.4.2 with amounts detailed below and the mixtures were degassed according to Exp.6.4.2 with addition of 1-hexanol (amounts detailed below), followed by sample removal for GC analysis.

The device was then connected back to the pump-head inlet of the reactor system, with a 1/32 " FEP tubing reactor coil in place around the flow reactor jacketed tube, giving a reactor irradiated volume of 3.8 mL and total system volume of 5.8 mL (Tubing 3 in **Exp. Table 1**).

Reactions were then performed according to Exp.6.4.2 at the required flow rate. Samples were taken according to Exp.6.4.2 and then the process repeated for each solution, until all experiments were completed, then the system shut-down according to Exp.6.4.2.

The reaction mixture giving a 0.43 M concentration used the following amounts:

- TMG (1.0136 g, 8.8 mmol), 4-bromoacetophenone (1.5915 g, 8.0 mmol), Ir-126 (0.0090 g, 0.008 mmol), dissolved in 8 mL MeCN.
- NiCl₂.glyme (0.0177 g, 0.08 mmol), dtbbpy (0.0214 g, 0.08 mmol), dissolved in 8 mL MeCN.
- 1.6 mL 1-hexanol was added (1.31 g, 12.8 mmol).
- A 0.05 mL aliquot was taken from each sample and diluted in 1.05 mL MeOH for GC analysis.

The reaction mixture giving a 0.47 M concentration used the following amounts:

- TMG (4.0591 g, 35.2 mmol), 4-bromoacetophenone (6.3742 g, 32.0 mmol), Ir-126 (0.0364 g, 0.032 mmol), dissolved in 40 mL MeCN.
- NiCl₂.glyme (0.0713 g, 0.32 mmol), dtbbpy (0.0865 g, 0.32 mmol), dissolved in 24 mL MeCN.
- 6.4 mL 1-hexanol was added (5.21 g, 51.0 mmol).

The reaction mixture giving a 0.85 M concentration used the following amounts:

- TMG (4.0532 g, 35.2 mmol), 4-bromoacetophenone (6.3680 g, 32.0 mmol), Ir-126 (0.0359 g, 0.032 mmol), dissolved in 16 mL MeCN.
- NiCl₂.glyme (0.0708 g, 0.32 mmol), dtbbpy (0.0857 g, 0.32 mmol), dissolved in 16 mL MeCN.
- 6.4 mL 1-hexanol was added (5.21 g, 51.0 mmol).

The reaction mixture giving a 1.14 M concentration used the following amounts:

- TMG (6.0913 g, 52.9 mmol), 4-bromoacetophenone (9.5542 g, 48.0 mmol), Ir-126 (0.0540 g, 0.048 mmol), dissolved in 16 mL MeCN.
- NiCl₂.glyme (0.1059 g, 0.48 mmol), dtbbpy (0.1288 g, 0.48 mmol), dissolved in 16 mL MeCN.
- 9.6 mL 1-hexanol was added (7.81 g, 76.4 mmol).

Conc. / M	Residence Time / min	Flow Rate / mL min ⁻¹	GC Yield / %
0.43	5	0.76	63
0.47	10	0.38	96
0.85	10	0.38	84
1.14	10	0.38	33

Exp.6.4.19 Procedure for Reactions in Table 5.4.17 Entries 6-8

Procedure for Entries 1-5 are covered by procedures above. Reaction solutions were prepared according to Exp.6.4.2 with amounts detailed below and the mixtures were degassed according to Exp.6.4.2 with addition of 1-hexanol (amounts detailed below), followed by sample removal for GC analysis.

The vessel was then connected to the pump-head inlet of the reactor system, with 2 1/32 " FEP tubing reactor coils in place around the flow reactor jacketed tube giving an irradiated volume of 7.6 mL and total system volume of 9.6 mL, or, 1 1/16 " FEP tubing reactor coil giving an irradiated volume of 15.2 mL and total system volume of 17.2 mL (Tubing 4 or 5 in **Exp. Table 1**, as appropriate).

Reactions were then performed according to Exp.6.4.2 at the required flow rate. Samples were taken according to Exp.6.4.2 and then the process repeated for each solution, until all experiments were completed, then the system shut-down according to Exp.6.4.2.

The reaction mixture giving a 0.85 M concentration used the following amounts:

- TMG (8.1193 g, 70.5 mmol), 4-bromoacetophenone (12.7403 g, 64.0 mmol), Ir-126 (0.0721 g, 0.064 mmol), dissolved in 40 mL MeCN.
- NiCl₂.glyme (0.1410 g, 0.64 mmol), dtbbpy (0.1727 g, 0.64 mmol), dissolved in 24 mL MeCN.
- 12.8 mL 1-hexanol was added (10.4 g, 102.0 mmol).

The reaction mixture giving a 0.45 M concentration used the following amounts:

- TMG (4.0591 g, 35.2 mmol), 4-bromoacetophenone (6.3863 g, 32.1 mmol), Ir-126 (0.1839 g, 0.16 mmol), dissolved in 40 mL MeCN.
- NiCl₂.glyme (0.1758 g, 0.80 mmol), dtbbpy (0.2146 g, 0.80 mmol), dissolved in 24 mL MeCN.
- 6.4 mL 1-hexanol was added (5.21 g, 51.0 mmol).

The reaction mixture giving a 0.47 M concentration used the following amounts:

- TMG (4.0678 g, 35.3 mmol), 4-bromoacetophenone (6.3760 g, 32.0 mmol), Ir-126 (0.0358 g, 0.032 mmol), dissolved in 40 mL MeCN.
- NiCl₂.glyme (0.0710 g, 0.32 mmol), dtbbpy (0.0858 g, 0.32 mmol), dissolved in 24 mL MeCN.
- 6.4 mL 1-hexanol was added (5.21 g, 51.0 mmol).

Conc. / M	Residence Time / min	Flow Rate / mL min ⁻¹	GC Yield / %
0.85	10	0.76	63
0.45	5	1.52	80
0.47	10	1.52	85

Exp.6.5 Chapter 6

Exp.6.5.1 Procedure for Synthesis of NHPI-Ester Starting Material

Cyclohexane carboxylic acid (1 eq.), *N*-hydroxy phthalimide (1 eq.) and *N*-dimethylamino pyridine (DMAP, 0.1 eq.) were added to a suitably sized round bottomed flask (amounts detailed below). These were then dissolved in DCM to a concentration of ~0.5 M (*w.r.t.* carboxylic acid). To this, dicyclohexylcarbodiimide (DCC, 1 eq.) was added slowly. Following the complete addition of DCC, a yellow solution with solids present would result. This was then stirred overnight in a fumehood, with the light off. The mixture turned white and stirring was stopped. The reaction mixture was then filtered through a ~1-2 cm pad of silica or celite and the solids washed with DCM/Et₂O. The filtrate was collected and the solvent from this removed on a rotary evaporator to afford the NHPI-ester as an off-white solid. Examples of reagent amounts and yields are given below for the synthesis using cyclohexyl carboxylic acid as the starting material, affording **NHPI** (cyclohexyl carboxylic acid NHPI-ester) as the product.

Amount Cyclohexyl Carboxylic Acid	Amount N-hydroxy Phthalimide	Amount DMAP	Amount DCC	Amount DCM	Isolated Yield* / %
6.41 g (50 mmol)	8.16 g (50 mmol)	0.61 g (5 mmol)	10.32 g (50 mmol)	100 mL	96
12.82 g (100 mmol)	16.33 g (100 mmol)	1.22 g (10 mmol)	20.62 g (100 mmol)	200 mL	83

*See Exp.5 and Appendix for characterisation.

Exp.6.5.2 General Procedure for Batch Decarboxylative C-O Coupling Reactions

To a flame dried Schlenk tube under an inert (Ar) atmosphere, NHPI-ester was added followed by [Ir(ppy)₂(dtbbpy)]PF₆ and the relevant Cu catalyst. This was dissolved in dry DCM and to this, the required amount of Et₃N was added. Following this, the vessel was immersed in liquid N₂ until full solidification of the mixture occurred and then put under a high vacuum on a Schlenk line (to a pressure of at least 0.4 mbar) for around 5 min. After this, the vessel was filled with Ar and thawed. A further two repeats of this freeze-pump-thaw cycle were applied, then, the required amount of phenol coupling partner was added. Following addition of the phenol, a further two repeats of this freeze-pump-thaw cycle were applied (five cycles in total, three before phenol addition, two after phenol addition).

The Schlenk tube containing the degassed mixture was then clamped in position above a stirrer plate ~1 cm away from a 3.5 W blue LED, or 5 x 12 W white LED block (details in Exp.3). The mixture was then stirred, and the light source turned on, with aluminium foil positioned around the set-up as a shield for the intense light. The mixture was then left for the required amount of time before stopping irradiation or for sampling. A fan was used to keep the mixtures cool, preventing DCM boiling. Where samples were taken, the light source was turned down to its lowest intensity, a N₂/Ar balloon inserted through the suba-seal, and samples taken with a syringe following air-sensitive protocols, before turning the light source back up to maximum intensity and continuing irradiation, until the final sample was taken.

Where products were isolated, a 0.2 mL sample was removed for ¹H NMR spectroscopic analysis of the crude reaction mixture. To the remaining mixture, EtOAc was added and this was washed twice with brine. The brine extractions were combined and washed twice with EtOAc. The organic extractions were then combined and dried over MgSO₄ before removing the solvent on a rotary evaporator. To the dried mixture, 2-3 heaped spatulas of silica gel and ~15 mL DCM was added. The solvent was then again removed on a rotary evaporator to furnish the crude material dry loaded on silica. This was then purified using automatic column chromatography with a Redisep R_f Gold column and an eluent of EtOAc along with cyclohexane, hexane or pentane.

Exact details for specific reactions conducted are given in the relevant subsequent sections.

Exp.6.5.3 General Procedure for Flow Decarboxylative C-O Coupling Reactions

To a flame dried Schlenk tube (or other suitable vessel) under an inert (Ar) atmosphere, NHPI-ester was added followed by [Ir(ppy)₂(dtbbpy)]PF₆ and the relevant Cu catalyst. This was dissolved in dry DCM and to this, the required amount of Et₃N was added. Following this, the vessel was immersed in liquid N₂ until full solidification of the mixture occurred and then put under a high vacuum on a Schlenk line

(to a pressure of at least 0.4 mbar) for around 5 min. After this, the vessel was filled with Ar and thawed. A further two repeats of this freeze-pump-thaw cycle were applied, then, the required amount of phenol coupling partner was added. Following addition of the phenol, a further two repeats of this freeze-pump-thaw cycle were applied (five cycles in total, three before phenol addition, two after phenol addition).

The Schlenk tube (or other vessel) containing the degassed mixture was then connected to the inlet of the Lightsabre flow reactor at one end of a three-way valve. To the other end was connected a flask of neat DCM, placed under an Ar atmosphere by 2 freeze-pump-thaw degas cycles. The inert, neat DCM was then flowed through the reactor until a minimum of 2 system volumes had passed through. The reactions were then performed according to a Standard Operating Procedure. Checks for leaks in the system were made whilst neat solvent was flushing doing so and, if leak free, the irradiated coil and jacketed tube shrouded with foil to prevent stray light. A recirculating chiller (connected to the inlet and outlet of the jacketed tube) was turned on and allowed to reach the desired temperature. Following shrouding and temperature equilibration, the Lightsabre LEDs were connected to a cold tap for cooling and turned on. The three-way valve was then opened to the reaction starting mixture and the pump started at the desired flow rate. A timer was started, and the reaction solution was pumped around the irradiated coil for the time taken for approximately 2 system volumes to pass through the reactor system. After this time, (usually) replicate samples were taken from the crude product outlet stream, each sample being taken a short time apart (to identify whether equilibration had not occurred, which would be suggested by subsequent samples giving observed yields significantly increasing with time).

An aliquot from each sample would then be taken and diluted in DCM for yield/conversion quantification using GC analysis. Typically, 0.5 mL aliquots were taken and dissolved in a further 0.5 mL DCM.

If multiple flow rates were being investigated using the same starting material mixture, following sampling, the flow rate would be set to the next desired flow rate. The three-way valve would then be switched to degassed DCM for a few minutes, before switching back to the starting material mixture and restarting the timer. The procedure for timing and sampling would then be repeated, as necessary. Following acquisition of the last samples, the three-way valve would then be switched to degassed DCM. The Lightsabre LEDs would then be turned off (and cooled with water for a further few minutes before closing the tap) along with the recirculating chiller. The foil shrouding would then be removed and the reactor allowed to flush with DCM until the reaction mixture was no longer visible. The sub-seal and tubing previously connecting the reaction mixture round bottomed flask to the three-way valve would then be removed from the flask and immersed in neat DCM so that the system was thoroughly flushed through. After this, the inlet tubings to the pump would be removed from the solvent and each allowed to flush through with air until the system emptied of solvent. The irradiated reactor coil would then be inspected for fouling. If a visible black coating on the entrance to the irradiate coil was noticed, the system would then be flushed through with ~100 mL H₂O before flushing through a small volume (~20–30 mL) of aq. HNO₃ (diluted to ~30%). The black coating would noticeably disappear from the tubing, at which point, the system would be flushed through with 1 M aq. NaOH (~100 mL) before flushing with H₂O until the aqueous outlet appeared neutral by indicator paper.

Exp.6.5.4 Procedure for Reactions in Table 6.4.1 Entries 3-6

The results presented in Entries 1 and 2 were obtained from the literature²¹⁸ as a comparison for work performed here. To a flame dried Schlenk tube under an inert (Ar) atmosphere, **NHPI** was added (82 mg, 0.30 mmol), followed by [Ir(dtbbpy)(ppy)₂](PF₆) (2.8 mg, 0.003 mmol) and Cu^I catalyst (detailed below)). This was dissolved in 3 mL dry DCM and to this, Et₃N (0.08 mL, 0.06 g, 0.6 mmol) was added, giving a homogeneous yellow solution. Following this, the vessel was immersed in liquid N₂ until full solidification of the mixture occurred and then put under a high vacuum on a Schlenk line (to a pressure of at least 0.4 mbar) for around 5 min. After this, the vessel was backfilled with Ar and thawed. A further two repeats of this freeze-pump-thaw cycle were applied, then, guaiacol (0.06 mL, 0.067 g, 0.55 mmol) was added. Following addition of guaiacol, a further two repeats of this freeze-pump-thaw cycle were applied (five cycles in total, three before phenol addition, two after phenol addition).

The Schlenk tube was then clamped in position above a stirrer plate ~1 cm away from a 3.5 W blue LED and a fan was used to cool the mixtures to prevent DCM boiling. The mixture was then stirred, and the light source turned on, with aluminium foil positioned around the set-up as shrouding. The mixture was then left for 2 h before removing samples for GC yield analysis, or for 18 h before obtaining an isolated yield. The light source was then turned off and the mixture remained a homogeneous yellow solution.

For isolation, 20 mL EtOAc was added and this was washed with 2 x 10 mL brine. The brine extractions were combined and washed twice with 2 x 10 mL EtOAc. The organic extractions were then combined and dried over MgSO₄ before removing the solvent on a rotary evaporator. To the dried mixture, silica gel was added until the all the crude mixture appeared to be adsorbed and ~15 mL DCM was added. The solvent was then again removed on a rotary evaporator to furnish the crude material dry loaded on silica This was then purified using automatic column chromatography with a Redisep R_f Gold column and an eluent of 95:5 pentane:EtOAc. Fractions were combined and the solvent removed to afford the desired product as a clear, colourless oil (0.0181 g, 29%). Characterisation details can be found in Exp.5 and Appendix.

Cu ^I Catalyst	Amount	Time / h	Yield / %
CuCl	0.0082 g, 0.08 mmol, 27 mol%*	18	29 (Isolated)
CuCl	0.0059 g, 0.06 mmol, 20 mol%	2	65 (GC)
Cu(OTf).benzene	0.0302 g, 0.06 mmol, 20 mol%	2	75 (GC)
Cu(OTf).4(MeCN)	0.0226 g, 0.06 mmol, 20 mol%	2	68 (GC)

*Calculation error (using molecular weight of CuCl₂ instead of CuCl) meant that the loading used in this experiment was 27 mol% as opposed to the intended 20 mol%.

Exp.6.5.5 Procedure for Reactions in Fig.4.1

To a flame dried Schlenk tube under an inert (Ar) atmosphere, **NHPI** was added (0.0818 g, 0.30 mmol), followed by [Ir(dtbbpy)(ppy)₂](PF₆) (0.0027 g, 0.003 mmol) and purified CuCl (0.0080 g, 0.08 mmol). This was dissolved in 3 mL dry DCM and to this, Et₃N (0.08 mL, 0.06 g, 0.6 mmol) was added, giving a homogeneous yellow solution. Following this, the vessel was immersed in liquid N₂ until full solidification of the mixture occurred and then put under a high vacuum on a Schlenk line (to a pressure of at least 0.4 mbar) for around 5 min. After this, the vessel was filled with Ar and thawed. A further

two repeats of this freeze-pump-thaw cycle were applied, then, guaiacol (0.06 mL, 0.067 g, 0.55 mmol) was added. Following addition of guaiacol, a further two repeats of this freeze-pump-thaw cycle were applied (five cycles in total, three before phenol addition, two after phenol addition). A 0.1 mL sample was removed for ^1H NMR spectroscopic analysis.

The Schlenk tube was then clamped in position above a stirrer plate ~1 cm away from a 3.5 W blue LED. The mixture was then stirred, and the light source turned on, with aluminium foil positioned around the set-up as a shield for the intense light and a fan used to keep the mixtures cool, preventing DCM boiling. The mixture was then left for the required amount of time before stopping irradiation or for sampling. A fan was used to keep the mixtures cool, preventing DCM boiling. Where samples were taken, the light source was turned down to its lowest intensity, a N_2/Ar balloon inserted through the suba-seal, and 0.1 mL samples taken with a syringe following air-sensitive protocols, before turning the light source back up to maximum intensity and continuing irradiation, until the final sample was taken.

The mixture was then left for a total of 7 h. The light source was then turned off and the mixture remained a homogeneous yellow solution. ^1H NMR spectroscopic analyses were used for qualitative assessments.

Note – calculation error (using molecular weight of CuCl_2 instead of CuCl) meant that the loading used in this experiment was ~27 mol% as opposed to the intended 20 mol%.

Exp.6.5.6 Procedure for Reactions in Table 6.4.2

To a flame dried Schlenk tube (or other suitable vessel) under an inert (Ar) atmosphere, NHPI-ester was added followed by $[\text{Ir}(\text{ppy})_2(\text{dtbbpy})]\text{PF}_6$ and CuCl (amounts detailed below). This was dissolved in dry DCM and to this, the required amount of Et_3N was added (amounts detailed below). Following this, the vessel was immersed in liquid N_2 until full solidification of the mixture occurred and then put under a high vacuum on a Schlenk line (to a pressure of at least 0.4 mbar) for around 5 min. After this, the vessel was filled with Ar and thawed. A further two repeats of this freeze-pump-thaw cycle were applied, then, the required amount of phenol coupling partner was added. Following addition guaiacol (amounts detailed below), a further two repeats of this freeze-pump-thaw cycle were applied (five cycles in total, three before phenol addition, two after phenol addition).

Soln.	Amount NHPI	Amount CuCl	Amount Ir-125	Amount Et_3N	Amount Guaiacol	Amount DCM
A	1.23 g, 4.5 mmol	89 mg, 0.90 mmol, 20 mol%	0.0405 g, 0.044 mmol, 1 mol%	1.2 mL, 0.87 g, 8.6 mmol, 1.9 eq.	1.0 mL, 1.11 g, 8.9 mmol, 2 eq.	45 mL
B	0.82 g, 3.0 mmol	59 mg, 0.60 mmol, 20 mol%	0.0270 g, 0.030 mmol, 1 mol%	0.8 mL, 0.58 g, 5.7 mmol, 1.9 eq.	0.65 mL, 0.72 g, 5.8 mmol, 1.9 eq.	30 mL
C	Amounts the same as solution B.					

Solution A was used for results in Entries 1-3. Solution B was used for results in Entries 4 and 6. Solution C was used for results in Entries 5 and 7. Reactions were then performed according to Exp.6.5.3, setting the recirculating chiller to the desired value and peristaltic pump to the required flow rate for each condition.

Time / min	Flow Rate / mL min ⁻¹	Temperature / °C	GC Yield / %
10	0.38	5	57
5	0.76	5	60
2.5	1.52	5	57
1	3.80	5	30*
1	3.80	5	33*
1	3.80	10	33
1	3.80	20	63

*Repeated results.

Exp.6.5.7 Procedure for Reactions in Table 6.4.3 Entries 2-7

Procedure for Entry 1 can be found in procedures above. To a flame dried Schlenk tube under an inert (Ar) atmosphere, NHPI-ester (0.41 g, 1.50 mmol) was added followed by [Ir(ppy)₂(dtbbpy)]PF₆ and CuCl (amounts detailed below). This was dissolved in 15.0 mL dry DCM and to this, Et₃N was added (0.4 mL, 0.29 g, 2.9 mmol, 1.9 eq.). Following this, the vessel was immersed in liquid N₂ until full solidification of the mixture occurred and then put under a high vacuum on a Schlenk line (to a pressure of at least 0.4 mbar) for around 5 min. After this, the vessel was filled with Ar and thawed. A further two repeats of this freeze-pump-thaw cycle were applied, then, the required amount of phenol coupling partner was added. Following addition guaiacol (0.32 mL, 0.36 g, 2.9 mmol, 1.9 eq.), a further two repeats of this freeze-pump-thaw cycle were applied (five cycles in total, three before guaiacol addition, two after guaiacol addition).

Reactions were then performed according to Exp.6.5.3, setting the recirculating chiller to 5 °C and peristaltic pump to 1.52 mL min⁻¹ (2.5 min residence time) for each condition.

Amount Ir-125	Amount CuCl	GC Yield / %
0.0135 g, 0.015 mmol, 1 mol%	0.0148 g, 0.15 mmol, 10 mol%	24
0.0135 g, 0.015 mmol, 1 mol%	0.0074 g, 0.075 mmol, 5 mol%	15
0.0068 g, 0.0074 mmol, 0.5 mol%	0.0148 g, 0.15 mmol, 10 mol%	43
0.0014 g, 0.0015 mmol, 0.1 mol%*	0.0148 g, 0.15 mmol, 10 mol%	24
0.675 mg, 0.00074 mmol, 0.05 mol%*	0.0148 g, 0.15 mmol, 10 mol%	13
0.338 mg, 0.00037 mmol, 0.025 mol%*	0.0148 g, 0.15 mmol, 10 mol%	12

*Measured from stock solution.

Exp.6.5.8 Procedure for Reactions in Table 6.4.4

To a flame dried Schlenk tube under an inert (Ar) atmosphere, NHPI-ester (0.41 g, 1.50 mmol) was added followed by [Ir(ppy)₂(dtbbpy)]PF₆ (amounts detailed below) and CuCl (0.0148 g, 0.15 mmol, 10 mol%). This was dissolved in 15.0 mL dry DCM and to this, Et₃N was added (amounts detailed below).

Following this, the vessel was immersed in liquid N₂ until full solidification of the mixture occurred and then put under a high vacuum on a Schlenk line (to a pressure of at least 0.4 mbar) for around 5 min. After this, the vessel was filled with Ar and thawed. A further two repeats of this freeze-pump-thaw cycle were applied, then, the required amount of phenol coupling partner was added. Following addition guaiacol (0.32 mL, 0.36 g, 2.9 mmol, 1.9 eq.), a further two repeats of this freeze-pump-thaw cycle were applied (five cycles in total, three before guaiacol addition, two after guaiacol addition).

Reactions were then performed according to Exp.6.5.3, setting the recirculating chiller to 5 °C or 20 °C where necessary and peristaltic pump to 1.52 mL min⁻¹ (2.5 min residence time) for each condition.

Temp. / °C	Amount Ir-125	Amount Et ₃ N	GC Yield / %
5	0.0014 g, 0.0015 mmol, 0.1 mol%*	0.4 mL, 0.29 g, 2.9 mmol, 1.9 eq.	24
5	0.0014 g, 0.0015 mmol, 0.1 mol%*	0.3 mL, 0.22 g, 2.2 mmol, 1.5 eq.	35
5	0.0014 g, 0.0015 mmol, 0.1 mol%*	0.2 mL, 0.15 g, 1.5 mmol, 1.0 eq.	38
5	0.0014 g, 0.0015 mmol, 0.1 mol%*	0.1 mL, 0.07 g, 0.7 mmol, 0.5 eq.	26
5	0.0068 g, 0.0074 mmol, 0.5 mol%	0.2 mL, 0.15 g, 1.5 mmol, 1.0 eq.	96
20	0.0068 g, 0.0074 mmol, 0.5 mol%	0.2 mL, 0.15 g, 1.5 mmol, 1.0 eq.	97

*Measured from a stock solution.

Exp.6.5.9 Procedure for Reactions in Table 6.4.5

To a flame dried Schlenk tube under an inert (Ar) atmosphere, NHPI-ester was added followed by [Ir(ppy)₂(dtbbpy)]PF₆ and CuCl (amounts detailed below). This was dissolved in dry DCM and to this, Et₃N was added (amounts detailed below). Following this, the vessel was immersed in liquid N₂ until full solidification of the mixture occurred and then put under a high vacuum on a Schlenk line (to a pressure of at least 0.4 mbar) for around 5 min. After this, the vessel was filled with Ar and thawed. A further two repeats of this freeze-pump-thaw cycle were applied, then, the required amount of phenol coupling partner was added. Following addition guaiacol (amounts detailed below), a further two repeats of this freeze-pump-thaw cycle were applied (five cycles in total, three before guaiacol addition, two after guaiacol addition).

Soln.	Amount NHPI	Amount CuCl	Amount Ir-125	Amount Et ₃ N	Amount Guaiacol	Amount DCM
A	0.41 g, 1.5 mmol	0.0148 g, 0.15 mmol, 10 mol%	0.0014 g, 0.0015 mmol, 0.1 mol%*	0.2 mL, 0.15 g, 1.5 mmol, 1.0 eq.	0.32 mL, 0.36 g, 2.9 mmol, 1.9 eq.	15 mL
B	0.82 g, 3.0 mmol	0.0297 g, 0.30 mmol, 10 mol%	0.0027 g, 0.003 mmol, 0.1 mol%	0.4 mL, 0.29 g, 2.9 mmol, 1.0 eq.	0.64 mL, 0.71 g, 5.7 mmol, 1.9 eq.	15 mL
C	2.05 g, 7.5 mmol	0.0742 g, 0.75 mmol, 10 mol%	0.0069 g, 0.0075 mmol, 0.1 mol%	1.0 mL, 0.73 g, 7.2 mmol, 1.0 eq.	1.60 mL, 1.78 g, 14.3 mmol, 1.9 eq.	15 mL
D	1.23 g, 4.5 mmol	0.0445 g, 0.45 mmol, 10 mol%	0.0210 g, 0.023 mmol, 0.5 mol%	0.65 mL, 0.47 g, 4.6 mmol, 1.0 eq.	1.0 mL, 1.1 g, 8.6 mmol, 1.9 eq.	30 mL
E	1.64 g, 6.0 mmol	0.0594 g, 0.60 mmol, 10 mol%	0.0274 g, 0.03 mmol, 0.5 mol%	0.8 mL, 0.58 g, 5.7 mmol, 0.95 eq.	1.30 mL, 1.4 g, 11.3 mmol, 1.9 eq.	30 mL

Solution A was used for the reaction in Entry 1 (reproduced from **Table 6.4.4**, procedure also given in Exp.6.5.8), Solution B for the reaction in Entry 2, Solution C for the reaction in Entry 3, Solution D for the reactions in Entries 4 and 6 and Solution E for the reactions in Entries 5 and 7 (all Entries relevant to **Table 6.4.5**). Reactions were then performed according to Exp.6.5.3, setting the recirculating chiller to 5 °C or 20 °C where necessary and peristaltic pump to 1.52 mL min⁻¹ (2.5 min residence time) for each condition.

Exp.6.5.10 Procedure for Reactions in Table 6.4.6

To a flame dried Schlenk tube under an inert (Ar) atmosphere, NHPI-ester was added followed by [Ir(ppy)₂(dtbbpy)]PF₆ and Cu catalyst (amounts detailed below). This was dissolved in dry DCM and to this, Et₃N was added (amounts detailed below). Following this, the vessel was immersed in liquid N₂ until full solidification of the mixture occurred and then put under a high vacuum on a Schlenk line (to a pressure of at least 0.4 mbar) for around 5 min. After this, the vessel was filled with Ar and thawed. A further two repeats of this freeze-pump-thaw cycle were applied, then, the required amount of phenol coupling partner was added. Following addition guaiacol (amount detailed below), a further two repeats of this freeze-pump-thaw cycle were applied (five cycles in total, three before guaiacol addition, two after guaiacol addition).

Solution	Amount NHPI	Amount Ir-125	Amount Cu Cat.	Amount Guaiacol	Amount Et ₃ N	Amount DCM
A	1.64 g, 6.0 mmol	0.0274 g, 0.03 mmol, 0.5 mol%	CuCl, 0.0594 g, 0.60 mmol, 10 mol%	1.30 mL, 1.4 g, 11.3 mmol, 1.9 eq.	0.8 mL, 0.58 g, 5.7 mmol, 0.95 eq.	60 mL
B	0.82 g, 3.0 mmol	0.0549 g, 0.06 mmol, 0.5 mol%	Cu(OTf).(4MeCN), 0.1130 g, 0.3 mmol, 10 mol%	0.64 mL, 0.71 g, 5.7 mmol, 1.9 eq.	0.4 mL, 0.29 g, 2.9 mmol, 1.0 eq.	30 mL
C	0.82 g, 3.0 mmol	0.0549 g, 0.06 mmol, 0.5 mol%	Cu(OTf).benzene, 0.1510 g, 0.3 mmol, 10 mol%	0.64 mL, 0.71 g, 5.7 mmol, 1.9 eq.	0.4 mL, 0.29 g, 2.9 mmol, 1.0 eq.	30 mL

Solution A was used for reactions in Entries 1-3, Solution B for reactions in Entries 4 and 5 and Solution C for reactions in Entries 6 and 7 (all Entries relevant to **Table 6.4.6**). Reactions were then performed according to Exp.6.5.3, setting the recirculating chiller to 5 °C or 20 °C as appropriate and peristaltic pump to the required flow rate (1.52 mL min⁻¹ for 2.5 min residence time, 2.28 mL min⁻¹ for 1.67 min residence time, 3.04 mL min⁻¹ for 1.25 min residence time) for each condition.

Solution	Temp. / °C	Residence Time / min	GC Yield / %
A	5	2.50	88
A	5	1.67	50
A	5	1.25	41
B	5	1.67	47
B	20	1.67	61
C	5	1.67	21
C	20	1.67	33

Exp.6.5.11 Procedure for Reactions in Table 6.4.7 Entries 2-7

Procedure for Entry 1 can be in procedures above. To a flame dried Schlenk tube under an inert (Ar) atmosphere, NHPI-ester (0.82 g, 3.0 mmol when using the 7.6 mL reactor, or, 1.64 g, 6.0 mmol when using the 15.2 mL reactor) was added followed by [Ir(ppy)₂(dtbbpy)]PF₆ (0.014 g, 0.015 mmol, when using the 7.6 mL reactor, or, 0.027 g, 0.030 mmol, when using the 15.2 mL reactor, 0.5 mol%) and CuCl (0.030 g, 0.3 mmol, when using the 7.6 mL reactor, or, 0.059 g, 0.6 mmol when using the 15.2 mL reactor, 10 mol%). This was dissolved in dry DCM (30 mL when using the 7.6 mL reactor, or 60 mL when using the 15.2 mL reactor) and to this, Et₃N was added (0.4 mL, 0.29 g, 2.9 mmol, 1.0 eq., when using the 7.6 mL reactor, or, 0.8 mL, 0.58 g, 5.7 mmol, 0.95 eq., when using the 15.2 mL reactor). Following this, the vessel was immersed in liquid N₂ until full solidification of the mixture occurred and then put under a high vacuum on a Schlenk line (to a pressure of at least 0.4 mbar) for around 5 min. After this, the vessel was filled with Ar and thawed. A further two repeats of this freeze-pump-thaw cycle were applied, then, the required amount of phenol coupling partner was added. Following addition guaiacol (0.64 mL, 0.71 g, 5.7 mmol, 1.9 eq., when using the 7.6 mL reactor, or, 1.30 mL, 1.4 g, 11.3 mmol, 1.9

eq., when using the 15.2 mL reactor), a further two repeats of this freeze-pump-thaw cycle were applied (five cycles in total, three before guaiacol addition, two after guaiacol addition).

Reactions were then performed according to Exp.6.5.3, setting the recirculating chiller to 20 °C and peristaltic pump to the required flow rate for a desired residence time, in a given reactor (detailed below). Further details regarding the reactor coils are found in Exp.2.2.

Reactor Coil Volume / mL	Residence Time / min (Flow Rate / mL min ⁻¹)	GC Yield / %
7.6	2.5 (3.04)	62
7.6	3.0 (2.53)	73
7.6	4.0 (1.90)	94
15.2	2.5 (6.08)	51
15.2	4.0 (3.80)	71

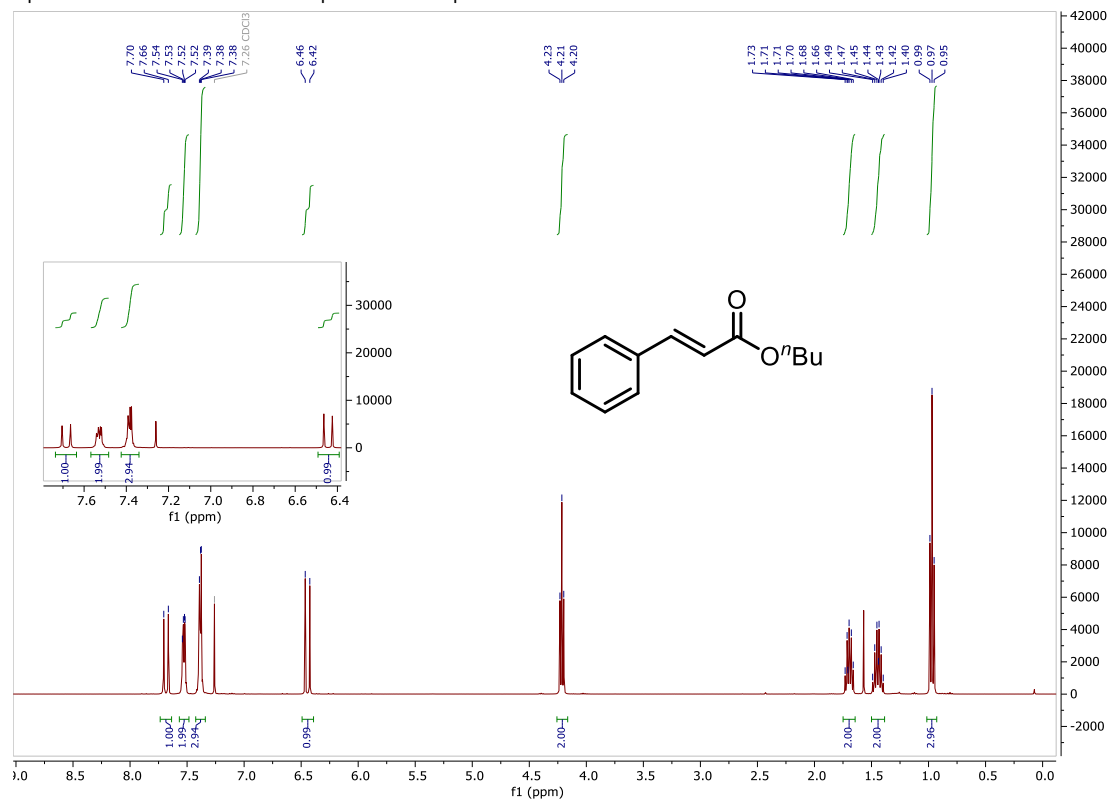
Appendix

Ap.1 Spectral Data

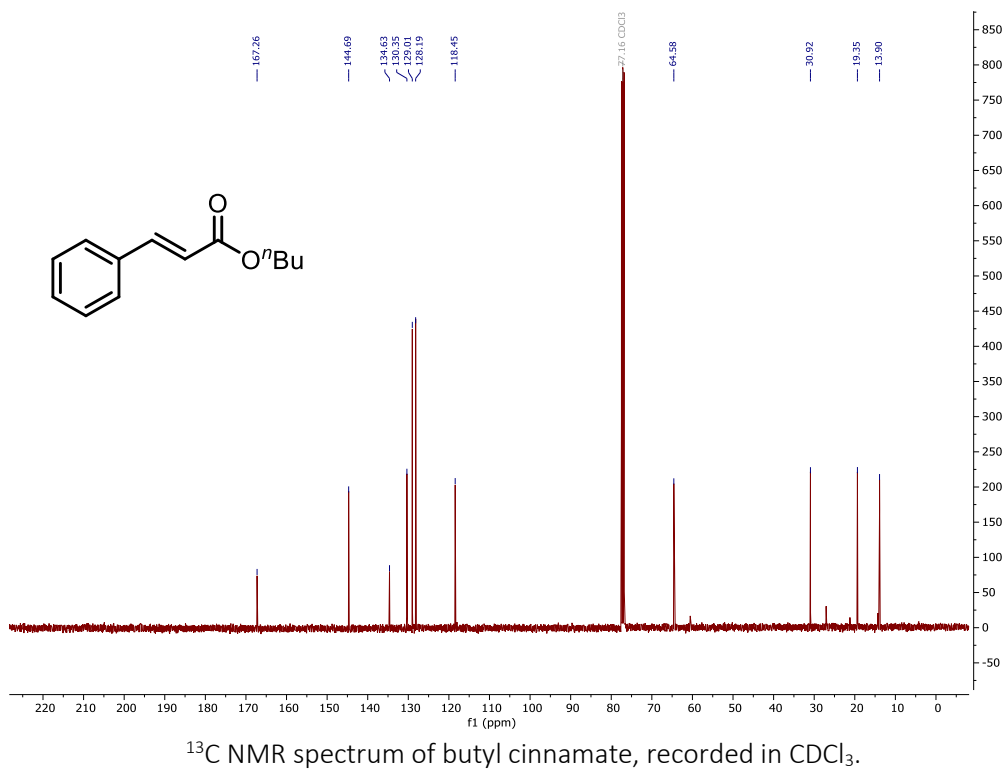
Ap.1.1 Chapter 2

Butyl Cinnamate

Spectra consistent with reports from previous literature.⁷⁶

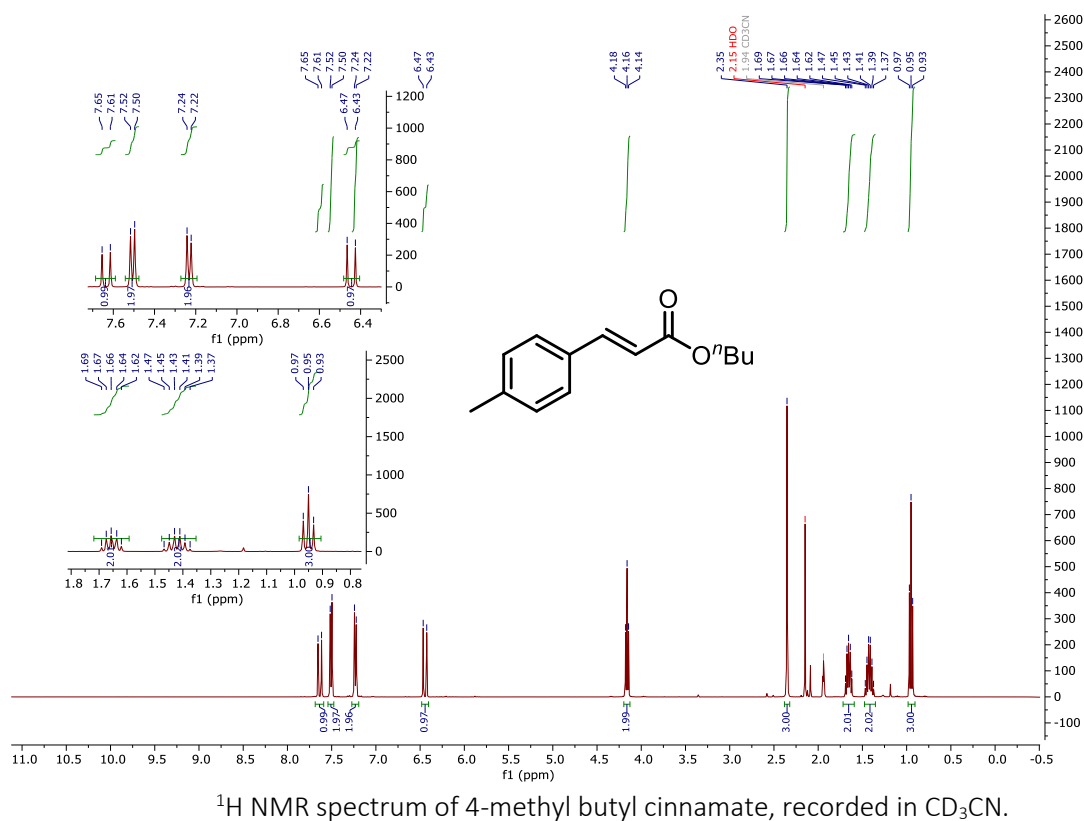


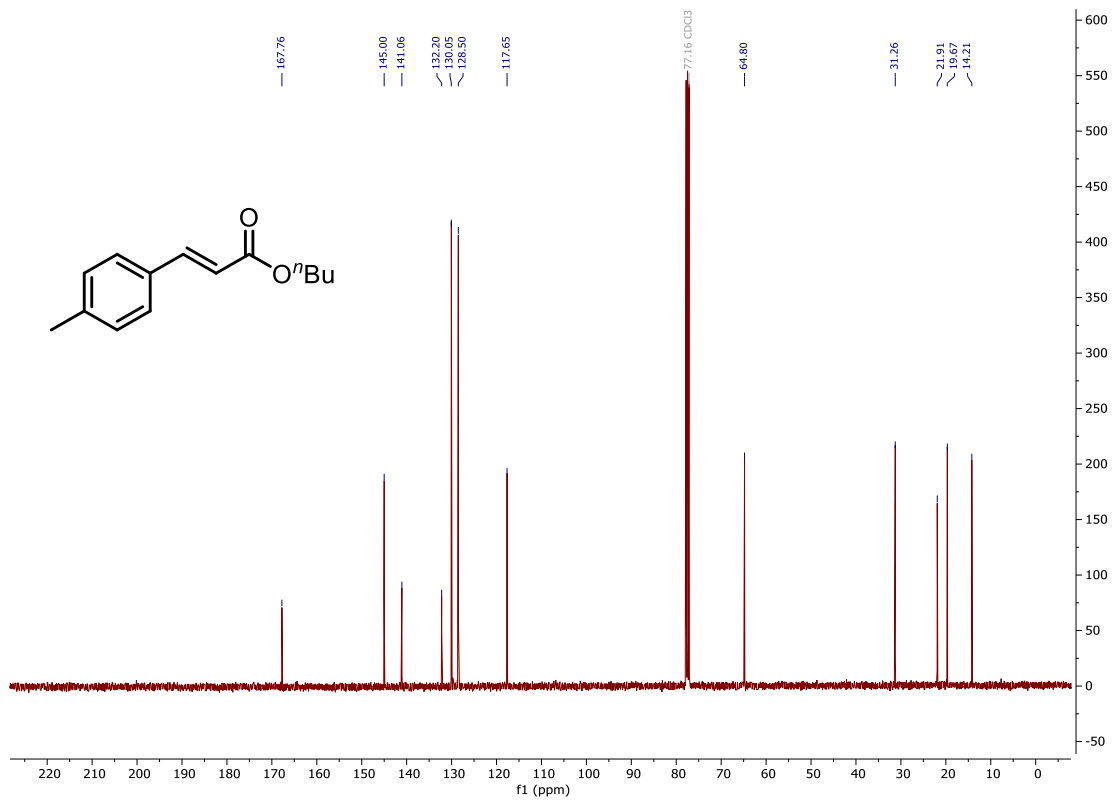
¹H NMR spectrum of butyl cinnamate, recorded in CDCl₃.



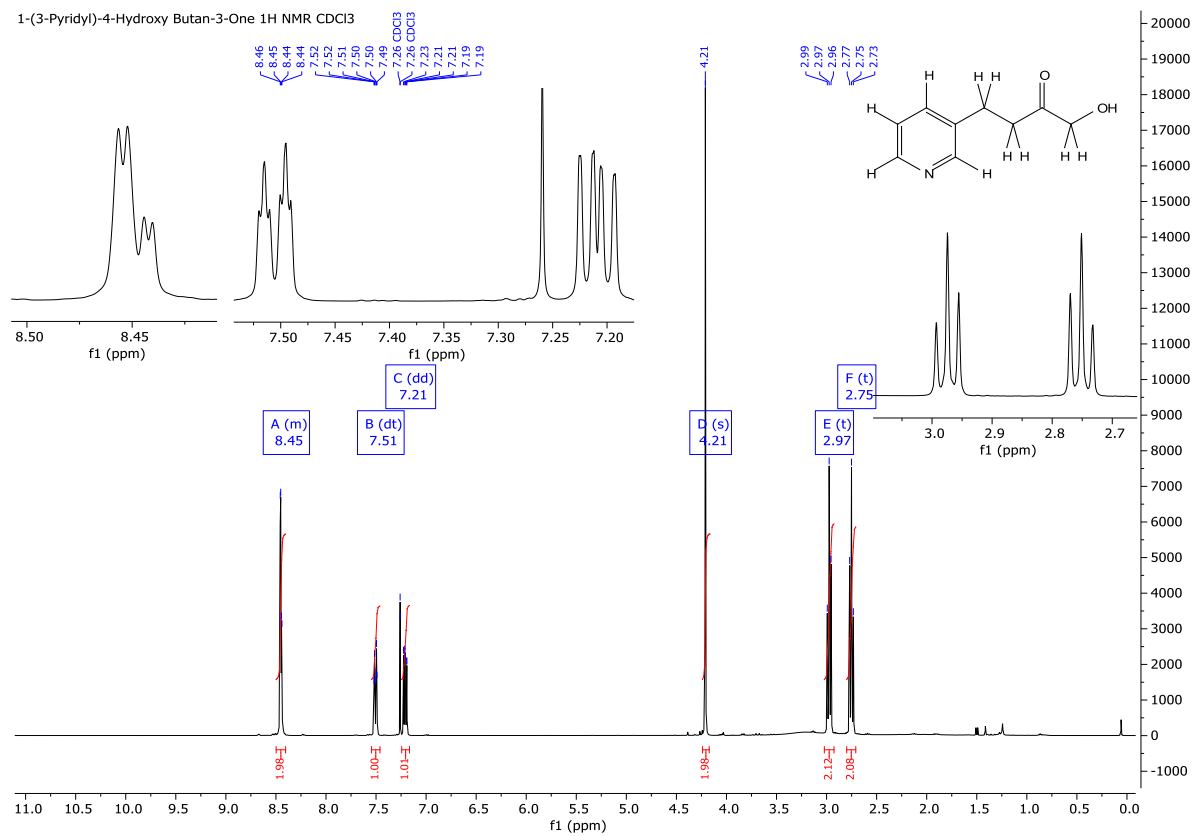
4-Methyl Butyl Cinnamate

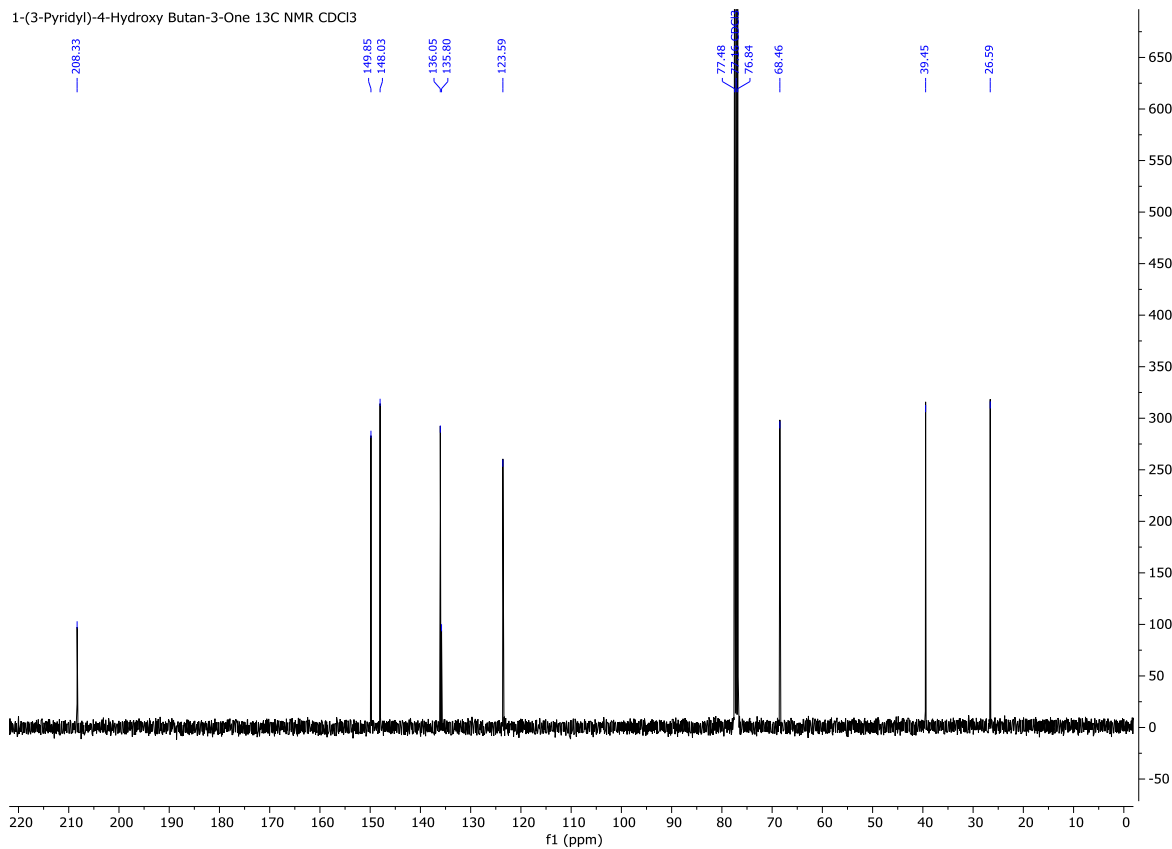
Spectra consistent with reports from previous literature.⁷⁶



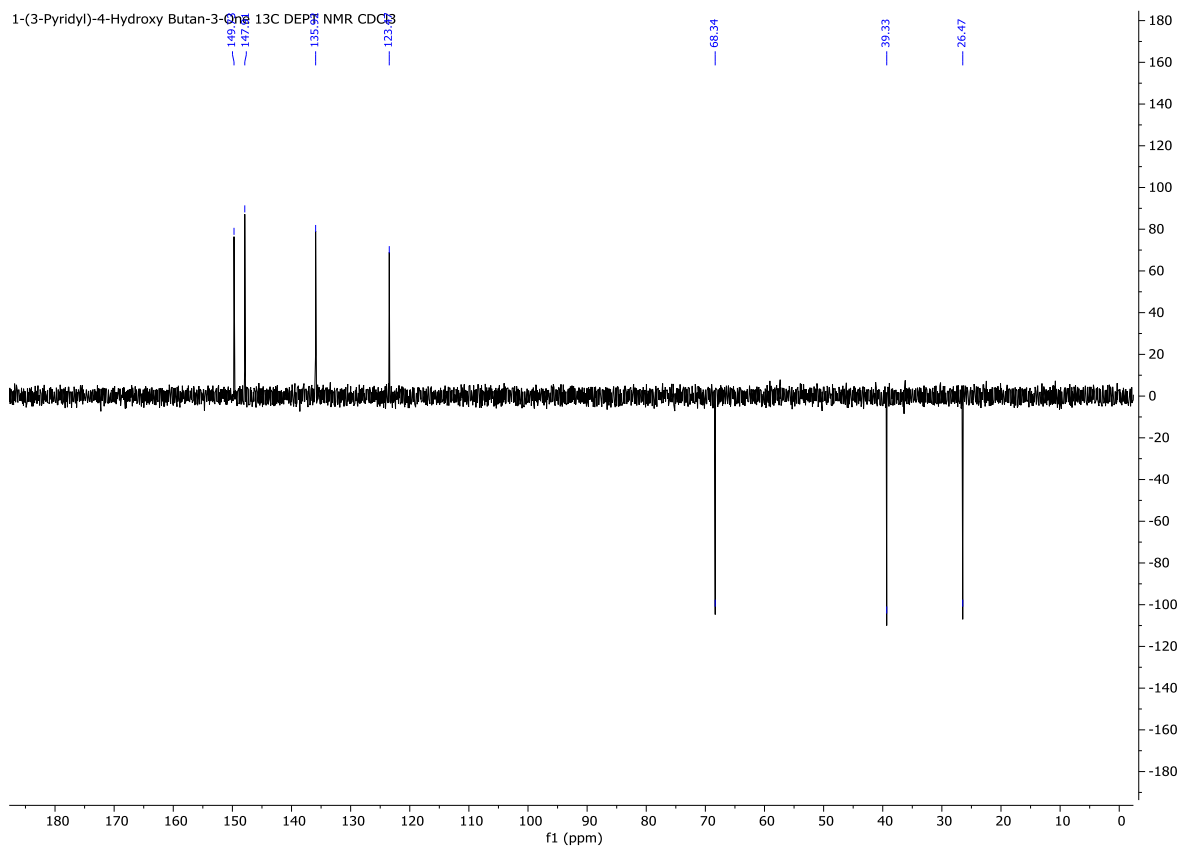


Ap.1.2 Chapter 3

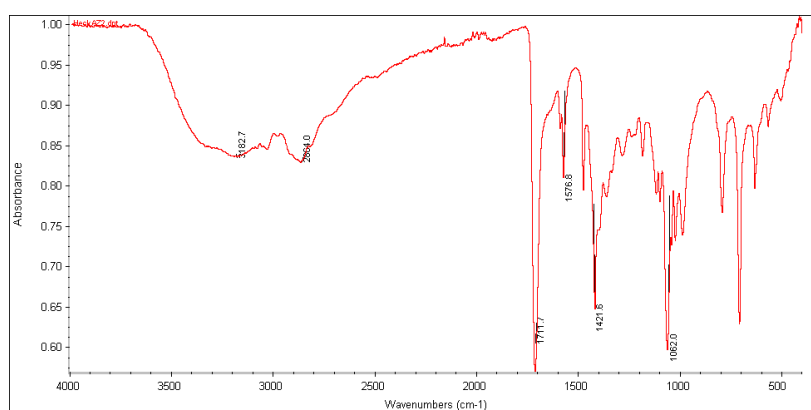




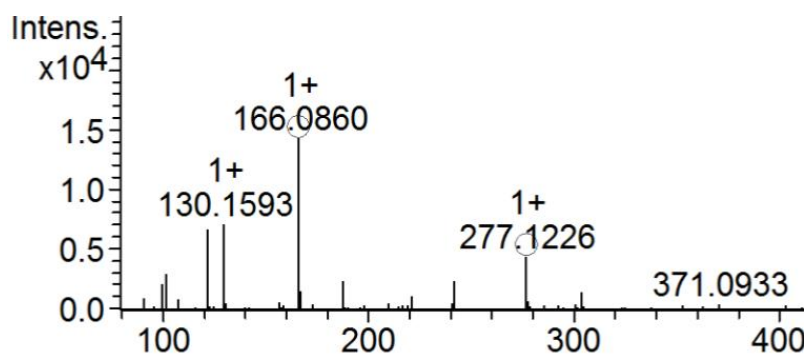
¹³C NMR spectrum of HPBO, recorded in CDCl₃.



¹³C DEPT NMR spectrum of HPBO, recorded in CDCl₃.



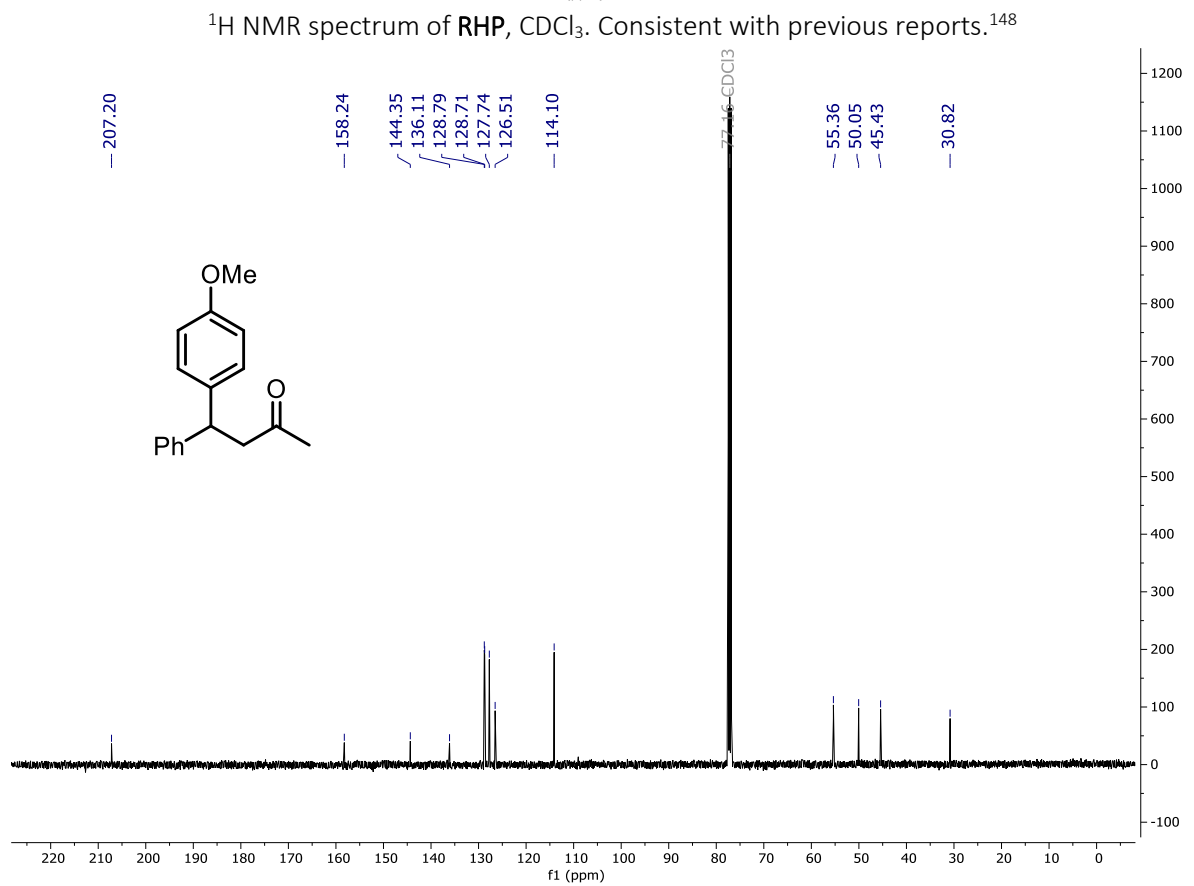
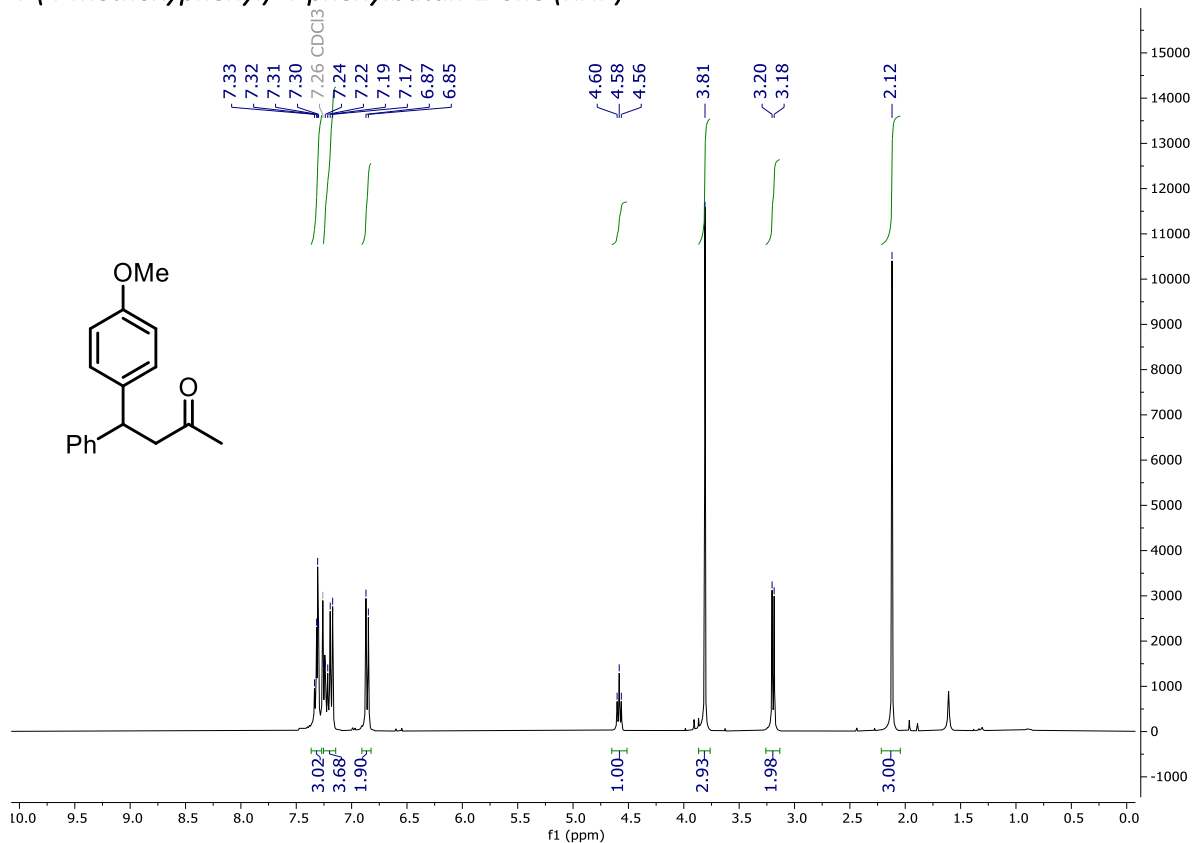
ATR IR spectrum of **HPBO**, recorded as a thin film, evidencing the presence of the C=O group in the product (1712 cm^{-1}) and the OH group (broad stretch, $\sim 3000\text{-}3500\text{ cm}^{-1}$).



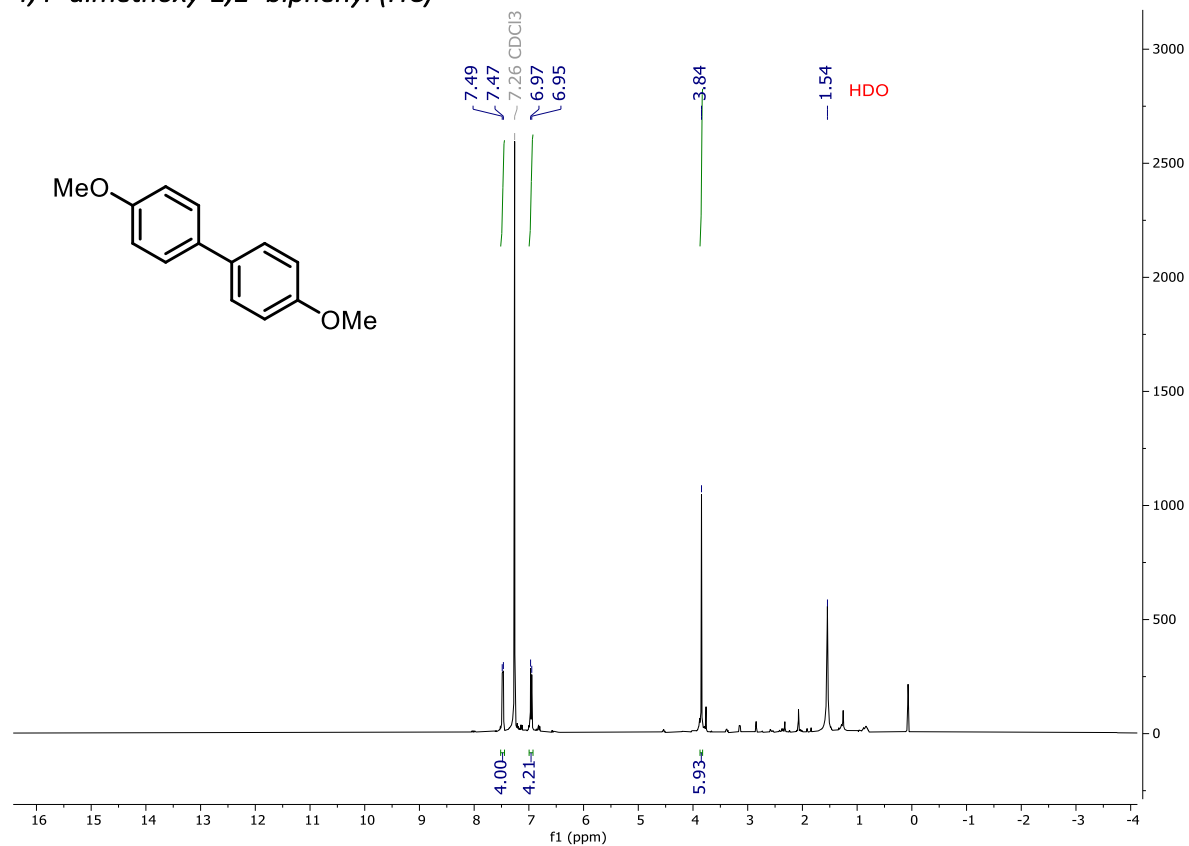
Mass spectrum of **HPBO**, recorded in MeCN, using electrospray ionisation.

Ap.1.3 Chapter 4

4-(4-methoxyphenyl)-4-phenylbutan-2-one (RHP)



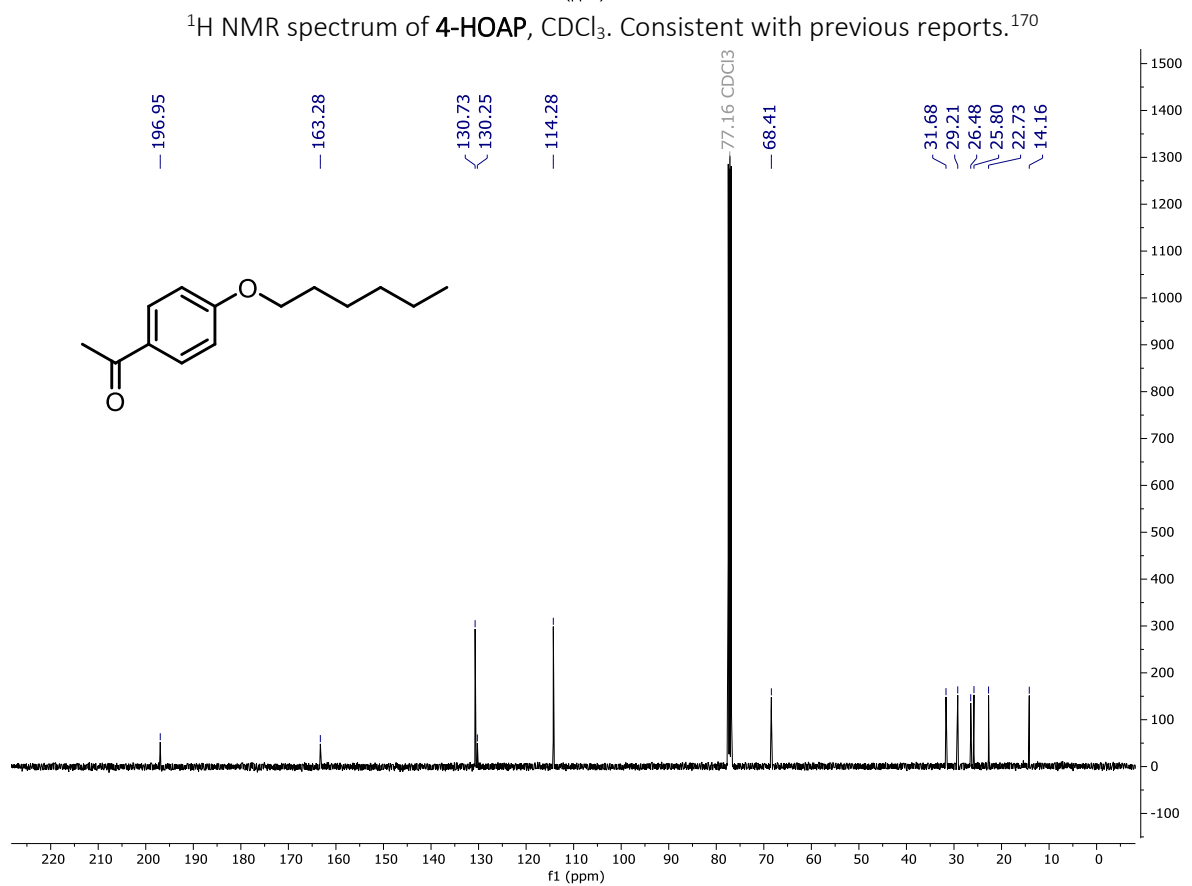
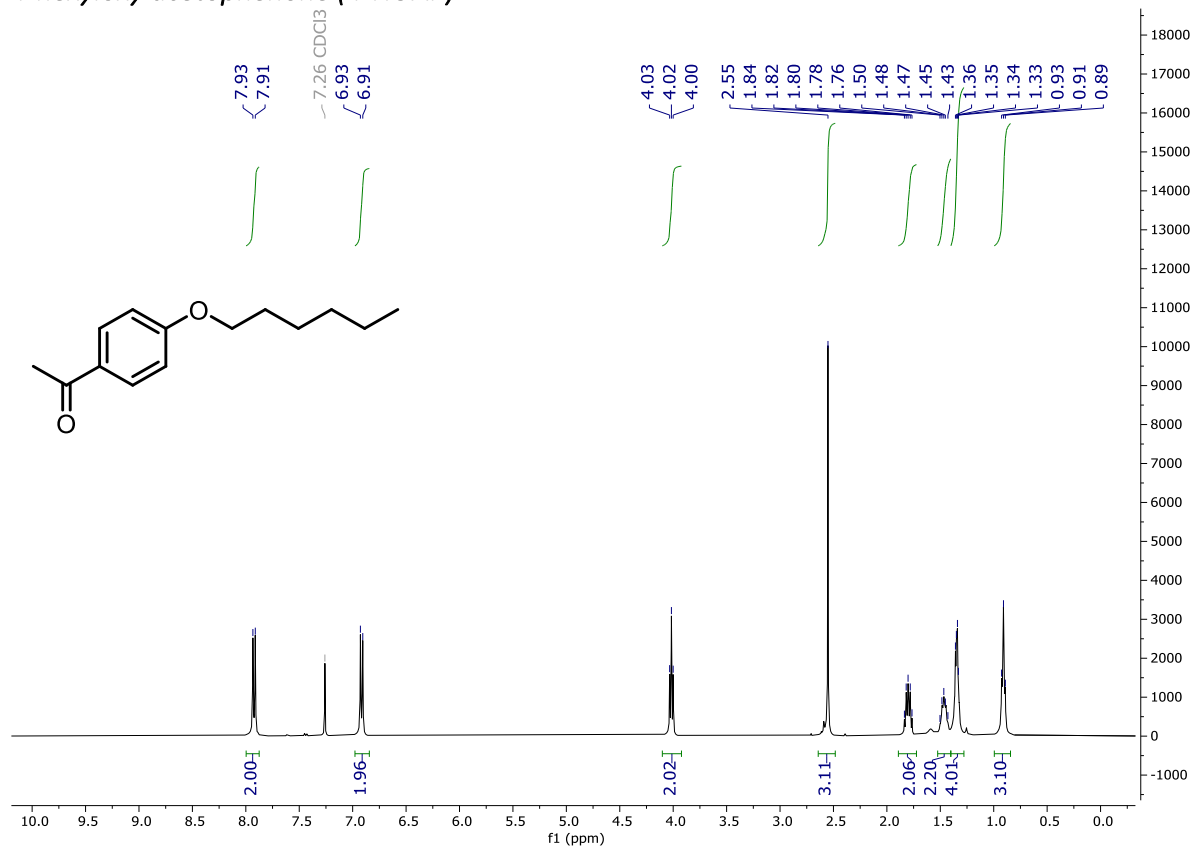
4,4'-dimethoxy-1,1'-biphenyl (HC)



¹H NMR spectrum of HC, CDCl₃ (isolated as a minor side-product, contaminated with water and greasy impurities).

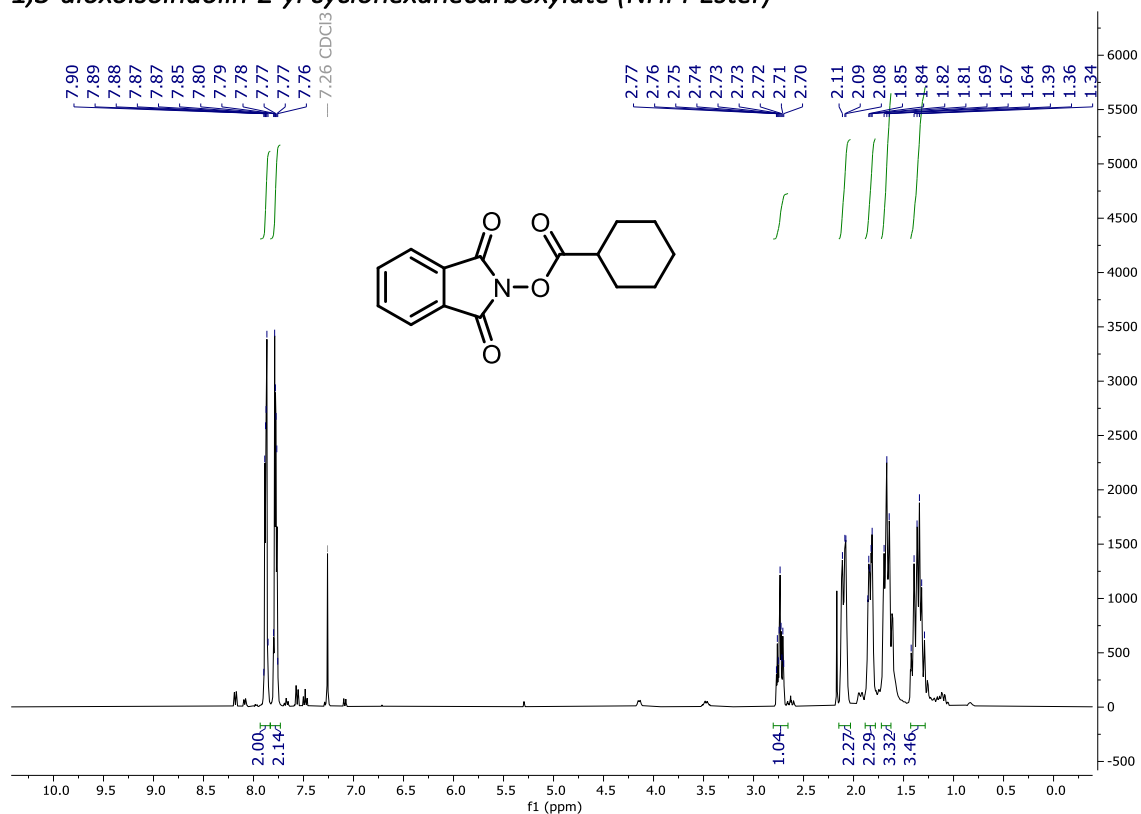
Ap.1.4 Chapter 5

4-hexyloxy acetophenone (4-HOAP)

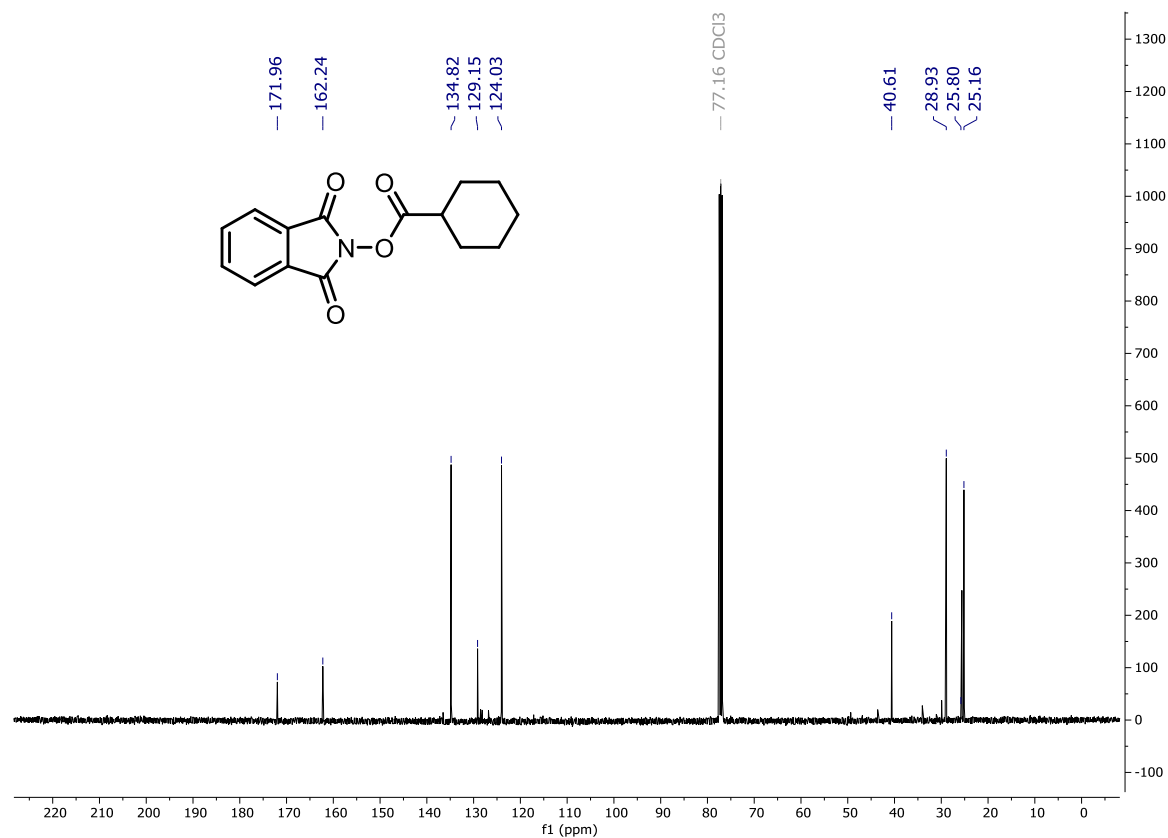


Ap.1.5 Chapter 6

1,3-dioxisoindolin-2-yl cyclohexanecarboxylate (NHPI-Ester)

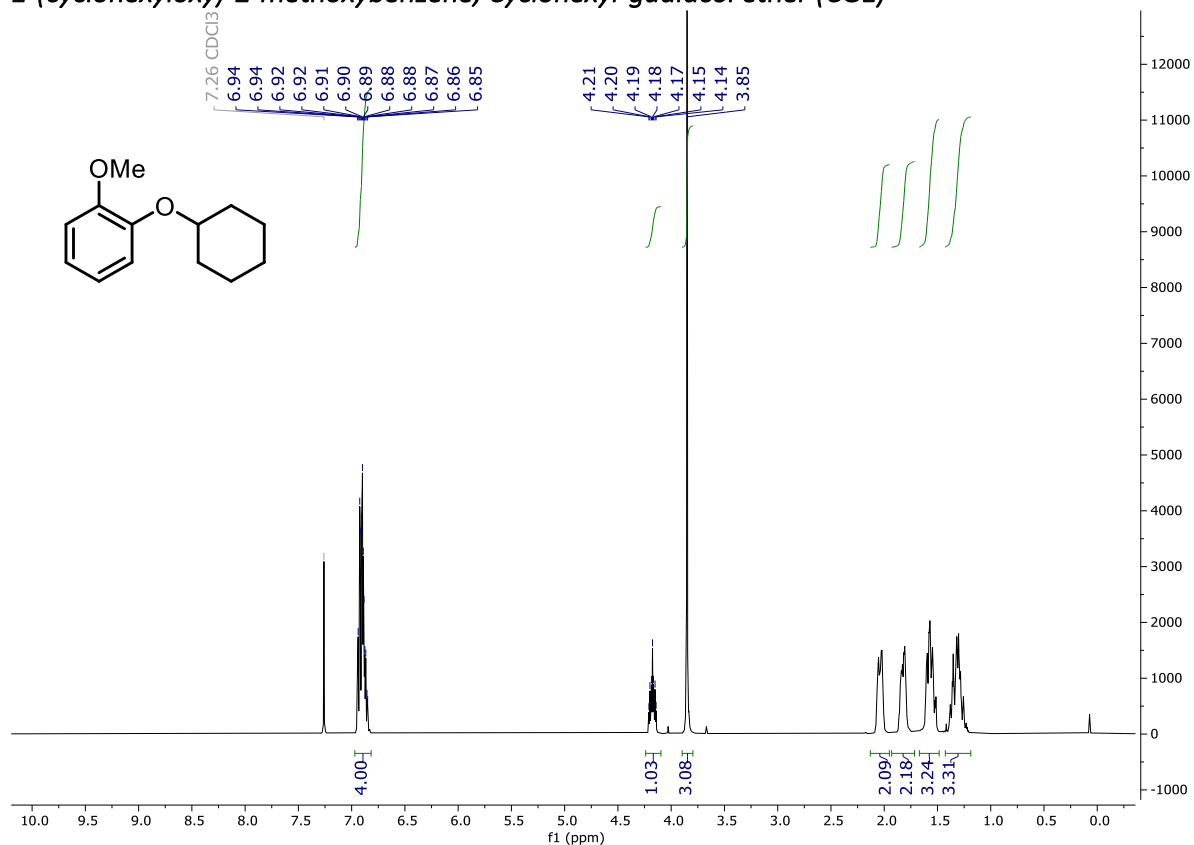


¹H NMR spectrum of NHPI, CDCl₃. Consistent with previous reports.²⁶⁴

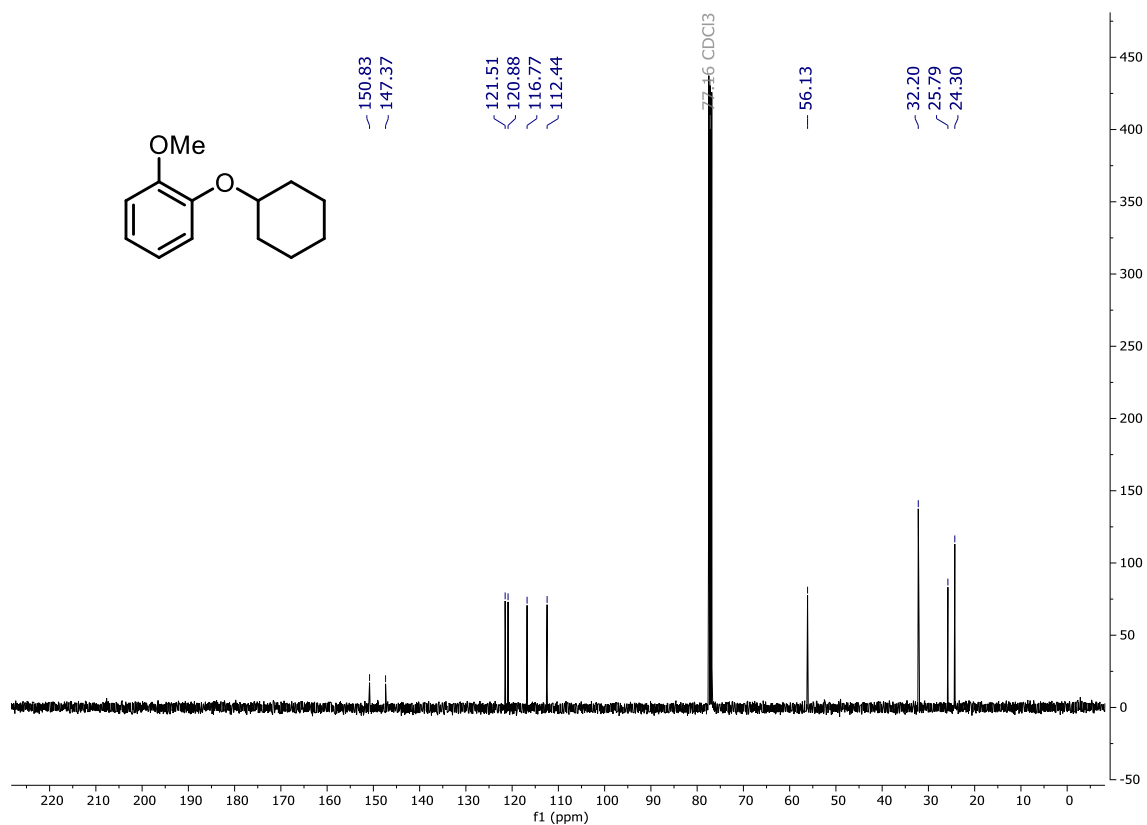


¹³C NMR spectrum of NHPI, CDCl₃. Consistent with previous reports.²⁶⁴

1-(cyclohexyloxy)-2-methoxybenzene, Cyclohexyl-guaiacol ether (CGE)



^1H NMR spectrum of CGE, CDCl₃. Consistent with previous reports.²¹⁸



^{13}C NMR spectrum of CGE, CDCl₃. Consistent with previous reports.²¹⁸

Ap.2 Analytical Yield Quantification (GC or ¹H NMR)

Ap.2.1 Chapter 2

Ap.2.1.1 GC Data for Butyl Cinnamate Yield Butyl Acrylate Conversion Quantification

Reported yields were GC analytical yields calculated using a calibration plot approach (details below). A Supelco SPB-170 column was used (described in the Experimental Chapter). The GC method used involved a temperature gradient from 50 °C to 300 °C, over 12.5 min, then holding at 300 °C for a further 5 min. Flame ionisation detection was used, with a temperature of 300 °C, and a 4 µL injection volume of sample (50.0 split ratio). He was used as the carrier gas (column flow rate of 1.36 mL min⁻¹). Reported yields were an average from replicate (usually triplicate) samples and quoted estimated uncertainties were the discrepancy between the reported average and the sample furthest away from the average.

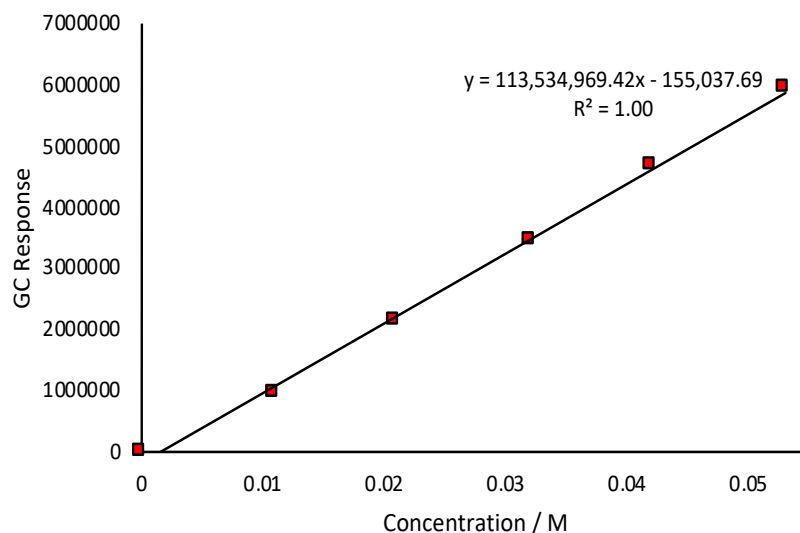
The conc. of starting solution was 0.43 M (*w.r.t.* **IB**), in all cases, as determined by the mass of **IB** added, and the total measured volume after addition of all reagents. Triplicate samples of ~0.5 mL were taken from the product solution to give crude reaction mixture samples. 0.1 mL aliquots of each sample were then taken and each was diluted in a further 1.0 mL MeOH to give a total GC sample volume of 1.1 mL. Yield was then calculated, using the calibration plot data, below. Conversion was quantified by calculating the ratio of the response of the limiting reagent signal in the product solution, and starting material solutions. Again, three 0.1 mL samples of starting solution were taken and diluted in 1 mL MeOH, prior to GC analysis. Yields were calculated as follows:

$$c_1 = \frac{y + 155038}{113500000}$$

$$c_2 = \frac{c_1 \times V_1}{V_2}$$

$$Yield = \frac{c_2}{c_{SM}} \times 100\%$$

Where: c_1 is the concentration of product in the GC solution, y is the response factor of product in the GC solution, c_2 is the concentration of product in the crude product solution *prior to dilution* for the GC sample, V_1 is the volume of the GC solution, prepared from the crude product sample *via* dilution in MeOH (1.1 mL in all cases in the table below), V_2 is the volume of crude product sample used, *prior to dilution* for the GC sample. (0.1 mL in all cases in the table below), c_{sm} is the concentration of the starting material solution used for the reaction – as the stoichiometric ratio between aryl halide and product is 1:1, this can be taken as a theoretical maximum yield of product obtainable.



GC calibration plot for butyl cinnamate.

Conversion was quantified by calculating the ratio (and then expressing as a percentage) of the response of the limiting reagent (iodobenzene) signal in the crude product solution (the same samples as those taken to determine the yield) and starting material solutions. Again, three 0.1 mL samples of starting solution were taken and diluted in 1 mL MeOH, prior to GC analysis (an average of three starting material samples was used for comparison against the limiting starting material signal in the crude product mixture). Again, the reported conversion was the average from the replicate samples and the estimated uncertainty was from the discrepancy between the average and the measurement furthest away from the average.

Ap.2.1.2 NMR Quantification Detail

¹H NMR spectroscopy was used to quantify the yields from initial work in the Vapourtec reactor, for model reactions between butyl acrylate with iodobenzene or 4-iodotoluene. Samples were taken in triplicate from the reaction and analysed as the crude reaction mixture.

From these spectra, yields were calculated using an external standard method, with the equations used detailed below. In all cases, 1,4-dinitrobenzene was used as the standard, with a sharp singlet at around 8.4 ppm. In the spectra, the integral trace for this singlet was set to 4.00. From this, the yields were determined from the integral traces of analyte (starting materials and products) signals relative to this signal, using the following equation:

$$n_x = n_{ES} \times \frac{I_x}{I_{ES}} \times \frac{H_{ES}}{H_x}$$

The terms in this equation are as follows: n_x is the number of moles of analyte (starting material or product), n_{ES} is the number of moles of external standard added to the NMR solution of crude product, I_x is the integral trace of the analyte NMR signal of interest, I_{ES} is the integral trace of the external standard NMR signal of interest, here, this was set to 4.00, being the signal around 8.4 ppm for 1,4-dinitrobenzene, H_{ES} is the number of protons responsible for the external standard NMR signal of interest, H_x is the number of protons responsible for the analyte NMR signal of interest.

The yield was then quantified by dividing the n_x determined by the number of moles of starting material (aryl halide) expected in a sample of the same volume, if the sample were to have been taken from the starting solution prior to reaction (then multiplied by 100 to give a percentage), rather than from the product outlet stream. For the analytes in the reactions studied by ^1H NMR spectroscopy in this work, the following signals were used to quantify yields:

Species	NMR Signal Used for Analysis
Iodobenzene	t, 7.08 ppm
Butyl Cinnamate (PhI Starting Material)	m, 7.50 ppm
4-Iodotoluene	d, 7.54 ppm
4-Methyl Butyl Cinnamate	d, 7.63 ppm

Ap.2.2 Chapter 3

Ap.2.2.1 GC Yield Analysis of 4PBO

Reported yields were GC analytical yields calculated using a calibration plot approach (details below). A Supelco SPB-170 column was used (described in the Experimental Chapter). The GC method used involved a temperature gradient from 50 °C to 300 °C, over 12.5 min, then holding at 300 °C for a further 10 min. Flame ionisation detection was used, with a temperature of 300 °C, and a 4 μL injection volume of sample (50.0 split ratio). He was used as the carrier gas (column flow rate of 1.36 mL min^{-1}). Reported yields were an average from replicate (usually triplicate) samples and quoted estimated uncertainties were the discrepancy between the reported average and the sample furthest away from the average.

In all cases, the conc. of starting solution was 0.48 M (*w.r.t.* **3IP**), in all cases, as determined by the mass of **3IP** added, and the total measured volume after addition of all reagents. Triplicate samples of ~0.5 mL were taken from the product solution to give crude reaction mixture samples. 0.1 mL aliquots of each sample were then taken and each was diluted in a further 1.0 mL MeOH to give a total GC sample volume of 1.1 mL. Yield was then calculated, using the calibration plot data, below. Yields were calculated as follows:

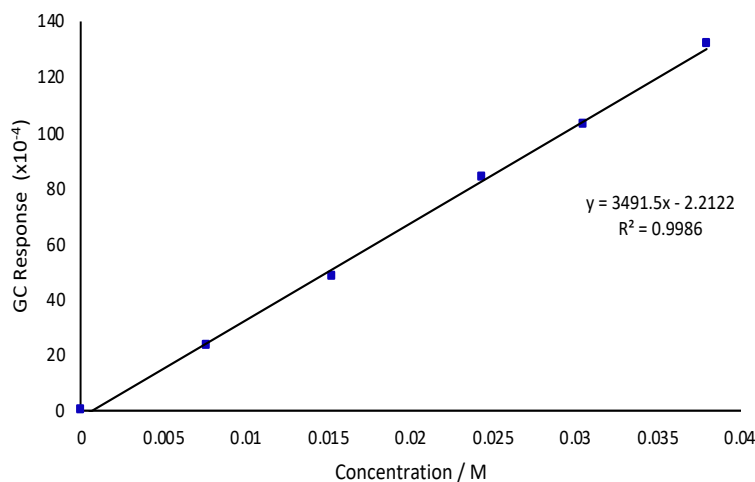
$$c_1 = \frac{y + 22122}{34915000}$$

$$c_2 = \frac{c_1 \times V_1}{V_2}$$

$$\text{Yield} = \frac{c_2}{c_{SM}} \times 100\%$$

Where: c_1 is the concentration of product in the GC solution, y is the response factor of product in the GC solution, c_2 is the concentration of product in the crude product solution *prior to dilution* for the GC sample, V_1 is the volume of the GC solution, prepared from the crude product sample *via* dilution in MeOH (1.1 mL in all cases), V_2 is the volume of crude product sample used, *prior to dilution* for the GC sample. (0.1 mL in all cases), c_{sm} is the concentration of the starting material solution used for the

reaction – as the stoichiometric ratio between aryl halide and product is 1:1, this can be taken as a theoretical maximum yield of product obtainable.



GC calibration plot for 4PBO.

Ap.2.2.2 GC Conversion Analysis of 3IP

Conversion was quantified by calculating the ratio (and then expressing as a percentage) of the response of the limiting reagent (**3IP**) signal in the crude product solution (the same samples as those taken to determine the yield) and starting material solutions. Again, three 0.1 mL samples of starting solution were taken and diluted in 1 mL MeOH, prior to GC analysis (an average of three starting material samples was used for comparison against the limiting starting material signal in the crude product mixture). Again, the reported conversion was the average from the replicate samples and the estimated uncertainty was from the discrepancy between the average and the measurement furthest away from the average.

Ap.2.3 Chapter 4

Ap.2.3.1 GC Yield Analysis of RHP

Reported yields were GC analytical yields calculated using a calibration plot approach (details below). A Supelco Equity-1701 column was used (described in the Experimental Chapter). The GC method used involved a temperature gradient from 50 °C to 280 °C, over 15 min, then holding at 280 °C for a further 5 min. Flame ionisation detection was used, with a temperature of 300 °C, and a 4 μ L injection volume of sample (50.0 split ratio). He was used as the carrier gas (column flow rate of 1.36 mL min⁻¹). Reported yields were an average from replicate (usually triplicate) samples and quoted estimated uncertainties were the discrepancy between the reported average and the sample furthest away from the average. Reported conversions were also averaged from the same replicate samples (as well as replicate samples of the starting material solution). Again, the reported conversion was the average from the replicate samples and the estimated uncertainty was from the discrepancy between the average and the measurement furthest away from the average.

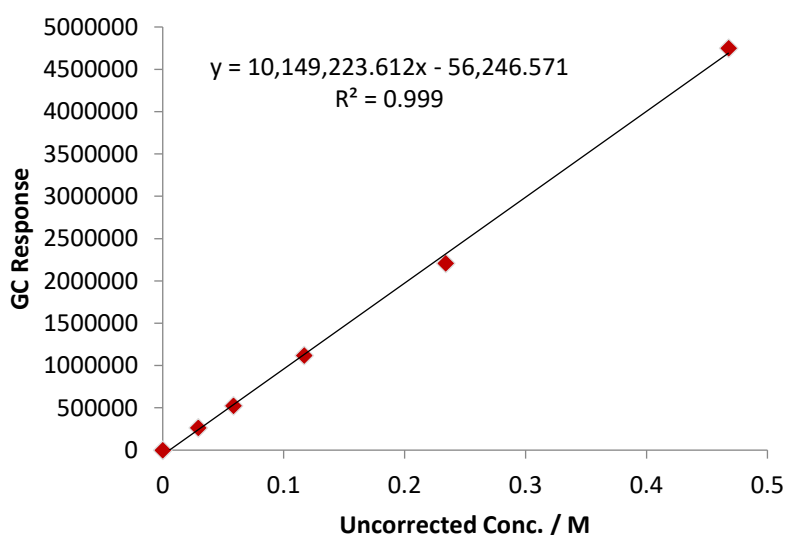
Starting material concentrations were determined from the weight of the limiting reagent and the total volume (measured after addition of reagents/solvent). Triplicate samples of \sim 0.5 mL were taken from the product solution to give crude reaction mixture samples. 0.1 mL aliquots of each sample were then

taken and each was diluted in a further 1.0 mL MeOH to give a total GC sample volume of 1.1 mL. Yield was then calculated, using the calibration plot data, below. Yields were calculated as follows:

$$c_{crude} = \frac{y + 56247}{10149224}$$

$$Yield = \frac{c_{crude}}{c_{SM}} \times 100\%$$

Where: c_{crude} is the concentration of product in crude mixture, y is the response factor of product of the analysed GC solution, c_{sm} is the concentration of the starting material solution used for the reaction – taken as a theoretical maximum yield of product obtainable, determined from the weight of limiting reagent added and the measured volume of starting solution.



GC calibration plot for RHP. Uncorrected conc. refers to the method for obtaining the calibration data where stock solutions were prepared (to a desired concentration in MeOH) which were then diluted further by taking 0.1 mL of stock solution and dissolving in an additional 1.0 mL neat MeOH. Uncorrected concentration refers to the stock solution concentration before addition of the additional 1.0 mL MeOH, taken in order to simplify yield calculations.

Ap.2.3.2 GC Conversion Analysis of HPBO (or 4IA)

Conversion was quantified by calculating the ratio (and then expressing as a percentage) of the response of the limiting reagent (HPBO or 4IA) signal in the crude product solution (the same samples as those taken to determine the yield) and starting material solutions. Again, three 0.1 mL samples of starting solution were taken and diluted in 1 mL MeOH, prior to GC analysis (an average of three starting material samples was used for comparison against the limiting starting material signal in the crude product mixture). Again, the reported conversion was the average from the replicate samples and the estimated uncertainty was from the discrepancy between the average and the measurement furthest away from the average.

Ap.2.4 Chapter 5

Ap.2.4.1 GC Yield Analysis of 4-HOAP

Reported yields were GC analytical yields calculated using a calibration plot approach (details below). A Supelco Equity-1701 column was used (described in the Experimental Chapter). The GC method used involved a temperature gradient from 50 °C to 280 °C, over 15 min, then holding at 280 °C for a further 5 min. Flame ionisation detection was used, with a temperature of 300 °C, and a 4 µL injection volume of sample (50.0 split ratio). He was used as the carrier gas (column flow rate of 1.36 mL min⁻¹). Reported yields were an average from replicate (usually triplicate) samples and quoted estimated uncertainties were the discrepancy between the reported average and the sample furthest away from the average.

Starting material (**4-BrAP**) concentrations were determined also using a GC method. Two calibration plots for both **4-HOAP** and **4-BrAP** were obtained, due to changing GC method during the course of the work. The calibration plots are given below alongside an example calculation of how yields were calculated. **4-BrAP** concentrations were determined as follows:

$$c_{SM} = \frac{y - 42338}{4672563}$$

Equations for yield determination using the Supelco Equity-1701 column and corresponding method.

$$c_{SM} = \frac{y + 5308}{6732304}$$

Equations for yield determination using the Supelco SPB-170 column and corresponding method.

Where y is the response factor of product of the analysed GC solution, c_{sm} is the concentration of the **4-BrAP** in the starting material solution used for the reaction (used as the theoretical maximum yield obtainable for **4-HOAP**).

Sampling involved taking replicate (usually triplicate) samples of ~0.5 mL from the product solution to give crude reaction mixture samples, or from the starting material solution for determination of starting concentration. 0.1 mL aliquots of each sample were then taken and each was diluted in a further 1.0 mL MeOH to give a total GC sample volume of 1.1 mL. Yield was then calculated, using the calibration plot data, below. Yields were calculated as follows:

$$c_{crude} = \frac{y + 47273}{7673880}$$

$$Yield = \frac{c_{crude}}{c_{SM}} \times 100\%$$

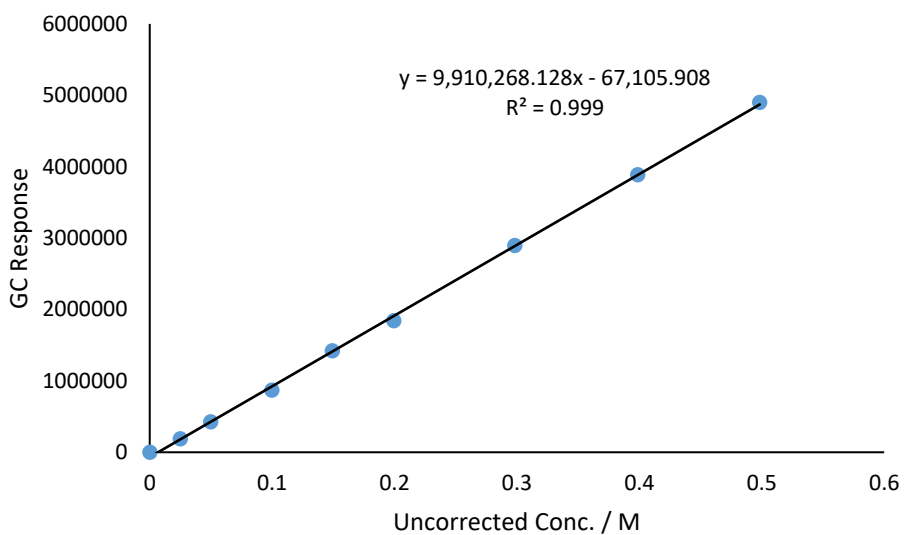
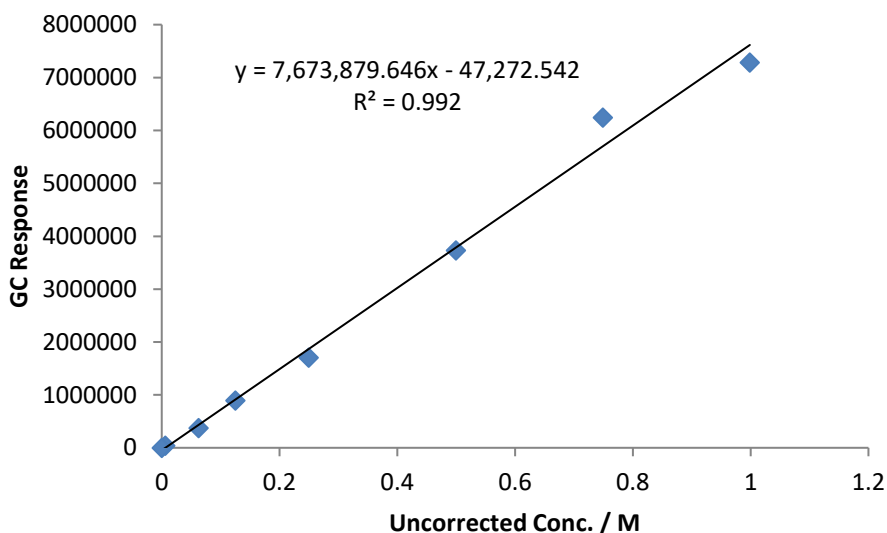
Equations for yield determination using the Supelco Equity-1701 column and corresponding method.

$$c_{crude} = \frac{y + 67106}{9910268}$$

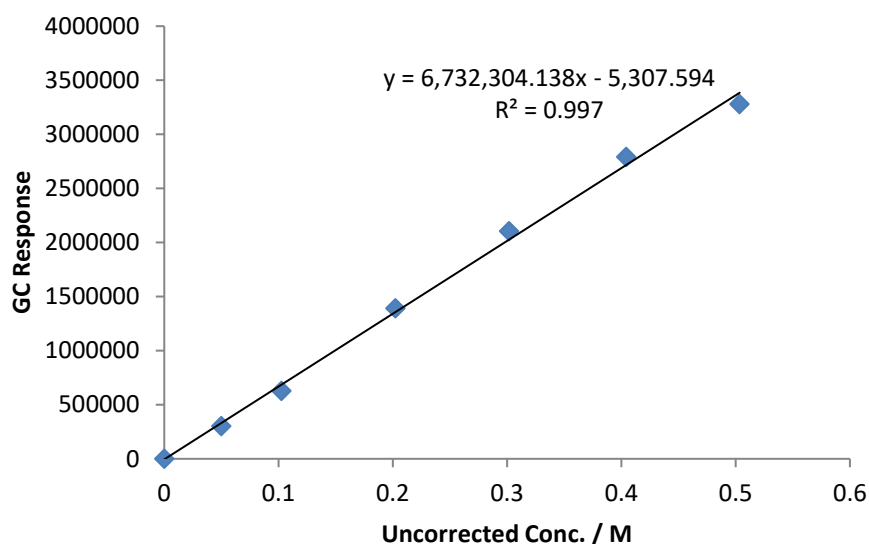
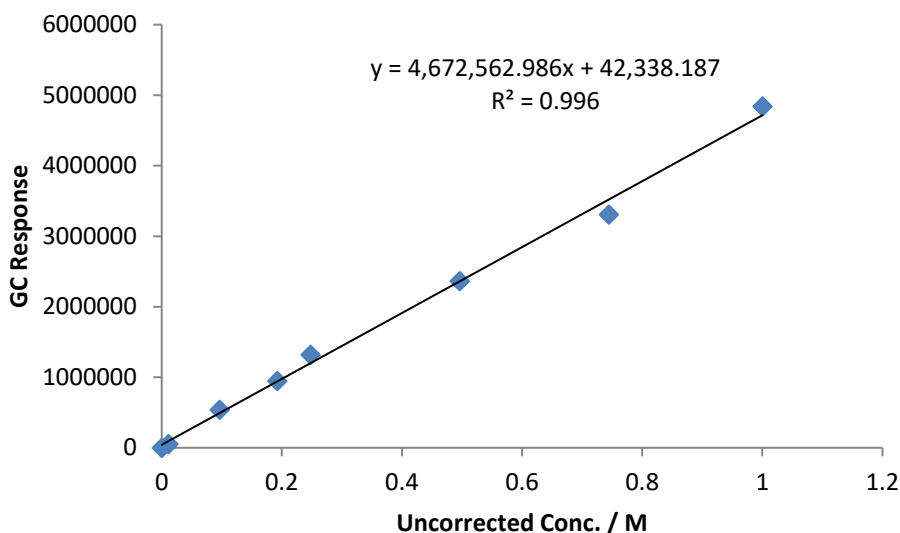
$$Yield = \frac{c_{crude}}{c_{SM}} \times 100\%$$

Equations for yield determination using the Supelco SPB-170 column and corresponding method.

Where: c_{crude} is the concentration of product in crude mixture, calculated using the calibration plot (below), y is the response factor of product of the analysed GC solution, c_{sm} is the concentration of the starting material solution used for the reaction – taken as a theoretical maximum yield of product obtainable, determined from 0.1 mL starting solution samples in a further 1.0 mL MeOH, using the calibration plots for **4-BrAP**, below.



GC calibration plots for **4-HOAP**, for the Equity-1701 column (above) and SPB-170 column (below). *Uncorrected conc. refers to the method for obtaining the calibration data where, as noted, stock solutions were prepared (to a desired concentration in MeOH) which were then diluted further by taking 0.1 mL of stock solution and dissolving in an additional 1.0 mL neat MeOH. Uncorrected concentration refers to the stock solution concentration before addition of the additional 1.0 mL MeOH, taken in order to simplify yield calculations.*



GC calibration plots for **4-BrAP**, for the Equity-170 column (above) and SPB-170 column (below). Uncorrected conc. refers to the method for obtaining the calibration data where, as noted, stock solutions were prepared (to a desired concentration in MeOH) which were then diluted further by taking 0.1 mL of stock solution and dissolving in an additional 1.0 mL neat MeOH. Uncorrected concentration refers to the stock solution concentration before addition of the additional 1.0 mL MeOH, taken in order to simplify yield calculations.

Ap.2.3.2 GC Conversion Analysis of 4-BrAP

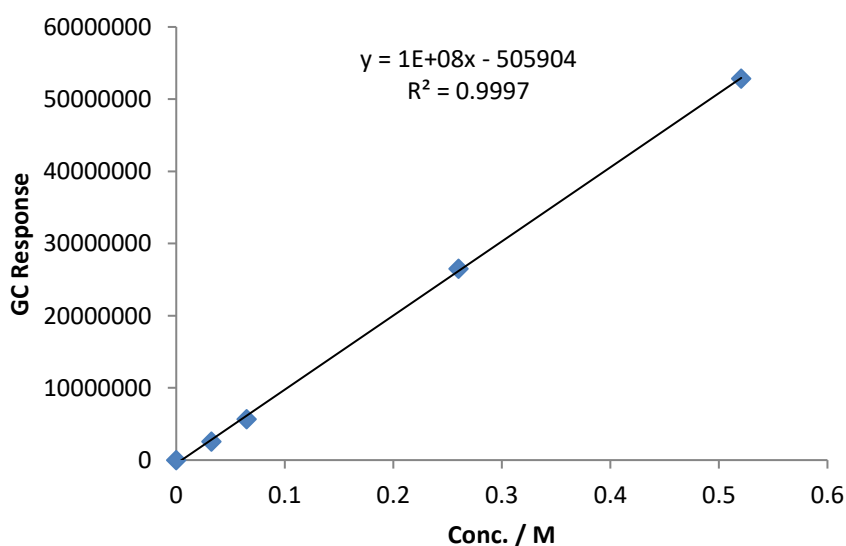
Conversion was quantified by calculating the ratio (and then expressing as a percentage) of the response of the limiting reagent (**4-BrAP**) signal in the crude product solution (the same samples as those taken to determine the yield) and starting material solutions. Again, three 0.1 mL samples of starting solution were taken and diluted in 1 mL MeOH, prior to GC analysis (an average of three starting material samples was used for comparison against the limiting starting material signal in the crude product mixture). Again, the reported conversion was the average from the replicate samples and the estimated uncertainty was from the discrepancy between the average and the measurement furthest away from the average.

Ap.2.5 Chapter 6

Ap.2.5.1 GC Yield Analysis of CGE

Reported yields were GC analytical yields calculated using a calibration plot approach (details below). A Supelco Equity-1701 column was used (described in the Experimental Chapter). The GC method used involved a temperature gradient from 50 °C to 280 °C, over 15 min, then holding at 280 °C for a further 5 min. Flame ionisation detection was used, with a temperature of 300 °C, and a 4 µL injection volume of sample (50.0 split ratio). He was used as the carrier gas (column flow rate of 1.36 mL min⁻¹). Reported yields were an average from replicate (usually triplicate) samples and quoted estimated uncertainties were the discrepancy between the reported average and the sample furthest away from the average. Reported conversions were also averaged from the same replicate samples (as well as replicate samples of the starting material solution). Again, the reported conversion was the average from the replicate samples and the estimated uncertainty was from the discrepancy between the average and the measurement furthest away from the average.

Starting material concentrations were determined from the weight of the limiting reagent and the total volume (calculated from addition of the volumes of liquid reagents/solvent added). Triplicate samples of >0.5 mL were taken from the product solution to give crude reaction mixture samples. 0.1 mL aliquots of each sample were then taken and each was diluted in a further 1.0 mL DCM to give a total GC sample volume of 1.1 mL. Alternatively, 0.5 mL aliquots of each sample were taken and 0.5 mL DCM added to give a total GC sample volume of 1.0 mL. Yield was then calculated, using the calibration plot data, below. Yields were calculated as follows:



GC calibration plot for CGE.

$$c_1 = \frac{x + 505904}{10^8}$$

$$c_2 = \frac{c_1 \times V_1}{V_2}$$

$$Yield = \frac{c_2}{c_{SM}} \times 100\%$$

Where: c_1 is the concentration of product in the GC solution, x is the response factor of product in the GC solution, c_2 is the concentration of product in the crude product solution *prior to dilution* for the GC sample, V_1 is the volume of the GC solution, prepared from the crude product sample *via* dilution in DCM (1.1 or 1.0 mL in all cases), V_2 is the volume of crude product sample used, *prior to dilution* for the GC sample. (0.1 mL or 0.5 mL in all cases), c_{sm} is the concentration of the starting material solution used for the reaction – as the stoichiometric ratio between NHPI-ester and alkyl-aryl ether product is 1:1, this can be taken as a theoretical maximum yield of product obtainable.

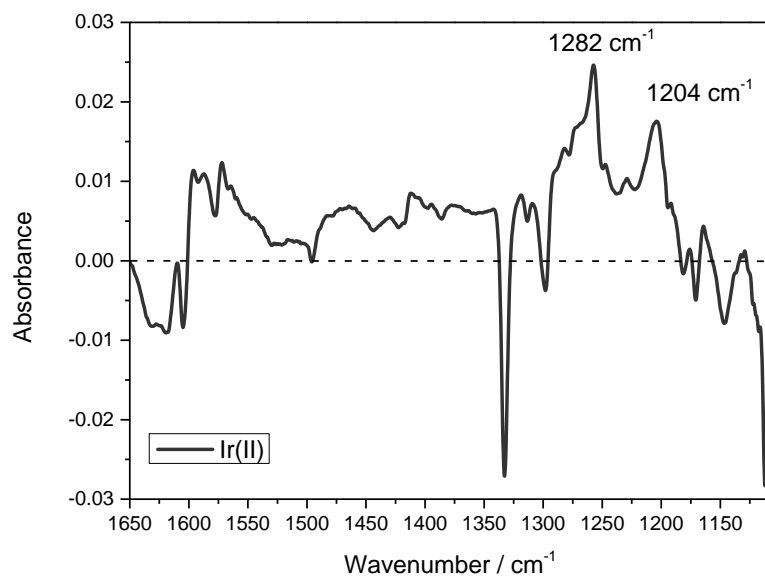
Ap.2.5.2 GC Conversion Analysis of NHPI-Ester

Conversion was quantified by calculating the ratio (and then expressing as a percentage) of the response of the limiting reagent (NHPI-ester) signal in the product solution and starting material solutions. Again, three 0.1 mL samples of starting solution were taken and diluted in 1 mL DCM, prior to GC analysis (an average of three starting material samples was used for comparison against the limiting starting material signal in the crude product mixture). Alternatively, 0.5 mL samples of starting solution were taken and 0.5 mL DCM. Reported conversions were also averaged from the same replicate crude product sample as used for yield determination (as well as replicate samples of the starting material solution). Again, the reported conversion was the average from the replicate samples and the estimated uncertainty was from the discrepancy between the average and the measurement furthest away from the average.

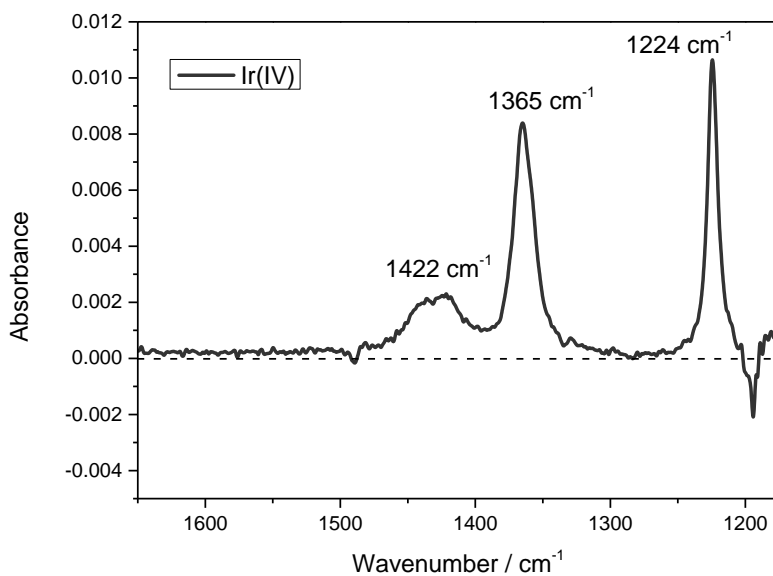
Ap.3 Spectroelectrochemistry Data

All spectroelectrochemical measurements were run as a solution in CD_3CN with 0.1 M tetrabutylammonium tetrafluoroborate electrolyte. Substrate concentrations were ~5 mM. Measurements were run in an optically transparent thin-layer electrochemical (OTTLE) cell with CaF_2 windows and a 200 μm path length. Pt electrodes were used as the working/counter electrodes and applied potentials were against a Ag reference electrode. Applied potentials were determined in advance from cyclic voltammetry measurements of the same solution. Cyclic voltammetry and spectroelectrochemical measurements were run by Katherine Reynolds.

Ap.3.1 Ir-126 Spectroelectrochemistry Data

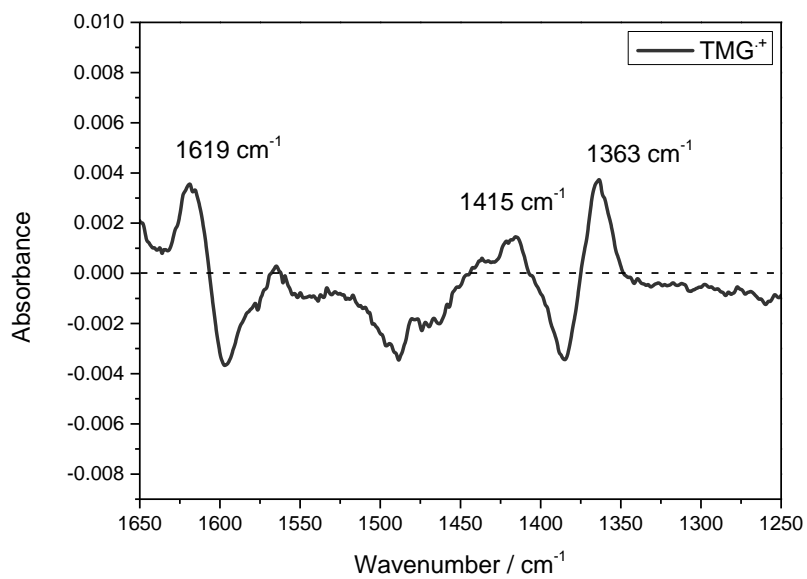


Spectroelectrochemistry spectrum for Ir-126 at -1.30 V.



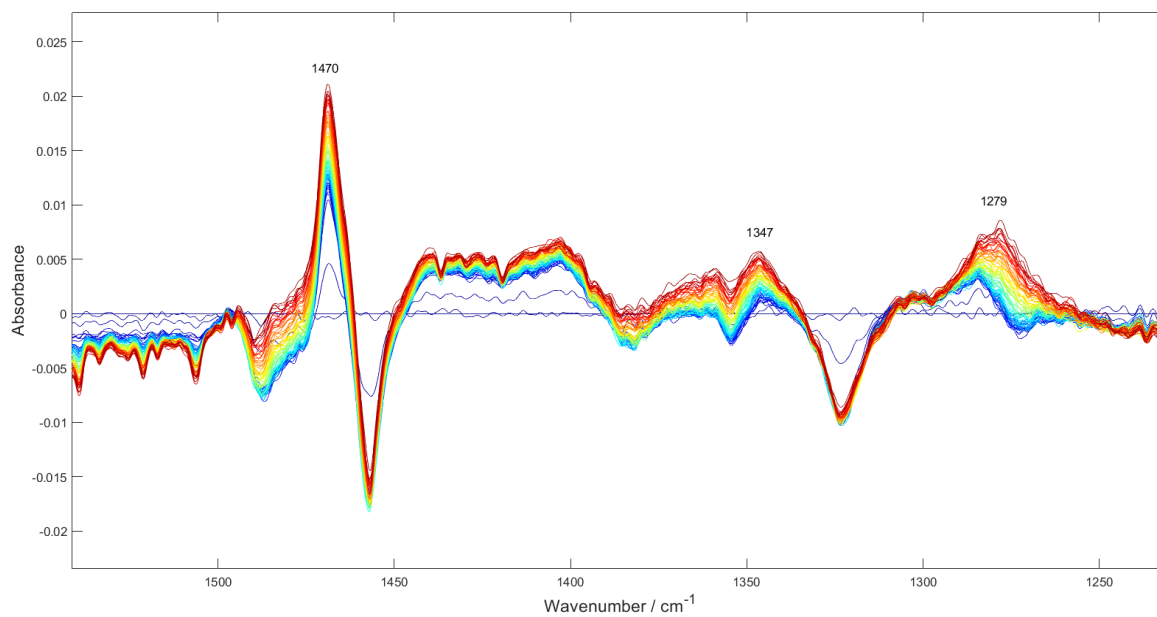
Spectroelectrochemistry spectrum for Ir-126 at 0.30 V.

Ap.3.2 TMG Spectroelectrochemistry Data

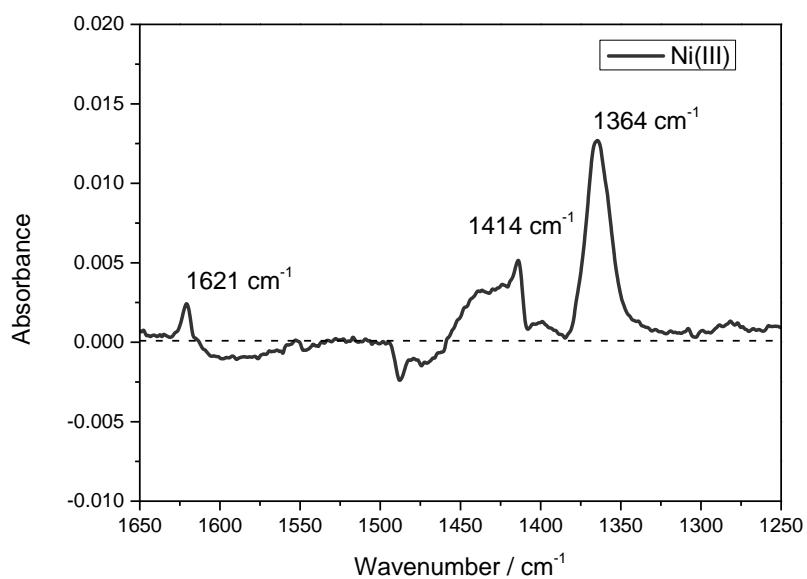


Spectroelectrochemistry spectrum for TMG at 1.30 V.

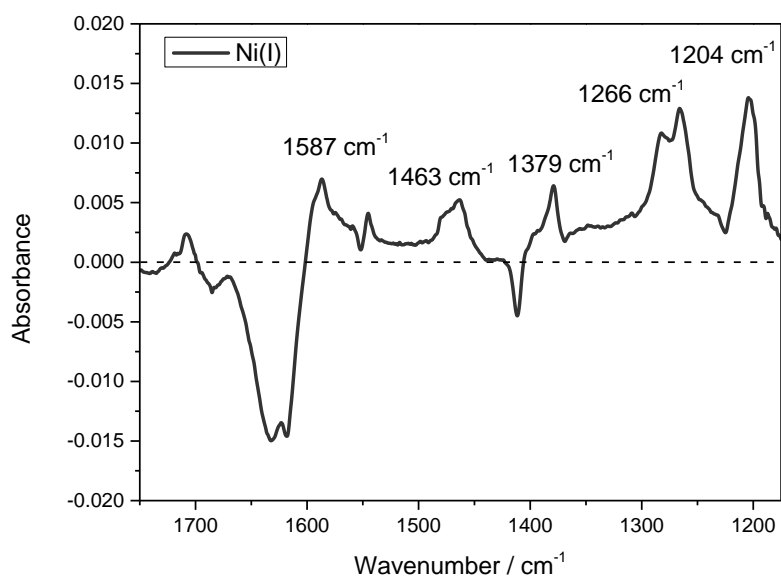
Ap.3.3 Quinuclidine Spectroelectrochemistry Data



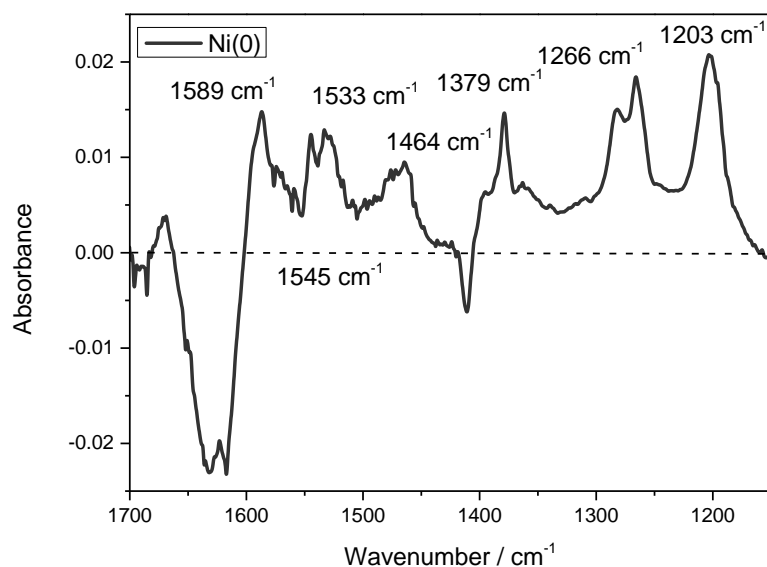
Ap.3.4 NiCl₂.glyme/dtbbpy Spectroelectrochemistry Data



Spectroelectrochemistry spectrum for NiCl₂.glyme/dtbbpy at 1.20 V.



Spectroelectrochemistry spectrum for NiCl₂.glyme/dtbbpy at -0.80 V.



Spectroelectrochemistry spectrum for NiCl₂.glyme/dtbbpy at -1.30 V.

Ap.4 Reactor Standard Operating Procedures

Ap.4.1 Thermal Flow Reactor Standard Operating Procedure

Start-Up:

1. Ensure sufficient preparation of reagent solution for the desired reaction adhering to safety and COSHH regulations.
2. Switch on the power to the system, supplying power to the temperature and pressure monitors and BPR.
3. Press the reset button on the trip, supplying power to the pump and heater (ensure the heater is not set to cause heating of the block at this point).
4. Using the Teflon three-way valve joining tubing 1, 2 and 3 (upstream of the pump, marked TWV on diagram), prime the pump firstly with the reagent solution, then, switching the open position of the three-way valve to the other inlet, prime the pump with reaction solvent. This is to ensure that after flushing the reactor with solvent and allowing desired pressures and temperatures to be reached, the pump inlet can be switched to the reagent solution without allowing air to enter the pump head.
5. Flush the reactor with at least two system volumes of reaction solution, checking the system for leaks.
6. When solvent begins to flow out of the reactor, set the system pressure using the BPR, again checking for leaks.
7. If leaks are found, the pressure should be reduced to atmospheric pressure and the fittings(s) tightened or replaced as needed and recorded in the logbook.

Heating:

8. Using the temperature control box, set the temperature for the heater.
9. Allow the set temperature to be reached whilst still flowing neat solvent through the reactor.

Reaction:

10. Using the Teflon three-way valve upstream of the pump, switch the pump inlet feed to the reagent solution (begin timing the reaction).
11. Allow equilibration time for the reaction (typically for 1.5 system volumes to be passed through the reactor).
12. Collect sample(s).

Shut-Down:

13. After passing through all reaction solution, use the T-piece to switch back to pumping neat reaction solvent.
14. When outlet solution becomes colourless (*i.e.* all reaction solution has left the system), set heater temperature to zero.
15. Allow the system to cool below the boiling point of the reaction solvent, then release the pressure step-wise (*e.g.* decrease 10 bar at a time) using the BPR interface.
16. When atmospheric pressure is reached, allow two system volumes of neat solvent to flush through to ensure cleaning of the reactor.
17. Stop the pumps and then turn off the system.

Emergency Shut-Down:

Turn off the heaters and pumps using the emergency stop button on the trip box. Allow the system to cool. When the system has cooled below the boiling point of the solvent (when all four thermocouples display a temperature below this value), the pressure can be released from the BPR.

In case of a fire, a CO₂ extinguisher should be used due to electrical components.

Cleaning:

As stated previously, the reactor should be thoroughly cleaned after use by flushing through with neat solvent. Due to the nature of the reactions of primary use (involving Pd-catalysis), occasional reconditioning of the reactor may be required. This can be determined by using a model reaction (*e.g.* between iodobenzene and butyl acrylate) in the absence of added catalyst. Upon analysis of the reaction, if conversion to the coupled product is seen, the reactor is likely somewhat fouled with Pd precipitate residue. If so, the reactor should be flushed with aqueous nitric acid for ~5 h at a flow rate of ~5 mL min⁻¹ (in a recycled system). If this is required, the sprung relief valve should be disconnected due to incompatibility between Kalrez seals and nitric acid. For this purpose, removing the valve is acceptable as no pressure or heat should be supplied to the system. After flushing with nitric acid, the system should then be flushed with deionised water for at least 10 system volumes to ensure complete removal of nitric acid residue. Prior to the next use, the reactor should then also be flushed thoroughly with the reaction solvent and the sprung relief valve reconnected before applying any pressure or heat.

Checklist:

- Check the tripbox is working including pressure/temperature trips and emergency stop.
- Ensure all electrical cables are properly connected.
- Carry out a leak test using blue paper.
- Ensure all tubing, reactor components and electricals appear undamaged.

Ap.4.2 Photochemical FEP Flow Reactor Standard Operating Procedure

Standard Start-Up, Performing a Reaction and Shut-Down Procedure:

1. Ensure suitable preparation of reaction solution has been performed according to the specific needs of the experiment, adhering to relevant COSHH and other safety regulations.
2. Switch on the power to the components of the system to be used (Lightsabre LEDs, pump and any cooling/heating devices). Ensure that the LED current dial on the LED control box is set to zero so that the LEDs do not immediately turn on.
3. Turn on the cooling (either from a recirculating chiller or water from a tap) to the Lightsabre LEDs – check for any leaks where appropriate. If leaks are found, turn off the cooling, attempt to repair the issue and repeat the test, until the issue has been resolved.
4. Repeat step 3 for heating/cooling being applied to the jacketed glass tube, if this is to be used in the reaction.
5. Begin pumping neat solvent (preferably using the solvent to be used for the reaction) through the system and perform a leak test – again, if leaks are found, stop the pump, attempt to repair the issue and repeat the test, until the issue has been resolved. The leak test should be performed at (at least) the maximum flow rate to be used for the reactions. After the leak test, the flow rate used to flush neat solvent through the system is not particularly important.
6. When the system is turned on, all possible components are free of leaks and neat solvent is flushing through the reactor coil, the reactor coil/jacketed glass tube should be shrouded, first with a loose covering with aluminium foil, and then a secondary shield placed in front of the reactor or in front of the containment unit. If removal of the shrouding is required at any time, appropriate safety glasses should be worn and others in the vicinity should be aware.
7. The Lightsabre LEDs can then be turned on to the desired current for the experiment, using the dial on the control box. Checks for any mistakes in the shrouding should be made and, if required, the dial turned back down to zero to turn off the LEDs and the shrouding adjusted appropriately. This step can then be repeated.
8. The temperature of the LEDs (as displayed on the control box) should be allowed to equilibrate and should be no higher than ~25 °C. If exceeding this temperature, the flow of water from the tap should be increased slightly (whilst ensuring no leaks appear – if so, the system should be turned off and the appropriate adjustments made until the issue has been resolved) or, the temperature of the recirculating chiller be lowered.
9. At this point – the flow rate required for the experiment should be set at the desired value. When the LED temperature has equilibrated to an acceptable level, the experiment can be started and the reaction begun. This could involve switching (using a three-way valve) from the neat solvent to the previously prepared reaction solution, or (so long as a peristaltic pump is being used) removing the pump-head inlet from the neat solvent and quickly immersing in the reaction solution. A timer should be started alongside this, for monitoring the time taken before taking samples, terminating the experiment etc.
10. If samples are required from the reactor outlet:
 - Ensure safety of the user and others by being aware that shrouding may be partially removed/compromised – wear appropriate safety glasses.
 - Remove the minimum amount of shrouding required for collecting a sample and undertake sampling whilst keeping on appropriate safety glasses and not looking directly at the light source.
 - Replace shrouding immediately after sampling.

11. After sampling, or, if samples are not required (the experiment involves collecting all of the mixture pumped through the system, for example) then the LEDs should be turned off, either by turning the current on the control box to zero, or by turning off at the plug outside of the containment unit (preferably, off at the control box first to avoid the LEDs unexpectedly turning on the next time the power supply to the control box is turned on at the wall). The inlet to the pump should again be switched back to neat solvent, following processing of all of the (or all of the required) reaction solution.
12. The shrouding should then be removed from the reactor system, whilst continuing to flush through neat solvent. The remaining reactor system components (Lightsabre control box, recirculating chillers/heaters) can be turned off, at the wall or unplugged), whilst the pump remains on.
13. At least ~5 system volumes of neat solvent should be flushed through the reactor to ensure thorough cleaning. It should be observed whether any build-up of contaminants has occurred (by visible observation of the transparent tubing) and, if necessary, perform further cleaning *e.g.* with other solvents, solutions *etc.*, which would likely be specific to the reaction performed and the relevant safety considerations in a COSHH form should be made.
14. The pump can then either be turned off to finalise the shut-down procedure, or, prior to this, the pump-head inlet can be removed from neat solvent and exposed to the air (presuming a peristaltic pump is being used) in order to empty the reactor system of any standing solvent. Following removal of the solvent from the system, the pump can then be turned off to complete the shut-down procedure.

Emergency Shut-Down:

If an emergency shut-down is required, this should be performed by turning off all system components at the wall plug outside of the containment unit, or, by unplugging or turning off the extension lead which all components are plugged in to, depending on how the system has been assembled.

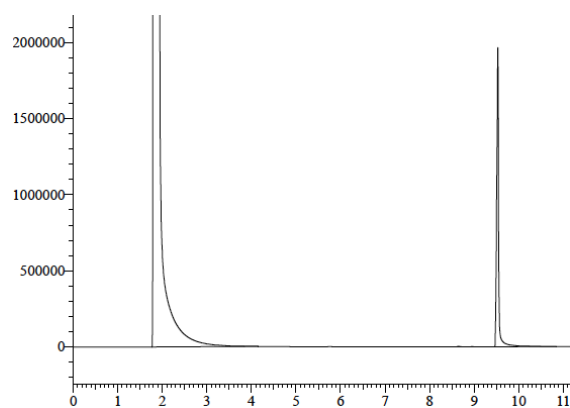
In case of fire in the proximity, a CO₂ extinguisher should be used, due to the presence of electrical components.

Checklist:

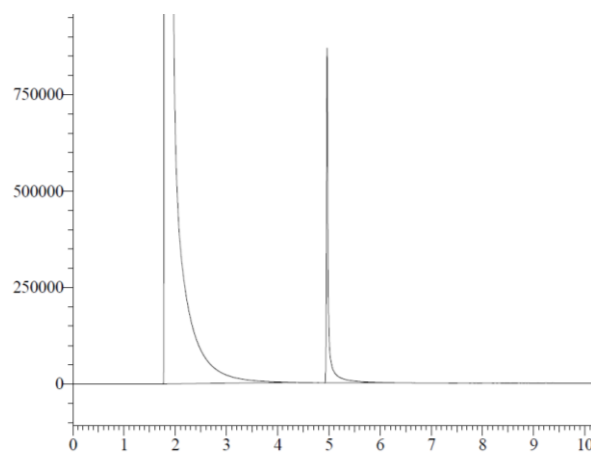
- Before use, ensure all components are appropriately positioned (*e.g.* electricals away from water or possible leaks, where shrouding can be appropriately positioned, suitable access to plugs/sockets for emergency shut-down *etc.*).
- Ensure all tubing, fittings/connections and components appear undamaged.
- Always perform a leak test prior to full operation for any fittings/connections where flowing liquids are involved.
- Ensure the Lightsabre control box has current set to zero before turning on the power to the box, so that bright light is not immediately emitted upon turning on the power.
- Ensure appropriate shrouding and safety glasses are available to the user before operation and that others in the vicinity are aware of the use of the light source.
- Ensure all COSHH forms and other safety considerations have been made before commencing the experiment.

Ap.5 GC Chromatograms

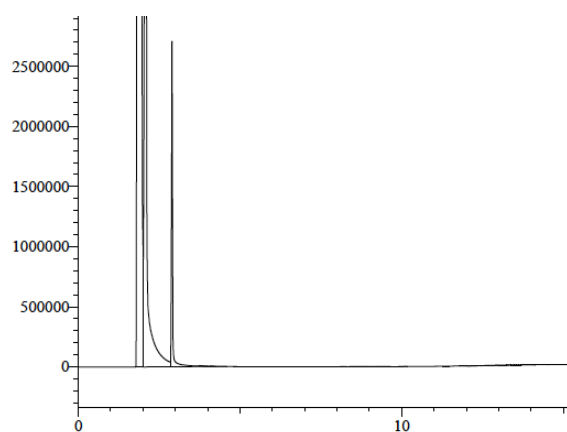
Ap.5.1 Chapter 2



GC chromatogram of **ButCin**, in MeOH, 0.053 M. Retention time ~9.5 min.

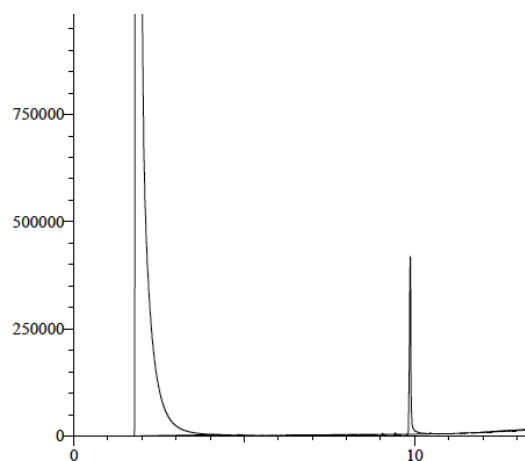


GC chromatogram of **IB** in MeOH. Retention time ~5.0 min.

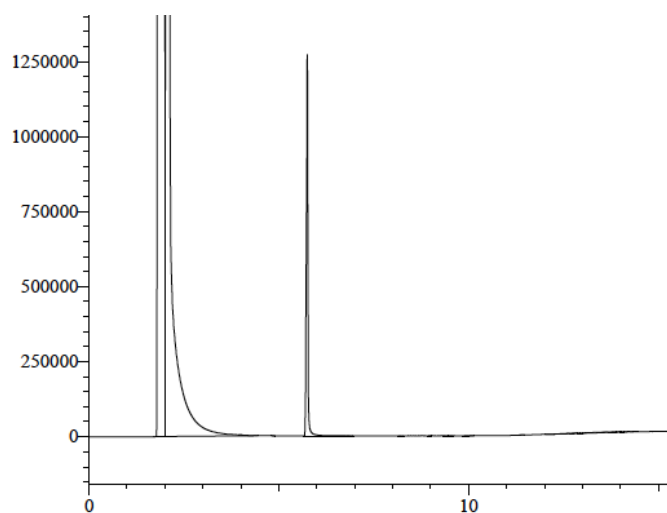


GC chromatogram of **DIPEA**. Retention time ~2.9 min.

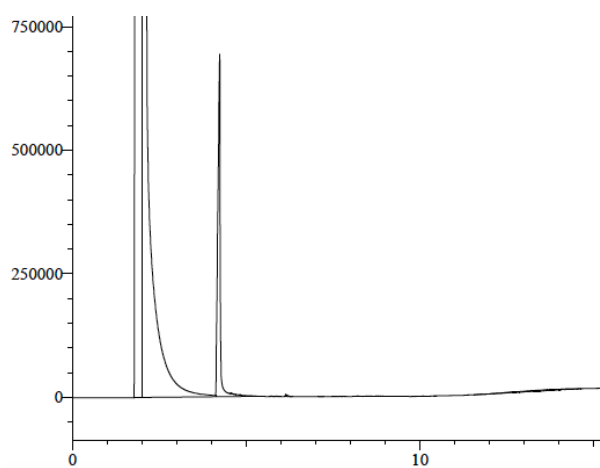
Ap.5.2 Chapter 3



GC chromatogram of **HPBO**, 0.038 M in MeOH. Retention time ~9.8 min.

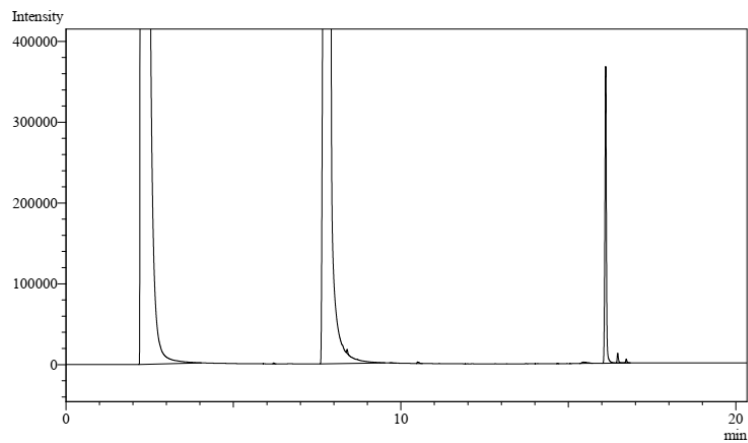


GC chromatogram of **3IP**. Retention time ~5.8 min.

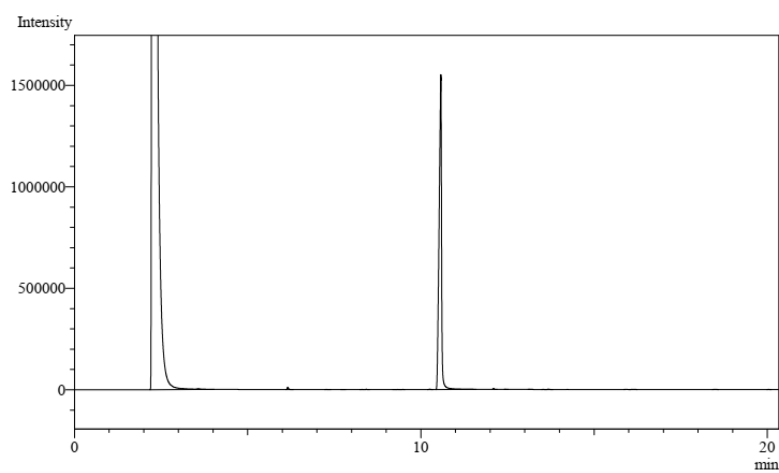


GC chromatogram of **DHB**. Retention time ~4.2 min.

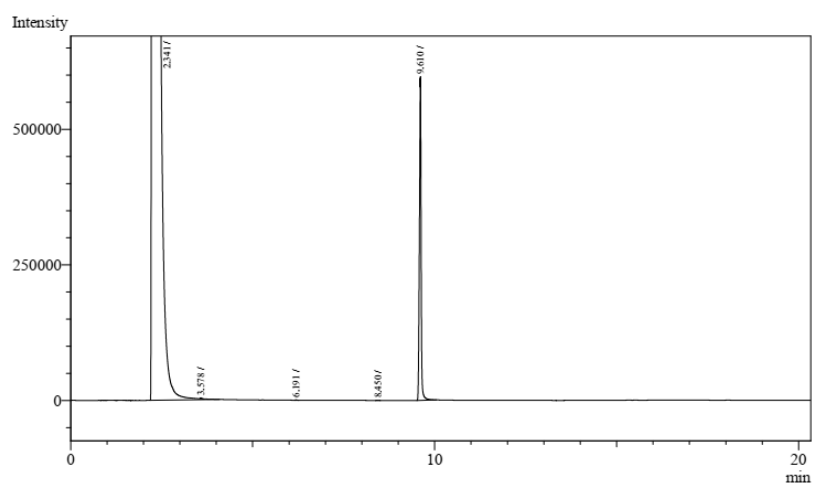
Ap.5.3 Chapter 4



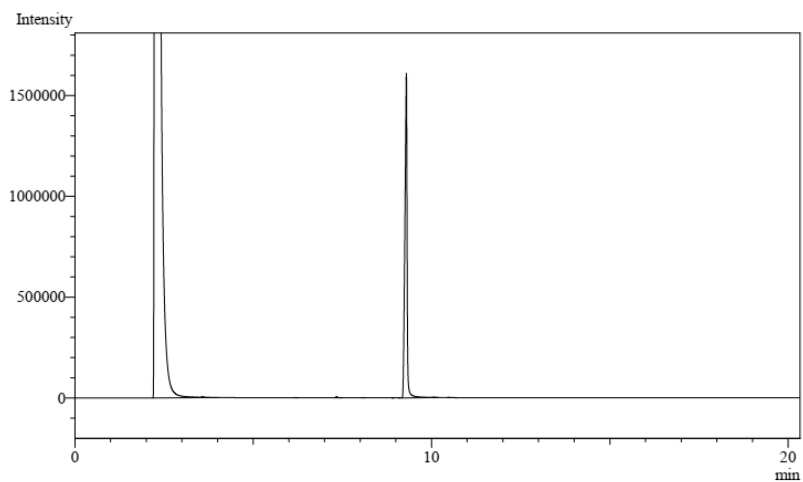
GC chromatogram of **RHP**, in MeOH/NMP (10:1). Retention time ~16.1 min.



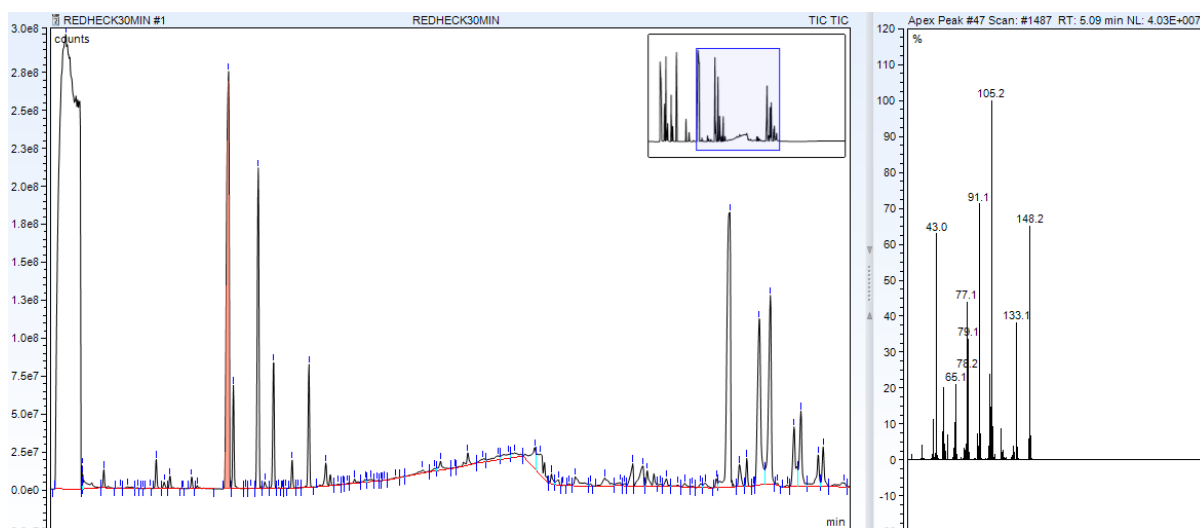
GC chromatogram of **4PBO**, in MeOH. Retention time ~10.6 min.



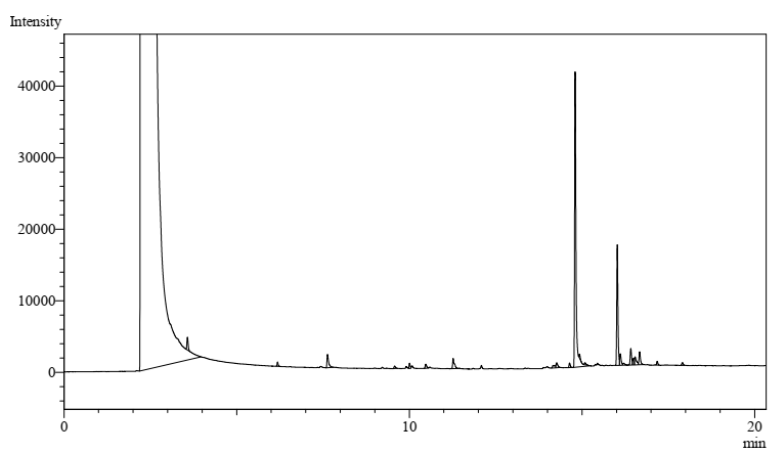
GC chromatogram of **4IA**, in MeOH. Retention time ~10.6 min.



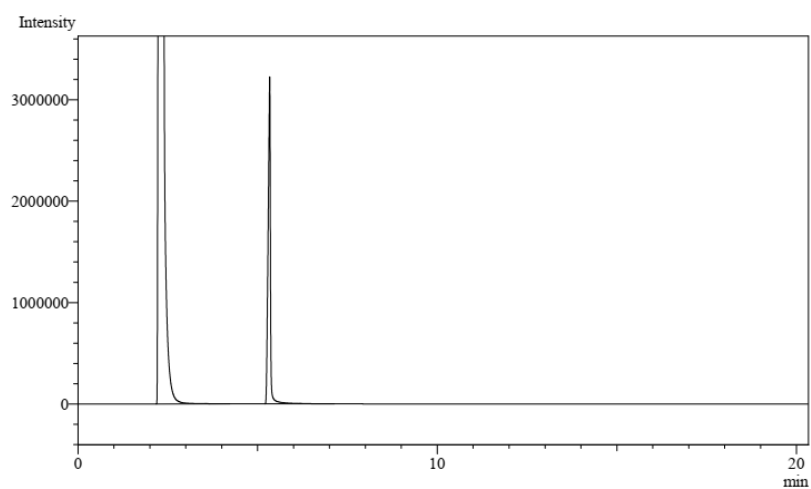
GC chromatogram of 4-phenylbutan-2-one RE, in MeOH. Retention time ~9.3 min.



GC-MS chromatogram/spectrum, suggesting the presence of a species with mass corresponding to that of RE.

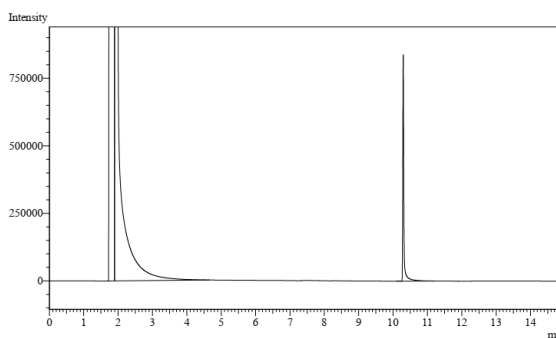
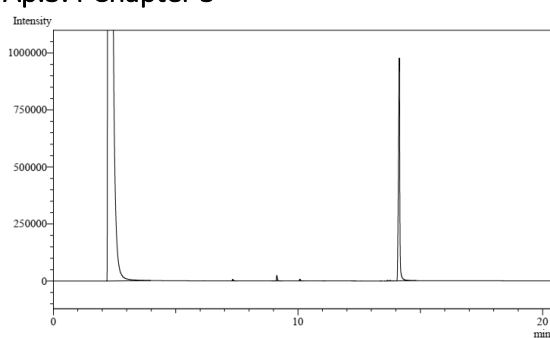


GC chromatogram of crude 4,4'-dimethoxy-1,1'-biphenyl HC, in MeOH. Retention time ~14.8 min.

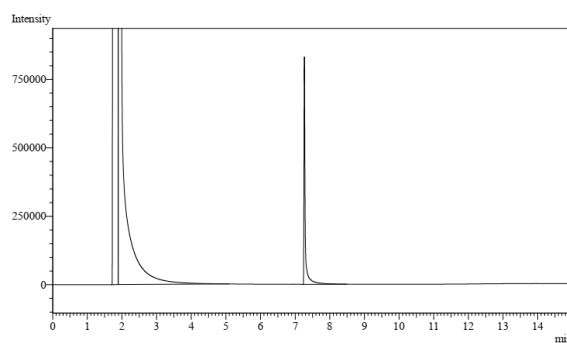
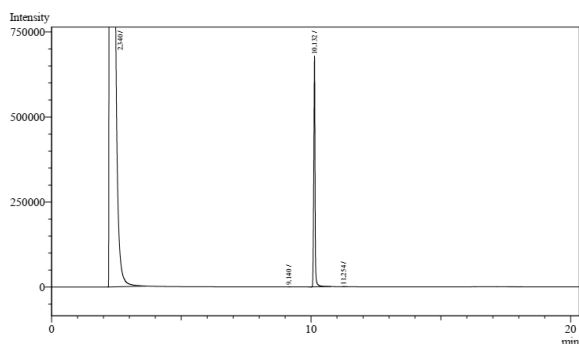


GC chromatogram of anisole, in MeOH. Retention time ~5.3 min.

Ap.5.4 Chapter 5

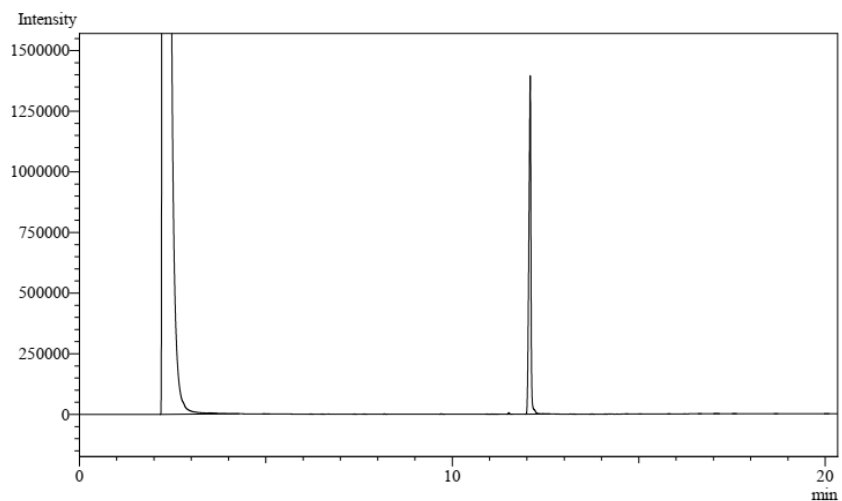


GC chromatogram of **4-HOAP**, in MeOH. Equity-1701 column (left) retention time ~14.1 min. SPB-170 column (right) retention time ~10.3 min.

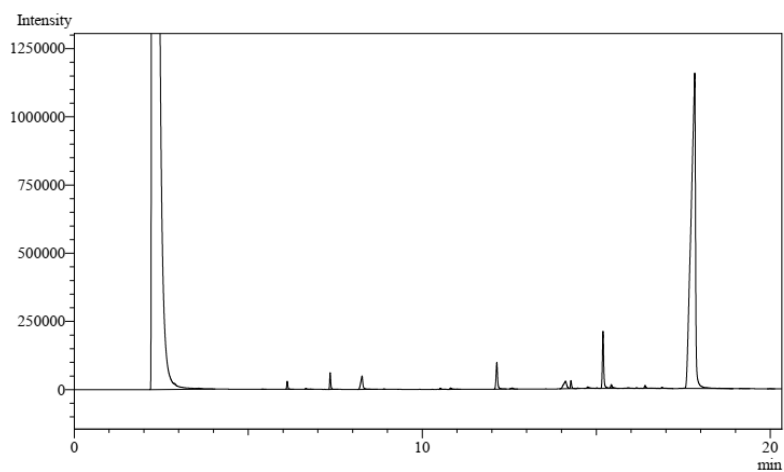


GC chromatogram of **4-BrAP**, in MeOH. Equity-1701 column (left) retention time ~14.1 min. SPB-170 column (right) retention time ~10.3 min.

Ap.5.5 Chapter 6



GC chromatogram of **CGE**, in MeOH. Retention time ~12.1 min.



GC chromatogram of **NHPI**, in MeOH. Retention time ~17.8 min.

